RELATIONSHIPS BETWEEN MICROMORPHOLOGY AND IMPACT PROPERTIES OF INJECTION MOULDED ISOTACTIC POLYPROPYLENE.

by

Mark William Murphy.

A Dissertation Submitted To Brunel University
For The Degree Of Doctor Of Philosophy.

Department Of Materials Technology
Brunel University
Uxbridge
Middlesex.

February 1986

Text cut off in original

Brunel University,
Department of Materials Technology,
Uxbridge, Middlesex. UB8 3PH.

Mark William Murphy

Relationships Between Micromorphology And Impact Properties Of Injection Moulded Isotactic Polypropylene.

Ph.D. Degree

1986

ABSTRACT

The micromorphology and properties of injection moulded semi-crystalline polymers can be significantly modified by changes in the injection moulding parameters and the design of mould. Further modifications to the microstructure and properties occur following the incorporation of additives into a thermoplastic compound, such as stabilisers, pigments, nucleants, etc. Many published papers refer to these changes in microstructure, but very little attention has been devoted to the detailed characterisation of the outer surfaces of injection mouldings, which play an important part in determining impact properties.

The main objective of this research project was to carry out a systematic examination of the micromorphology of a range of isotactic polypropylene injection mouldings, paying particular attention to the outer layers which are difficult to characterise and to then relate the micromorphology revealed to the impact properties. Models which relate the mechanism of impact failure to microstructure and processing route have been developed as a result.

Particular attention was given to the careful production of injection mouldings to ensure reproducible micromorphologies and mechanical properties for set processing conditions. This was carried out prior to very comprehensive characterisation of micromorphology using a range of analytical techniques including, straightforward microtomy and optical microscopy, x-ray diffraction, Differential Scanning Calorimetry and the application of a new etching and replication method for transmission electron microscopy studies. The impact properties of mouldings were determined by instrumented falling-weight and instrumented Izod impact test methods.

Injection mouldings revealed a complex skin-core morphology, the width, degree of orientation, crystal form (α or β) and spherulite size of the various layers were found to be strongly dependent on the moulding parameters and additives incorporated. The role of such factors in determining the impact properties was identified providing valuable information to commercial moulders of polypropylene.

ACKNOWLEDGEMENTS

I would like to thank Professor M.J. Bevis and Mr. K. Thomas for supervising this work with the guidance and encouragement required.

In addition, I would like to thank the National Physical Laboratory and the Science and Engineering Research Council for their financial support.

Thanks are also due to Dr. D. Norton for his valuable assistance with the etching and replication technique and to Miss. E. Thompson for her assistance with the x-ray diffraction studies. To my colleagues Dr. P. Allen, Dr. J. Bowman and Mr. C. Watson for valuable discussions and suggestions.

Finally, I would like to thank Sharon Forder for typing this thesis so diligently.

CONTENTS

./.....

CHAPTER I

INTRODUCTION AND LITERATURE SURVEY

1.1 INTRODUCTION

It is widely recognised that the mechanical properties of injection moulded semi-crystalline thermoplastics are strongly dependent on the morphology of the polymer, the orientation of the polymer chains and the existence of residual stresses. Studies of various moulded semi-crystalline polymers have shown that three or more morphological regions are discernible and these range from a non-spherulitic highly oriented surface layer to a spherulitic relatively unstrained central core. The effect of injection moulding variables, compound additives and mould design on this morphology and the quality of the moulded part are an important aspect of moulding technology.

A number of detailed systematic studies on the effects of processing parameters on skin-core morphology and resultant mechanical properties of semi-crystalline thermoplastics have been carried out (1-25). However, although certain common trends have been noted between morphology variations and property variations, it is apparent that the development of relationships between processing conditions, morphology and mechanical properties remains a complex problem. The complexity of the problem becomes apparent when one considers the many interdependent combinations of machine settings, mould designs and percentage loadings of compound additives that can be used to produce a moulded article and the effects of these parameters on the mechanical working thermal history and resultant microstructure.

A systematic study was therefore initiated by The National Physical Laboratory and Brunel University to improve our current knowledge on the effect of moulding conditions, mould geometry, compound additives and molecular weight on the mechanical properties of isotactic polypropylene homopolymer, iPP. It was considered that impact loading would present the most severe test for the material and so this has been the test method used to assess the quality of the mouldings throughout the research programme.

The ultimate aim of the study was to develop a model relating processing variations to micromorphology and impact properties of iPP homopolymer and report this to a depth not previously attempted. This work should then indicate how to improve the quality of iPP moulded parts particularly where fine control of surface microstructure is required. It is well known that isotactic polypropylene is a complex polymer in that it can crystallize into more than one crystallographic form and that these are incorporated into spherulites of different types depending on the rate of cooling and the level of stress and pressure during crystallization. It was therefore intended to also establish the role of crystallite size and type, surface morphology and shear induced morphologies on the impact properties of iPP injection mouldings. To this end careful selection and incorporation of commercially available additives was required to assess the effects of enhancing or suppressing certain crystallographic features and determine resultant related changes in impact performance. The known crystalline architecture of iPP will be described in the following section.

This dissertation is divided into six chapters.

Chapter 1 deals with a comprehensive review of the existing literature concerned with crystallization of polymer melts, structure development in injection moulded semi-crystalline polymers and impact property-process condition relationships established for numerous injection moulded polymers. Within this literature review aspects such as nucleation and growth mechanisms, the spherulitic and lamellar morphology of melt crystallized iPP, crystallization under the influence of shear and extensional flow, skin-core morphologies and the effects of additives on the structure and properties of melt crystallized iPP are discussed.

Chapter 2 is concerned with the selection and preparation of materials, instrumentation and control of the injection moulding machines, instrumented impact test methods, and a detailed explanation of the characterization techniques employed to resolve the micro-morphology of injection moulded iPP plaques. This chapter is an extension to the literature survey since many relevant papers were found which have applied the testing and characterisation techniques to iPP mouldings in a similar manner. In some cases previous studies provided useful guidelines on the interpretation and quantification of results.

Chapter 3 presents the experimental procedure and results of studies on the effects of processing conditions on the micro-morphology and impact properties of injection moulded iPP.

Of particular interest as regards technical advancement in characterisation of micromorphology was the application of -

(i) the permanganic etching technique to reveal the micro-morphology of injection mouldings which clearly illustrated the structural heterogeneities present,

(ii) the x-ray diffractometer to study the concentration and distribution of the two crystalline phases (α and β) along the flow direction of iPP mouldings and furthermore, to quantify the degree of molecular orientation and crystallinity, and

(iii) the Vickers Microhardness testing of bulk mouldings to gain quantitative information about the hardness through the thickness of selected areas exhibiting banded morphologies.

Both impact test methods employed in this research project have sophisticated instrumentation to provide as much information as possible on the impact event. An analysis of some typical force/time and energy/distance^2 curves is given to assess the mechanisms of crack initiation and propagation. In addition fracture surface studies were made using the Scanning Electron Microscope (SEM) to reveal the crack initiation site and fracture topography of Izod test pieces.

Chapter 4 presents the experimental procedure and results of studies on the influence of molecular weight distribution on the micromorphology and impact performance of iPP injection mouldings. This study revealed interesting modifications of the size and distribution of the two polymorphs (α and β) and the shear zone with molecular weight which had profound effects on the selected area impact properties. X-ray diffraction studies revealed noteable sensitivity of the β phase nucleation to molecular weight levels.

Chapter 5 is concerned with the study of the effect of low percentage additions of commercially available compounds on the micromorphology and impact properties of injection moulded iPP. In this study the Differential Scanning Calorimeter was used to generate thermal data on the melting and recrystallization behaviour of moulded plaques and to assess the relative proportions of α and β crystallites produced. An interesting correlation between crystallization temperature, Tc, and impact strength was found due to the nucleating effect of some additives i.e. noticeably reducing the degree of supercooling. X-ray Diffraction studies revealed preferential heterogeneous nucleation of one polymorph or the other and significant variations in the degree of crystallinity with certain additives.

The discussion of the results presented in Chapters 3, 4 and 5 is given in Chapter 6 with reference to previously published literature. The presentation of two models relating impact properties to micromorphology and processing conditions, as well as proposed theories on the contribution of α and β crystallites and surface morphologies to impact strength of iPP mouldings are given. In addition, we have gained quantitative information on the effects of heterogeneous nucleating agents and molecular weight on the micromorphology and impact properties.

The industrial importance of this work is highlighted in the discussion with reference to some additional characterisation and testing of commercial iPP injection mouldings supplied by the Addis Company (26).

1.2 CRYSTALLIZATION OF POLYMER MELTS

1.2.1 Spherulitic Development

When a polymeric melt is allowed to cool in the absence of stress from quasiextensional flow a spherulitic structure is formed as shown in Figure 1 for a polypropylene grade.

Detailed investigations (27, 28, 29) of the spherulitic microstructure show that they are composed of radially directed thin platelets of lamellae ribbon-like crystals, which are very long in comparison to their thickness. The thickness of the crystal ribbon is in the order of 100-500Å and since the thickness is only a fraction of the polymer chain length the polymer chain may enter a given crystal ribbon many times - Figure 2. The chains are oriented approximately parallel to the thin dimensions of the ribbon and 'tie chains' connect individual crystal ribbons. The inter-ribbon region is generally termed amorphous composed of tie chains, chain ends, loose loops or even totally unincorporated chains. The spherulite structure is seen often as a banded structure under polarised light and this is due to natural twisting of the ribbonlike crystals about their molecular axes. The reader is referred to the original papers of Keith and Padden (30, 31), of Keller (32) and Price (33) for further details on the optical extinction effects of spherulites.

Precisely how a spherulite develops depends, in the first instance, on how it is nucleated. A common, but not essential progression is that depicted in Figure 3, beginning with a fibre and evolving through sheaf-like embryos before attaining a spherical envelope. When spherulites impinge upon one another they become polyhedral. Mature spherulites have the same crystallographic axis along every radius.

Figure 1 Typical iPP spherulitic structure.

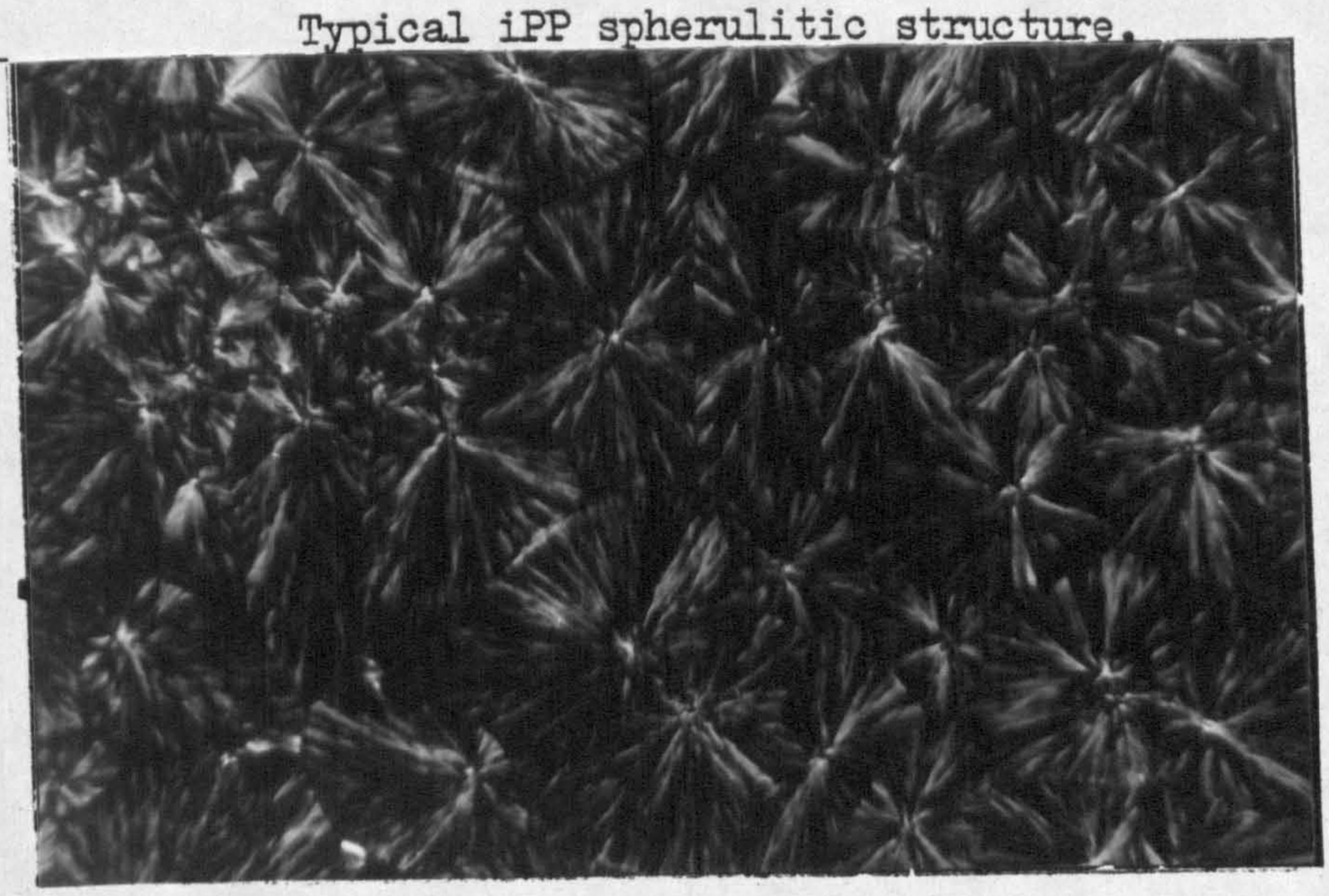

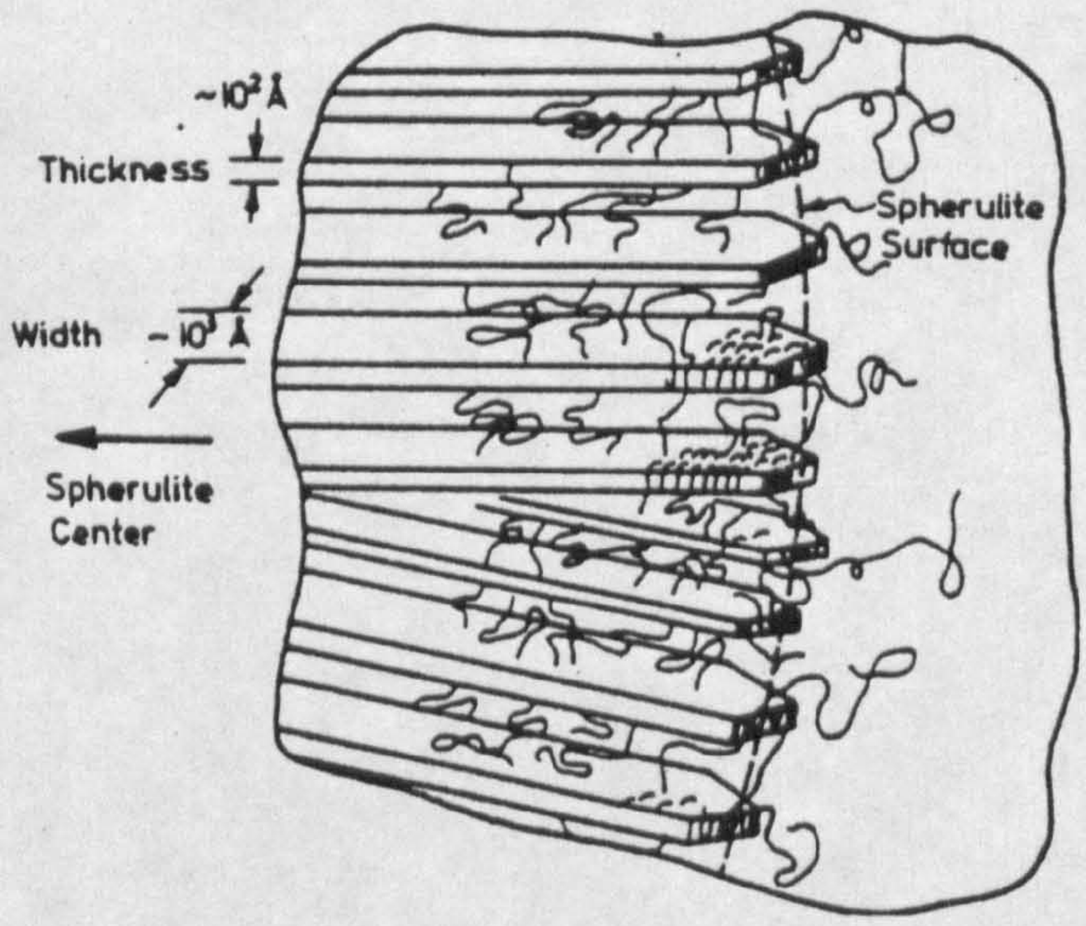

Figure 2 Schematic representation of spherulite.

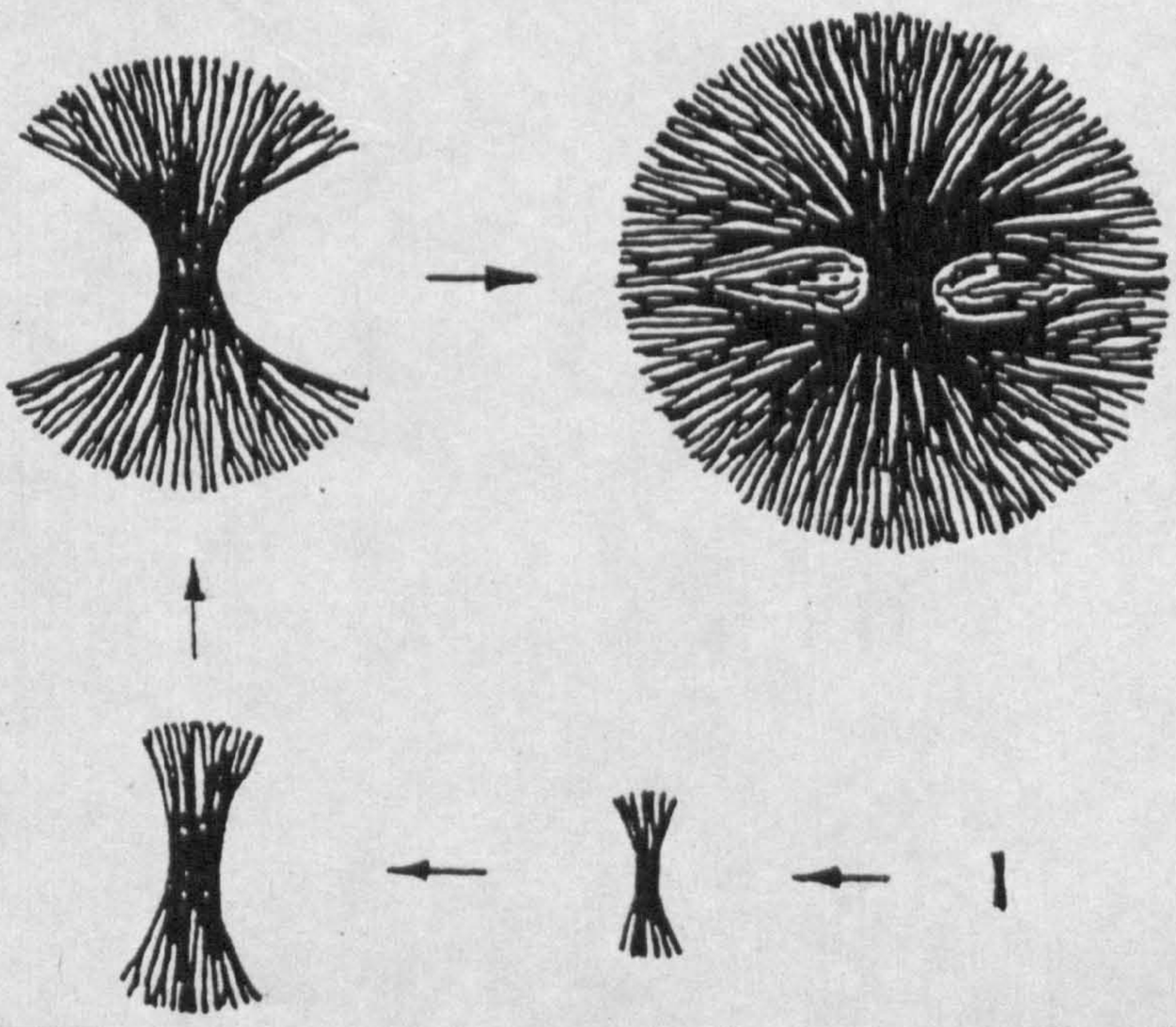

Figure 3 Progression of spherulite growth beginning with a fibre and evolving through sheaf like embryos.

1.2.2. Nucleation and Growth

The polarizing microscope has been much used to study the growth rates of spherulites, i.e. the velocity of radial advance. All studies show that this quantity is remarkably linear with time at a given temperature, except when spherulites near impingement or when the viscosity of the melt is deliberately reduced. This is, in fact, a critical point in the understanding of spherulitic growth. The variation with temperature typically takes the form of Figure 4. It has long been recognized, however, that the characteristic shape is a consequence of growth being slowed by increasing viscosity at lower temperatures and by diminishing thermodynamic drive (i.e. supercooling) as the melting point is approached. For polyethylene, growth is so fast that only the higher end of this curve can be realized while for other polymers such as iPP and isotactic polystyrene the whole range can be measured.

The extent over which growth rate can be measured depends on spherulite size and this in turn depends on the relation between nucleation rate and growth rate. In simple terms, if nucleation is slow and growth rate fast by comparison, a few large spherulites will result. Conversely, rapid nucleation will lead to a profusion of spherulites which may well be immature. If spherulite size is to be controlled and this can be a desirable end in just the same way as control of grain size is important in metallurgy, then it is through varying nucleation rates that it is best attempted.

This is possible because, almost always, nucleation in polymers is heterogeneous in origin i.e. it is initiated on non-polymeric particles. Were it homogeneous forming on the polymer itself, many fewer possibilities would present themselves. In a bulk sample once heterogeneous nucleation has started growth will proceed through the entire sample. This is the basis of adding heterogeneities deliberately to samples to control spherulite size and development.

No matter whether nucleation is heterogeneous or homogeneous it is still strongly affected by molecular weight, with longer molecules usually initiating crystallization of the polymer. Presumably this is because the longer a molecule is, the greater chance of being able to adopt a suitable conformation. The loss of longer molecules by degradation leads to the creation of additional very short ones which helps to grow fewer and more open spherulitic structures.

Crystal growth is usually governed by diffusion, either of heat or matter. Keith and Padden (34) formulated a theory based upon the diffusion of impurities away from growing crystal surfaces to account for the development of radial fibrosity at isothermal constant growth rates. Keith and Padden's proposal is essentially as follows:- Consider a supercooled polymer melt within which crystallization is proceeding at a finite rate. Although there must be local temperature gradients to allow the heat of crystallization to be dissipated, the uniform linear growth rate shows that these must be small and the system may be regarded as effectively isothermal. Let there be an equilibrim concentration $C_{\infty 0}$ of effective impurities at points remote from growing crystals.

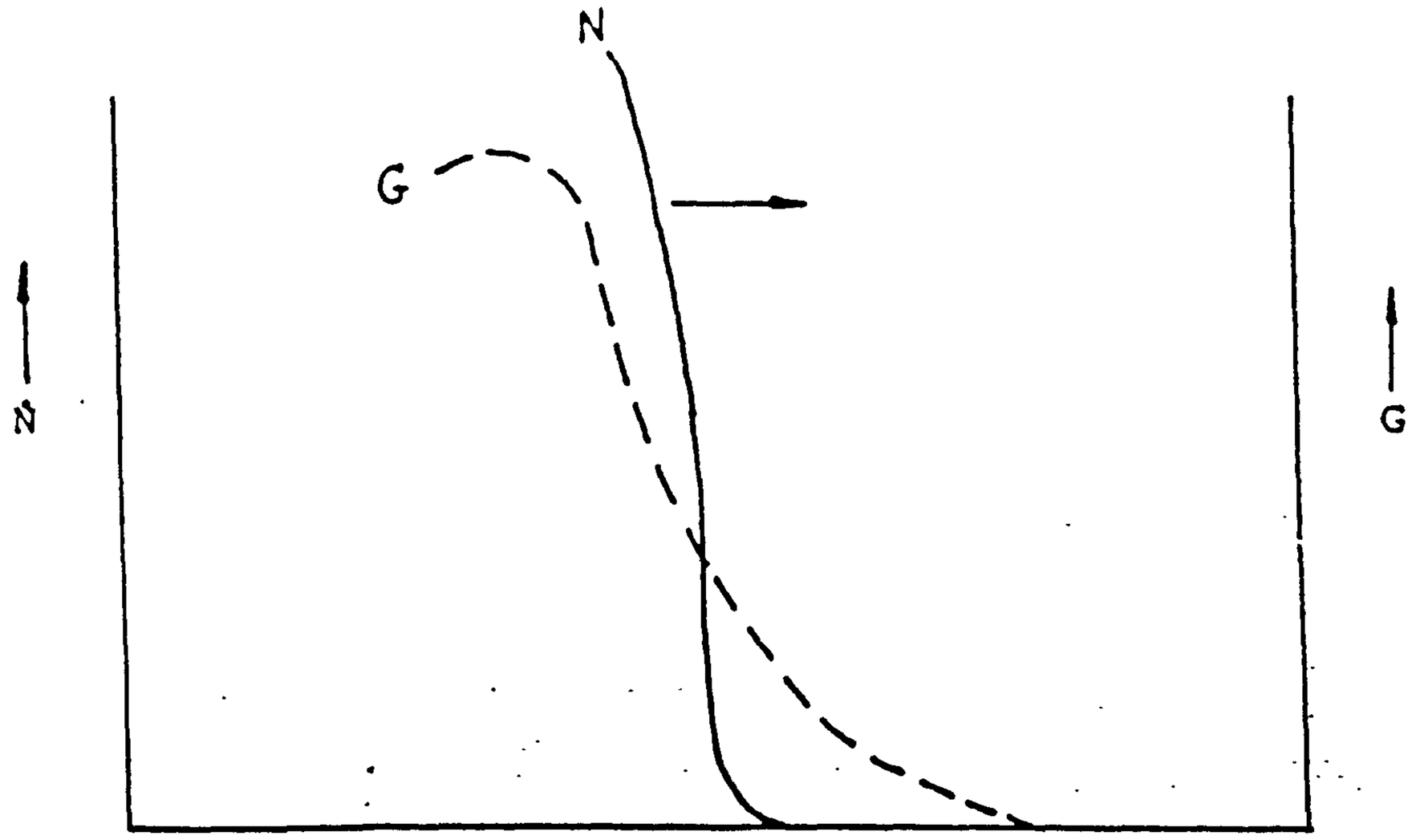

Figure 4 Relative temperature dependences of polypropylene nucleation rate N and spherulitic growth rate G.

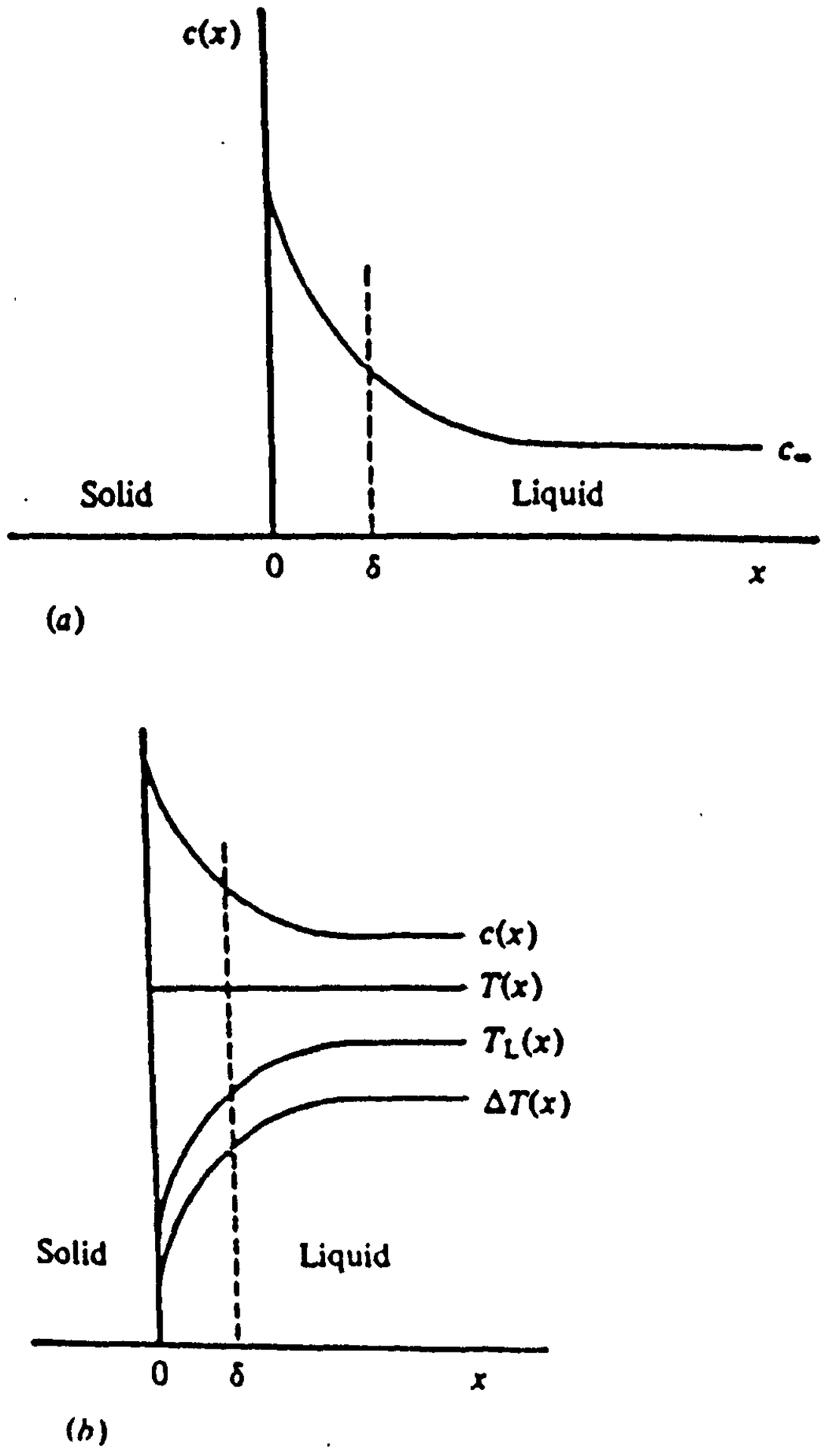

Figure 5 (a) The schematic dependence of impurity concentration C with distance ahead of a growing crystal surface.

(b) Corresponding variations in ambient temperature T, liquidus temperature T_L and supercooling $\Delta T = (T_L - T)$ produced by varying concentration C; arbitrary units.

The distribution of such impurities is dependent on the rate of advance of a crystal surface G and the diffusion coefficient for 'impurities' D. The distance at which the concentration of impurities is enhanced is determined by the length $\delta = D/G$ as shown schematically in Figure 5(a). The effect of this build up of impurities at the crystal/melt interface on further crystallization, depicted in Figure 5(b), is to depress the equilibrium melting temperature T_L (liquidus temperature). The effective supercooling $T=T_L-T$ is correspondingly decreased and the thermodynamic drive for crystallization to proceed reduced. In polymers, fibrils develop in interspherulitic regions because the poorly crystallizable components segregate between them and delay or stop solidification of the intervening melt. The diameter of these fibrils was predicted by the workers to be $\sim\delta$ because this is the scale of the diffusion field at each growing tip.

In addition to fibrillation there must be small-angle branching to give spherulites their spherical symmetry. A correlation of finer fibres and more frequent branching has been rationalized by Keith and Padden (34), who point out that it is consistent with new fibrils initiating at misaligned surface nuclei near the tips of existing units. If a new fibril should start it will only survive if its 'diameter' is commensurate with δ.

1.2.3. Kinetics

Spherulitic growth proceeds in two essentially different ways which must be, and indeed are, reflected in isothermal growth kinetics. The first stage, primary crystallization, consists of outward growth of lamellar or fibres until impingement,

the second, secondary crystallization, which may well overlap the first, is growth filling in the interstices. The relative sizes of these two effects can vary widely, depending on the constitution of the melt and growth history.

Modern theories of the lamellar thickness are kinetic theories, that is they assume that the observed lamellar thickness responds to changes in crystallization temperature and rate. The application of kinetic theories, established for solution grown polymers, to melt crystallized polymers is an empirical rather than fundamental matter which is complex and not yet fully established on a quantitative level. The reader is referred to an excellent and comprehensive review of kinetic theories given by Bassett (35) based on early work by Hoffman, Davis and Lauritzen (36), Sanchez (37) and the more recent theories on chainfolding and time dependent crystallization summarised by Schultz (38). It was not thought relevant to this work to include these complex theories in the literature study.

1.2.4. The Spherulitic and Lamellar Morphology of Melt-Crystallized Isotactic Polypropylene

The chosen polymer for this research project, iPP, has a crystalline architecture which is complex and multifaceted. The conventional and most widely occuring crystal structure of polypropylene is the one determined first by Natta and Corradini (39), with a monoclinic lattice as illustrated in Figure 6, referred to later when other polymorphs became apparent as the 'α' structure. Soon after a polymorph with a hexagonal lattice, shown in Figure 7, the hexagonal or 'β' structure was recognised (40–43) known to be favoured by high

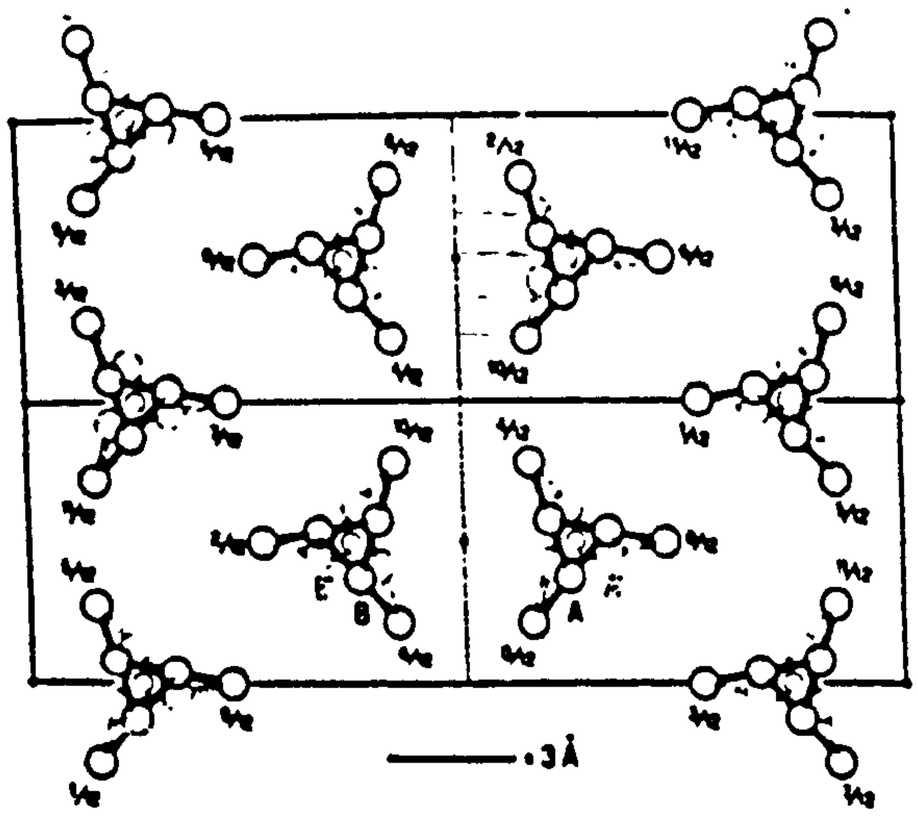

Figure 6 Monoclinic lattice of the α polymorph of iPP as determined by Natta and Corradini (39).

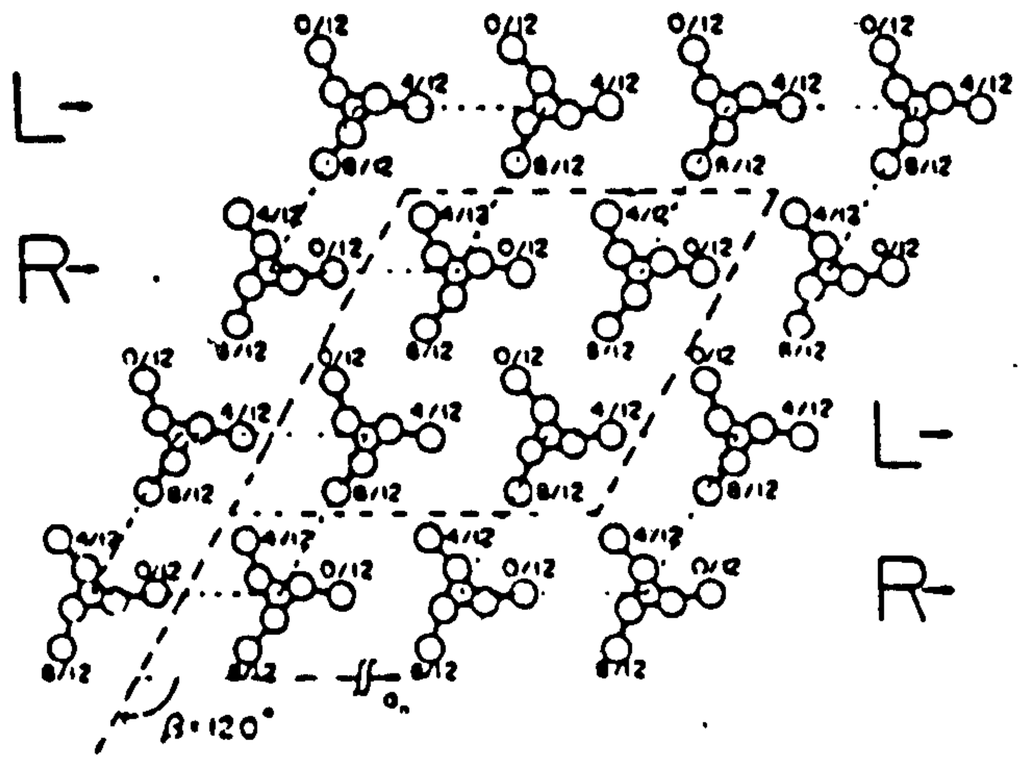

Figure 7 Hexagonal lattice of the β polymorph of iPP.

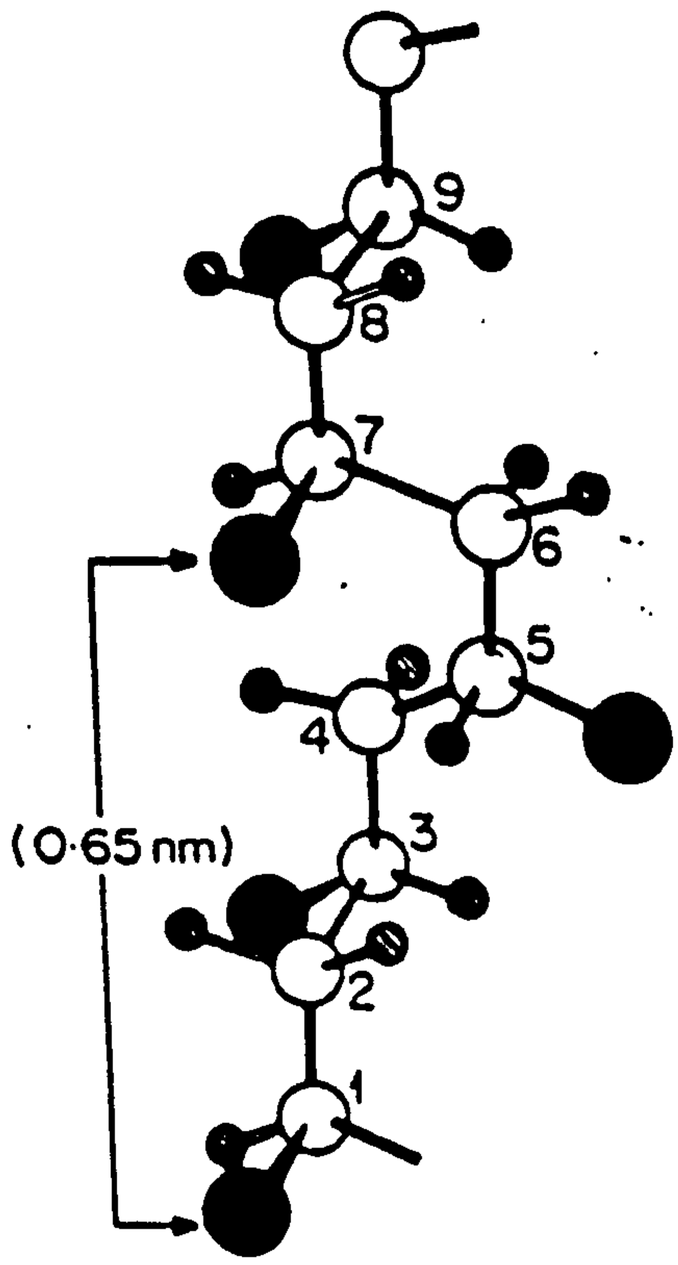

Figure 8 The (3_1) three fold polypropylene helical form. Working from carbon 1 the following sequence is followed; 1 and 4 are trans to each other, carbons 2 and 5 are gauche, 3 and 6 are trans, 4 and 7 are gauche and so on. Carbon 1 repeats at carbon 7, hence this helix is three fold with three monomer residues constituting one complete turn.

shear rates (44), fast cooling from the melt (45) and certain heterogeneous nucleants (46-48). This 'β' structure only appears as a minority constituent of the bulk sample when it does occur. Following this an even rarer third polymorph based on a triclinic lattice, the so-called 'γ' structure was identified by Turner-Jones et. al.,(41). Subsequent workers found that the formation of this structure is promoted by hydrostatic pressure (49-51). There is also mention of a 'δ' structure found in polypropylenes with a high percentage of amorphous material (52). The chain conformation in all these structures ($\alpha, \beta, \gamma, \delta$) is identical and corresponds to the familiar three fold (3_1) helix, illustrated in Figure 8, the stacking geometries of these helices determining the different polymorphs.

On the resolution level of the polarizing microscope, there exists a variety of spherulite types classified by their appearance between cross-polaroids, including sign and nature of birefringence. Four distinct spherulite types and some mixed forms were identified by Keith and Padden (53). Types I and II, known as the α-modification are composed of monoclinic unit cells. Their birefringence is low, positive for the first and negative for the second. The spherulites of type III and IV are composed of hexagonal unit cells and were categorised as the β-form spherulites. They are much more negative in birefringence and are easily distinguished by their highly luminous appearance in polarized light, surrounded by much less bright α spherulites. Type IV shows a characteristic banded structure. Examples of all these spherulities are presented in Figure 9. The defining properties of all the

TABLE 1 Characteristics of iPP spherulite types.

SPHERULITE TYPE	I	MIXED	II	III	IV
	MONOCLINIC			HEXAGONAL	
CRYSTAL STRUCTURE	α	α	α	β	β
MAGNITUDE OF BIREFRINGENCE	0.003	+0.002	0.002	0.007	0.007
SIGN OF BIREFRINGENCE	+ve	+ve/-ve	-ve	-ve	-ve
CONCENTRIC BANDING	No	No	No	No	Yes
ISOTHERMAL Tc (°C)	<134	134-138	>138	<122	126-132

Figure 9 Different iPP spherulite types I-IV, viewed in polarized light a)-type I; b)-type II; c)-type III; d)-type IV; e)-mixed.

a)

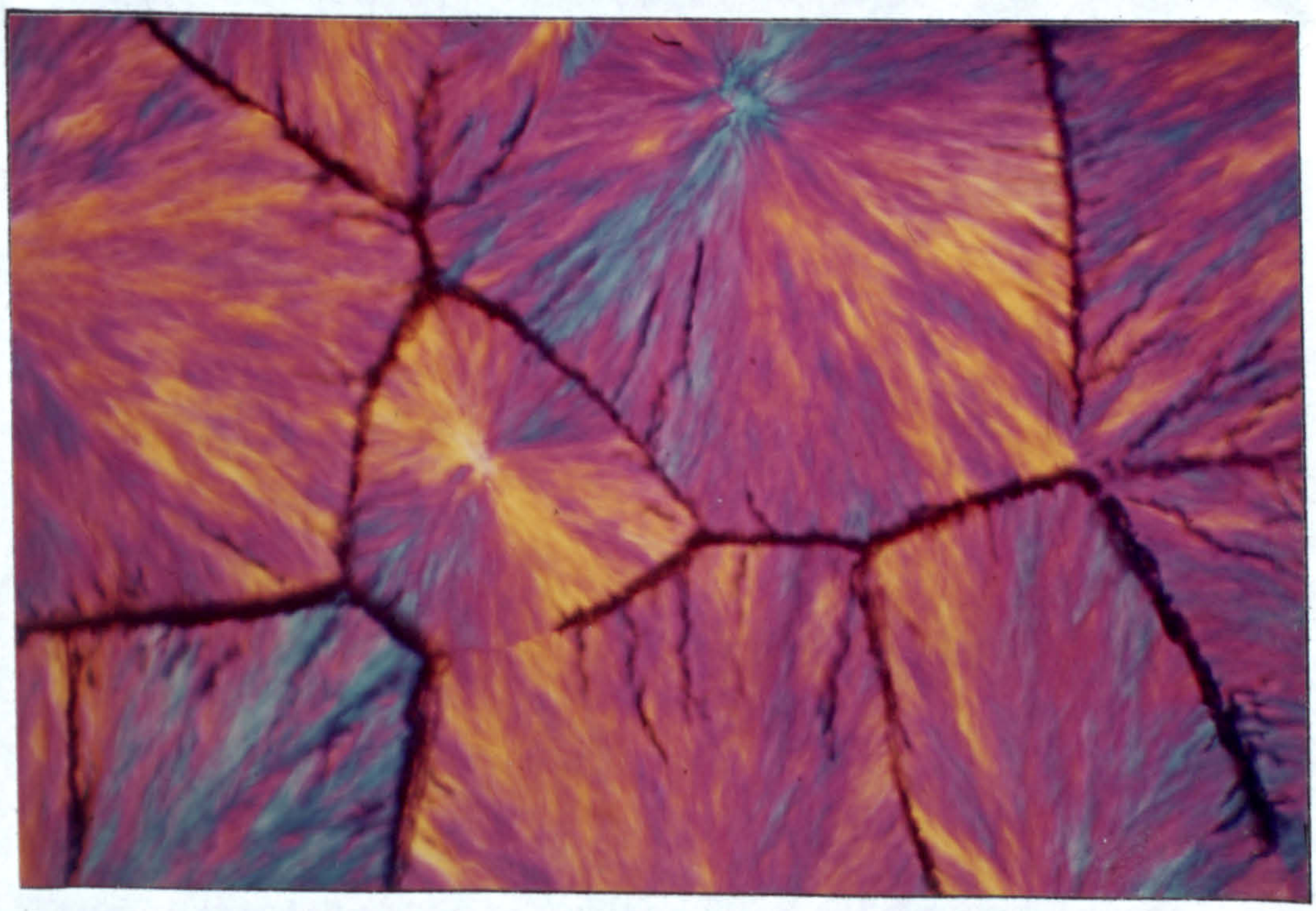

b)

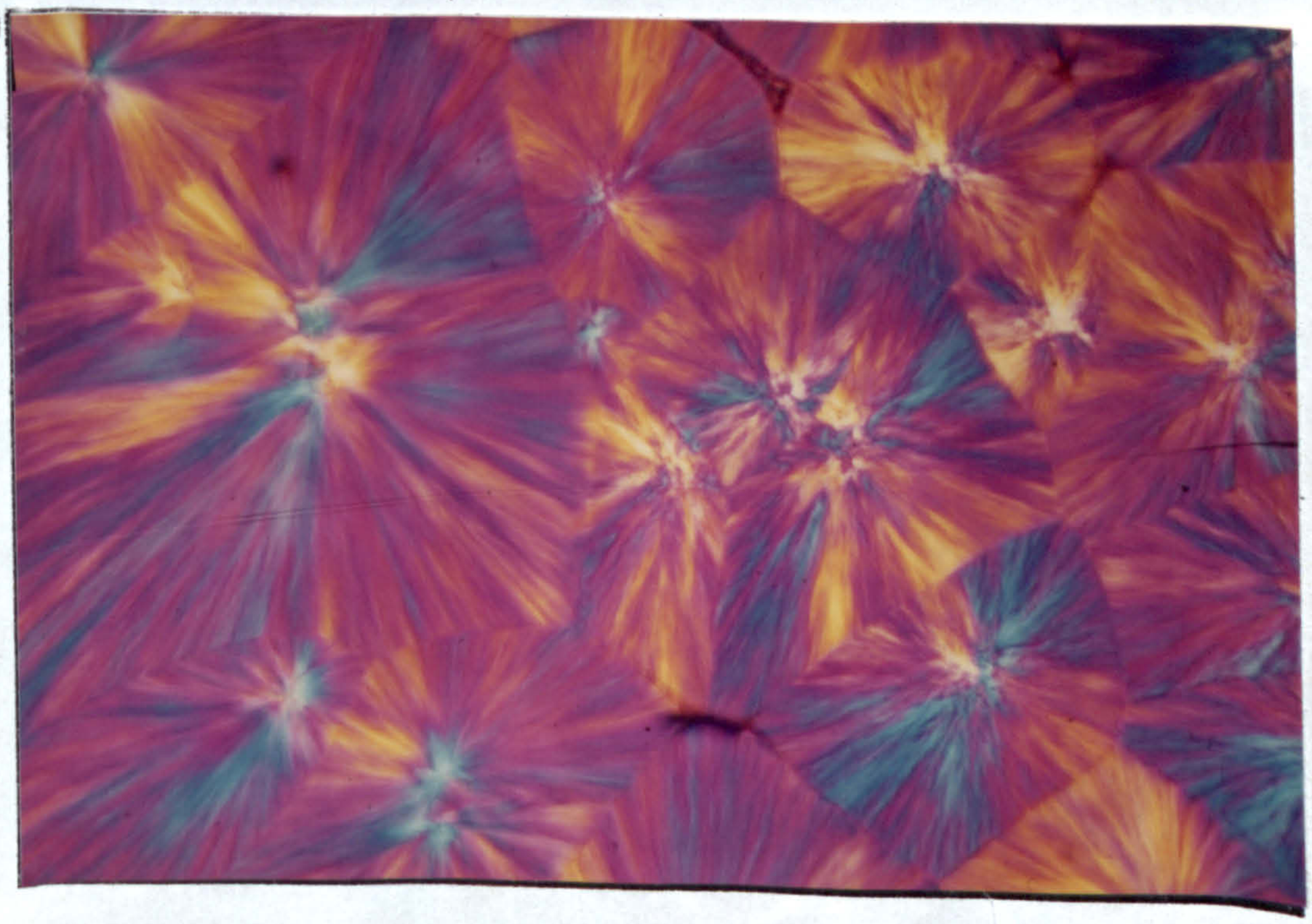

c)

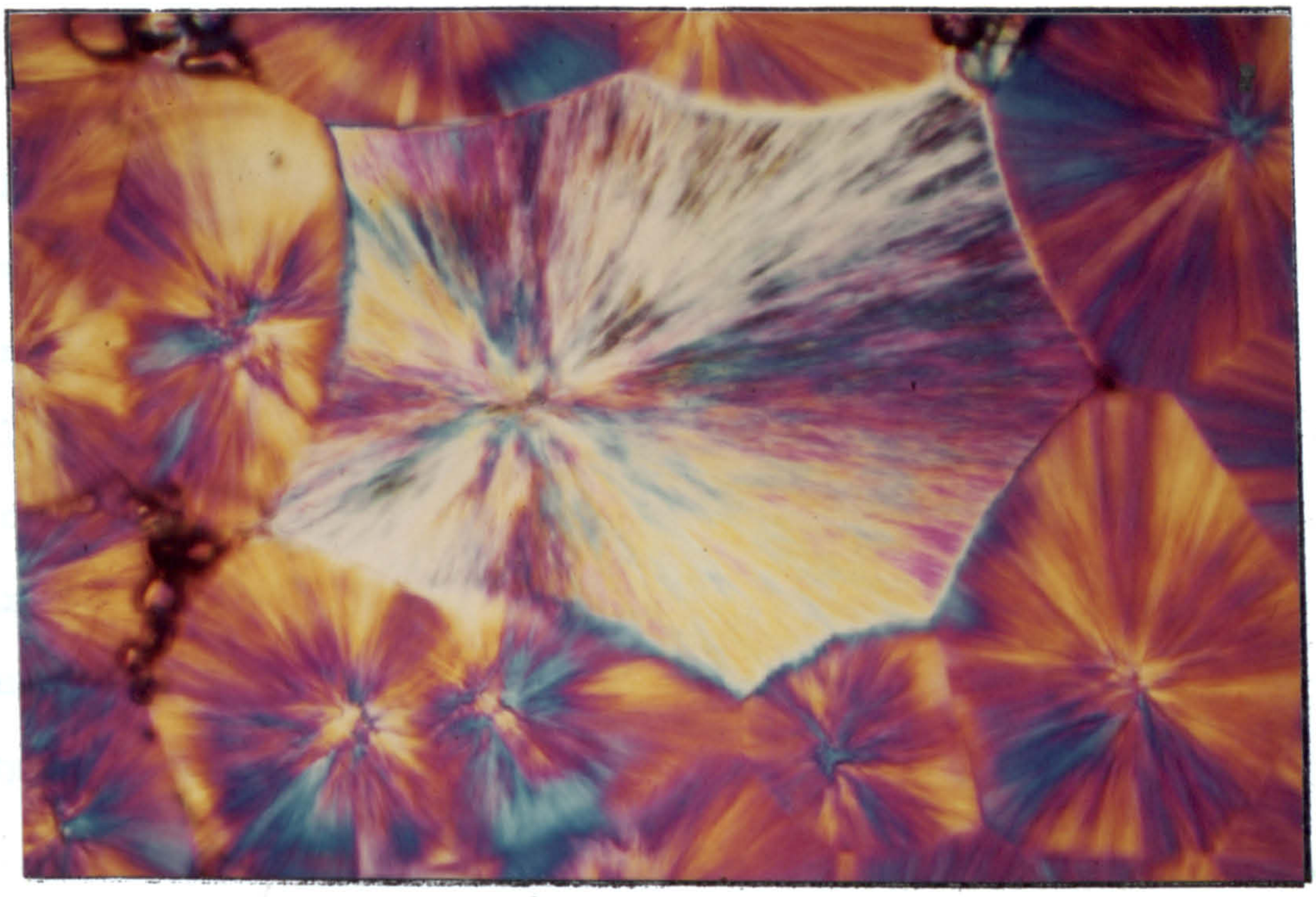

d)

e)

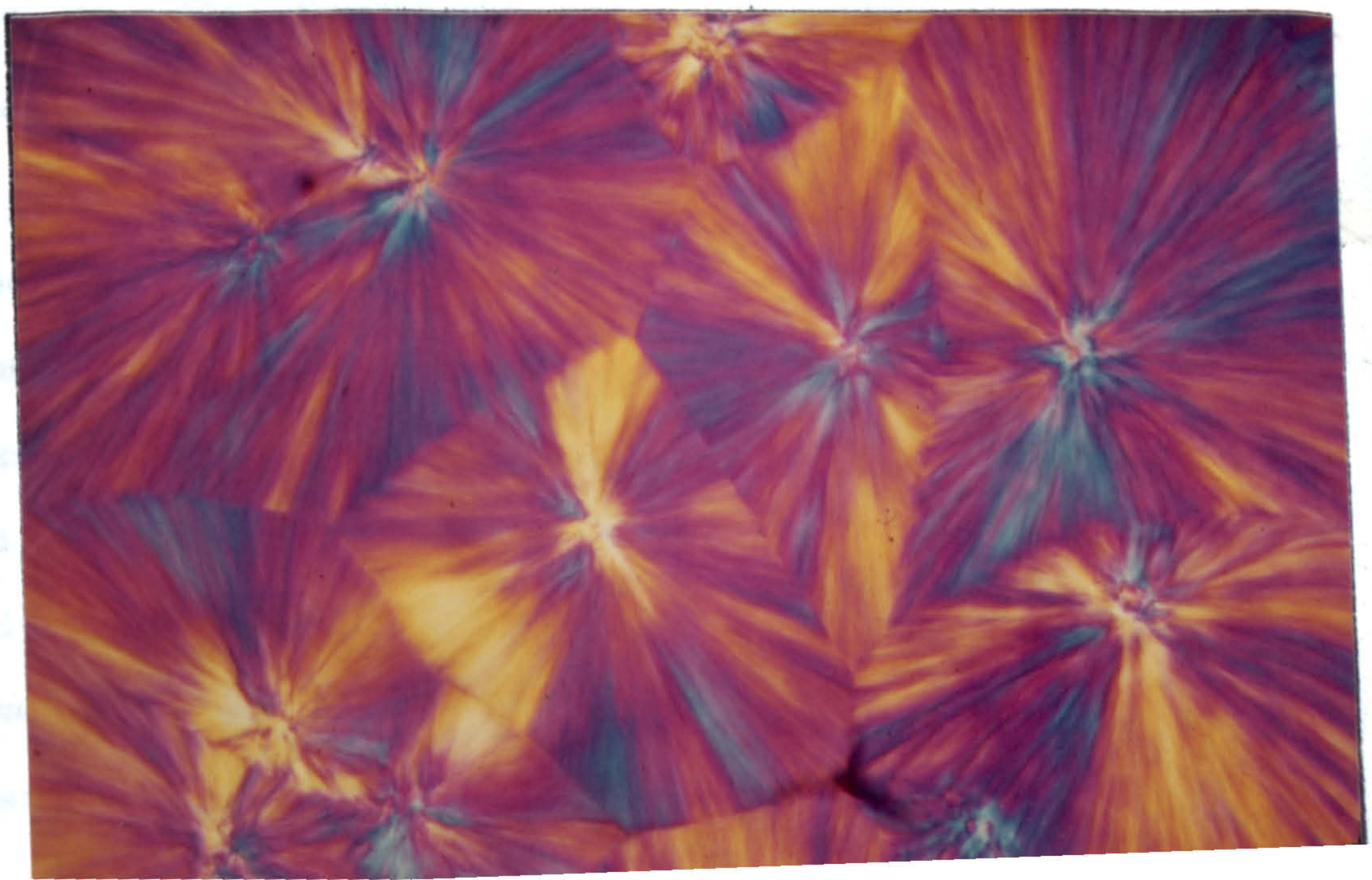

spherulites perceived by previous studies, mainly ref. 11, are given in Table 1. Intriguingly, the spherulites of most bulk crystallized samples belong to the so-called 'Mixed' spherulite type. These spherulites exhibit random distributions of positively and negatively birefringent regions where the birefringence is of a low and often not measurable value. The unit cell of the mixed category is the monoclinic, α, variety.

According to Lovinger et al., (45) the two crystal forms α and β are also distinguished by their crystallization kinetics. Types III and IV nucleate at a much lower rate than types I and II, but once nucleated they grow faster by between 20 and 70%.

The lamellar morphology on the resolution level of the electron microscope is also complex. iPP is exceptional among polymers insofar as its most common α polymorphic form crystallizes with a tightly 'cross-hatched' dendritic habit incorporated within the usual spherulitic structure. This unique morphology was noted early on in both solution (54, 55) and melt grown (56-59) specimens of α polypropylene. It was examined in detail by Khoury (55) who, in a most thorough study, found that solution grown dendrites consist of "twinned" crystals forming an acute angle of 80.67°. The consequence of such twinning provides a natural explanation for the changing birefringence of spherulites of monoclinic iPP. The net birefringence depends on the relative proportions of twinned and untwinned components. The gradual change from positive to negative birefringence for iPP spherulites with increasing crystallisation temperature may thus be interpreted in terms of a reduction in the degree of twinned component (56).

A new preparative microscopic technique of permanganic etching (60, 61) was applied recently by Bassett and Olley (62) and Norton and Keller (63) to reveal the lamellar detail of iPP melt grown spherulites. Both studies put forward mechanisms for the formation of the α cross hatched morphology which will be discussed in the following section with reference to earlier theories. More importantly both studies verified that it is the radial component of the iPP α spherulite which imparts the observed increasingly negative birefringence with increasing crystallisation temperatures. The work of Norton and Keller (63) also revealed the lamellar texture of β-form spherulites. They were found to consist of broad locally stacked parallel lamellar organised in an entirely radial manner just as in the spherulites of other polymers. Numerous hexagonal etch terraces were shown to develop during growth of the β spherulite, as illustrated in Figure 10, indicating the possibility that screw dislocation growth mechanisms were operative.

1.2.5. The Origin of Lammellar Cross-hatching in Polypropylene

The problem of understanding cross-hatching in monoclinic polypropylene is one of long standing. Khoury (55) made the reasonable supposition that there was an epitaxial relationship between parent and twin. The branching angle of $80^{\circ}\ 40'$ corresponds to parallelism of the a and c axes in one lattice with the -c and -a axes respectively of the other. Figure 11, is a schematic representation of the 'cross-hatched' morphology taken from Norton (63). On this figure the direction R represents the radial direction within the spherulite whilst the direction T represents the branched, tangential direction, characteristic of the cross-hatched overgrowth. The mismatch of the a and c lattice parameter is however about 2.3%.

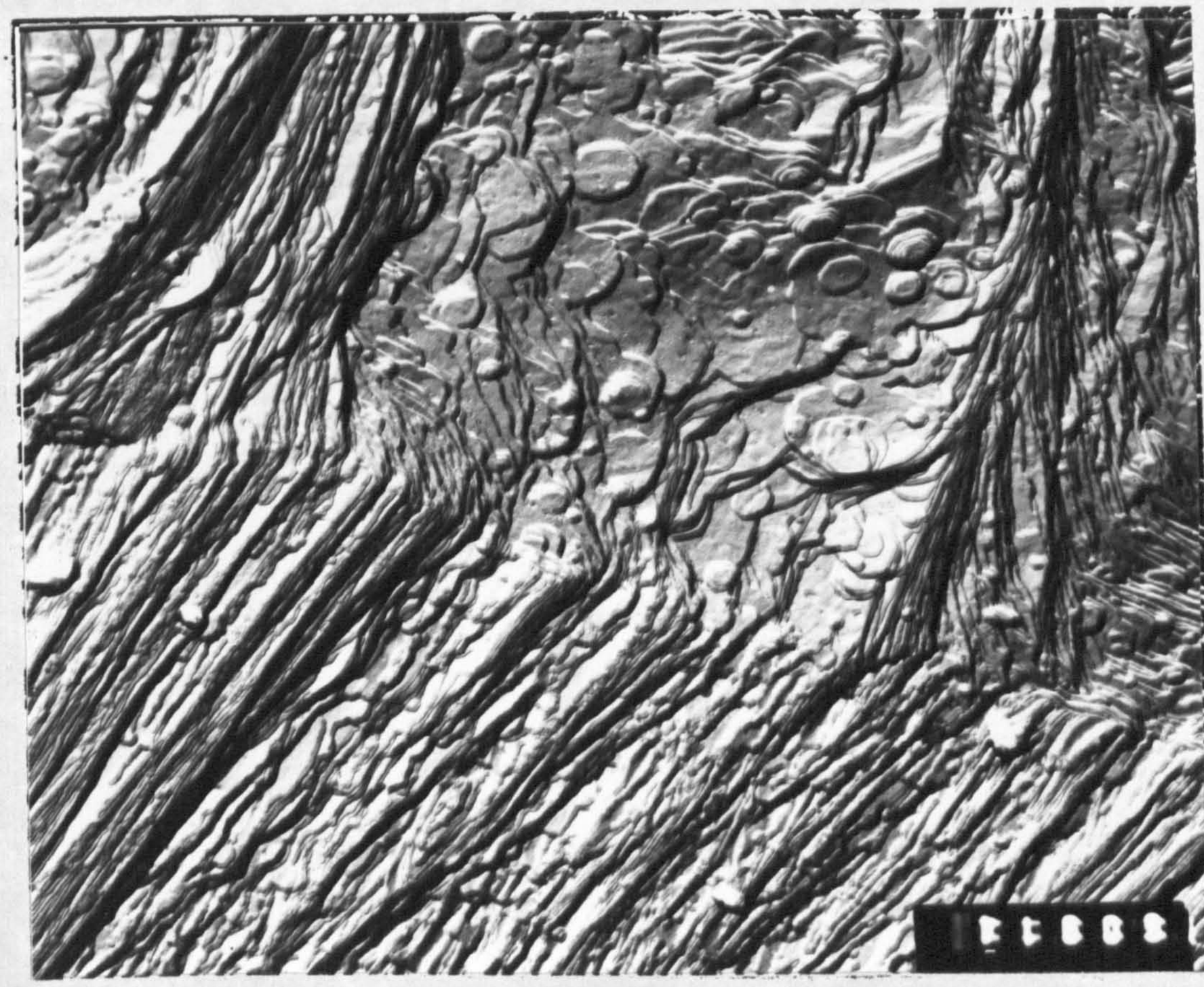

Figure 10 Hexagonal etch terraces at the centre of a type III spherulite (after Norton and Keller (63).

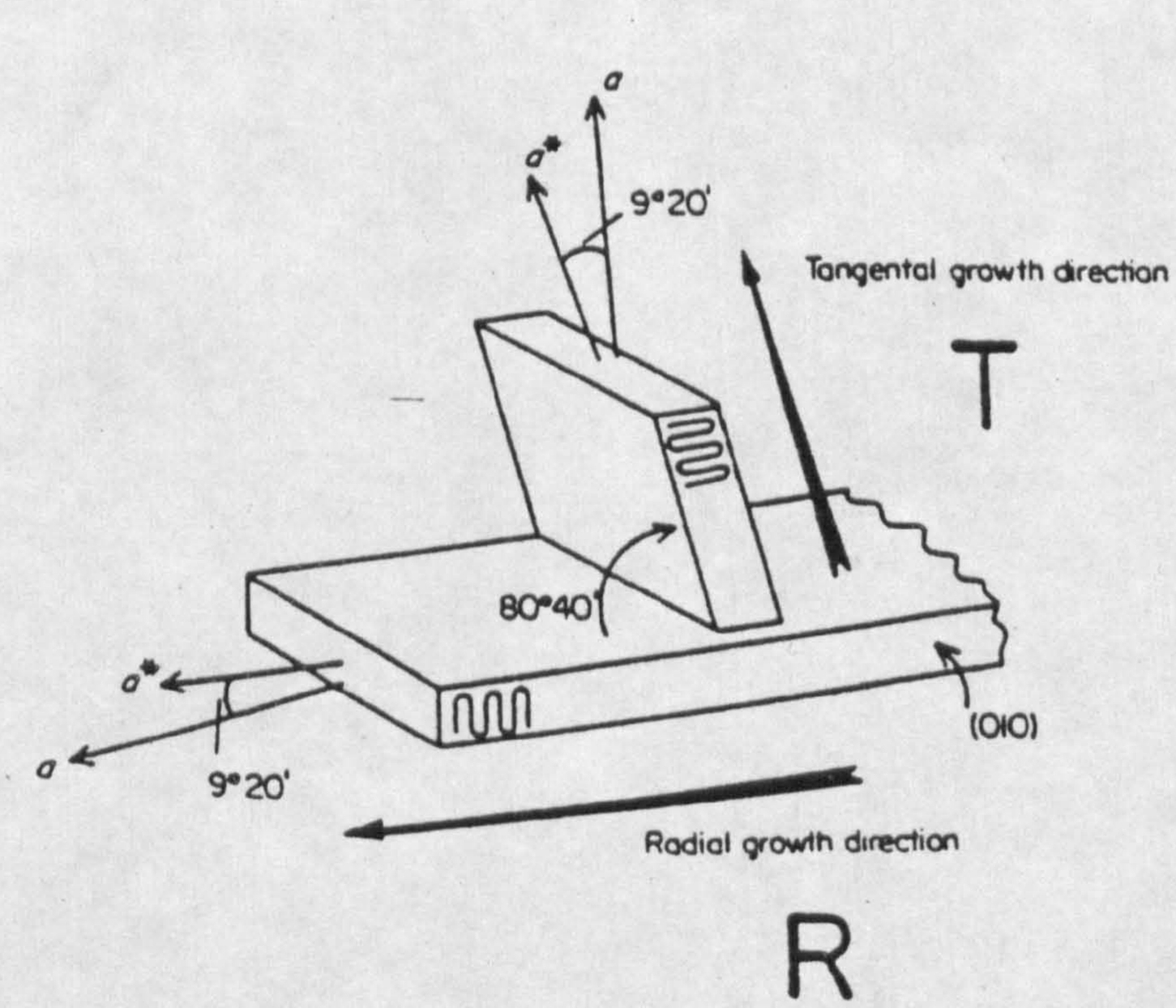

Figure 11 Schematic representation of cross-hatch morphology.

Indicating the epitaxial deposition of one branch. The $80^{\circ}40'$ branch angle corresponds to parallelism of the a and c axes of one lattice with the -c and -a axes respectively, of the other.

Subsequently, Padden and Keith (56) proposed that the cross-hatch is initiated at the lateral (010) edges of lamellae and involves the deposition of minute patches of γ-phase, triclinic, iPP. This gives a match between the a axis of the α and c axis of the 'γ' phases of around 0.6%. Drawing upon results of Turner-Jones (41) they also suggested that the formation of the intervening γ phase was related to the segregation of medium and high mass stereoblock molecules.

Recently Basset and Olley (62) observed that profuse cross-hatching starts at the edges of, and to a lesser extent within, γ sheaves which is support for the link between segregated polymer and cross-hatching. Furthermore, the latter found that the maximum temperature, 155°C, at which the formation of cross-hatching occurs is near the upper limit of the stability range of γ-phase. In another study by Clark and Spruell (64) on the crystallization of melts during flow, another hypothesis was formulated: the epitaxial fit is between the separation (13.1 Å) of two chain folds in the primary lamellae (R lamellae) and the spacing between two turns of the iPP helix (13.0 Å). Finally, it should be noted that if the a* axis is the growth direction, (a* reciprocal lattice constant), hence by implication the corresponding lateral axis of the lamellae, the lamellar fold surface is not (001), but rather a surface inclined at 9°20' to it (the difference between the a and a* axes), i.e. ($\bar{1}$06) (59, 64).

The most recent study on the origin of cross-hatching in α-polypropylene was made by Norton and Keller (63). The authors presented evidence that appeared to favour some form of pure epitaxy, i.e. one that is related to some fundamental lattice constant rather than a method of branch propagation by the deposition of an intermediate γ-phase. Extensive experiments with electron diffraction studies of thin and irregular amounts of iPP, which fortunately remained adhered to the replica surface, produced only scarce evidence of the γ phase. In addition, the lamellar fold surface was shown to be $(\bar{1}06)$ in agreement with Clark and Spruell (64) which the authors proposed requires the development of (001)/(100) 'microfaceting' giving a jagged geometry to the fold surface on the scale of a few fold repeats, this in turn might promote the initiation of the cross-hatched lamellae.

Whether the cross-hatch develops concurrently with the radial growth of the spherulite or subsequently from material left uncrystallized during isothermal crystallization is another as yet unsolved problem. However, Norton and Keller (63) noted that a positively birefringent α spherulite is seen positive during isothermal growth which implied that the cross-hatch responsible for the positive character must already be present at an early stage of growth. Interestingly at high crystallisation temperatures ca.Tc = 148°C differences in the relative thickness of the two components was identified, the radial lamellae being slightly thicker : ca. 50 nm for the radial component and ca. 40 nm for the tangential component. These spherulites exhibited a negative birefringence as a result. The authors explained the lower

thickness of tangential lamellae in terms of reduced isothermal thickening effect in that they formed at a slightly later stage than their radial counterparts which is contrary to their initial interpretation.

In spite of the difficulty in understanding the complex morphologies iPP displays at least some system has emerged, which descriptive as it may be, should assist in subsequent identification of the crystal structures. It has been established that in the α-spherulites the ratio of the cross-hatch versus radial lamellae directly influences the spherulite type, furthermore that the radial orientation of the R lamellae is a*, which correspondingly is also the crystallographic growth direction of the spherulite irrespective of whether cross-hatching is present or not. For the hexagonal β-phase structures the regular radial growth is along the <300> crystallographic direction allowing ease of identification by both optical and by electron microscopic techniques.

1.2.6. Thermal Behaviour Of Melt Crystallized iPP

The melting behaviour of α- and β- form material differs signficantly. Samples containing the α- form show only one melting differential scanning calorimetry (DSC) peak at about 168°C, while if both forms are present, multiple peaks can be observed depending on the heating rate as well as on the crystallization temperature (45, 65-67). A double melting behaviour of β-form crystals has been observed, particularly at slow heating rates. After the initial melting at about 145°C another structure showing faint positive birefringence may appear, that, according to Fujiwara (66) still has a

hexagonal lattice. This recrystallised form, β', melts at around 152°C and is succeeded by a monoclinic α- form. Melting of this recrystallised α-form may happen at a higher temperature than original α- crystals in the same specimen. As has already been indicated, crystallization from unstressed melts produces a great majority of α-form spherulites, while the β form are usually scarce. However, the random occurrence of β crystallites seems to be favoured by rapid cooling from the melt to temperatures between 100 and 130°C, by the presence of some nucleating agents, or by crystallization during melt shear (44-48). The thermal studies applied by these workers are reviewed in Chapter 2 under the heading "Application of DSC To Melt Crystallized iPP."

1.3 STRUCTURE DEVELOPMENT IN INJECTION MOULDED SEMI CRYSTALLINE POLYMERS

Injection moulded semi-crystalline parts often show a complex skin-core morphology, consisting generally of a layer of oriented material near the mould wall, an intermediate shear zone and a core with randomly oriented spherulites. The width degree of molecular orientation, crystal form and spherulite size of the various layers are strongly dependent on the moulding parameters. By varying them, mouldings showing distinctly differing morphologies can be obtained. The following sections review the current state of knowledge regarding the interrelations within processing, and micro-structure of moulded polymers.

1.3.1 Crystallization Under Stress

The orientation of crystals relative to the primary stress direction is critical to the mechanical properties of a moulded article. In the crystalline state, polymer chains are aligned parallel to one another and in general bonding

along the chain is covalent while bonding perpendicular to the chain is of weak hydrogen or Van de Walls type. Consequently, it is found that tensile moduli parallel and transverse to the chains may differ by two orders of magnitude. Similarly, shear moduli on the plane of the chain are much lower than shear moduli on planes cut by the chain. Crystals exhibit a range of orientations over a moulded article but locally can be highly oriented.

The crystallisation mechanism for a highly stressed polymer melt injected into a cooled cavity must be considered since this gives rise to a very different pattern of crystallization than isothermal experiments. Solidification under moderate degrees of deformation fosters the development of 'shish kebab' or row nucleated lamellar morphologies. The 'shish kebab', as it is now universally known, is a morphology that is seen to be a composite structure of narrow central thread (~30 nm in diameter) strung with small platelets as shown in the schematic diagram of Figure 12. In short the shish kebab is regarded as nucleation of fibrils followed by epitaxial overgrowth of lamellae sharing a common chain-axis orientation along the fibre. The fibre itself results from strain-induced crystallization i.e. from distorted molecular conformations in which chains have been brought and maintained parallel for long enough to nucleate crystallites. It has been found that shear flow does not promote nucleation whereas extensional flow does. The fundamental requirement is that molecules be brought together extended and remain so for long enough to allow nucleation. Shear flow cannot do this, but extensional flow may. The parallel lamellar nature of the morphology is the cause of substantial stiffening along the lamellar normal direction (i.e. fibre axis). The extended

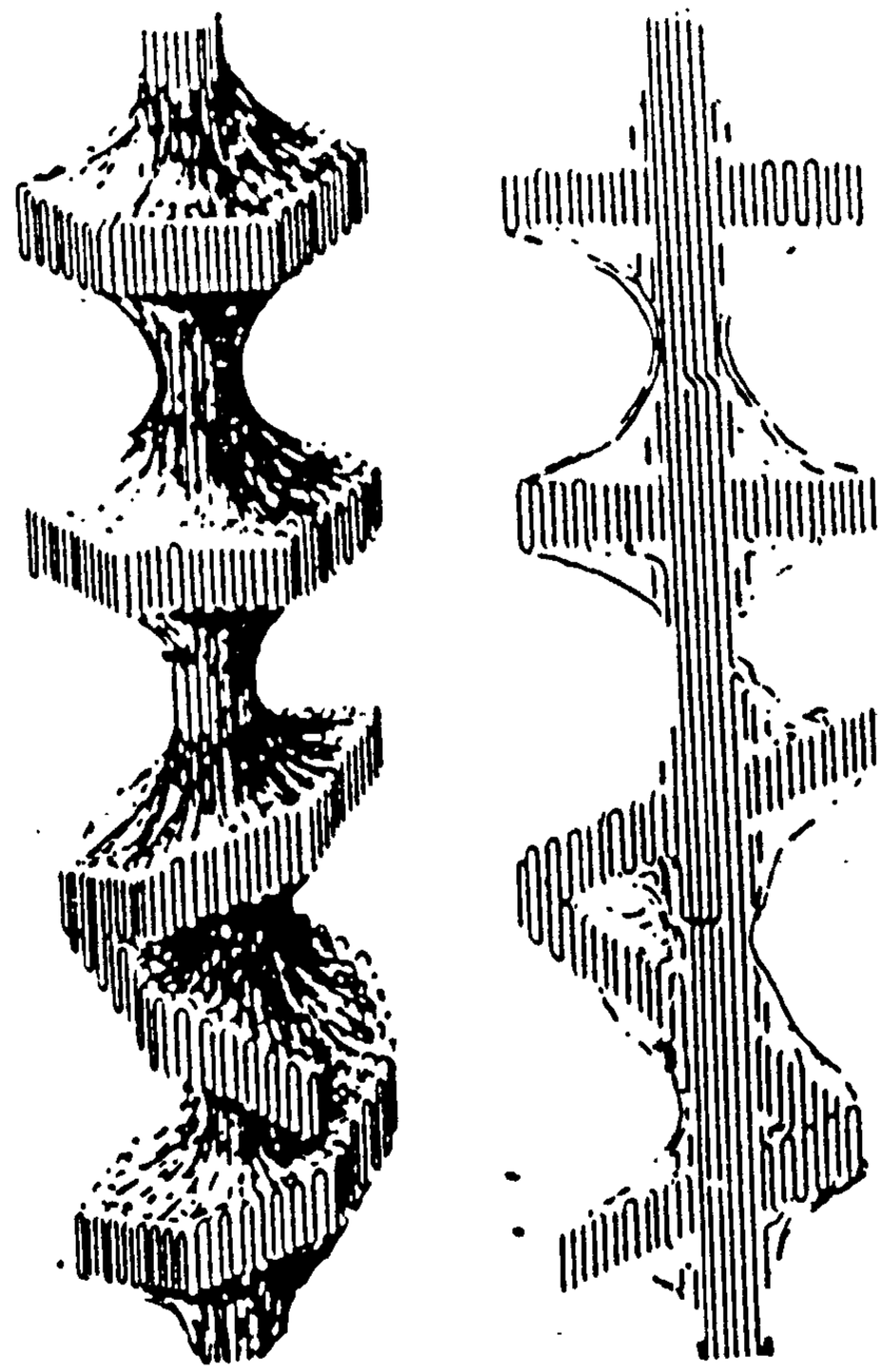

Figure 12

Schematic molecular model of the shish kebab morphology.

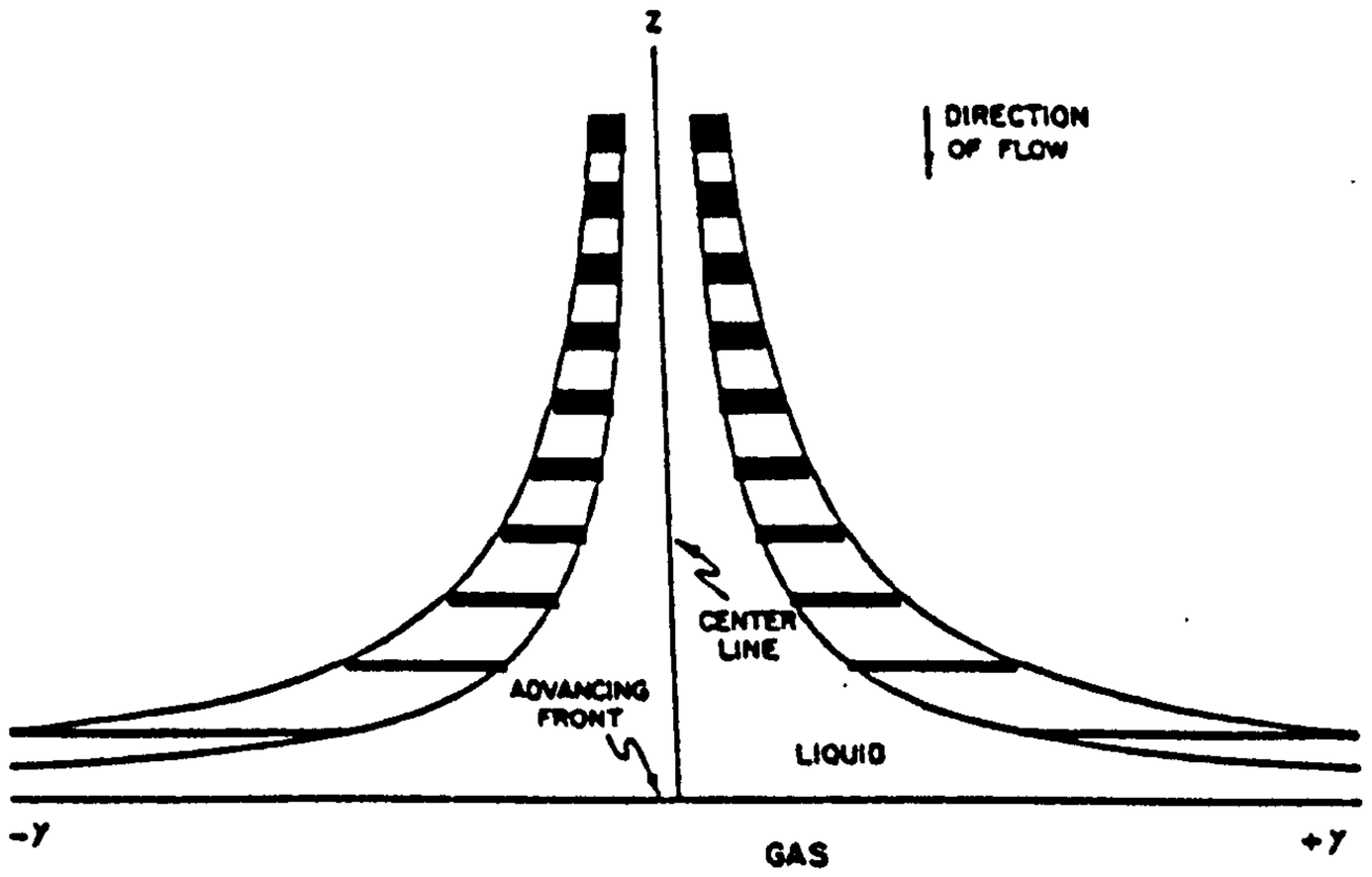

Figure 13

Schematic representation of the flow pattern in the central portion of an advancing melt front between two parallel plates (70).

chain cores themselves do not contribute significantly to the high modulus but they provide a framework for the oriented parallel interlocking arrangement of lamellar giving a zip fastening effect conducive to good mechanical properties.

Odell et al., (68) demonstrated the ultra-high modulus that can be achieved by extruding oriented plugs of polyethylene under appropriate programming of crystallization temperature. Bashir et al., (69) in a recent extension of this work demonstrated how the extreme high end of the molecular weight distribution is instrumental in the attainment of such structures. The longest chains, even if present in very small amounts, produce fibrous crystals during extrusion which serve as nuclei for lamellar crystallization throughout.

Row nucleation in crystallization from the melt also occurs when the melt is under strain, increasing the probability of bringing chains parallel for long enough to nucleate a crystal embryo. Once a crystallite has formed, by whatever means, its high Young's modulus will accentuate the stress field increasing the probability of a further nucleus along its own axis. The chance of generating a row nucleus in this way will increase with strain and with crystallization temperature (by reducing the free enthalpy driving alternative crystallization). Once a row nucleus has formed it is likely to initiate growth transverse i.e. perpendicular to the direction of strain, not least because the nucleated filaments will tend to become load bearing and so remove stress from residual material. The lamellae become wider ($\geqslant$1mm) as the strain decreases obscuring the central filament that may under higher extensions and lower crystallization temperatures cause shish kebab morphologies.

This transverse growth of lamellar is equivalent to that along the radius of a spherulite, possessing the same crystallographic axis and may appear as a 'burst' of spherulitic nucleation under conditions of fast cooling. This type of spherulitic growth is termed 'transcrystallinity' and is discussed in detail in Chapter VI of this thesis.

1.3.2 Flow Patterns In Injection Moulding

The importance of the flow pattern during mould filling in determining the details of the microstructure, and hence the properties, cannot be over emphasised. The generally accepted flow pattern of an advancing melt front is that proposed by Tadmor (70) and is illustrated in Figure 13. The direction of transport and the change of shape of fluid elements (shown as the dark regions) is depicted. The fluid elements in the central space deccelerate as they approach the slower-moving interface and aquire a radial component of velocity as they spill toward the wall region. The fluid particles are known to follow a curved path until they reach the mould wall, as shown in Figure 14. At this point, the orientation of the fluid elements and macromolecules is parallel to the mould wall. Thus, the orientation is induced by elongational flow in the flow direction in the case of a wide cavity. At some point upstream from the advancing front the velocity profile is quite close to that of a fully developed laminar flow. This will give rise to shear induced orientation. Thus both, elongation and shear flow fields are present and should be expected to have pronounced effects on the local orientations. The material behind the advancing front and between the solidified layers at the mould wall experiences a velocity and shear rate profile that has a zero shear adjacent to the skins and at the centre of the moulding, with maximum shear in between as illustrated in Figure 14.

Figure 14

Flow pattern in the advancing melt front, indicating the orientation of the particles arriving at the cold walls (70).

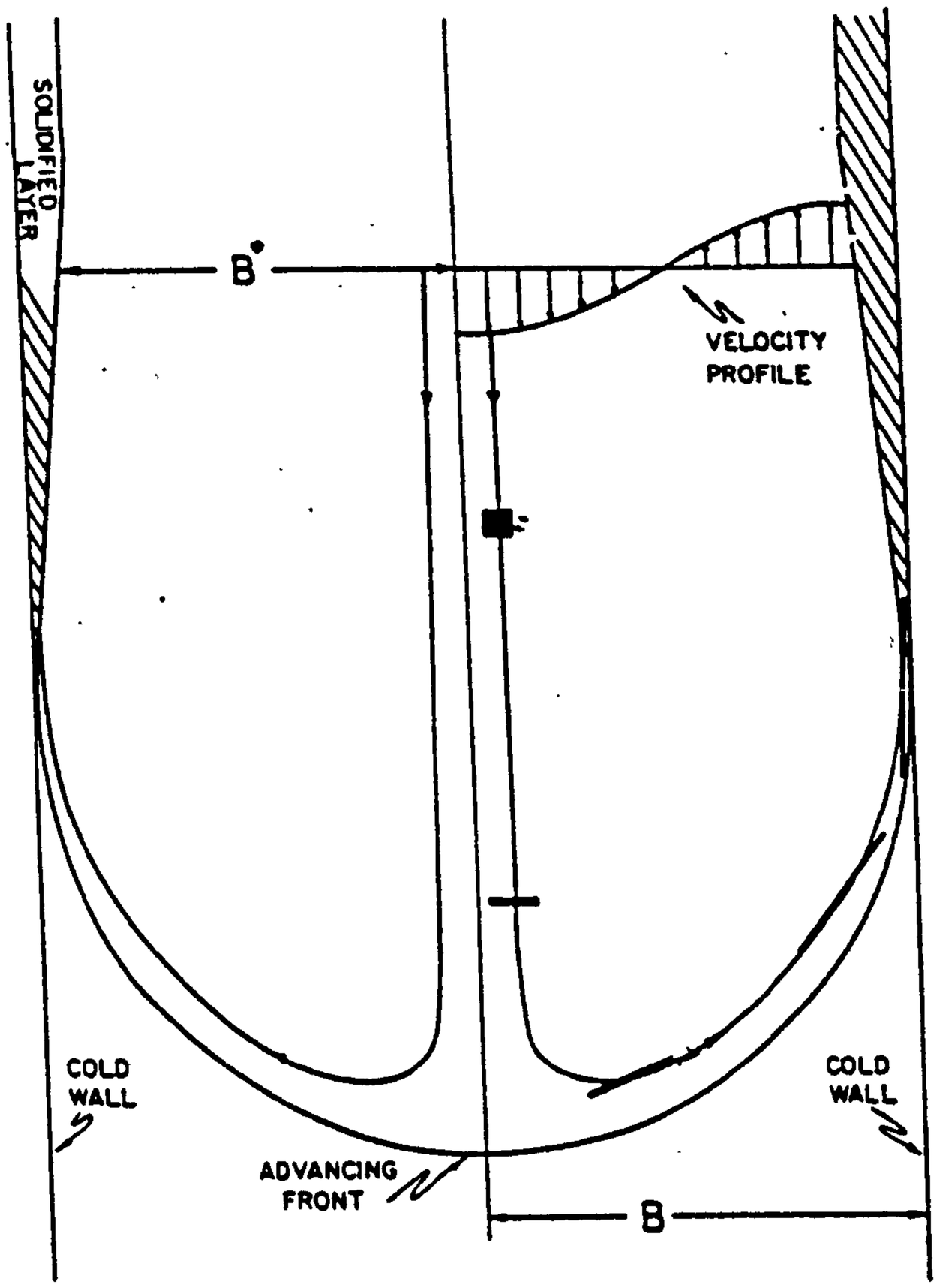

Figure 15

Progression of the melt front in a rectangularly cross-sectioned cavity as a function of fill time $t_1 < t_2 - < t_{10}$.

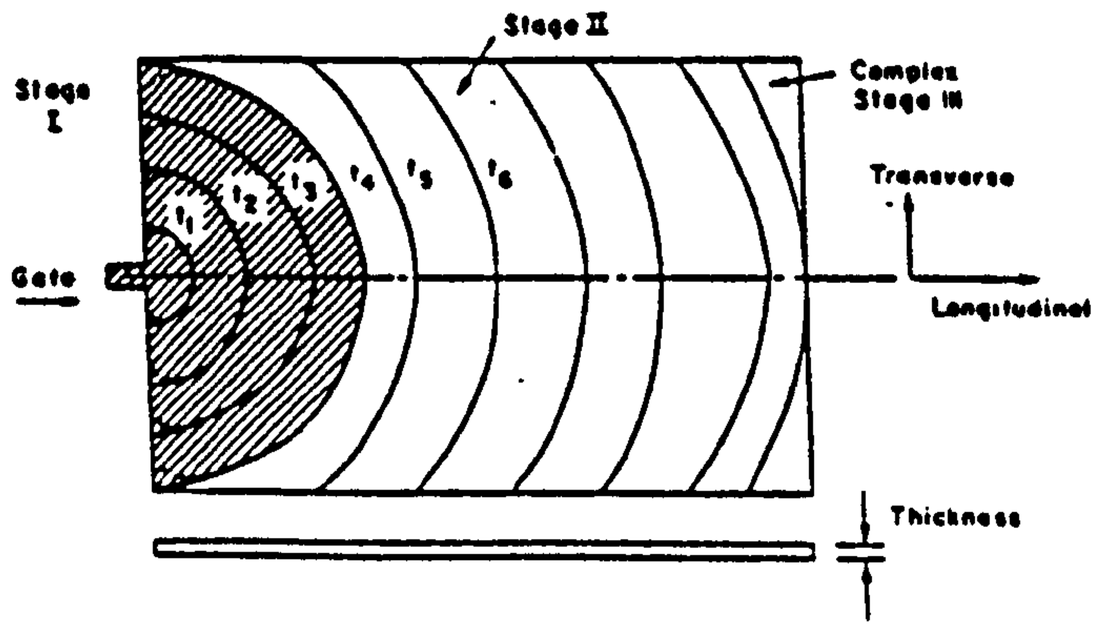

In the case of a tensile bar moulding, as the melt enters the tensile bar gauge section from the neck, the reduction in the cross-sectional area of the channel causes normal stresses to develop, which means that the moulding must accommodate the elastic strain energy. As the melt enters the enlarged cross-section on the side opposite the gate, the velocity is reduced, and the bulk of the stored elastic strain energy is relieved by elastic recovery, similar to die swell in extrusion.

In the case of a rectangular cross-sectioned cavity as used in this research study, the flow front is as shown in Figure 15. In stage 1, a biaxial orientation would be expected. In stage II, orientation both in the direction of flow and transverse to it would be expected. However, the longitudinal orientation should be much greater than the transverse orientation because, along the centre line, only longitudinal orientation should be observed. Transverse orientation should be insignificant at the centre and increase as one goes towards the edges. In stage III, the flow front position is complex as is the orientation in this region.

1.3.3 Skin-Core Morphologies

Polyethylene

Kamal and co-workers (71, 72) have studied the morphological zones and orientation in injection moulded polyethylene. A variety of techniques were employed including density, polarised light microscopy infrared measurements and differential scanning calorimetry. They observed four distinct zones, a non-spherulitic skin-zone with a certain degree of

transcrystallinity revealed, a second zone containing very fine asymmetric spherulites of almost uniform size nucleated at fast rates, a third zone containing asymmetric larger spherulites and a fourth zone of randomly oriented and nucleated spherulites.

Heise and co-workers (73, 74) presented a detailed orientation study of injection moulded linear and branched polyethylene. This work is reviewed by Katti and Schultz (75) in some detail to emphasise the changes in orientation from strong radial c-axis (chain axis) orientations at points nearest the gate to a biaxial a + b axes pattern and then still further from the gate, where radial stresses are smaller and ribbons undergo twisting, an orientation in wich b axis is tangential and a and c are random about the tangent lines.

The work by Heise (73, 74) also considered thickness dependence of quarter circle mouldings. As the thickness increases from 1mm to 4mm, the average degree of orientation through the sheet becomes lower.

Heckmann and Johnsen (76) studied the orientation distribution with depth in the case of injection moulded polyethylene. It was noted that, under their conditions, the highest degree of orientation is found about 200 μm below the surface. They also revealed a strong maximum in modulus and in melting temperature at the same depth. Although the photomicrographic evidence was not given, it was suggested that a transcrystalline surface layer was present. The authors offered no explanation, however, as to why the melt strain should increase toward a maximum away from the mould surface.

Polypropylene (PP)

Kantz (5, 6) studied the effects of processing conditions on morphology and crystalline orientation of injection moulded polypropylene tensile bars. Three distinct layers were identified:

(i) A highly oriented non-spherulitic skin.

(ii) A row nucleated spherulitic shear zone.

(iii) A typical isotropic spherulitic core.

Studies by polarised transmission light microscopy revealed evidence of spherulites nucleating along negatively birefringent rows in the shear zone. These spherulites were identified as the metastable hexagonal β- crystal form type III spherulites, as classified by Keith and Padden (53) with the assistance of x-ray diffraction techniques. The core region contained larger but more randomly size spherulites of the positive birefringent type I variety characteristic of the stable monoclinic α-structure.

Further studies by Fitchmun and Mencik (77, 78) and Menges et al., (79) confirmed the existence of five distinct layers, a surface zone of four layers and a core. On the extreme surface layer no spherulitic structure is noticed at all, but from the second layer the spherulitic structure is seen to develop with spherulites decreasing in size gradually to a point around the centre of the third layer. After passing this point the spherulites become larger again. X-ray texture work by both authors revealed orientation patterns for each layer. The surface layer consisted of poorly oriented a + c axes orientation, in layer 2 a low order of preferred orientation of the a axis close to layer 1 was seen and in layer 3 c-axis and a-axis orientations were observed.

Isotropic rings were seen from sections of the core indicating no preferred orientation. The oriterion used by Fitchmun and Mencik to assess the preferred orientation by x-ray diffraction is described in more detail in Chapter II.

From the studies on polypropylene referred to above Clark (4) gave the following unified approach from his interpretation of Kantz et al's publications:-

"The skin can be interpreted as that portion of the polymer crystallised during the filling stage. A large number of fibril nuclei are produced under the high stress of quasi-extensional flow and lamellar overgrowths have a planar conformation. This structure has a fibrous type molecular orientation with ideally all chain segments of the crystals (both lamellae and fibrils) being parallel to the injection direction. The fold surfaces do not contribute to the x-ray diffraction spots and in any case are a minor component.

The shear zone can be attributed to the portion of melt crystallised during the packing stage. Stress is lower, fewer fibrils are formed and the overgrowths of lamellae twist during growth. This results in a distinctive differ-ence of appearance in optical micrographs. With fewer fibrils present the lateral extent of the lamella may be greater than under high stress. These structures can appear as oblate spherulites with their short axes parallel to the injection direction.

With the removal of quasi-extensional stress in the cooling stage no mechanism is present for creation of fibril nuclei and a normal spherulitic structure is observed in the core."

Polyoxymethylene (Acetal Resin)

Extensive work by Clark (2, 3, 4) on the morphology of injection moulded bars of acetal resin revealed three crystalline morphologies consistent with those already discussed. However, the skin layer in acetal mouldings is much thinner than in polypropylene and in fact two zones were elucidated in longitudinally cut sections. The combined volume of these two zones is small compared to the volume of the bar indicating either slower crystallisation rates or faster filling and packing stages. A region of twisted lamellae (transcrystallinity) and a spherulitic core are the two types of morphology formed during the cooling stage of polyoxymethylene.

The volume of work published on other polymeric systems is limited but includes articles on TPX (9), polytetramethylene terephthalate (80), polypropylene-ethylene copolymers (8) and polybutylene terephthalate (81), all of which show a marked dependence of microstructure and properties on processing conditions.

In the case of polytetramethylene terephthalate Callear and Shortall (80) revealed four zones characterized as non-spherulitic, loosely packed flow lines, a region without visible flow lines and tightly packed flow lines.

Henke et al.,(8) investigated the morphology of a polypropylene-polyethylene copolymer and found the usual three-layer morphology. Interestingly, these workers found that the molecular weight of the skin was higher than that of the shear region but not significantly different from the core.

Thus the higher molecular weight species crystallize preferentially as nonspherulitic material on the edge of the mould.

In the case of polybutylene terephthalate Hobbs and Pratt (81) found that a nonspherulitic skin of variable thickness is developed. A continuous density increase occurs through the depth of this region, with the fractional crystallinity of the core approaching 0.25. The degree of orientation is low, and the complicated multiple zone morphologies reported in other systems are absent. The low level of orientation in the skin is indicative of rapid stress relaxation in the low viscosity melt during cooling.

The morphology studies of injection moulded TPX (copolymer based on poly 4-methylpentene-1) by Bowman et al., (9) revealed four zones characterized as highly oriented, edge equiaxed crudely spherulitic, and highly oriented and equiaxed spherulitic. The distribution of the regions exhibiting different microstructures varied in a systematic way with moulding conditions.

1.3.4 Influence of Processing Conditions on Microstructure

To present information of direct relevance to the moulder a number of papers are now reviewed to indicate the effects of processing conditions on the morphology ofpolyolefins. The moulder is interested in fast cycle times gained by using low melt and mould temperatures and high injection pressures and speeds. However, the ranges and limits through which these and many other variables can be varied are determined by the intrinsic properties of the polymer grade including: melting temperature, heat of fusion, temperature and shear rate dependence of viscosity, and processing stability.

Kantz and co-workers (5, 6) studied the effect of polymer melt temperature and injection pressure on the overall morphology of an impact modified ethylene propylene copolymers and isotactic polypropylene homopolymer. Melt temperatures of 190, 218, 233 and 275°C under injection pressures ranging from 400 to 1300 psi were used. The mould temperature was held at 30°C for both materials.

One of the principal findings of this study was that the area fraction of skin (A_S) in both polymers increases markedly with decreasing melt temperature. Injection pressure affects A_S only slightly, if at all. It did however, cause noticeable differences in spherulite appearance and in the area fraction of the shear zone (A_I). It was noticed that A_S for the copolymer is more sensitive to variations in melt temperature than is the homopolymer. Also, the injection pressure affects the area fraction of the shear zone much more in the case of the copolymer. The authors also looked at the combined area fractions of the skin and shear zones A_{SI} and noted a linear variation of A_{SI} with melt temperature and a clear effect of injection pressure for the homopolymer, but a complicated effect of melt temperature for the homopolymer.

The flow behaviour of the copolymer changes abruptly in the temperature interval between 233° and 275°C to give very large values of A_I. Noticed also was a reversed effect of injection pressure on A_{SI} for each polymer. It was also shown that moulding close to or at the melting point would give crystallisation of a highly oriented morphology throughout the specimen. Similar but non-linear variations of A_{SI} for polypropylene was found by Fitchmum and Mencik (77), by Bowman et al., (9) for TPX and by Tan and Kamal (71) for polyethylene.

Henke and co-workers (8) studied the effect of mould temperature on the morphology and properties of polypropylene and polypropylene co-polymers. The authors found that varying the mould temperature affected the width of the shear zone and strongly influenced the average size of spherulites within the specimen. The width of the skin did not vary, in contrast to observations by Kantz (5, 6). The skin region was found to possess a molecular weight higher than that of the interior which has not previously been reported. General conclusions from this study have shown that small spherulites and wide shear bands are characteristic of low mould temperatures whereas larger spherulites and thinner shear zones are characteristic of higher mould temperatures.

The thickness of the oriented skin layer is influenced by processing parameters since the degree of molecular orientation is controlled by the shear gradient which imposes the basic conditions necessary for rapid growth of fibril crystals. A cold mould gives rise to large temperature gradients promoting ribbon-like growth parallel to the lines of heat flow. However, high wall-shear stress and a large shear gradient would cause the same effect.

Xavier, Tyagi and Misra (24) studied the influence of injection moulding parameters on the morphology of glass reinforced composites. The authors stated that higher injection pressures increase shear rate and flow rate, but reduce the viscosity at the centre of the melt. If the increase in shear rate is higher than the decrease in viscosity, then the orientation will increase in unfilled polypropylene. They also studied injection speed and have shown that as injection speed is increased, the shear rate is also increased, and this results

in greater number of polymer chains orienting along the elongating force direction. Menges and Wubken (79, 82) also observed that an increase in injection rate increased shrinkage caused by the molecular orientation at the surface and changed the distribution.

A comprehensive paper was presented recently by Guo and Bowman (22) dealing with the processing - mechanical property relationships in polybutylene injection mouldings. The overall structure of the injection mouldings was revealed to be composed of an essentially spherulitic core and a highly oriented and birefringent skin. The influence of barrel temperature and mould temperature on the extent of highly oriented skin and density profiles through the thickness of the mouldings were also given. From these results the following conclusionswere made:-

(i) Increasing the barrel temperature reduced the overall density of mouldings.

(ii) The thickness of the highly oriented skin decreased with increasing barrel or mould temperature.

(iii) The density of the core of the mouldings was controlled primarily by the mould temperature.

(iv) The maximum density observed in the material comprising the skin of the mouldings was a function of both barrel temperature and molecular weight.

(v) The thickness of the highly oriented skin was not significantly influenced by molecular weight but the density was greatly influenced.

The authors explained (v) by considering the increase in relaxation times associated with increasing molecular weight. The increase in relaxation times would lead to longer retention times of preferred orientation, and subsequent crystallisation

and growth from the oriented melts in high molecular weight material would occur.

The influence of mould temperature on structure distribution was explained in terms of the effects of temperature gradient. As the temperature gradient is reduced, so the rate of heat withdrawal decreases and consistent with the barrel temperature effect the thickness of the skin decreases. The density distribution within the mouldings also changed as mould temperature was increased, this was accounted for by the density and spherulite size increase of the core material due to reduced rates of cooling.

For polyoxymethylene, or acetal, a semicrystalline thermoplastic Bowman (25) studied the relationships between moulding conditions, moulding microstructure and component mechanical properties in injection mouldings. It had been established by Clark (2, 3, 4) that barrel temperature exerts the most powerful influence, of all practical moulding variables, on microstructure and mechanical properties for a single grade of plastic. The acetal copolymer was consequently moulded at six barrel temperatures all with one mould temperature and cooling time. The microstructures of the mouldings were examined by polarised light microscopy of thin microtomed slices and for further studies DSC, x-ray pole figure analysis and density measurements were employed. Five distinct layers found within the acetal copolymer plaque mouldings and their textures and microstructures were described and mechanisms for the development of the preferred orientation were proposed. The influence of barrel temperature on the extent of structures 1 to 5 was also studied and the following conclusions were made of the study as a whole:

(a) At all barrel temperatures the microstructure of the mouldings was layered and symetrical about the centre line. Five layers were identified, the outer three possessed significant preferred chain-axis orientation, while the inner layers, layers 4 and 5 exhibited little preferred orientation.

(b) The melt that formed the outermost layers 1 and 2, probably underwent extensional flow at the melt front, thus inducing a significant preferred chain axis orientation which was retained by the quenching effect of the cold mould wall. Layer 3 possessed a sheared microstructure probably formed as the viscosity in the core flowing melt increases as that melt cooled. Layers 4 and 5 possessed little preferred orientation.

(c) Increases in barrel temperature relaxed the texture and preferred chain-axis orientation in layers 1 and 2 as the melt had longer to relax. The size of spherulites in layers 5, 4 and 2 increased with barrel temperature, reflecting the preference for spherulite growth to nucleation at the slower cooling rates.

(d) Increases in barrel temperature reduced the extent of the highly oriented layers 1, 2 and 3 and increased the extent of layers 4 and 5.

1.4 IMPACT PROPERTY - MICROSTRUCTURE AND PROCESS CONDITION RELATIONSHIPS

Process variables have significant effects on the microstructure and, hence, on the properties of a moulded article. The effect of injection moulding conditions on the impact strength of thermoplastics is reviewed below.

The results of Kantz, et al.,(5, 6) for the variation in Izod impact strength with A_{SI}, shows a linear increase in tensile yield strength with increasing A_{SI} for polypropylene polymers. The reason for this correlation was clarified by x-ray diffraction patterns at adjacent portions of the central region of the tensile specimen. Qualitative differences in orientations in specimens moulded at different temperatures was revealed with a considerably higher degree of preferred orientation found in samples moulded from a lower melt temperature of 190°C compared to those moulded at 275°C. The skin of the moulding was basically a fibre structure having biaxial orientation and the impact strength was found to increase with increasing fraction of A_{SI}. The samples in this work were notched and at low A_{SI} the skin will have been penetrated and the effects of A_{SI} not noticed, this may explain the apparent minima observed.

Okamoto et al., (15) studied the relationships between Izod impact strength and various moulding conditions for polyethylene. The authors found that as melt temperature increased Izod impact strength in the longitudinal direction decreased while the strength in the direction transverse increased. This result corresponded to their earlier conclusions that the percentage of skin layer was reduced with mould temperature, melt temperature and injection speed.

Williams and Bevis (16-20) noted the effect of variations in barrel temperature on microstructure and morphology during a study of polypropylene copolymer injection mouldings. Increasing the melt temperature from 185 to 225°C not only reduced the thickness of the skin layer in the moulding but also reduced the degree of molecular orientation in the

mouldings, as observed by the elimination at the rows of β-shear nucleated type III spherulites. At melt temperatures above 245°C the character of the skin changed from that of a featureless highly oriented structure to one more characterisric of a spherulitic structure. The highly oriented molecules in the skin formed at lower melt temperatures offered greater resistance than the more spherulitic skin formed at higher melt temperatures when impact tested at room temperature. However, when tested below the ductile failure mode at -10°C the influence of internal stress and molecular orientation becomes more important than the character of the skin. This was clearly demonstrated by a reduction in impact strength of plaques prepared at 185°C and a marked rise in impact strength of mouldings prepared at higher barrel temperatures.

Henke and co-workers (8) studied the relationship of mould temperature with Izod impact strength. The impact strength of the propylene ethylene copolymer samples decreased with increasing mould temperature up to about 160°C. Consequently, the Izod impact strength decreased with increasing spherulite size. This makes sense if we consider that the polymer will fracture interspherulitically, basically by rupture of the tie molecules as the spherulites become larger. If the sample has small spherulites there will be more tie molecules and consequently a higher impact strength. An increase of the Izod impact strength with decreasing spherulite size was noted also in high density polyethylene by Ohlberg, Roth and Raff (1).

Impact strength then has been found not to be purely a function of the width of the skin and shear zones but also of the average spherulite size variance. Additionally, for example, Way, Atkinson and Nutting (7) studied the effect of spherulite

size on the fracture morphology of polypropylene and found that an average spherulite radius R = 0.08 mm, produced by a cooling rate of 0.03°C Sec^{-1}, gives the optimum tensile properties of a particular isotactic polypropylene.

Cole (83) presented a paper entitled the relevance of impact tests to the quality of injection mouldings. Within this paper the author outlines factors which influence impact behaviour namely; flow into the mould, mechanical anisotropy, gate and mould design, moulding parameters and moulded in stress, which vary with location and through the thickness. The author suggested that such factors favour the use of falling-weight tests on complete mouldings. The most recent paper published on the effects of injection moulding parameters on the impact strength of thermoplastics is given by Crawford and McGonagle (84). The authors presented a case against moulding simple geometries of test pieces stating that these do not simulate the flow paths which are experienced by the melt in practical mouldings. It is generally accepted that melt flow patterns are an extremely important aspect of injection moulding and have a very significant effect on the properties of the moulding. In an effort to provide information of more direct relevance to the moulder a programme of work on the properties of pseudo mouldings specially designed to incorporate typical features present in commercial mouldings was carried out.

Experience had shown (85-88) the authors that weld lines present a major problem to moulders and so multigated moulds, up to a maximum of six gates, were used to provide a range of filling patterns and weld line positions since any of the

gates could be blocked off. A variety of gate sizes could also be used since each gate was a button insert. A range of injection rates, pressures, melt temperatures and mould temperatures were studied in detail on four different shape mouldings. The material used was a polypropylene homopolymer and test pieces were cut for instrumented tensile impact testing, both plain and notched samples were tested at temperatures over the range -40° to 20°C. The results of this work may be summarised as follows:-

(1) Effect of Injection Rate

In notched samples no injection rate effect was noticed on impact strength due to the severe stress concentrations being the overiding factor rather than inherent weaknesses in the samples. Un-notched samples showed that a slight reduction in impact strength was noticed at high and low injection rates. At low injection rates higher viscosities, and the freezing off with little orientation in the flow direction, were said to account for low impact strengths. At high injection rates stress crystallisation effects may account for low impact strengths.

(2) Effect of Injection Pressure

As with injection rate the inclusion of sharp and blunt notches in the samples did not provide any useful information. The poor impact strength at high injection pressures was associated with high residual stresses in the moulded article. Although low pressures minimise residual stresses it is clear that if welds are present in a moulding then sufficient pressure is required to provide good knitting of the weld fronts and expulsion of trapped air from the weld zone.

(3) Effect of Melt Temperature

The major factors contributing to the observed behaviour was thought to be molecular orientation. At high temperatures the longer cooling times result in less orientation in the test direction so that the samples were weaker than those produced at low temperatures. However, at very low melt temperatures (170°C) other effects such as freezing off and stress crystallisation had a dominant influence.

(4) Effect of Mould Temperature

Tests on moulding using mould temperature in the range 20-60°C revealed consistent reductions in impact strength with increasing mould temperatures. When mouldings are quenched quickly a high degree of molecular orientation occurs in the flow direction, at higher mould temperatures the orientation has time to relax out.

(5) The gate size had a large effect on impact strength and in all the tests, the larger gate was seen to give higher impact strength values.

(6) The geometry of the moulding had an effect on the impact strength of the product and in many cases this effect was larger than could be caused by variations in the processing conditions.

(7) Depending on the mould filling pattern it was possible to get larger variations in the impact strength of different sections of a moulding. Different melt flow patterns determined the strength of a weld i.e. whether the angle of approach was oblique or flat.

(8) The impact strength of a rib was less than other sections of the moulding due to undesirable transverse orientation of the molecules in these sections.

(9) It is apparent that there was a machine effect in that mouldings produced under apparently identical conditions on different machines did not have the same impact strength.

The fatigue properties of injection moulded polypropylene copolymer have also been invesitaged in a systematic manner (21) using several processing conditions and with different gating systems to produce a range of typical spherulitic microstructures. In addition to internal weld lines, some specimens were joined to form external mirror plate butt-welds. The effect of the different microstructures on the fatigue and impact properties as a function of two test temperatures of 23 and -10°C were reported. The influence of different microstructures resulted in significant differences in load-bearing ability.

The fatigue studies were co-ordinated with systematic studies of the effect of different pigments, concentration of recycled plastic and exposure to ultra-violet light (natural and artificial) on the structure and properties of injection moulded polypropylene (17-20). A marked dependence of impact properties on pigment type was reported and indicates the importance of additives on structure and properties. However, the most dramatic influence on mechanical properties is the internal weld line caused by merging flow fronts within the mould cavity. Substantial decreases in mechanical properties

associated with internal weld lines have been reported for reinforced thermoplastics (89, 90) as well as unreinforced thermoplastics (91-94). Unpublished results (95) are being collated at Brunel University and should be sufficient to indicate the magnitude of the effect of pigments and internal weld lines on the tensile properties of injection moulded test bars and particularly in the case of the fibre reinforced plastic.

1.5 EFFECT OF ADDITIVES ON THE STRUCTURE AND PROPERTIES OF MELT CRYSTALLISED POLYPROPYLENE

It has been shown that certain materials may be added to a polymer in small quantities in order to bring about crystallization at a higher temperature and to produce a fine homogeneous spherulitic morphology. Such materials are termed heterogeneous nucleating agents and are of great commercial importance since they considerably change the density, clarity and mechanical properties. However, compounds vary widely in their effectiveness as heterogeneous nucleating agents.

In an early study by Beck (96) on the heterogeneous nucleating agents for polypropylene crystallization the author stated that nucleation at the interface of a foreign phase requires at least five of the following characteristics:-

(a) It should be capable of reducing the interfacial surface free energies involved i.e. it should be wet by the polymer or absorb polymer on its surface at and below the polymer melting point.

(b) It should be insoluble in the polymer at and below the polymer melting point.

(c) It should melt above the polymer melting point and preferably without decomposition.

(d) It should be non volatile, stable and unreactive towards its environment i.e. polymer, oxygen, moisture and miscellaneous additives.

(e) Also, if possible, it should possess a crystalline structure similar to that of the polymer.

Considering property (a) the basic idea underlying most pictures of heterogeneous nucleation is that the total interfacial free energy of the crystalline embryo is reduced by a foreign phase which already provides part of the interface to be formed; this brings about a reduction in the activation free energy for nucleation and thereby a decrease in the degree of supercooling required for nucleation. The higher the preference of the crystalline phase to absorb at the foreign material rather than the liquid phase, the lower the activation free energy for nucleation will be. One might expect a good solvent for polypropylene, such as a hydrocarbon, to be an important constituent of the structure of a good nucleating agent for polypropylene crystallization. Property (b), of course, implies that the nucleating agent must present a solid surface to the polymer in a temperature range of importance for crystallization. It also suggests that another constituent of this good nucleating agent would be a group capable of rendering the molecule insoluble in the polymer. Such an insolubilizing group might be a highly polar substituent. Such a model nucleating agent may be represented by an organocarboxylic acid salt. The authors studied the effects of metal cations, substituent groups and length of aliphatic groups of a wide range of different compounds, sodium benzoate and basic aluminium di-benzoate were among the most ideal representatives of the model nucleating agent found so far for

polypropylene. Aromatic organic groups were found to be better constituents of the nucleating agent than aliphatic groups.

Binsbergen (97, 98) tested about 2000 substances for their possible nucleating effect on the crystallization of polyolefins. It was found that the nucleating agents were insoluble in the polymer melt and were probably always crystalline substances. The great majority of which exposed a surface consisting of hydrocarbon groups resembling moderate to good solvents for the polymer, their insolubility being due to a layer-like arrangement of their strongly polar and non-polar groups at the seed crystal surface. Epitaxy was ruled out as a mechanism for the nucleating effect, since the nucleating agents were active in all polyolefins tested, regardless of lattice dimensions. He also concluded that the activity of agents is strongly dependent on the degree and sometimes on the method of dispersion and that orientation of the nucleating particles in the polymer melt causes oriented crystallization of the polymer.

Fitchmun and Newman (99) showed that transcrystallinity occured at the surface of polypropylene and polyethylene in contact with mylar and teflon, while aluminium and copper oxides showed little effect on surface morphologies of crystallizing melts. The occurence of transcrystallinity was attributed to heterogeneous nucleation induced at the mould surface. However, contrary to claims in the literature, the surface energy of the mould surface and temperature gradients across the melt surface did not play a primary role in transcrystalline formation. The authors proposed that the similarity in chemical structures of the various active mould surfaces and specifically known nucleating agents was the determining factor.

Chatterjee and Price (100, 101) studied the nucleating abilities of various substrates (mostly polymeric) on the melt crystallization of iPP, poly (ethylene oxide), poly (butene -1) and polycaprolactone using hot stage microscopy. The activity of the substrate as a nucleant was assessed and ranked on whether it was very active inducing transcrystallinity, moderately active or inactive. From a survey of 43 substrate-crystallizing polymer pairs they concluded that the necessary conditions for a strong nucleating action in polymer melt crystallization were as follows:-

(a) Similarity of chemical structure of substrate and crystallizing polymer.

(b) Similarity of crystallographic unit cell type of the chosen pair.

(c) Close match of crystal lattice parameters of the chosen pair.

Furthermore, they concluded that the surface energy of a substrate does not indicate its nucleating ability. Low energy surface polymers were capable of inducing transcrystallinity. In fact contrary to the claims of Fitchmun and Newman (99) that only high-energy surfaces can induce transcrystallinity, it was revealed that low-energy surfaces can even surpass high energy surfaces in nucleating ability.

The use of graphite fibers as a nucleating agent for polypropylene was investigated by Hobbs (102). Crystallization from the melt showed that only graphite fibres with crystals of the size of the fold length of the polypropylene lamellae were active nuclei and produced transcrystallinity. A match of the helical period of the polymer with the H-absorption sites of graphite was suggested to enhance nucleation.

Although Binsbergen (97) has excluded lattice matching type epitaxy as the major mechanism for heterogeneous nucleation, recent work now suggests that structural similarities between some of the nucleating agents and polymer are quite common.

Wittman and Lotz (103) suggested that structural similarities between some of the apolar parts of nucleating agents and polyethylene are striking and indicated a need for re-examination of epitaxial correlations across the particle-polymer interface. The authors based their proposal on studies on the nucleating effect of benzoic acid for various polymers. They reported an epitaxial relationship between polyethylene, n-paraffins or aliphatic polyesters and benzoic acid which was characterized by a unique orientation of the polymer mass parallel to the substrate plane.

Garborczyk and Paukszta (104) studied the influence of additives on the structure and properties of polymers. Small amounts (0.5%) of stabilizers were dispersed in acetone and mixed with powdered iPP. Crystallization from the melt was examined by hot stage microscopy followed by x-ray diffraction structural investigations. The stabilizers used were aromatic amines and their sulphur analogues. Samples containing 2-mercaptobenzimidazole (MBIM) and triphenodithiazine (TPDT) preferentially nucleated the β hexagonal form. The authors proposed that the shape of the stabilizer crystal is one of the reasons why the β form was nucleated. The cyrstals of MBIM and TPDT have the form of plates or needles elongated in the c-axis direction and belong to the centrosymmetric space group $P2_1/C$. In addition these compounds have similar structures in which sulphur atoms are placed above the planes of the phenyl rings.

The observations of Garbarczyk nad Paukszta (104) provide a possible explanation for the preferential nucleation of the β-form by γ Quinacridone Red E pigment reported by Leugering (46) and Duswalt and Cox (65) in that this also has a structure similar to TPDT.

More fundamental work was carried out by Wellinghoff, Rybnikar and Baer (105), they observed the growth of thin epitaxial films of polyethylene on the surface of alkali halides. The epitaxial growth was postulated to have been induced mainly by the interaction of polyethylene molecules with the short range dispersion forces originating from the alkali halide surface and also from packing considerations. Rybnikar (106) extended this principle to the nucleation of polyethylene by talc, suggesting the polymer molecules are orientated by electrostatic forces emanating from talc.

Ronca (107) more recently established an epitaxial relationship for polyethylene, polypropylene, polyoxymethylene (POM) and polyhydroxybutyrate (PHB) nucleated with talc and boron nitride. The relationship was made after taking electron micrographs from the particles which formed the centre of spherulites produced in recrystallisation of solvent cast films of the compounds. With respect to iPP (ICI Grade GXM43), preferential growth of spherulites along the (040) plane with the chain axis oriented parallel to the surface of the substrate was observed. Two dimensional lattice matching of the polymer with talc and boron nitride was identified. The former substrate revealed a repeated configuration with a periodicity of nine polymer chains and the latter with a periodicity of thirteen polymer chains. The author also demonstrated a close

epitaxial growth of polyethylene POM and PHB with talc and boron nitride with excellent crystal matching between polymer and substrate. Ronca concluded that epitaxial growth is the most probable mechanism for induced nucleation and that perfect crystal matching of the polymer and substrate will ensure a maximum shift in the crystallization temperature. It was concluded that a good nucleant should have -

(i) homogeneous and easy dispersion,

(ii) a small particle size and narrow size distribution,

(iii) well developed cleavage or growth facets of a suitable size,

(iv) good epitaxial correlation at particle - polymer interface,and,

(v) a sufficiently high melting point and chemical stability.

Very little work has been published on the effects of iPP additives on the structure and impact properties of polypropylene. As previously mentioned Williams and Bevis (17, 18, 19, 20) noted a marked dependence of impact properties on pigment type and concentration incorporated in an iPP copolymer. The heterogeneous nucleating effect of phthalocyanine blue caused dramatic reductions in impact performance despite its excellent protection against photodegradation. Incorporation of Ultramarine blue pigment caused preferred nucleation of the β-type spherulites accompanied by slight reductions in impact properties.

The authors were unable to offer any mechanism of nucleation or reasoning for the drop in impact properties and it was suggested that this was an area of work requiring more attention.

Hutley and Darlington (108, 109) recently published two papers concerned with an established linear correlation between the impact strength and rate of crystallization for a series of highly filled polypropylene compounds. To confirm whether the nucleating phenomena discovered affected impact strength the authors have stated that a high priority in their further investigations will be to obtain direct evidence of the differences in polymer morphology. The results of this work are dealt with in more detail in Chapters II and VI.

****

The totality of the literature reviewed above indicate the importance of processing conditions, compound additives and mould design in influencing the mechanical properties of moulded parts. The utilisation of the information presented above and in the referenced papers should help in the optimisation of the mechanical properties of moulded parts although, regrettably, the systematic study of the reported effects and in particular those relating to performance after weathering and long lifetime remains a complex and relatively neglected subject. The use of straightforward microtomy from moulded parts and transmission electron microscopy of replicas provides for a very effective method for microstructure characterisation in unfilled and low percentage filled thermoplastics. Clearly the need to establish structure-impact property relationships in isotactic polypropylene requires the preparation, testing and characterisation of a whole range of injection mouldings exhibiting various structural modifications.

CHAPTER 2

SELECTION AND PROCESSING OF MATERIALS, AND EXPERIMENTAL TECHNIQUES.

2.1 SELECTION OF MATERIALS

2.1.1 Selection of Polypropylene

The iPP homopolymer used throughout the research programme, namely GXM43, was supplied by I.C.I. GXM43 is a commercial, medium flow (X), fast cycling, general purpose (G) injection moulding grade (M) with a Melt Flow Index measured at 230°C, according to ASTM D1238, of 9.0 grams per 10 minutes. This grade was chosen because of its wide application to domestic and automative components.

2.1.2 High and Low Molecular Weight Tails

In order to study the effects of incorporating low percentages of both high and low molecular weight polypropylenes on the micromorphology and impact properties of GXM43, suitable grades were selected as follows:-

(i) A general purpose pipe extrusion grade (GSE16), with a Melt Flow Index measured at 230°C of 0.8 grams per 10 minutes, was selected from the ICI literature for the high molecular weight additions.

(ii) Likewise, a general purpose, easy flow, injection moulding grade (GYM45), with a Melt Flow Index measured at 230°C of 15.0 grams per 10 minutes, was selected from the ICI literature for the low molecular weight additions.

All three grades used in the research programme were supplied in granular form, stabilised adequately for applications involving intermittent exposure to high service temperatures, but free of Ultra-Violet stabilisers. A data summary of physical properties for the three grades is given in Table 2, the data was collated from various I.C.I. technical leaflets (110, 111).

TABLE 2

Physical Properties of Polypropylenes Selected

Property	Test Method	Unit	Homopolymer Grade GXM43	GSE16	GYM45
Density		g/cm^3	0.905	0.905	0.905
Tensile yield stress	ISO-R 527	kg/cm^2	350	337	350
Melt flow index (MFI)	230°C/2.16 Kg	g/10min	9.0	0.8	15.0
Flexural Modulus	ASTM D790	kg/cm^2	18,000	16,800	18,000
Izod impact strength	ISO R 180 23°C	J/m notch	40	65	40
	ASTM D256 0°C		25	35	25
	(0.25mm notch) -20°C radius		20	25	20
Rockwell hardness	ASTM D785	R Scale	95	93	95
Softening temperature	ISO-R306	°C	148	148	148
Heat distortion temperature	ISO-R75				
4.6 kg/cm^2 (455 kN/m^2)	ASTM D648	°C	68	105	68
18.6 kg/cm^2 (1820 kN/m^2)		°C	105	-	105
Flammability	FMVSS 302 (3mm thickness)	Burning rate mm/min	20	20	20
Co-efficient of thermal expansion at 20°C		K^{-1}	1.1×10^{-4}	-	1.1×10^{-4}
Moulding shrinkage at 20°C		%	1-2	-	1-2
Weight Average * Molecular Wt.		Mw	284,000	490,000	249,000

* Results received from RAPRA Polymer Supply and Characterization Centre.

2.1.3 Mineral Fillers

The addition of mineral fillers such as talc or chalk to polypropylene increases the rigidity and dimensional stability of moulded parts. Grades containing 10-40% by weight are not uncommonly used to provide a wide spectrum of properties and beneficial cost savings. For the purpose of the research project two such fillers were used in low percentage additions to assess whether any modifications to the existing micromorphology and resulting impact properties could be achieved. The two mineral fillers chosen for this work are described below:

(i) Chalk

A very fine, high purity calcite filter (crystalline calcium carbonate of Urgonian origin) was chosen from the Omya range of fillers (112). The high degree of fineness and whiteness give this filler almost pigmentary qualities. Low oil absorption, good resistance to weather and ageing are amongst its favourable properties. Its application to injection moulded polypropylene gives tougher and less stiff mouldings than grades with similar levels of talc. The chalk supplied by Omya had a mean particle size quoted at 1.5 mm and a chemical composition as follows:

Chemical analysis of Omya hydrocarb	$CaCO_3$	99.75
	MgO	traces
	Fe_2O_3	0.02
	SO_4^{2-}	0.06
	Colloidal aluminium silicate	0.10
	Moisture (DIN 53198)	0.30
	Particle shape (crystalline)	rhombohedral

The crystalline system of chalk is based on the hexagonal unit cell with lattice parameters a = 4.989Å and c = 17.062Å.

(ii) Talc

This is a proven, powerful α-phase heterogeneous nucleant for polypropylene. Recent studies by Ronca (107) on the heterogeneous nucleation of iPP reported crystallization temperature shifts upwards in the order of 12°C for concentrations of 1wt% or more. Talc is incorporated into polypropylene at various levels ranging from 10% to 40% by weight for commercial applications requiring improved rigidity. The increase in rigidity of mouldings is accompanied by reductions in the co-efficient of linear expansion and in mould shrinkage. Because of the filler, however, the natural colour of talc filled mouldings is light grey, and there is a reduction in surface gloss. Also, impact strength declines with increasing levels on filler. The talc used was supplied by I.C.I. (113) along with a powder grade of GXM43 polypropylene (GX543M) to assist in dispersion during pre-compounding.

The structure of talc is such that it reveals a plate-like crystal form exhibiting a large surface area in relation to its mass. The internal structure of talc has its most polar groups situated, on the materials surface, at the ends of the platelets where bonds have been broken as illustrated in Figure 16. The chemical formula of talc is given as $Mg_3Si_4O_{10}(OH)_2$, with the chemical name Magnesium Silicate Hydroxide. The crystalline system of talc is based on the monoclinic unit cell with lattice parameters a=5.287Å, b=9.171Å, c=18.964Å and β=99.61°.

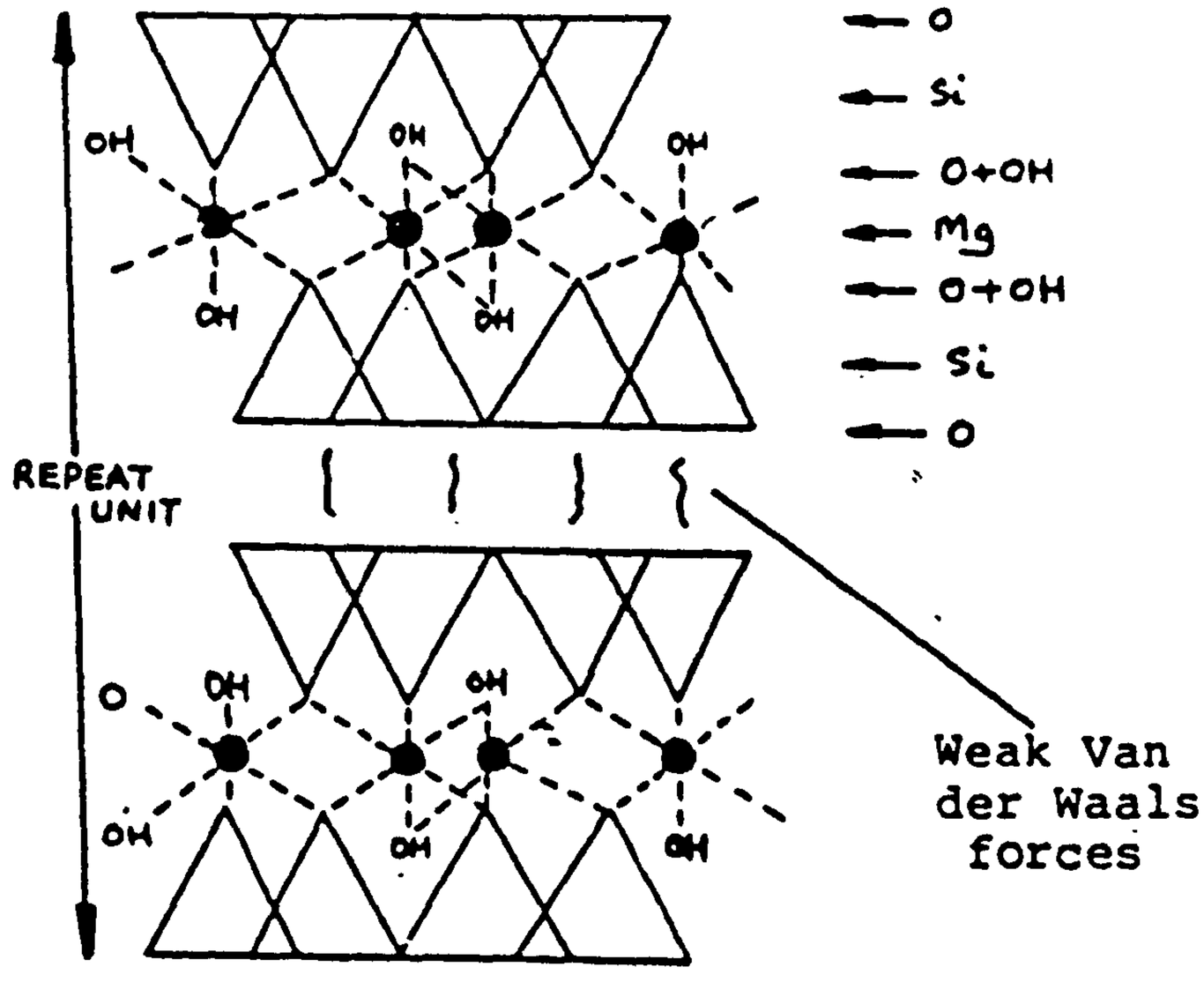

(a) Talc. $Mg_3(OH)_2Si_4O_{10}$

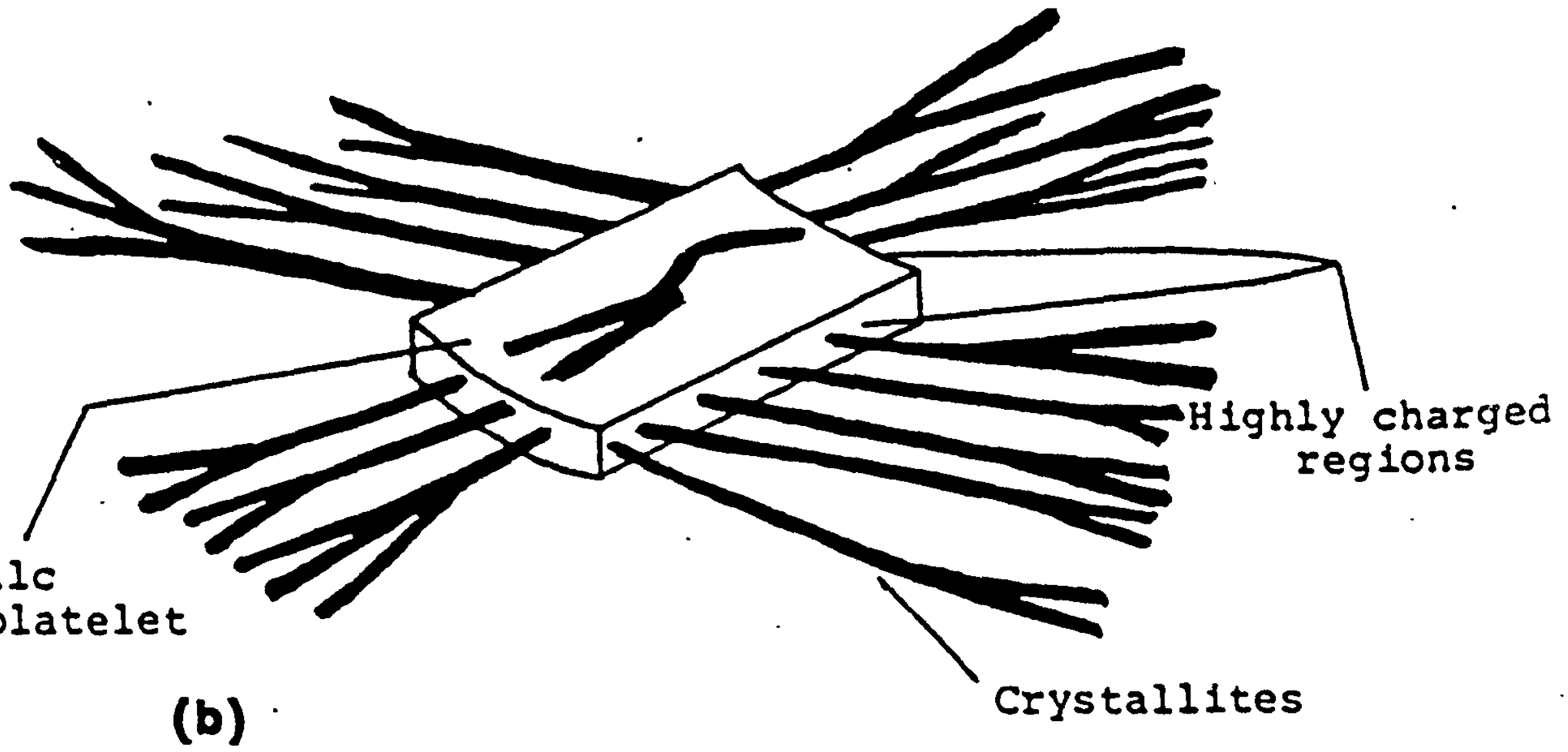

(b)

Figure 16 (a) The internal structure of talc.
(b) Nucleation model for the PP/talc system.

2.1.4 Pigments/Nucleants

Four pigments known for their nucleating ability in polypropylene were selected by careful surveyance of the existing literature. Preferential nucleation of either the α- or the β- iPP crystalline form was of particular relevance in the selection criteria used. The pigments chosen for this work and a brief synopsis of the existing literature on their application to iPP is given below:-

(i) Ultramarine Blue

The incorporation of Ultramarine blue pigment at low loadings (0.1 - 2.0 wt.%) in polypropylene copolymer injection mouldings was studied by Williams and Bevis (16-20). The latter found that increasing the percentage of pigment gave rise to an increase in the proportion of β-phase spherulites with an accompanying decrease in the impact strength of mouldings. For this reason it was decided to study the effects of low loadings of Ultramarine blue on the micromorphology and impact properties of polypropylene homopolymer as an extension to previous work.

Ultramarine is a member of the nosean-sodalite family of minerals which have a three dimensional alumino-silicate lattice carrying a negative charge. In the interstices, and cavities, in the lattice cations are located to neutralize the negative charges. Ultramarine contains sodium sulphide and sulphur, the colour of this inorganic pigment changing from green to blue with increasing sulphur trapped in the cavities in the form of free radicals. The composition for the blues is said to lie between $6(Na\ Al\ SiO_4)_6\ \ 2S$ and $6(Na\ Al\ SiO_4)_6$.

Na_2S, 3S. Ultramarine blue is used widely in the colouring of polypropylene, it is non-migratory and non-chalking with excellent resistance to heat, light and alkali. Its main disadvantage is poor resistance to acids. The grade chosen for this work was 08 supplied by Reckitts Colours Limited. It lies in the middle of the range of shades available, both with respect to cost and tinting strength. 08 is very soft and easily dispersed is polymers which favours its application as a nucleant. The crystalline system of Ultramarine blue is based on the cubic unit cell and the mean particle size was quoted as 2.4 μm (114).

(ii) Phthalocyanine Blue

Williams and Bevis (16-20) also studied the effects of incorporating low loadings (0.1-2 wt%) of a phthalocyanine blue pigment on the structure and impact properties of a polypropylene copolymer. The use of phthalocyanine blue gave rise to mouldings which exhibited poor impact properties as a result of its powerful nucleating properties reported previously by Rybnikar (105). However, the pigment afforded 50% protection against photodegradation in copolymer having no additional ultra-violet stabilizer. It was decided to include phthalocyanine blue in the research programme to investigate its nucleating characteristics in polypropylene homopolymer, and to assess the resultant effect on impact properties.

Phthalocyanine blue is an organic pigment with outstanding heat, light and non-migratory properties. It is

however a difficult pigment to disperse and requires careful application of pre-compounding techniques. Its basic structure is an extremely stable copper complex shown below:-

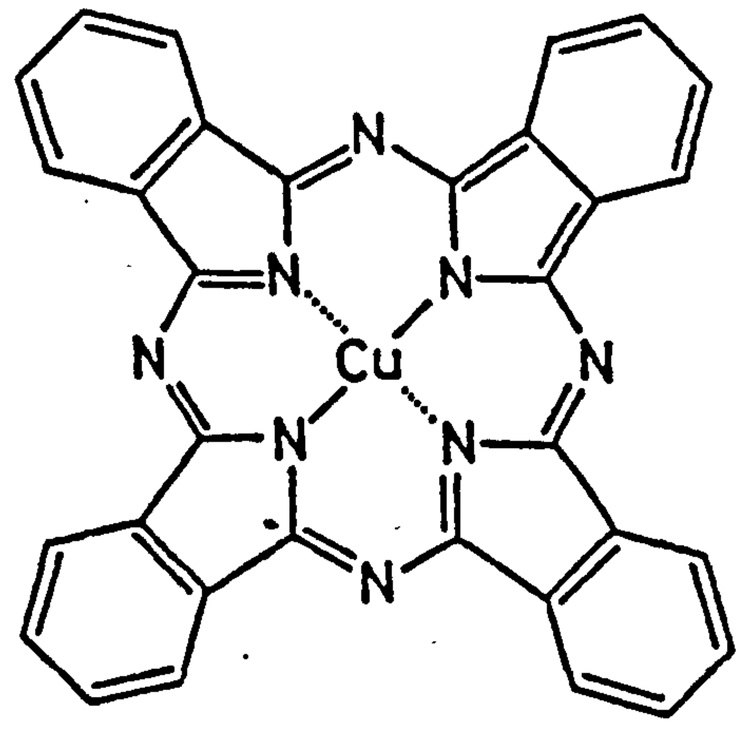

copper phthalocyanine

It has a monoclinic unit cell with a space group of $P2_1/c$ and lattice parameters a = 14.68Å, b = 4.98Å, c = 19.60Å, $\beta = 121.5^{\circ}$.

(iii) Quinacridone Pigments

Work by H.J. Leugering (46, 48) at Hoechst has shown that small amounts of a quinacridone colourant, Permanent Red E3B, preferentially nucleated the β-form of polypropylene. This compound is one of the very few known, effective nucleators, found to be only effective in its 'γ' crystalline form. Quinacridones can also exist in α and β modifications which apparently do not nucleate the β polymorph. Other β phase nucleators described in the literature are the bisodium salt of O-phthalic acid (115) the aluminium salt of 6 - quinizarin sulphonic acid (116) and to a lesser degree isophthalic and terephthalic

acids (115). A more recent thermal study of the β- form by Duswalt and Cox (47) found that nucleation was affected by both the rate of cooling during crystallization and level of E3B nucleator used. Optimum β- phase nucleation was found at cooling rates of -20°C/minute using 10^{-4}-10^{-5}% of nucleator. However, appreciable amounts of crystallinity was produced even at nucleator levels of 10^{-8}%.

In an attempt to relate the level of β phase to impact properties in injection moulded polypropylene, it was decided to incorporate a low percentage of E3B to preferentially nucleate the β-form. The pigment was supplied by Hoechst UK, along with technical data (117-120). The structure of linear trans-quinacridone is given below:

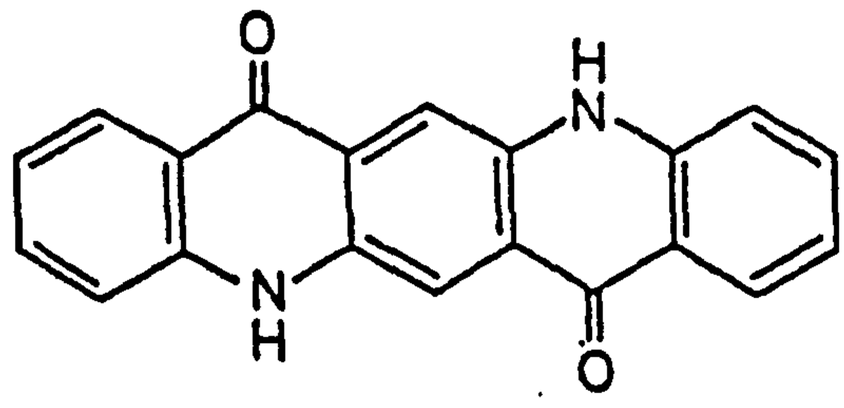

linear-trans-quinacridone

It has a monoclinic unit cell with a space group of $P2_1/C$ and lattice parameters a = 14.116Å, b = 3.885Å, c = 13.377Å and β = 107.22°.

The pigment was supplied in powder form with a mean particle size of 0.11μm, it is a rather yellowish quinacridone red with very high light and solvent fastness. According to Hoechst literature it is suitable in application to rigid PVC, plasticised

PVC, polyolefines and polystyrene.

In addition to low percentage incorporation of the γ form of quinacridone a β form was also chosen from the literature for comparison of nucleating properties. Among those available, Fast Pink E was chosen because of its simularity to E3B in particle size distribution and suitability to polyolefines. This pigment has a distinct violet tinge with simularly high light fastness, thermal and migration stability. The mean particle size of both quinacridones was quoted at 0.11 μm.

2.2 PREPARATION OF FEEDSTOCKS

2.2.1 Natural Compounds

The Natural GXM43 iPP granules were injection moulded in the as supplied condition for the initial work, reported in Chapter 3, to determine the effects of processing parameters on the micromorphology and impact properties.

2.2.2 Incorporation Of High And Low Molecular Weight Tails

Feedstocks consisting of 5, 10, 20, 30 and 100 wt% of high and low molecular weight polypropylenes, GSE16 and GYM45, respectively, were also prepared. The compounds were mixed with natural GXM43 granules for a set time of 5 minutes using a Winkworth tumble mixer. The feedstocks were then moulded direct using a Sandretto 6GV/50 injection moulding machine.

To assess the degree of dispersion of the high and low molecular weight additions moulded plaques were granulated and sent to the Polymer Supply and Characterization Centre at the Rubber and Plastics Research Association (RAPRA). An

analysis of the molecular weight distribution using Gel Permeation Gas Chromatography was carried out by RAPRA. The results of this analysis, given in Chapter 4, revealed an excellent correlation between weight average molecular weight and percentage addition of high or low molecular weight material indicating good dispersion.

2.2.3 Pigmented Compounds

Feedstocks consisting of 0.1wt.% pigmented polypropylene GXM43 were also prepared by tumble mixing for 5 minutes, followed by extrusion on a single screw Reifenhauser S45, using the conditions in Table 3, and granulation. To assist in the dispersion of phthalocyanine and Ultramarine blue pigments a small quantity of spindle oil (c.a.0.01 wt.%) was mixed with the natural granules prior to pigment addition. The dispersion of pigments in the moulded plaques was assessed by taking microtomed sections and viewing them in transmitted light.

2.2.4 Mineral Filled Compounds

Feedstocks containing 1 wt.% chalk were prepared in the same manner as pigmented Feedstocks. However, the incorporation of 5 wt.% talc to the natural polypropylene homopolymer by tumble mixing and single screw extrusion led to poor dispersion with distinct agglomeration of the talc particles. To overcome this dispersion problem ICI supplied the natural polymer in its powder form, GX543M. A good dispersion was achieved by using a specially modified twin screw extruder, designated Model TS40-DV-L. The TS40 is a co-rotating intermeshing unit featuring modular screw and barrel sections for flexibility, twin ports for devalatilizing and/or feeding additives,

Table 3 S45 Single Screw Extrusion Conditions

Heater Zone 1	170°C	Screw Speed 11.5 rpm
Heater Zone 2	180°C	Motor Current 7.0 amps
Heater Zone 3	200°C	Haul Off 2 m/min
Heater Zone 4	210°C	
Heater Zone 5	220°C	
Heater Zone 6	220°C	
Heater Zone 7	220°C	

Table 4 TS40 Twin Screw Extrusion Conditions

Screw diameter	40 mm
Center distance	35 mm
Flight depth	5 mm
L/D ratio	17:1 (from front of feed port)
Flight pitch	Feed 24mm Compression 16 mm Metering 16 mm
Screw Speed	120 rpm
Motor Current	8 Amps
Heater Zone 1	185°C
Heater Zone 2	195°C
Heater Zone 3	205°C
Heater Zone 4	210°C
Heater Zone Nozzle	215°C
6 strand die	
Constant maximum compression monitored by pressure transducer at screw tips	200 psi or 1378.96 kNm^{-2}

efficient temperature control, and a special barrel withdrawal design that facilitates replacement and material analysis. A typical screw configuration used for the preparation of heavily filled compounds of calcium carbonate in polypropylene is shown in Table 4 together with the processing conditions used.

2.3 INJECTION MOULDING

A Bone Cravens Daniels 320-120 tonne, 250g shot, and a Sandretto 6GV/50 tonne injection moulding machines were instrumented to prepare reproducible mouldings for this research project as described in the following sections.

2.3.1 Instrumentation and Control of Daniels 320-120 Injection Moulding Machine

For the initial study on the effects of processing conditions on micromorphology and impact properties the Daniels injection moulding machine was used. Mould filling and reproducibility was optimised using the Hunkar Model 315 Adaptive Ram Programmer System. The model 315 offered the capability of controlling cavity hold pressure profile, shot size, injection velocity profile, hydraulic pressure, holding and plasticate pressure simultaneously, as well as other machine variables that effect the residence time and stress conditions of the part. The system operates with a specially designed high response- high flow servo valve; and feedback transducers for cavity pressure, injection velocity, hydraulic pressure and ram position, providing accurate closed-loop control of all functions. The system should give parts with consistent shrinkage uniform weight and diminished stress.

The most important control system operations are outlined below with reference to the schematic representation shown in Figure 17.

(i) Shot Control is achieved by using a shot control logic circuit that determines the line stroke of the ram to give the desired cavity pressure with identical polymer volume in front of the ram on each shot, a shot memory and correction circuit to ensure consistent decompression of the melt after plasticising, and accurate shot size control is also provided. In addition, the shot control links with the programmable servo system to give exact control of the ram position.

(ii) Injection velocity control is achieved through the closed loop feedback system which consists of; a servo valve to control the flow of oil and pressure to the ram cylinder to move the ram through a pre-set velocity profile, a ram position transducer to feedback ram position and injection velocity, and a velocity programme panel to provide 10 velocity command points for a given shot i.e. dividing the shot into 10 equal increments.

(iii) Cavity pressure control is achieved through a closed loop feedback control system also. The system components are a servo valve controlling flow of oil and oil pressure simultaneously for the ram cylinder and a force load cell that measures cavity pressure transmitted through an ejector pin in the mould. In addition, a cavity hold pressure programme panel to provide six hold pressure command points is provided, i.e. dividing the cushion into six equal increments. A maximum cavity pressure cut off control is achieved by a closed loop feedback control system comprising of a servo valve and

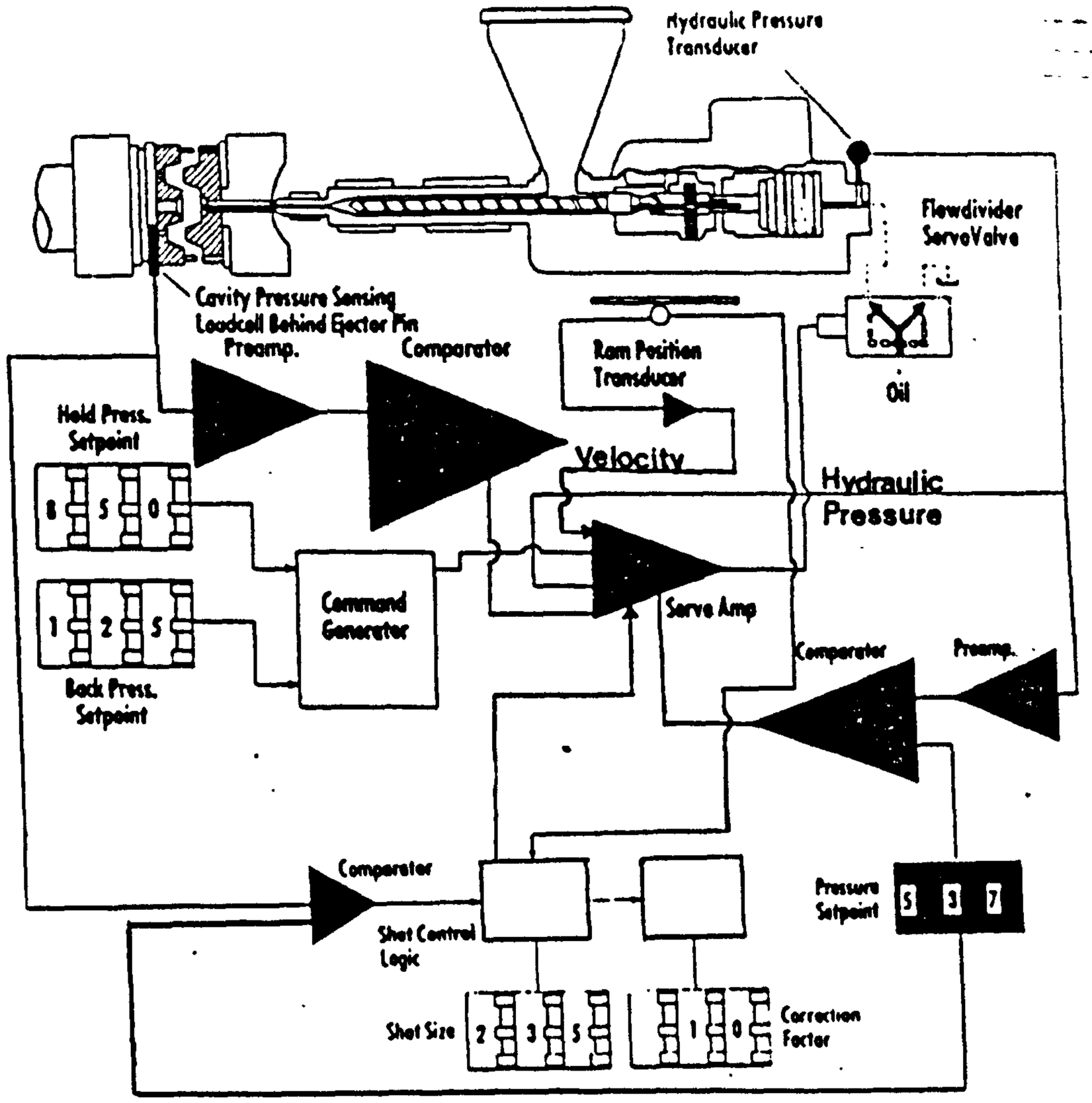

Figure 17 Schematic representation of Hunkar control system operations.

a hydraulic pressure transducer linked to a self compensating programmable servo system.

2.3.2 The NPL Mould

The Daniels was fitted with a specially designed mould, Figure 18, invented by K. Thomas of the National Physical Laboratories according to Patent Specifications 1577 034 (121). The mould was designed in order to achieve economy in the usage of mould components and to permit some variability in the form of the mould cavity in a particular mould. This was achieved by use of replaceable impression units, each unit offering variable arrangements of fluid ducts to enable optimum cooling to be maintained with different forms of mould cavity. Two replaceable impression units were assembled, namely a 90 mm diameter disc cavity and a 90 mm square cavity, in addition double tensile bar construction and double impact bar cavities were available as shown in Figure 18 . Changes in the thickness of the parts produced can be effected by replacing the packing plate and spacing ring with other such rings of different thicknesses. In addition Gate pads are provided for a variety of gate designs and sizes which are easily inserted. Balanced runner systems for single or double gating are also provided. The runner layout for the disc and squares is illustrated in Figure 19. For the purpose of the research project 3mm and 2mm depth cavities only were used with edge/ pin gates (3mm Deep x 1½mm wide).

Two Kistler cavity pressure transducers were inserted, one behind a dummy ejector pin in the 90mm square cavity and one near the gate in the runner system. The mould temperatures were constantly monitored by use of two thermocouples each located in the opposite fixed platen exactly central as regards

Figure 18 NPL mould, showing replaceable impression units.

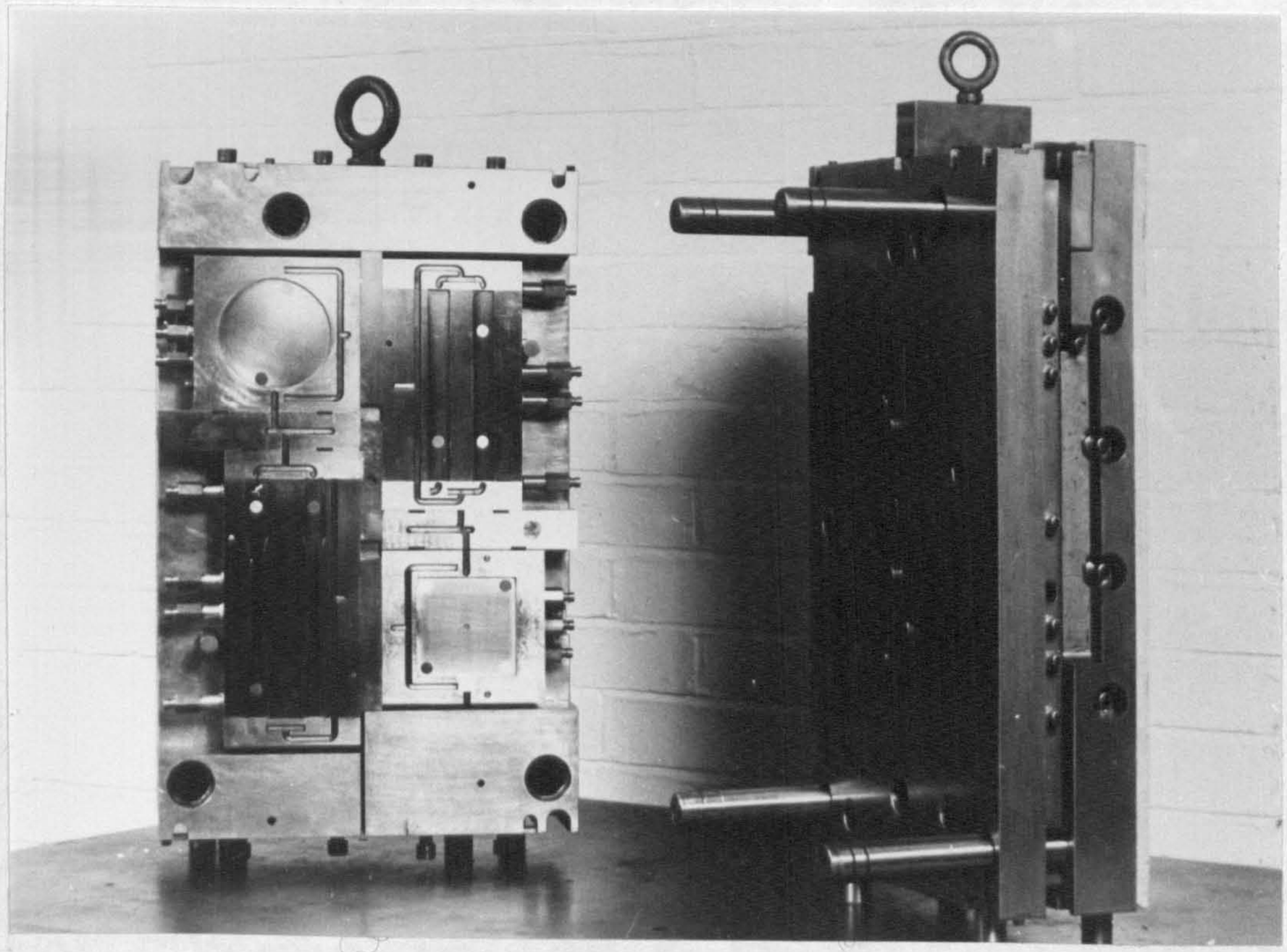

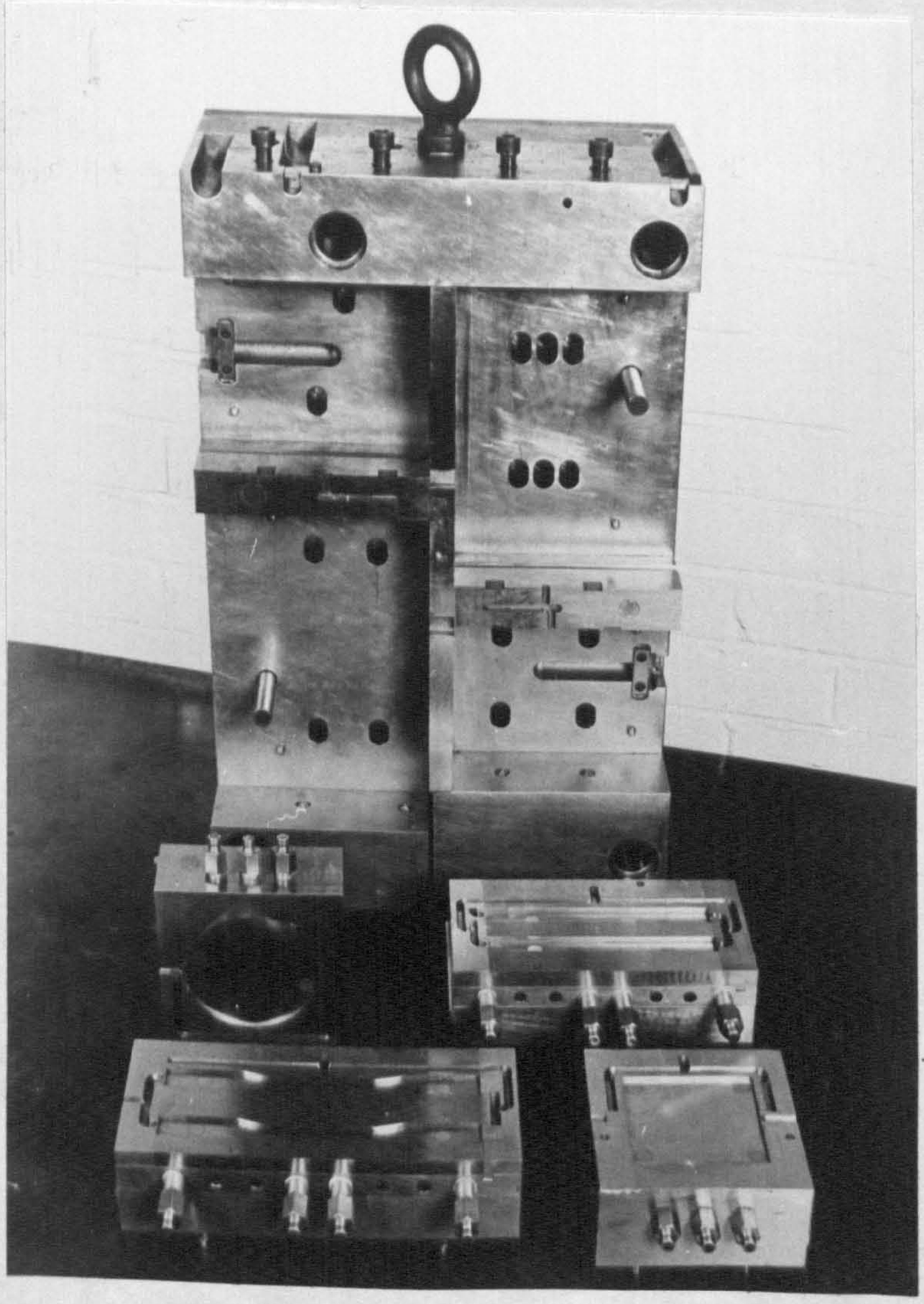

Figure 19 Runner layout for discs and squares.

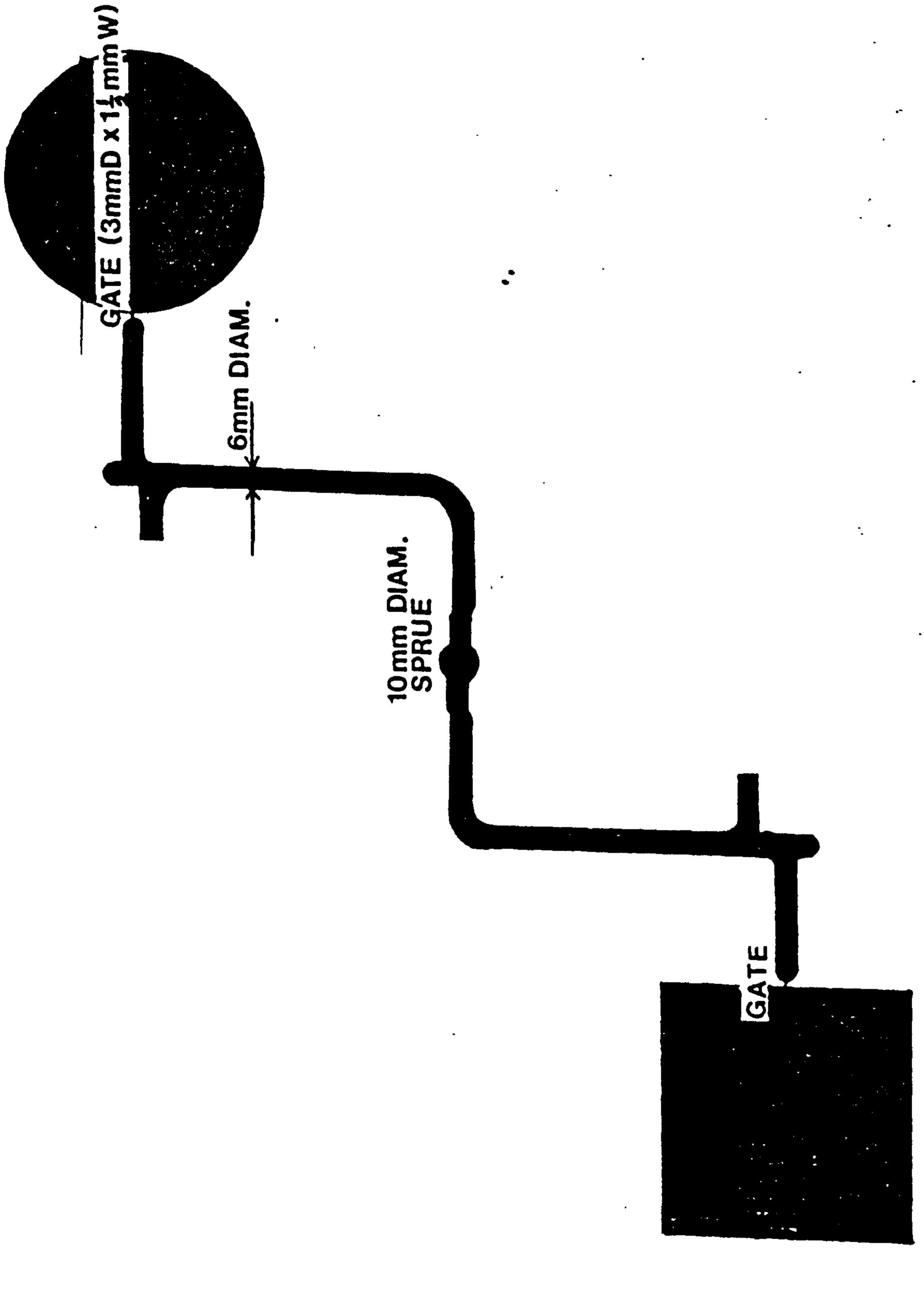

the cavities they were monitoring. The melt temperature at the nozzle was also monitored by use of a thermocouple. In total four chart recorders were set up with the ability to record the following:-

(i) Mould temperature ..... Recorder 1

(ii) Nozzle (melt) temperature ..... Recorder 2

(iii) Cavity Pressure Profile or Runner Pressure Profile ..... Recorder 3 (connected to Hunkar monitor via X output)

The fourth chart recorder was linked to the Hunkar monitor output Y to read amount of -

(iv) shot size
(v) hydraulic pressure
(vi) speed of ram

} Switchable using monitor selector

In order to accurately record the injection velocity the speed of ram output, Z, was linked to an oscillocope.

2.3.4 INSTRUMENTATION AND CONTROL OF THE SANDRETTO 6GV150 INJECTION MOULDING MACHINE

For subsequent studies, on the effect of gate geometry and incorporation of a wide range of additives on the micromorphology and impact properties of polypropylene injection mouldings, the Sandretto 6GV/50 tonne injection moulding machine was used.

It soon became impractical to consider using a range of processing conditions for a range of additives in view of the time and cost involved in moulding and the critical assessment of the performance of the moulded parts. Therefore, one set of moulding conditions was used throughout keeping all machine parameters constant.

The Sandretto is linked to an E82 microprocessor closed loop control unit which gives accurate control of injection moulding variables, with a 10 stage injection speed profile and 5 stage injection pressure profile to give maximum control of the injection stage. However, there was no facility for cavity hold pressure profile monitoring or maximum cavity pressure switch over which is vital to ensure good reproducibility of mouldings. For this reason, a Dynisco FT444, 100lb, ¼ inch pin diameter, strain gauge transducer was located behind a dummy ejector pin, and the changes in cavity pressure during mould filling were continuously monitored to ensure good reproducibility and optimum mould filling.

2.3.5 The Brunel Mould

The mould used on the Sandretto was a 3mm thick, double film-gated plaque mould. The geometry, location of mould temperature and cavity pressure sensor are shown in Figure 20. To improve the mould temperature control two Churchill heater/chiller units were employed. The melt temperature was monitored at the nozzle using a melt thermocouple linked to a digital readout.

The optimum conditions for injection moulding virgin granules were identified, and included a consideration of first and second stage pressures, mould andmelt temperatures cooling and injection times and the geometry of the moulds and sprues. Optimization of cavity pressure profiles in relation to the magnitude and timing of injection and hold-on pressures was made to ensure good mould filling. Once optimum conditions for the virgin granules had been established they were kept constant for the feedstocks containing various additives, so

Figure 20

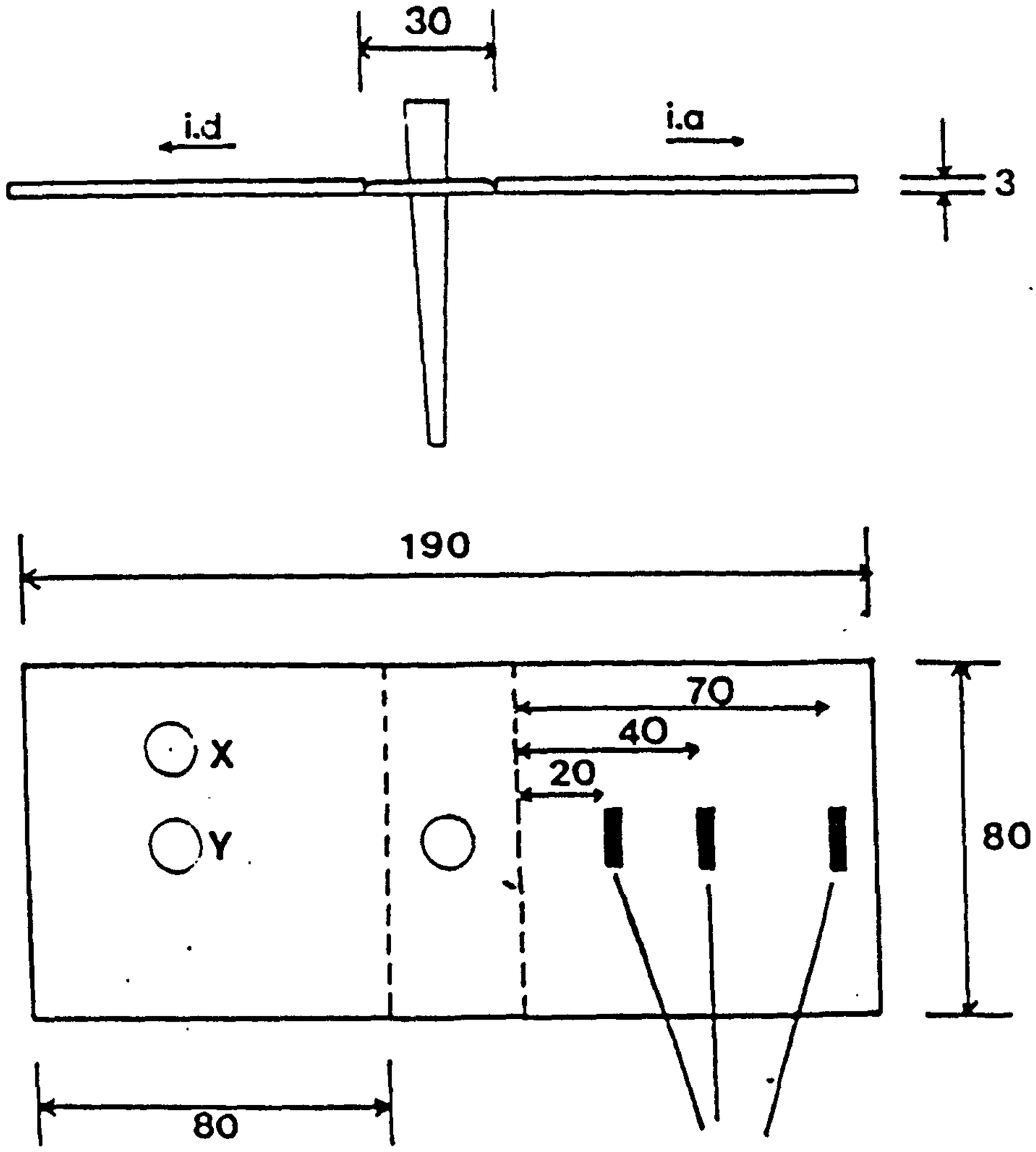

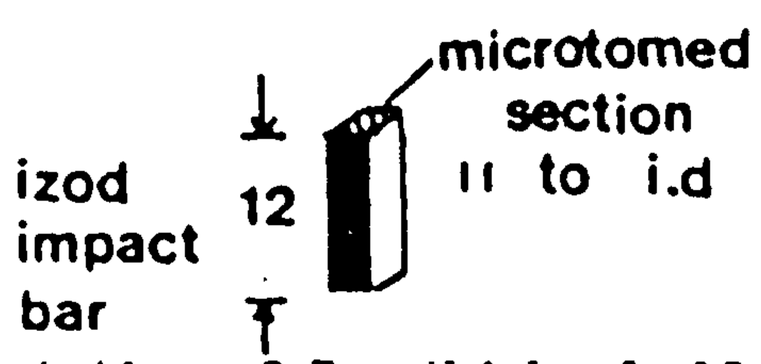

Figure 20 Schematic representation of 3mm thick, double film gated plaque mould, indicating mould temperature sensor X cavity pressure sensor Y and position of Izod test pieces.

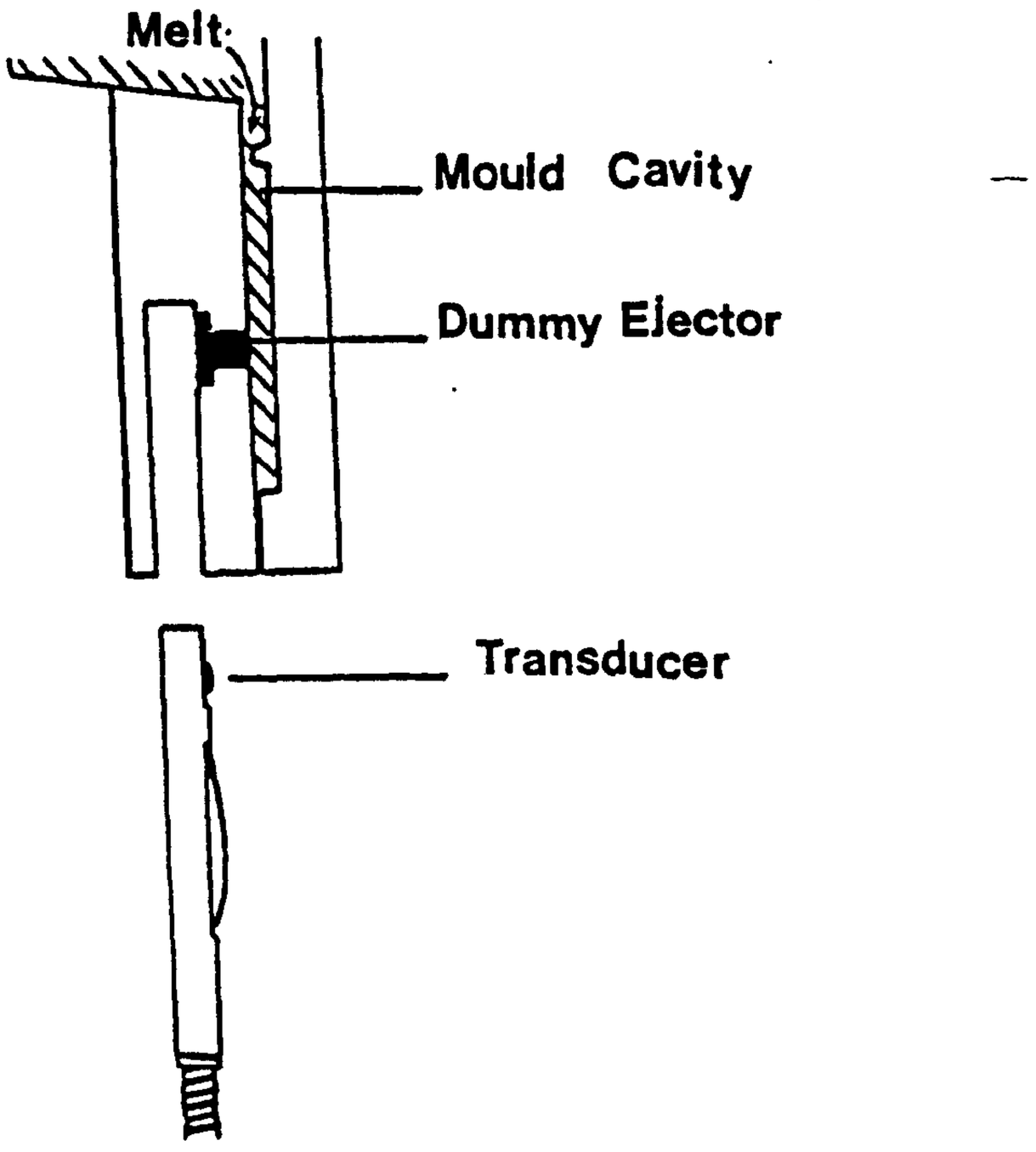

that any differences in properties would be due to differences in the formulation of compounds and not to changes in the machine variables. All mouldings were weighed directly after moulding to give some indication of reproducibility and changes in volume shrinkage from one condition to another.

2.4 INSTRUMENTED IMPACT TESTING

2.4.1 Introduction

An impact test appears initially to be an attractive and quick method of assessing quality. However, the number of specimens required to establish the significance of small changes in failure resistance may reduce its appeal. Some factors such as flow into the mould, skin and core morphology and moulded -in strains and stresses, which vary from location and through the thickness, may also cause scatter in the data produced by tests on specimens taken from larger mouldings.

Typical impact tests are the Izod test (ASTM D-256,ISO R-180) employing a cantilevered beam sample , the Charpy test (ASTM D-256, DIN 53453, ISO R-179) employing a three point bending sample, and tests in which samples in the form of plaques are impacted by a falling weight or tup, such as the Gardner test, or similar tests specified in ASTM D-3029 or DIN53443 and more recently ISO 6603/1. These standard tests are most useful for ranking materials in order of increasing toughness but because of the geometrical differences involved (types of stress and strain fields), it is not uncommon to find that different tests rank the same set of materials in different orders. The results of such tests are usually presented as a single number, such as the energy to break a sample in the Izod and Charpy tests, or the drop height required to produce an agreed 50% failure of all samples for a typical falling-

weight test. This single number result is a disadvantage since the more detailed aspects of the behaviour of the material under impact conditions are ignored. Energy may be absorbed in two clearly distinct ways; by elastic bending of the sample up to the point at which major craking occurs; and then by plastic deformation of the resin matrix. There may also be an intermediate stage of reduced rigidity following the initial formation of cracks, particularly in the case of drop-weight testing, where resistance to crack propagation is higher.

A number of instrumented impact testers have been described in the literature (122-132) which aim to follow both sample deflection and force between striker and sample over relatively short impact times (in the order of 1 milli-second). For the measurement of deflection, optical devices are generally used since many other displacement transducers, such as linear variable differential transformers, are too slow. For force measurements, strain gauges or piezo-electric crystal force transducers have been used successfully. Cessna et al., (126) appear to have been the first to realise that it is possible to obtain both kinematic (deflection, velocities) and dynamic (forces and energies) information from a single accelerometer attached to the tup or pendulum. The use of an accelerometer to instrument an impact tester is based on elementary physics. According to Newton's law acceleration in the impact direction (measured by the accelerometer) immediately yields the total force on the striker in the impact direction, the force between striker and sample can be obtained by subtraction. In addition, as long as the force between sample and striker is different from zero (i.e. that the sample and striker are in contact), then the velocity of the sample at the contact point is equal

to the velocity of the striker, and the deflection of the sample at the contact point is equal to the displacement of the striker. The velocity and displacement of the striker, in turn, can be obtained from the acceleration by integration at successive intervals.

For the purpose of the research project the need to study the impact properties of selected areas in a wide range of moulded articles required the use of an instrumented test to assess the performance of miniature unnotched bars. In addition the need to test whole mouldings for directional weakness was also required. It was decided therefore to use both an instrumented izod impact test and an instrumented falling weight test to gain as much information as possible on the impact performance of mouldings and their dependence on structural heterogeneity.

2.4.2 Instrumentation of Falling Weight Machines

The Daventest Rosand Instrumented Impact-test (132) used in this work can be briefly described as follows:-

1) Mechanical Design

The mechanical design is very simple. The velocity of the impacting body can easily be varied by changing the drop-height h, thus

$$Vo = \sqrt{2gh} \qquad \text{(i)}$$

Where Vo is the velocity at impact and g is the acceleration due to gravity (9.81 ms^{-2}).

The sample holder is a raised ring of 40mm internal diameter mounted on a base plate below the vertical drop tube which guides the striker to impact. The drop height available is 2000mm allowing 6 m/s maximum impact velocity

of a 27kg.striker and carriage,mass. In addition the impact machine is fitted with specially designed constant deceleration shock-absorbers, automatic triggering from an infra-red switch and a fully automated cycle (including retrieval of the drop weight assembly, sample stripping and damping). The striker is designed with a reversed taper (to prevent drag in ductile materials) and hemi-spherical end with a diameter of 20mm.

2) Data Aquisition and Evaluation

Figure 21 shows the equipment used for data aquisition and evaluation. A piezo-electric quartz kistler transducer, specially modified to have an enhanced combination of load capacity and frequency response, puts out a voltage proportional to acceleration. The signal is amplified and filtered with a 12 dB/octave frequency range 1 to 30 kHz (switched). The charge converter and amplifier have a switchable sensitivity from 0.01 - 40 kN full scale deflection in steps of 1, 2, 5, 10, etc., (to enable a whole range of impact properties to be analysed). The information is then transferred to a transient recorder system showing directly the force-time curve, the force-distance curve can be worked out by an integral microprocessor and can also be displayed. The transient recorder is a basic unit with better than 100 kHz sampling rate, 1024 sample points, 8 bit accuracy (=0.4%) and sweep times set at 10, 20, 50 ... 1000 ms as required. This is adequate for most general testing. In order to analyse the curve stored by the transient recorder system, a computer can:-

(a) display the curve for full calculation of force, distance and energy absorbed up to any point (making full allowance for any deceleration of the probe resulting from the energy absorbed by the specimen)

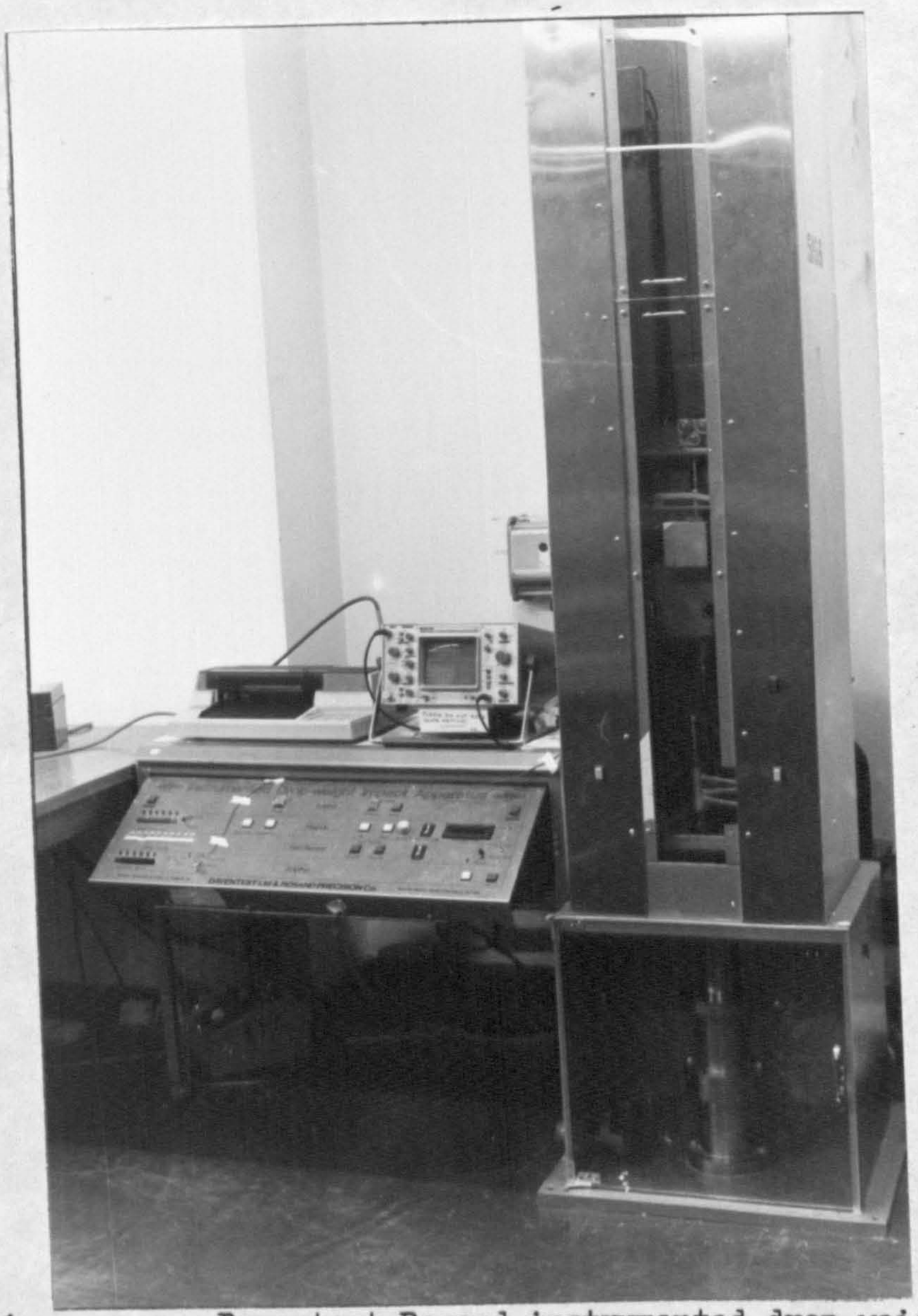

Figure 21 Daventest Rosand instrumented drop-weight impact test machine.

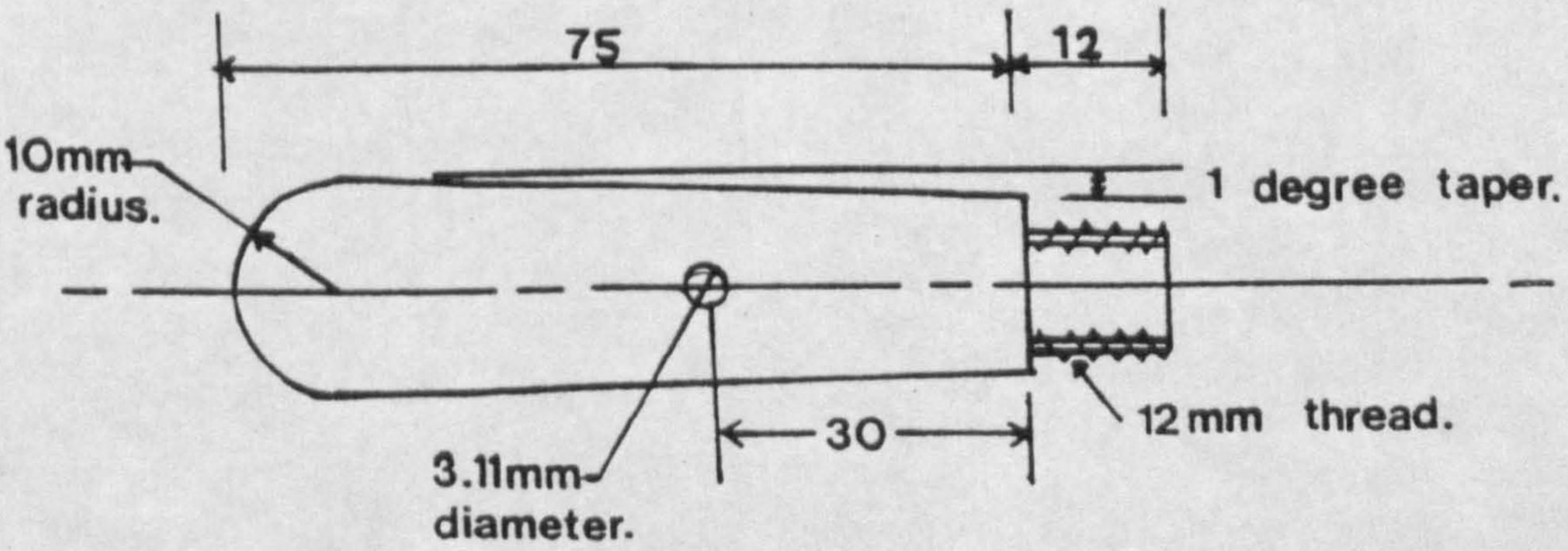

Figure 22 Dimensions of impact tup used in drop-weight impact test.

(b) Print out results as required

(c) Store data as required and

(d) Plot graphs of Force-Time, Force-Distance, Energy-Distance^2 and Velocity-Time, as required.

The computer calculates the impact velocity Vo (eqn(i)), and impact energy, Eo,from :-

$$Eo = mgh \qquad \text{\_\_\_\_ (ii)}$$

where m is the mass of the striker. The digitized voltage-time information, u(t), is transferred to the calculator and converted to acceleration, a(t). (Convention: u(t)>0 for positive acceleration in the direction of fall, i.e. u(t)<0 during impact).

$$a(t) = g \quad [\, u(t)/S \,] \qquad \text{\_\_\_\_ (iii)}$$

where a(t) is the acceleration (ms^{-2}), u(t) is the voltage (mV), and S is the sensitivity of the accelerometer (mVg^{-1}) supplied.

The acceleration immediately yields the force, F(t), exerted on the sample by the falling weight

$$F(t) = m \quad [\, g \, - a(t)] \qquad \text{\_\_\_\_ (iv)}$$

where m is the mass of the falling weight (kg), and F(t) is the force (N) (F>0) in downward direction.

The acceleration data are then integrated to yield the velocity of the falling weight as a function of time.

$$V(t) = Vo + \int_{t_o}^{t} a(t')\, dt' \qquad \text{\_\_\_\_ (v)}$$

where t_o is the moment of impact and Vo is the impact velocity. The integration of the velocity against-time data yields the displacement of the falling weight

$$x(t) = x(t_o) + \int_{t_o}^{t} V\,(t')\, dt' \qquad \text{\_\_\_\_ (vi)}$$

where $x(t_c)$ is the displacement at the time of impact ($x > o$ in the downward direction).

The quantity

$$d(t) = x(t) - x(t_o) = \int_{t_o}^{t} V(t') \, dt' \qquad \text{(vii)}$$

represents the deflection of the sample as long as the falling weight is in contact with it. Finally, the energy $\Delta E(t)$, transferred from the falling weight to the sample for $t > t_o$ can be calculated from the change in kinetic and potential energies of the falling weight:

$$\Delta E(t) = (m/2)\left[V_o^2 - V^2(t)\right] + mgd(t) \qquad \text{(viii)}$$

2.4.3 Falling-Weight Impact Test Procedure

The injection moulded circular plaques were freely supported on a raised ring of 40mm internal diameter and impacted with a 20mm diameter tup, Figure 22. In this respect the test procedure conformed to the ISO/DIS 6603/1 specification. The impact test conditions used throughout the research project are summarised in Table 5.

Table 5 Falling Weight Impact Test Conditions.

Impact speed $3ms^{-1}$	Support Ring I/D 40 mm
Sweep time 10-20ms	O/D 60 mm
Sensitivity 1-2 kN	Striker hemisphere 20mm diameter
Drop height 458 mm	Mass striker 27kg
Delay 9ms	Unclamped
Test temperature 23°C	No filter

A minimum of five test for each moulding condition were made and the force/time; force/distance and Energy/distance^2 curves were plotted for each test.

2.4.4 NPL Instrumented Izod Impact Test Procedure (133, 134)

Impact testing on square bars (3 x 3 x 12mm) cut from the mouldings at various positions was performed with a widely used small pendulum machine (Hounsfield Tensometer). To allow clamping the normal Charpy test supports were replaced by a single clamp, positioned so that one peak only of the double peak impact head struck the test bar 4mm from the clamp. The clamp was fitted with constant torque closure to ensure reproducible clamping force. The dial of the machine registers the rest position reached by the pendulum after breaking the test bar, and hence gives the total energy absorbed from the pendulum.

In order to determine the behaviour during breaking, the pendulum was fitted with a Brüel and Kjoer (B.and K) Type 8307 accelerometer (quartz crystal) of weight 0.5g, held in a centrally drilled hole in the impact head. The overall mass of the pendulum was 0.113 kg providing an initial velocity of 2.45 m/s. The force/time behaviour of the pendulum during impact was thus determined.

The unnotched specimen breaks in about 1ms and so a Datalab DL 905 transient recorder was used to record the signal during the test, which was amplified by a B. and K. Type 20626 conditioning amplifier set to filter between 3Hz and 10kHz. The signal containing 1000 data points was analysed using an oscilloscope and BBC microcomputer system linked to a Hewlett Packard RS232 7470A plotter. The filtering used was sufficient to dampen superimposed subsidiary shock waves, too much filtering makes a 'ringing' of the accelerometer after fracture of test piece appearing as a spurious deceleration peak on the record.

The signal is integrated to provide velocity and distance data in the same manner as with the drop-weight impact machine using the trapezoidal method of integration.

The Instrumented Izod Impact set-up can be seen in Figure 23, and the testing geometry complete with clamping arrangement is shown in Figure 24. Each sample had its cross-sectional area at the point of impact measured prior to testing.

2.5 MICROTOMY AND OPTICAL MICROSCOPY

Optical microscopy proved a rapid and most valuable technique in the characterization of the as-moulded microstructure in iPP injection mouldings. Selected areas were microtomed to provide thin (4-5 μm) sections which were subsequently examined in polarised transmission light using a Reichert Zetopan Nr365467 microscope. The quality of such sections was governed by several important factors summarised below:-

(i) Sledge microtome condition and performance.

(ii) Blade quality/sharpness.

(iii) Blade facet angle/tilt angle to sample.

(iv) Cutting angle to specimen.

(v) Cutting speed.

(vi) Specimen temperature.

(i) Sledge Microtome

An MSE sledge microtome, fitted with -

(a) a bilateral knife holder which can be set at angles from 90° to about 120° to the cutting direction.

(b) an object mounting mechanism with a tilting range of 15° in all directions.

(c) an object feed adjusted in steps from 1 to 20μm and,

Figure 23 NPL instrumented Izod impact test.

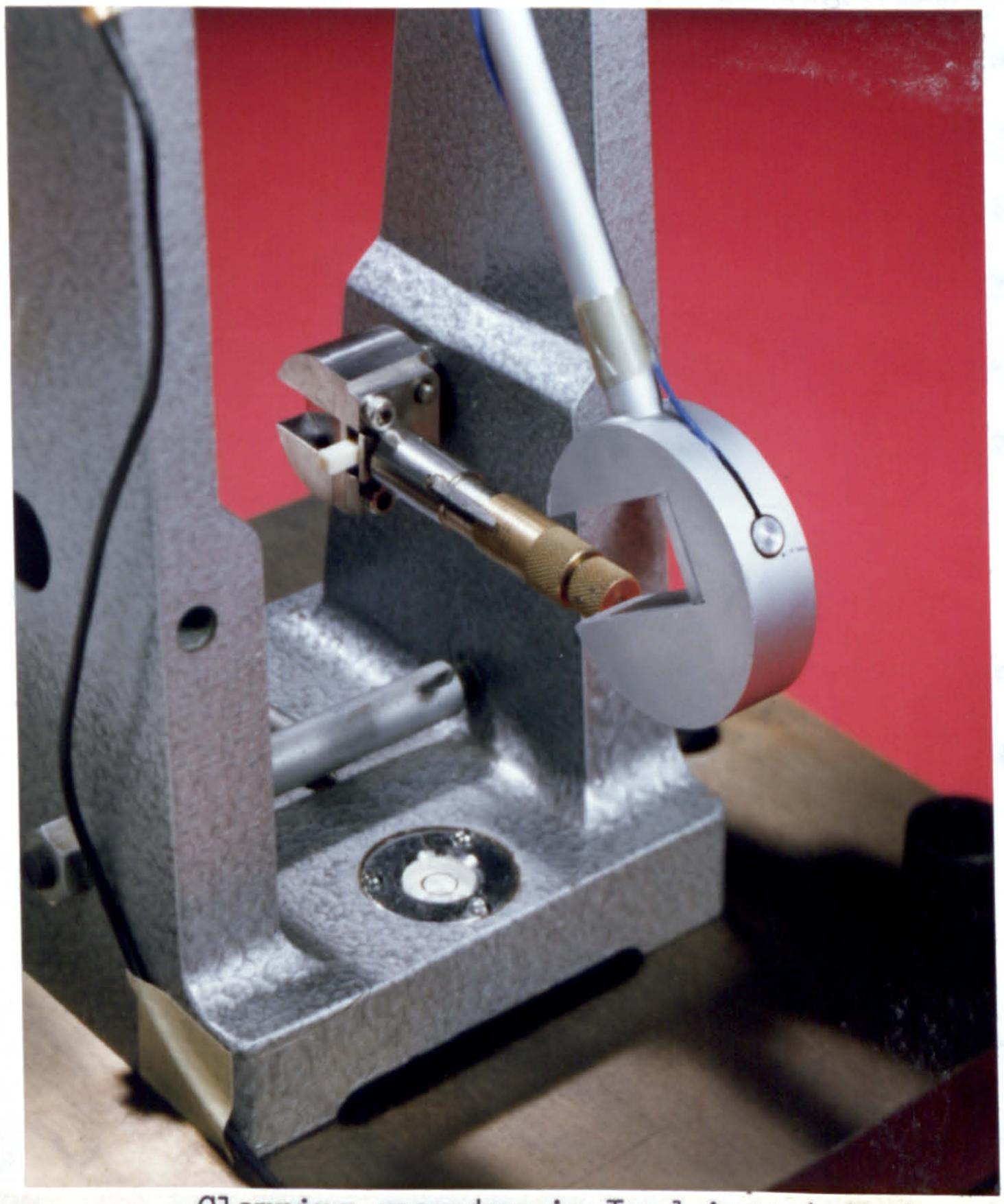

Figure 24 Clamping geometry in Izod impact test.

(d) a Mectron (Frigistor) microtome cooling stage, was used to provide the quality of sections required to meet the stringent demands of microscopic investigations. The most important structural feature of the microtome is the free movement of the object towards the fixed knife. The object is raised through the required μm value before each cutting action.

(ii) Blade Quality and Sharpness

A conventional mild steel Glen Creston blade with a 37° facet angle was recommended for this work. In order to keep this blade in A1 condition a sharpening schedule was adhered to after prolonged use. A Shandon and Southern Autosharp IV machine fitted with soft copper alloy (Kemet) lapping plates and 8 and 3μm diamond pastes was used for this schedule which routinely takes under 2 hours to complete. The blade was inspected using reflected light microscopy to ensure that no scratches > 3μm or any burrs remained.

(iii) The Tilt Angle of the Blade to the Sample

This did not appear to have any significant effect on quality of sections but for convention an angle of 4° was chosen.

(iv) The Cutting Angle To The Specimen

This was set at 90° so as not to impart differing forces on either side of the section by having a leading edge. Samples were all cut parallel to the flow direction since samples cut perpendicular to flow did not reveal the bright β type spherulites.

(v) The Cutting Speed

This was controlled manually and therefore a difficult factor to assess. However, The National Physical Laboratory allowed use of their microprocessor controlled LKB sledge microtome which enabled the effects of cutting speeds to be examined. No significant effect was found on quality of sections with speed of cut.

(vi) Specimen Temperature

A Mectron (Frigistor) microtome cooling stage designed specifically for the MSE sledge microtome was used to control the sample temperature at -24°C. The cooling stage works on the principles of the Peltier effect whereby a current flows along the junction A of two metals in series, heat is evolved or absorbed at A depending on the current direction, that is, a cooling is produced at the junction of two metals in one direction and an evolution of heat in the other direction. The Frigistor microtome stage comprises; a frigistor module mounted on a water cooled heat exchanger to which the adaptor for the specific microtome is fitted, in addition harnessed water tubes and power leads run into the heat exchanger and module respectively. An AC/DC power supply which converts the AC mains input to the required DC is also required such that the stage temperature is simply adjusted by increasing or decreasing the current (maximum current of 15 Amps supplies a cooling effect down to -24°C).

Microtomy of polypropylene samples below its glass transition temperature, Tg (10°C) improved the quality of sections and increased our confidence in true representations of the as-moulded microstructures revealed. Cutting at -20°C reduced the possibility of deformation (tearing or dragging) and curling of sections, allowing simply brittle fracture of sections away from the bulk.

The use of the cold stage also improved clamping by exploiting the contraction of fluids with freezing, a solvent named O.C.T compound used for research in histology, pathology, zoology and botany was provided by Leitz and proved to have extraordinary clamping qualities at low temperatures (Polycell paste also proved effective).

Sections prepared were mounted in immersion oil on glass slides and secured with coverslips. Details of selected areas for microtomy and light microscopy of a range of mouldings are given in each relevant chapter with micrographs.

2.6 DIFFERENTIAL SCANNING CALORIMETRY STUDIES (DSC)

2.6.1 Basic Principles of DSC

The use of differential scanning calorimetry for examining the thermal behaviour of thermoplastics has gained wide acceptance and is of great importance for studying and understanding both their processing behaviour and end-use properties.

At present several types of DSC are commercially available. The DSC 2 and thermal analysis data station (TADS) manufactured by Perkin Elmer is being used within our laboratory.

The main parts of these instruments consists of a platinum sample holder and an identical reference holder, both having a built-in heating element and a temperature sensor. The sample, varying in weight from 0.1 mg to 25 mg, is placed in a small aluminium pan; a similar empty pan is normally used as a control . (Both solid and liquid samples can be analysed the solid samples can be in film, powder or granular form). Both sample holders can be cooled or heated at various fixed rates (from 0.5°C/min to about 320°c/min) in a controlled atmosphere or isothermal measurements can be carried out. During an experiment the temperature of both sample holders is kept the same, this means that when some thermal transition takes place in the sample, the heat flow to it has to be changed to keep it at the same temperature as the reference holder. The difference in heat flow per unit of time is recorded as a function of the temperature or the time.

The measurement of specific heat is the most obvious application of the DSC apparatus. Using a linear temperature programme, the heat flow rate is directly proportional to the instantaneous specific heat of the sample. By recording this heat flow rate as a function of temperature and comparing it with the heat flow rate into a standard material of known specific heat under the same conditions, the specific heat of the sample can be determined as a function of temperature.

2.6.2 Application of DSC to Polymers

Most semi-crystalline materials melt upon heating and thermoplastic materials generally melt over a wide temperature range. This behaviour is related to imperfections in the crystallites and non-uniformity in their size; the smaller, less perfectly formed crystallites melt at lower temperatures. In consequence

polymer melting behaviour will be influenced by factors which influence the degree of crystalline perfection such as mechanical and thermal history. Double melting peaks may also result with polymers which have been subject to orientation. This close relationship between crystallinity and heat changes during melting makes DSC a useful technique for determining the degree of crystallinity.

For calorimetric determinations the enthalpy change, ΔH_{Tmin}^{Tmax} Tmax is measured between a limiting low (room) temperature value (Tmin) where the crystallinity of either component is expected to have reached its limiting value, and a temperature (Tmax) above the melting point (Tm) of the polymer. The mean specific heats of solid and molten polymer over the temperature ranges Tmin → Tm and Tm → Tmax are given by $\bar{C}p,s$ and $\bar{C}p,l$ respectively. The quantity (Cp,s (Tm-Tmin) + Cp,l (Tmax - Tm)) is then subtracted from ΔH_{Tmin}^{Tmax} to give the heat of fusion from which the degree of crystallinity can be calculated using literature values for heats of fusion of perfectly crystalline samples.

Generally, materials that melt on heating will crystallize on cooling. This crystallization shows up as an exothermal change in the DSC trace. In addition to the intrinsic polymer variables which affect melting the crystallization behaviour is very much affected by the presence of nucleating agents in the sample, and the degree of supercooling. Isothermal crystallization exotherms are often used in routine work to measure the crystallization rate from the peak width at half height. In addition, during cooling studies the onset temperature of crystallization is sometimes used as an indication of the rate of re-crystallization.

Several considerations must be made, in order to calculate the rate of crystallization:

(a) Thermal history - Variations in the heating conditions before crystallization is believed to affect the nucleation process. Morgan (135) proposed the existence of small crystalline regions above the observed melting point of a polymer, the greater the perfection of such crystalline regions the higher the temperature required to melt it. These crystalline entities may induce crystallization on cooling. If a sample is heated to a different temperature than another, with which if is being compared, varying nucleation may result from a difference in the number and size of persistent crystalline areas in each sample.

(b) Rate of cooling - The nucleation density of a polymer is affected by the cooling rate, slow cooling produces a lower nucleation density than quenching. The formation of a large number of nuclei brings about rapid crystallization. The effect of cooling rate upon the supercooling of polypropylene was shown by Beck (136), Figure 25. Supercooling is the slowing down of growth by increased viscosity at lower temperatures and the diminishing thermodynamic drive as the melting point is approached.

(c) Concentration of nucleator - Beck (136) also investigated the effect of concentration of nucleating agent (aluminium dibenzoate) on the crystallization temperature of polypropylene. The largest effect was observed at very low concentrations i.e. less than 0.5% as illustrated in Figure 26.

(d) Dispersion of nucleator - The degree of dispersion is important for the nucleating effect. Adequate dispersion of the substrate in polymer is not always obtained due to the tendency of some materials to agglomerate e.g. Talc.

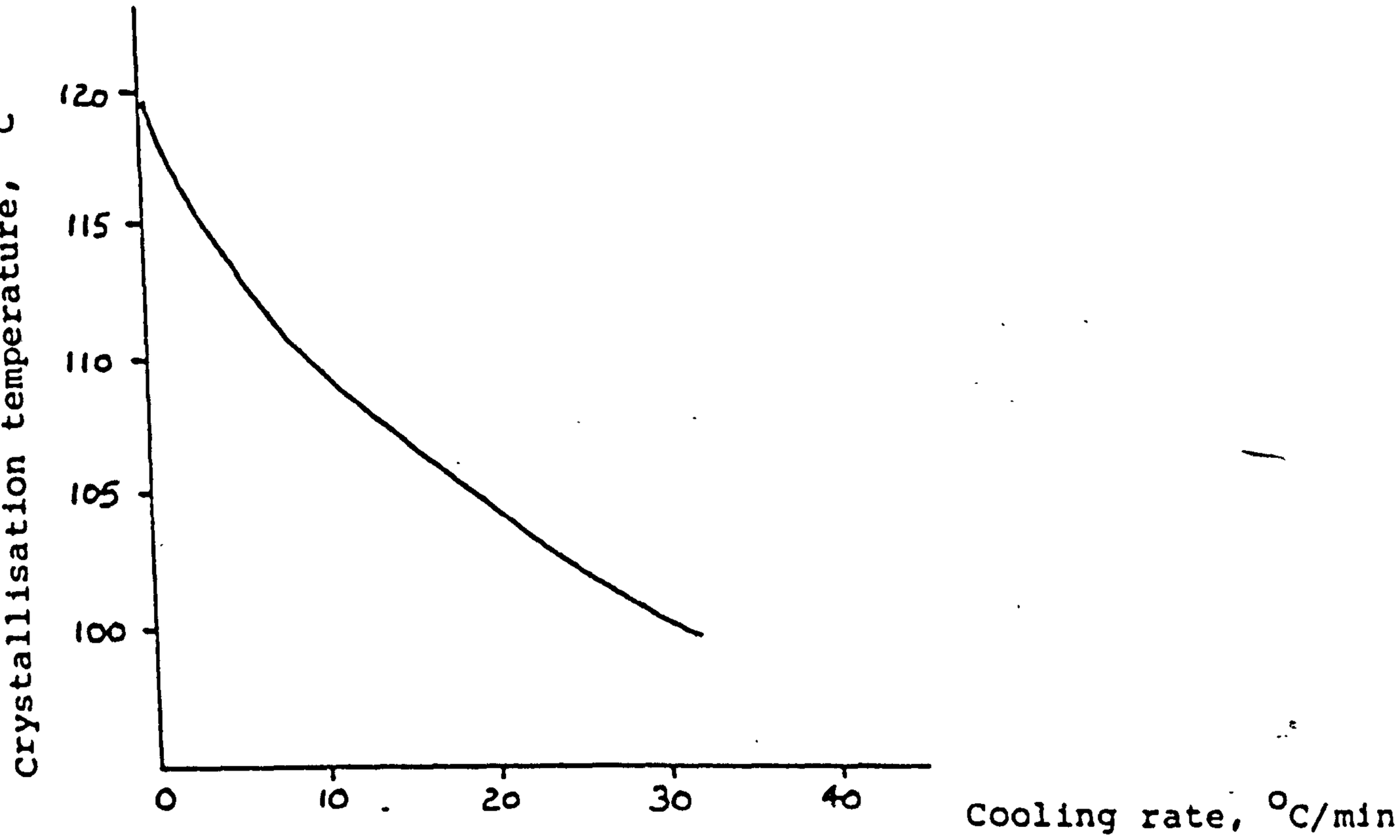

Figure 25 Effect of cooling rate on the supercooling of iPP.

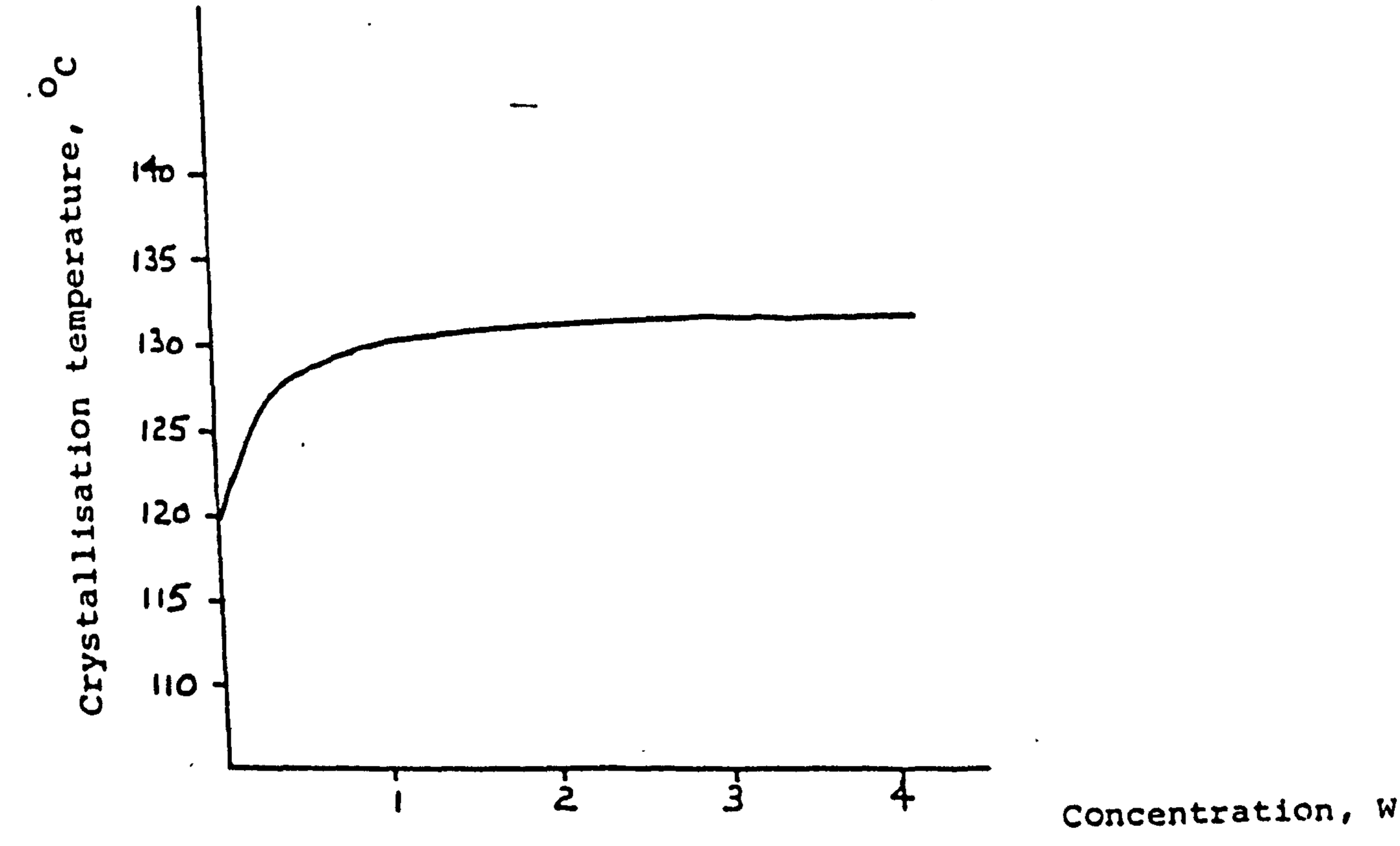

Figure 26 Effect of concentration of nucleant on crystallisation temperature of iPP.

The DSC technique is also widely used to measure the glass transition temperature, Tg, which is an important parameter for polymer characterization since it determines the upper or the lower limit of the service temperature range of a polymer. In addition it has been known for a long time that certain mechanical properties of glassy polymers strongly depend upon their thermal history. The loss of general ductile behaviour on ageing or annealingbelow Tg is of particular concern and DSC measurements are of importance in studying such annealing phenomena.

Another major application of DSC is in the study of the thermal stability of polymers. The degradation process can be followed by measuring the heat of reaction under scanning or isothermal conditions. In order to isolate the thermo-oxidative from the purely thermo-degradative processes the measurements can be carried out in either an oxidative or an inert atmosphere.

2.6.3 Application of DSC to Melt Crystallized iPP

The existence of multiple crystalline forms in isotactic polypropylene has been well established. Padden and Keith (53, 58) were the first to study the growth rates and determined that the α phase (types I and II spherulites) grow at the same rates which is about 20% slower than the faster growing β phase spherulites. The authors could only observe the β form sporadically with growth between 401 and 405 K.

Use of a pigment, Permanent Red E3B, has been reported by Leugering (48) and Duswalt (49) to result in preferential nucleation of the β form. The former showed that at crystallization temperatures below 403K the pigment at 10^{-4} to 10^{-5} wt.% preferentially nucleated the β phase, whereas the latter showed

that crystallization at an optimum temperature of 409K and concentrations of 10^{-6} wt.% pigment produces appreciable amounts of the β form. However, in both cases differential thermal analysis (DTA) showed a peak twice as intense for the α-phase endotherm than for the β-phase. Turner-Jones et al., (41, 42) produced large amounts of the β form by quenching a sample very rapidly to below 403K.

Lovinger et al., (45) reported DSC melting curves for polypropylene crystallized under various conditions. Their result at a heating rate of 10 K/min indicated a β melting endotherm at 425 K and an α endotherm at 440 K. The relative sizes of the two peaks depended on crystallization conditions. They also observed that slow heating rates (1 to 3 K/min) in the DSC apparatus led to extensive β to α conversion.

Richardson et al., (137) found that rapid quenching of polypropylene films from 445 K to room temperature results in crystalline material exclusively in the lower melting β form. Annealing at temperatures below 443K, or approaching this temperature slowly, has the effect of converting β material to α in agreement with Lovinger et al., (45). The overall degree of crystallinity does not seem to be influenced by this conversion.

As previously mentioned, Hutley and Darlington (108, 109) recently established a correlation between the onset temperature of recrystallization and the impact strength of an injection moulded highly limestone filled polypropylene copolymer. A linear increase in the falling weight impact strength with decreasing crystallization temperature was found. The implication that a nucleation phenomenon was occuring that gives rise

to enhanced rates of crystallization but also to a morphology with reduced toughness was made.

Ronca and Vesely (138) recently published work on the heterogeneous nucleation of polypropylene for a range of nucleants. Talc proved to be the most effective α-phase nucleant in film samples prepared by a melt mixing technique on heated glass slides. The authors found that a temperature shift of the crystallization temperature from 387.92K upto 399.77 was observed for polypropylene with 10% by wt. talc. It was clear however, that the change in crystallization temperature with increasing nucleant content was rather strong upto 1%, beyond this value increasing concentrations of talc had little effect. The spherulite sizes were reduced from 100-200 μm to 40-50 μm diameter with just 0.25% by wt. additions of talc to polypropylene.

Oliveira and Hemsley (139) reported on the thermal behaviour of α and β-form iPP spherulites recently in a paper concerned with hot plate welds. A double melting behaviour of β-form crystals was observed, particularly at slow heating rates. After the initial melting at about 418K of the original β another melting peak occured at around 425K thought to be a recrystallized β' form. The influence of pre-and post- welding annealing of the polypropylene was also investigated and revealed an apparent 'memory' of the β-form crystallization despite heating well above the hexagonal to monoclinic conversion temperature given by Fijiwara (66). This work raises many questions as to the occurence and persistence of the type III$ spherulites in polypropylene.

Figure 27 Indium melting curve.

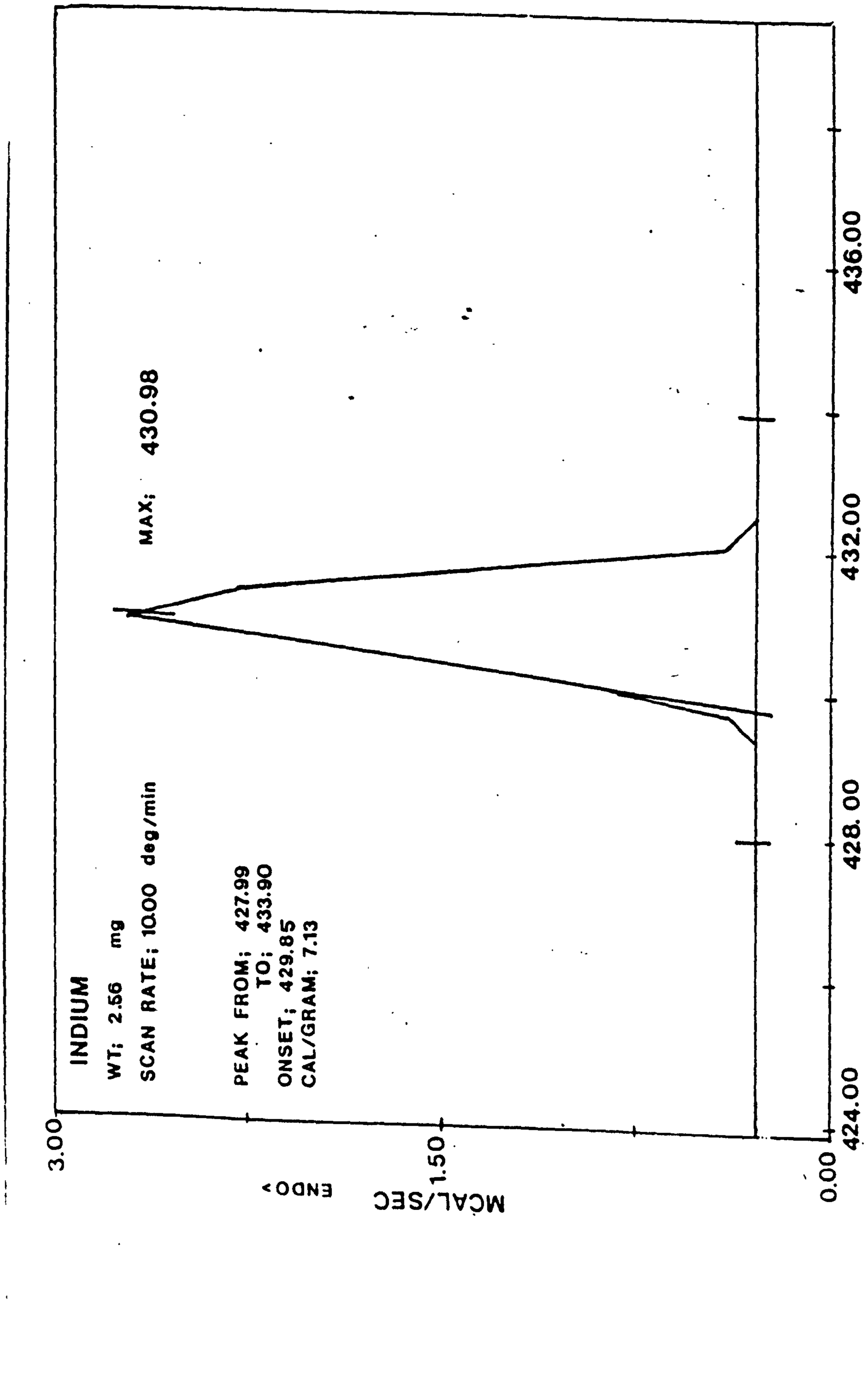

2.6.4 Experimental Procedure Employed

As part of the general research programme a particular study on the melting and recrystallization behaviour of iPP injection mouldings was made. The purpose of this study was to assess the degree of crystallinity, the level of α and β phase nucleation and in particular the rate of recrystallization in a range of mouldings. From this assessment a fundamental connection between thermal and impact properties similar to that found by Hutley and Darlington (108, 109) is suggested. In this study samples (~5mg) were taken from selected areas of injection mouldings and heated to 500K at 10K min^{-1}, which is 50K above the melting point of isotactic polypropylene, held for 10 minutes (to remove previous thermal history), followed by programmed cooling at -10K min^{-1}.

The DSC was calibrated using an indium sample, the resulting Indium melting curve is shown in Figure 27 revealing only a small error in temperature calibration.

The effects of processing conditions and incorporation of small percentages of low and high molecular weight polypropylene, and various nucleants on the melting and recrystallization behaviour was examined. Subsequent plots of impact strength versus crystallization temperature are presented in Chapter 5.

2.7 PREPARATION OF SPECIMENS FOR ELECTRON MICROSCOPY

2.7.1 Background

Various etching techniques have been tried to examine the internal microstructure of crystalline polymers, employing, ions gas discharges, solvents and perhaps most successfully strong oxidising acids.

Nitric acid has been widely used on polyethylene (though it is much less effective on polypropylene) following Palmer and Cobbold's (140) demonstration that this reagent is able to degrade polyethylene into lamellar fragments. However, revealing fine detail has proved elusive and nitric acid rapidly attacks polyethylene causing it to become friable and difficult to handle.

Fitchman and Newman (141) successfully used two different etching procedures on iPP surfaces prior to scanning electron microscopy (SEM). In the first process, as-moulded samples were swollen for 10-15 min in an aqueous dispersion of turpentine (10%) and a fluorinated surfactant at 70°C and then oxidised for 5-10 min at 80°C in a bath containing 20% sulphuric acid saturated with chromium trioxide (CrO_3). The fluorinated surfactant was added to enhance the wetting of the polymer surface by the oxidising medium. In the second process samples were immersed in a 6M aqueous chromium trioxide solution for 5 days at 75°C. With the former technique the crystalline morphology was obscured by an artificial morphology due to oxidative stress-induced cracking, these artefacts were minimized using as etchant a dilute aqueous chromic anhydride solution similar to that used by Armond and Atkinson (142). The degree of relief in the texture revealed was improved, but attempts to study fine lamellar detail proved impossible.

The use of chlorosulphonation as a technique for the electron microscopy of polymers has been pioneered by Kanig (143) (although there is an earlier report by de Korosy and Zeigerson (144)). Despite early reference to its use for isotactic polypropylene in practice it has found application

almost exclusively to polyethylenes. These are treated by immersion of small samples (~ 10 mg) in chlorosulphonic acid, commonly at 60°C, for some hours. After subsequent washing with freezing acetone then water it is usual to soak specimens in uranyl acetate for 3hrs or more. This reagent tends to avoid image contrast fading. The contrast observed in sections was found to be primarily due to sulphur and chlorine staining. Chlorosulphonation is manifestly a valuable technique which, in principle, can reveal the total lamellar morphology. However, the technical difficulties of so doing should not be underestimated. Samples are considerably changed by staining treatment (colour, melting point, enthalpy of fusion), Basset and Hodge (61, II) found that chlorosulphonation alone gave lamellar thicknesses different from other techniques (reduced by some 30 nm).

A relatively recent development in the field of morphological research studies has been the introduction of the permanganic etching technique. Basset, Hodge and Olley (60) discovered that solutions of potassium permanganate in concentrated sulphuric acid etch upto 2μm depth from the surface of crystalline polyolefines selectively in such a manner as to reveal fine lamellar detail. This may be examined, after suitable washing, either by replication and the transmission electron microscope or directly with scanning electron microscopy. The best high resolution instruments can approach the resolution of replicas (~ 5nm) but the lower resolution of conventional scanning microscopy can be misleading. Intensive studies by the forementioned authors on the morphology of melt crystallised polyethylene (61, I, II, III) has given great confidence both in sensitivity to morphological environment and in the reliability of the textures revealed.

The potential of the method when used with iPP has recently been demonstrated by Basset and Olley (62) and Norton and Keller (63) mentioned in the literature review. The former studied the lamellar structures within melt grown spherulites of the monoclinic α form, whereas the latter successfully characterised the particular lamellar morphology of the five different spherulite types, as identified optically by Kieth and Padden (53). In all previous work using the permanganic etchant the studies have been confined to melt grown thin films, the aim of our work was to utilize and modify the technique to study the micromorphology of real iPP injection mouldings exhibiting banded structures.

In order to apply the permanganic etching technique several important considerations must be taken into account. Firstly, the reagent described originally was a 7% w/v solution of potassium permanganate ($KMnO_4$) in sulphuric acid (H_2SO_4) but a less severe treatment is now preferred (145). The reason for this was to minimize the precipitation of pinkish brown crystal artefacts on the scale of 10 μm thought to be $Mn_2(SO_4)_3 . H_2SO_4 . 4H_2O$. The presence of these crystals inhibits etching but they are subsequently removed in the washing procedure leaving the shapes of the artefact behind. A mixture of H_2SO_4 and ortho phosphoric acid (H_3PO_4) helps to minimize this precipitation. Secondly, the need to avoid relaxation of residual strain of moulded samples requires a more delicate etch at a lower temperature than the original 60-100°C originally used. Thirdly, the hexagonal β form of polypropylene is particularly amenable to permanganic etching and this may lead to complications when etching samples with mixed spherulitic and lamellar morphologies of differing resistance to the etch. It was, therefore, necessary to experiment with carefully controlled etching parameters to optimise as far as possible

the concentration of etch, the time and temperature of etching, and the cleansing stage before replication.

2.7.2 Preparation of Specimens for TEM Studies

Etching Procedure

(i) Make up a 50:50 mixture of orthophosphoric acid and Analar grade (minimum assay 98%) sulphuric acid in a pre-dried stoppered ground glass test tube. Place the stoppered mixture in an ultra-sonic bath for 30 seconds, and then leave to cool for at least 5 minutes.

(ii) Add ½ wt.% potassium permanganate. Support the test tube in an ultra-sonic bath, switch on and leave for approximately 1 hr, during which the temperature of the bath should rise to 40°C. The active species $O_3MnO - SO_3H_3$ produces a dark green precipitate. If at this stage the precipitate is blue it indicates water contamination and should be discarded.

NB. The time taken to disolve the permanganate is faster if dry phosphoric acid is used and the reagent appears to be more stable during long etching times, also the possibility of undisolved permanganate crystals is reduced.

(iii) Samples to be etched (microtomed surfaces) are placed surface side downward into the etchant. Good results occur with etch times varying from 15 minutes to 2 hrs; 1 hr usually being sufficient with the assistance of ultra-sound.

After the desired treatment the following five stage cleansing recipe is recommended:-

(i) Wash the specimen in a mixture of 2 parts sulphuric acid to 7 parts of distilled water*, which has been precooled at -20°C for 2 minutes in the ultrasonic bath or until

precipitate completely dissolves.

* These proportions are approximately those giving the lowest freezing mixture which is helpful in preventing the heat of dilution of the original acid affecting the sample.

(ii) Transfer the specimen to a 30% solution of hydrogen peroxide (to remove manganese dioxide) for 1 minute in ultrasound.

(iii) Transfer to distilled water for 1 minute.

(iv) Rinse in acetone for 1 minute.

(v) Finally dry in a vacuum oven for about 1 hr at around 40°C.

Replication Procedure

Olley et al., (60) examined samples using a standard two-stage replication process, making a first impression in cellulose acetate and then shadowing this with gold/Palladium (Au/Pd), then depositing a Carbon film for improved mechanical strength. The cellulose acetate - Au/Pd-C sandwich is then mounted onto grids and the cellulose acetate layer is dissolved away using acetone vapour.

Norton (146), however, used a much more direct method whereby the etched and cleaned specimens are immediately shadowed with a very thin (15-20Å) platinum/palladium (Pt/Pd) 80/20 alloy layer at an angle of 20-40°. A thicker and vertical backing of carbon follows. The Pt/Pd-C layer is then removed by using a small blob of aqueous polyacrylic acid (PAA) which upon drying (~2hr) spreads and adheres tightly to the carbon. The Pt/Pd-C-PAA sandwich can be easily removed by prising away with a razor blade, it is then placed PAA side down in distilled water and after a sufficient time (~2 hr) to allow the PAA to disolve the replica is floated onto hexagonal mesh 200 and 400 type copper grids for transmission electron microscopy.

Two stage plastic/carbon replicas can give a distorted image of the surface by contraction during the drying of the cellulose acetate film or by deformation during dry stripping. In addition to this the liklihood of impurities being introduced via the cellulose acetate or the acetone are increased using this technique. It was decided therefore to use the more direct replication technique.

The etching and replication was initially carried out at Bristol University with the assistance of Dr. D.R. Norton to perfect the technqiue and subsequent experiments to optimise the etching times and concentrations were performed at Brunel University. The samples were replicated using an Edwards 306 vacuum coater as follows:

(i) 1 cm length of 0.5mm diameter Pt/Pd 80/20 alloy in wire form is wound around a thicker pre-prepared tungsten wire filament.

(ii) The evaporant to specimen distance was set at 10 x 10^{-2}m.

(iii) The sample was shadowed at $\alpha = 40^{\circ}$ such that gas phase atoms were emitted from the evaporation source at a pressure maintained at $\sim 10^{-6}$ mm Hg. This gives emitted atoms a mean free path length of the order of the chamber and a thickness of coating (t) according to the equation:-

$$t_{coating}(nm) = \frac{m3 \times 10^{9} \sin \alpha}{16 \pi d^{2} \rho}$$

where m = mass wire evaporated (g)
α = shadow angle
ρ = density of wire (gcm^{-1})
d = sample to filament distance (cm)

(iv) The shadow is then backed using 2cm of carbon fibre (diameter 2mm), under the same conditions, except for a change in the low tension selector from 10v/0.1 to

Examination of the replicas by TEM was performed using a Philips EM301 and a JEOL 100CX, both equipped with a eucentric goniometer ($\pm$ 60°) and nitrogen cold stage.

2.7.3 Scanning Electron Microscopy

A Cambridge Stereoscan S250Mk2 Scanning Electron Microscope was used in the analysis of representative fracture surfaces of Izod impact tested samples. To minimize charge effects an accelerating voltage of typically 10kV was used with a spot size of 4. The samples were splutter coated with gold for four minutes, prior to examination. A detailed discussion and presentation of fracture surface studies for each moulding conditions is given in the relevant chapters.

2.8 X-RAY DIFFRACTION

2.8.1 Basic Principles

The application of x-rays to the study of materials makes it possible to determine detailed information on the state of order or disorder of the system. The diffraction of x-rays by liquids or gases gives rise to diffuse haloes; the diffraction of x-rays from crystalline substances gives rise to sharp circles or spots. More detailed information on the state of order of a crystalline material may be obtained from the analysis of the intensity, position and line width of the diffraction lines. In the case of semi-crystalline polymers, the x-ray analysis, at various levels of sophistication, may give data concerning:

(a) identification of material,

(b) its crystallinity,

(c) the relative disposition and geometry of the crystallites, and

(d) the relative disposition of the atoms in the crystallites.

The crystallinity and texture of the polymeric material may be studied as functions of the thermal and mechanical treatment that the material has undergone.

All crystalline polymers, when irradiated by x-rays, give patterns containing both relatively sharp lines and diffuse haloes. It is now generally agreed that in polymeric materials of high crystallinity the major part of the material is made up of crystals, in the form of thin platelets, in which chains run perpendicular, folding many times within the crystal. The presence of dislocations, chain folds and chain ends in the crystals could explain the persistence of amorphous haloes.

2.8.2 Structural Determinations for iPP

From the Bragg angles at which diffraction from a crystal occurs it is possible to obtain information concerning the unit cell dimensions of a crystalline polymer. From a detailed analysis of the intensities it is often possible to deduce also the molecular geometry and mode of packing of chains. A typical procedure goes through the following steps:-

The identity period along the chain axis is deduced from the seperation of the layers represented in Figure 28. In the case of polypropylene, c= 6.5 $\pm$ 0.1Å.

The indexes of the reflections on the 0^{th} layer are of the type hK0, the indexes of the 1^{st} layer are of the type hk1, the indexes of the reflections of the 2^{nd} layer are of the type hk2, and so on. The 2θ values of the hk0 reflections may be directly measured on the spectrum; through the Bragg law we deduce from them the corresponding values of $1/d_{hk0} = |\vec{S}_{hk0}|$.

The next step involves the determination of three reciprocal lattice constants a*, b*, γ^* (in our case $\gamma^* = 90^\circ$), consistent with all the observations of $1/d_{hk0}$. When this is done the appropriate h and k indexes may be assigned to each reflection.

An analogous procedure is followed to determine the indexes of the hk1 reflections, and to establish the values of α^* and β^*. From the reciprocal lattice it is easy to go by a straightforward mathematical procedure to the unit cell constants of the direct lattice.

The number of monomeric units in the unit cell is then deduced by comparing the calculated with the observed density, in the case of iPP, the denisty calculated for twelve units per cell is 0.96 g/cm^3; the observed density of a highly isotactic sample is 0.93g/cm^3 (due to lower density of amorphous regions).

In the case of polypropylene an analysis of the data shows that all possible reflections having h+k = 2n + 1 are absent, this fact establishes the symmetry of the unit cell, and the fact that four macromolecular chains must be running through it.

Once the unit cell constants have been deduced the chain conformation and the mode of packing must be fixed by trial and error until an acceptable agreement between calculated and observed intensities is made.

In the case of polypropylene, the reasonable assumption of a helicoidal chain conformation, having successive trans and gauche internal rotation angles along the chain, Figure 8, from Natta et al., (39) is generally recognised.

2.8.3 X-Ray Diffraction Studies of Isotactic Polypropylene

As previously stated iPP is exceptional among polymers insofar as its most common polymorphic form crystallizes with a tightly cross-hatched dendritic habit incorporated within the usual spherulitic structure. This polymorph (α-form) has been widely studied in melt crystallised samples. The α structure was first determined by Natta and Corradini (39), to consist of molecular chains ordered in a 3_1-helical conformation packed monoclinically, the unit cell having dimensions:-

$a = 6.65 \pm 0.05$ Å, $b = 20.96 \pm 0.15$ Å and $c = 6.50 \pm 0.04$ Å

$\alpha = 90^\circ$ $\beta = 99 \pm 1^\circ$ $\gamma = 90^\circ$

A typical indexed α-phase diffraction pattern is shown in Figure 29. Soon after the β-form was discovered, a polymorph with a hexagonal lattice. The β structure was recognised by Keith and Padden (40) and later by Turner-Jones et al., (44, 42) who calculated the unit cell dimensions to be:-

$a = 19.08$ Å $b = 19.08$ Å $c = 6.49$ Å

$\alpha = 90^\circ$ $\beta = 90^\circ$ $\gamma = 120^\circ$

A typical indexed β-phase diffraction pattern is schematically represented in Figure 30. This structure was found to be favoured by rapid cooling and only occuring occasionally.

Following this an even rarer third polymorph based on a triclinic lattice, the so called γ structure was identified by Turner-Jones et al., (42). The structure was found to be favoured by hydrostatic pressure (49, 50, 51). The unit cell dimensions were first reported by Turner-Jones et al., (42), but modified more accurately by Morrow and Newman (49), in samples of very low molecular weight fractions, to be as follows:-

$a = 6.54$ Å $b = 21.40$ Å $c = 6.50$ Å

$\alpha = 89^\circ$ $\beta = 99.60^\circ$ $\gamma = 99^\circ$

Figure 28 X-ray diffraction pattern of iPP.

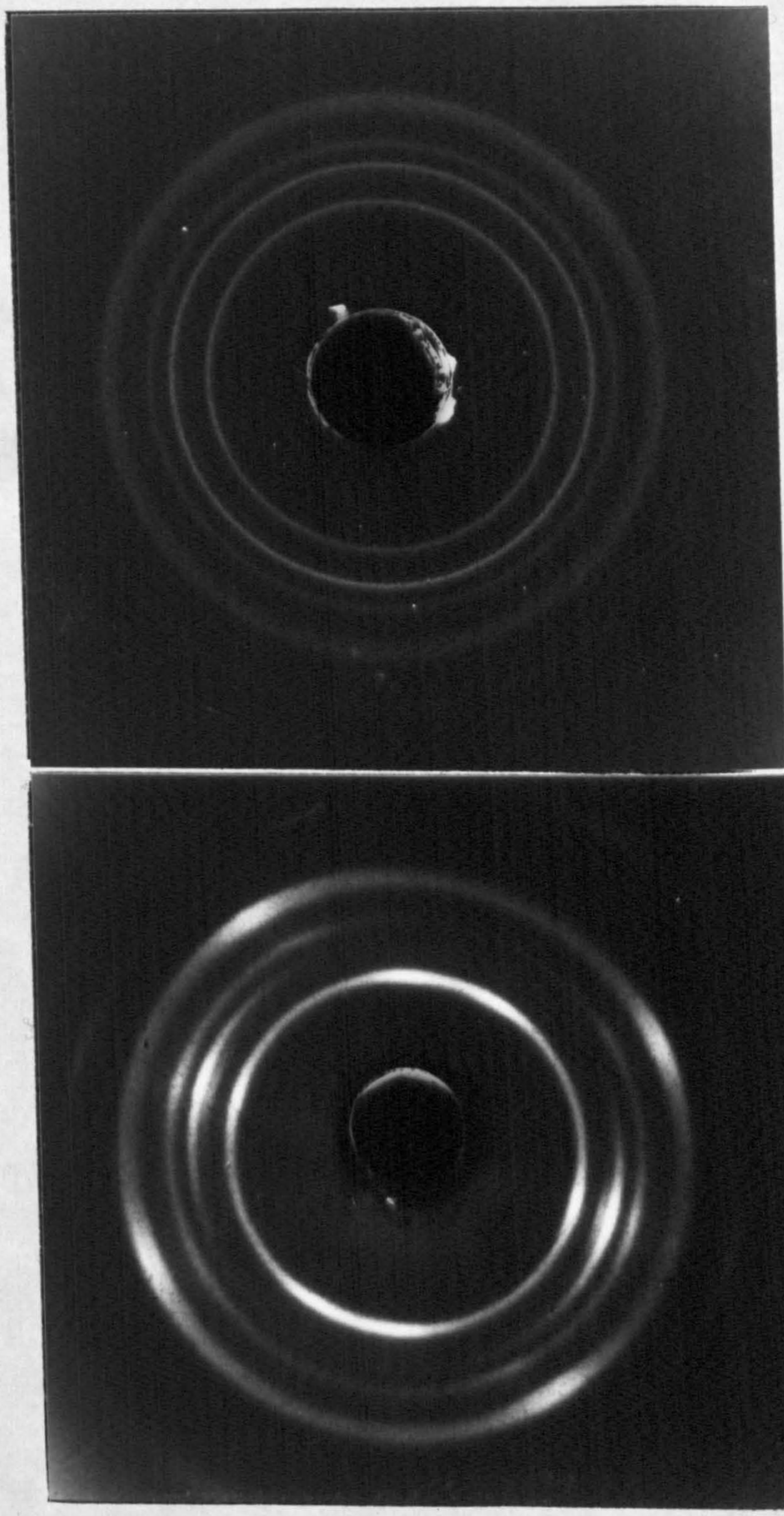

Figure 29 A typical indexed x-ray diffraction pattern of injection moulded iPP α form spherulites.

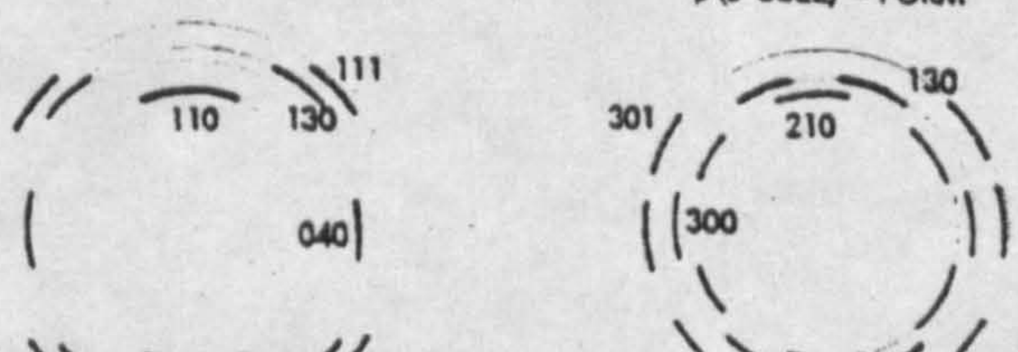

hkl	d* (α)
110	0.246
040	0.2945
130	0.322
111	0.3705

d* (β)	hkl
0.247	210
0.280	300
0.3335	130
0.367	301

Figure 30 A schematic representation of some reflections from α and β-form crystals in iPP.

Addinck and Beinteria (52) reported a fourth polymorphic δ form, found in polypropylenes with a high percentage of amorphous material, but the structure of this was only tentatively proposed as being based on a base -centred orthorhombic cell. In all these structures ($\alpha, \beta, \gamma, \delta$) the chain conformation is identical and corresponds to the familiar three fold (3_1) helix, the different stacking geometries of these helices account for the different polymorphs identified.

The generally agreed Turner-Jones indexed reflections are given in Table 6 with observed intensities and calculated reciprocal spacings for iPP α, β and γ forms.

2.8.4 Application of X-ray Diffraction Techniques to Real iPP Injection Mouldings

Kantz et al., (6) took thin sections (5-10 μm) from the midpoint of tensile bar specimens perpendicular and parallel to the flow direction. The x-ray diffraction patterns were recorded using a flat plate camera to make qualitative comparisons of the degree of preferred orientation through the thickness of the mouldings. The authors concluded that the skin was highly crystalline and biaxially oriented. The crystallites in the core of the moulding were seen to possess some degree of preferred orientation but mainly random. Regions between skin and core exhibited a very high degree of orientation of crystallites in both directions parallel and perpendicular to the flow axis. This work was found to be consistent with work done on biaxially oriented polypropylene film by Uejo and Hoshino (147). A tentative proposal that the degree of preferred orientation is the principal parameter governing tensile strength, impact strength and shrinkage was made.

TABLE 6 Turner-Jones indexed iPP α, β and γ diffraction pattern data.

LINE NO.	Iobs	d*calc	INDEX (hkl)	CRYSTAL PHASE
1	s	0.246	110	α
2	s	0.280	300	β
3	s	0.295	040	α
4	s	0.322	130	α
5	w	0.348	140	γ
6	s	0.371	301	β
7	s	0.371	111	α
8	s	0.378	$\bar{1}31$	α
9	w	0.425	041	β
10	w	0.425	131	α
11	m	0.422	060	α
12	w	0.462	200	α
13	w	0.485	330	β
14	m	0.491	220	α
15	w	0.560	600	β

TABLE 7 X-ray diffraction data of the crystalline phases of iPP.

α-PHASE			β-PHASE		
MILLER INDICS h,k,l		2θ (degrees)	MILLER INDICES h,k,l		2θ (degrees)
110	(α_1)	14.1			
			300	(β_1)	16.1
040	(α_2)	16.9			
130	(α_3)	18.5			
111	(α_4)	21.3			
$\bar{1}31$	(α_4)	21.8			
041	(α_4)	21.9			
			221	(β_2)	23.1
060	(α_5)	25.5			

Mencik and Fitchmun (78) examined injection mouldings of polypropylene by x-ray diffraction for texture and orientation patterns as a function of the distance from the surface and of moulding conditions. The assessment of preferred orientation of polymer crystallites was made using the following criteria:

(i) The c-axis orientation was determined if the (110) and (130) rings had spots of increased intensity in the direction perpendicular to flow;

(ii) The a-axis orientation was determined if the (110) and (130) rings had spots of increased intensity on the first layer line, the flow direction being considered as the fiber axis. These criteria refer to exposures with the X-ray beam perpendicular to the original flow.

As employed here the a-axis orientation serves to describe a uniaxial orientation in which polymer crystallites are aligned with their crystallographic a axes, preferentially in the direction of flow. Similarly the uniaxial c-axis orientation has the c-axes lying preferentially in the direction of flow. The unit cell employed here is that found by Natta et al., (39).

The authors found that the morphology was made up of four distinct layers. The first layer usually consisted of poorly a + c oriented crystallities, the second layer some 100-700 μm below the surface was seen to exhibit preferred a axis close to the extrusion direction. The equator of the diffraction pattern in layer 2 was formed by strong (040) and weak (060) arcs. Layer 3 was shown to exhibit both a-axis and c-axis orientation while layer 4 consisted of a system of istotropic rings typical of the monoclinc phase of polypropylene of random orientation.

Some evidence of the β-phase (hexagonal) polymorph was also found in the core, identified by a reflection of the (300) arc with d = 5.52 Å. The x-ray texture of individual layers was correlated with morphology for two different injection velocities.

The structure of the skin layer of an injection moulded polypropylene was also studied by means of WAXS by Fujiyama (10-14) the c-axis was found to be highly oriented parallel to the flow direction and the plane of the lamellar structures of about 160Å in thickness were oriented normal to the flow direction. The authors proposed a so-called "shish-kebab"-like structure to the skin layer.

Scherpereel (148) discovered the presence of β-form spherulites, in the gate region of iPP injection mouldings, these were row nucleated near the underside of the skin. The growth of the β-crystal modification was shown to be enhanced by high mould temperatures.

2.8.5 Application of X-ray Diffractometry to Study Crystalline Polymorphism In Injection Moulded iPP

In injection mouldings of iPP where spherulitic morphology is encountered, β crystallinity is normally found at the few percent level as row nucleated spherulites. These row spherulites contain various amounts of β phase depending on the orientation of the melt and the cooling rate from the melt to the crystallisation temperature. Since nucleation of the β form occurs much more rarely in a moulded sample than that of the predominant α form (including the mixed type) it has not been easy to study the effect of percentage β-form present on the impact behaviour of mouldings. However, by x-ray diffraction the spatial

distribution of the two crystalline phases (α and β) of iPP injection moulded samples can be studied. Turner-Jones et al., (41, 42) proposed an index based on the peak heights in the diffractogram to calculate β phase concentrations. This method was used recently by Trotignon et al., (149) to study the β-phase distribution (and some other crystallographic data) in injection-moulded tensile test bars of iPP. The authors carried out quantitative determinations on α_1, α_2, α_3, α_4, and β peaks whose characteristics are shown in Table 7.

This table shows that α_1, α_2, α_3 and β peaks are representative of crystalline orientations parallel to the surface of the sample. A routine approach based on peak heights can be used to determine the following indices:

(i) a crystallinity index C where

$$C = \frac{h\alpha_1 + h\alpha_2 + h\alpha_3 + h\alpha_4 + h\beta}{5\,ha}$$

NB: C cannot be directly related to the overall crystalline fraction since this would require accurate seperation of the background curve as reported by Natta et al., (39), Weidinger et al., (150), and Ullman (151), where corrections for incoherent radiation, thermal scattering, polarization and Lorentz factors as well as numerous other uncontrollable assumptions need to be made. The purpose of measuring C is to allow comparibility with B and A indices and suitability for manual routine measurements.

(ii) a β-phase index B where

$$B = \frac{h\beta}{h\alpha_1 + h\alpha_2 + h\alpha_3 + h\beta}$$

(iii) an α-phase orientation index A where

$$A = \frac{h\alpha_1}{h\alpha_1 + h\alpha_4}$$

A=1 when no α_4 peak

A=0 when no α_1 peak

$h\alpha_1$, $h\alpha_2$, $h\alpha_3$, $h\alpha_4$ and $h\beta$ are the heights of the corresponding crystalline peaks taken from the amorphous background and ha is the maximum height of the amorphous background. Trotignon et al., (149) confirmed the importance of molecular orientation on crystallization processes during injection moulding and have shown that a strong morphological heterogeneity exists along the melt flow direction.

It was decided to use these quantitative determinations to study the effects of structural heterogeneity on the drop weight and Izod impact properties along the flow direction. The technique proved particularly valuable in relating the extent and level of β phase nucleation in the surface layers to changes in processing parameters and to the type of nucleants added. Furthermore, the level of β phase nucleation on impact properties became clear.

Experimental Procedure

Injection moulded plaques from every variable studied were sectioned through the gate as shown in Figure 31, producing eight 10 x 10 x 3 mm^3 samples. The samples were mounted surface skin side up on the spinning stage of a Philps PW1050 Diffractometer linked to a PW1710 control terminal and software. The crystallographic analysis was made by scanning nickel filtered Cukα radiation, collimated through a 0.2mm slit, through 2θ values between 12 and 30° at a scan rate of 2 degrees/minute. The reflections from the spinning surface were then collected through a 1 mm slit to the counter. A typical set up is shown in Figure 32 and the Diffractometer with its control terminal is shown in Figure 33.

Figure 31 Sectioning of injection moulded iPP plaques for x-ray diffraction studies.

Figure 32 X-ray diffractometer set up.

Figure 33 X-ray diffractometer and control terminal.

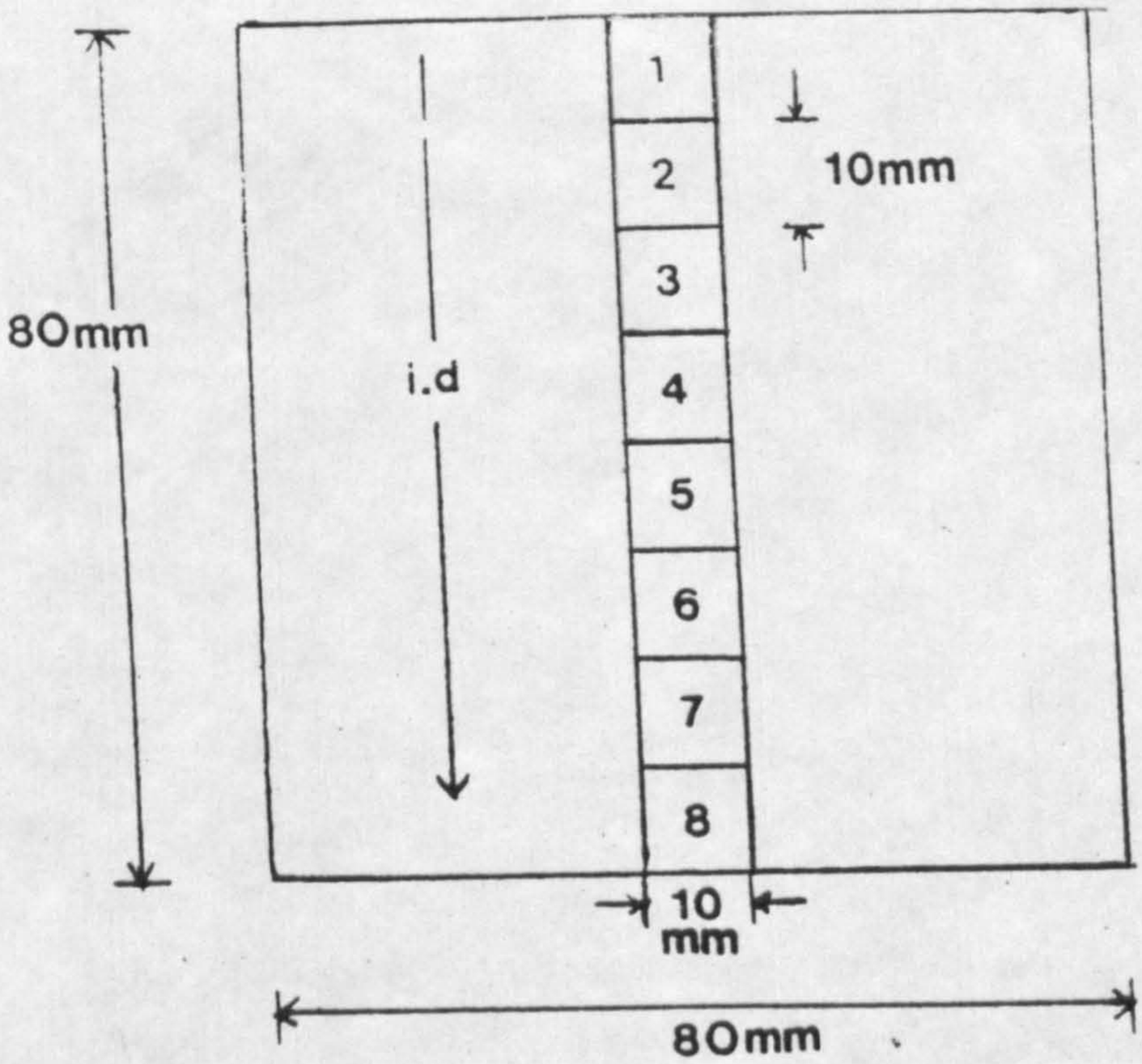
80mm
i.d
1
2
3
4
5
6
7
8
10mm
10
mm
80mm

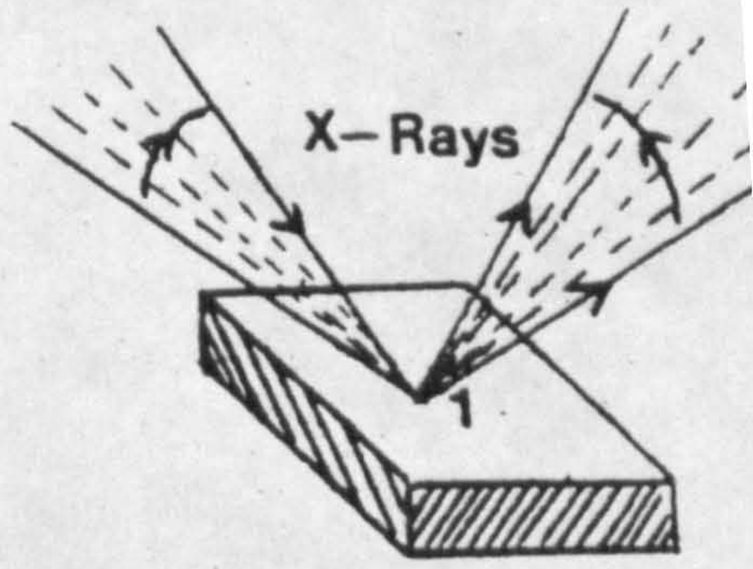
X-Rays
1

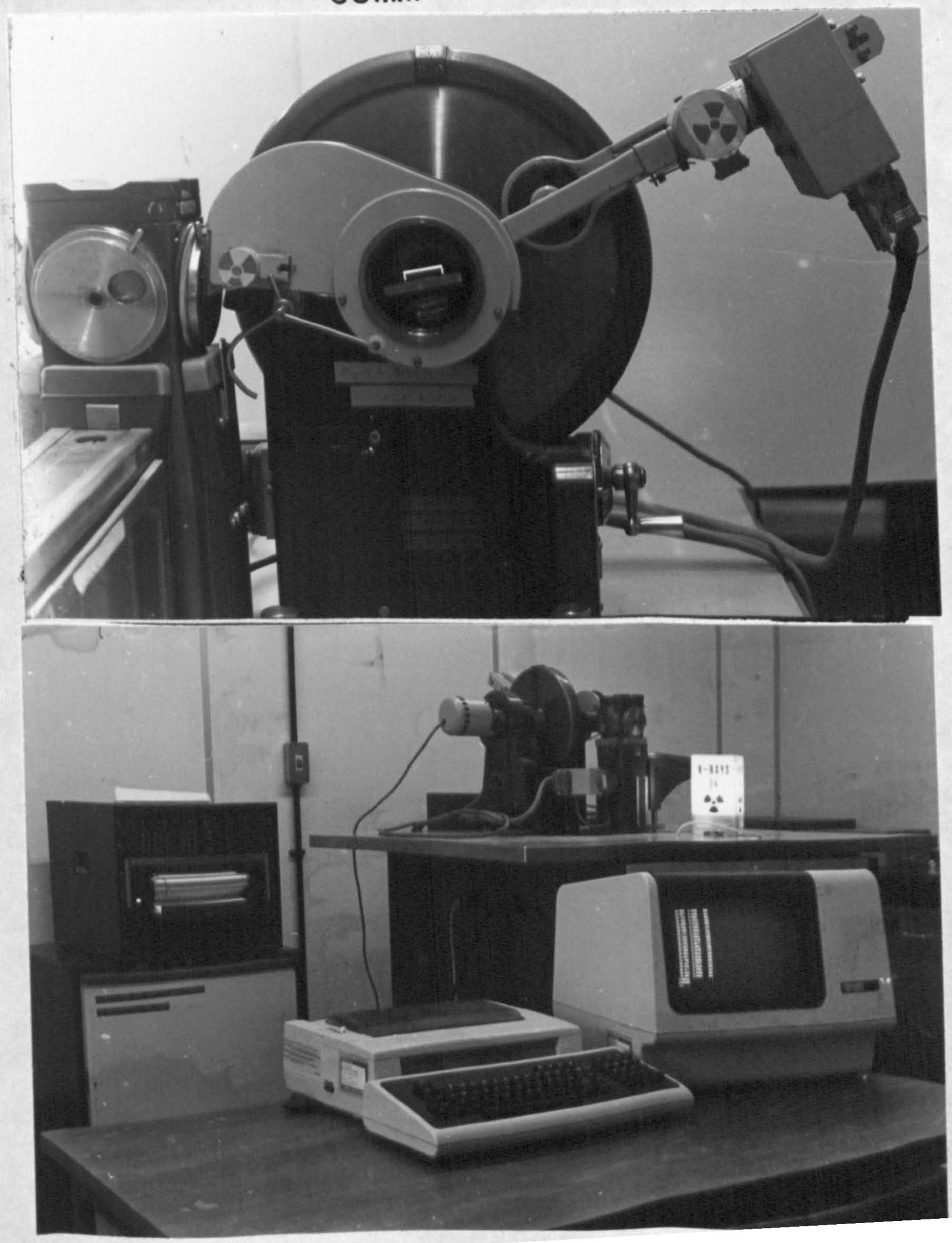

The diffractograms recorded were analysed using the Trotignan criteria for measurement of peak heights as shown in Figure 34.

2.8.6 Application of Flat Plate WAXS To Study Orientation of Individual Morphological Bands

A sample close to the gate of a moulding was used to characterize individual morphological layers by optical microscopy TEM, microhardness and x-ray diffraction. In order to assess the degree of preferred orientation of different morphologies it was necessary to microtome layers off the surface. Specimens as obtained were mounted in a Philips Micro Camera, having a 500 μm diameter collimater, so that the Ni filtered Cukα x-ray beam was parallel to the thickness of the specimen but perpendicular to the moulded surface and melt flow direction. A film to sample distance of 50 mm was used throughout the experiment and exposure times of 2 hours were required. A typical set up is shown in Figure 35.

2.9 MICROHARDNESS TESTING

2.9.1 Definition of Microhardness

In indentation hardness testing the hardness number is defined as the ratio of the applied load to the contact area of indentation. This has the dimensions of pressure and by convention units are kg f mm^{-2} although these are seldom quoted. In a standard Vickers hardness test the indenter is a sqaure based pyramid with angle between opposite faces being 136°. In this case the Vickers Hardness number, Hv is given by:

$$Hv = \frac{F}{\frac{1}{2} D^2/\sin\frac{1}{2}(136^{\circ})} = 2 \sin 68 \, (F/D^2)$$

$$= 1.8544 \, (F/D^2). \; kg/mm^2$$

Figure 34 A typical iPP diffractogram analysis.

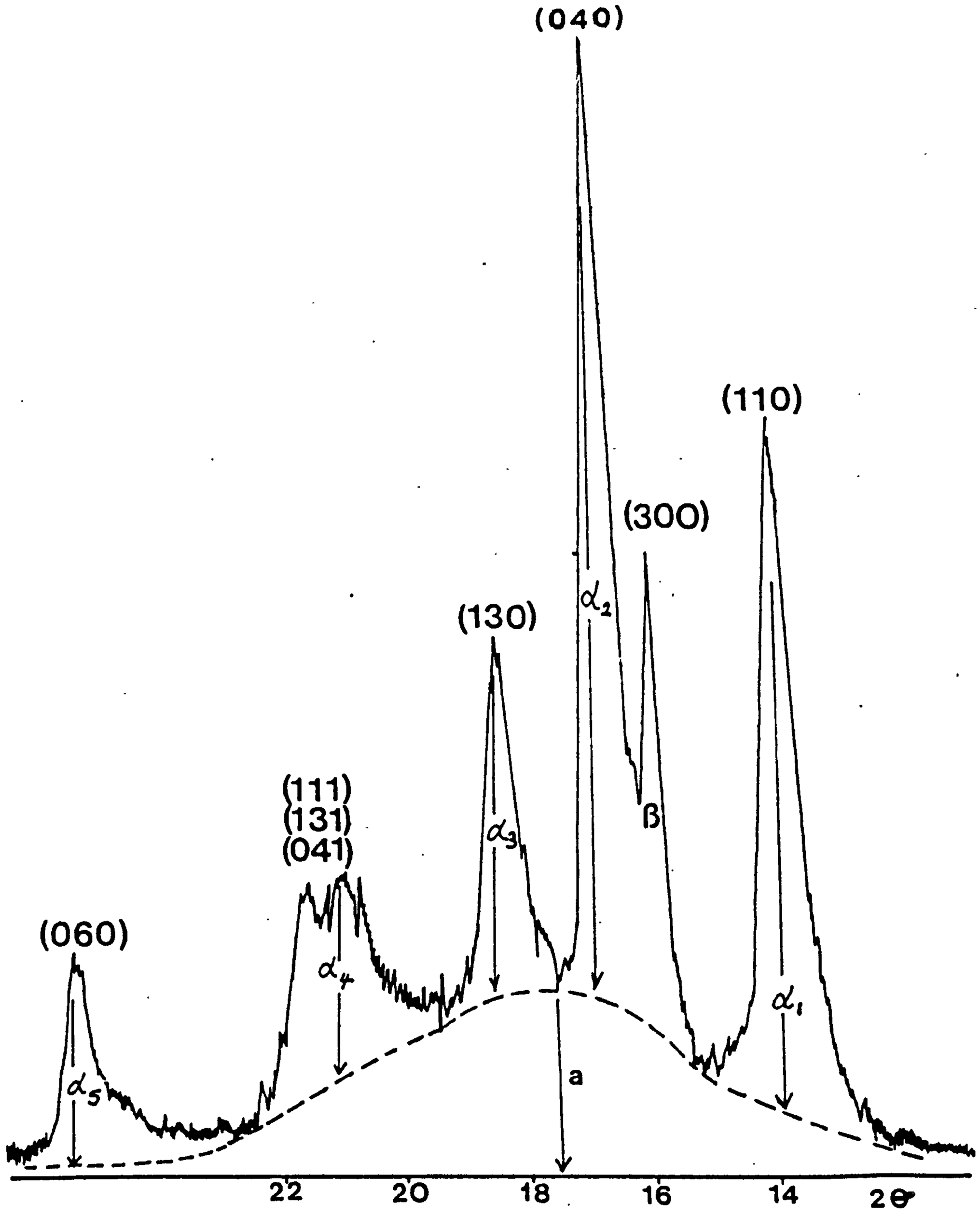

$$\frac{h\alpha_1 + h\alpha_2 + h\alpha_3 + h\alpha_4 + h\beta}{5ha} = \text{Crystallinity Index C}$$

$$\frac{h\beta}{h\alpha_1 + h\alpha_2 + h\alpha_3 + h\beta} = \beta\text{-Phase Index B}$$

$$\frac{h\alpha_1}{h\alpha_1 + h\alpha_4} = \alpha \text{ Phase Orientation Index A}$$

Figure 35 Flat plate WAXS set up.

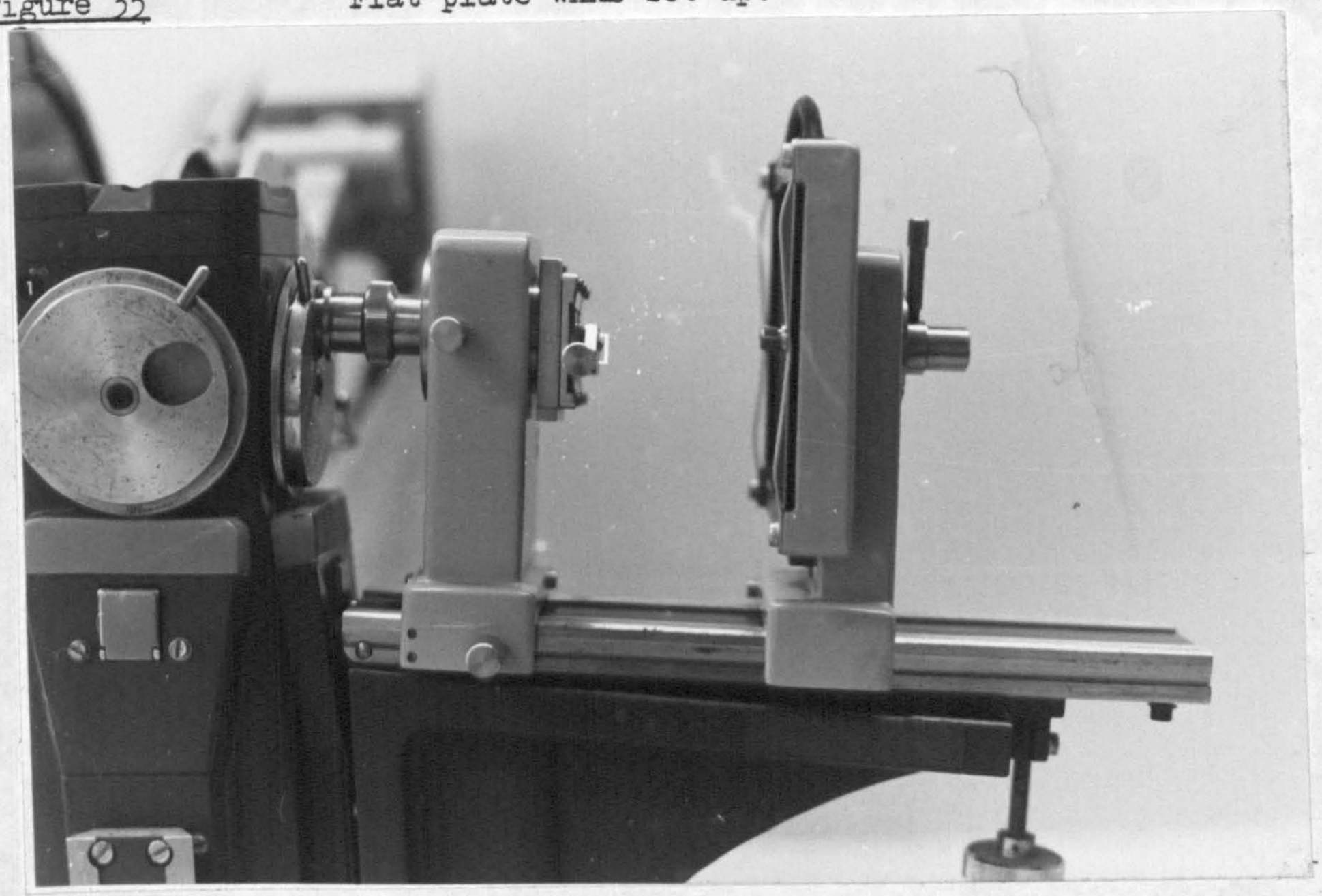

Figure 36 Shows a microhardness plot for an iPP moulding (after Bowman and Bevis (155).

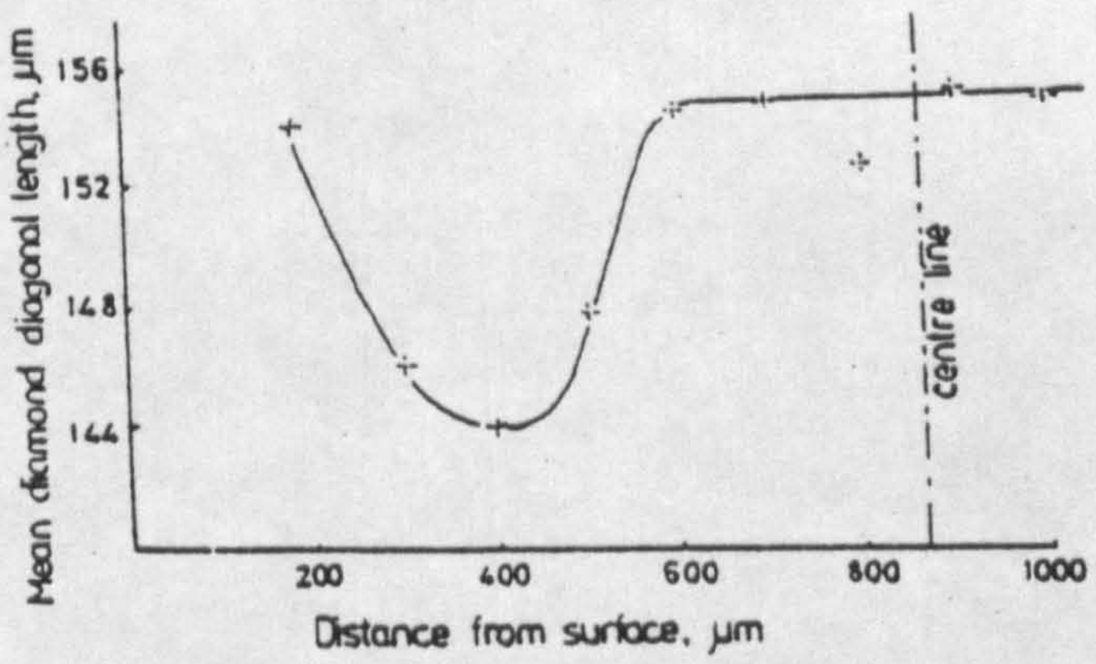

Figure 37 Microhardness indenter alignment relative to the injection direction.

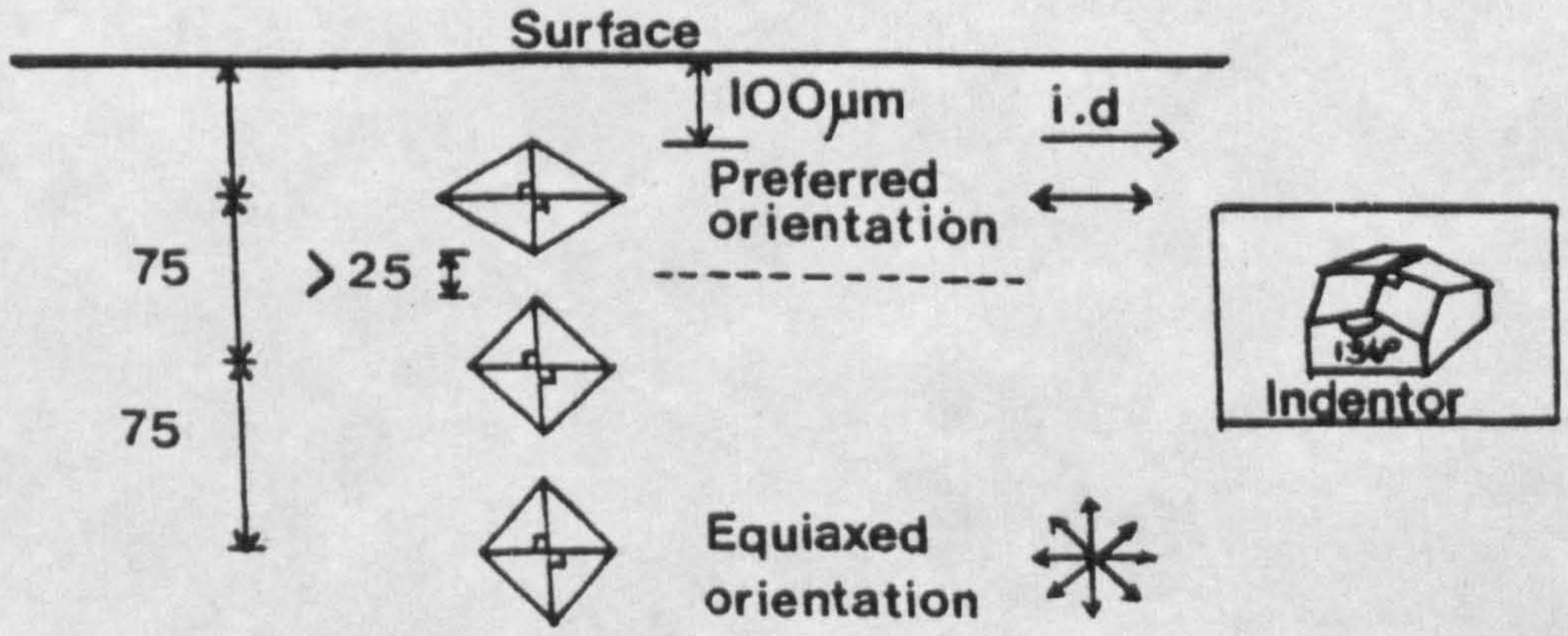

Where F is the applied load (in kg) and D is the length of the diagonal of the indent (in mm) produced after removal of the load.

It should be noted that in some cases the indent may be distorted, for example, a rhomboid instead of a square, but this does not necessarily mean the indenter shape is wrong. The shape of the indent is dependent on the directional properties in the material under test.

2.9.2 Microhardness Testing of Thermoplastics

Micro-indentation testing has been used as a method of measuring the surface hardness of metal products for about 50 years (152). The method differs from conventional hardness testing in that the loads applied to the indenter are less than 1kg and the test equipment needs to be extremely sensitive so that the very small indent (~40 μm) can be measured accurately. Due to its relative simplicity and non-destructive nature the microhardness test has been particularly useful in situations where it can be used as an indication of surface durability and in some cases as an indication of strength. In recent years an interest has been aroused in the hardness testing of plastics. However, it has been found that the viscoelastic behaviour of plastics has a significant effect on the hardness measurement taken. In all cases, material properties such as yield stress, elastic modulus, tensile strength, brittleness etc., all play a part in the determination of a hardness number.

Theoretical analysis of hardness of plastics is difficult because the stress system in the vicinity of the indenter is complex.

Also when creep occurs the depth of penetration of the indenter will progressively increase, but under constant load, the creep effect will decrease with time since the area of the impression is increasing. The time dependent recovery when the load is removed is another factor which must be considered when measuring the size or depth of penetration of the indent.

Despite these considerations hardness testing of plastics is potentially a very useful, non-destructive method of assessing the quality of moulded parts. It has already been used to investigate areas such as moulded in stresses by Kent et al., (153) and density variations by Crawford et al., (154) and in addition interesting correlations have been reported between microhardness and morphology of injection moulded plastics by Bowman and Bevis (9, 155, 156). More recently Kent et al., (157, I, II) have used a variation of conventional hardness testing techniques to investigate orientation effects in moulded parts.

Load & Loading-time Dependence

Eyerer and Lang (158) have investigated the applicability of the Vickers microhardness test and, for nineteen different commercial plastics, they concluded that with a standard loading procedure the deviation of lengths of diagonals under load and after removal of the same (measuring from 5s upto 24hr after removal of the load) does not on average exceed 2.5%. Crawford (159, 160) carried out Vickers microhardness tests on polymethyl methacrylate (PMMA) plasticised Poly vinyl chloride (PVC), polypropylene and acetal copolymer using two different test methods. In one case the depth of the penetration is measured during application of the load and in the other case the size of the indent has been measured after load removal.

The author concluded that:-

(i) the microhardness of plastics is dependent on the applied load to the indenter and time of application of load.

(ii) when the indenter is removed there is a large (50-70%) recovery of the depth of the indent, but only a small recovery (~ 5%) of the diagonals.

(iii) the vast majority (90%) of the recovery occurs in the first few seconds after load removal.

(iv) for polypropylene, unplasticised PVC and PMMA the amount of recovery is dependent only on the duration of the applied load but for acetal it is also dependent on the value of load.

This small recovery in the length of the diagonals occuring a few seconds after load removal is in agreement with the observations of Eyerer and Lang (158), Balta Calleja and Basset (161) and Phillips and Ramakrishnan (162).

2.9.3 Application to Injection Moulded Thermoplastics

Microhardness is then an attractive method for investigation of the microstructure of semicrystalline polymers, especially because the indentation is highly localised to a small volume element and responds to small changes in texture and morphology. Microhardness is furthermore a very useful property which provide a direct measure of the anisotropy developed within an injection moulded polymer as a consequence of high orientation of molecular chains. The object of the present study was to assess variations in micromorphology throughout an iPP injection moulding, similar to that reported by Bowman and Bevis (9, 155, 156) for TPX and acetal mouldings. Figure 36 shows a microhardness plot of polypropylene specimens also reported by the afore mentioned authors.

2.9.4 Testing Procedure

The Vickers microhardness tester is similar in appearance to a bench microscope but differs in that it has a special indenter ojective. The principle of operation is that the surface of the sample under test is brought into focus and the standard Vickers pyramid indenter is forced down onto the surface with a pre-selected load. After release of the load the indenter is removed from the surface and the image of the indent may be viewed and measured at the filar micrometer eyepiece focal plane of 75X using the M022952 50X objective and magnification changer set to 1.4X. The lengths of both diagonals of the indent can then be converted into a Vickers hardness number according to the equation given previously.

Each surface to be tested was exposed using a sledge microtome and then mounted in polyester resin. The specimens were then ground wet to 600 emery followed by polishing on 6, 3, and 1 μm diamond paste wheels respectively. The polished surface was examined to ensure it was free from gross (1-2 μm) scratches which is of paramount importance in microhardness testing. The samples were then mounted and clamped securely on the Vickers microscope stage and tested using the following standardized procedure adopted from previous work (9, 155). The indenter was aligned so that one diagonal was parallel and one perpendicular to the injection direction as shown in Figure 37. A load of 10 grammes was applied for 1 minute, in all tests followed by a subsequent 2 minute recovery period before measurement of diagonals. Hardness readings were taken well away (100 μm) from free edges on the sample and the space between each indent centre was 75 μm thus allowing at least 25 μm between apexes consequently reducing the possibility of any one indent effecting another.

The microhardness indentation was sufficiently small to allow it to exist within and respond to changing morphologies and anisotropies.

****

CHAPTER 3

EFFECTS OF PROCESSING CONDITIONS ON MICROMORPHOLOGY AND IMPACT PROPERTIES OF INJECTION MOULDED iPP.

3.1 INJECTION MOULDING

3.1.1 Optimization of Mould Filling

The volume of plastics mouldings is much affected by temperature and pressure and, up to a point, by time. It is very difficult to accurately predict component shrinkage which in the case of partially crystalline materials such as polypropylene can be as much as 15-30%. Compression reduces the volume of a polymer melt by about 6-7% and it is this compressibility in polymer melts which enables shrinkage during moulding to be kept within acceptable limits by what is known as 'holding pressure.'

There are two types of shrinkage:

(i) Processing Shrinkage, defined as the difference between the dimensions of the cold mould and the cold moulding at $23^{\circ}C \pm 2^{\circ}C$, 24 to 168 hours after moulding, and

(ii) Post Shrinkage, which is defined as dimensional changes occuring in the course of time in the finished moulding. Post shrinkage can also be minimised by controlling processing conditions (e.g. high mould temperature and high holding pressure).

The easiest way of determining the factors which influence processing shrinkage is by weighing the mouldings. The relationship between the weight of a moulding and its volume is as follows:-

$$V = \frac{m}{\rho} = mv \qquad \text{with } v = \frac{1}{\rho}$$

where ρ = density

v = specific volume

V = moulding volume

m = moulding weight

Since the density of an injection moulding varies but little at room temperature, changes in weight give a clear indication of volume changes and changes in volume shrinkage.

The optimum mould filling conditions were identified in our research programme by firstly, determining the shot size required to fill the cavity, by the short shotting technique whereby a gradual increase in the shot weight is used with 1st stage high injection pressures until flashing of excess material occurs, and secondly, at this point a switch over to a second stage holding pressure is made utilizing a pre-set melt cushion size. The material is then packed, according to a cavity hold pressure profile, until gate freeze-off occurs preventing any more material entering the cavity. Optimization of the mould filling process is achieved with the aid of cavity pressure profiles recorded from the cavity pressure transducer signal. A typical cavity pressure profile is shown in Figure 38.

The decisive factor for shrinkage, and thus for the dimensions, of the finished part is the point where cavity pressure reaches atmospheric since it is at this point that the moulding becomes detached from the cavity wall i.e. starts to shrink. By increasing the holding pressure time moulding quality is improved, but there is little point in holding much beyond gate freeze-off since no further melt can be forced into the cavity.

3.1.2 Daniels Injection Moulding Conditions and Data Monitored

Injection mouldings of GXM43 iPP, 3mm plaques, were prepared in the Daniels machine using the NPL mould and full instrumentation as described in section 2.3.1. In order to initially study the effects of extremes of processing parameters on micromorphology and impact properties the moulding programme in Table 8 was chosen using the set processing parameters summarized in Table 9.

TABLE 8 Daniels moulding programme.

MOULD TEMPERATURE (°C)	MELT TEMPERATURE (°C)	FILL TIME (secs)
35	220	1.35
80	220	1.35
35	220	2.60
35	220	4.00
35	280	1.35
35	280	4.00
80	280	1.35
80	280	4.00

TABLE 9 Set Processing parameters used for Daniels injection mouldings.

NOZZLE HEATER (°C)	220	280
HEATER BAND 1 (°C)	210	260
HEATER BAND 2 (°C)	200	240
HEATER BAND 3 (°C)	190	220
HEATER BAND 4 (°C)	180	200
SHOT SIZE (INCHES)		1.85
CUSHION SIZE (INCHES)		0.40
PLASTICATE PRESSURE (Nm^{-2})		89631.88
MAX.CAVITY PRESSURE RANGE (MPa)		27.58-31.03
HOLD PRESSURE PROFILE (%)	50,55,60,60,65,65,70,70,75,75	
INJECTION VELOCITY PROFILE (%)	R2,65,65,65,65,65,65,65,60,55,50	
	R1,65,65,65,65,65,65,65,60,55,50	
	R1,30,30,30,30,30,30,30,30,30,30	
COOLING TIME (secs)		30
HOLD TIME (secs)		30

A total of 40 continuous mouldings for each of the eight processing conditions was produced with a minimum of 20 mouldings scrapped during start-up of each condition to ensure equilibrium of machine variables. All machine parameters were kept constant and the machine was kept scrupulously clean to avoid anomolies due to contamination.

In addition, 2mm thick injection moulded plaques were prepared using melt temperatures of 220°C and 280°C with a fixed mould temperature of 35°C and a cavity fill time of 1.35 seconds. These additional mouldings were used to enable a study of the effect of mould thickness on micromorphology and impact properties to be made.

3.1.2.1 Analysis of Data Monitored

Typical cavity pressure profiles are illustrated in Figure 39, the following observations were made from these traces with respect to gate-freeze off times:-

(i) Reducing the cavity fill time, i.e. increasing the injection velocity, increases the gate freeze-off time and allows longer hold pressure times to be maintained. Shrinkage is therefore expected to be reduced with cavity fill time.

(ii) Increasing the mould temperature significantly increases the gate-freeze-off time. Shrinkage usually increases with increasing cavity wall temperature, although, in some instances the reverse may happen e.g. if pressure transfer is greatly improved because of the higher mould temperature.

(iii) Increasing the melt temperature also significantly increases the gate freeze-off time. This is due to improved pressure transfer into the mould which should

Figure 38 A typical cavity pressure profile.

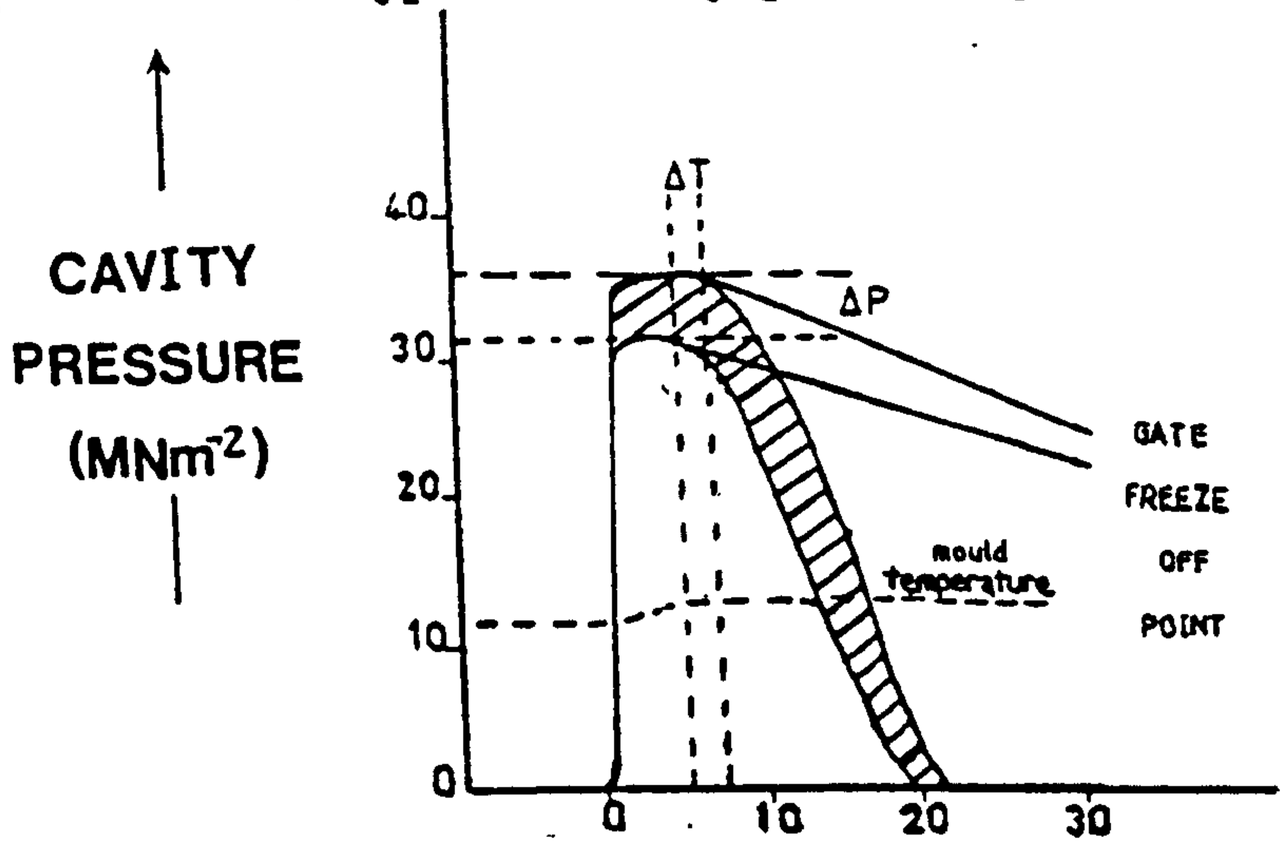

Figure 39 Typical cavity pressure traces recorded for iPP injection mouldings.

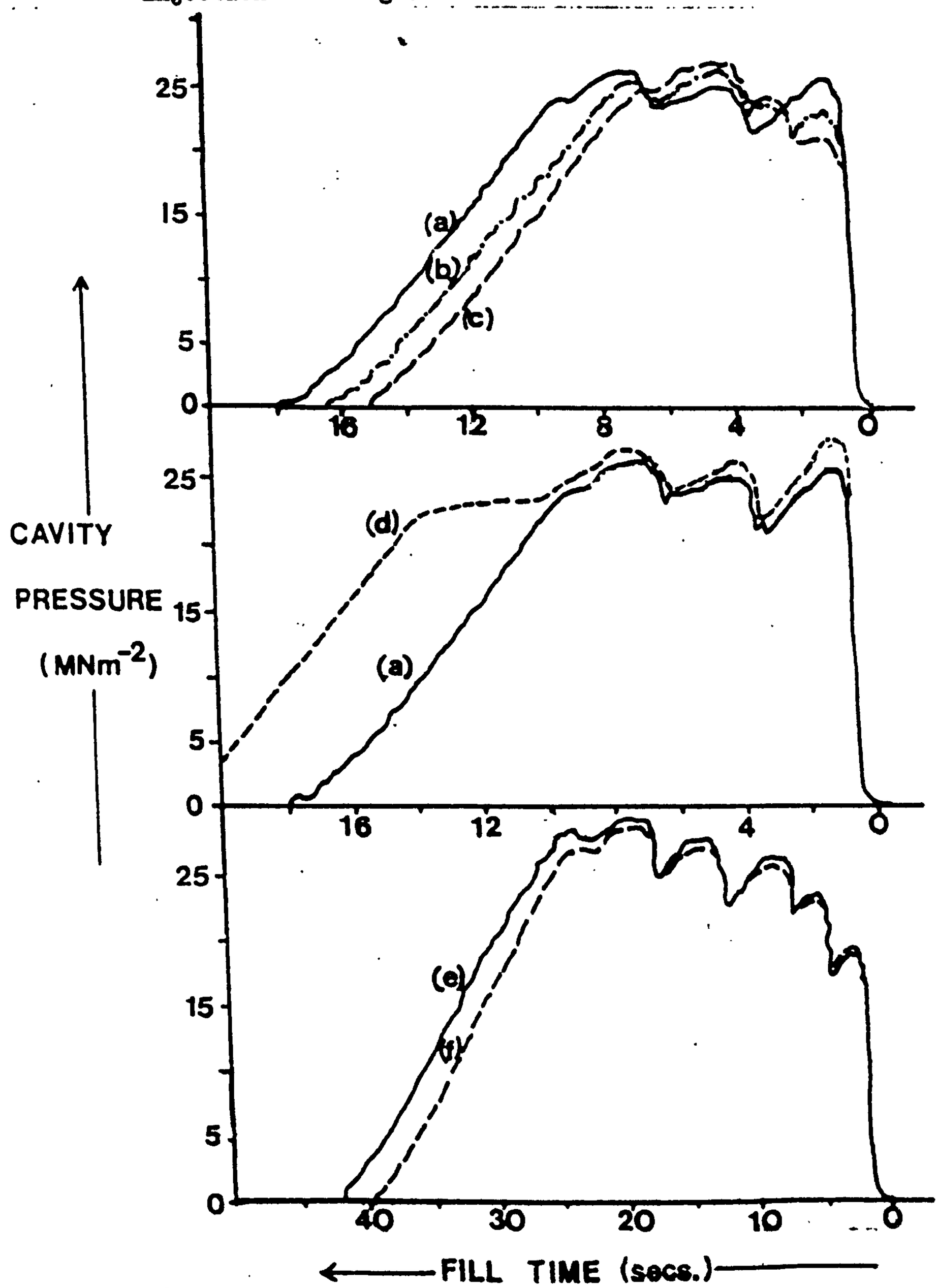

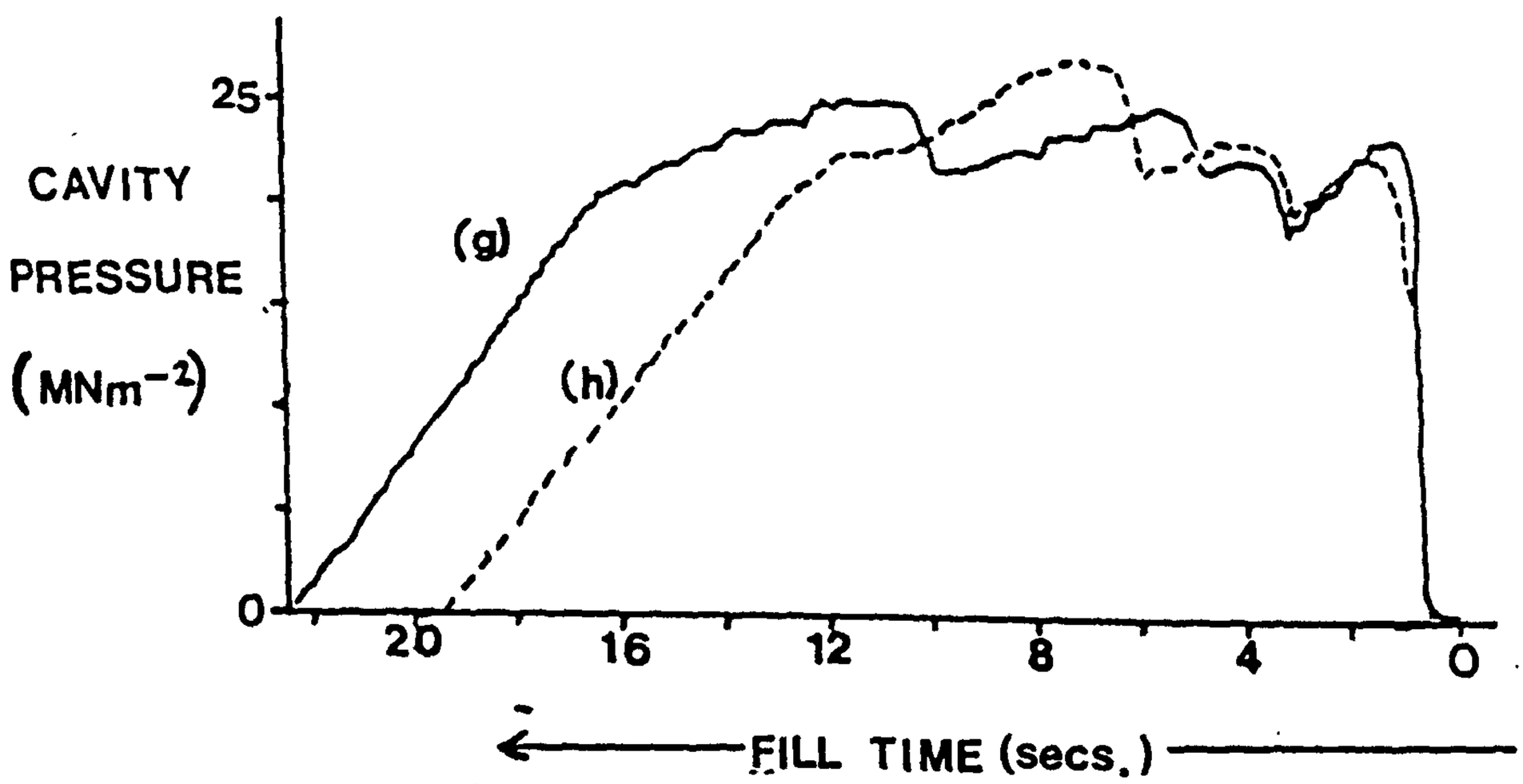

Moulding Condition			Key
Mould °C	Melt °C	Fill (secs)	
35	220	1.35	(a)
35	220	2.60	(b)
35	220	4.00	(c)
80	220	1.35	(d)
80	280	1.35	(e)
80	280	4.00	(f)
35	280	1.35	(g)
35	280	4.00	(h)

(iv) The shortest gate freeze-off time was found with low mould and melt temperatures combined with slow injection.

(v) The longest gate freeze-off time was found with high mould and melt temperatures combined with fast injection.

In order to study the influence of cavity pressure profiles on the weight of mouldings/shrinkage factor, each moulding was weighed. Data of mean; shot weight, gate freeze-off time, effective holding pressure time, peak cavity pressure and volume shrinkage are presented in Table 10. Figures 40-42 illustrate graphically the relationship between shot weight and peak cavity pressure and the variations in shot weight, gate freeze-off time and effective hold pressure time with processing conditions.

From the data monitored during this carefully controlled moulding programme the following conclusions were made:-

(i) The reproducibility of mouldings from each processing condition was excellent revealing a shot weight standard deviation maximum of 0.049 g in any run.

(ii) The volume shrinkage of mouldings did not exceed 6% which is within acceptable limits considering the extremities of processing conditions attempted. Furthermore, this observation suggests adequate packing during the hold pressure time.

(iii) The shot weight was found to increase linearly with increasing peak cavity pressure, gate freeze-off time, and effective hold pressure time.

(iv) High melt temperatures and fast cavity fill times improved the volume shrinkage of mouldings as predicted in Section 3.1.3. However, the effect of mould temperature on mould shrinkage is not entirely clear.

TABLE 10 Summary of data monitored during Daniels injection moulding.

MOULDING CONDITION °C/°C/secs	SQUARE WEIGHT (g) $\bar{x}$	s.d	CIRCLE WEIGHT (g) $\bar{x}$	s.d	GATE FREEZE TIME (secs)	HOLD PRESSURE TIME (secs)	PEAK CAVITY PRESSURE (MNm^{-2})	VOLUME SHRINKAGE (%)	CAVITY DEPTH (mm)
35/220/1.35	19.88	.037	20.82	.048	9.50	15.00	28.10	5.30	3.00
80/220/1.35	19.80	.030	20.70	.034	17.00	21.40	26.60	5.90	3.00
35/220/2.60	19.79	.069	20.68	.045	8.00	16.40	24.60	6.00	3.00
35/220/4.00	19.76	.027	20.69	.029	6.80	18.00	25.60	6.00	3.00
35/280/1.35	19.90	.037	20.77	.049	16.50	22.20	28.00	5.60	3.00
35/280/4.00	19.88	.026	20.76	.029	11.50	19.40	27.30	5.70	3.00
80/280/1.35	20.06	.024	20.99	.032	30.00	42.00	30.50	4.60	3.00
80/280/4.00	20.05	.030	20.95	.027	28.50	40.00	28.60	4.80	3.00
35/220/1.35	13.66	.052	14.57	.027	6.30	10.00	30.80	0.60	2.00
35/280/1.35	13.95	.028	14.85	.056	14.20	18.00	29.30	0.10	2.00

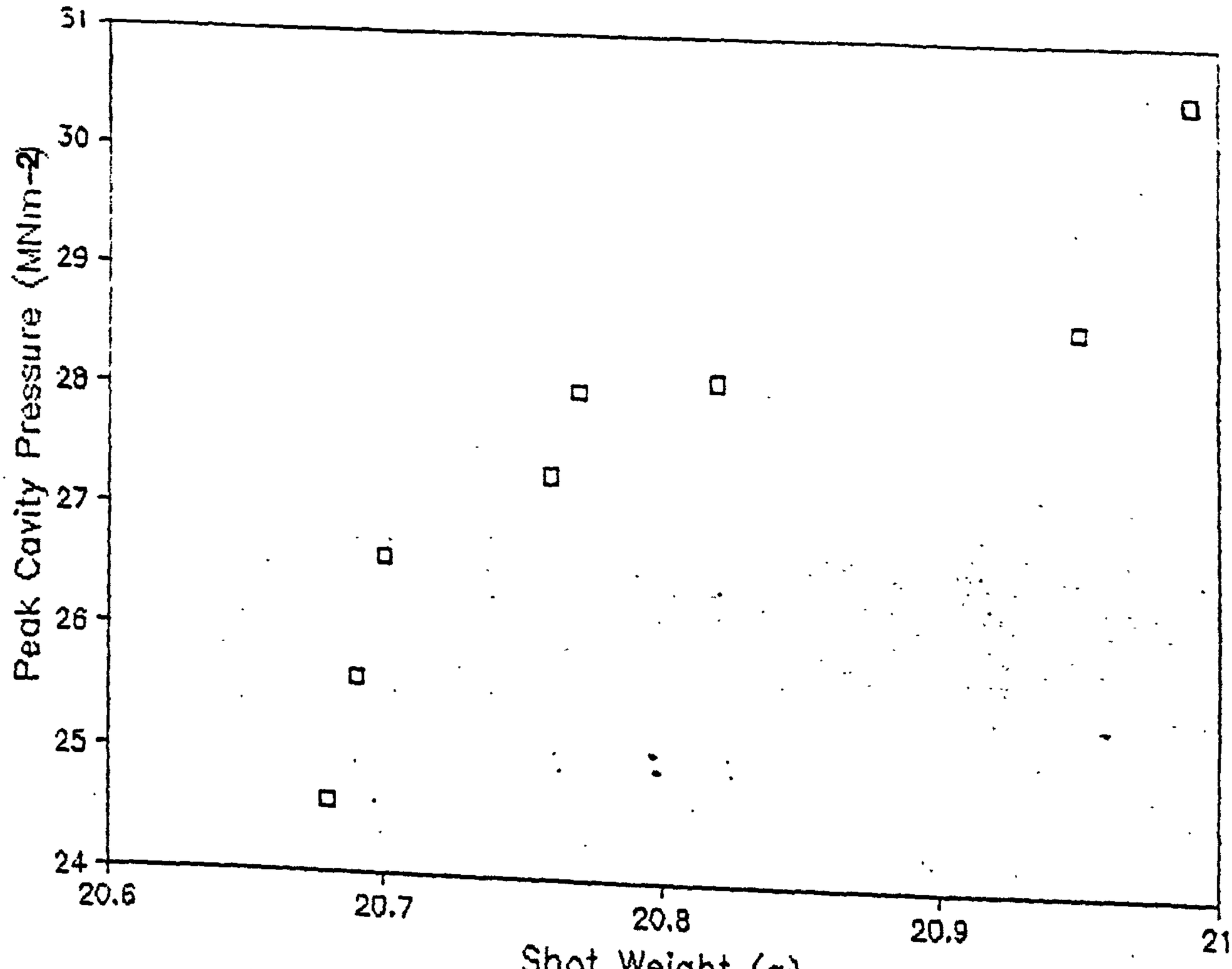

Figure 40 (a) Relationship between shot weight and peak cavity pressure.

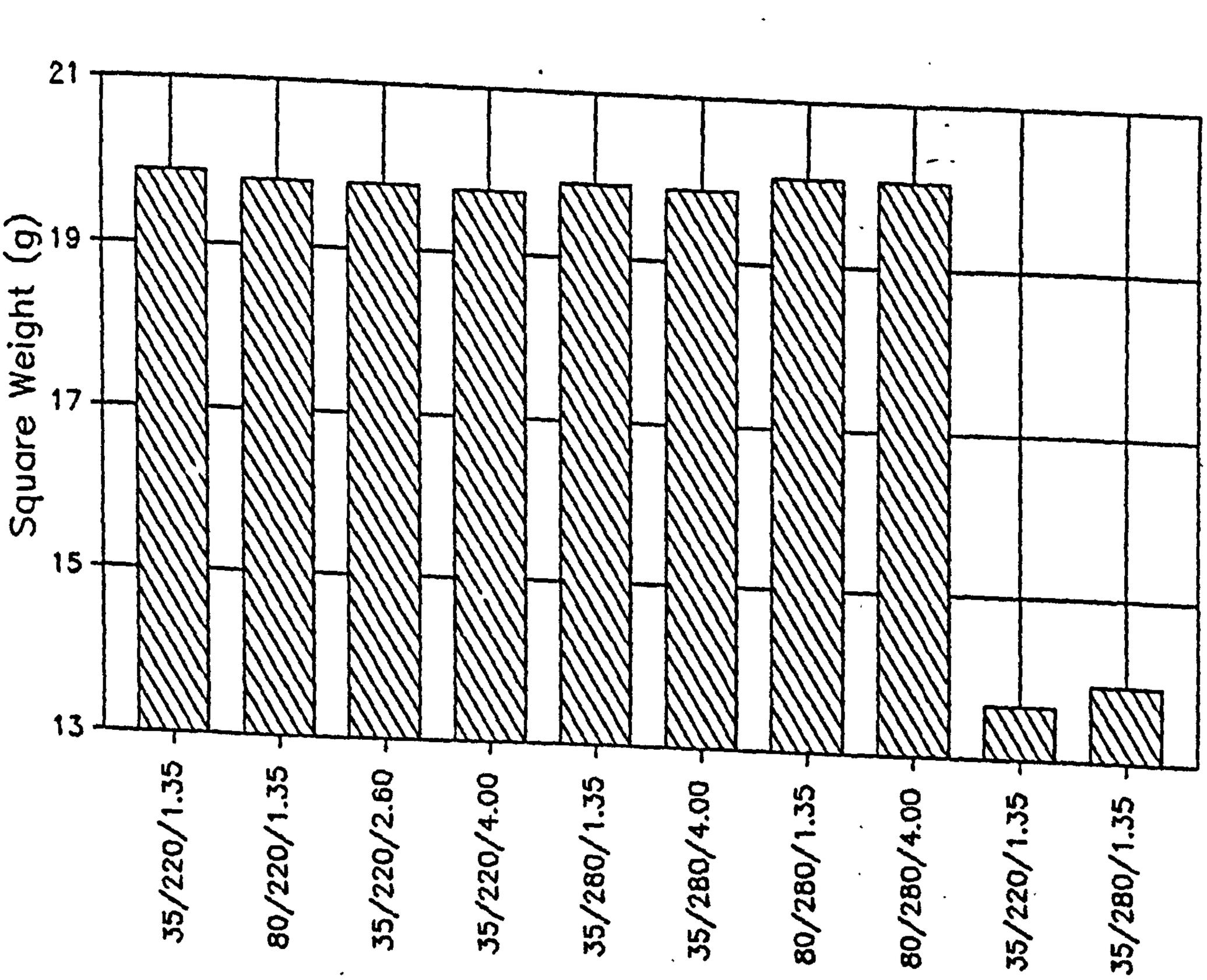

Figure 40 (b) Variation of shot weight with processing condition.

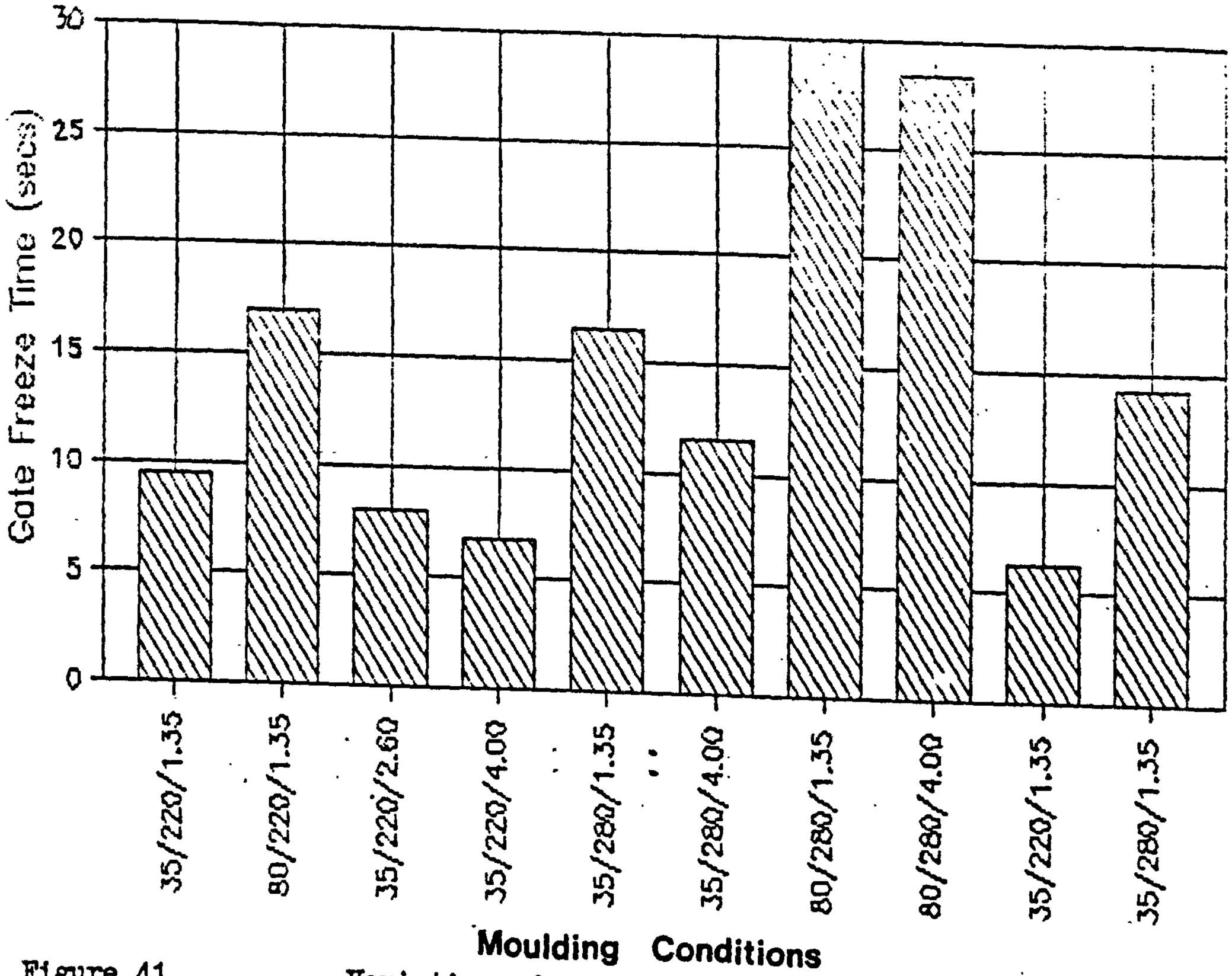

Figure 41

Variation of gate freeze time with moulding conditions.

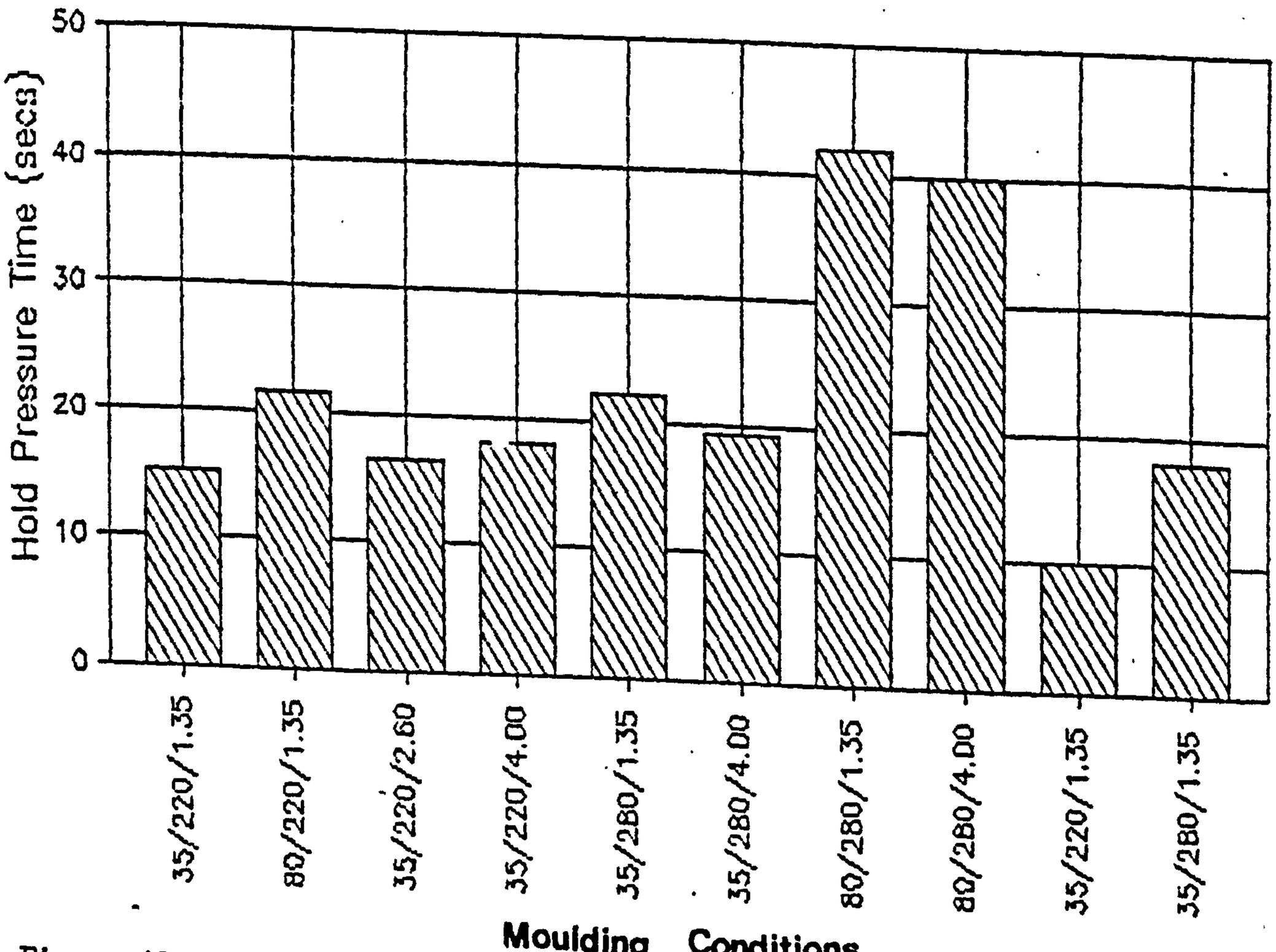

Figure 42

Variation of hold pressure time with moulding conditions.

3.1.3 Sandretto Injection Moulding Conditions

In an attempt to compare the effects of gate geometry and to study in more detail the effects of processing conditions, the Sandretto 6GV/50 tonne injection moulding machine was used fitted with the 3mm thick double-film gated plaque mould as described in the previous chapter. The availability of the Sandretto moulding machine favoured its use for the remainder of the research programme. The injection moulding programme used is summarized in Table 11 and the set processing parameters programmed into the microprocess controller are given in Table 12.

3.1.3.1 Results of Data Monitored

The changes in cavity pressure during mould filling, melt and mould temperatures, and shot weight were continuously monitored during the injection moulding programme. The mouldings were weighed 24 hours after moulding prior to removal of sprue and runner sections. A total of 30 complete mouldings were made for each processing condition with 20 mouldings scrapped during start up to ensure equilibrium of machine variables.

Table 13 summarizes the data monitored for each processing condition and gives an estimate of the percent volume shrinkage that occurred. From these results it was concluded that:

(i) The mouldings produced on the Sandretto with the Brunel double film gated mould were not as reproducible as the Daniels pin gated mouldings. However, a shot weight standard deviation maximum of around 0.4 grammes was quite acceptable given that no cavity pressure control facility was available. The variations in shot weight with processing conditions is shown in Figure 43.

TABLE 11 Sandretto moulding programme.

MOULD TEMPERATURE (°C)	MELT TEMPERATURE (°C)	FILL TIME %	FILL TIME (secs)
30	220	15	7.15
30	220	30	4.20
30	220	45	2.67
50	220	30	4.20
70	220	30	4.20
30	250	30	4.20
30	280	30	4.20

TABLE 12 Set processing parameters used for Sandretto injection mouldings.

NOZZLE HEATER (°C)	220	250	280
HEATER BAND 1 (°C)	210	240	270
HEATER BAND 2 (°C)	190	220	260
HEATER BAND 3 (°C)	170	200	240
1st STAGE PRESSURE (MPa)	91.7		
2nd STAGE PRESSURE (MPa)	78.6		
3rd STAGE PRESSURE (MPa)	72.0		
PLASTICATE PRESSURE (%)	5		
1st STAGE INJECTION TIME (secs)	2		
2nd STAGE INJECTION TIME (secs)	16		
3rd STAGE INJECTION TIME (secs)	4		
INJECTION SPEED (%)	15	30	45
CYCLE TIME (secs)	44.65		

TABLE 13 Summary of data monitored during Sandretto injection moulding.

MOULDING CONDITION			MEAN SHOT WEIGHT (g)		MEAN PEAK CAVITY PRESSURE (MNm^{-2})		VOLUME SHRINKAGE (%)
°C	°C	%	$\bar{x}$	s.d	$\bar{x}$	s.d	
30	220	30	40.05	.283	25.23	.551	4.65
30	250	30	40.33	.273	25.42	.861	3.98
30	280	30	40.79	.111	25.73	.423	2.89
15	220	30	39.81	.228	25.06	.513	5.22
45	220	30	40.23	.355	25.36	.928	4.22
30	220	50	40.66	.105	25.65	.485	3.21
30	220	70	41.32	.159	26.09	.491	1.62

(ii) The shot weight was found to increase linearly with peak cavity pressure as illustrated in Figure 44. This observation is in good agreement with that made for the Daniels moulding programme.

(iii) The volume shrinkage of mouldings improved considerably with increasing melt and mould temperatures and injection velocity. These trends are also in good agreement with those noticed for the Daniels mouldings.

3.2 IMPACT TESTING OF INJECTION MOULDED iPP PLAQUES

3.2.1 Instrumented Izod Impact Testing of Daniels Mouldings

3.2.1.1 Preparation of Test Pieces for Izod Impact Test

Instrumented Izod impact tests on miniature (3 x 3 x 12mm) test pieces cut from selected areas of mouldings were performed using the NPL pendulum machine and procedure outlined in Section 2.2.4. A total of fifteen samples from each processing condition were tested, that is,five samples tested from each of three positions relative to the flow direction as shown schematically in Figure 20. The preparation of test pieces was in accordance with the following careful procedure to ensure defect free surfaces:-

(i) A 3 x 90 x 13 mm or 3 x 80 x 13 mm strip, depending on the size of plaque (80 x 80 x 3mm or 90 x 90 x 3mm for the Sandretto and Daniels mouldings respectively), was cut from a central area of each moulding using a band saw i.e. running from the gate region to the far side of the moulding.

(ii) This strip was then accurately milled to give a defect free 3 x 90 x 12mm specimen.

(iii) This specimen was then mounted in a specially designed 12 mm wide clamp arrangement on the low speed diamond saw, to facilitate progressive sectioning of 3 x 3 x 12mm test pieces using a Buehler 350µm wide diamond waffering

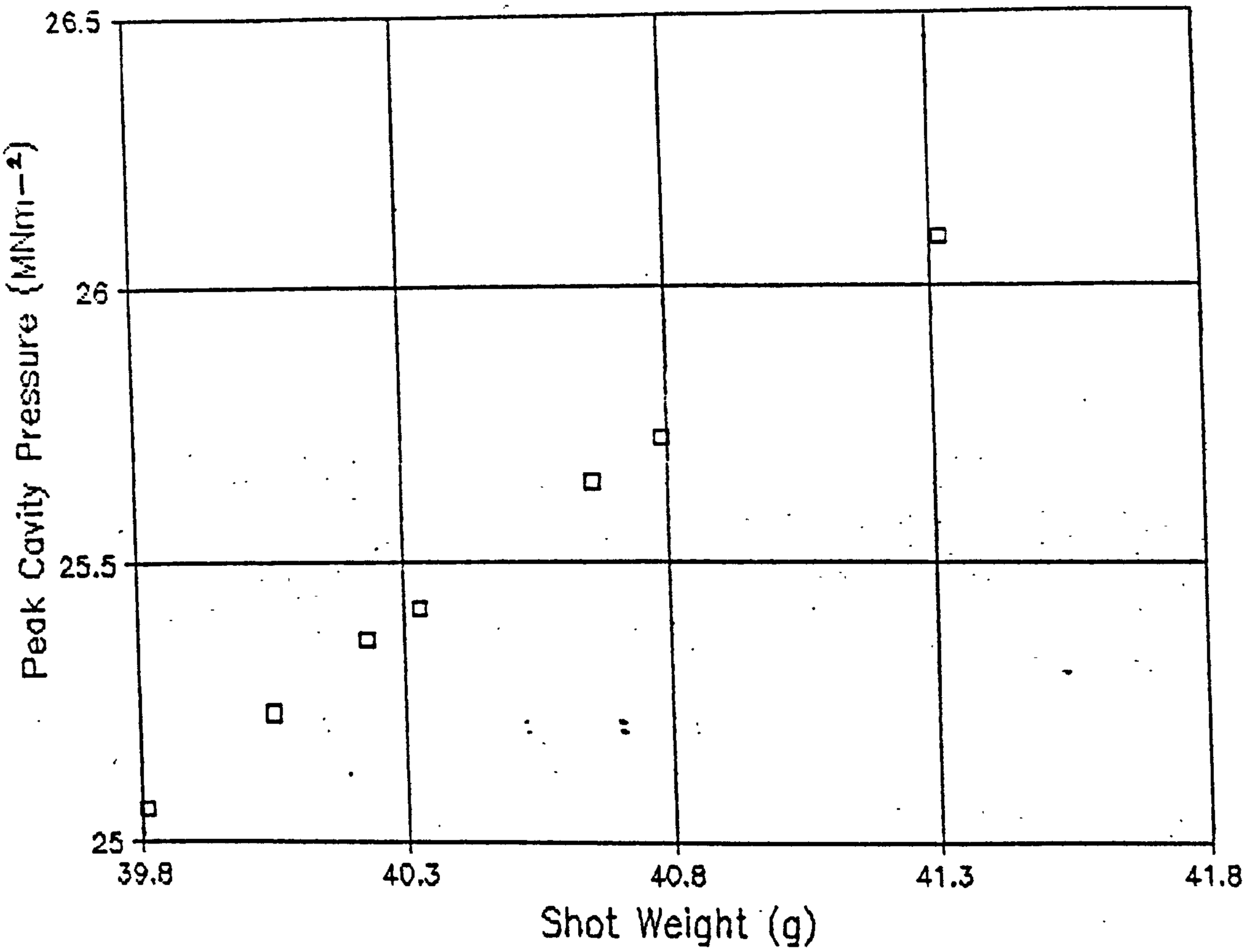

Figure 44 Relationship between shot weight and peak cavity pressure for Sandretto iPP injection mguldings.

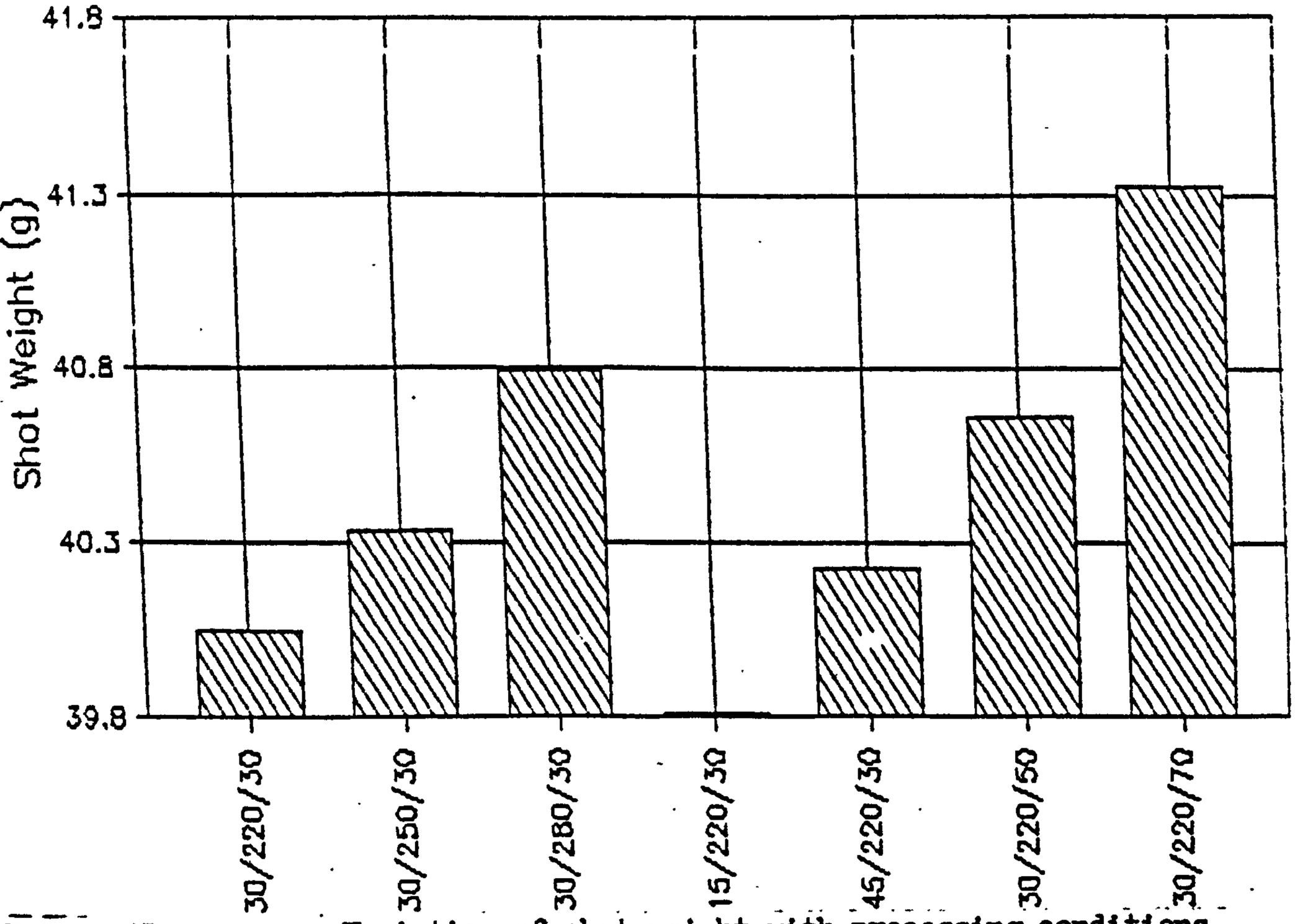

Figure 43 Variation of shot weight with processing conditions.

3.2.1.1 Izod Impact Test Results For Daniels Injection Moulded iPP Plaques

Test pieces taken from 20 mm, 45 mm (centre) and 70 mm along the flow path were prepared according to the procedure above. These test pieces were then impact tested in a controlled, 20°C, temperature environment. A summary of the accelerometer output reading impact energy to failure data collated is given in Table 14(a), calculated with prior knowledge of the cross-sectional area of each test piece. The statistical mean and standard deviation of 5 samples is given in each case. The dial energy readings were continuously monitored on the Hounsfield machine to check the accuracy of the computer calculated results.

For the purpose of this work it was found adequate to compare only Force/time and energy/distance^2 records. A thorough analysis of all records would have proved far too time consuming. The relation between energy absorbed from the pendulum and the square of the distance x, moved by the point of impact upto crack propagation, is linear and the gradient of this curve provides an effective elastic modulus of the sample (134). This modulus is in fact a combined shear and bending modulus due to the obvious end effects associated with clamping. The mean and standard deviation data for the energy to crack over distance squared (E/d^2) are also given in Table 14(b) for this reason. From this impact test study Figure 45 illustrates typical Force/time and energy/distance^2 curves shown for 35/220/1.35 controlled moulding conditions.

The following observations were made from the Izod impact test results illustrated graphically in Figures 46-52:-

TABLE 14(a) Instrumented Izod impact test results for Daniels mouldings.

MOULDING CONDITIONS MOULD (°C)	MELT (°C)	FILL (secs)	I.S 20 mm (kJm^{-2}) $\bar{x}$	s.d	I.S 45 mm (kJm^{-2}) $\bar{x}$	s.d	I.S 70 mm (kJm^{-2}) $\bar{x}$	s.d
35	220	1.35	4.04	0.33	12.90	2.70	16.44	2.05
80	220	1.35	3.55	0.51	5.90	1.40	6.63	0.28
35	220	4.00	4.71	0.42	6.64	0.30	18.73	0.71
35	280	1.35	9.19	0.73	15.40	0.51	19.97	1.49
35	280	4.00	6.17	0.84	9.56	1.50	12.42	5.00
80	280	1.35	5.77	0.58	6.65	0.20	6.80	1.20
80	280	4.00	5.23	0.92	5.80	0.60	7.15	1.07

TABLE 14(b) Effective modulus data calculated from energy/distance^2 curves.

MOULDING CONDITIONS MOULD (°C)	MELT (°C)	FILL (secs)	E/d 20 mm (kJm^{-2}) $\bar{x}$	s.d	E/d 45 mm (kJm^{-2}) $\bar{x}$	s.d	E/d 70 mm (kJm^{-2}) $\bar{x}$	s.d
35	220	1.35	61.30	2.0	60.0	3.0	67.0	3.0
80	220	1.35	60.0	3.0	60.0	5.0	65.0	6.0
35	220	4.00	58.0	5.0	62.0	4.0	60.0	2.0
35	280	1.35	62.0	3.0	65.0	1.0	62.0	7.0
35	280	4.00	59.0	2.0	66.0	2.0	60.0	3.0
80	280	1.35	58.0	4.0	68.0	1.0	68.0	2.0
80	280	4.00	54.0	4.0	66.0	2.0	60.0	5.0

Figure 45

Typical Force/time and energy/distance^2 curves for samples impact tested at 20mm and 70mm along the flow direction of a 35/220/1.35 moulding.

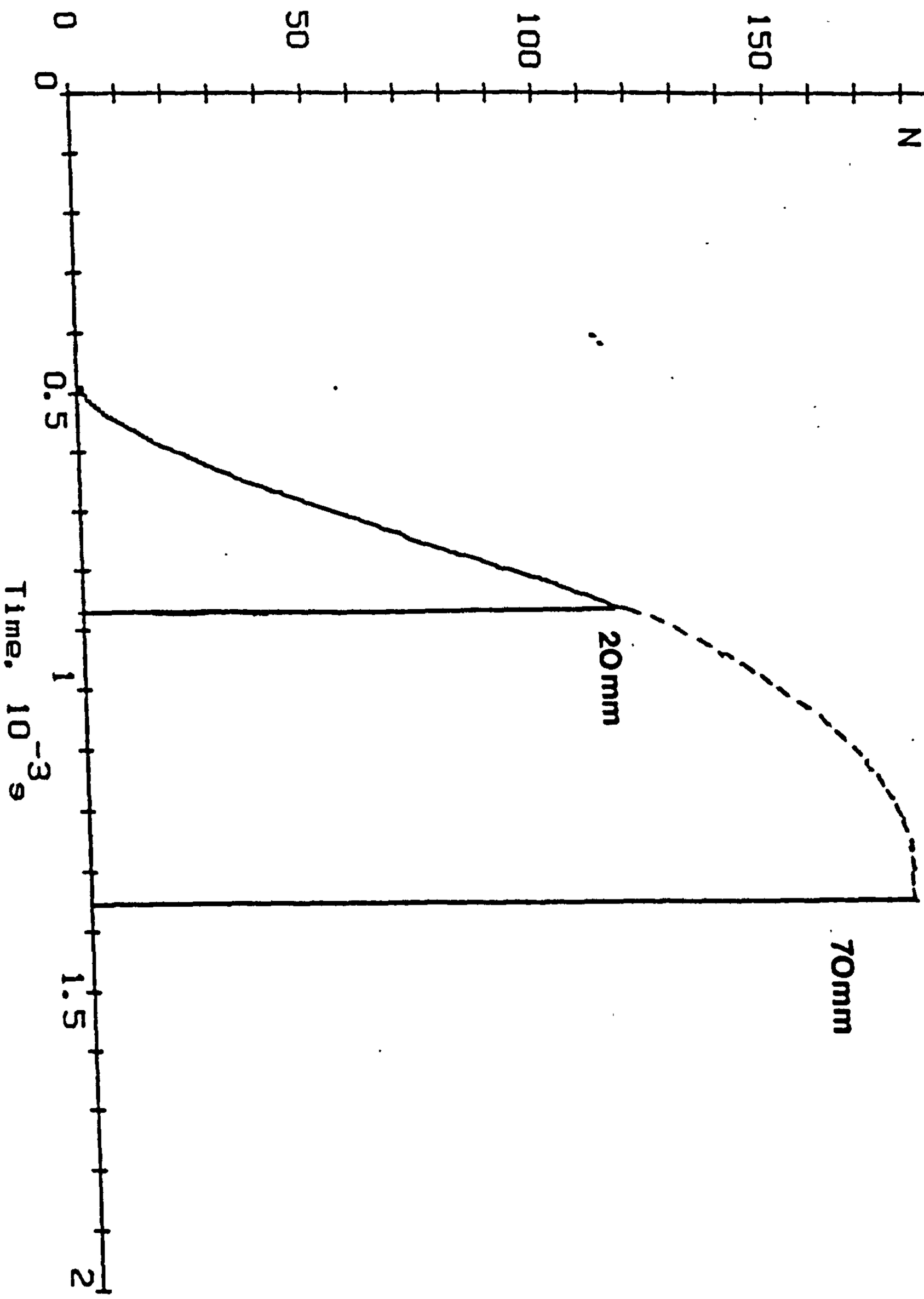

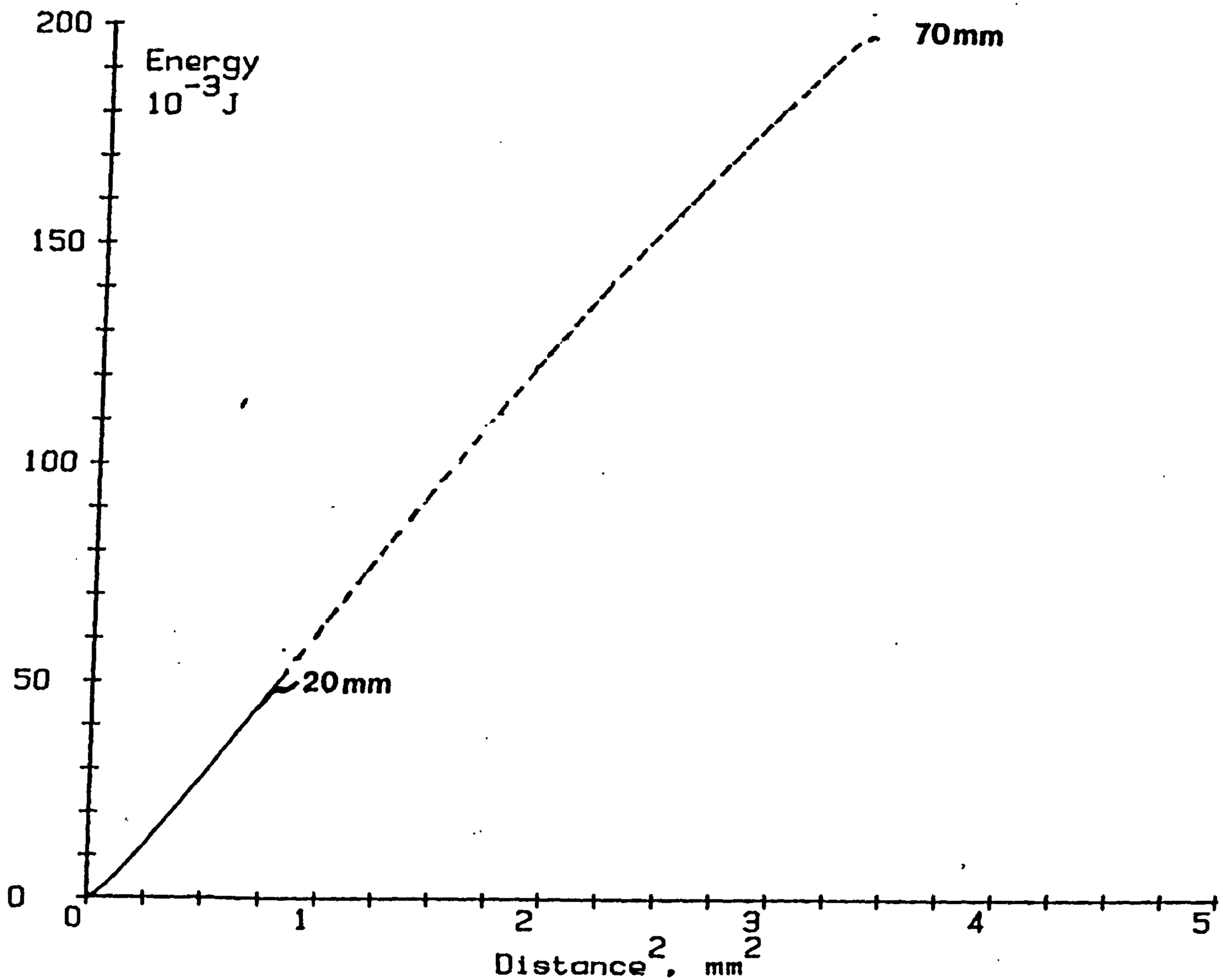
200
150
100
50
0
Energy
10^{-3} J
70mm
20mm
0
1
2
3
4
5
Distance^2, mm^2

Figure 46

Presentation of Izod impact strength data and selected area micrographs for 35/220/1.35. Scale bar = 100 um.

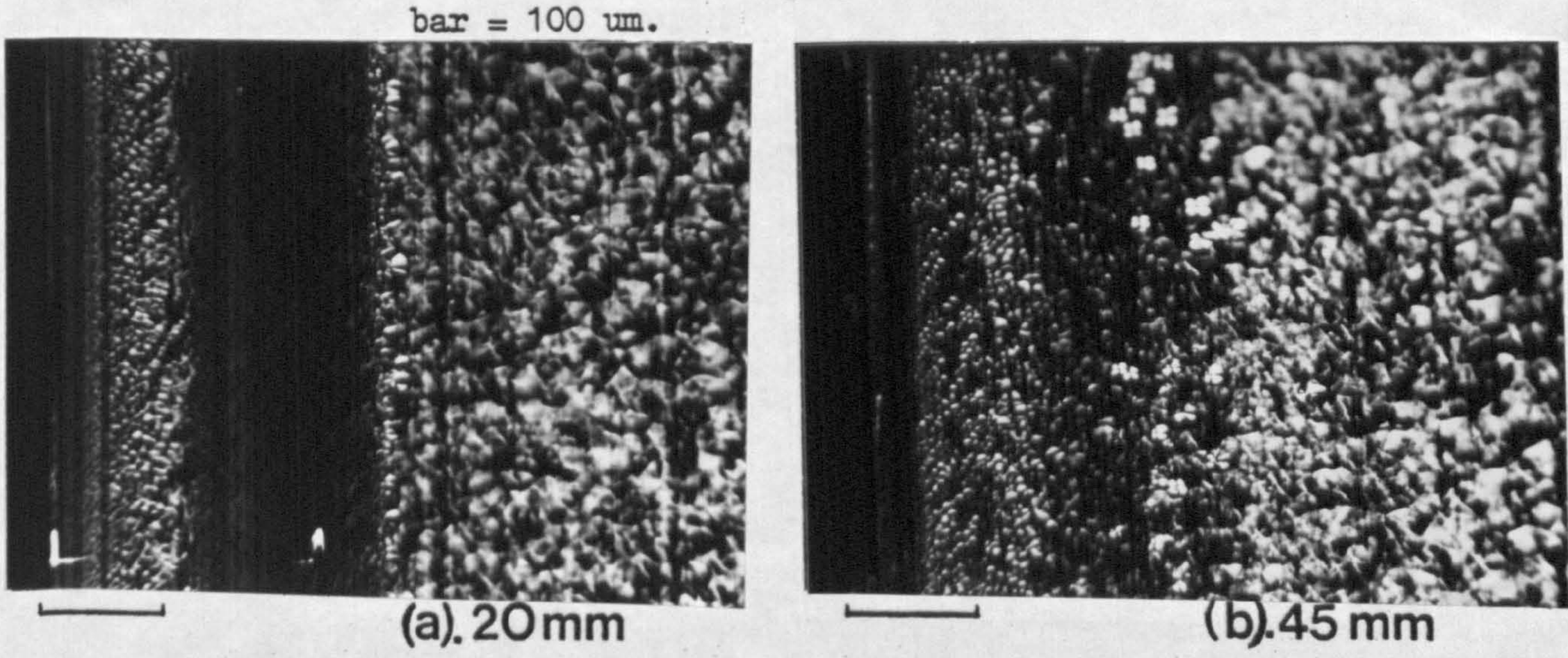

Figure 47

Presentation of Izod impact strength data and selected area micrographs for 35/220/4.00 moulding conditions.

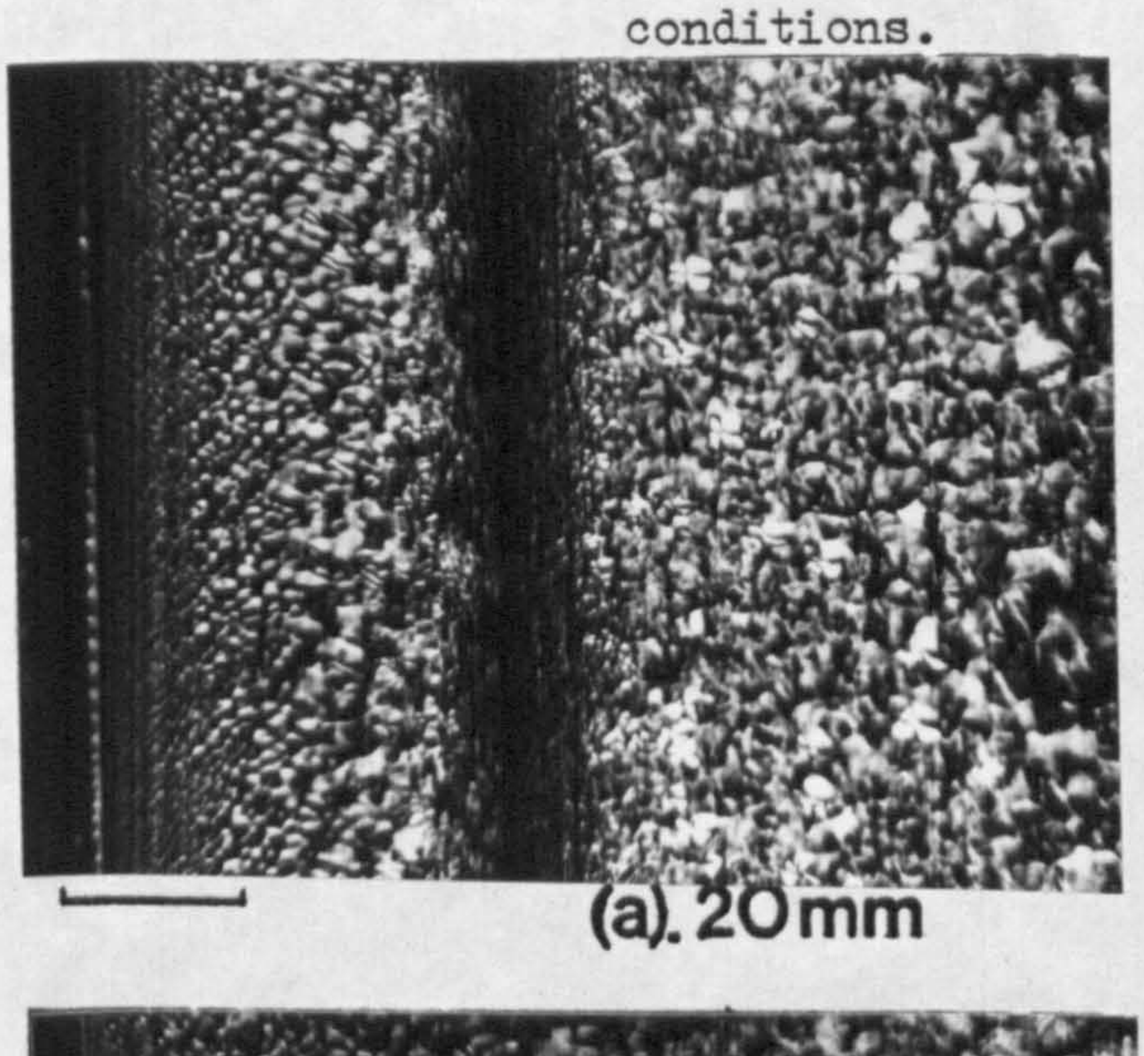

Scale bars = 100 μm

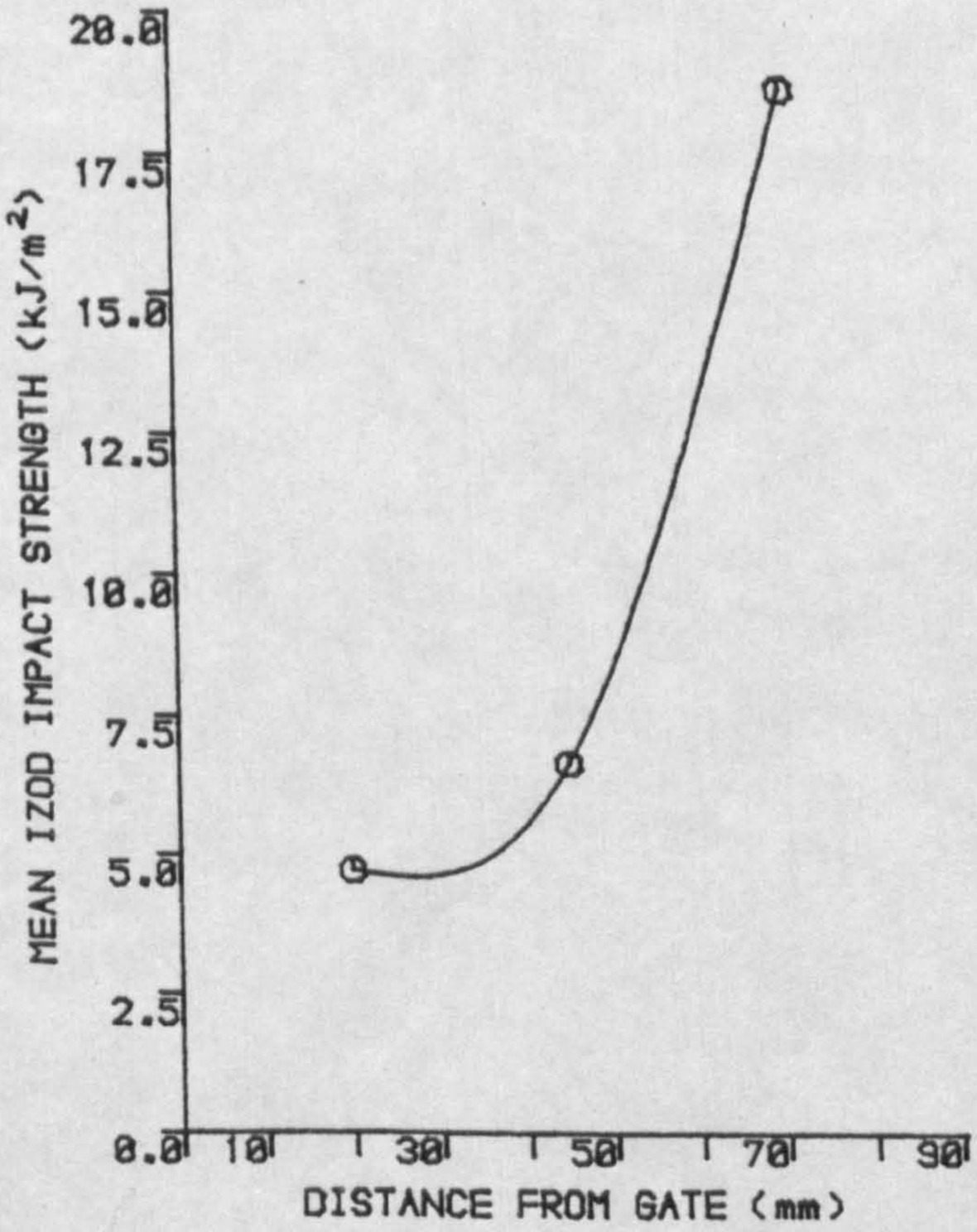

Figure 48 Presentation of Izod impact strength data and selected area micrographs for 35/280/1.35 moulding conditions.

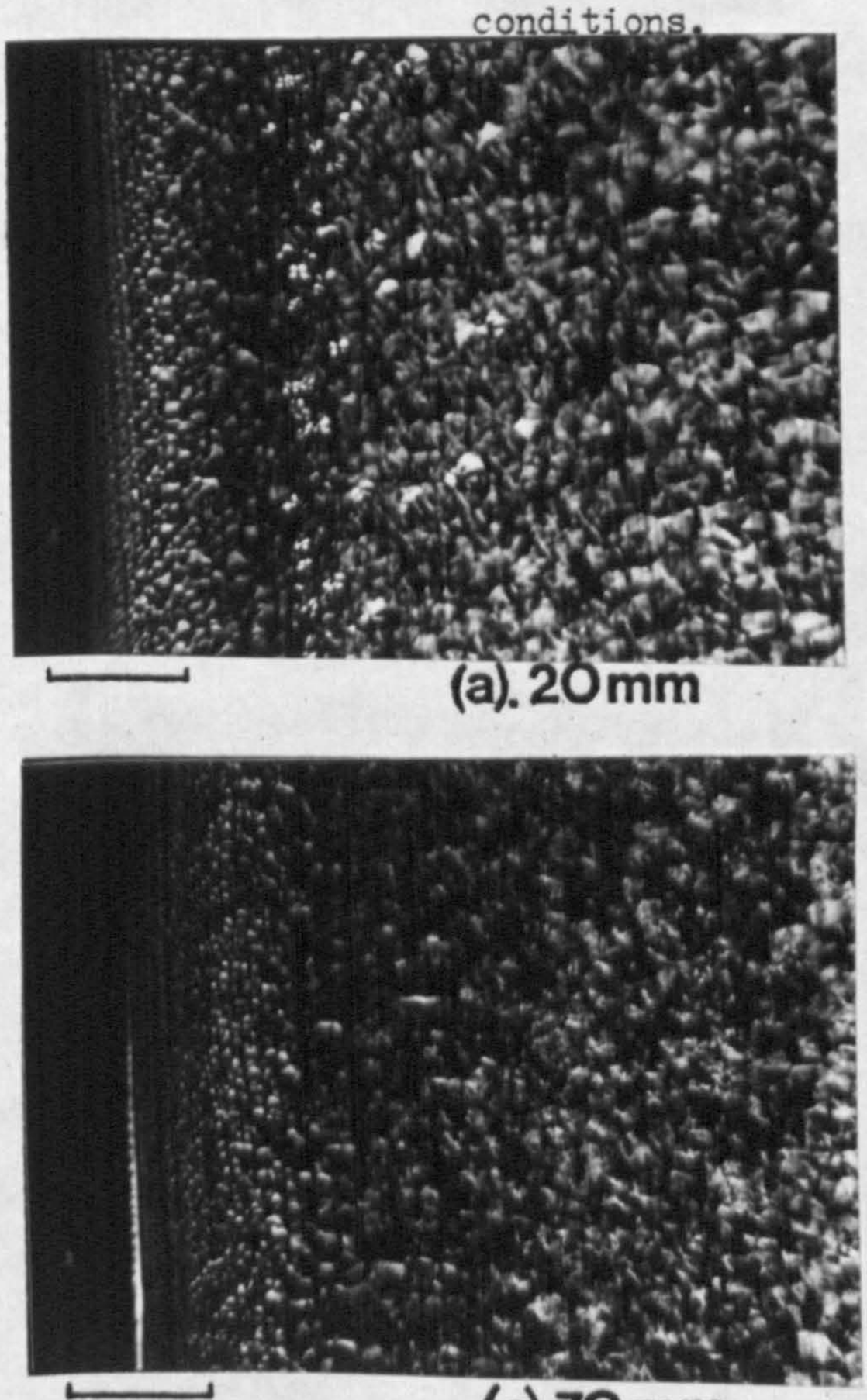

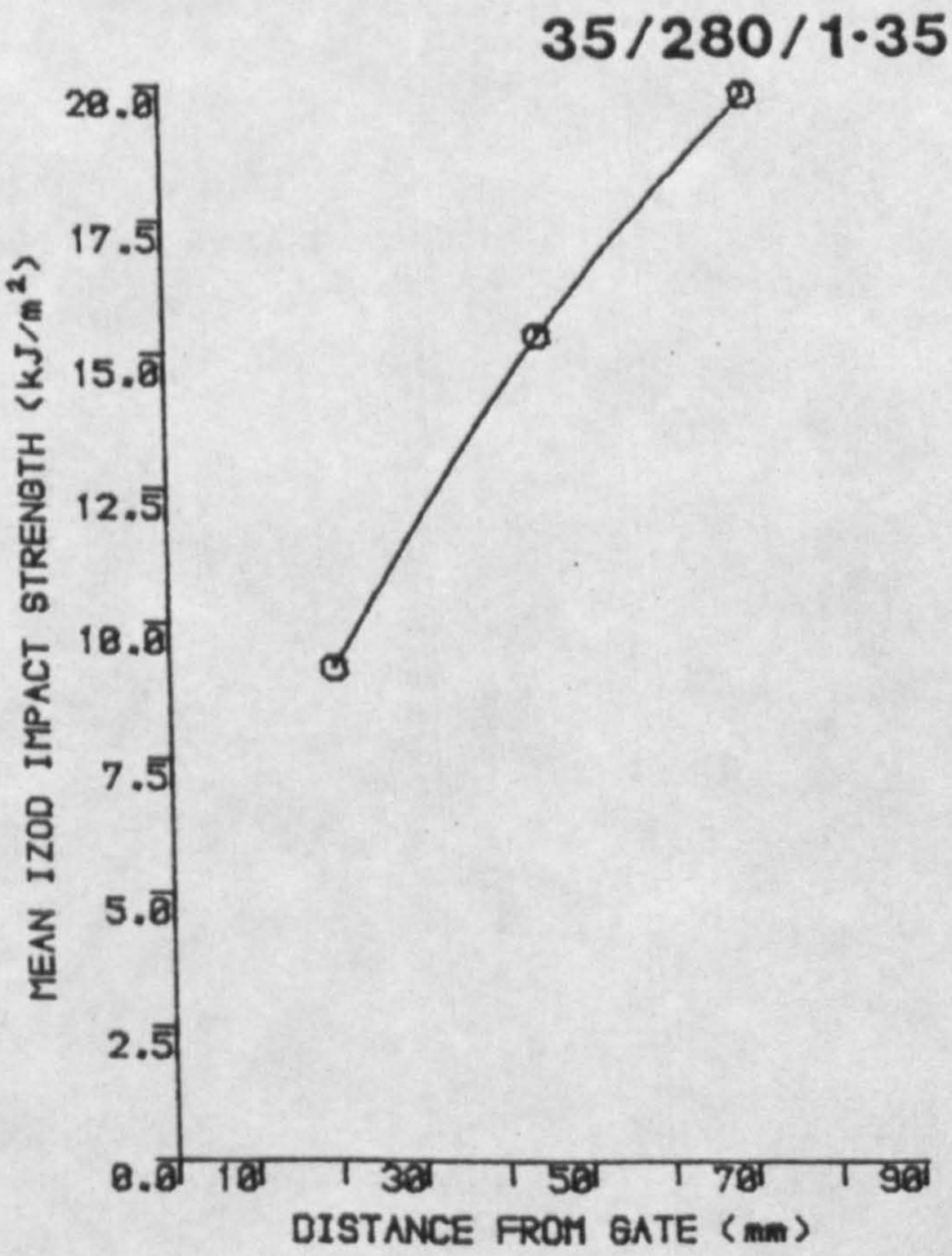

Figure 49

Presentation of Izod impact strength data and selected area micrographs for 35/280/4.00 moulding conditions.

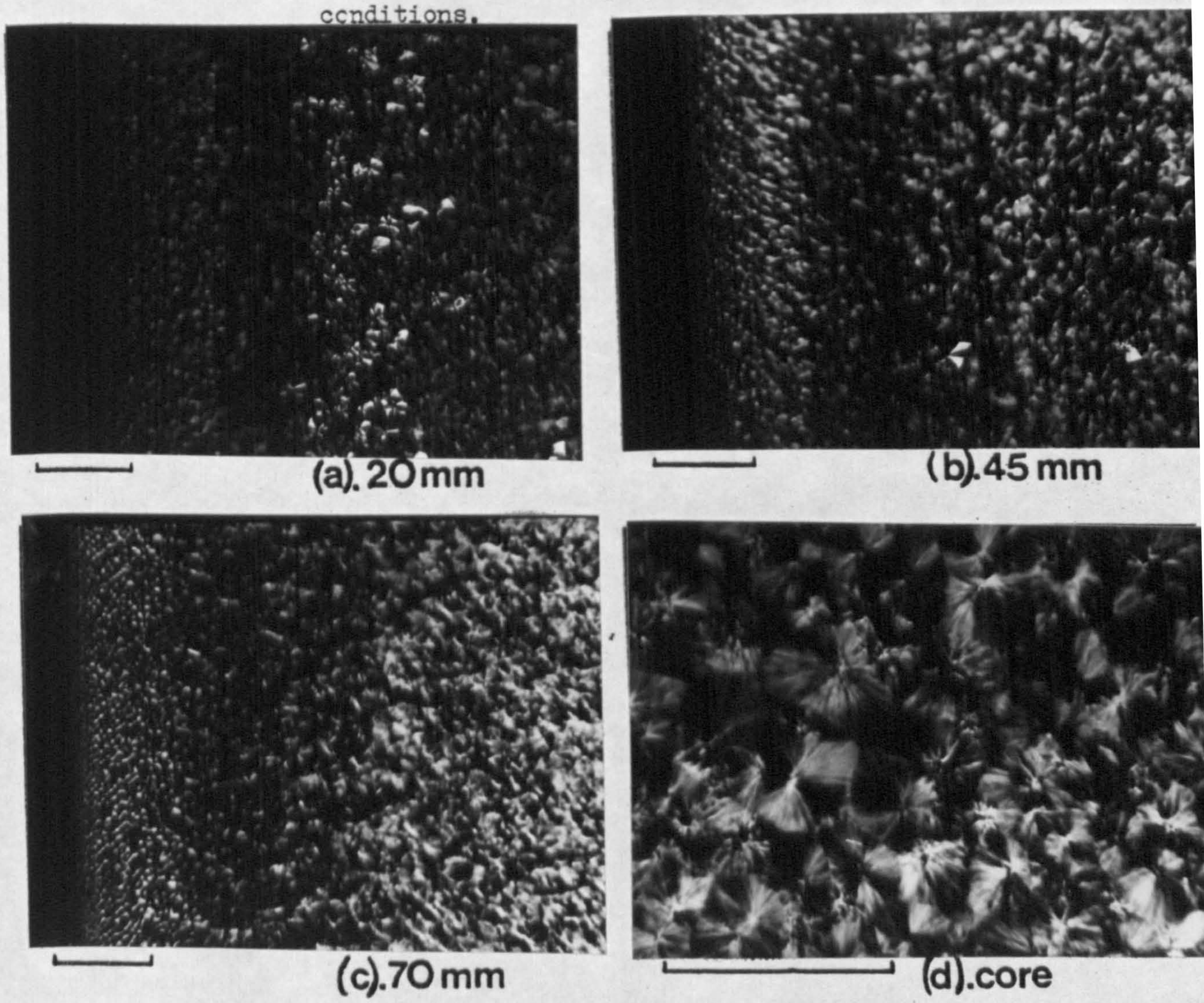

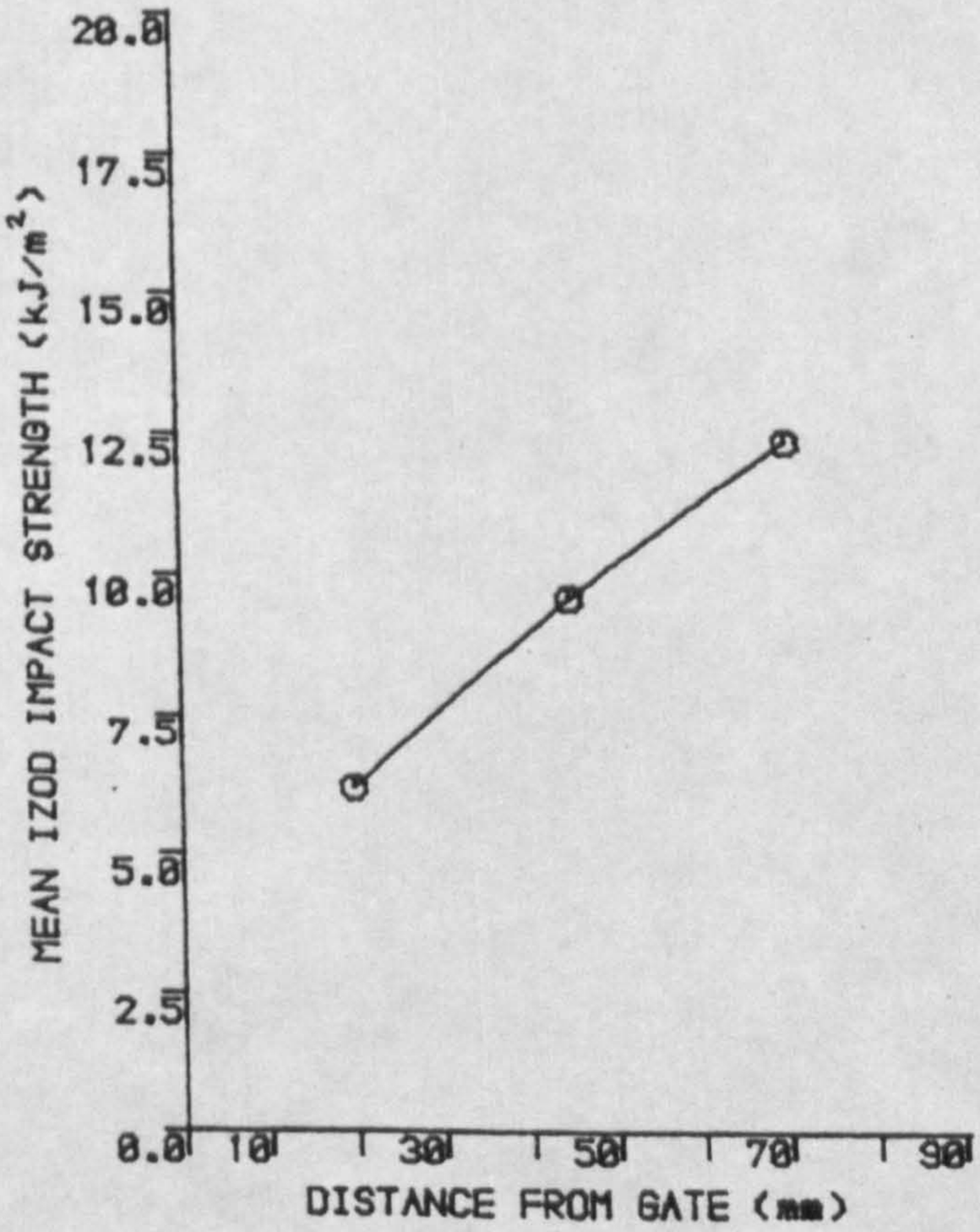

Figure 50

Presentation of Izod impact strength data and selected area micrographs for 80/220/1.35 moulding conditions.

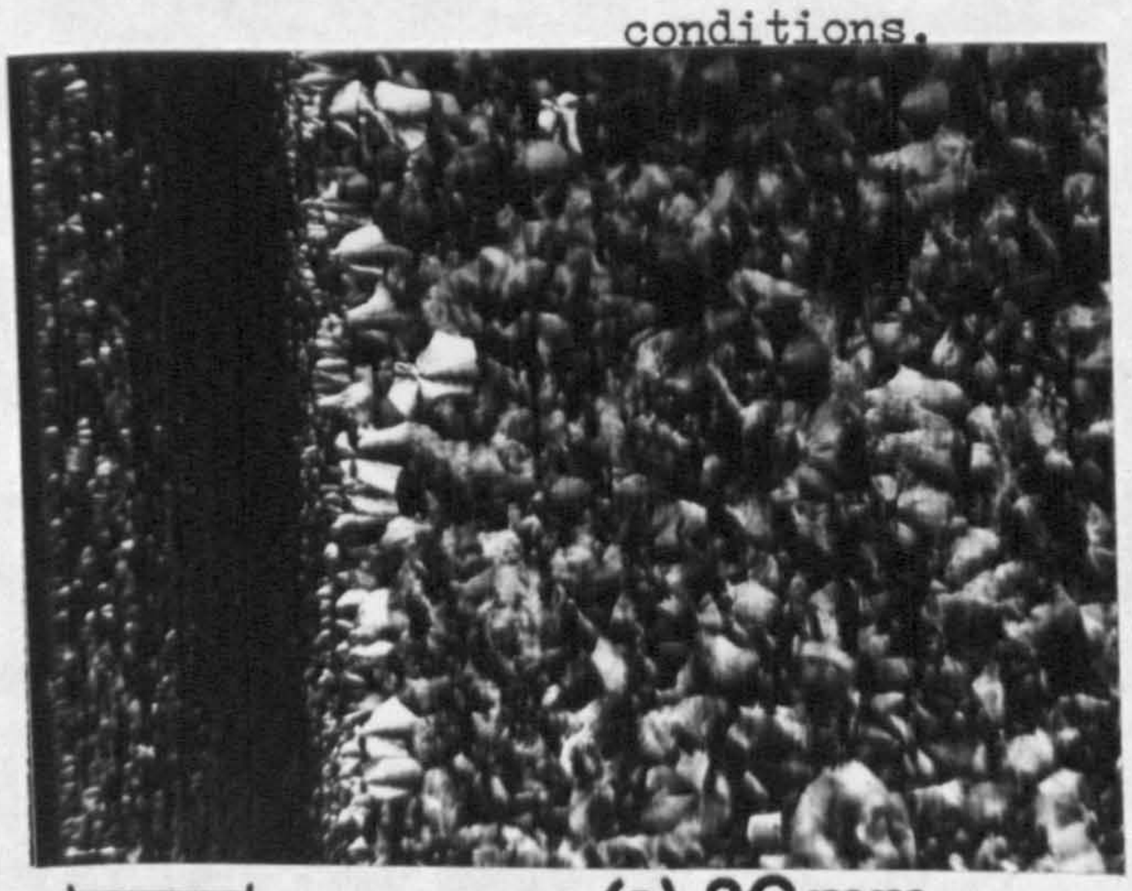

(a). 20 mm

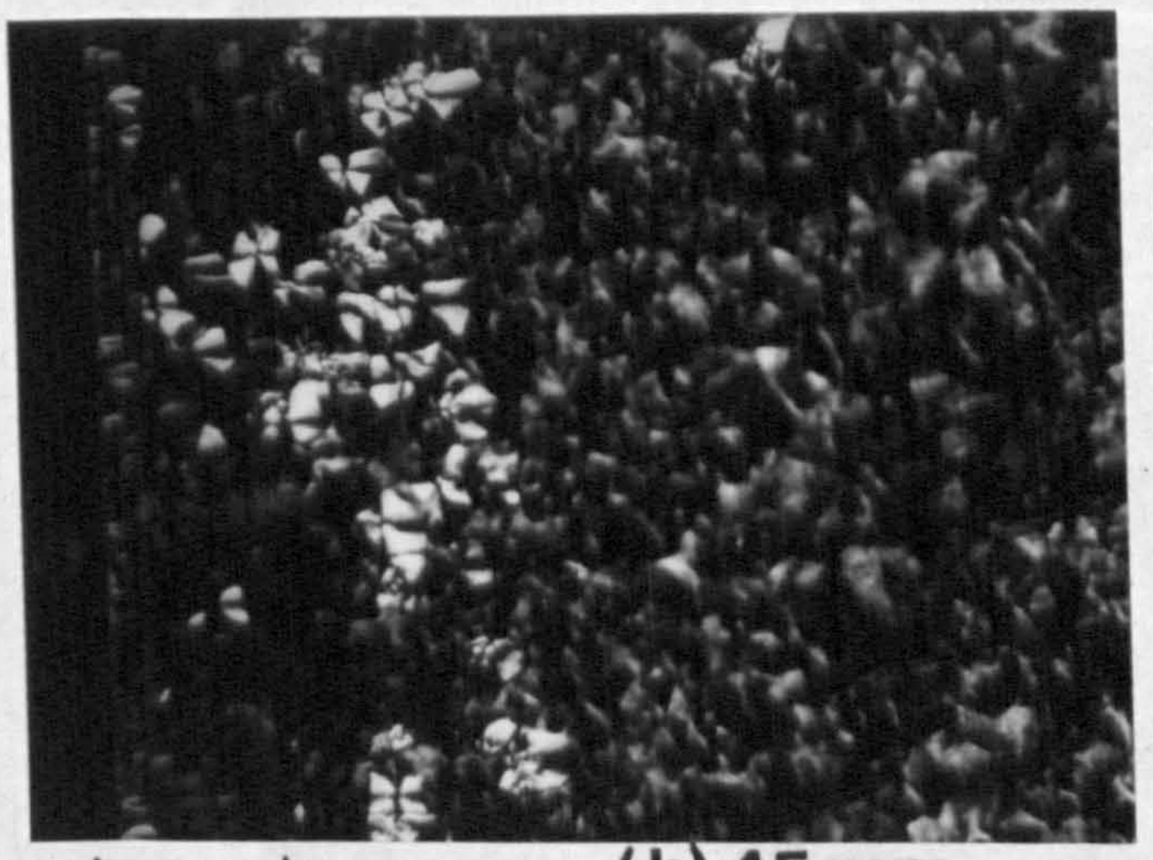

(b). 45 mm

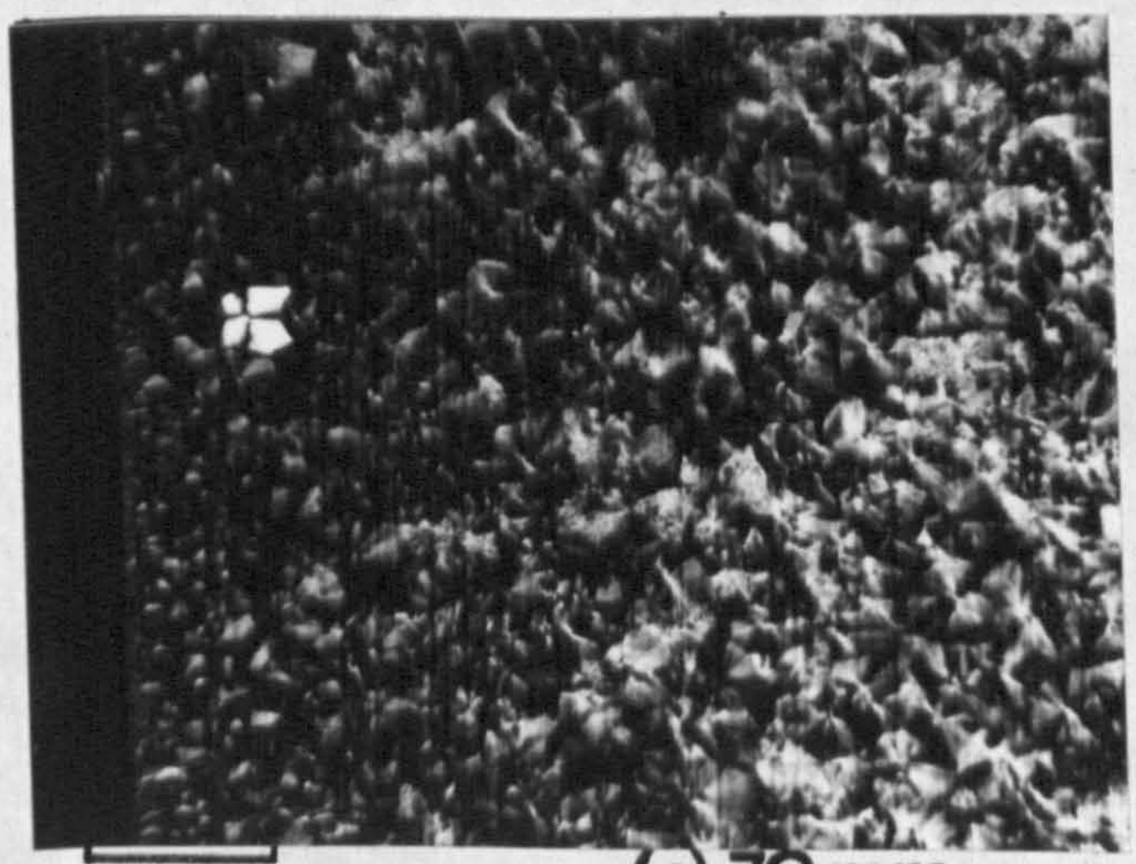

(c). 70 mm

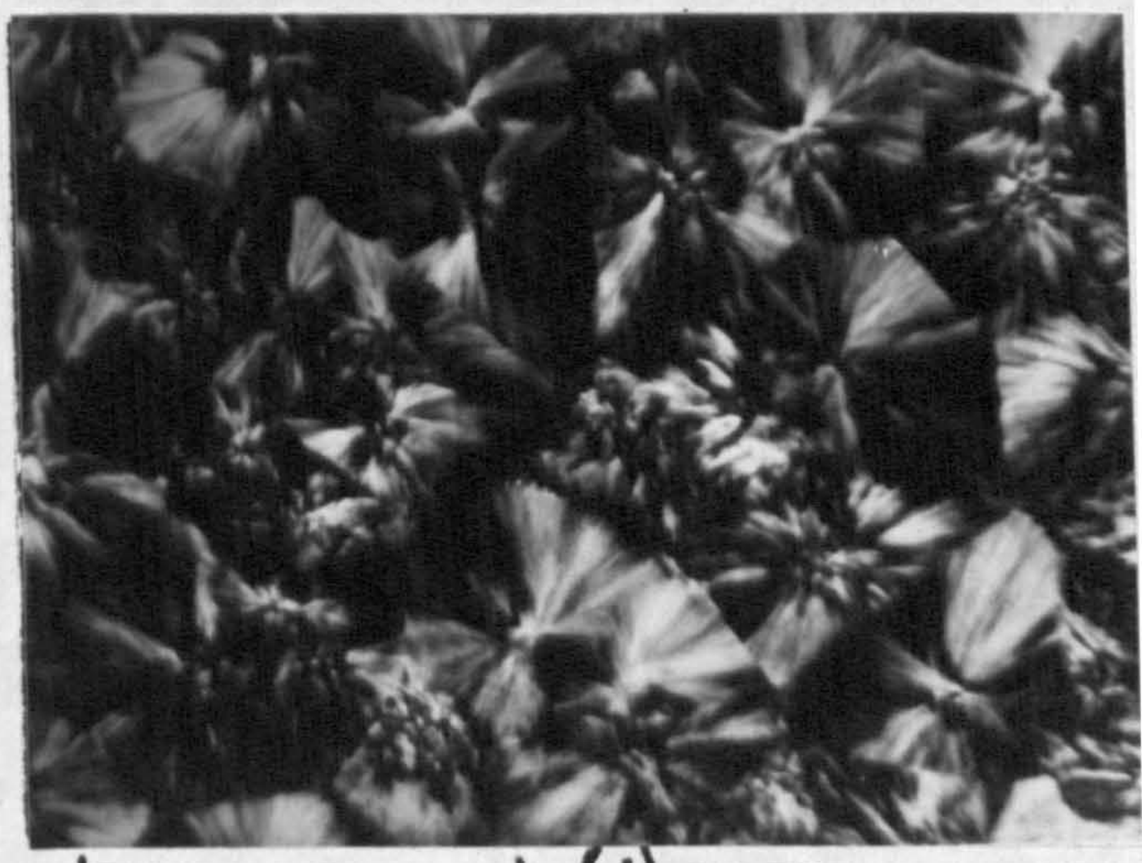

(d). core

Scale bars = 100 μm

80/220/1·35

Figure 51

Presentation of Izod impact strength data and selected area micrographs for 80/280/1.35 moulding conditions.

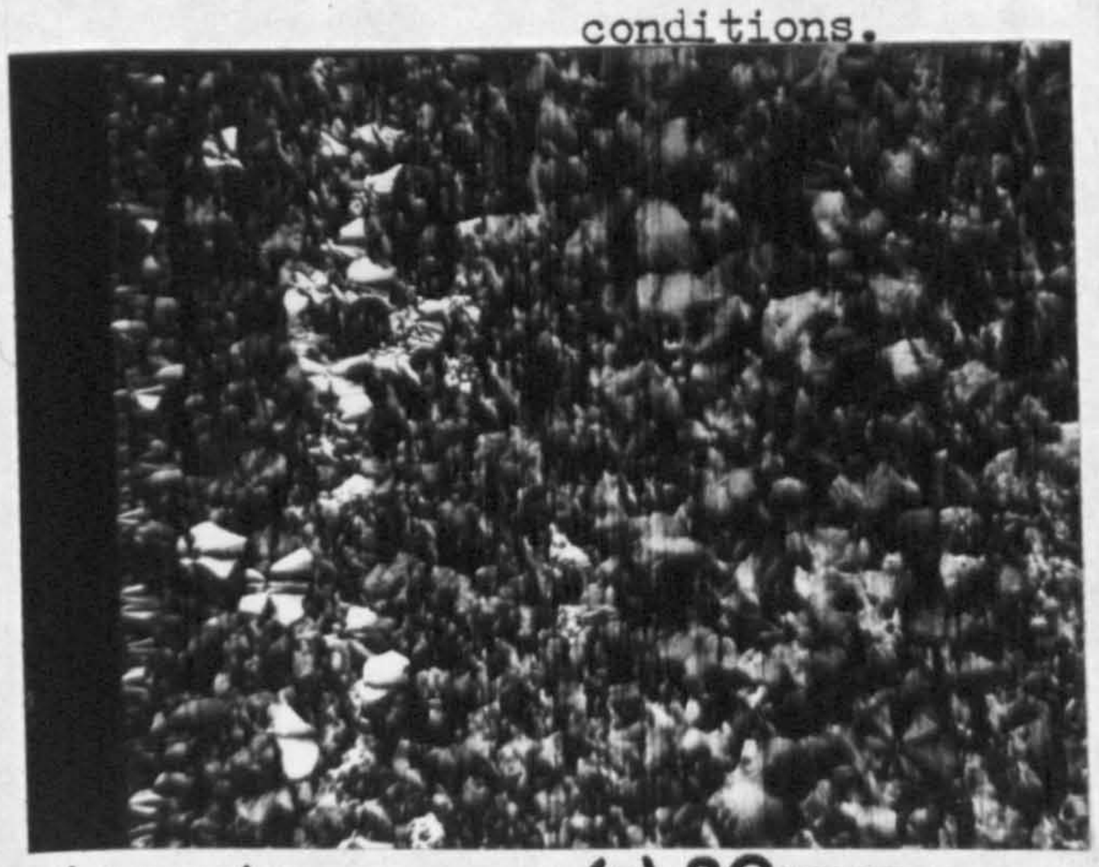

(a). 20 mm

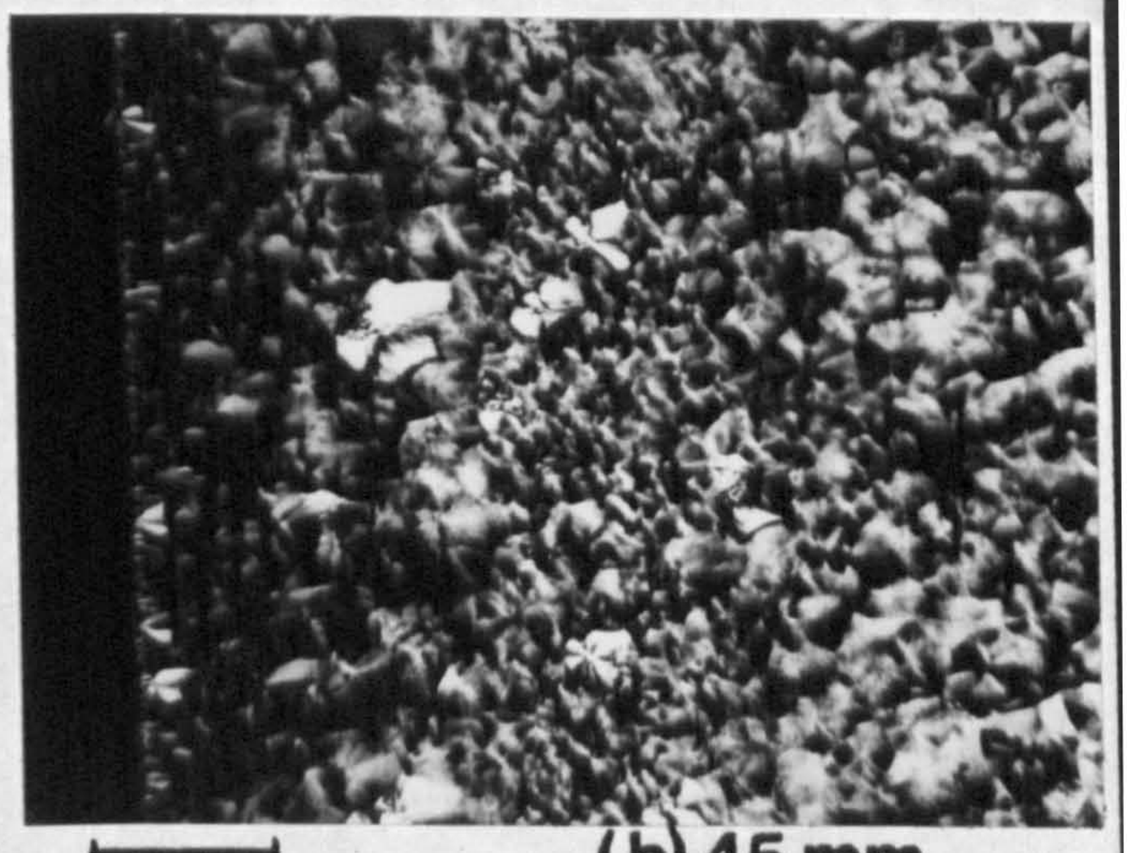

(b). 45 mm

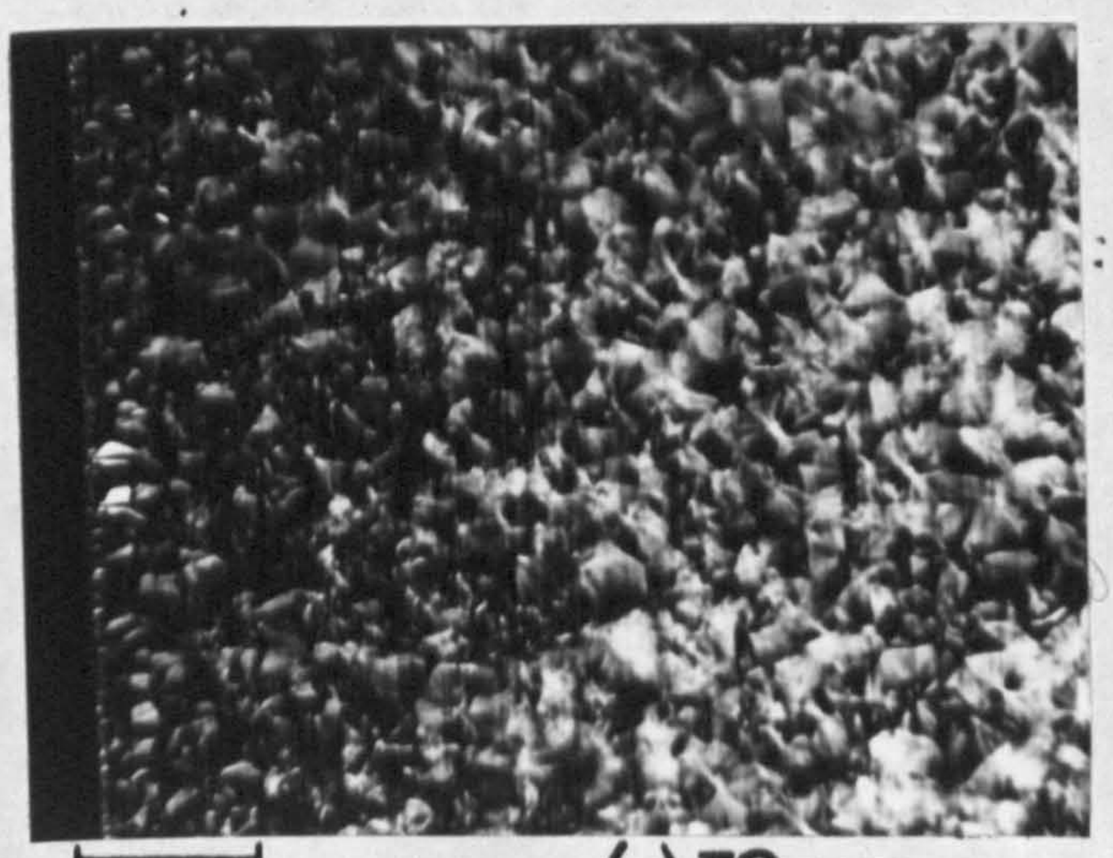

(c). 70 mm

(d). core

Scale bars = 100 μm

80/280/1·35

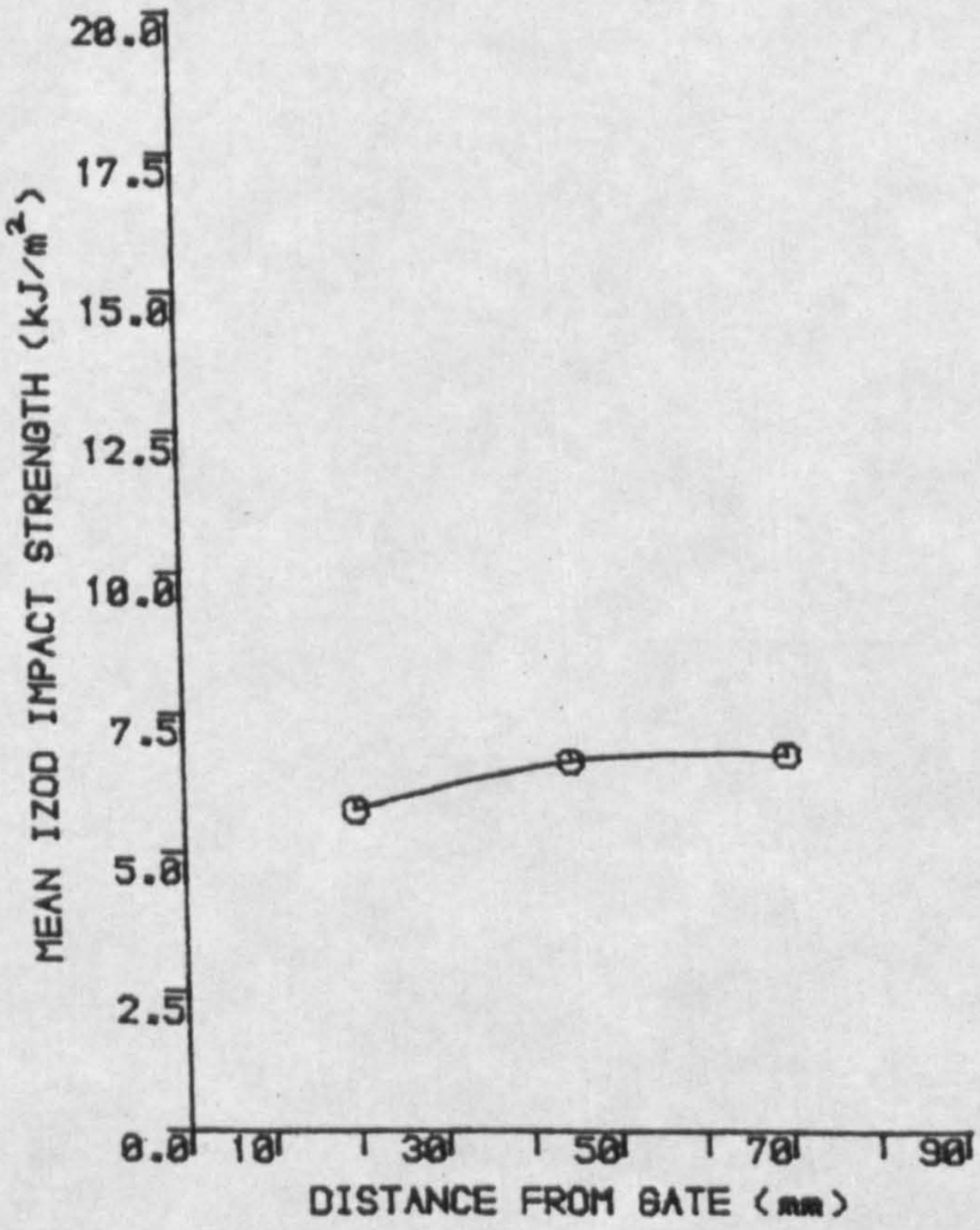

Figure 52

Presentation of Izod impact strength data and selected area micrographs for 80/280/4.00 moulding conditions.

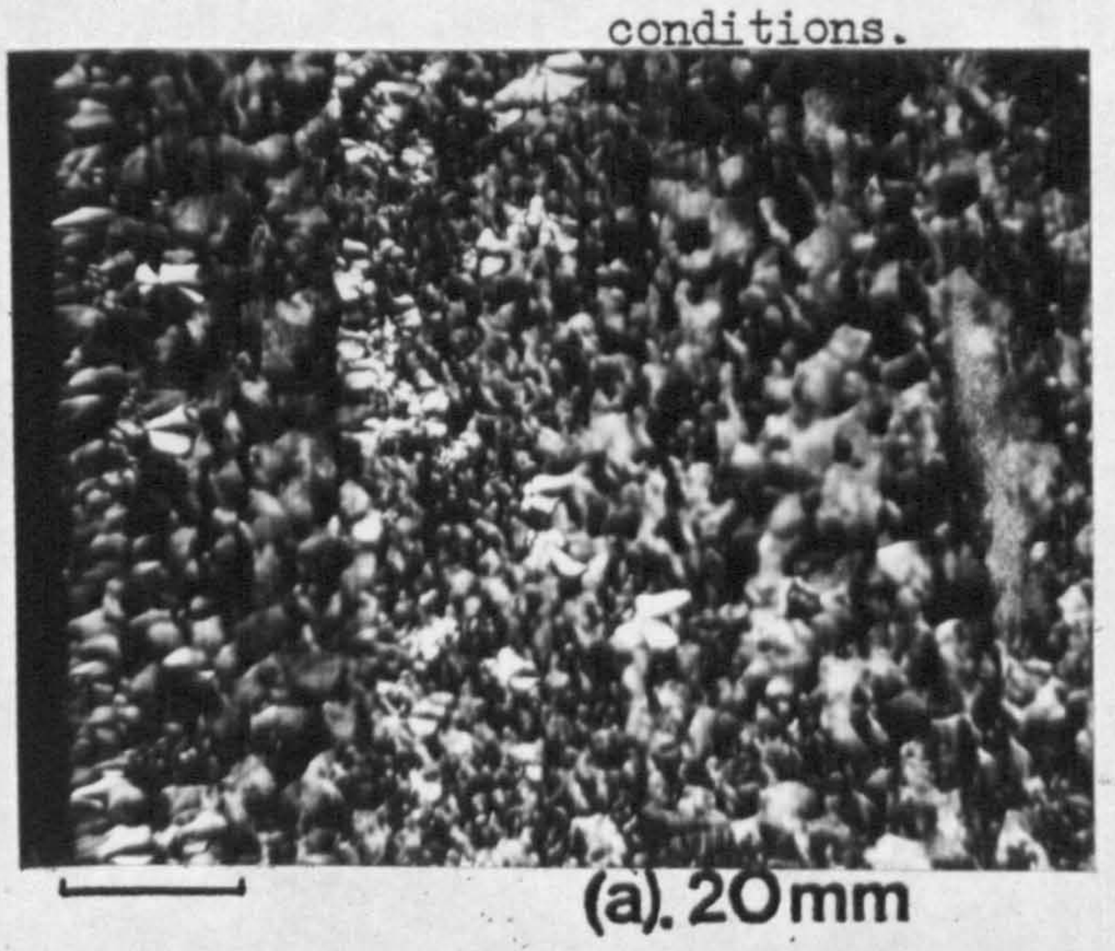

(a). 20 mm

(b). 45 mm

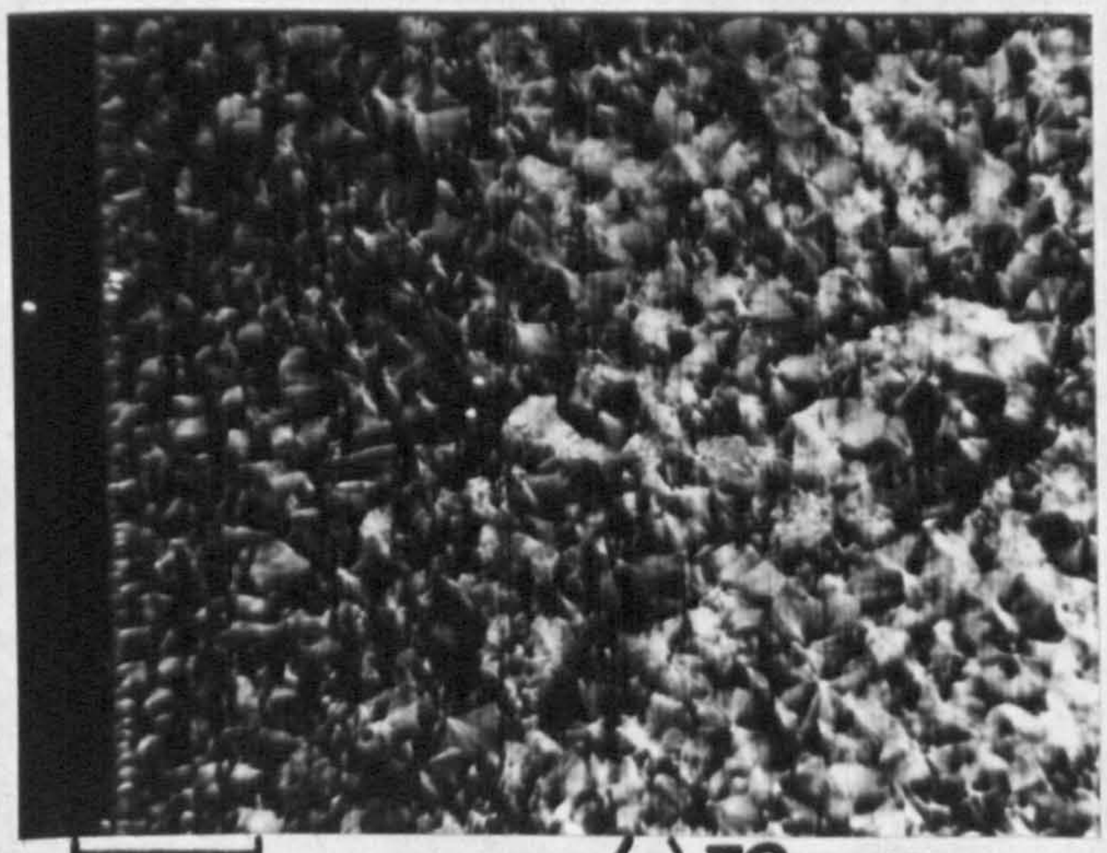

(c). 70 mm

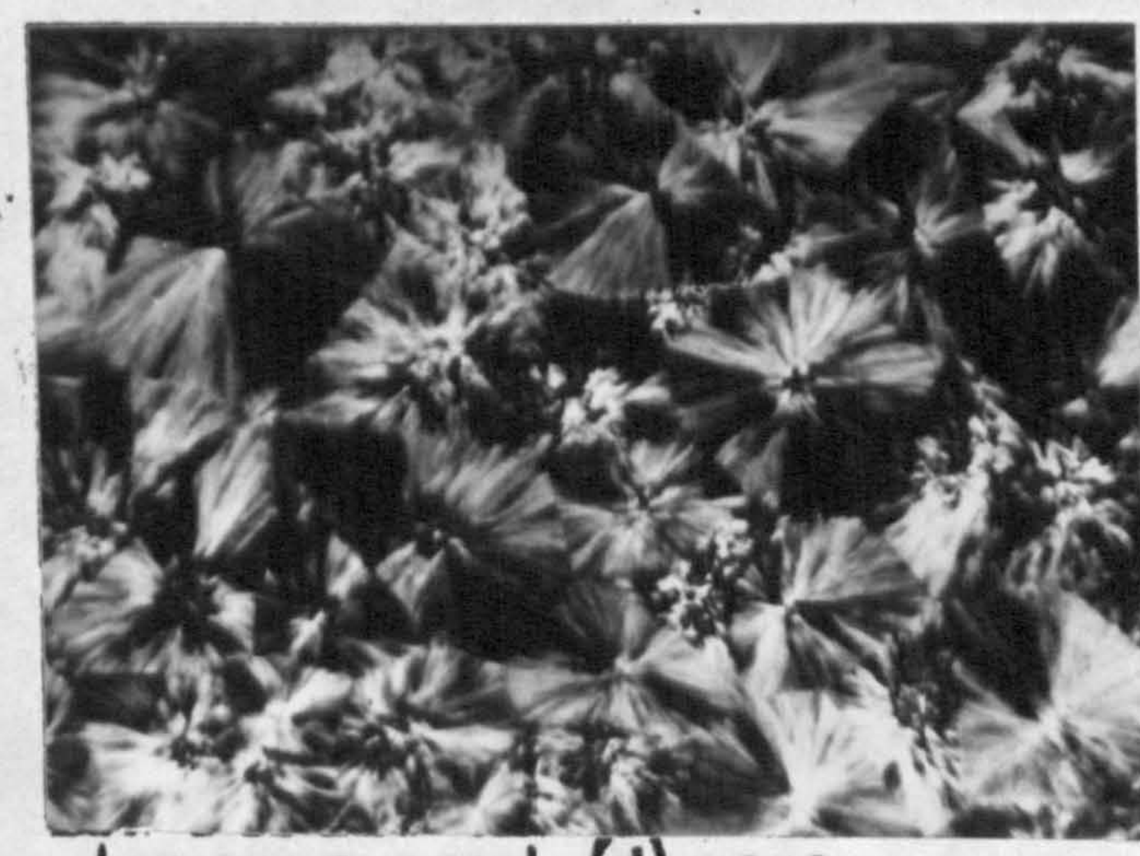

(d). core.

Scale bars = 100 μm

80/280/4·00

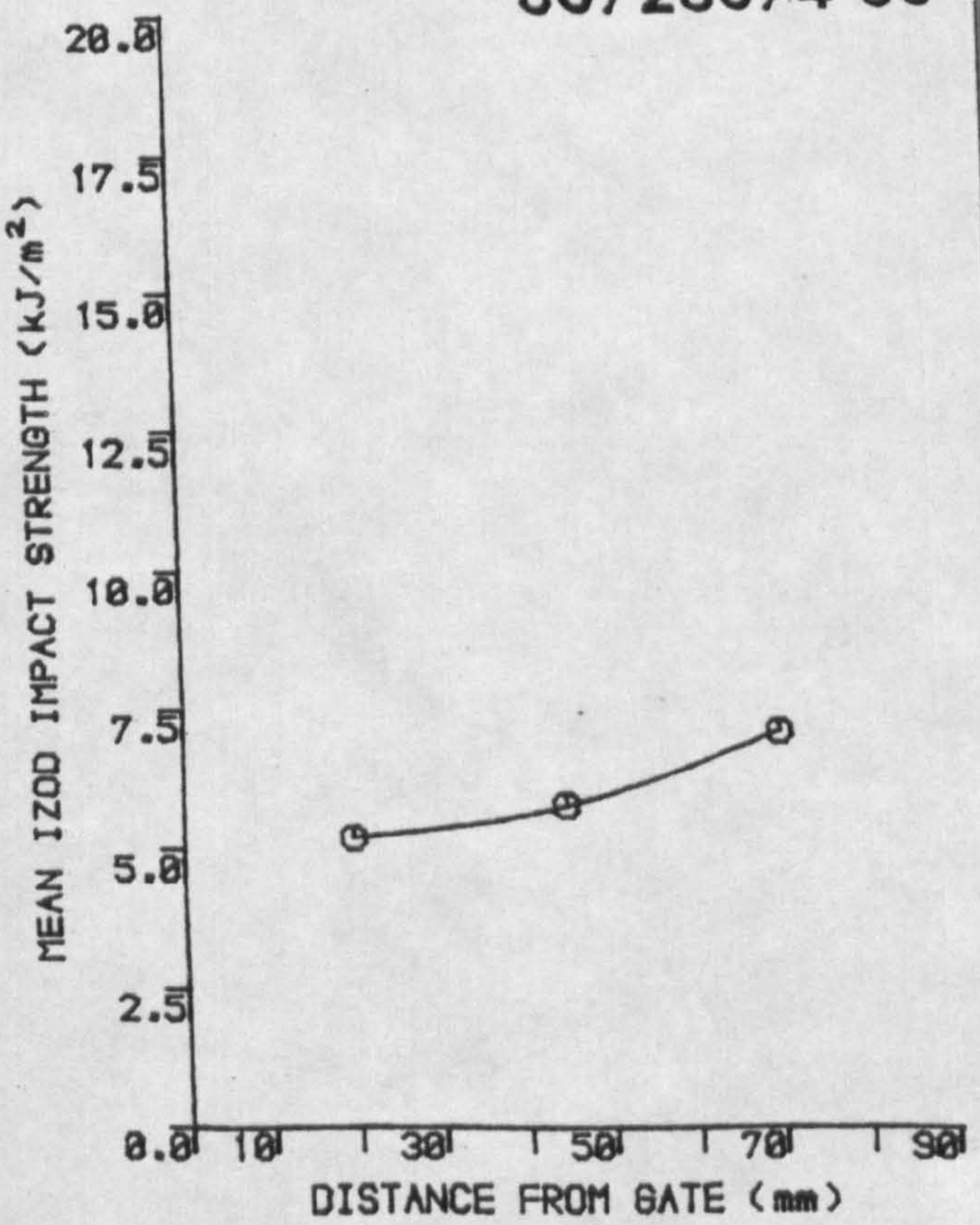

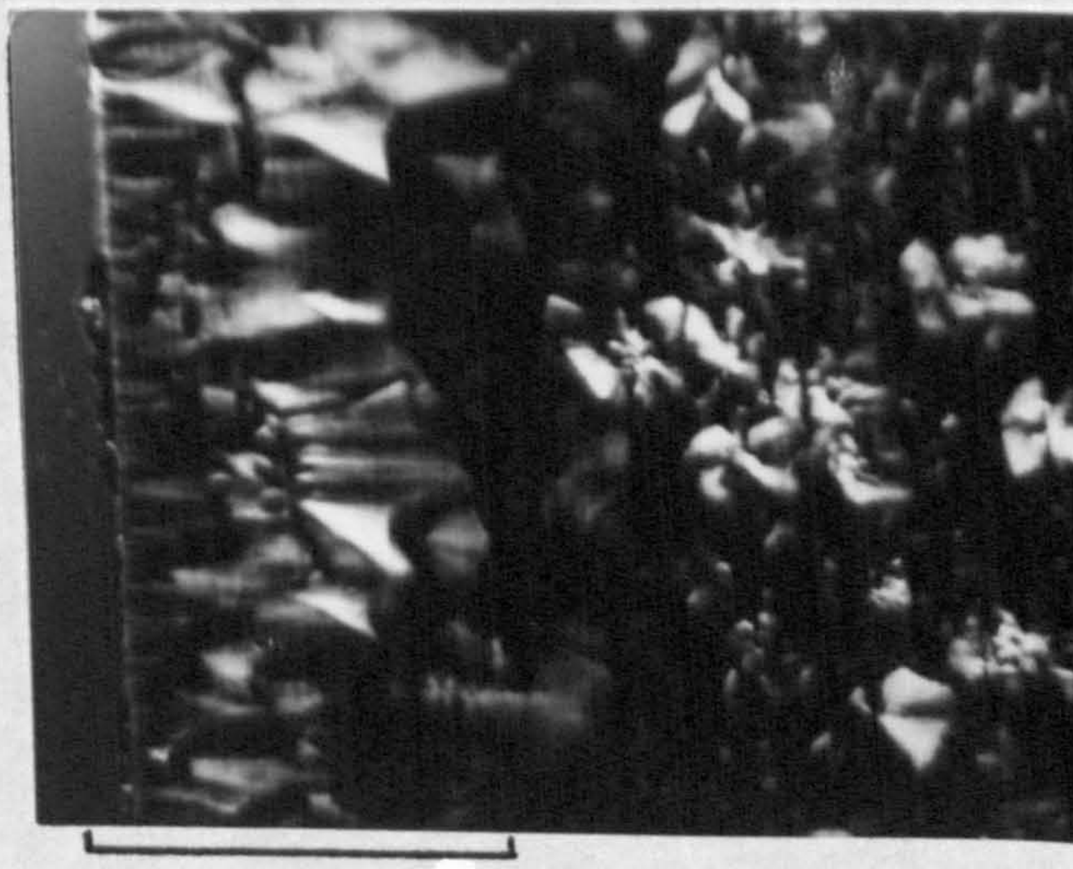

(e). Transcrystalline surface.

(i) The validity of results for 12 x 3 x 3 mm test bars was established by showing that dial readings and computer calculated results were in excellent agreement (better than 94% in each individual test). There are therefore no significant 'hidden' energy losses to be accounted for.

(ii) It was found in almost every case that a plot of energy absorbed vs. distance squared is linear almost up to the point of failure. We therefore conclude that most energy is absorbed by elastic bending of the beam and that only a small additional energy is absorbed during crack propagation, after the linear portion of the curve.

(iii) All samples failed in an essentially brittle manner. However, a distinct toughening effect was observed with distance along the flow direction for every moulding condition.

(iv) High melt temperature mouldings gave much higher impact strengths close to the gate than those moulded at low melt temperatures.

(v) High mould temperature mouldings exhibited inferior impact properties with little improvement with position of sample relative to the flow direction.

(vi) Little effect of injection velocity on impact properties of moulded plaques was noted. However, a slight improvement in centre of moulding impact strength was noticed with increasing cavity fill time.

(vii) The most marked improvement in impact strength with distance along the flow direction was observed when a combination of low mould temperature, low melt temperature and fast cavity filling were used to product iPP plaques i.e. those conditions that give maximum shear and preferred molecular orientation.

Fig. 48
BEST:
35|280|1.35

(viii) No significant variation in effective modulus E/d^2 was observed with changes in processing conditions or position of test piece, relative to the gate of injection moulded iPP plaques.

3.2.1.3 A More Detailed Systematic Impact Test Analysis of Selected Mouldings

A more detailed investigation was required to establish whether the increase from low to high impact properties with distance from the gate is a gradual or sharp transition. For this reason, samples that exhibited this trend in properties were selected i.e. plaques moulded with low mould temperatures and fast injection times. The plaques (35/220/1.35 and 35/280/1.35) were sectioned along their flow direction to give 26 (3 x 3 x 12mm) test pieces which were impact tested in the same manner as before, the impact test results are given in Table 15 and illustrated graphically in Figure 53. The following observations were made:-

(i) Mouldings produced using a low melt temperature (220°C) revealed a steady increase in impact strength up to approximately 49 mm along the flow path, whereupon a transition from 8 kJm^{-2} to 15 kJm^{-2} occurred over some 6 mm further along the flow path. The impact strength in the remaining 35 mm of flow was found to increase steadily to around 17.5 kJm^{-2} before dropping down to 13 kJm^{-2} at the extreme end of the moulding.

(ii) In contrast, a moulding produced using a high melt temperature (280°C) revealed a steady increase in impact strength upto 8kJm^{-2} at 38 mm from the gate, whereupon an improvement to 15kJm^{-2} occurred within the space of about 10 mm. The impact properties remained at around 15kJm^{-2} for a further 35 mm along the flow path eventually increasing to a maximum of about 19kJm^{-2} at the far side of the moulding.

TABLE 15 Results from the systematic Izod impact test analysis of Daniels injection mouldings.

DISTANCE FROM GATE (mm)	35/220/1.35 I.S (kJm-2)	35/280/1.35 I.S (kJm-2)
0.0- 3.0	2.53	2.67
3.5- 6.5	3.78	4.03
7.0-10.0	3.23	4.25
10.5-13.5	3.40	4.46
14.5-17.0	3.29	6.23
17.5-20.5	4.39	8.81
21.0-24.0	4.62	7.89
24.5-27.5	5.08	7.64
28.0-31.0	4.18	8.34
31.5-34.5	5.13	7.87
35.0-38.0	5.59	8.54
38.5-41.5	7.14	10.73
42.5-45.0	8.54	13.17
45.5-48.0	8.17	12.89
49.0-52.0	13.53	15.07
52.5-55.5	14.17	14.75
56.0-59.0	15.18	14.54
59.5-62.5	16.22	16.65
63.0-66.0	16.69	15.84
66.5-69.5	17.17	15.87
70.0-73.0	17.40	17.05
75.0-76.5	17.63	18.22
77.0-80.0	16.61	18.05
80.5-83.5	14.04	15.84
84.0-87.0	13.36	19.39
87.5-90.0	13.30	18.76

Figure 53 Variation of Izod impact strength with distance from the gate for Daniels iPP mouldings produced at 220°C and 280°C melt temperatures.

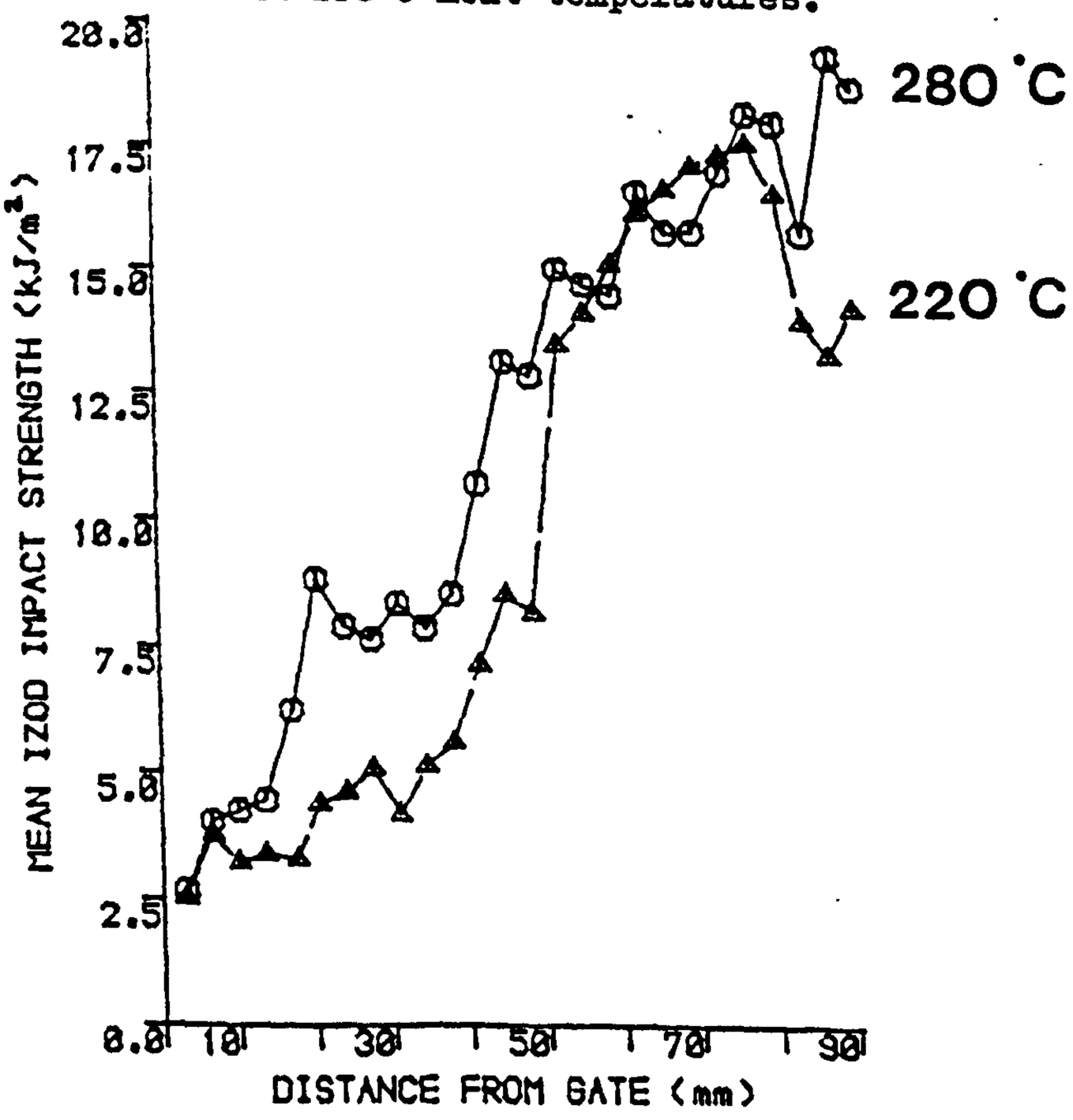

3.2.2 Instrumented Drop-Weight Impact Testing Of Daniels Injection Moulded iPP Plaques

In order to provide a realistic assessment of directional weakness in the as-moulded plaques, prepared over the range of conditions specified, the Daventest Rosand Instrumented drop-weight impact test machine was used in accordance with the procedure given in Section 2.4.3. The centre of plaque impact test results are summarized in Table 16, providing mean first peak energy, mean final energy, and mean first peak force data of five circular plaques from each processing condition. A bar chart representation of mean first peak energy versus moulding condition is given in Figure 54.

3.2.2.1 Analysis of Impact Curves

From the force/distance and energy/distance^2 curves plotted, typically illustrated in Figure 55, the following observations were made:-

(i) The force/time curves were complicated by shock wave effects, so that one cannot necessarily attribute each serration to a major cracking event.

(ii) An intermediate stage of reduced rigitity following the initial peak was observed in every test followed by several significant broad energy absorption peaks.

(iii) The peaks following the initial one correspond to an energy which can be upto 16 times greater than that associated with the first peak value, and approaches the total energy for the complete event.

(iv) The first peak on the force/distance curves corresponds to the energy required to initiate major cracks i.e. the energy required to bend the samples beyond their elastic limit as shown in the energy/distance^2 curves. A drop in energy absorption accompanies the reduced rigidity of plaques as they crack and this is shown on

TABLE 16 Instrumented drop-weight impact test results for Daniels injection mouldings.

MOULDING CONDITIONS MOULD (°C)	MELT (°C)	FILL (secs)		PEAK ENERGY (Nm) $\bar{x}$	s.d	FINAL ENERGY (Nm) $\bar{x}$	s.d	PEAK FORCE (N) $\bar{x}$	s.d
35	220	1.35	A	0.536	0.187	3.592	0.348	534.39	74.88
80	220	1.35	B	0.190	0.069	2.998	0.810	342.78	55.38
35	220	4.00	C	0.654	0.216	4.382	0.364	574.22	84.27
80	280	1.35	D	0.262	0.028	2.693	0.699	398.97	15.37
80	280	4.00	E	0.271	0.009	2.330	0.216	406.27	5.55
35	280	1.35	F	0.763	0.591	5.096	1.408	608.58	218.46
35	280	4.00	G	0.310	0.077	4.714	0.338	416.42	52.12

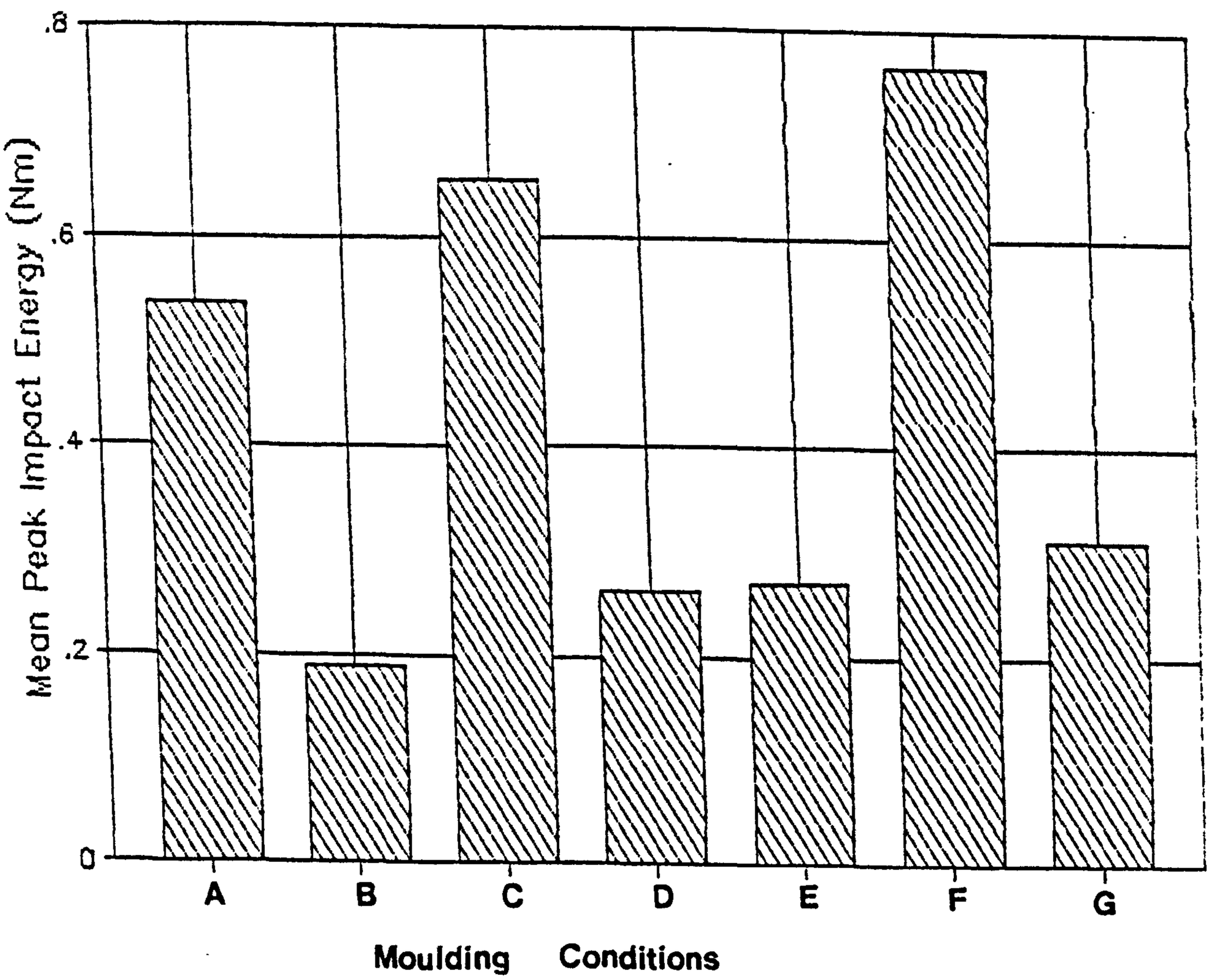

Figure 54 Bar chart representation of mean first peak drop-weight impact energy versus moulding condition.

MATERIAL CODE MM161C SAMPLE DETAILS GXM43 80/280/1.35

DATE 12/03/84 TEMP 23 DEG C IMPACT VELOCITY 3 M/S

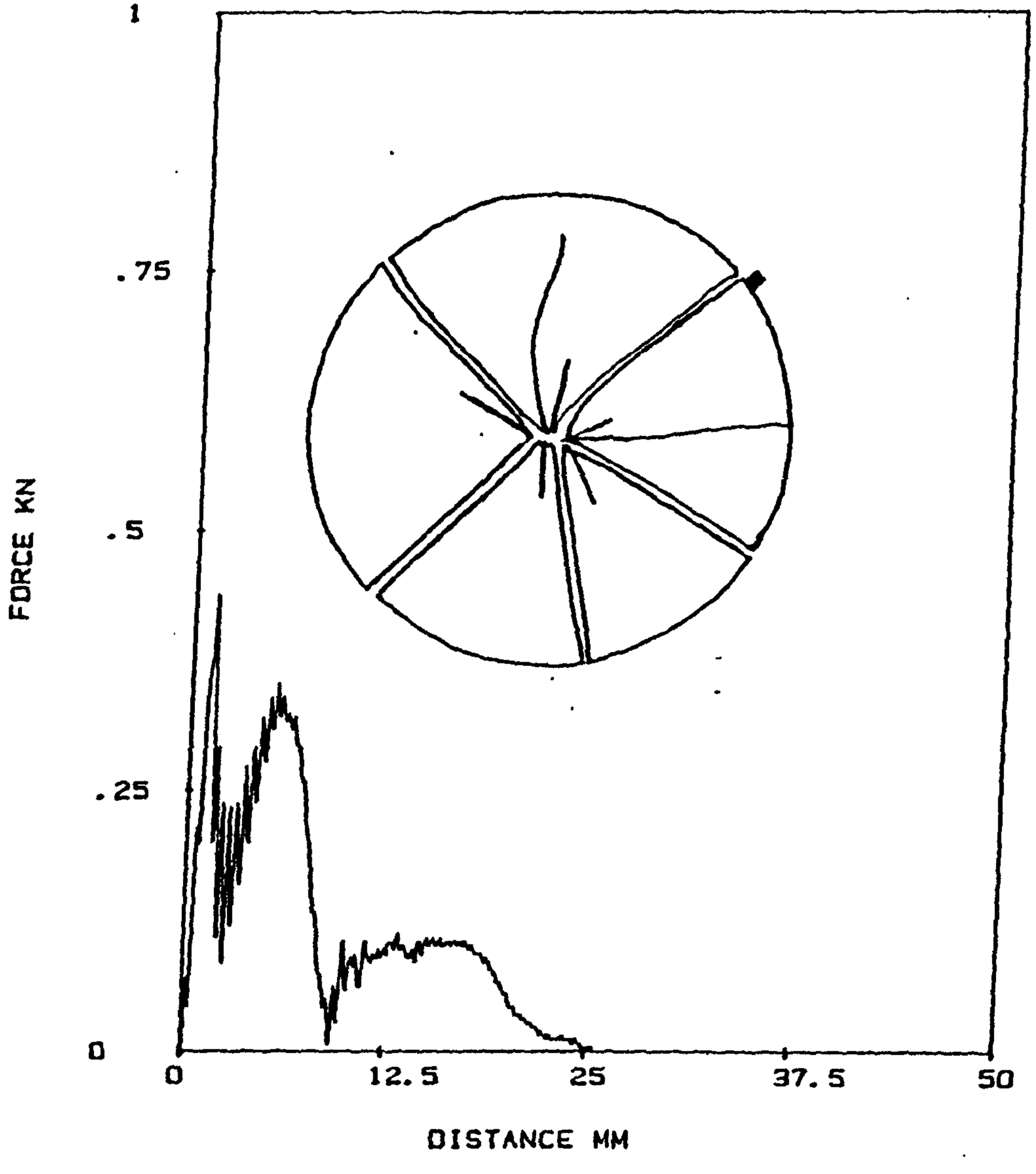

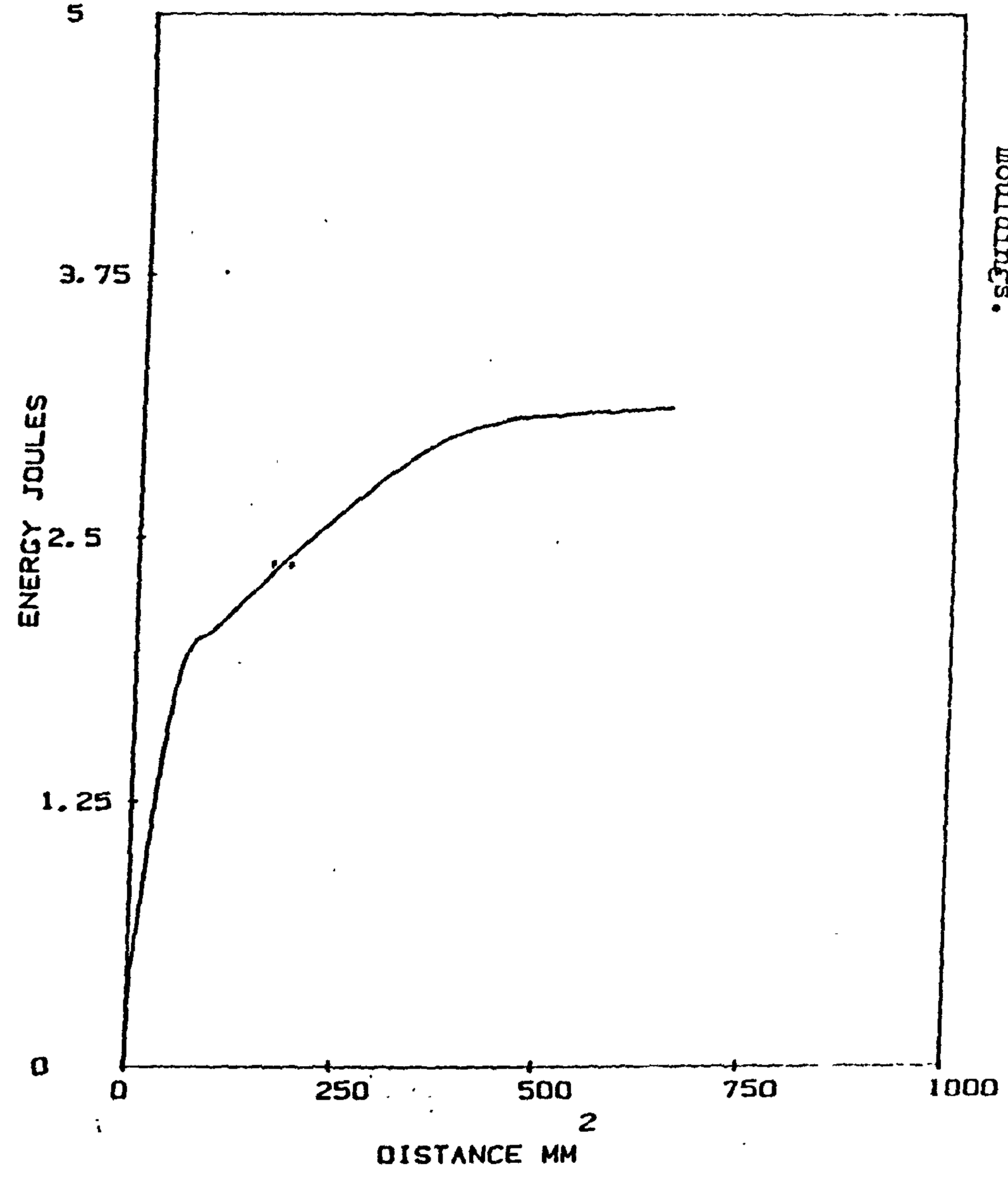

Figure 55

Typical force/distance and energy/distance^2 curves from drop-weight impact tests of Daniels iPP mouldings.

the energy/distance^2 curve as a deviation from the initial linear relationship.

(iv) The subsequent peaks on the force/distance curves are associated with the increased energy absorption required to propagate cracks through the lateral dimensions of the plaque.

3.2.2.2 Analysis of Results

An inspection of the broken test plaques to identify the fracture patterns, revealed typically five or six major radial cracks and a number of minor cracks (i.e. which did not travel the extent of the plaque) which varied in number depending on the processing conditions used to mould the plaque. Typically different fracture patterns are presented with the force/distance and energy/distance^2 curves in Figures 56 and 57. A summary of approximate number of major and minor cracks is given in Table 17. There appeared to be more minor cracks as the Peak impact energy increases, this was particularly notable in the case of high melt temperature/low mould temperature mouldings where up to 18 minor cracks were observed.

From this study the directional weakness in mouldings was assessed, it appears that in low melt temperature mouldings a major crack always runs directly through the gate region, it is thought that this is the first crack to propagate. This hypothesis corresponds to an observed weakness in mouldings close to the gate found in Izod testing. In the case of high melt temperature mouldings the directional weakness was not easily assessed but a high proportion of mouldings did show a crack propagating towards the gate region.

MATERIAL CODE MM139C SAMPLE DETAILS GXM43 35/280/1.35

DATE 09/03/84 TEMP 23 DEG C IMPACT VELOCITY 3 M/S

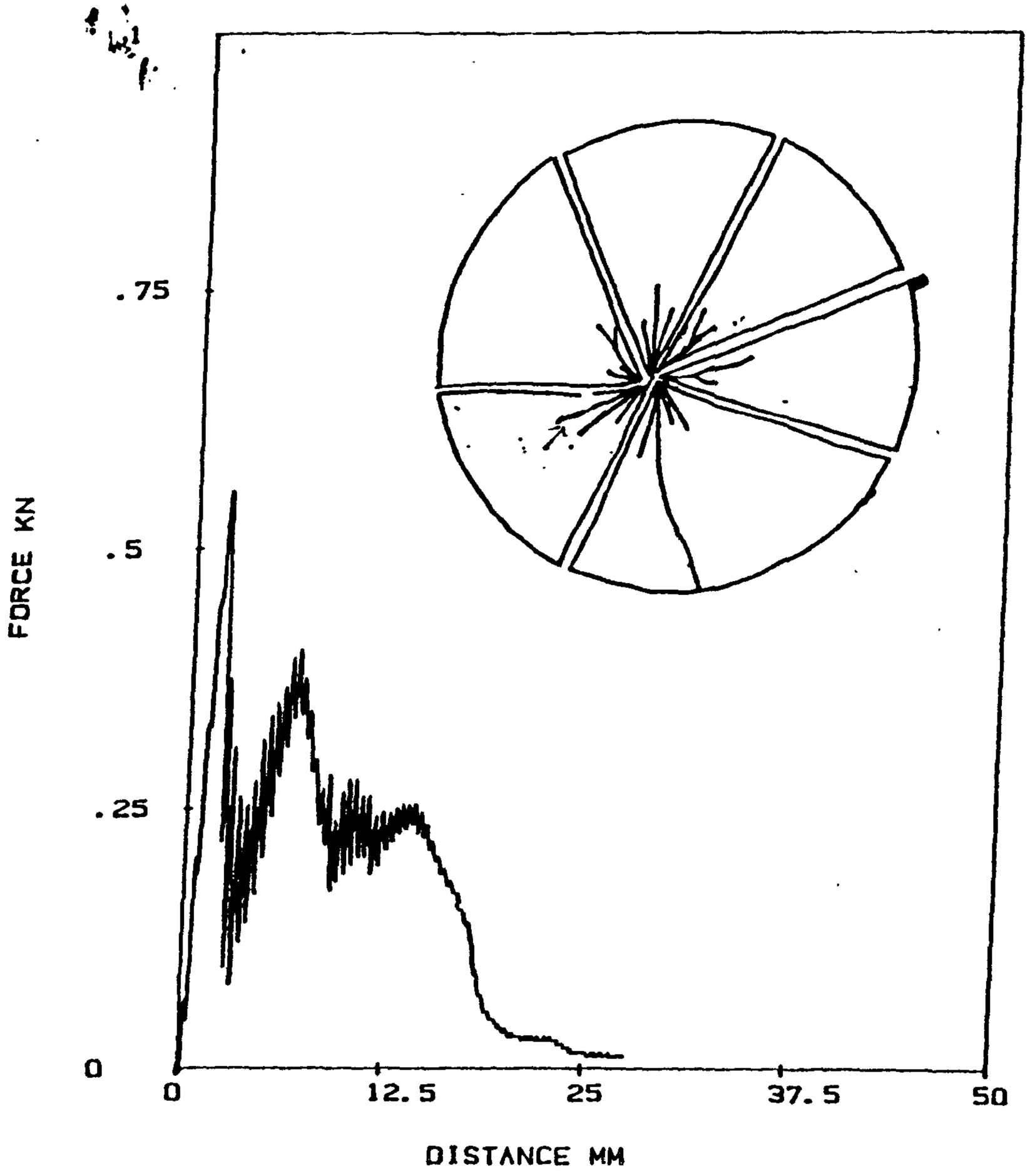

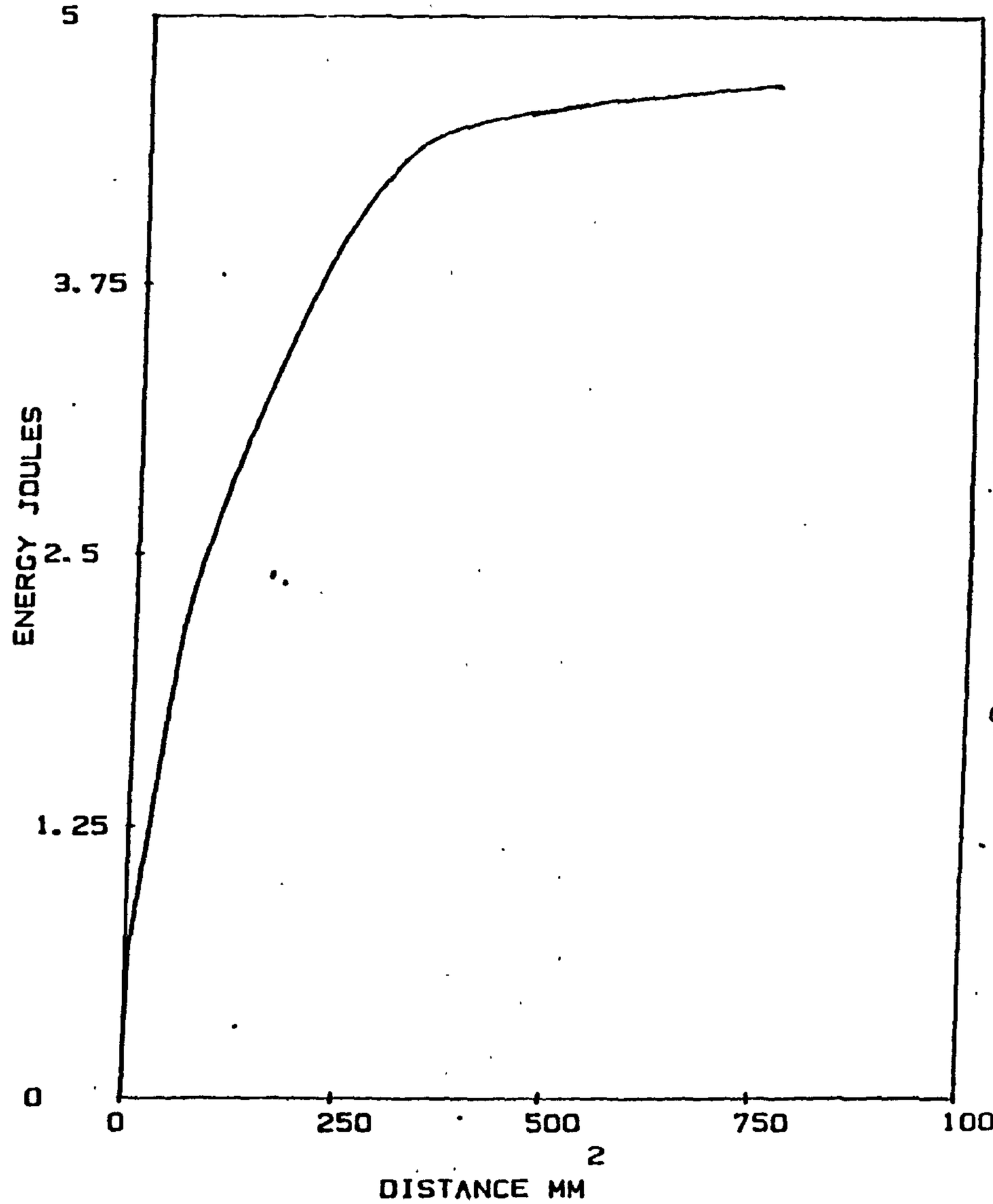

Figure 56

Typical force/distance and energy/distance^2 curve presented with the associated fracture pattern for an 80/280/1.35 iPP moulding.

Figure 57

Typical force/distance and energy/distance² curve presented with the associated fracture pattern for a 35/280/1.35 iPP moulding.

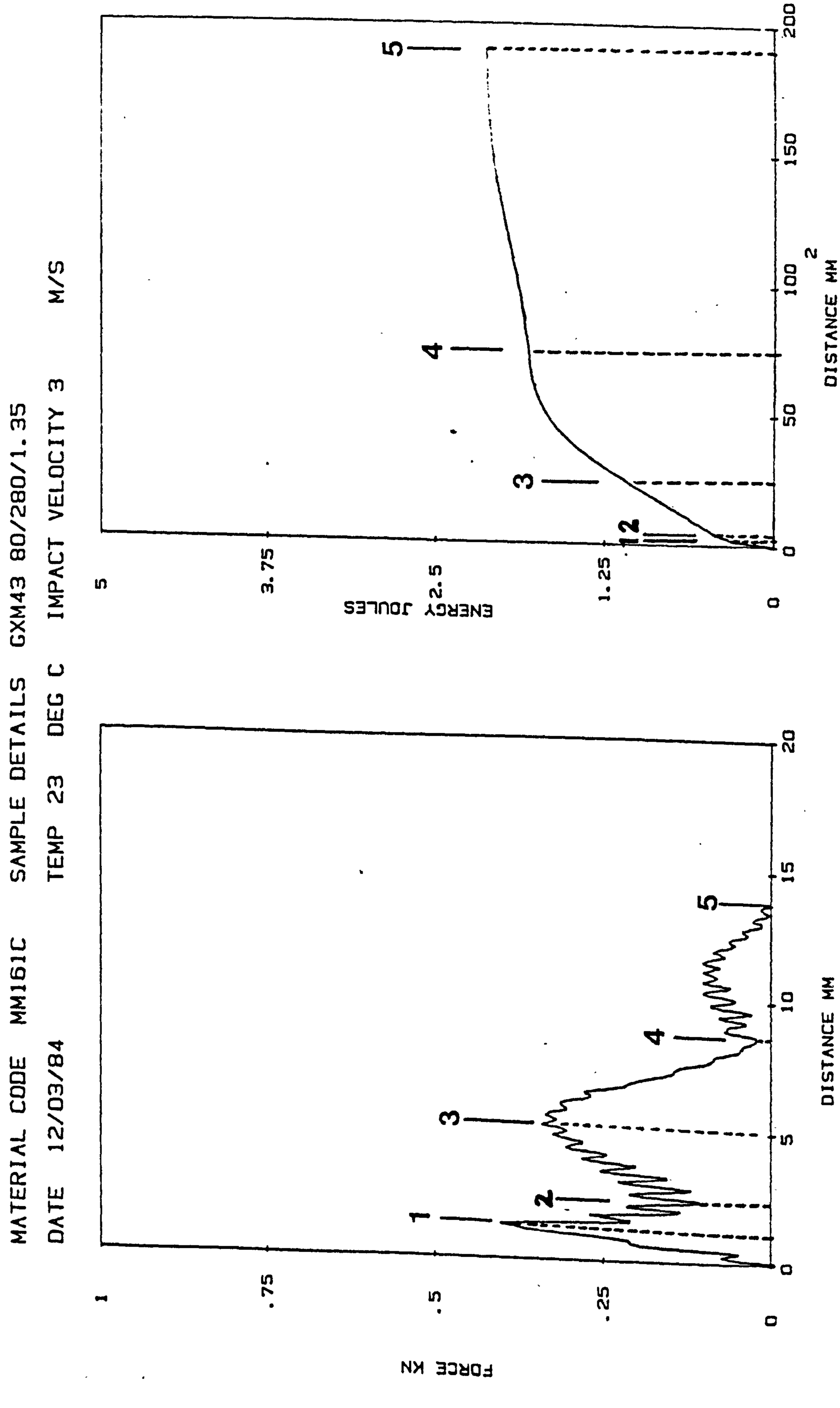

Figure 58 A fracture pattern sometimes found for high melt temperature/low mould temperature iPP mouldings.

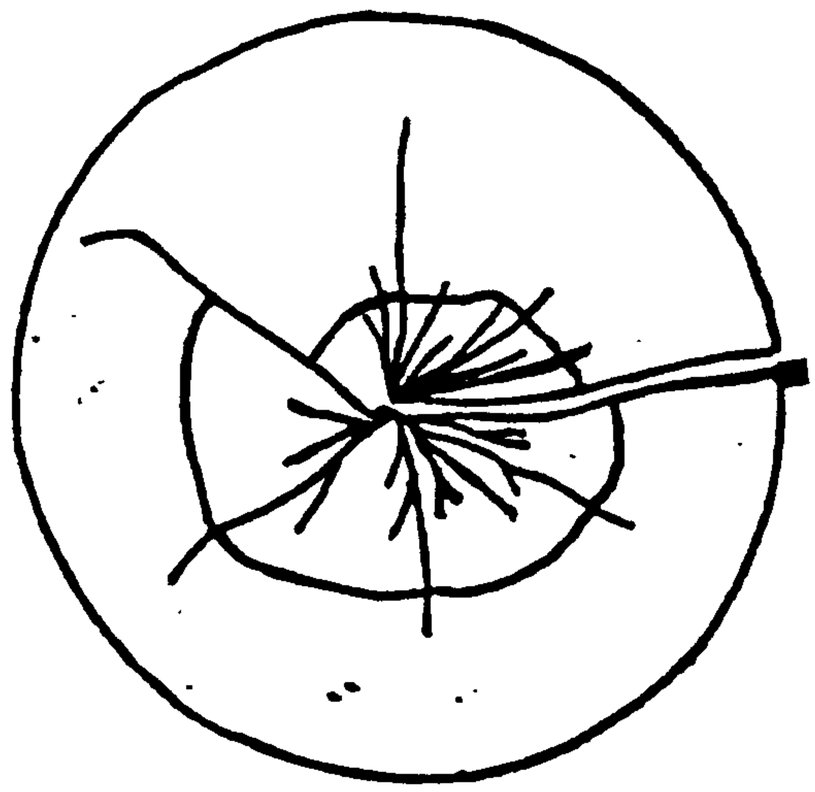

TABLE 17 Results of a fracture pattern analysis of Daniels drop-weight impact tested plaques.

MOULDING CONDITIONS MOULD (°C)	MELT (°C)	FILL (secs)	NUMBER OF MINOR CRACKS	NUMBER OF MAJOR CRACKS
35	220	1.35	9	6
80	220	1.35	5	5
35	220	4.00	10	5
35	280	1.35	18	6
35	280	4.00	10	5
80	280	1.35	5	5
80	280	4.00	7	5

TABLE 18 Instrumented Izod impact test results for Sandretto mouldings.

MOULDING CONDITIONS MOULD (°C)	MELT (°C)	FILL (%)	I.S 20 mm (kJm^{-2}) $\bar{x}$	s.d	I.S 40 mm (kJm^{-2}) $\bar{x}$	s.d	I.S 70 mm (kJm^{-2}) $\bar{x}$	s.d
30	220	30	4.45	0.79	6.64	0.81	13.08	5.18
30	250	30	8.52	1.50	11.52	0.40	14.92	0.50
30	280	30	11.99	2.30	15.96	0.26	16.67	0.68
50	220	30	4.25	0.57	4.39	0.72	9.45	0.43
70	220	30	4.13	0.83	4.25	0.85	5.63	1.39
30	220	15	4.92	0.65	6.99	0.23	14.62	0.74
30	220	45	4.02	0.43	7.34	0.71	13.05	1.03

Some high melt temperature/low mould temperature mouldings revealed the fracture pattern in Figure 58, in this case only one major crack reached the edge of the disc and it does so very close to the gate supporting the hypothesis.

A good overall agreement was found between Izod and drop-weight impact test results as regards trends in impact properties with variations in moulding parameters. This agreement can be summarized as follows:-

(i) An improvement in impact properties occured with plaques moulded at elevated (280°C) melt temperatures.

(ii) A reduction in impact properties occured with plaques moulded at elevated (80°C) mould temperatures.

(iii) Little effect of injection velocity on the impact properties except when slow injection times/high melt temperatures and low mould temperatures were used to mould plaques which resulted in poor impact properties compared to fast injection times.

3.2.3. Instrumented Izod Impact Testing of Sandretto Injection Mouldings

As with the Daniels injection moulded pin gated plaques selected area test pieces were prepared from Sandretto fan gated mouldings for subsequent Izod impact testing. Initially 5 test pieces from 20mm, 40mm (centre) and 70 mm along the flow direction respectively were tested for each processing condition. The accelerometer output impact energy readings were converted to impact strength values with knowledge of the cross-sectional area of each test piece and the mean and standard deviation of the impact strengths for each moulding condition are given in Table 18.

From the results presented in Table 18 the mean Izod impact strength versus distance from gate curves were plotted to show

the effect of melt temperature,mould temperature and injection velocity on the impact strength at selected areas along the flow direction. These curves are presented in Figures 59 to 61. The following observations were made from these results:-

(i) The impact strength increases with distance along the flow direction for all mouldings. The degree of improvement is dependent on the processing conditions used to mould the plaques.

(ii) Increasing the melt temperatures during moulding led to plaques with significantly improved impact properties particularly in the gate region.

(iii) Increasing the mould temperatures during moulding led to plaques with inferior impact properties across the entire moulding, with very little improvement with position relative to the gate.

(iv) The effect of increasing injection velocity was to slightly reduce the impact properties of mouldings.

As with the Daniels mouldings the plaques produced with high and low melt temperatures and low mould temperatures were selected for more detailed examination to establish the transition region from low to high impact strength values. The results of this experiment are given in Table 19 and plotted in Figure 62.

From the plot of impact strength versus distance from the gate for high and low melt temperatures shown in Figure 62 it can be seen that a substantial increase in impact strength occurs at 21 mm and 70 mm for the 220^{o}C and 280^{o}C mouldings respectively. A similar observation was made in the case of Daniels mouldings previously reported.

Figure 59 Effect of melt temperature on Izod impact strength.

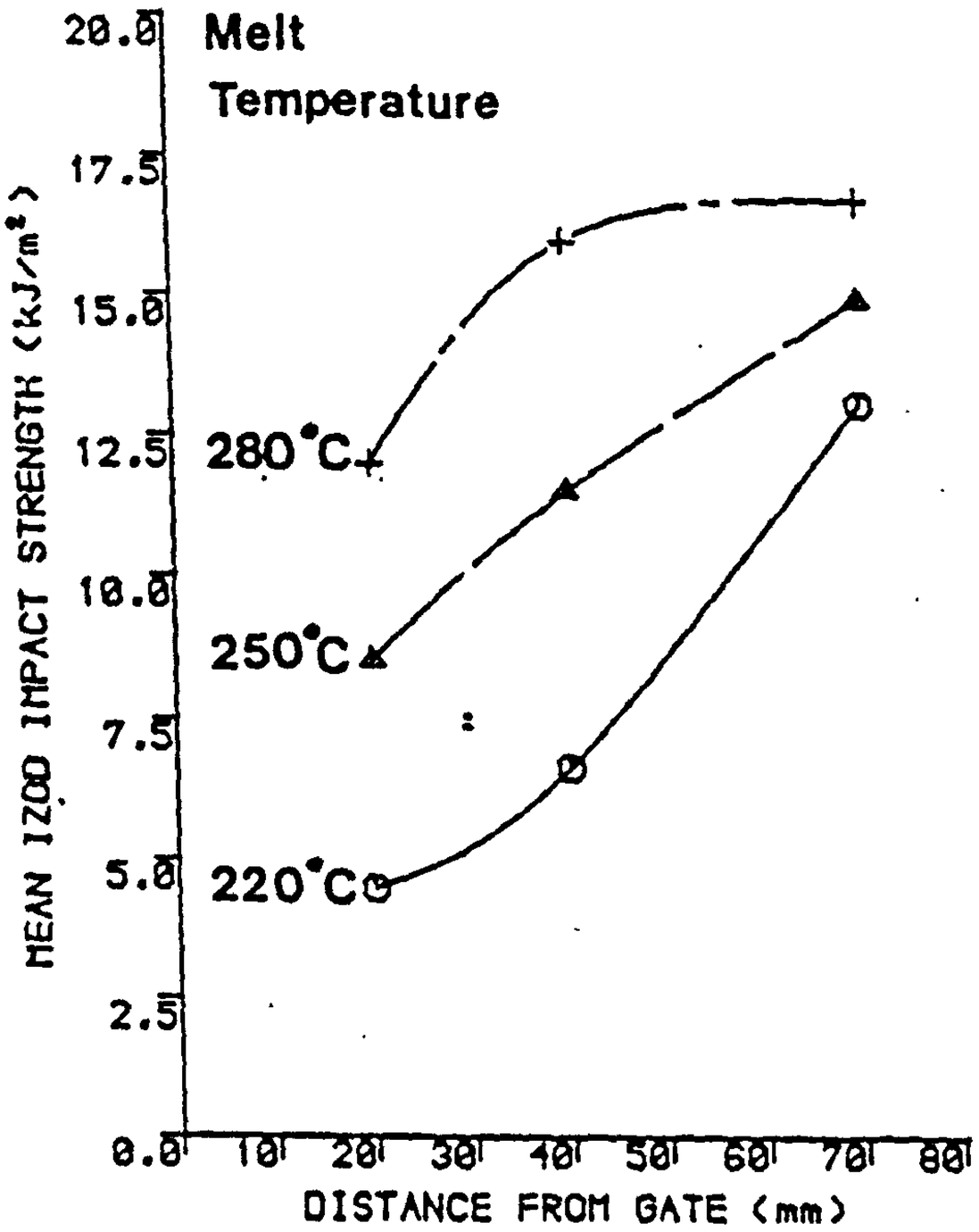

Figure 60 Effect of mould temperature on Izod impact strength.

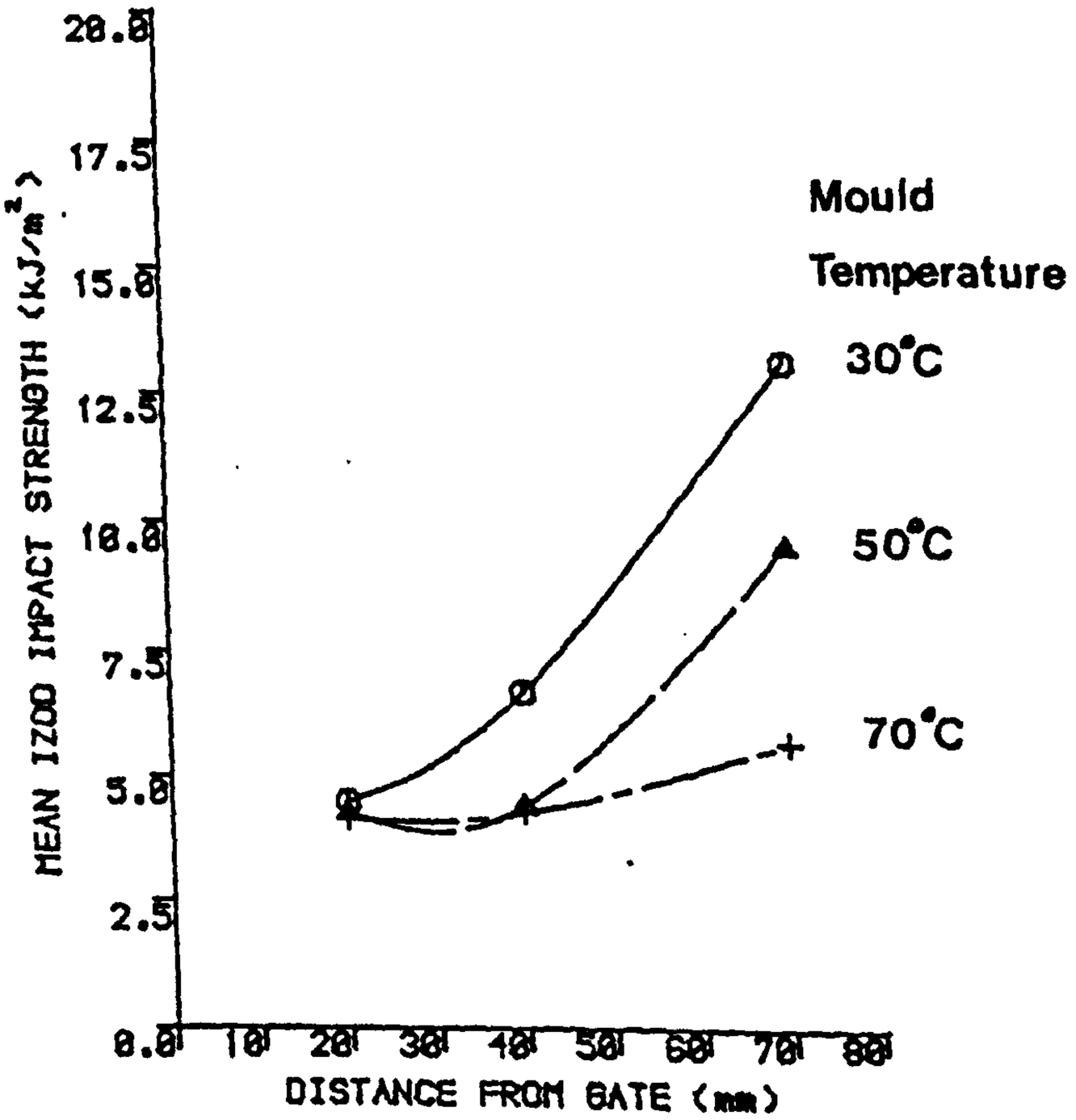

Figure 61 Effect of injection velocity on Izod impact strength.

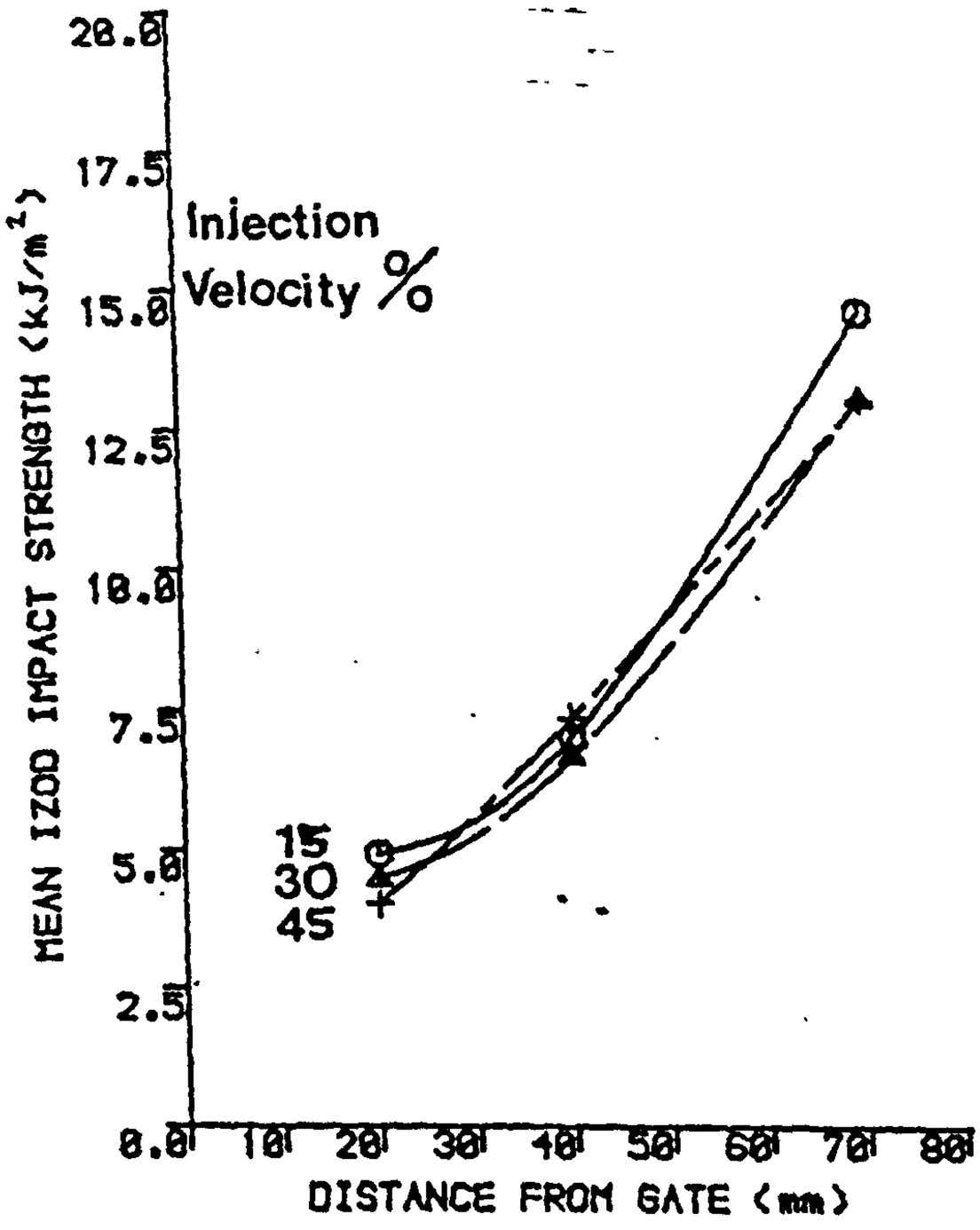

TABLE 19 Results from the systematic Izod impact test analysis of Sandretto injection mouldings.

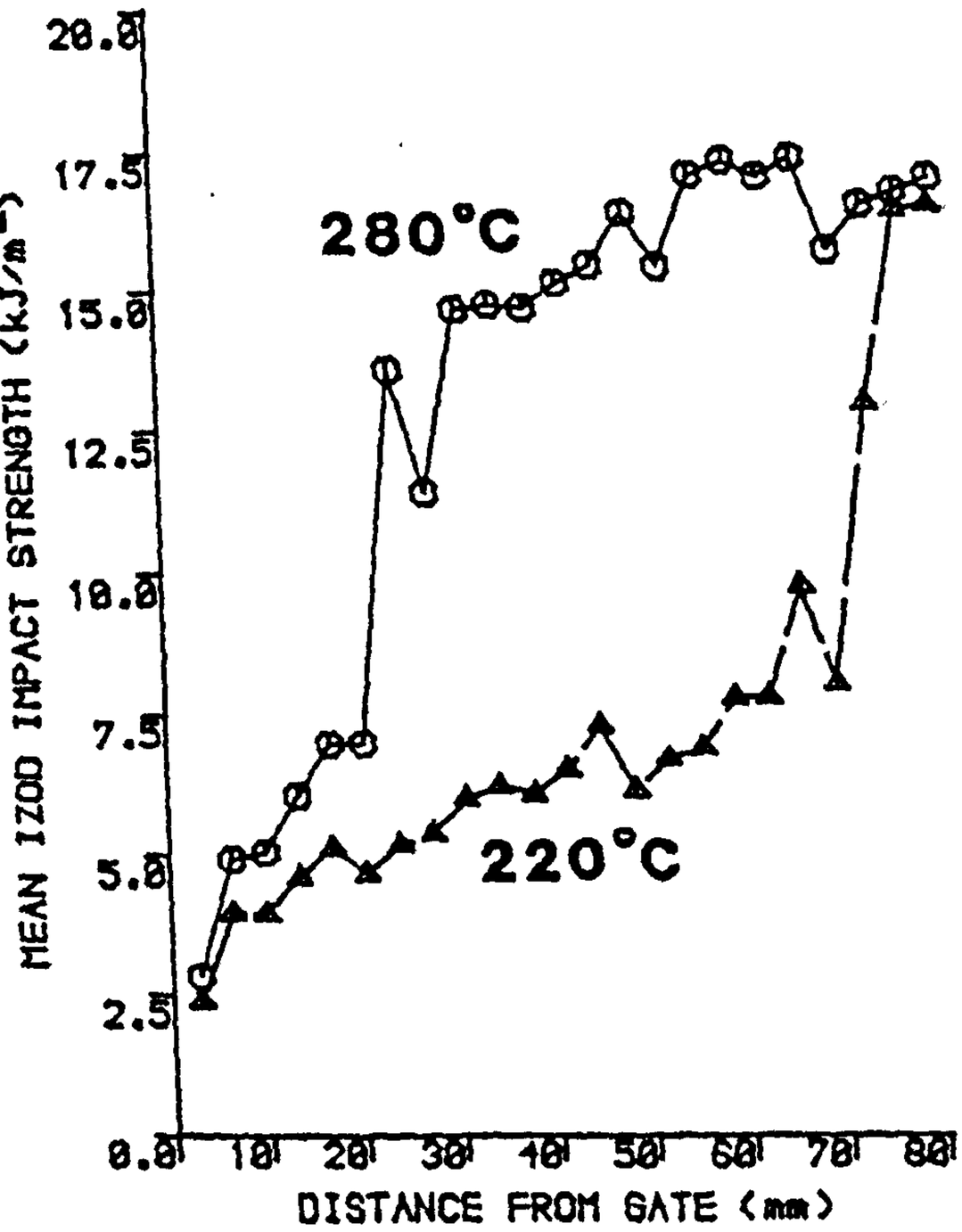

DISTANCE FROM GATE (mm)	30/220/30 I.S (kJm^{-2})	30/280/30 . I.S (kJm^{-2})
0.0- 3.0	2.39	2.84
3.5- 6.5	3.95	4.89
7.0-10.0	3.96	5.03
10.5-13.5	4.60	6.07
14.5-17.0	5.12	6.99
17.5-20.5	4.65	7.01
21.0-24.0	5.19	13.63
24.5-27.5	5.40	11.45
28.0-31.0	6.06	14.73
31.5-34.5	6.27	14.83
35.0-38.0	6.14	14.77
38.5-41.5	6.58	15.24
42.5-45.0	7.37	15.26
45.5-48.0	6.22	16.49
49.0-52.0	6.79	15.55
52.5-55.5	6.99	17.16
56.0-59.0	7.89	17.42
59.5-62.5	---	17.14
63.0-66.0	9.86	17.47
66.5-69.5	8.15	15.83
70.0-73.0	13.09	16.64
75.0-76.5	16.56	16.88
77.0-80.0	16.63	17.12

Figure 62 Variation of Izod impact strength with distance from the gate for Sandretto mouldings produced at 220°C and 280°C melt temperatures.

3.2.4 Instrumented Drop-Weight Impact Testing of Sandretto Injection Moulded iPP Plaques

As with the Daniels injection moulded plaques the Sandretto mouldings were tested using the Daventest-Rosand instrumented drop-weight impact test machine to provide a realistic assessment of directional weakness.

The centre of the 80 x 80 x 3 mm as-moulded plaques was impacted for five samples from each of the processing conditions used to prepare them. These results are summarized in Table 20 and illustrated by the bar chart in Figure 63 and by the graphs in Figures 64 and 65.

3.2.4.1 Analysis of Force/Distance and Energy/Distance^2 Curves

From the typical Force/distance and energy/distance^2 curves shown in Figure 66, similar observations to the Daniels impact test curve analysis were made. Namely, that:-

(i) the force/distance curves are complicated by shock wave effects,

(ii) an intermediate stage of reduced rigiditily occurred

(iii) the occurrence of two broad peaks, corresponding to the propagation energy, after the initial peak were apparent, and

(iv) the first peak on the force/distance curve corresponded to the linear portion of the energy/distance^2 curve.

3.2.4.2 Analysis of Results

The fracture patterns of typical impact failures are presented in Figures 67 and 68, and a summary of major and minor crack data is given in Table 21. It was again noticed that at least 4 major cracks were observed in every case, however, the number of minor cracks varied considerably from one processing condition to another. The following trends were observed with drop-weight impact testing:-

TABLE 20 Instrumented drop-weight impact test results for Sandretto injection mouldings.

MOULDING CONDITIONS MOULD (°C)	MELT (°C)	FILL (%)		PEAK ENERGY (Nm) $\bar{x}$	s.d	FINAL ENERGY (Nm) $\bar{x}$	s.d	PEAK FORCE (N) $\bar{x}$	s.d
30	220	15	A	0.235	0.024	2.032	0.271	241.30	40.28
30	220	45	B	0.282	0.058	2.191	0.521	275.00	32.40
30	220	30	C	0.242	0.017	2.073	0.308	261.70	13.25
30	250	30	D	0.533	0.128	2.004	0.338	356.10	41.87
30	280	30	E	0.799	0.158	1.864	0.378	443.76	58.77
50	220	30	F	0.221	0.047	1.892	0.493	231.26	18.89
70	220	30	G	0.202	0.037	1.528	0.195	218.26	25.81

Figure 63 Bar chart representation of mean first peak drop-weight impact energy versus Sandretto moulding condition.

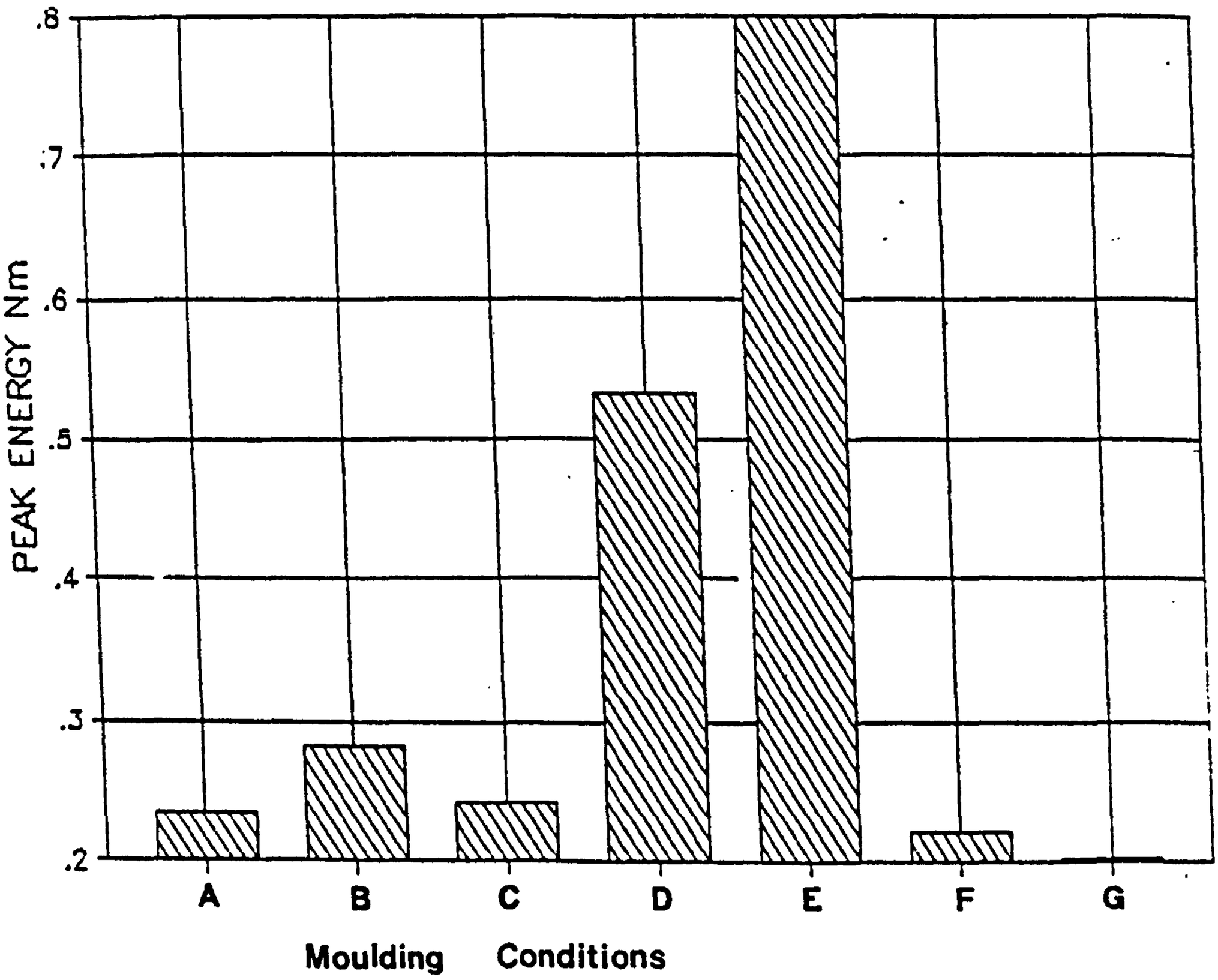

Figure 64 Mean peak drop-weight impact energy versus melt temperature.

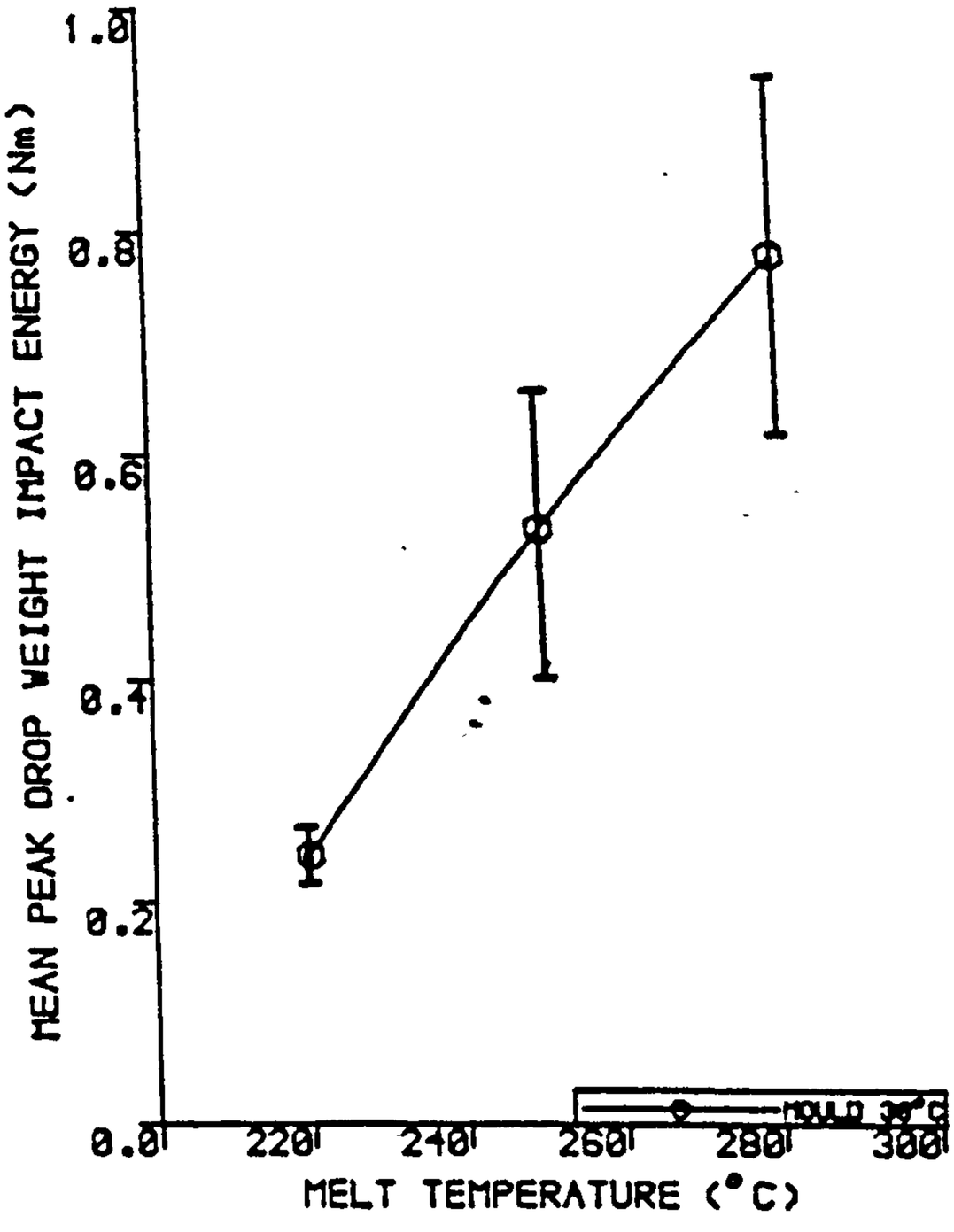

Figure 65 Mean peak drop-weight impact energy versus mould temperature.

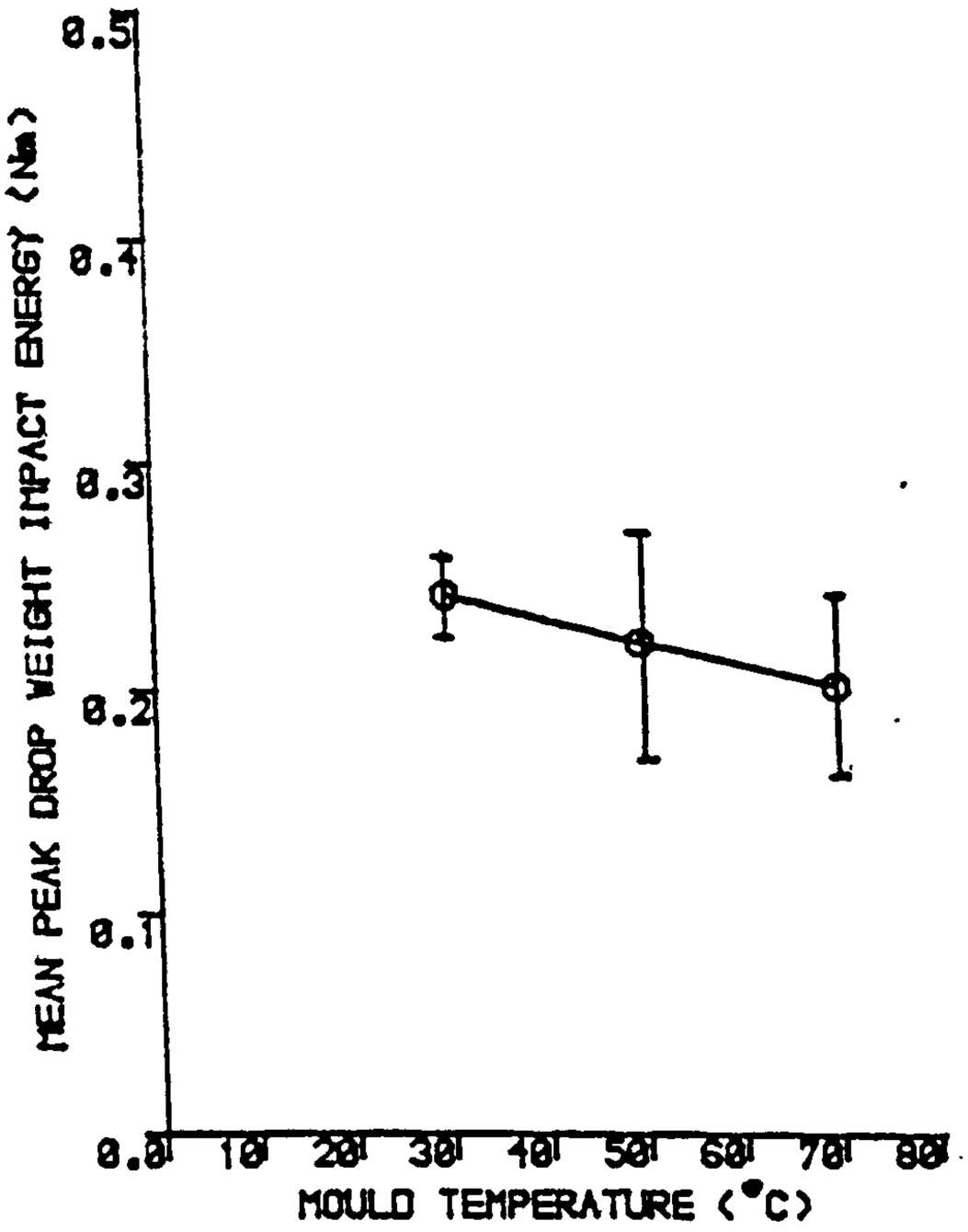

Figure 66

Typical force/distance and energy/distance^2 data from drop weight impact tests of Sandretto iPP mouldings.

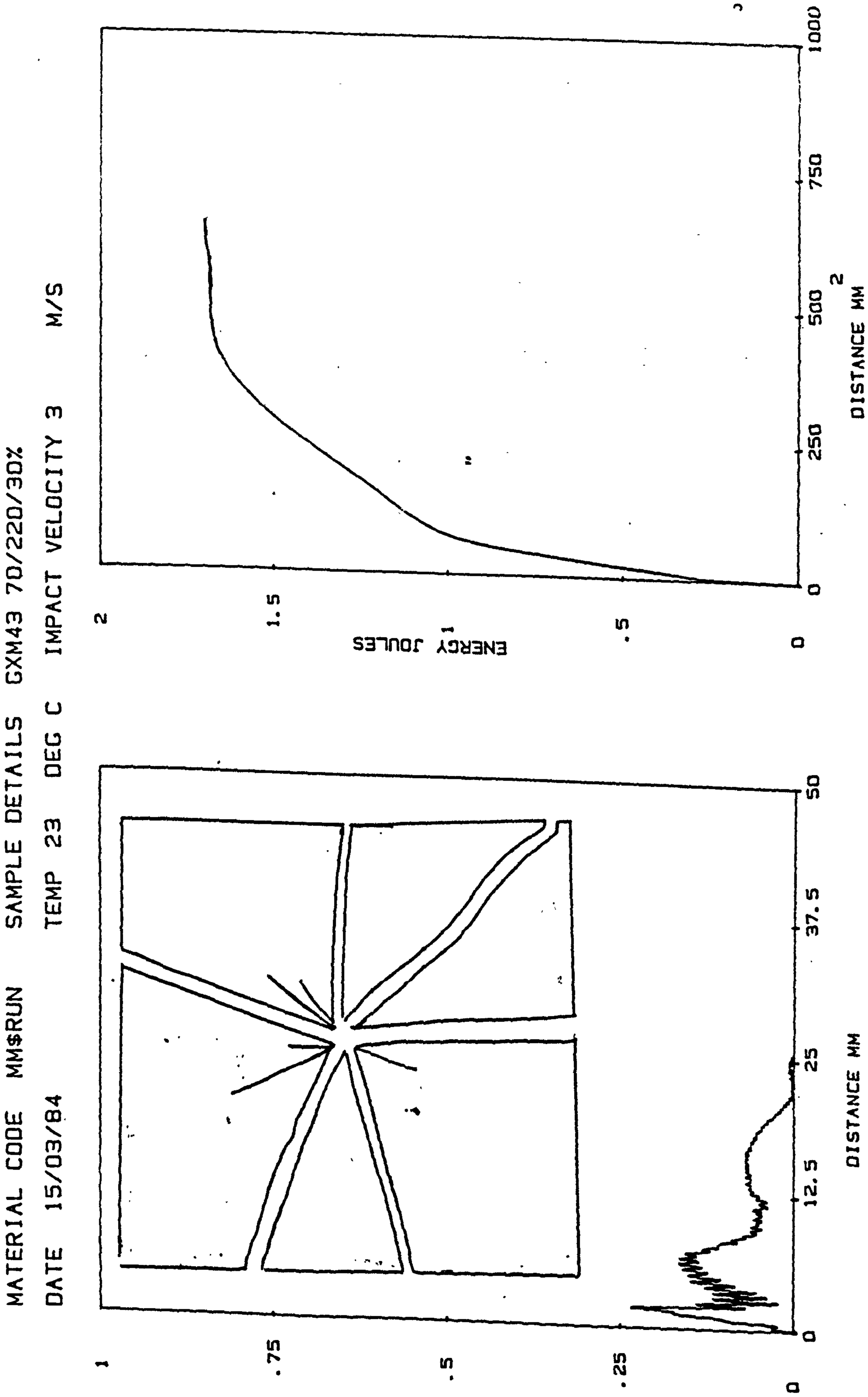

MATERIAL CODE MM$RUN SAMPLE DETAILS GXM43 30/220/30%

DATE 15/03/84 TEMP 23 DEG C IMPACT VELOCITY 3 M/S

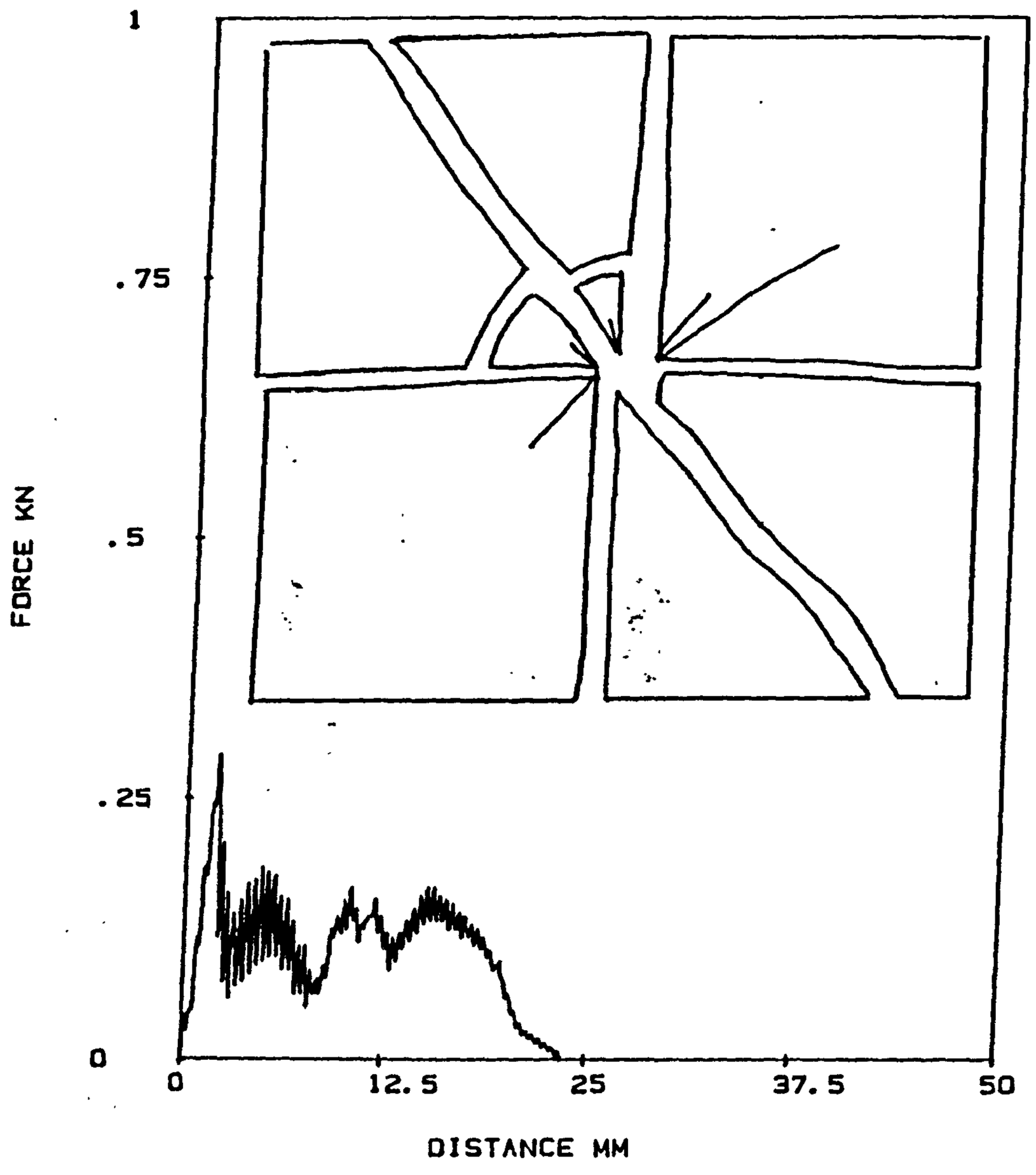

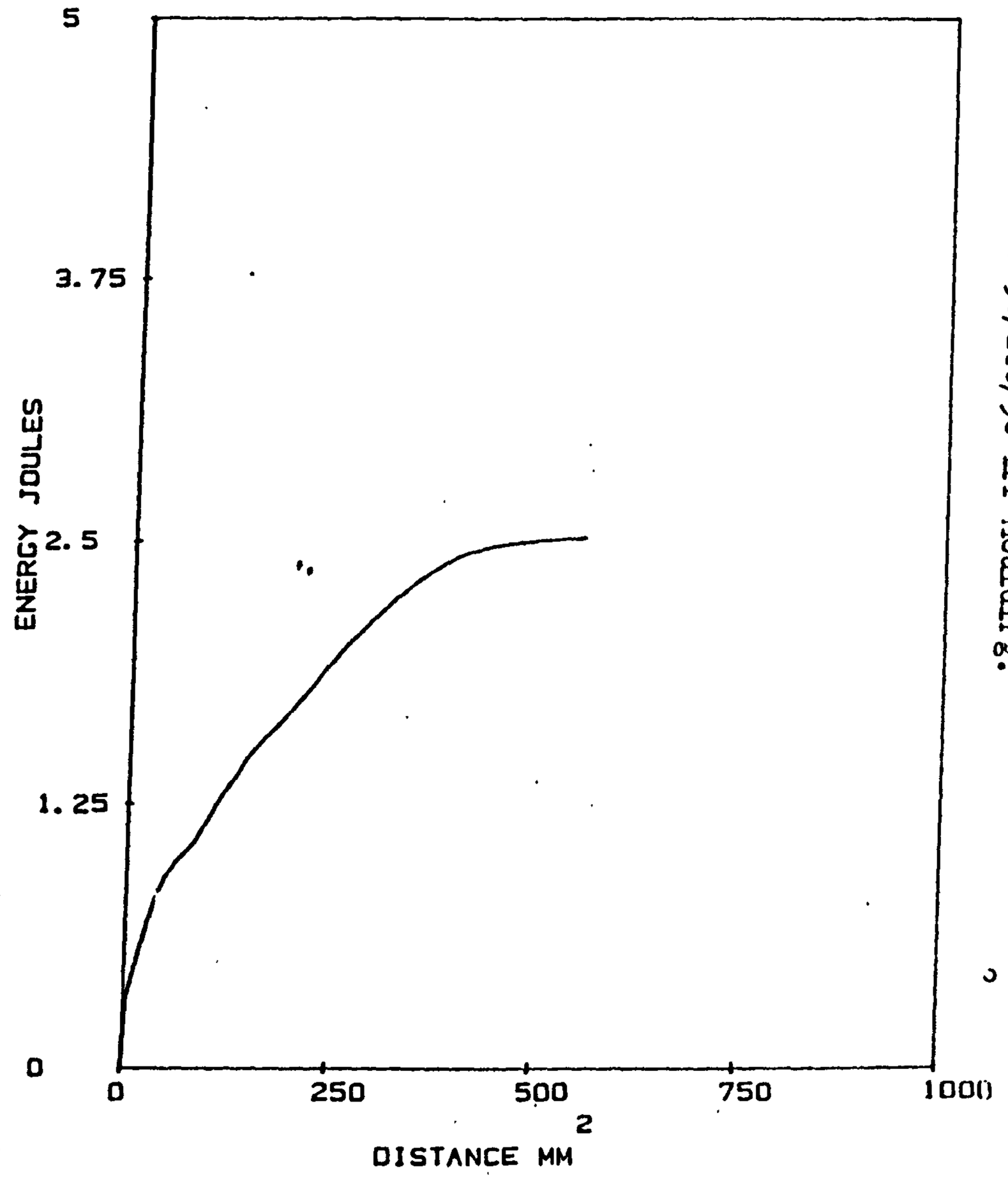

Figure 67

Typical force/distance and energy/distance^2 data presented with the associated fracture pattern for a 30/220/30 IPP mouldirg.

Figure 68

Typical force/distance and energy/distance^2 curves presented with the associated fracture pattern for a 30/280/30 iPP moulding.

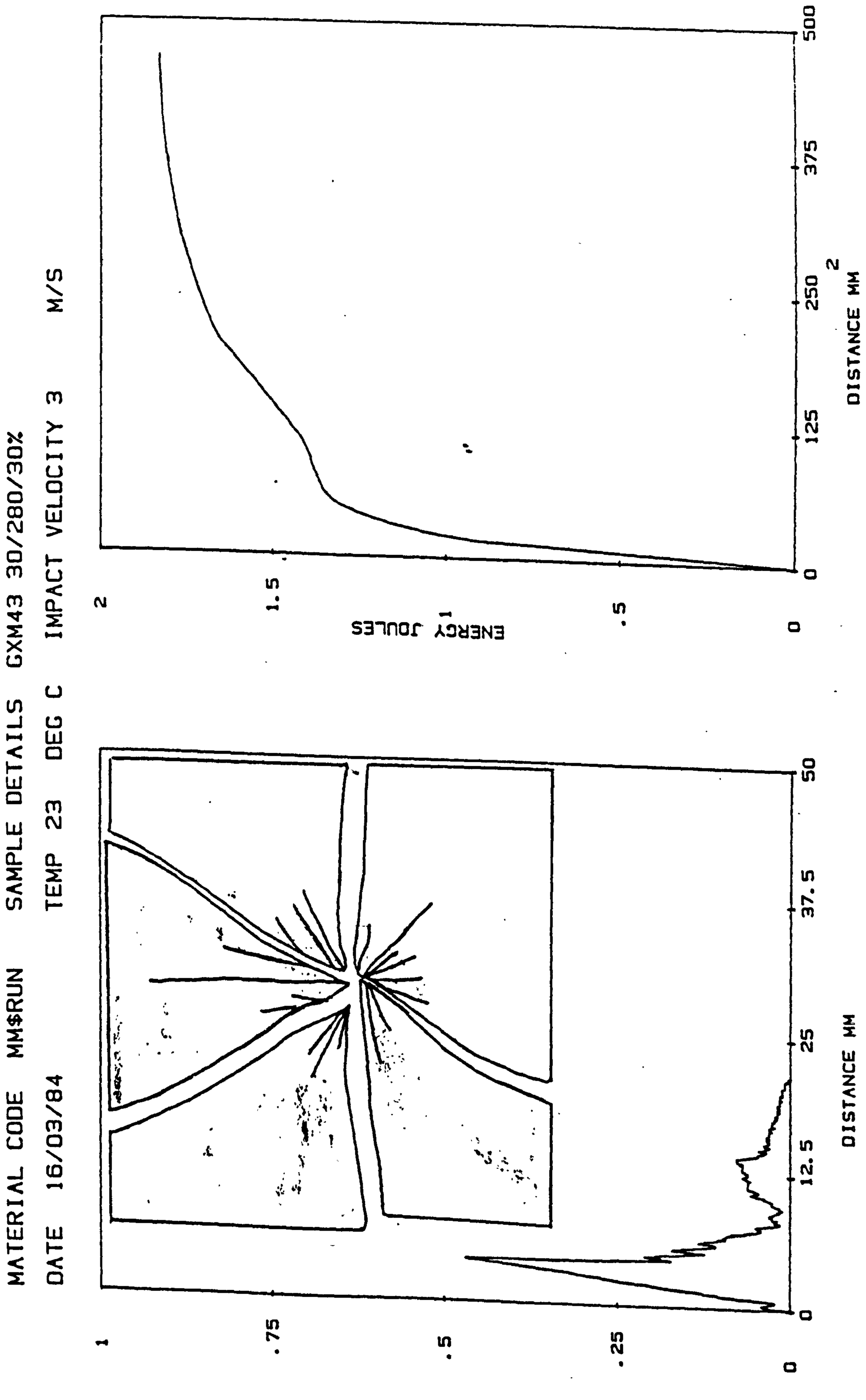

TABLE 21 Results of fracture pattern analysis of Sandretto drop-weight impact tested plaques.

MOULDING CONDITIONS MOULD (°C)	MELT (°C)	FILL (secs)	NUMBER OF MINOR CRACKS	NUMBER OF MAJOR CRACKS
30	220	15	7	4
30	220	30	7	6
30	220	45	8-9	4
30	250	30	18	4
30	280	30	>20	5
50	220	30	7	4
70	220	30	4-5	6

(i) Increasing the melt temperature of mouldings appears to lead to the occurrence of far more minor cracks before any major crack is produced. This type of fracture pattern was associated with high 1st peak forces and impact energies i.e. a toughening effect was observed.

(ii) A decrease in the number of minor cracks in the impact fracture pattern was found with increasing the mould temperature to produce mouldings. This was accompanied by a respective drop in 1st peak energy.

(iii) The effect of injection velocity on the impact fracture patterns similarly showed this trend. An increase in the 1st peak energy was associated with an increase in the number of minor cracks produced, as the cavity fill rate was increased.

For these mouldings it was difficult to assess directional weakness due to the variation in direction and number of major cracks propagating through each plaque. However, as with Daniels mouldings one crack was found to propagate directly towards the gate (with little deviation) in all low melt temperature mouldings.

In addition, a good correlation in trends between centre of moulding Izod impact strength and Peak Falling weight impact energy was found with variations in moulding conditions, namely, an improvement with increasing melt temperature and deterioration with increasing mould temperature.

3.2.5 Summary of Impact Test Results

It has been clearly illustrated from these impact property studies, of a range of injection moulded 3mm thick polypropylene

plaques, that melt and mould temperatures exhibit the greatest influence on the impact strength of mouldings. Furthermore, that the impact strength may increase substantially part-way across mouldings,this transition appears to be highly dependent on the melt processing temperature used and very probably an the resultant heterogeneity in micromorphology.

There is good correlation between Izod impact test and falling weight impact test results despite the difference in geometry. of test. The Izod test has been invaluable in assessing the dependence of impact strength on postion of test piece within a moulding, whereas the falling weight test has been instructive as to directional weakness and fracture mechanisms expected in as-moulded samples.

It was clearly necessary to identify the micromorphology of regions within an injection moulding and associated processing conditions, which give rise to the impact property variations. For this reason a light microscopy study was undertaken on representative samples from each processing condition.

3.3 OPTICAL CHARACTERISATION OF THE AS-MOULDED MICROSTRUCTURES

3.3.1 Introduction

The micromorphology of the injection moulded plaques was initially characterized by polarised light microscopy examinations of thin films, 2-6 μm thick, prepared by microtomy of Izod test pieces. Sections examined on the Reichert Zetopan microscope revealed up to six distinct morphological zones through the thickness of the mouldings. These morphological zones varied in width and extent with position along the melt flow path and with changes in processing conditions.

Typical gate area banded morphologies are shown in Figure 69, they are all composed of a highly oriented and birefringent non-spherulitic skin and a spherulitic core. The morphology between the skin and core was found to consist of an apparently oriented structureless band similar to, but distinct from, the skin with row nucleated β-phase spherulites ahead of it. This structureless band probably forms because it is the last material to enter the mould and consequently is unaffected by the flow of additional material. The drop in pressure, the rapid cooling and the lack of material flow do not allow sufficient molecular reorganisation for the development of a spherulitic morphology. The presence of row nucleated β phase spherulites indicate a transformation occuring as material flow and temperatures increase towards the core. In fact, the structureless zone appears to transform totally to row nucleated spherulites as the melt flow direction is traversed.

The extent and width of the structureless region as well as the nucleation and growth of the β phase spherulites appear to be extremely sensitive to processing conditions. The results of this study are presented with a view to explaining the Izod impact test behaviour of mouldings, for this reason micrographs are correlated with Izod impact strength versus Distance from gate curves previously discussed.

3.3.2 Analysis of Daniels Mouldings Microstructure By Optical Microscopy

Micrographs of the as-moulded microstructure of Daniels injection mouldings microtomed from Izod test samples cut at 20 mm, 45 mm, and 70 mm along the flow direction are presented in Figures 46 to 52 for each processing condition.

Figure 69 Typical gate area banded morphologies found in Sandretto iPP injection mouldings.

300µm

Moulding Conditions

30/220/30

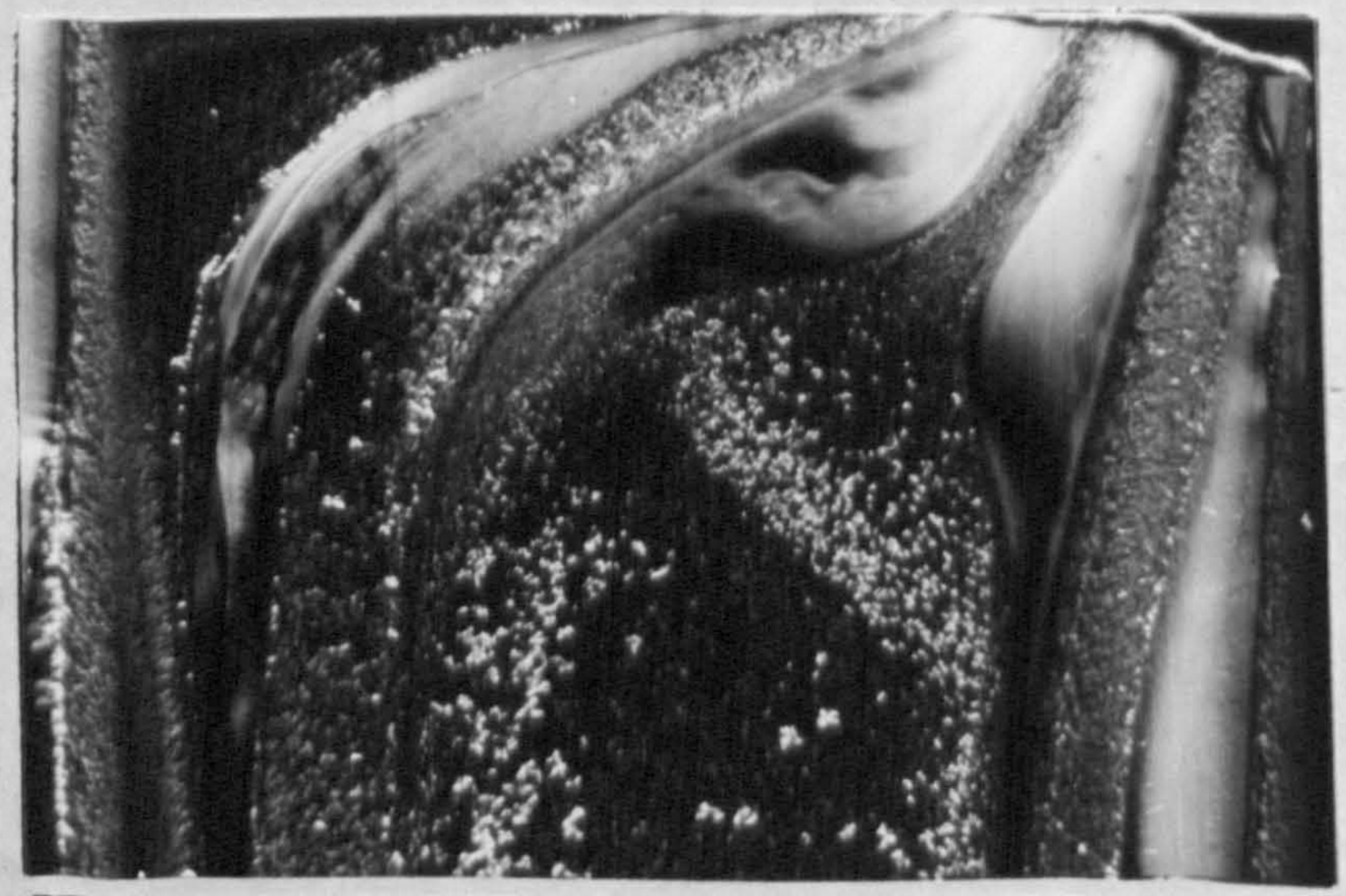

30/250/30

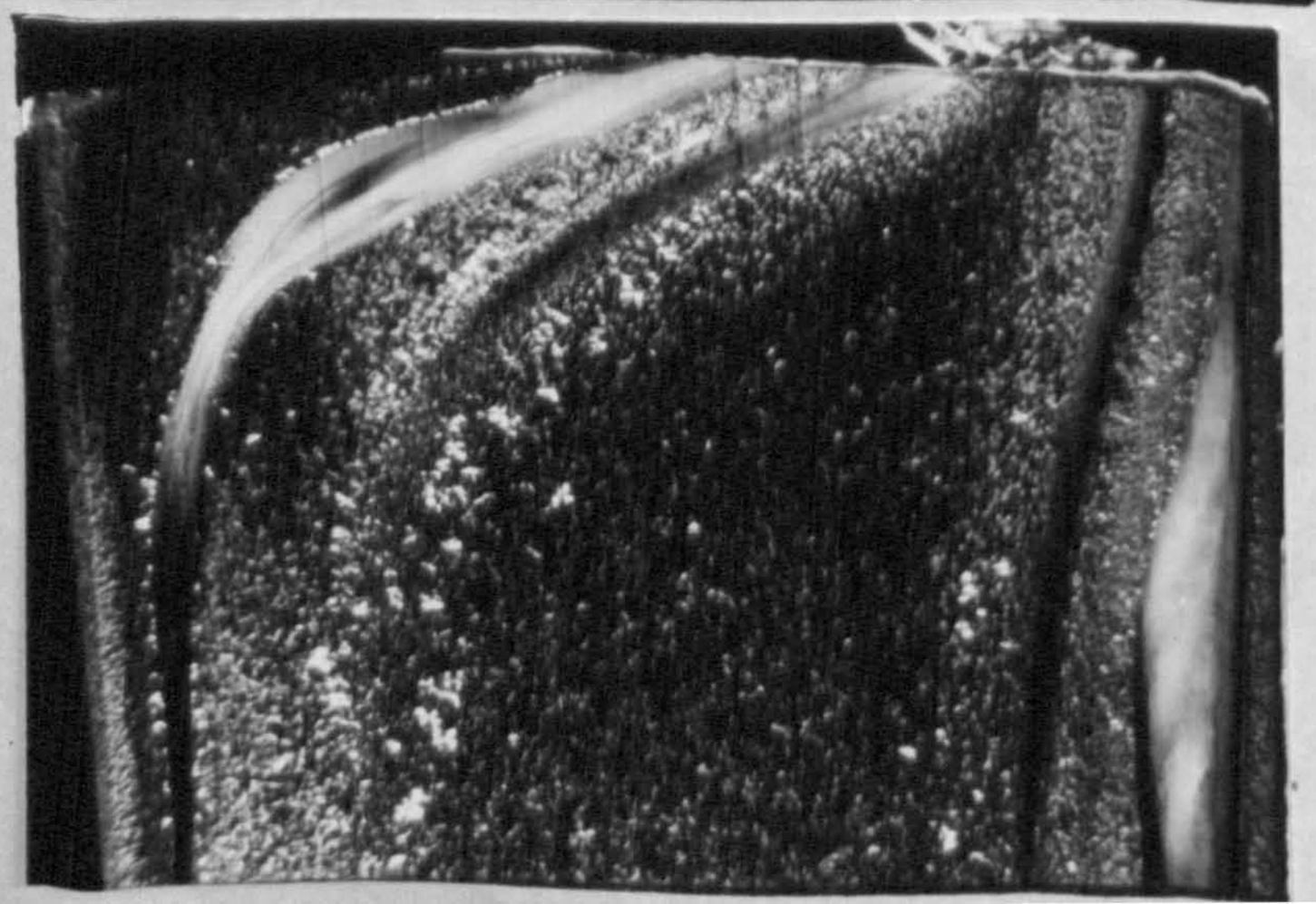

30/280/30

300µm

30/220/15

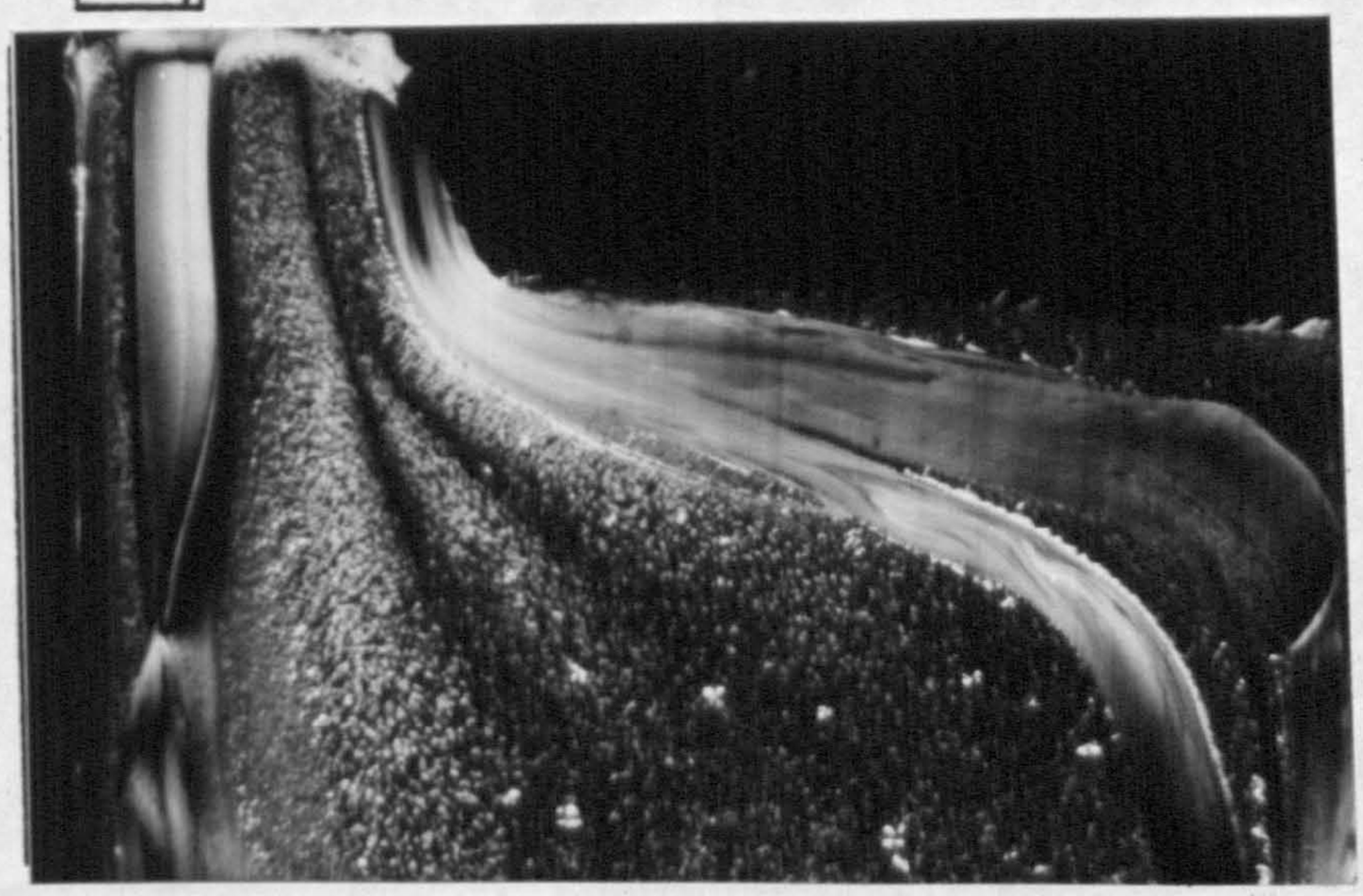

30/220/45

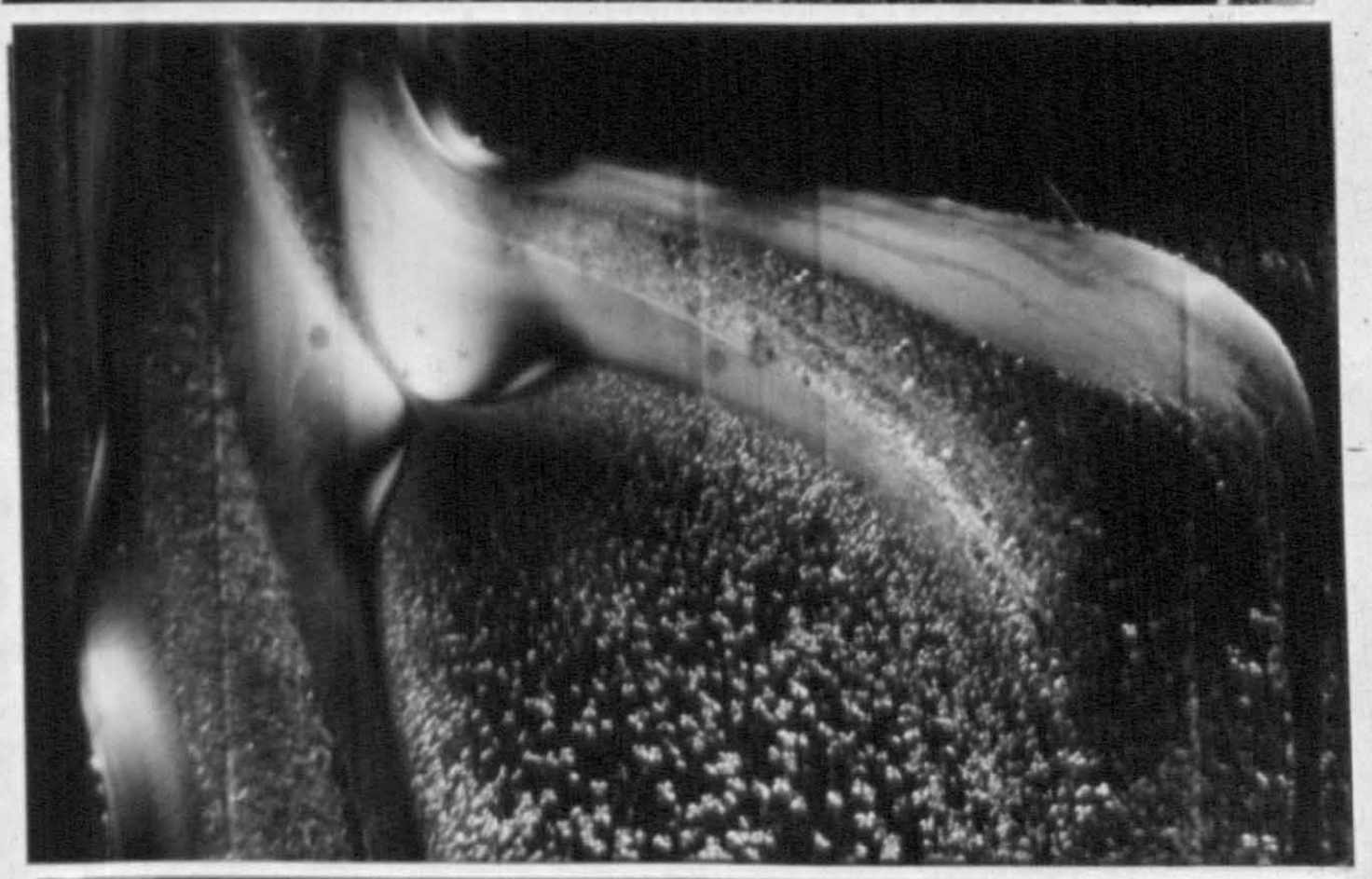

50/220/30

70/220/30

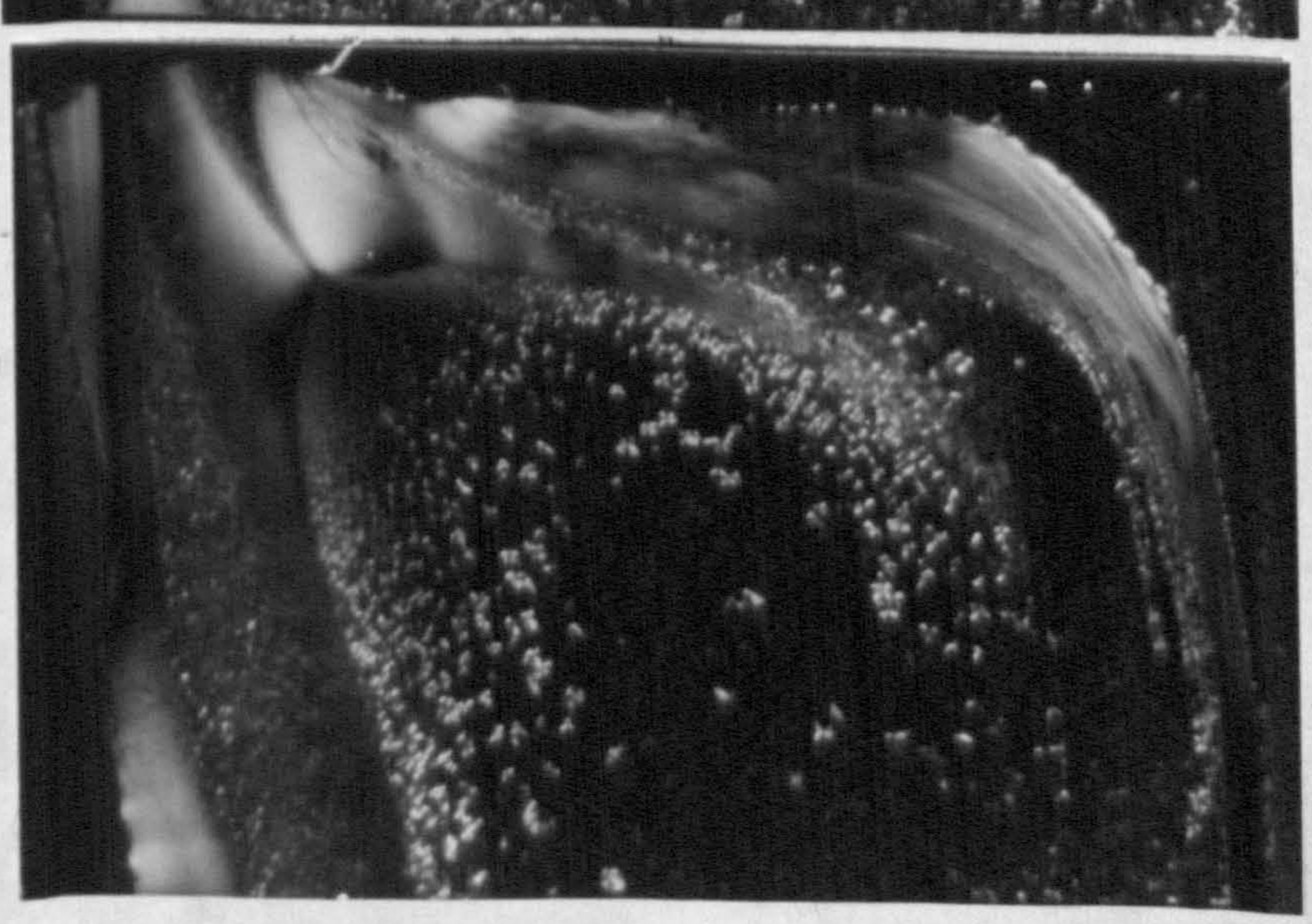

The following observations were made with reference to Table 22 which summarizes the extent and width of the morphological bands in each respective area:-

(i) Highly sheared melts i.e. low melt temperature mouldings exhibit well defined banded morphologies in sections taken 20 mm from the gate. The structureless band described and row nucleated β phase structures are associated with low impact properties. As mouldings are traversed these banded morphologies die away and impact properties are seen to improve dramatically.

(ii) Mouldings produced at high melt temperatures do not reveal this structureless band 20 mm from the gate but do show rows of β-phase spherulites which die away as the moulding is traversed. The impact strength is seen to be higher close to the gate than low melt temperature mouldings, but still inferior to the excellent impact strengths found at the far side of the mouldings.

(iii) The size of row nucleated β phase spherulites close to the gate are seen to be very much dependent on the mould temperature used. High mould temperatures and melt temperatures combined, for example, revealed β-spherulites upto 40 μm in diameter in the gate region, Figure 51(a) illustrates this point.

(iv) Increasing the mould temperature also induced a trans-crystalline surface microstructure in contrast to the frozen oriented skin found in low mould temperature mouldings. Low impact strengths are found in high mould temperature mouldings along the entire melt flow direction, this suggests that the transcrystalline layer is the overiding weakness.

(v) Reducing the cavity fill time increases the nucleation of β-phase spherulites close to the gate and reduces

the width of the structureless band. Generally slightly lower impact properties are revealed with slower injection velocities.

(vi) The size of core α -phase spherulites increases marginally with increasing mould temperatures and melt temperatures as illustrated in micrograph (d) of each Figure 46 to 52.

The systematic microtomy of the Izod test pieces prepared from low and high melt temperature mouldings, selected for more detailed impact property studies, was also carried out. This was done to gain a better understanding of the microstructural changes responsible for the impact property variations illustrated in Figure 53.

Micrographs are presented in Figures 70 and 71 for the low and the high melt temperature mouldings respectively. These micrographs reveal that in areas close to the gate in both mouldings a structureless band and some row nucleated β phase spherulites exist. As the mouldings are traversed the structureless band width reduces and the density of nucleation of β phase spherulites increases, this is correlated in both cases to a gradual improvement in impact properties. It is not, however, until the β spherulites disappear at some point along the flow direction that the impact properties increase dramatically. This transition occurs at 49 mm and 38 mm along the melt flow path for the 220°C and 280°C melt temperature mouldings respectively. The impact properties beyond these transition points appeared to become increasingly dependent on the frozen skin thicknesses, which are c.a. 20 μm for the 220°C moulding and c.a. 10 μm for the 280°C moulding, since little variation in core α spherulite size was observed in these mouldings.

Figure 70

The microstructure, revealed from Izod test pieces, along the melt flow direction of a Daniels 35/220/1.35 iPP moulding.

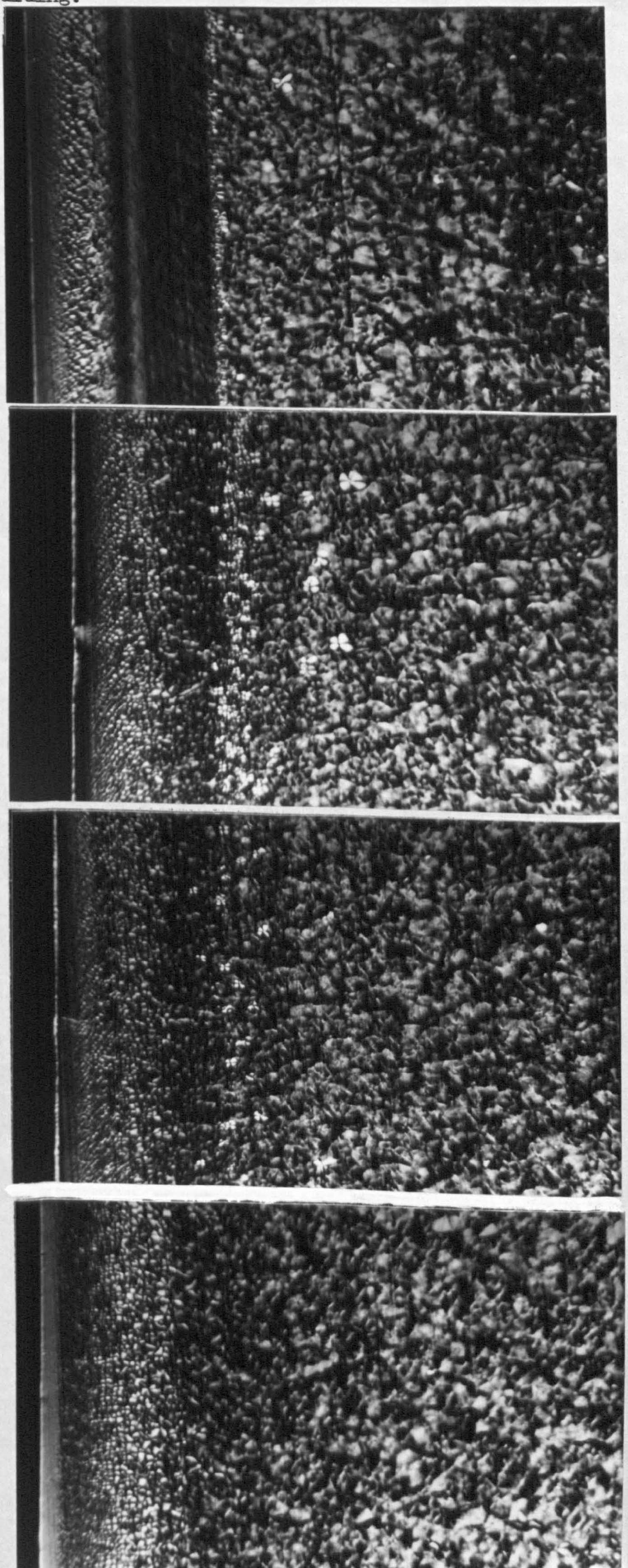

Figure 71

The microstructure, revealed from Izod test pieces, along the melt flow direction of a Daniels 35/280/1.35 iPP moulding.

Distance from gate (mm)

14.5–17.5

100µm

31.5–34.5

49.0–52.0

66.5–69.5

3.3.2.1 Summary of Results

The observations above reveal the microstructural features governing the impact properties of the Daniels pin-gated iPP plaques. It was found that structural heterogeneity in the form of banded morphologies is cause for concern, particularly where row nucleation of the β -form is enhanced, in injection mouldings of iPP. In addition, transcrystallinity at the surface of mouldings, produced using high mould temperatures, should be avoided as this leads to very poor impact resistance across the entire moulding.

The optimum conditions suggested for the moulding of 3mm thick pin-gated plaques of iPP, with good impact properties, are low mould temperatures (30°) high melt temperatures $(280^{\circ}C)$ and fast cavity fill times (c.a. 1 second).

3.3.3 Analysis of Sandretto Mouldings by Optical Microscopy

Due to the structural variations that occur along the melt flow direction in injection moulded plaques of polypropylene it was decided to carry out a far more detailed optical characterization of Sandretto mouldings.

The preparation of sixteen 5mm x 3mm microtomed sections from plaques of each processing condition was made, these sections were taken at consecutive intervals along the melt flow direction as shown in Figure 72. The optical micrographs shown in Figures 73 to 79 provided detailed information on the sensitivity of the banded morphologies to processing conditions. A summary of the extent and width of the structural features in Sandretto iPP injection mouldings is given in Table 23.

The observations made were in good agreement with those made on the Daniels mouldings, namely that high melt temperatures used

Figure 72

Sectioning of Sandretto injection moulded iPP plaques for detailed optical microscopy.

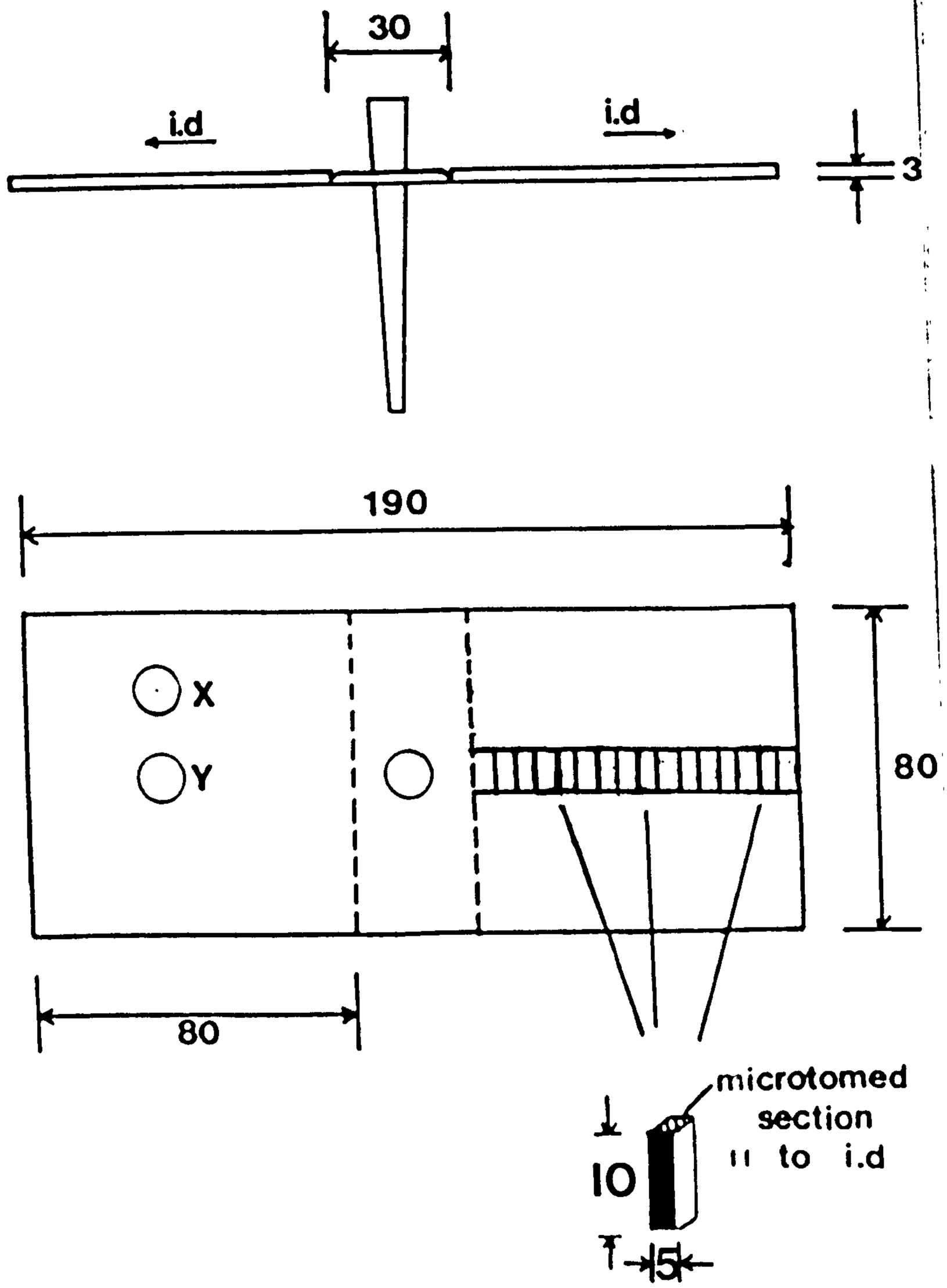

All dimensions in millimetres

Figure 73

The variation in surface morphology along the flow direction of a Sandretto 30/220/30 moulding.

Melt Temperature	220°C
Mould Temperature	30°C
Injection Velocity	30%

100μm

Distance Along Flow Path (mm)

5–10

10–15

20–25

25–30

30–35

35–40

45–50

55–60

Figure 74

The variation in surface morphology along the flow direction of a Sandretto 30/250/30 moulding.

Melt Temperature 250°C

Mould Temperature 30°C

Injection Velocity 30%

100μm

Distance Along Flow Path

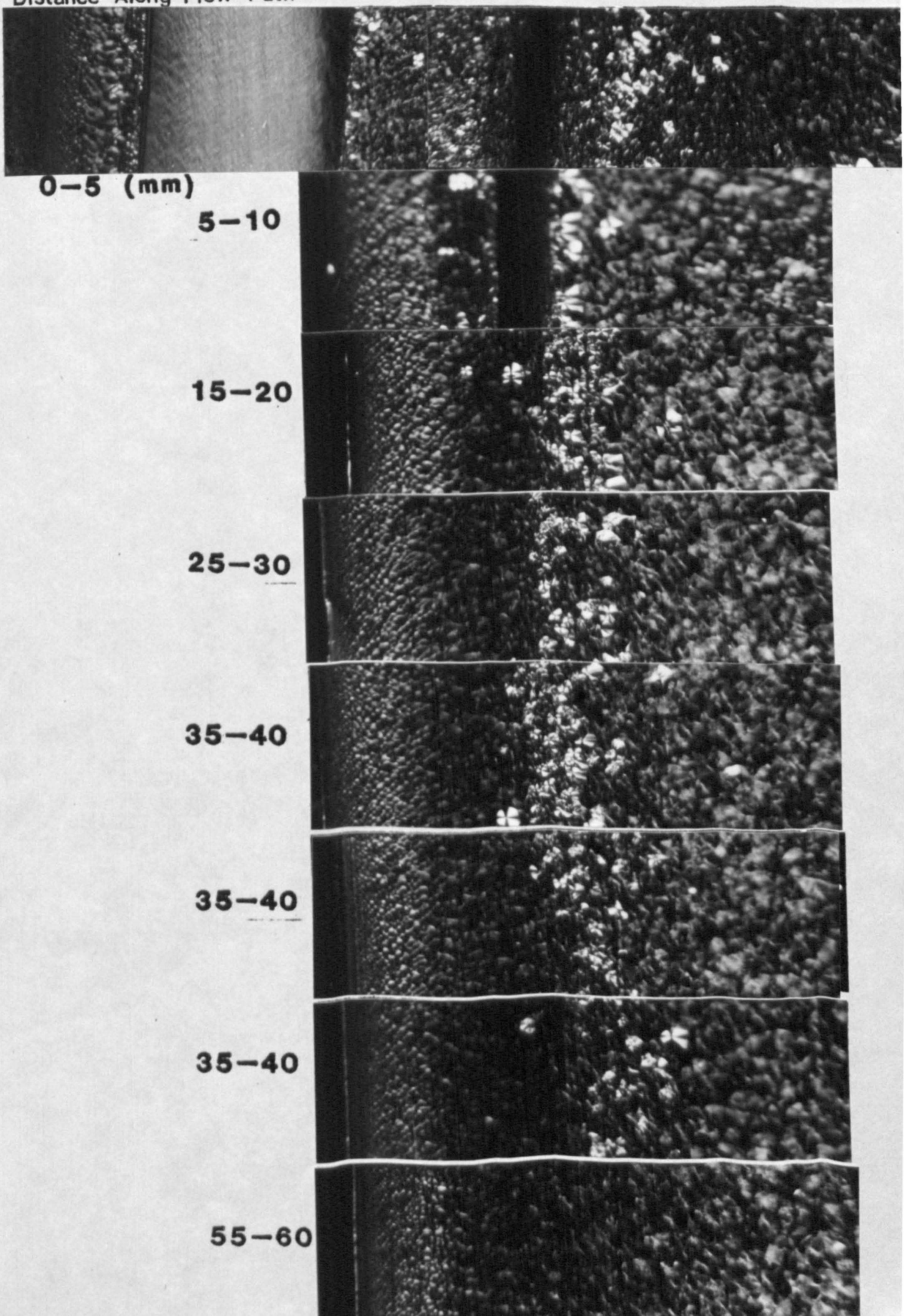

Figure 75

The variation in surface morphology along the flow direction of a Sandretto 30/280/30 moulding.

Melt Temperature 280°C

Mould Temperature 30°C

Injection Velocity 30%

100µm

Distance Along Flow Path (mm)

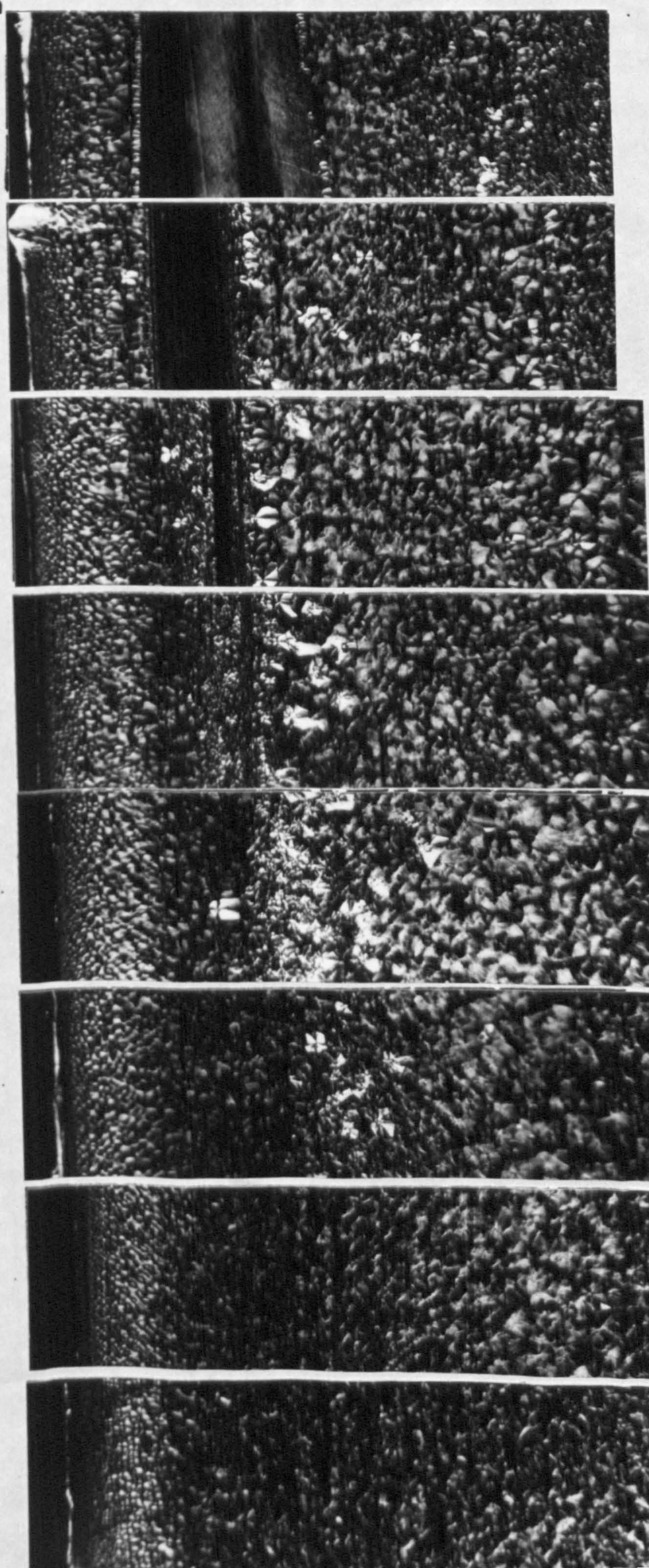

0-5

5-10

5-10

10-15

15-20

25-30

35-40

55-60

Figure 76

The variation in surface morphology along the flow direction of a Sandretto 50/220/30 moulding.

Melt Temperature **220°C**

Mould Temperature **50°C**

Injection Velocity **30%**

100μm

Distance Along Flow Path (mm)

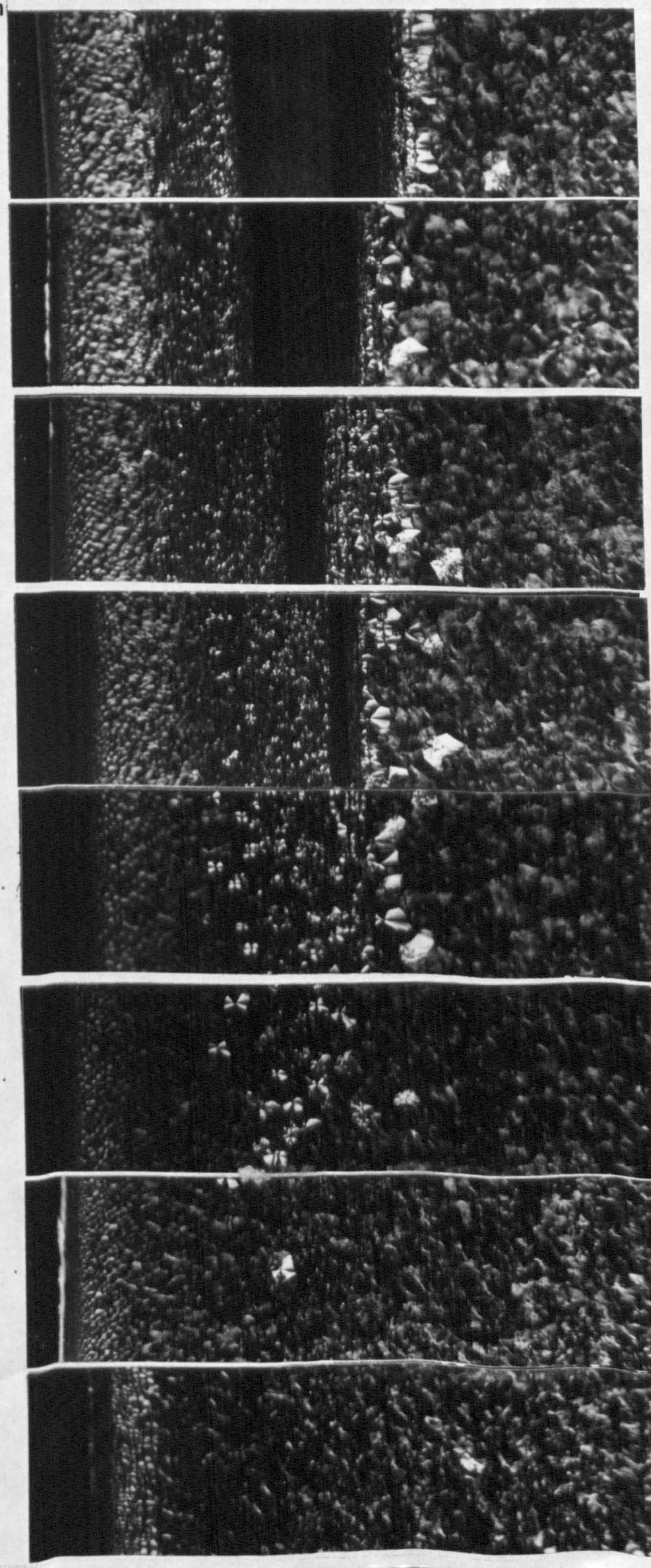

0–5

0–5

10–15

15–20

25–30

35–40

45–50

55–60

Figure 77

The variation in surface morphology along the flow direction of a Sandretto 70/220/30 moulding.

Melt Temperature	220 C
Mould Temperature	70 C
Injection Velocity	30%

100μm

Distance Along Flow Path

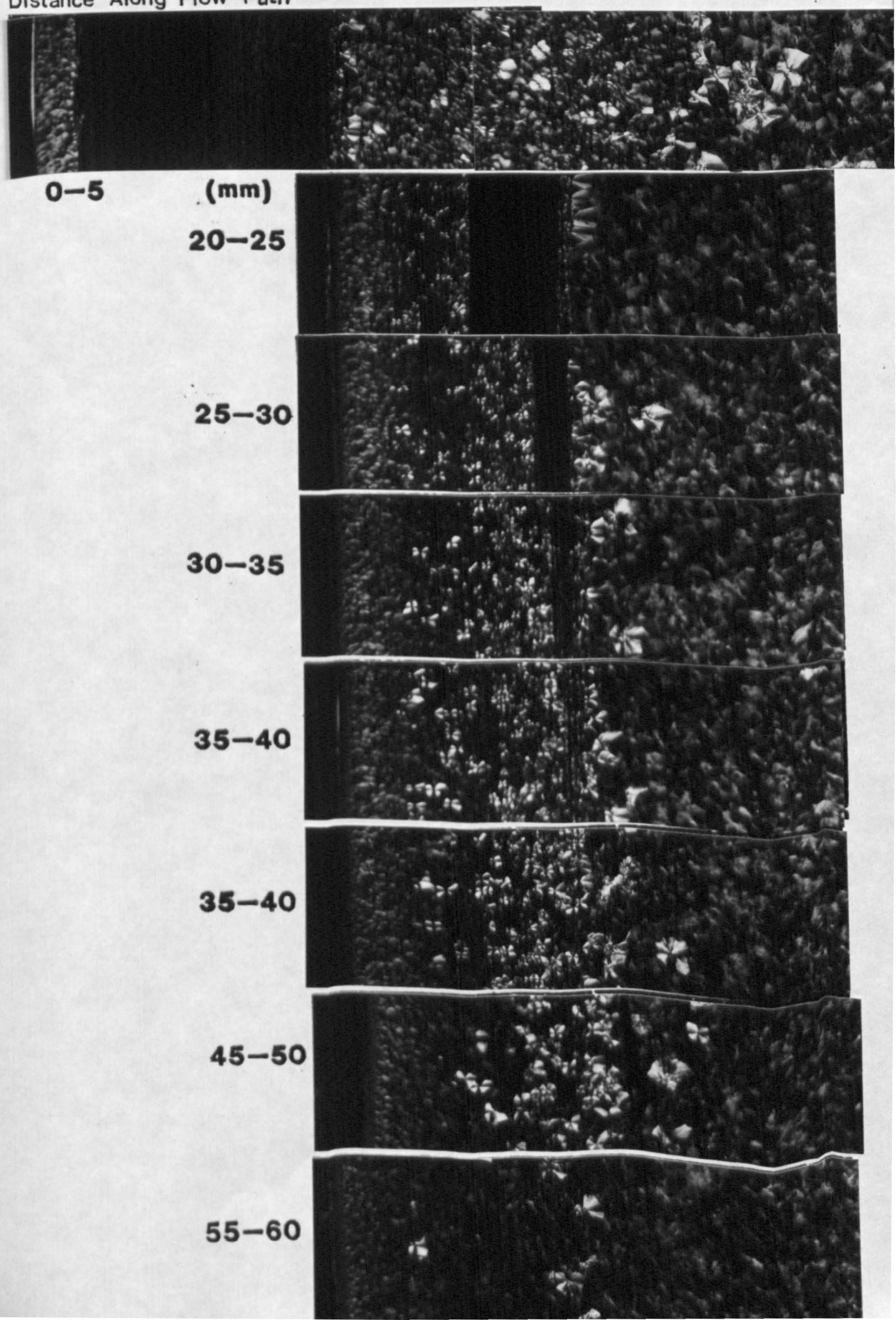

Figure 78

The variation in surface morphology along the flow direction of a Sandretto 30/220/15 moulding.

Melt Temperature 220 C

Mould Temperature 30 C

Injection Velocity 15%

100μm

Distance Along Flow Path (mm)

0–5

15–20

35–40

35–40

40–45

55–60

55–60

75–80

Figure 79

The variation in surface morphology along the flow direction of a Sandretto 30/220/45 moulding.

Melt Temperature 220°C

Mould Temperature 30°C

Injection Velocity 45%

100μm

Distance Along Flow Path

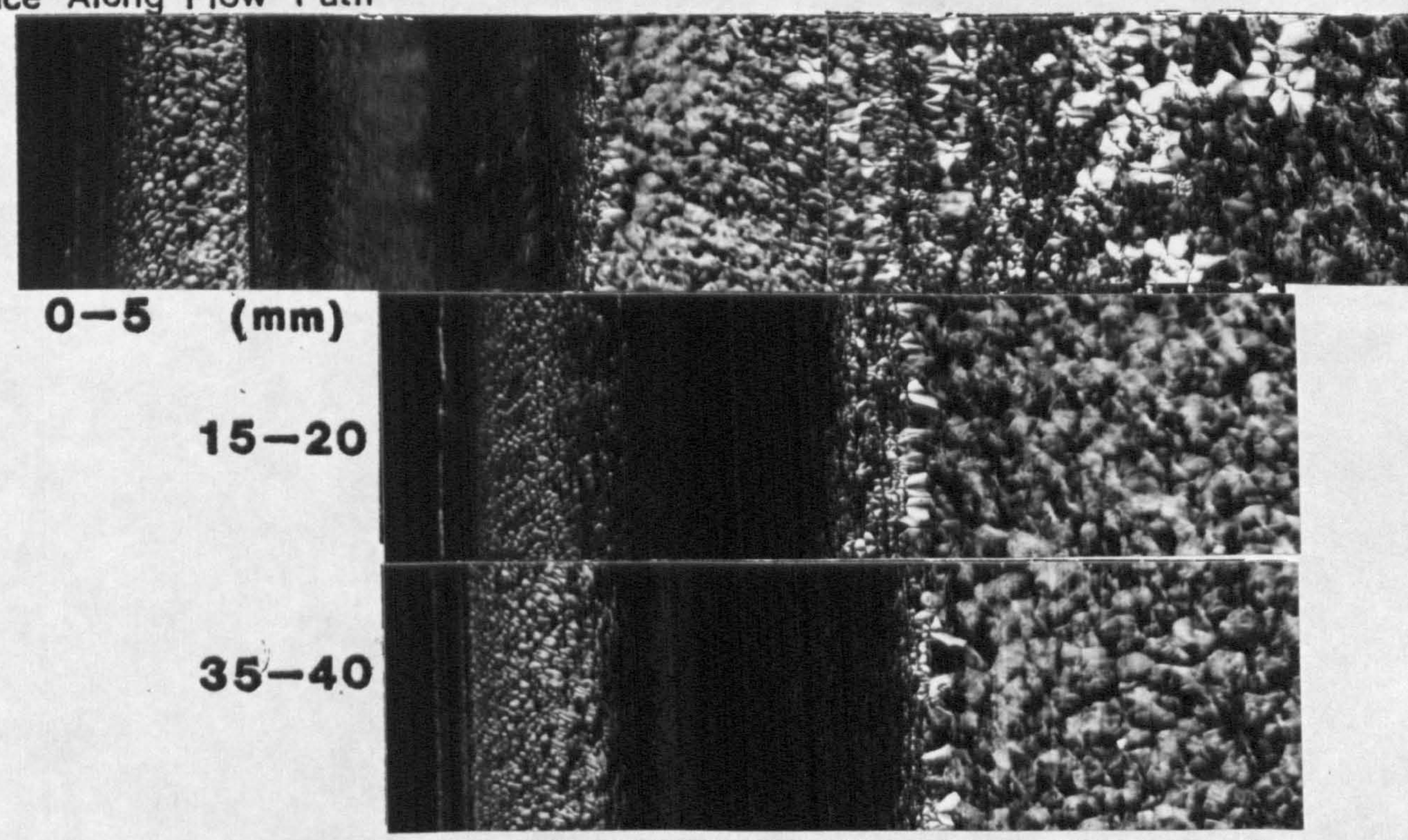

0–5 (mm)

15–20

35–40

35–40

40–45

40–45

55–60

75–80

TABLE 22 Distribution of morphological bands in Daniels injection moulded iPP plaques.

MOULDING CONDITIONS MOULD (°C)	MELT (°C)	FILL (secs)	SKIN THICKNESS (μm)	EXTENT OF STRUCTURELESS BAND (mm)	EXTENT OF B PHASE ROW NUCLEATION (mm)	MAX β DIAMETER (μm)	MAX α DIAMETER (μm)
35	220	1.35	20	>20	45-50	~20	30-40
35	220	4.00	15	20-25	45-50	~20	30-40
35	280	1.35	10-15	<20	40	~30	45-50
35	280	1.35	10-15	<20	<45	~30	45-50
80	220	4.00	trans.	20-30	>45	~60	50-60
80	280	1.35	trans.	<20	>45	~70	60-80
80	280	4.00	trans.	<20	>45	~60	60-70

TABLE 23 Distribution of morphological bands in Sandretto injection moulded iPP plaques.

MOULDING CONDITIONS MOULD (°C)	MELT (°C)	FILL (%)	SKIN THICKNESS (μm)	EXTENT OF STRUCTURELESS BAND (mm)	EXTENT OF β PHASE ROW NUCLEATION (mm)	MAX β DIAMETER (μm)
30	220	30	15-20	30	50	<35
30	250	30	10	15	40	<35
30	280	30	5	10	35	35-40
50	220	30	30	25	45	<60
70	220	30	20	35	45	20-30
30	220	15	20	45	60	<60
30	220	45	<10	40	45	<60

to produce mouldings reduced the extent of banded morphologies, and high mould temperatures significantly reduced the skin thickness and induced transcrystalline growth at the surface. The point along the flow direction at which β phase spherulites die away corresponded well to the increase in Izod impact strength, particularly with increasing melt temperature.

The low magnification gate area micrographs presented provide interesting comparisons of the degree of β phase nucleation, and formation of this structureless band in the final packing stage, from one processing condition to another. See Figure 69.

It can be seen that mouldings produced at high melt temperatures significantly reduced the β phase nucleation and width of the structureless band. However, changes in mould temperature appear to have had no significant effect on structural heterogeneities below the surface of mouldings.

The role of the frozen skin thickness on impact properties was also better understood from these studies. In the absence of a skin layer (i.e. in mouldings produced at high mould temperatures) the impact properties were severely impaired. However, in mouldings with relatively thick skins (i.e. in mouldings produced using slow cavity fill times or low melt temperatures) the properties were also impaired when banded morphologies and in particular β-phase spherulites were present. It appears that the influence of the skin is only appreciated at the point where β-phase spherulites disappear, for example, note the marked improvement in properties in low melt temperature mouldings and slowly injected mouldings at the far side of plaques where only skin-core morphologies are present.

As with the Daniels mouldings the microtomy of Izod test pieces prepared from low and high melt temperature mouldings, selected for more detailed impact property studies was carried out. The impact property variations illustrated in Figure 62 were then related to the micrographs presented in Figures 73 and 75 for the low and high melt temperature mouldings respectively.

The obvious dependence of impact properties on the row nucleated β phase spherulites was again revealed since significant improvements in the impact properties occured at the point where these structures die away. This transition occurs at 21mm and 70mm for the 220°C and 280°C melt temperature mouldings respectively which is significantly different to that found in Daniels mouldings.

3.3.4 Impact Properties of 2mm Thick iPP Injection Mouldings With Surface Layers Machined Off

To assist in the understanding of the influence of processing conditions on structure development and consequent impact properties the surface layers of 3mm thick Daniels mouldings were removed by Fly-Cutting. Removing 500 μm from each surface successfully eliminated shear nucleated β-phase spherulites and banded morphologies to leave essentially 2mm of α-phase spherulitic structures. These machined plaques were found to have sufficiently smooth surfaces to dismiss any need for polishing before impact testing.

The samples were impact tested, using the procedures outlined previously, in both Izod and drop-weight modes and their resultant properties compared to as-moulded 2mm thick plaques prepared under identical conditions. This simple experiment provided a means of measuring the impact properties of

mouldings with and without banded morphologies and row nucleated β-phase structures. The results are shown in Table 24 for selected Izod tests and in Table 25 for centre of moulding drop-weight tests. These results are presented graphically in Figures 80 and 81.

From these results a significant improvement in impact properties with removal of 500 μm of surface material was observed. The improvement for low melt temperature moulded plaques was particularly impressive up to halfway across with an increase in Izod impact strengths by a factor of 2.6x and drop-weight impact strengths by a factor of 11.6x. Low melt temperature mouldings revealed far more extensive row nucleation of the β-phase spherulties which explains the improvement in impact properties with the removal of these weakening structures.

These results highlight the possibility that the α-phase of polypropylene produced by slow cooling can provide a mechanism of improving the impact properties. Typical microstructures of the as-moulded and fly cut Izod samples are presented in Figure 82 (a-d).

3.4 TRANSMISSION ELECTRON MICROSCOPY STUDIES (TEM)

A sample revealing typical banded morphologies in polarised light was chosen for replication and etching to provide information on lamellar microstructures. A surface through the thickness parallel to the flow direction was exposed by microtomy and then ground wet to 600 emery followed by careful polishing to a 1 μm finish using diamond paste wheels. The surface was ultrasonically cleaned and then etched according to the permanganic etching technique described in Section 2.7 using 1 wt% of $KMnO_4$ and an etching time of 30 minutes

TABLE 24 Selected area Izod test results for 2mm thick as-moulded and 2mm thick fly-cut iPP plaques.

MOULDING CONDITIONS	I.S 20 mm (kJm-2) $\bar{x}$	s.d	I.S 45 mm (kJm-2) $\bar{x}$	s.d	I.S 70 mm (kJm-2) $\bar{x}$	s.d
35/220/1.35	3.47	1.14	3.69	0.72	10.51	3.27
35/220/1.35 FLY CUT	7.40	1.71	9.54	3.12	12.02	1.51
35/280/1.35	4.55	0.27	9.27	2.35	11.13	1.71
35/280/1.35 FLY CUT	5.74	0.35	10.95	2.40	13.05	1.05

Figure 80 Mean Izod impact strength versus distance from gate for 2mm thick fly cut and as-moulded iPP plaques.

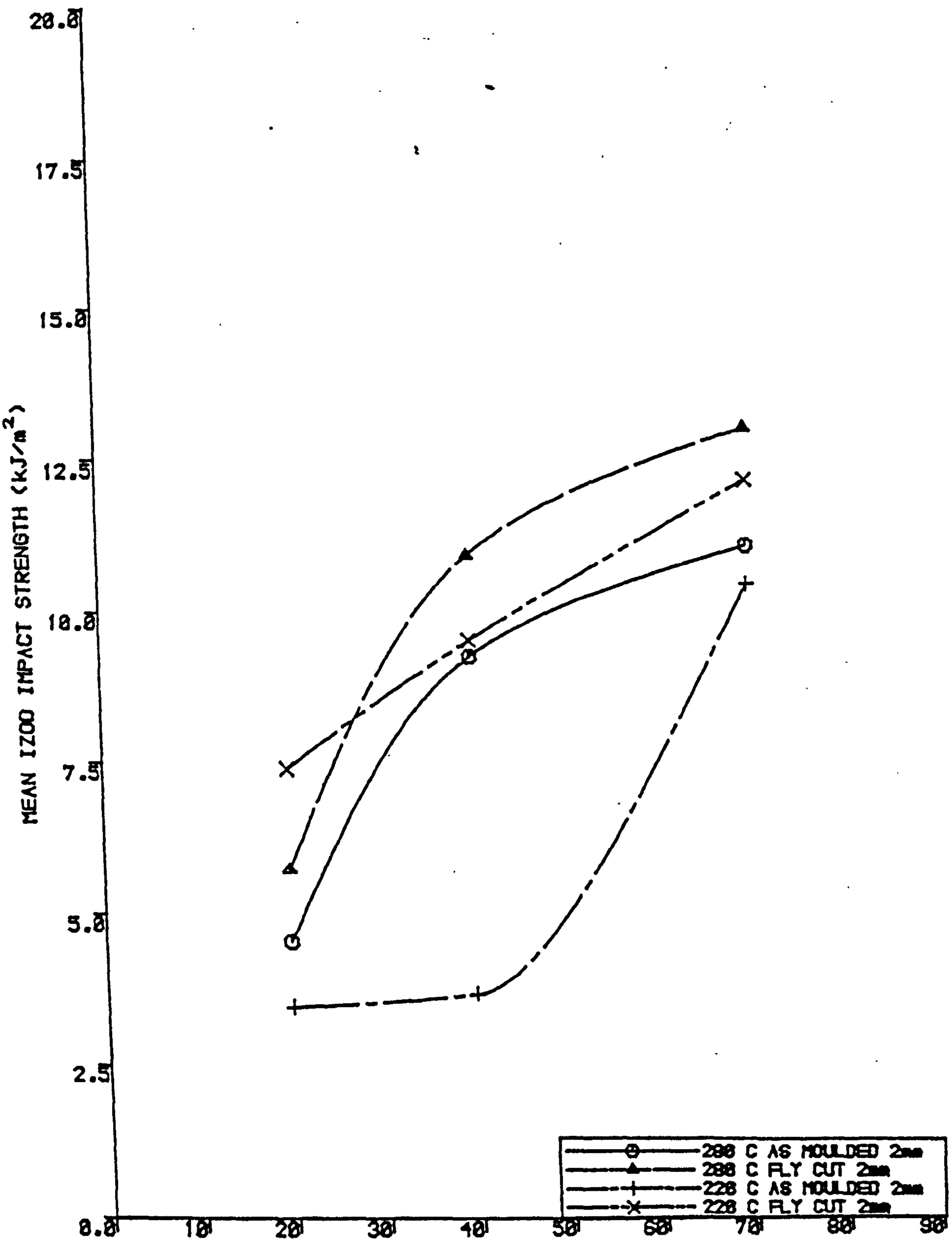

TABLE 25 Instrumented drop-weight impact test results for 2mm thick as-moulded and 2mm thick fly-cut iPP plaques.

MOULDING CONDITIONS	PEAK ENERGY (Nm) $\bar{x}$	s.d	PEAK FORCE (N) $\bar{x}$	s.d
35/220/1.35	0.151	0.038	171.02	28.88
35/220/1.35 FLY CUT	1.750	0.340	941.32	134.06
35/280/1.35	0.801	0.117	528.26	53.15
35/280/1.35 FLY CUT	2.037	0.753	1010.82	275.12

Figure 81 Mean peak drop-weight impact energy versus moulding condition for 2mm thick fly cut and as-moulded iPP plaques.

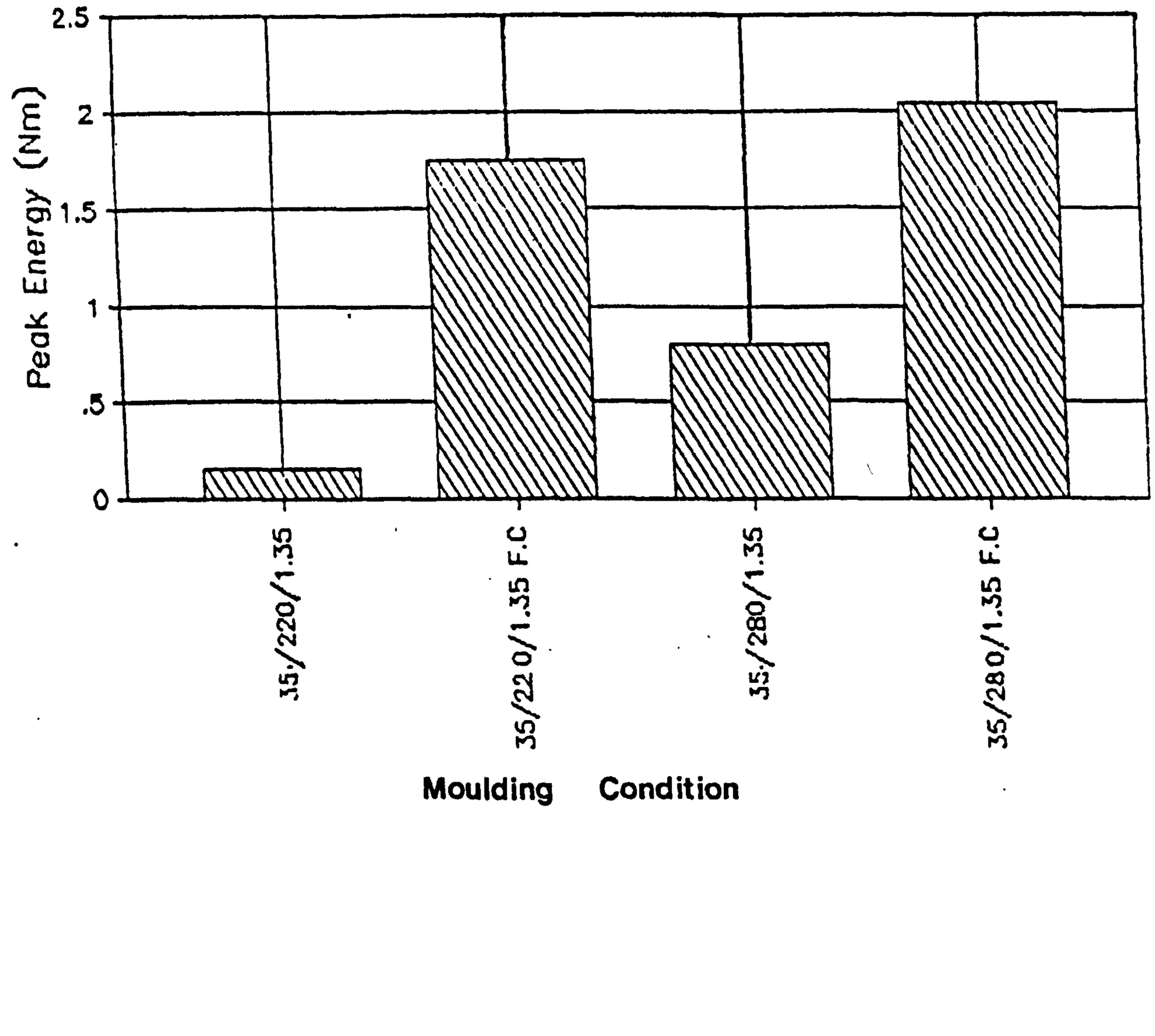

Figure 82

(a) Variation in surface microstructure of a low melt temperature as moulded 2mm thick plaque.

(b) Surface microstructure of a low melt temperature fly cut 2mm thick plaque.

(a) 2mm thick as-moulded plaque.

scale bars = 100μm

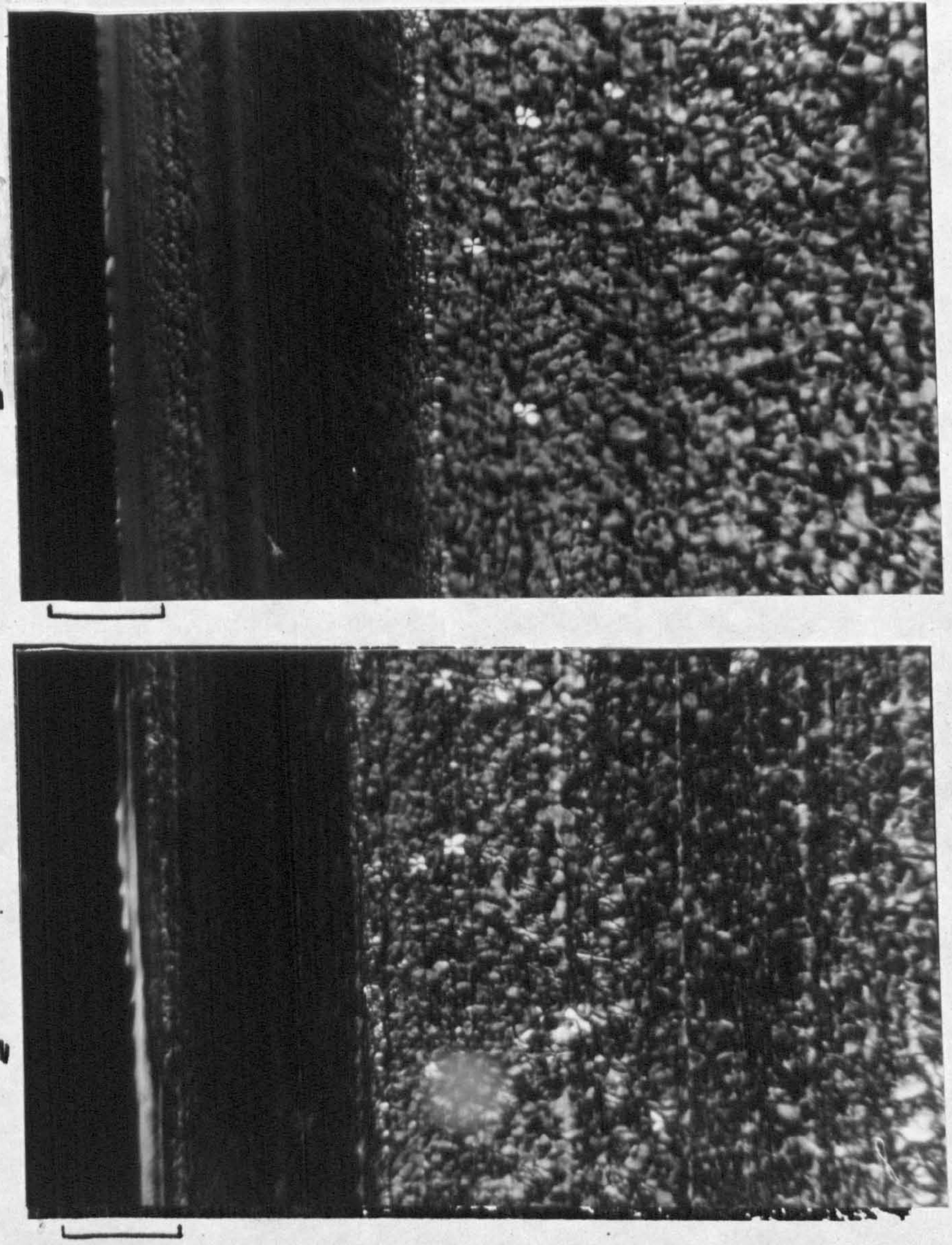

20mm

45mm

70mm

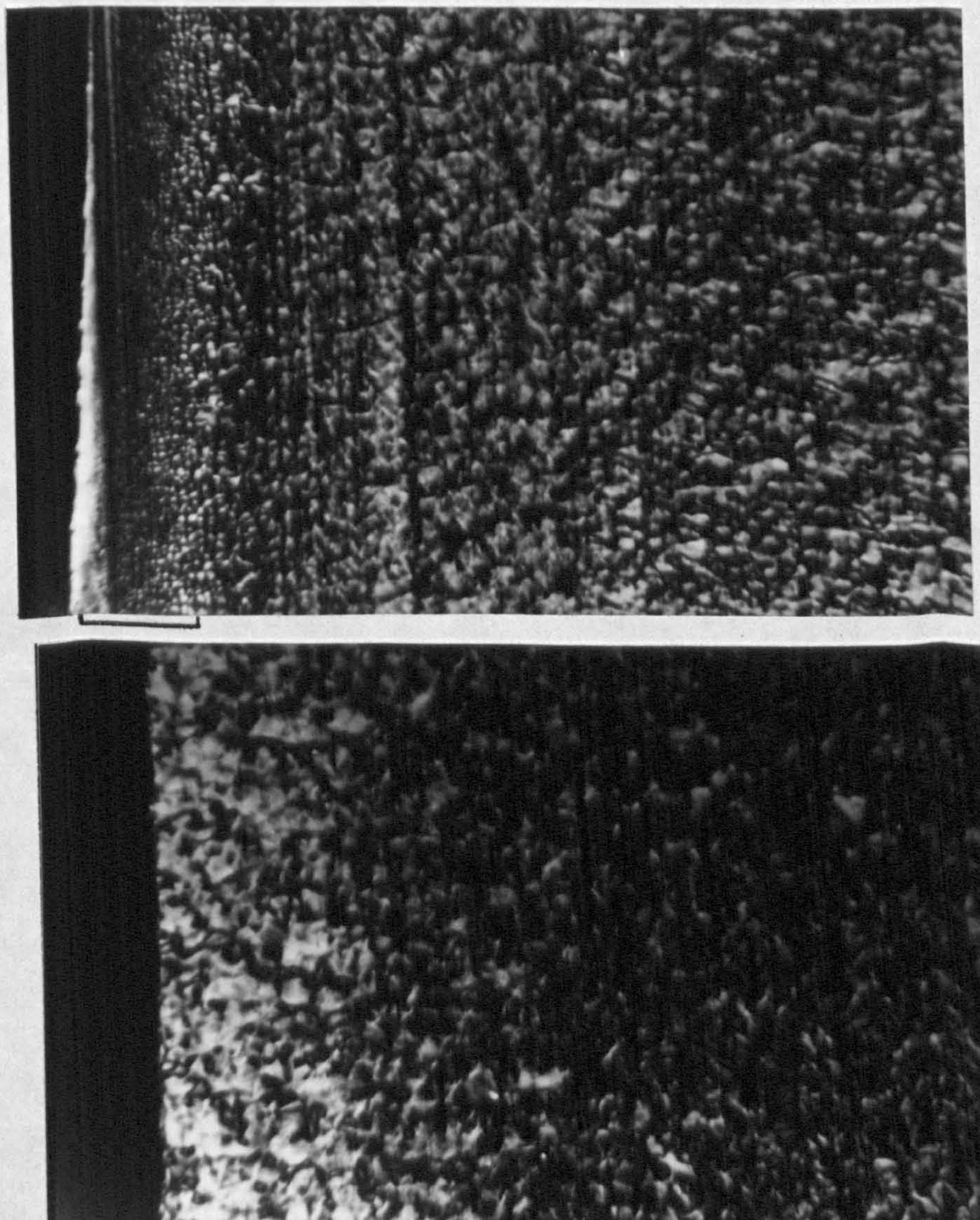

(b) 2 mm thick fly-cut plaque.

(c) Variation in surface microstructure of a high melt temperature as moulded 2mm thick plaque.

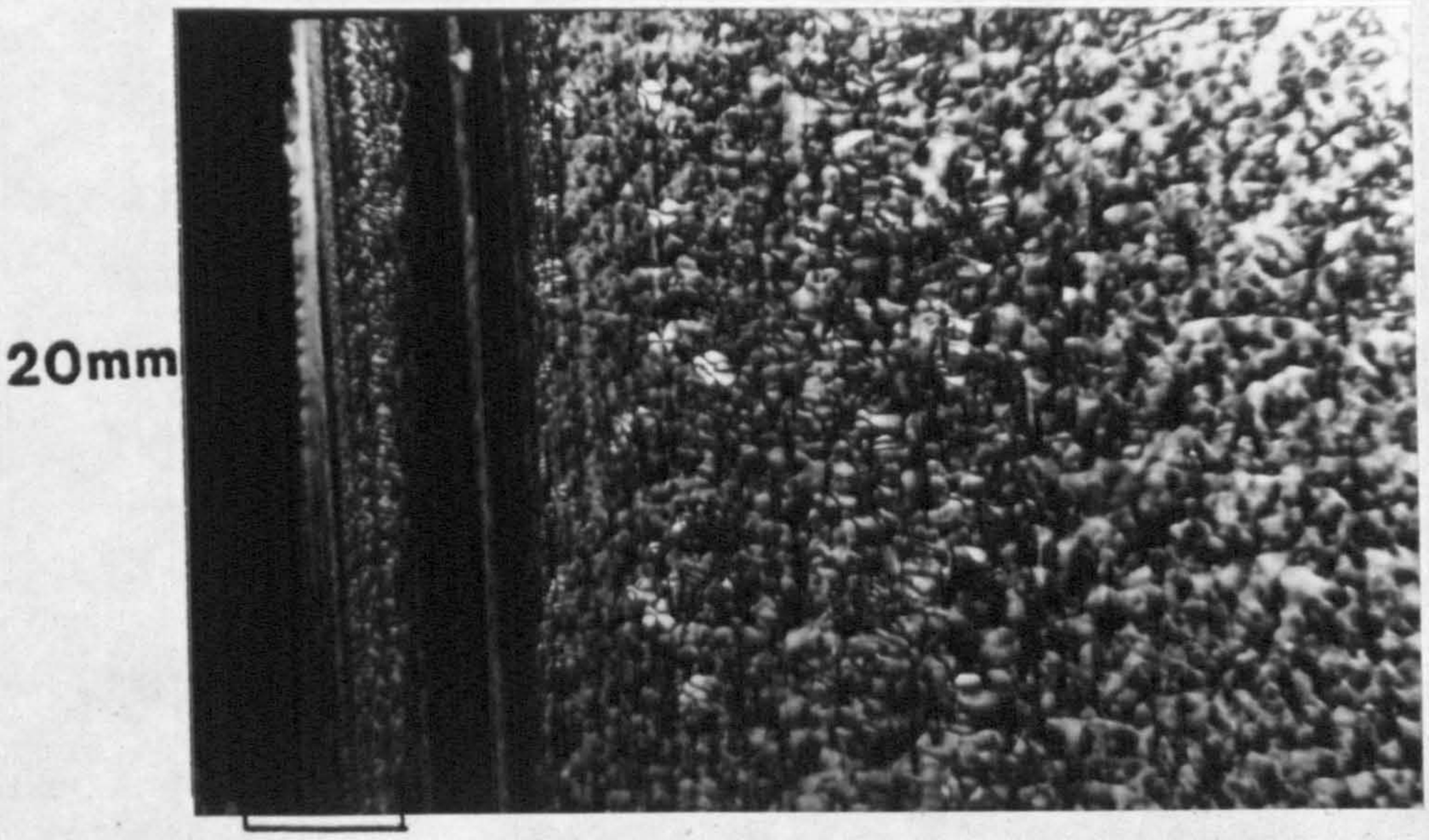

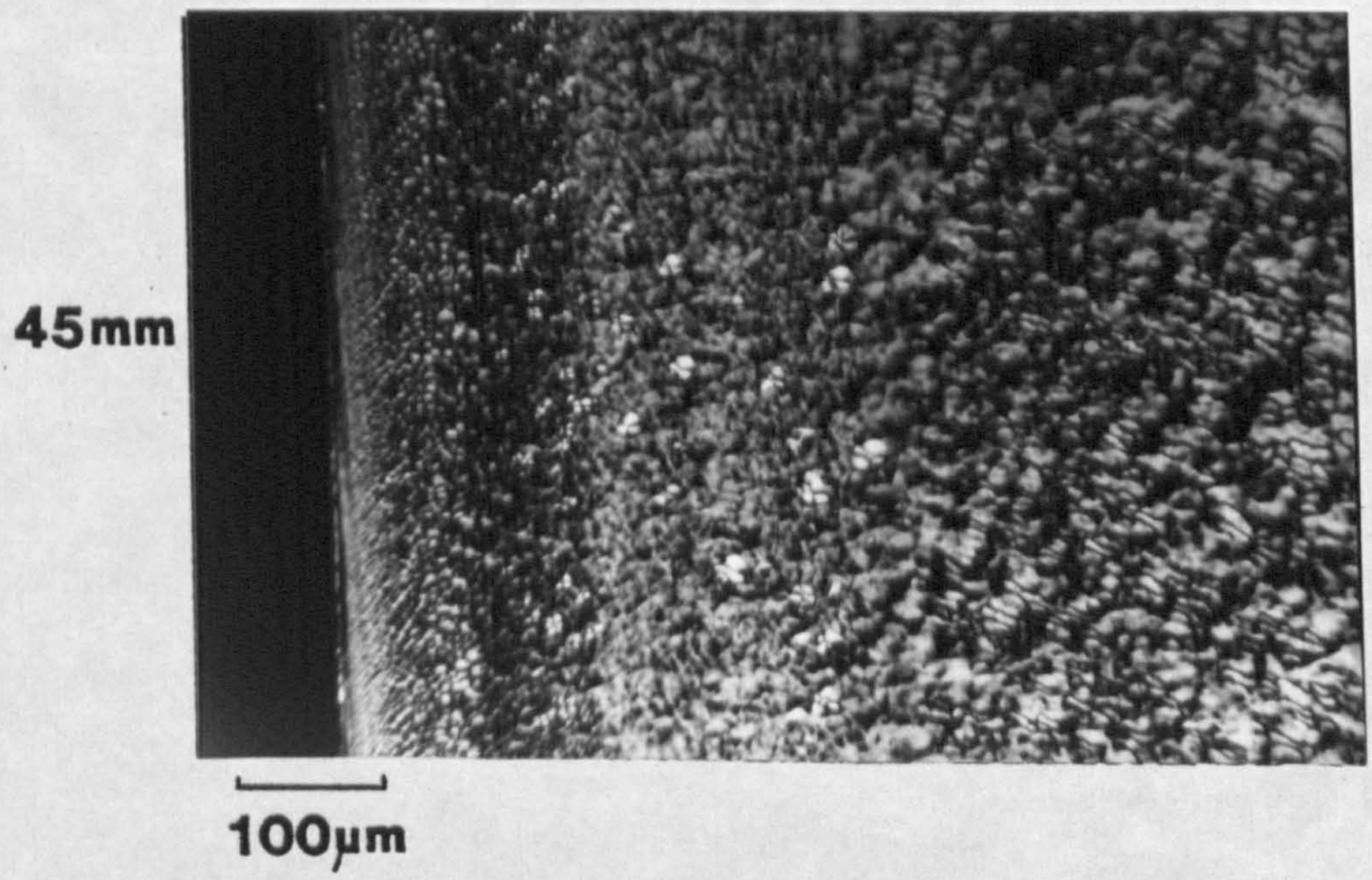

(d) Surface microstructure of a high melt temperature fly cut 2mm thick plaque.

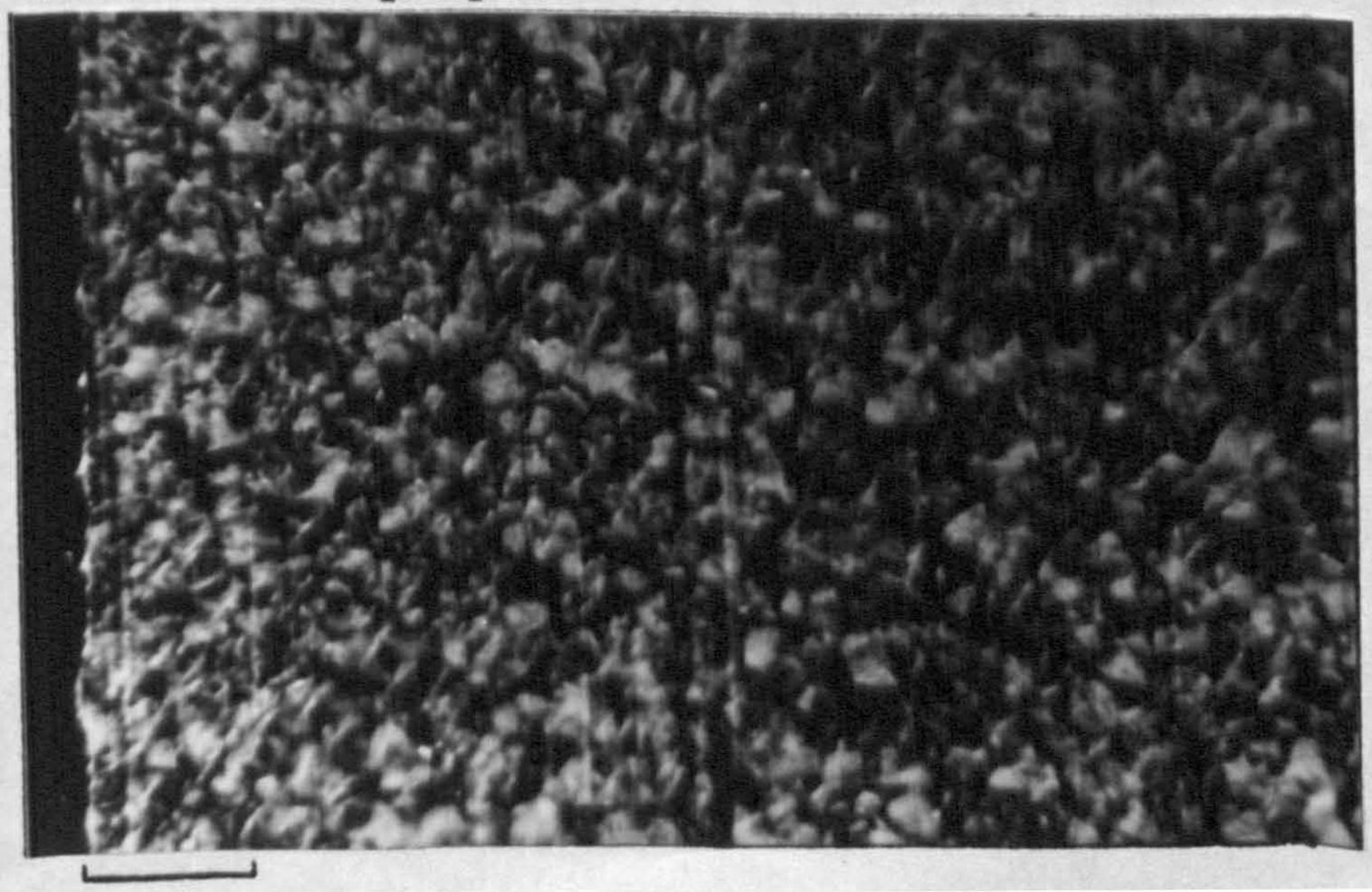

(found by trial and error to give the best results). The etched surface was cleansed using the 5 stage treatment before replication using the Norton (63) technique previously described. Examination of replicas by TEM was performed using a Philips EM301 and Jeol 100CX microscope. The resultant micrographs are presented with detailed examinations.

Figure 83 shows the low magnification micrographs montaged to reveal the skin, structureless band, βphase spherulites and typical core spherulites remarkably similar to that seen in polarised light microscopy. At this low magnification the fine detail of the non-spherulitic morphologies are not revealed but it is immediately clear that the band of what was originally thought to be structureless material is infact essentially lamellar in nature. It is of interest to note that this region above the spherulitic core has cracks running perpendicular to the injection direction, a similar observation was found by Fitchmun and Mencik (77) with aqueous chromium trioxide etchant and chromic-sulphuric acid etchants.

This low magnification study established an important point as a result of the similarity in layered morphologies observed in both types of microscopy. The layers represent real differences in crystalline morphologies and not artifacts associated with the methods of sample preparation.

At higher magnifications, some of the fine features of the individual layers became visible. The skin layer was found to have very little structure, as shown in Figure 84, with a slightly pebbled fibrous pattern with apparently all lamellae oriented in the flow direction. This layer probably consists of chain extended material typical of highly oriented melts.

Figure 83

Low magnification TEM micrographs montaged to reveal the skin, structureless band, β phase spherulites and core spherulites typical of iPP mouldings.

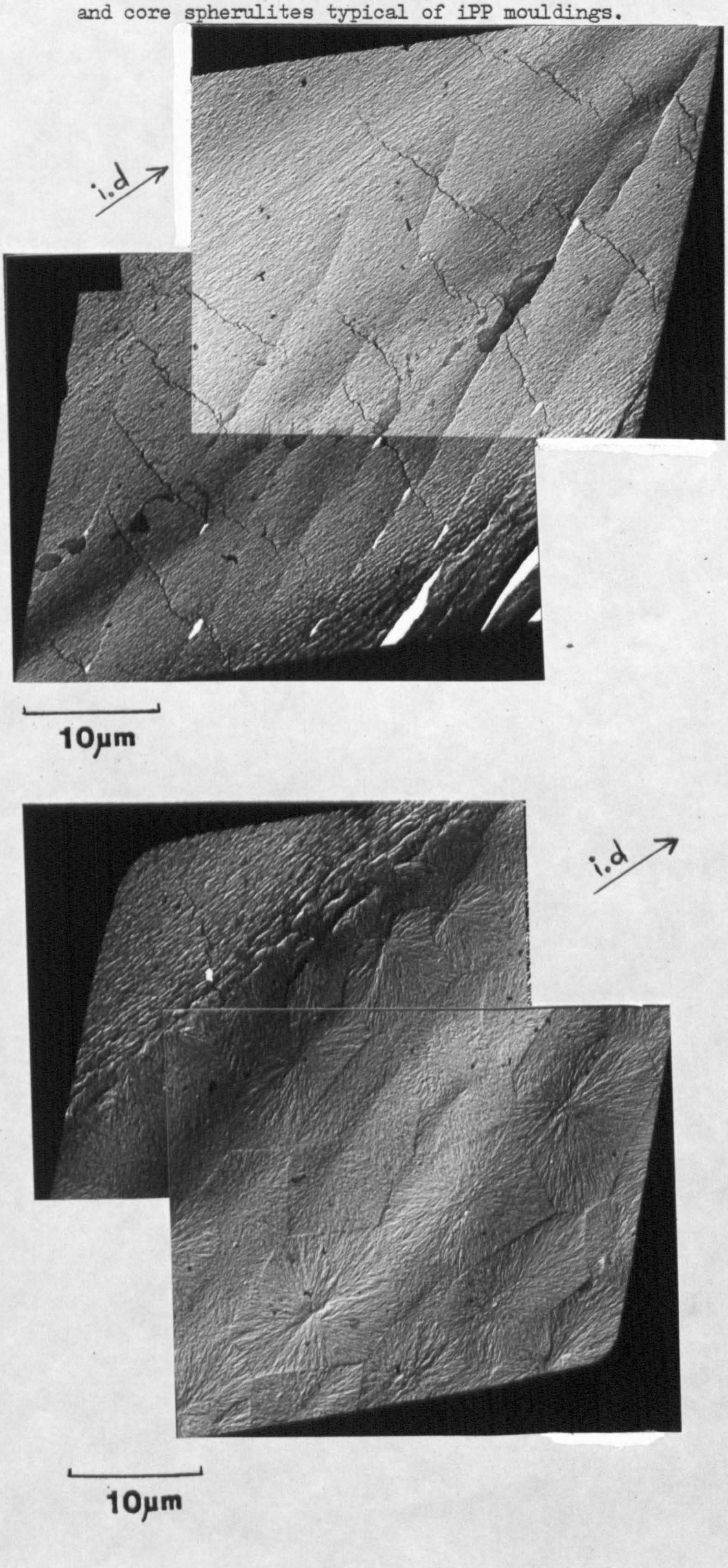

Figure 83 cntd.

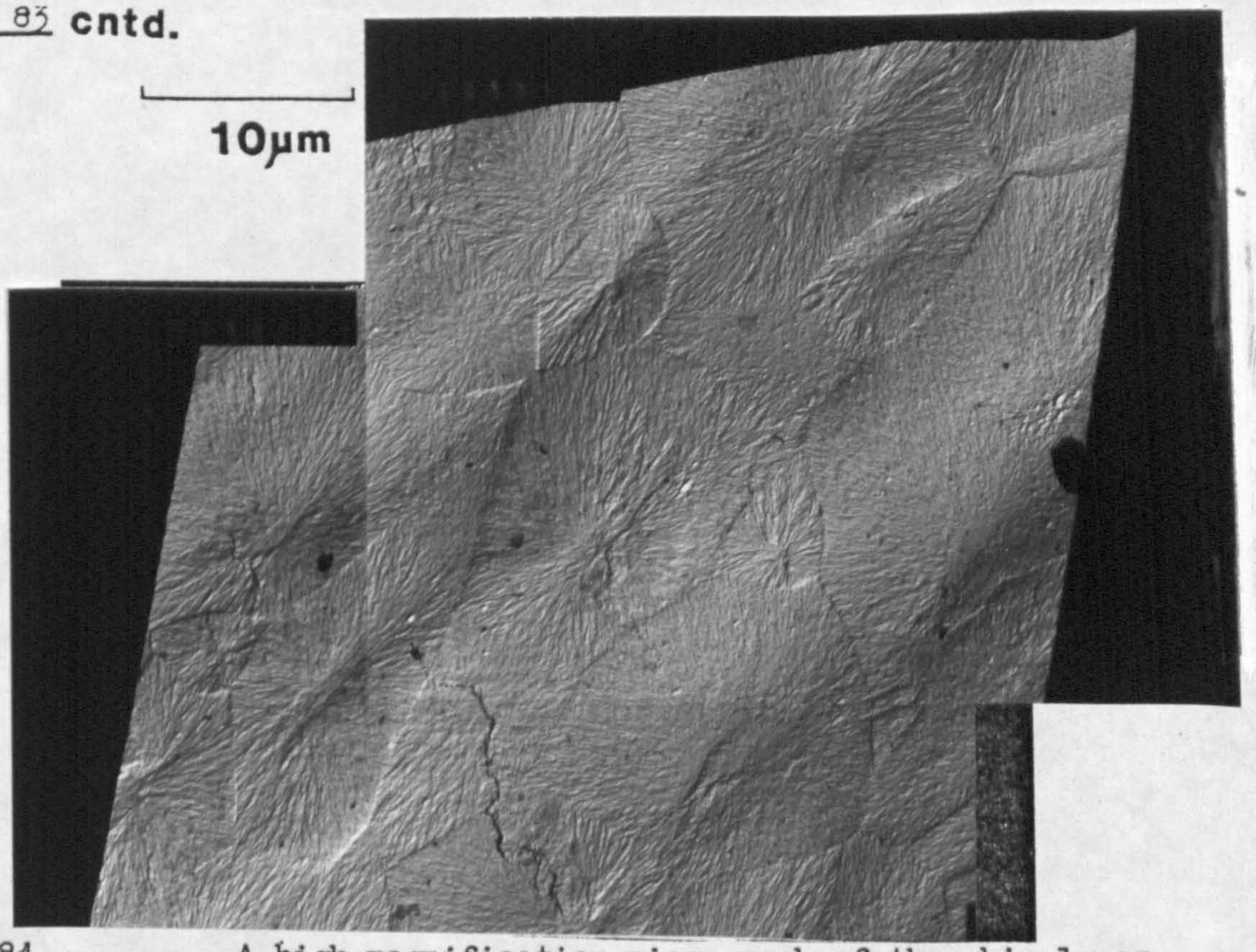

Figure 84 A high magnification micrograph of the skin layer revealing very little structure but a high degree of alignment of fine lamellae.

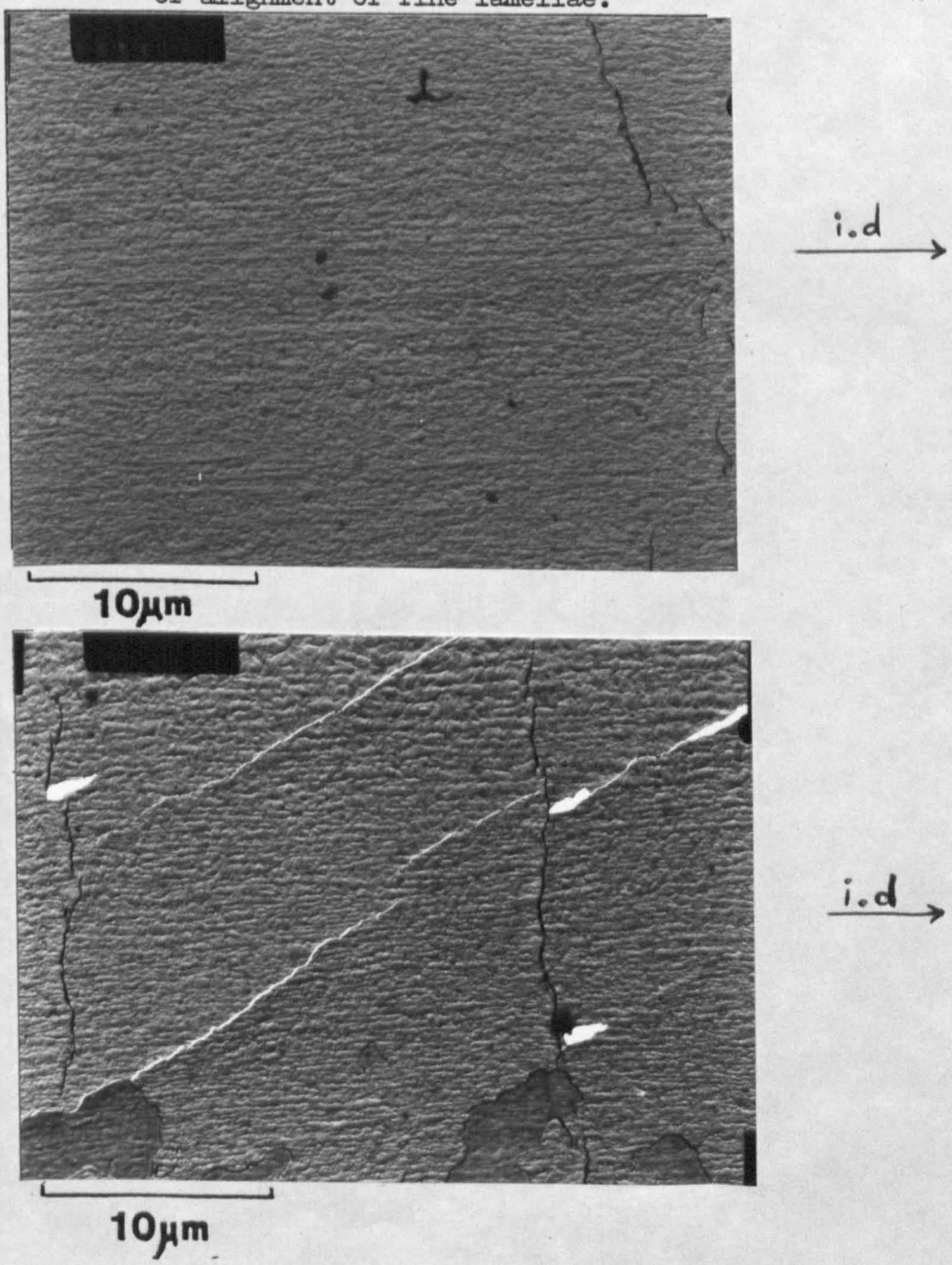

Figure 85(a),(b) The morphology in the highly sheared region revealed typical row nucleation of lamellae lying perpendicular to the flow direction.

Figure 86 A high magnification micrograph of the row nucleate lamella region.

(a)

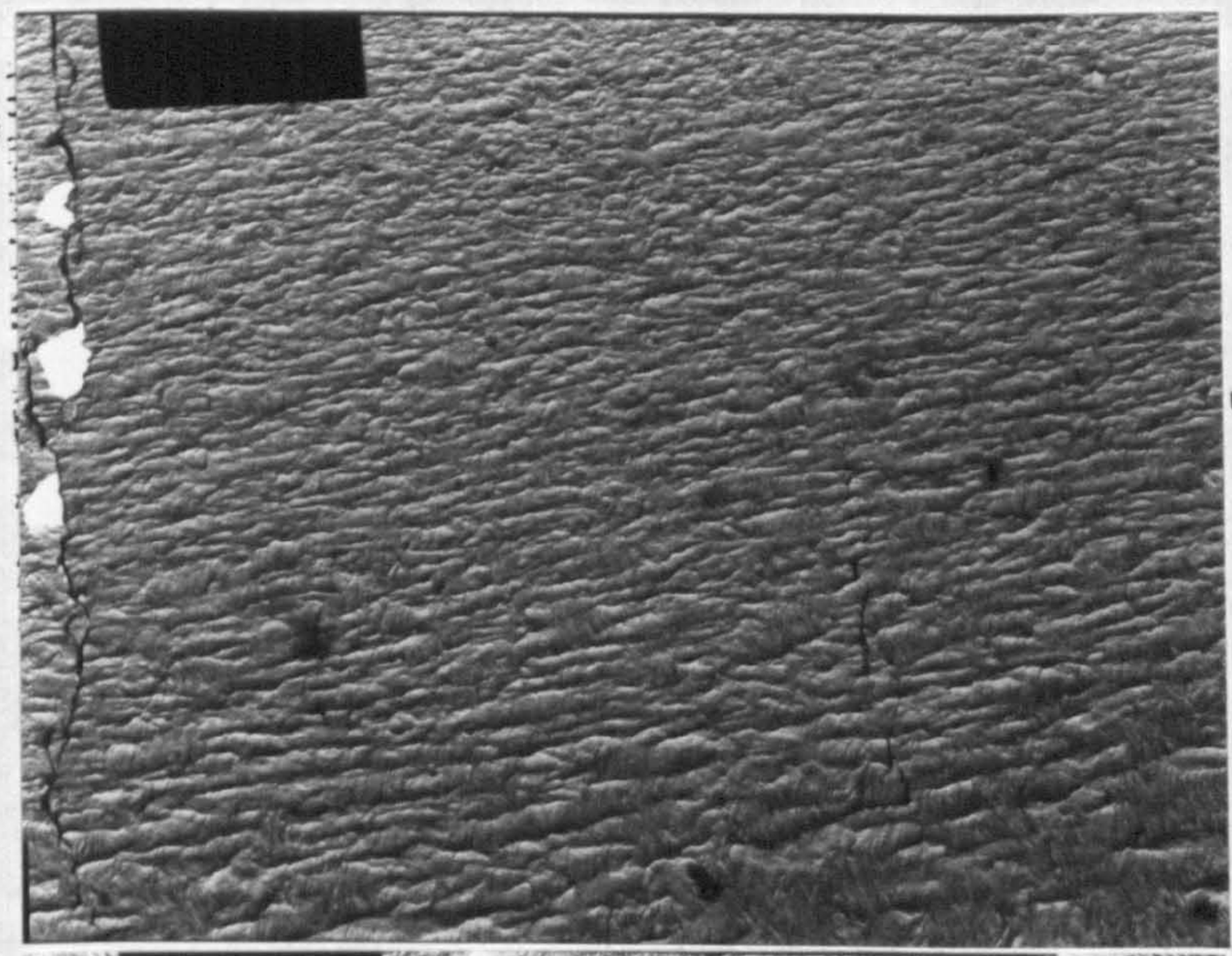

10μm

1.d

(b)

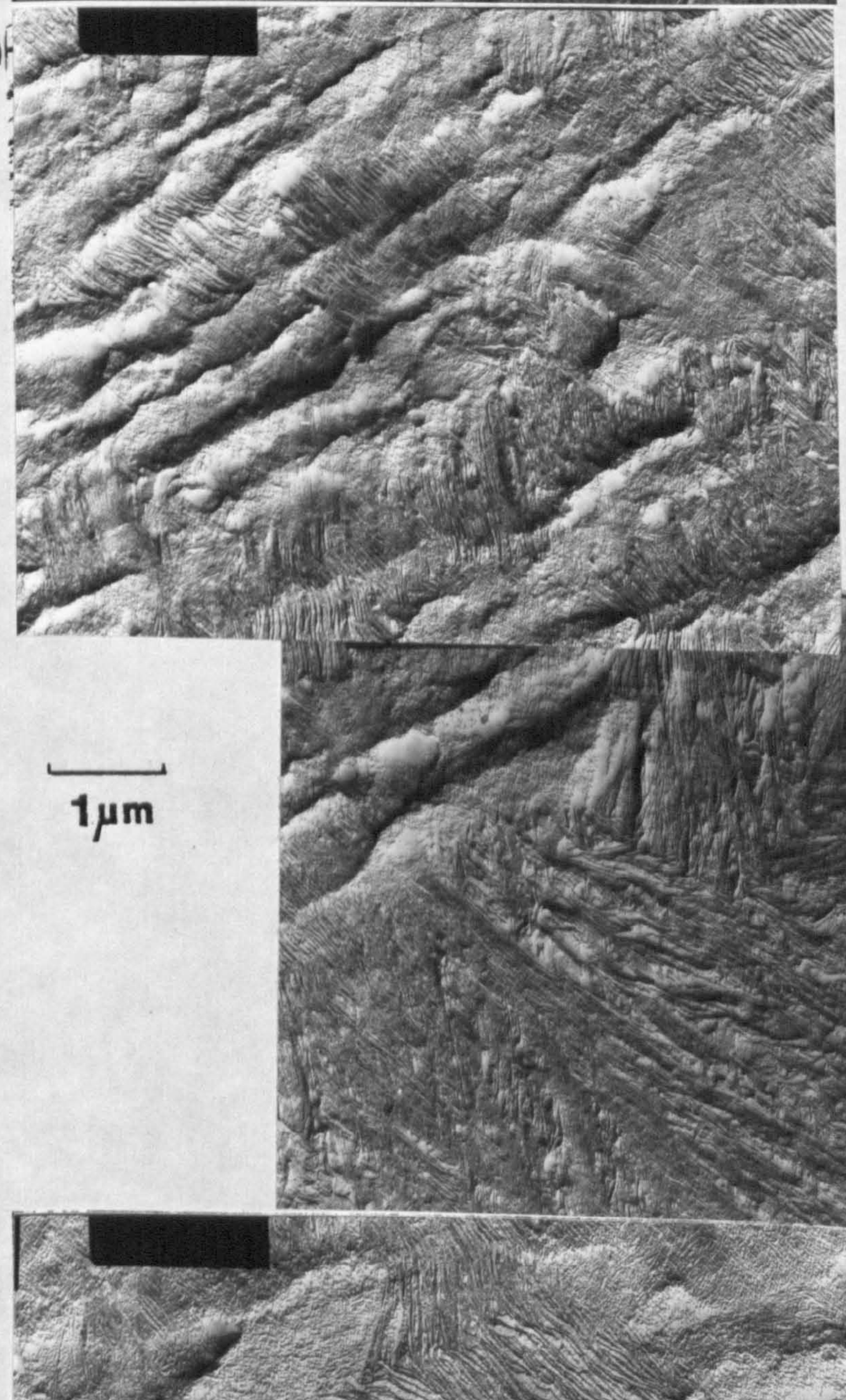

1.d

1μm

1μm

Frozen in fibrous type molecular orientation with all chain segments of the crystals both lamellae and fibrils aligned parallel to the injection direction occurs due to the high degree of shear that the polymer melt is under before freezing. This type of morphology is universally known as shish-kebab.

The morphology in the band of material below the skin revealed typical row nucleation of lamellae lying perpendicular to the highly aligned fibrous growths seen in the skin layer. This transverse growth of lamallae is shown in Figure 85 at 13.7k and in Figure 86 at 17k. The lamellae are in the order of 100Å in width and upto c.a. 4 μm in length. The length of lamellae and the degree of row nucleation was found to increase towards the centre of the moulding. In the case of an injection moulding the crystallisation temperature increases away from the cold mould wall as do shearing stresses to a certain point depending on the melt temperature and injection velocity. Both of these factors will enhance row nucleation as has been seen in the micrographs.

The nucleation of typical row β spherulites at the boundary with this fibrous band was observed as shown in Figure 87. These structures result from the massive nucleation along lines due to flow and shear within the material. With so many nuclei, growth can only proceed perpendicular to the original line of flow, this transverse growth is equivalent to that along the radius of a spherulite possessing the same crystallographic axis. The size of these spherulites is of the order of 5-10 μm.

Figure 87 (a) The row nucleation of β spherulites at the boundary with the row nucleated lamellar region.
(b) & (C) At increasing magnifications the β spherulites reveal entirely radial organisation of lamellae.

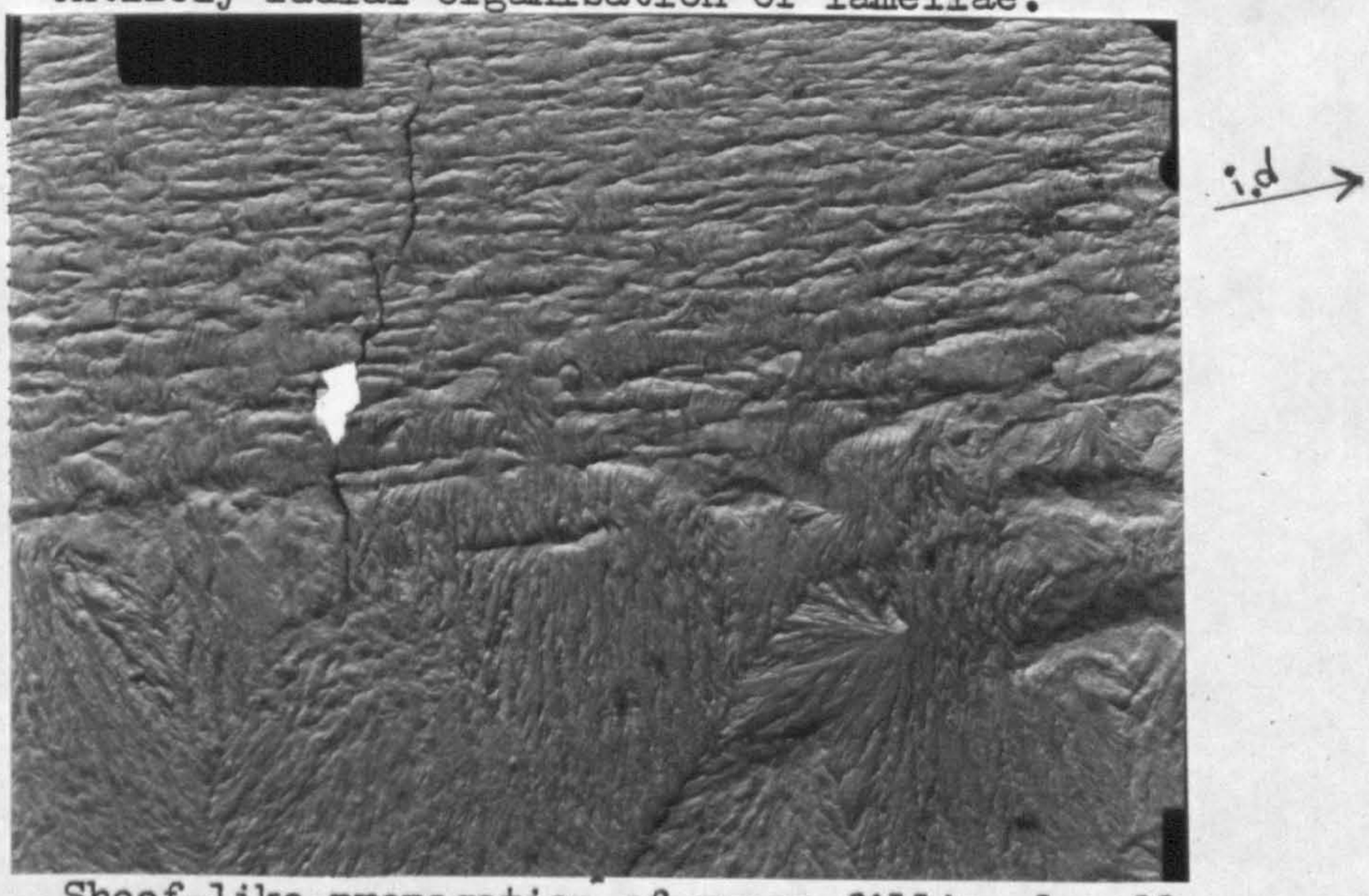

Figure 88 Sheaf-like propagation of space filling lamellae to form a spherulite as sketched in Figure 3.

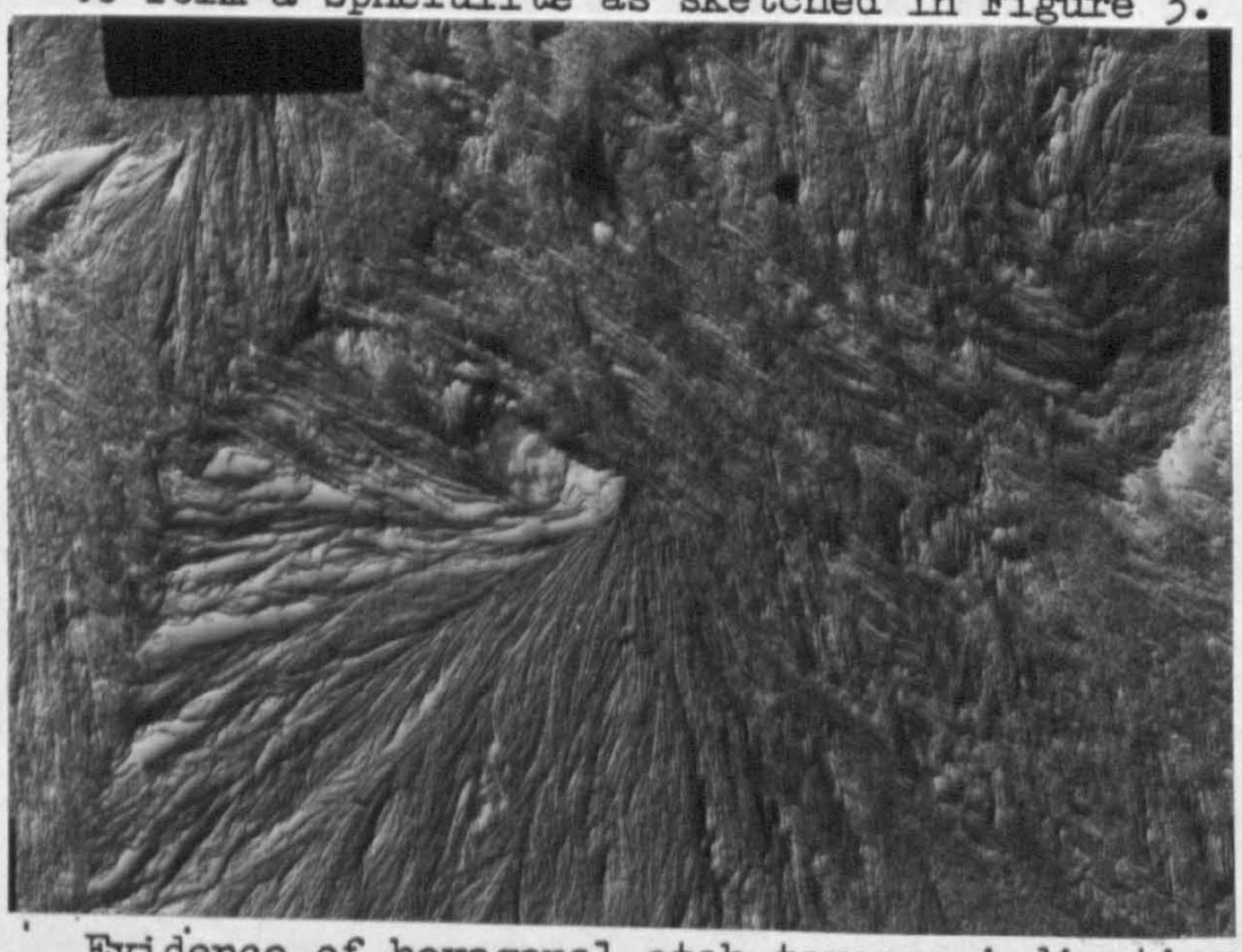

Figure 89 Evidence of hexagonal etch teraces indicating the possibility of screw dislocation growth mechanisms.

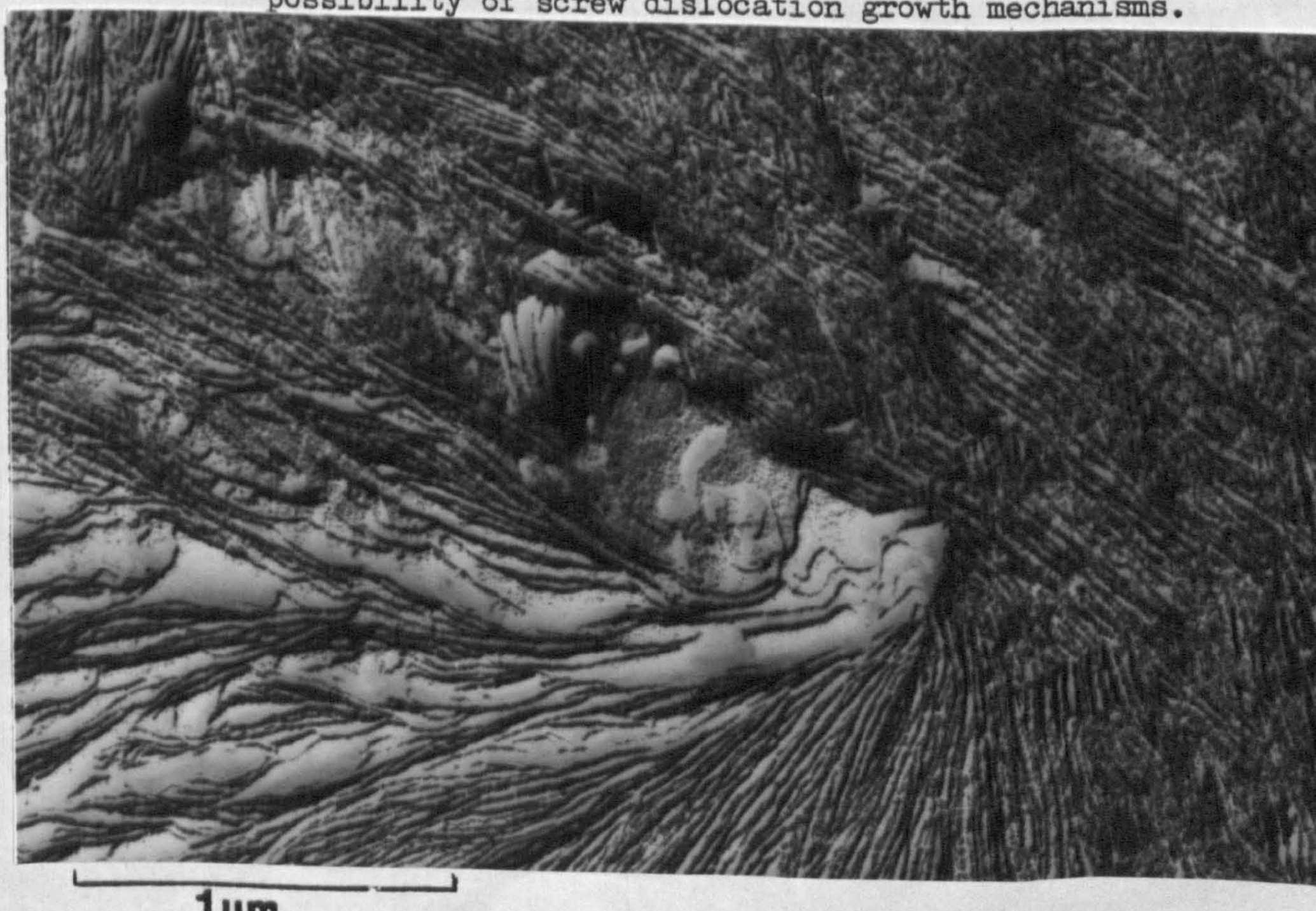

At increasing magnifications of 13.7K and 48K the spherulites revealed entirely radial organisation of lamellae typical of the β phase spherulites found by Norton and Keller (63) in melt grown crystals. The broad locally parallel stacked lamellae, just as in other polymer spherulites, revealed a sheaf like progagation of the space filling lamellae as sketched in Figure 3. In Figure 88 it can be seen that on the right hand side lamellae are stacked parallel and edge-on, a typical b-axis profile, whilst the left hand side illustrates the situation when the lamellae are viewed flat-on, i.e. closely along the c-axis or molecular chain direction. Some evidence of the development of numerous hexagonal etch teraces indicating the possibility of screw dislocation growth mechanisms was found, these are shown in Figures 89 close to the sheaf-like propagation. These observations are in agreement with the observed β -phase spherulites found nucleating along rows in optical microscopy studies.

The core spherulites reveal the unique and puzzling feature of cross-hatch type lamellar branching identified to occur in all types of α-phase monoclinic polypropylene (55,62,63). Figure 90 illustrates a low magnification appearance of these spherulites which occur upto 40 μm in diameter towards the centre of mouldings. Figure 91 illustrates how the branching affects the underlying lamellar morphology bestowing upon it what is essentially a bimodal orientation where radial lathlike lamellae nucleate tangential and cross-hatched overgrowths of lamellae are oriented nearly orthogonally. Figure 92 shows the essential appearance and features of the cross-hatched morphology. On this figure R represents the radial direction within the spherulite whilst the direction T represents the branched, Tangential direction, characteristic of the cross-

Figure 90

Low magnification micrograph of the α phase monoclinic iPP spherulites.

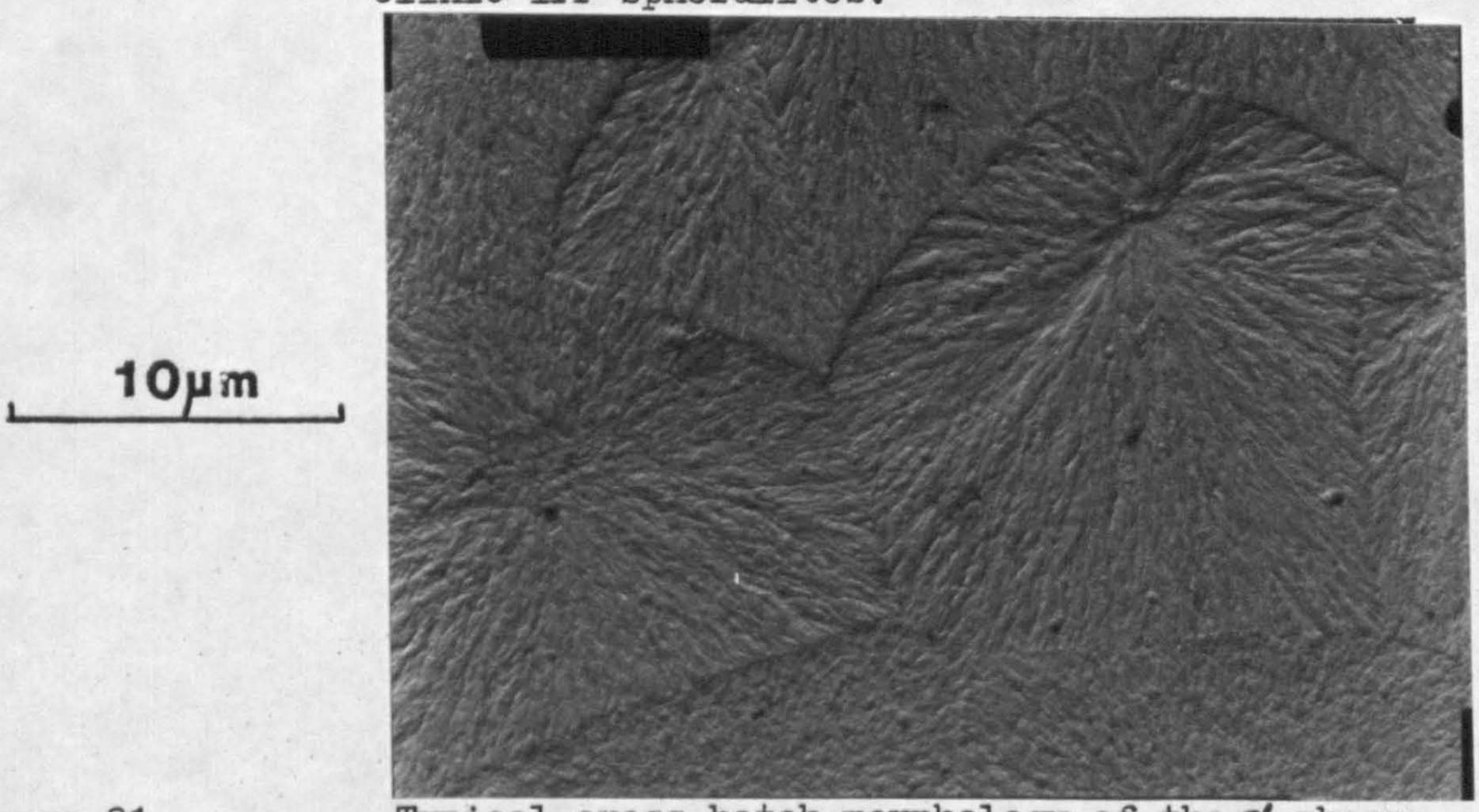

Figure 91

Typical cross-hatch morphology of the α phase spherulite.

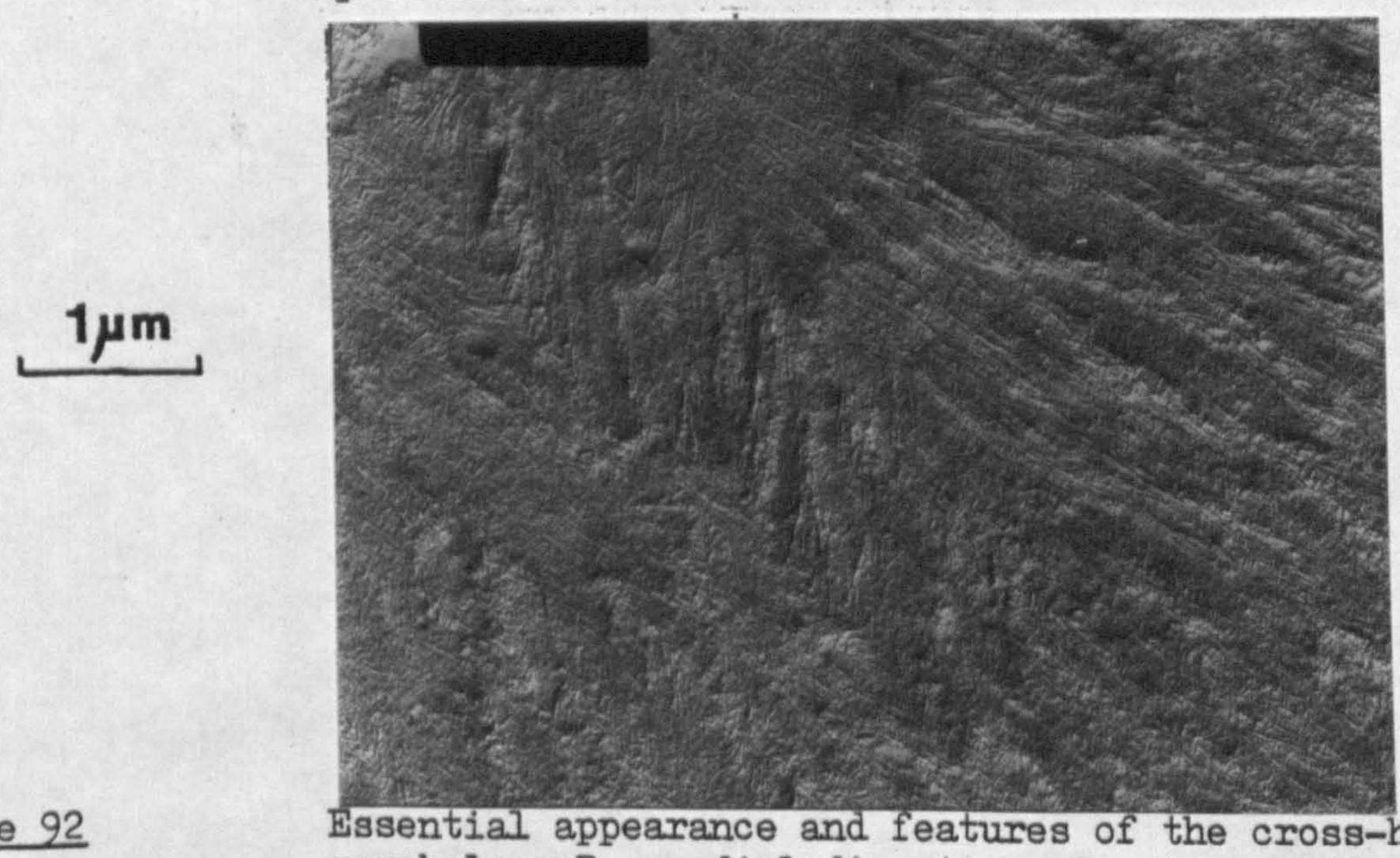

Figure 92

Essential appearance and features of the cross-hatched morphology R = radial direction, T = tangential direction; with N = 'nodular' structures.

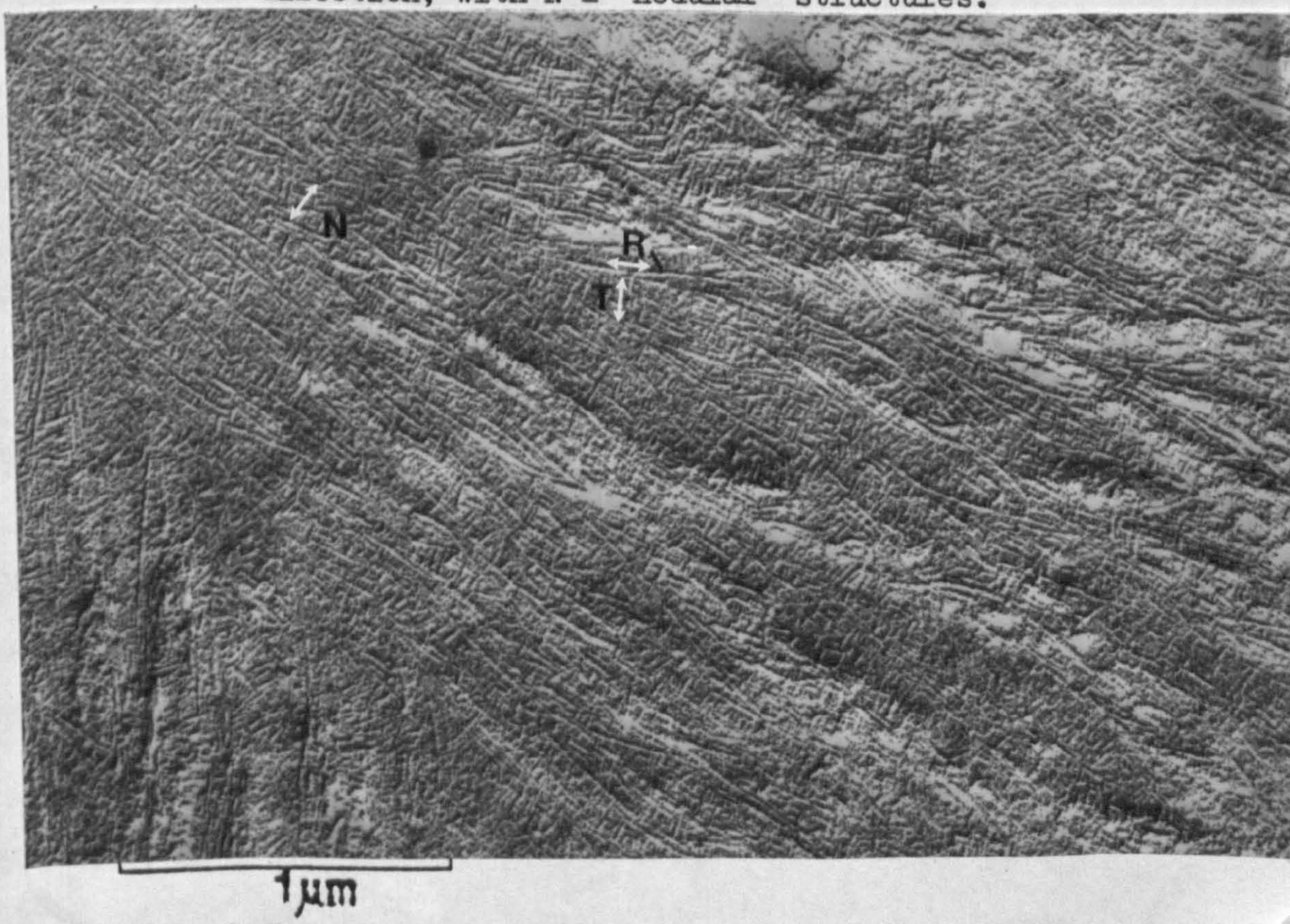

hatched overgrowth. The intercrossing and shorter lamellae, T, were measured to be at angles of around 80° with respect to the radial direction which is in good agreement with observations by Khoury (55). Norton (63) found that at crystallisation temperatures of 148°C the differences in the respective thicknesses of the two components revealed that radial lamallae were slightly thicker c.a. 50 nm compared to c.a. 40 nm for the tangential component.

The consequence of such twinning provides a natural explanation for the changing birefringence of spherulites of monoclinic polypropylene. The net birefringence and its sign depend on the relative proportions of twinned and untwinned components. Lamellae with radial growth display negative birefringence (as with β spherulites) whereas lamellae with tangential growth display positive birefingence. It then follows that in Type I α-phase spherulites the T and in Type II α-phase spherulites the R lamellae should predominate in the cross-hatch. In spherulites observed (close to the row nucleated β spherulites a greater fraction of the tangentially oriented component was found. In numerous places the texture appears 'nodular' rather than lamellar, this is thought to represent the earliest stages of branching, marked N in Figure 92. As the core of mouldings is approached it is thought that increasing temperatures should lead to a progressive reduction in the proportion of tangential lamellae and a subsequent change in the birefringence.

The few chosen examples of Figure 93 (a-c) illustrate the appearance of the α/α phase boundary morphologies, there are regions of an excess of radial or tangential component. Typical areas where these differences occur are

Figure 93 (a - c) A few chosen examples of the appearance of the α/α phase boundary morphologies. Regions marked F = flat on views of lamellae;

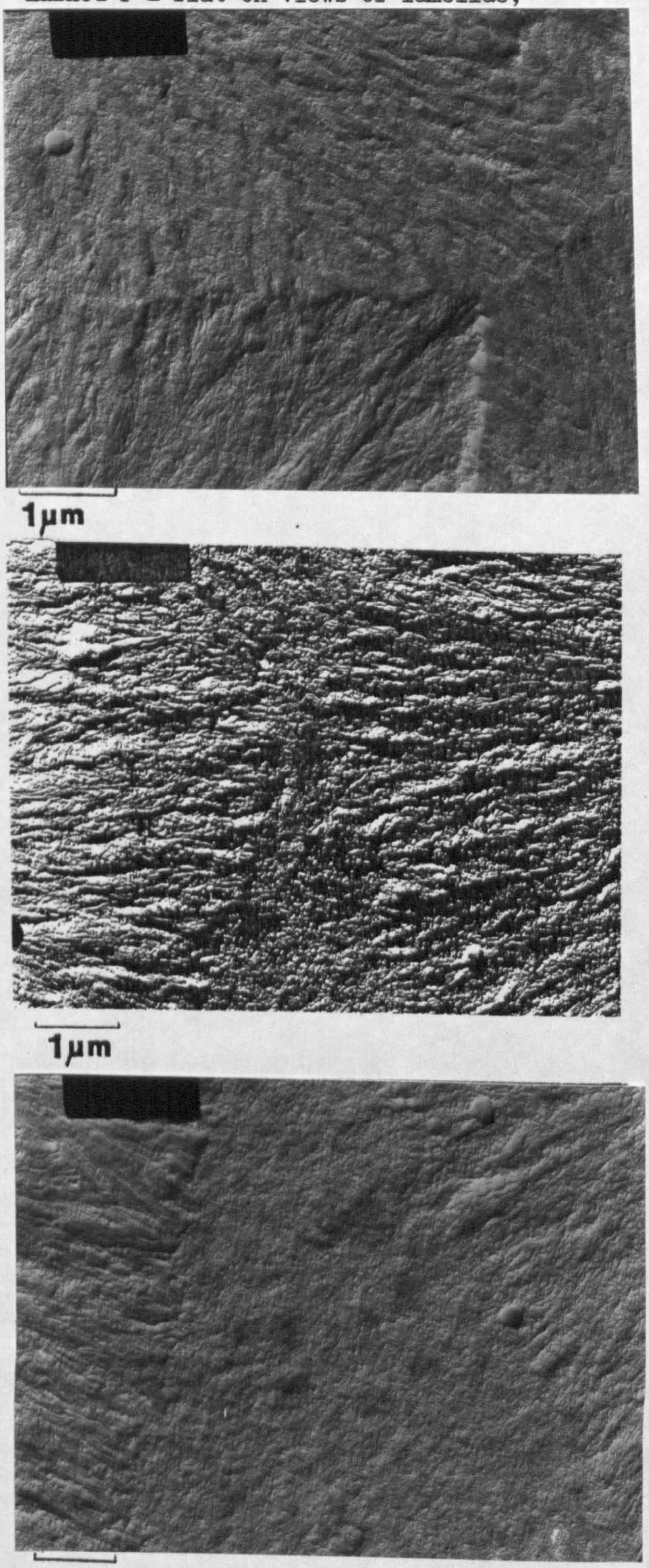

marked R, F and T respectively (Regions marked F represent flat-on views of lamellae, they should display zero biregringence).

3.5 SCANNING ELECTRON MICROSCOPY (SEM) STUDIES OF FRACTURE SURFACES

The fracture surfaces of representative Izod impact tested samples from each processing condition used in the Daniels injection moulding programme were analysed using a Cambridge Stereoscan SEM as described in Section 2.7.4. The presentation of low magnification micrographs proved adequate in assessing variations in fracture initiation sites and fracture topography in selected areas of the moulding.

Typical impact fracture surfaces revealed at 20mm, 45mm and 70mm along the melt flow direction are shown in micrographs for the various processing conditions in Figure 94 (a-d). The following general observations were made at this stage:-

(i) The gate area (20mm along flow) test piece in low mould and melt temperature samples showed two distinct surfaces corresponding to an initiation region and the final, brittle, fracture region. The former corresponded to the row nucleated region of mouldings found some 100 μm below the surface observed in optical studies. This initiation site appeared to be very smooth, similar to the mirror zone seen in amorphous polymers, at the onset of fracture. The latter corresponded to the typical spherulitic texture of the moulding, this fracture surface is seemingly fibrillar with random crack propagation through the thickness of the moulding. As the flow direction is traversed the crack initiation site is seen to move in towards the centre of mouldings, becoming smaller and more fibrillar as it does so.

Figure 94 (a - c) Typical impact fracture surfaces revealed at 20mm, 45mm and 70mm along the melt flow directior for the various processing conditions.

(a) Low melt and low mould temperatures.

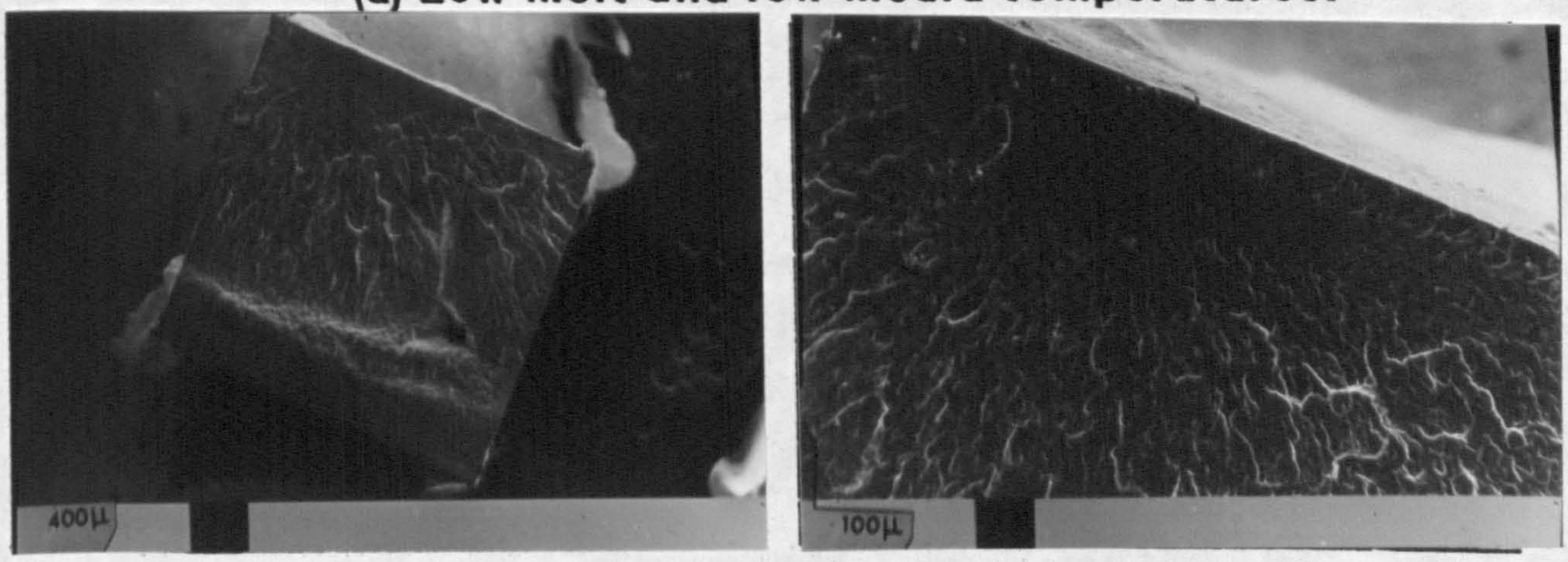

20mm

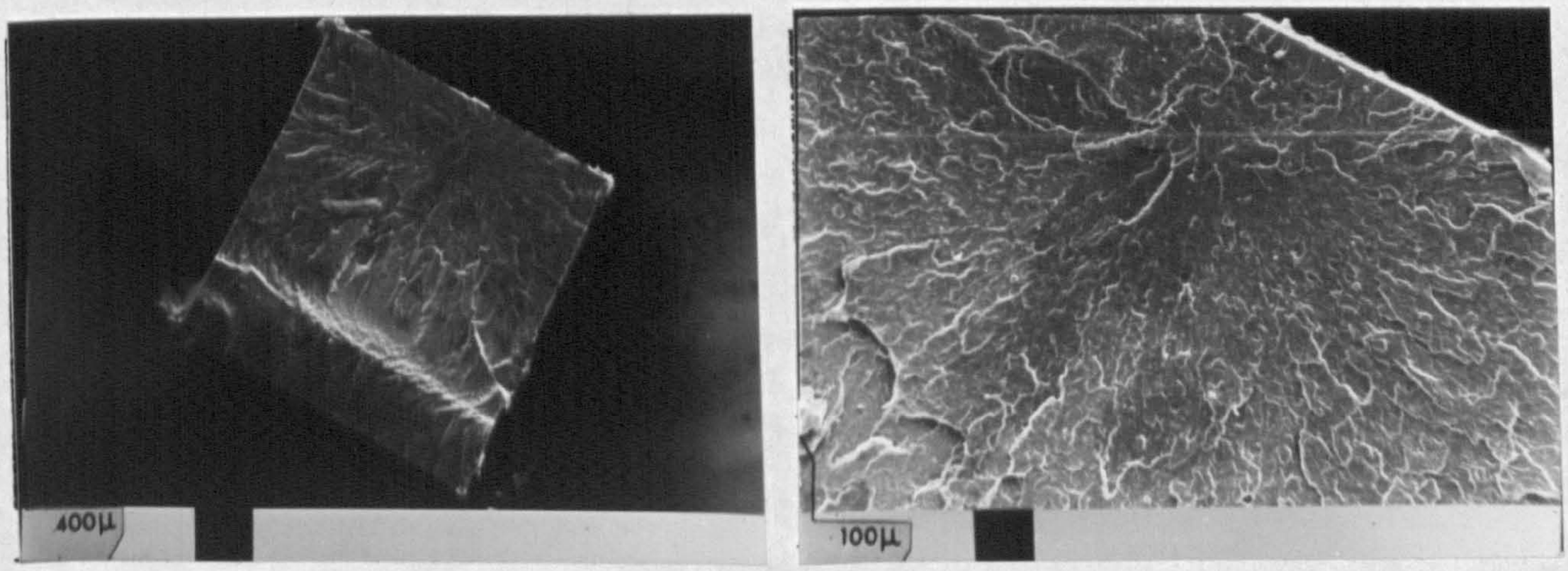

45mm

70mm

(b)High melt and low mould temperatures.

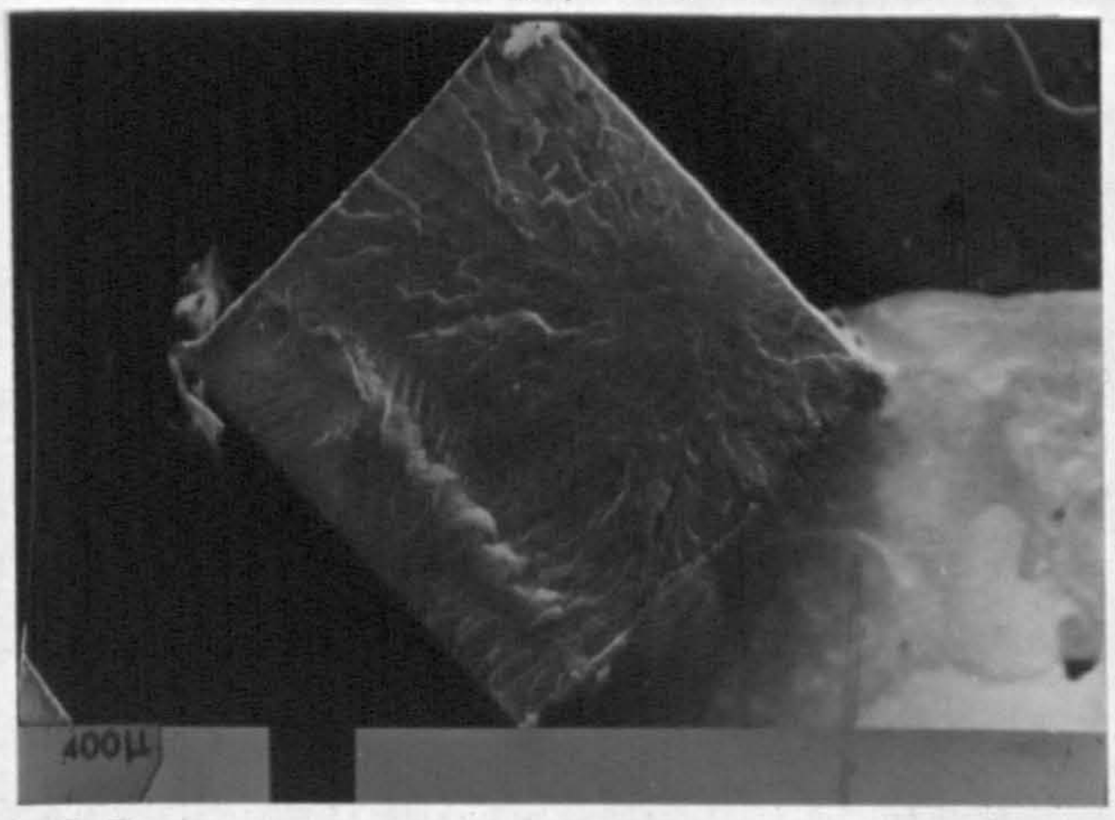

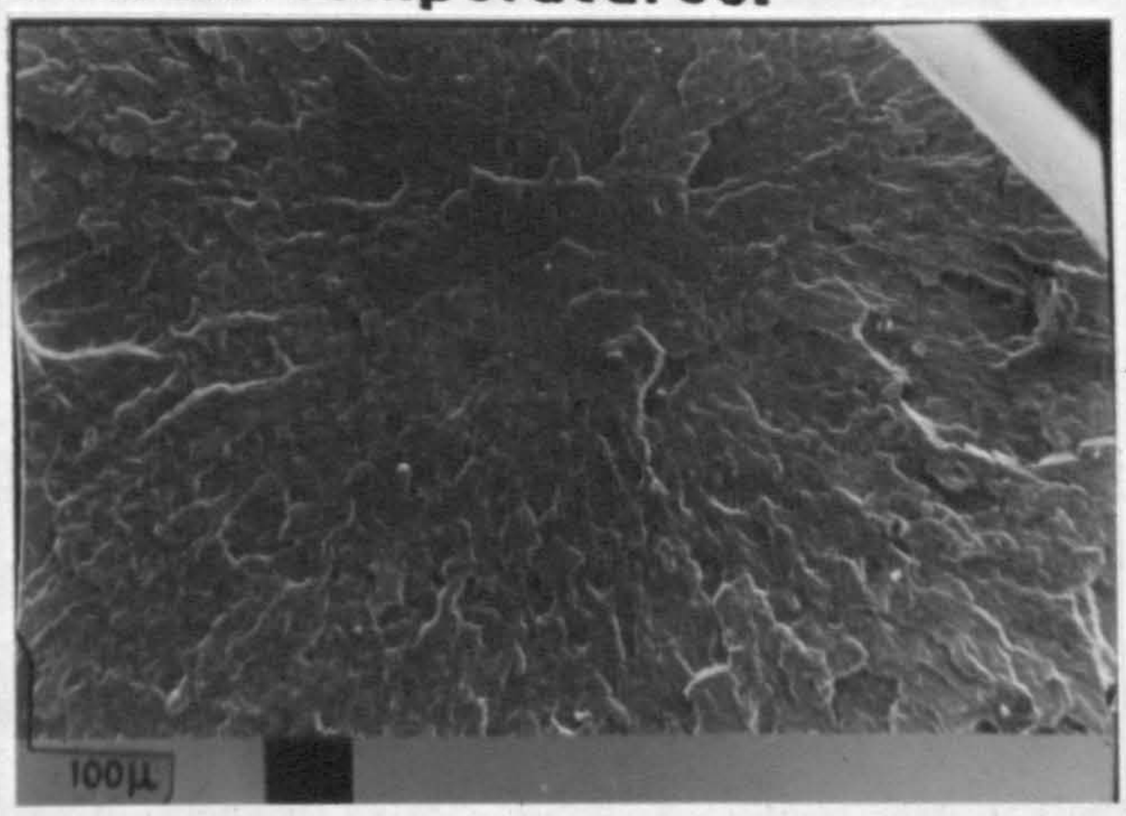

20mm

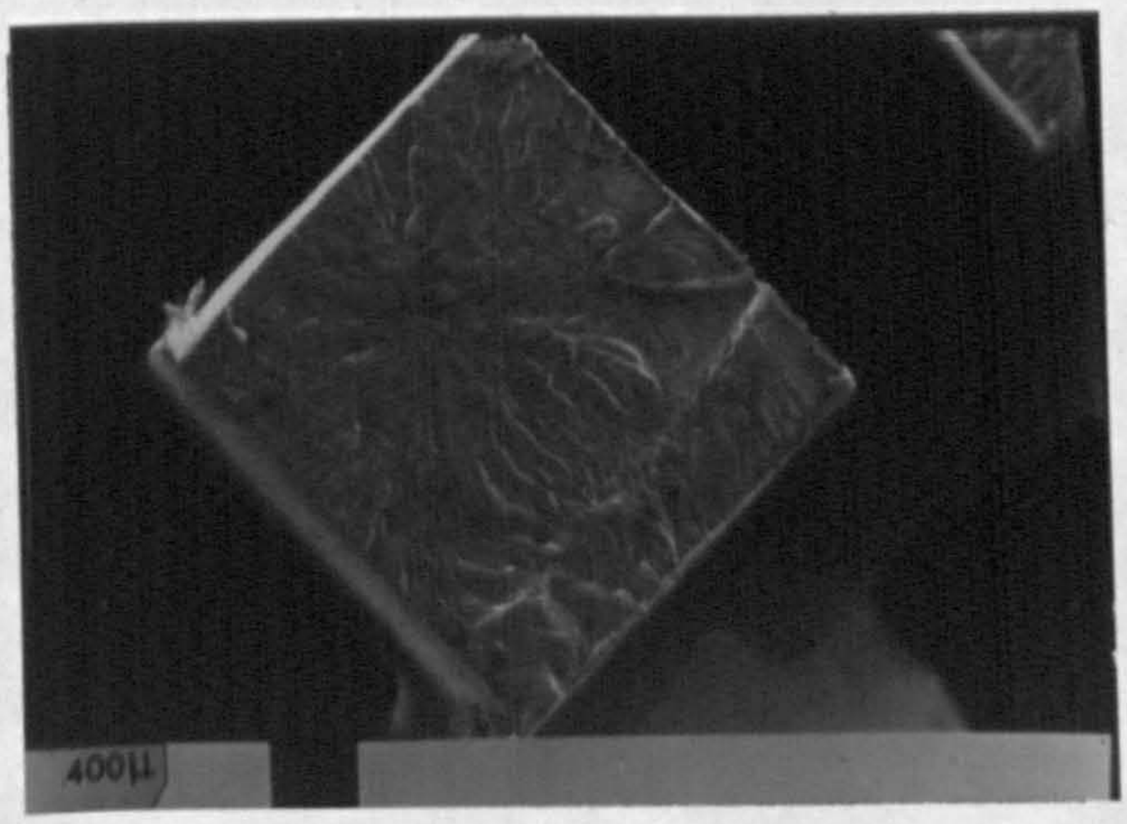

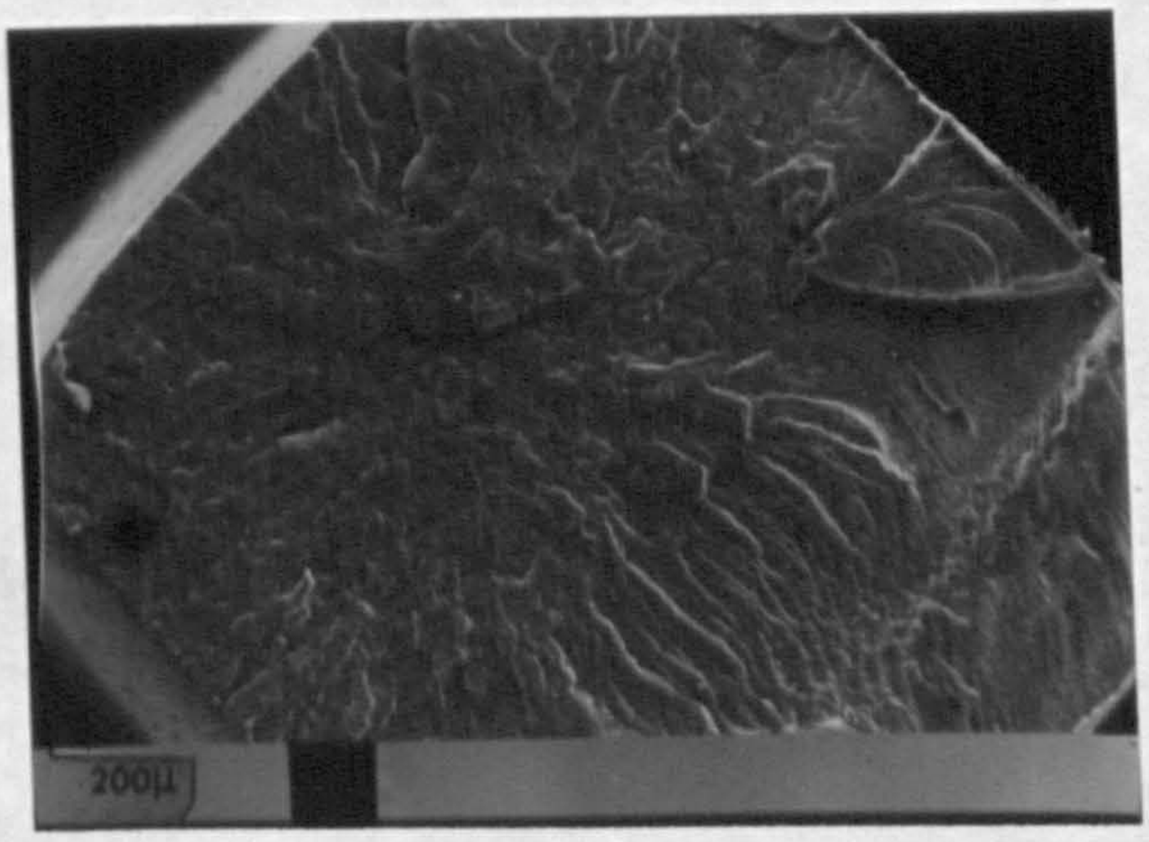

45mm

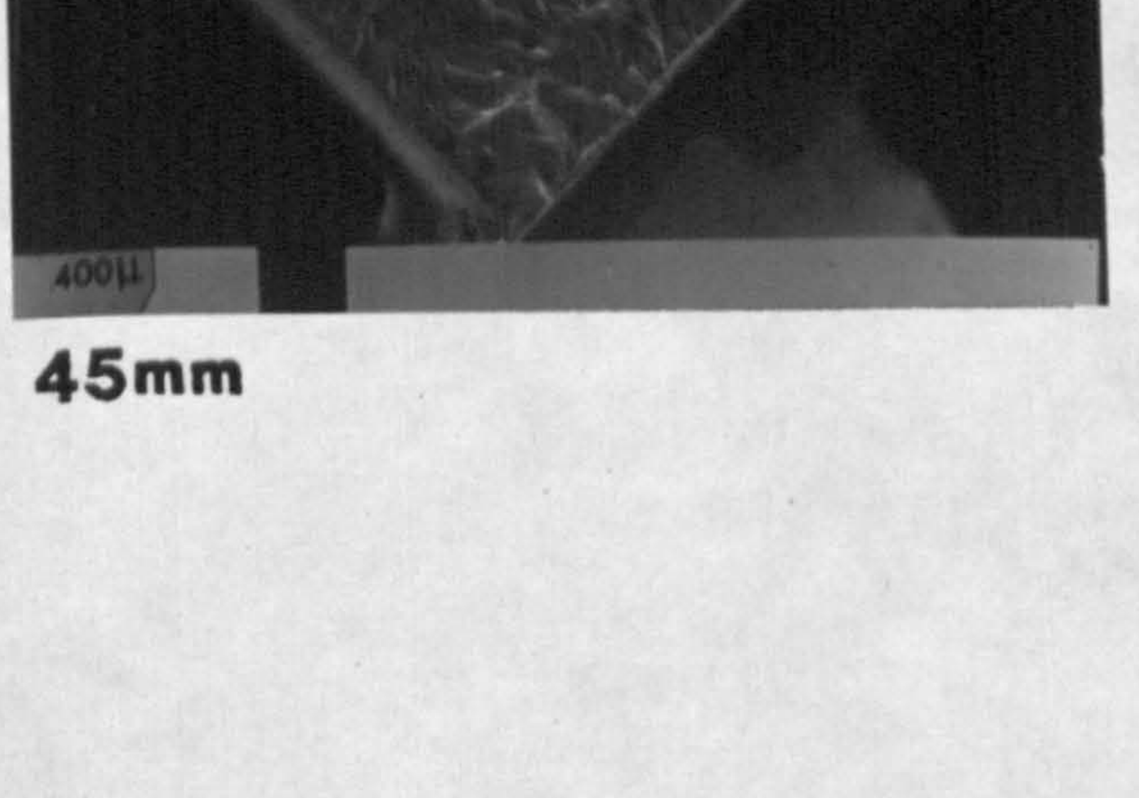

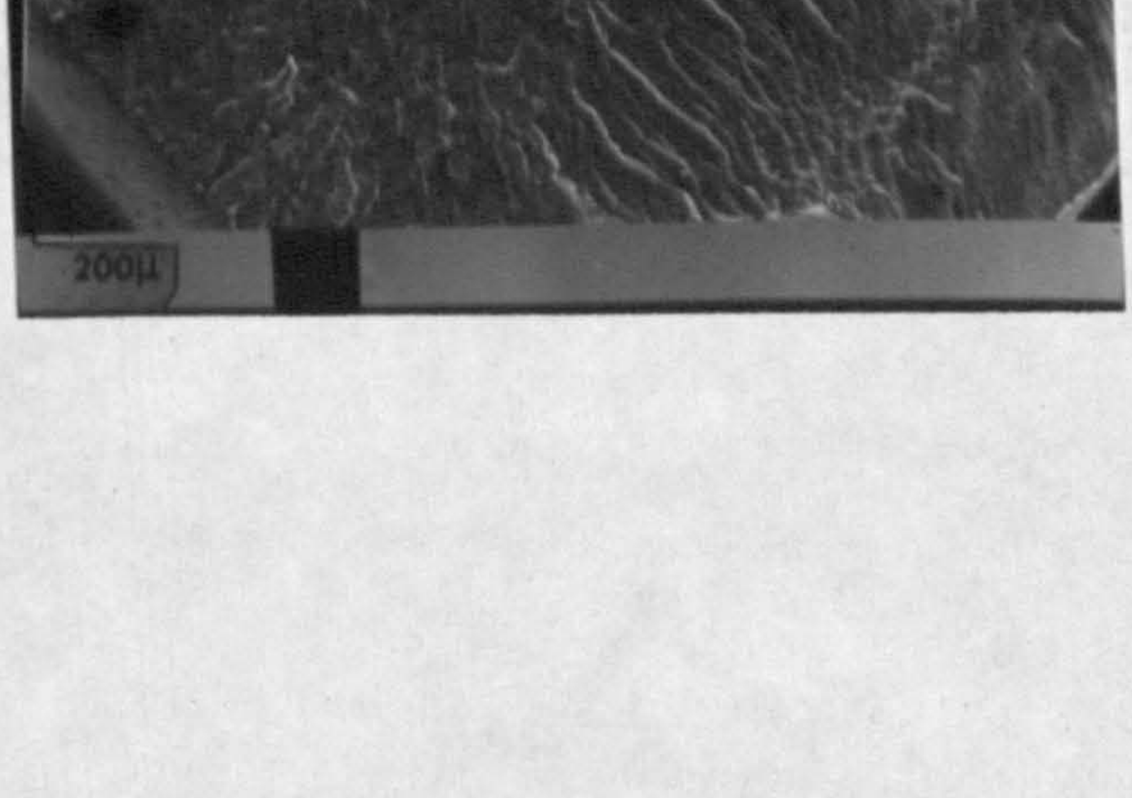

70mm

(c) High melt and high mould temperatures.

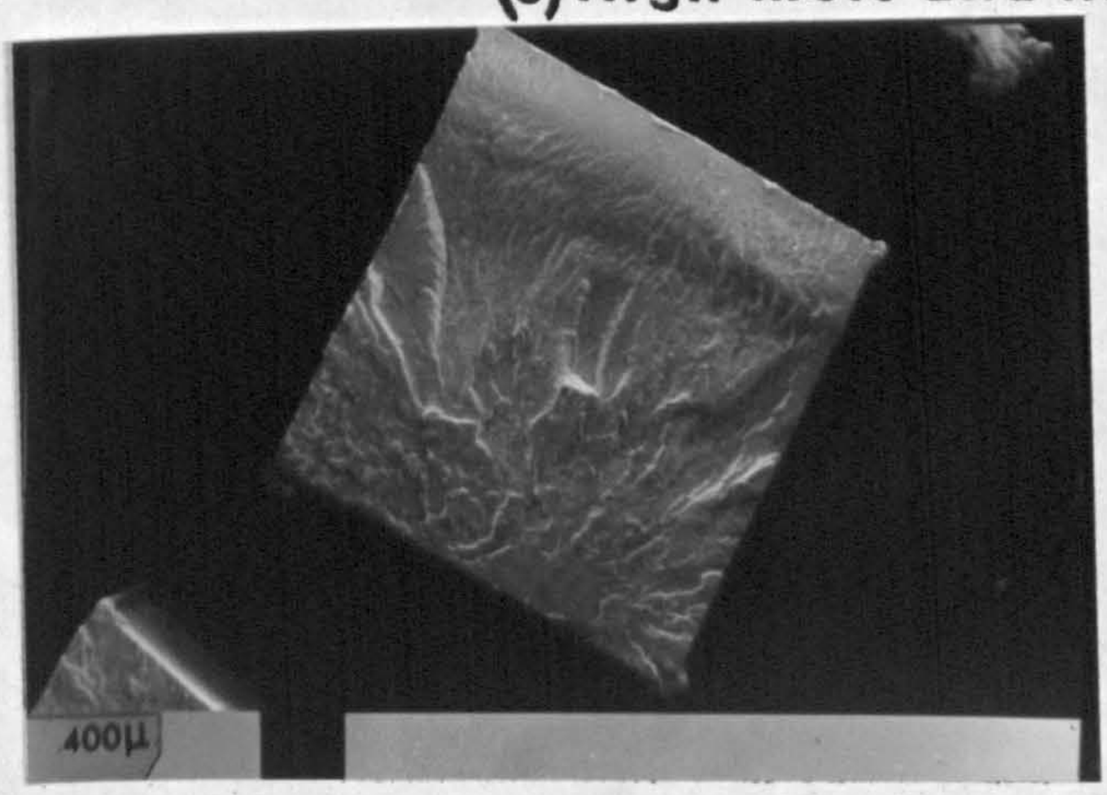

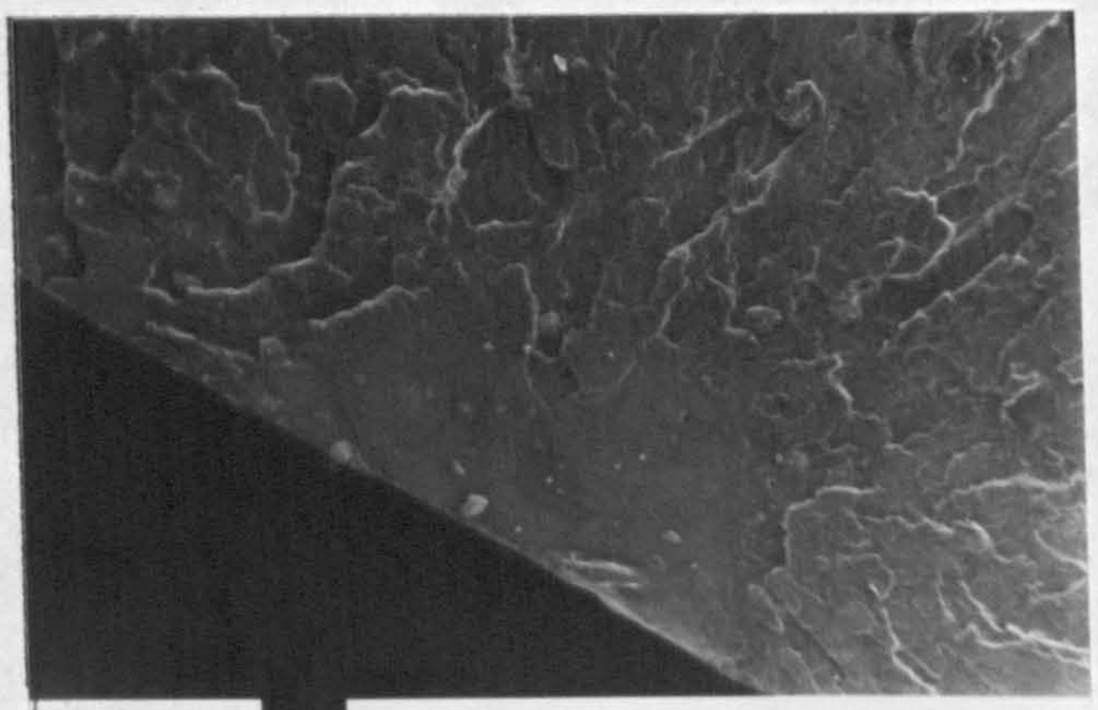

20mm

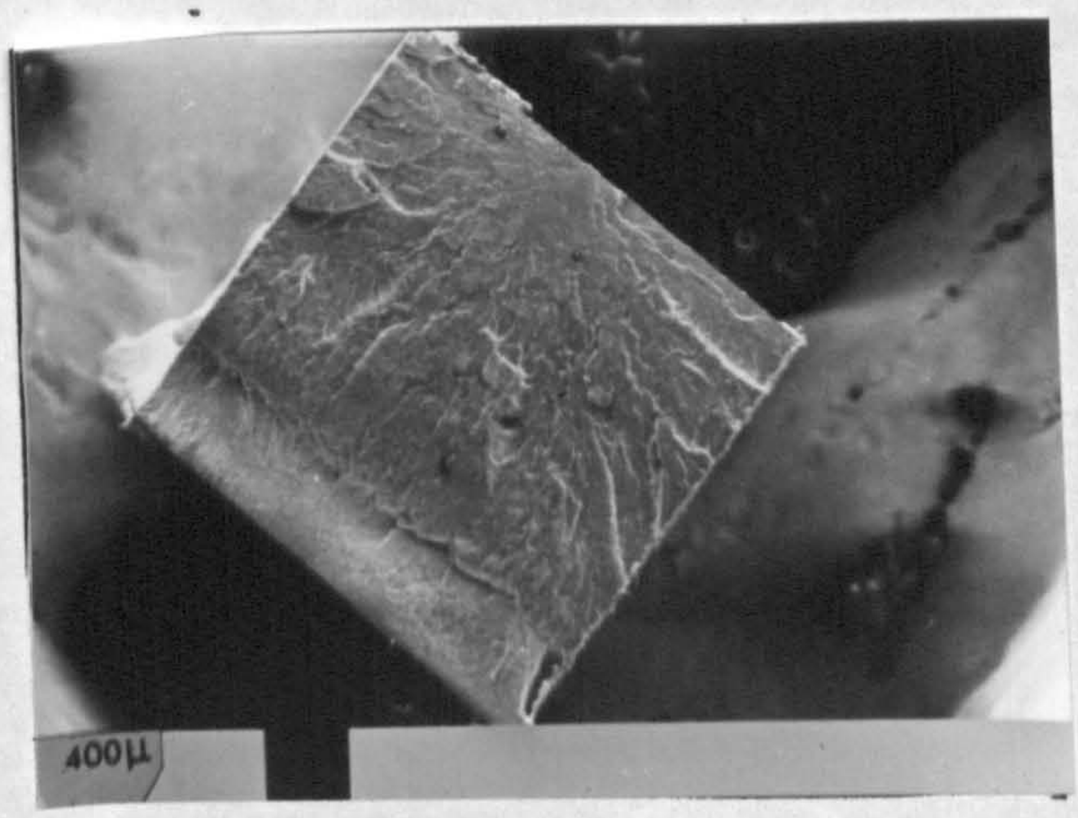

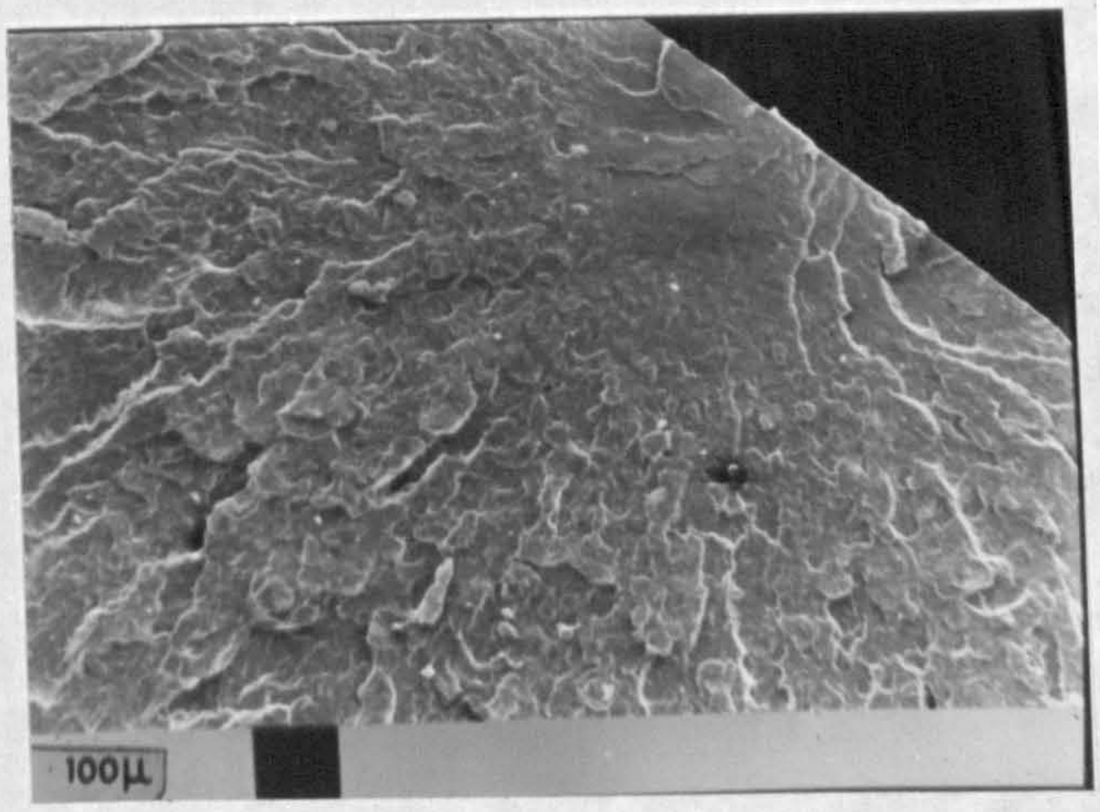

45mm

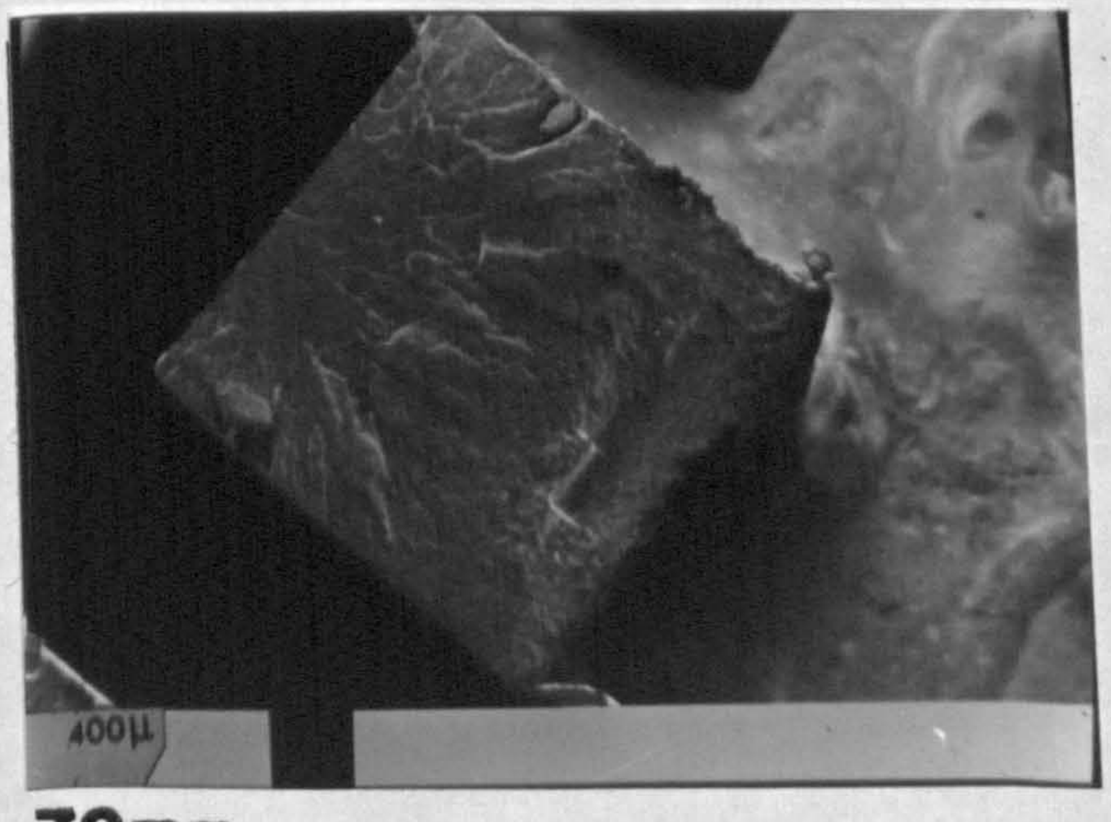

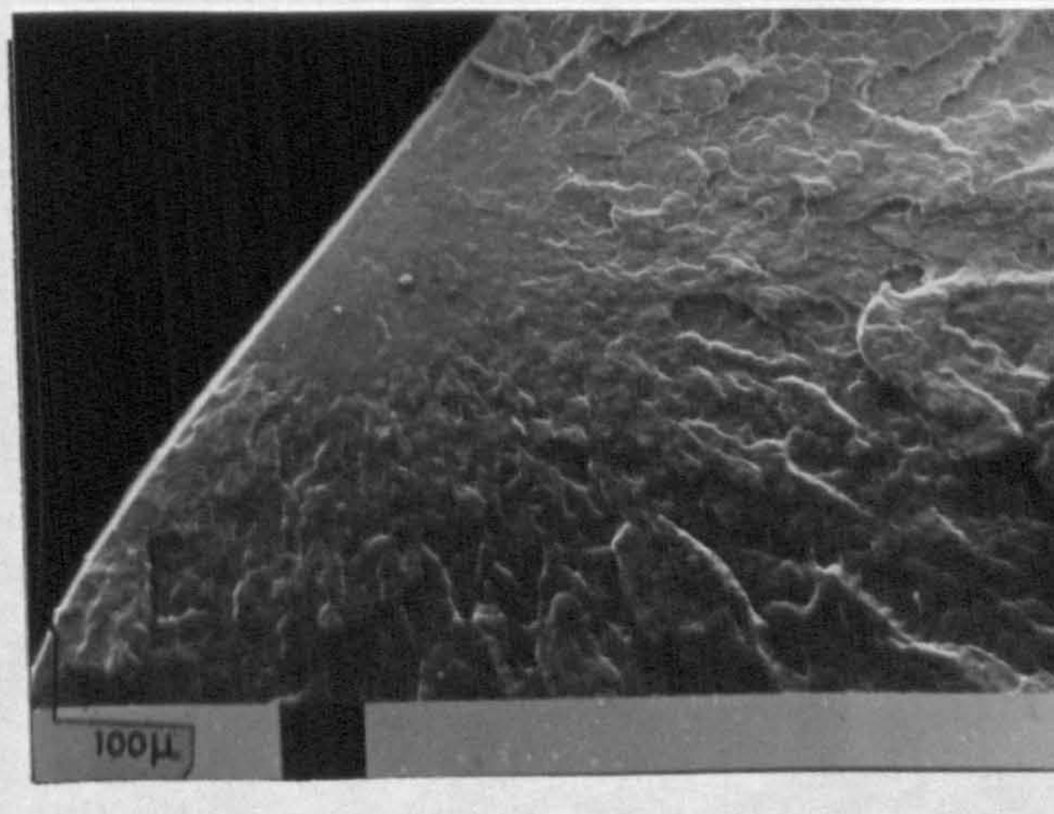

70mm

(ii) The gate area in high melt temperature, low mould temperature mouldings revealed a fracture initiation site some 100 μm below the surface also. However, this region was distinctly fibrillar in contrast to the smoothness of the low melt temperature mouldings. Optical microscopy revealed the absense of a row nucleated fibrous region in this area of the moulding, but did reveal the presence of the β phase spherulites approximately 100 μm below the surface. As with low melt temperature mouldings the crack initiation site was seen to move in towards the centre of the moulding as the melt flow direction was traversed.

(iii) The initiation of cracks in high mould temperature mouldings occurs at the surface in all areas of the moulding looked at. These findings support the theory that it is a transcrystalline surface layer causing the overall weakness in these mouldings.

(iv) In all test pieces a hinging effect was noted at approximately 400 μm from the surface skin opposite the point of impact.

The fracture surfaces of Izod samples selected for more detailed studies of impact strength variations with melt flow direction were also analysed. Both Daniels and Sandretto low melt temperature and high melt temperature samples were examined to establish whether the sharp transition in impact properties was related to a change in the fracture initiation sites and/or mode of fracture. The micrographs for selected Daniels mouldings shown in Figure 95(a) reveal a distinct shift from edge initiation to centre initiation at 49 mm and 38 mm for low and high melt temperature mouldings respectively. This corresponds to the sharp transition in impact properties shown in Figure 53 Like-wise the Sandretto samples selected revealed a shift in

Figure 95 (a) Fracture surface micrographs for selected Daniels iPP mouldings showing a distinct shift from edge initiation to centre initiation at 49mm and 38mm for low and high melt temperature mouldings respectively.

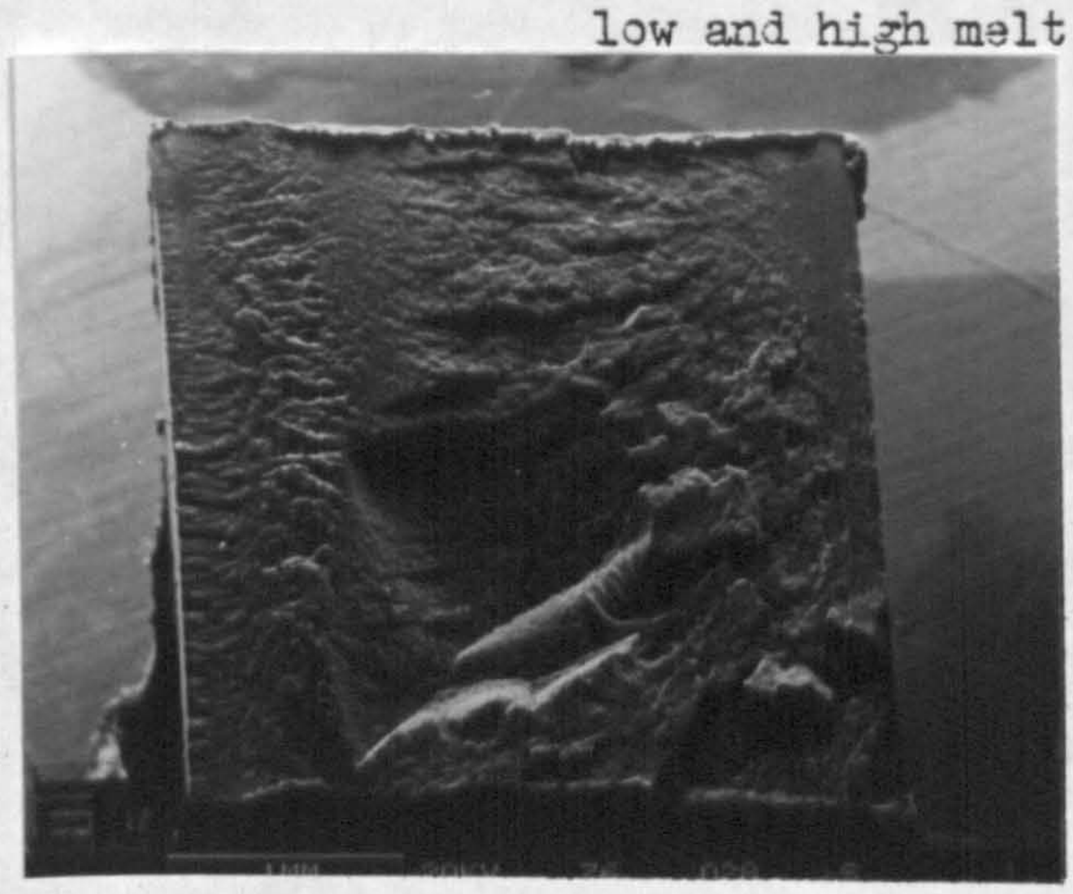

LOW MELT

10.5—13.5mm

HIGH MELT

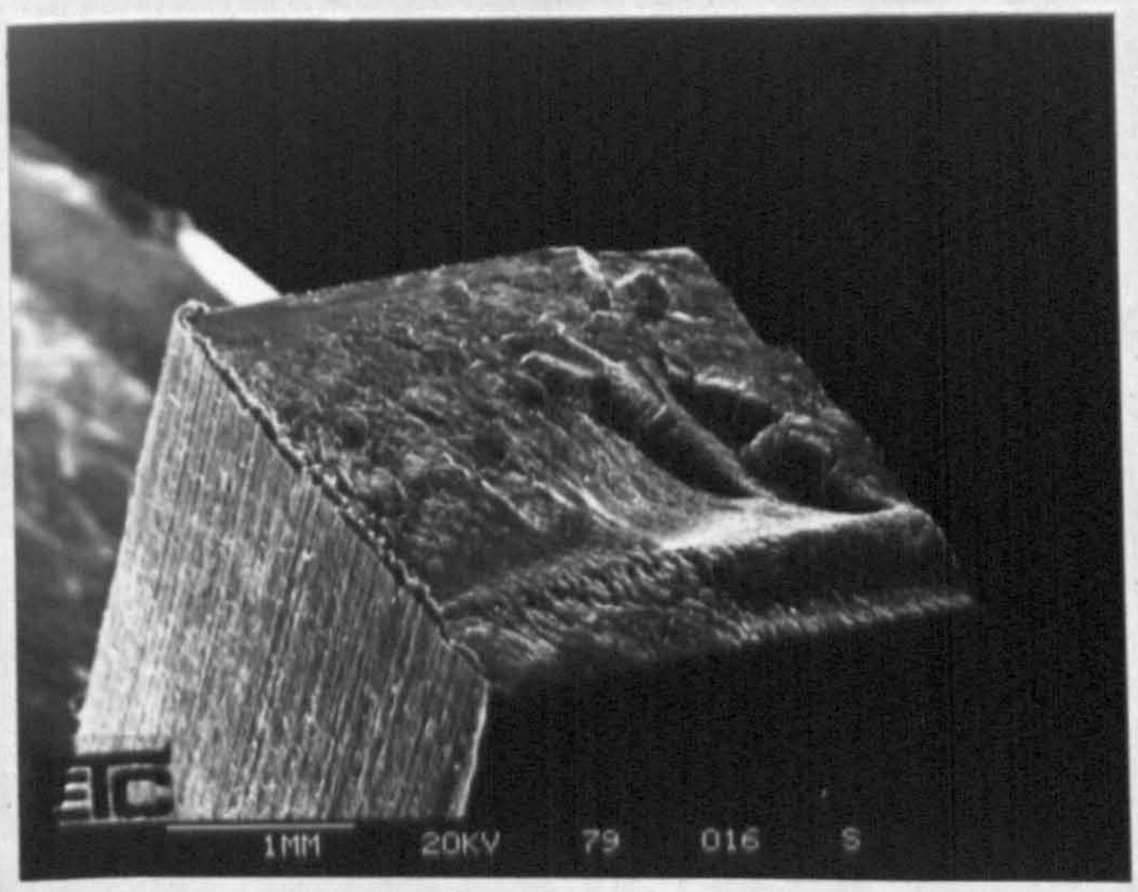

45.5—48.5mm

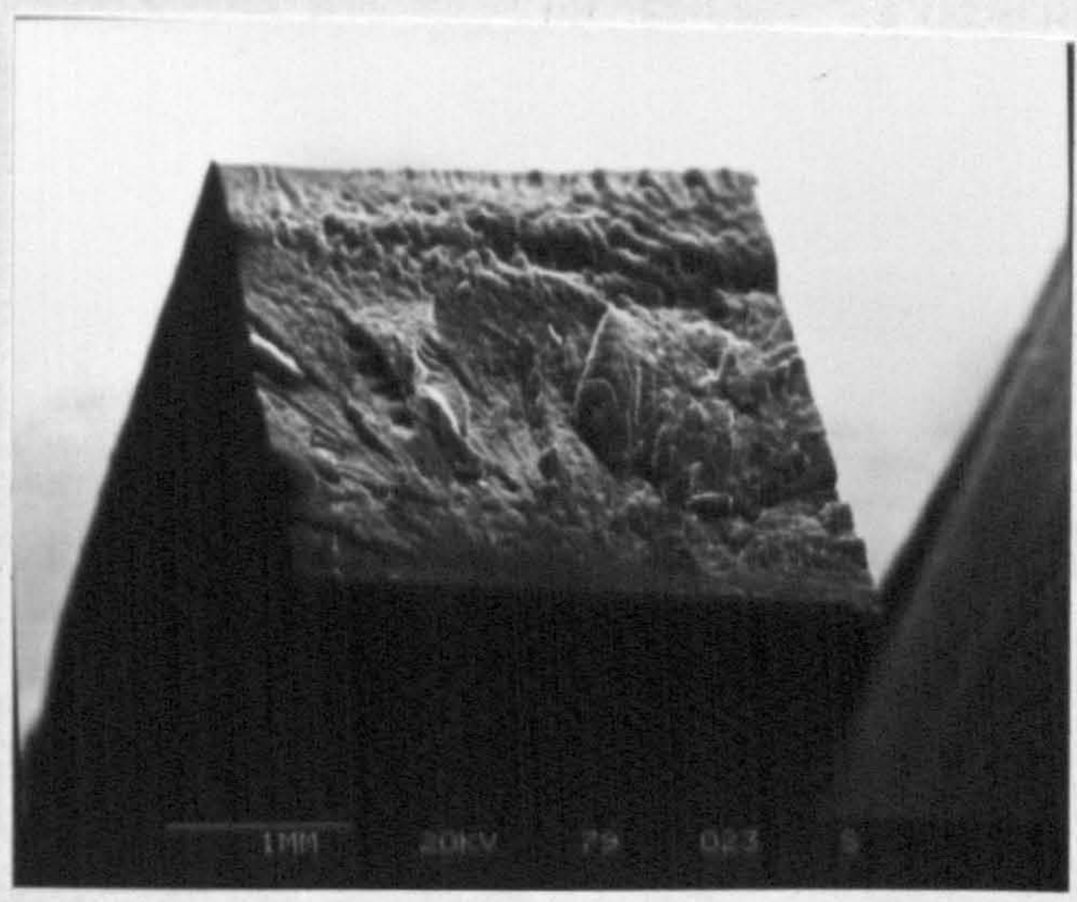

35.0—38.0mm

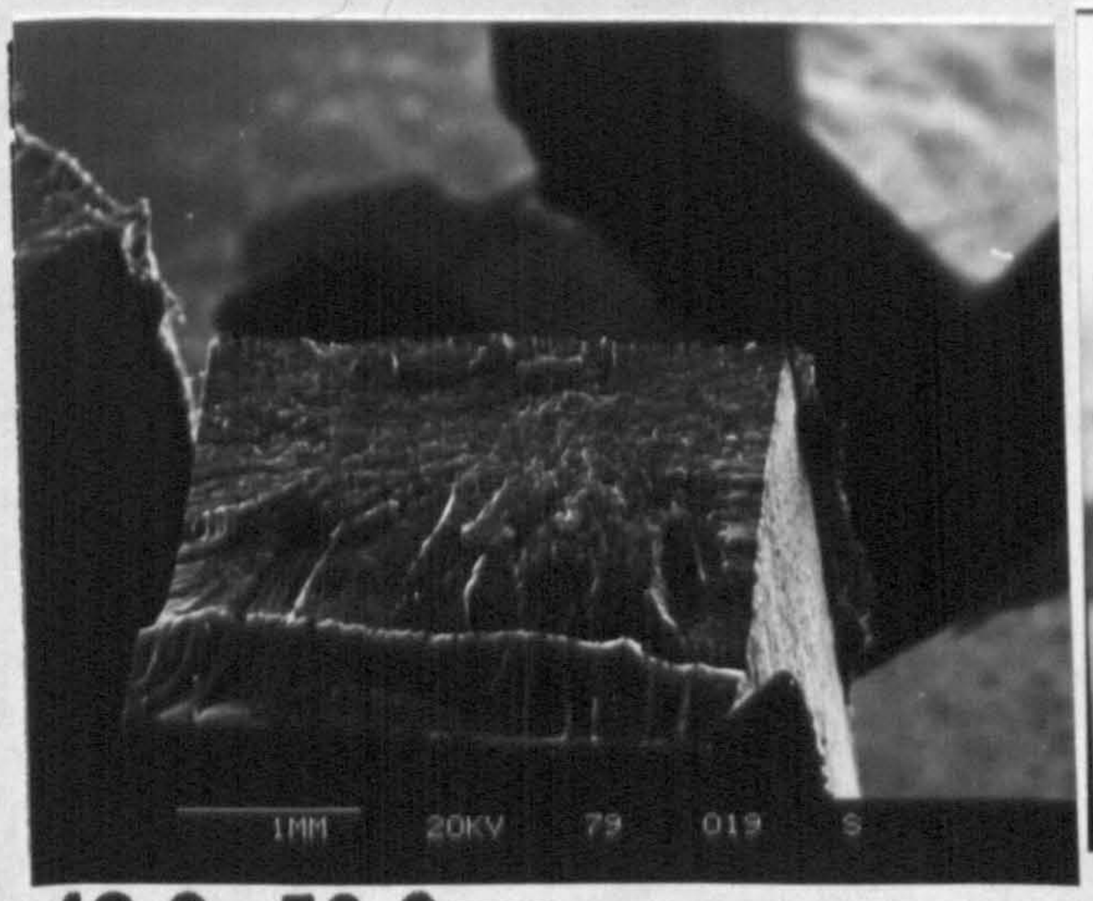

49.0—52.0mm

38.5—41.5mm

Figure 95 (b) Fracture surface micrographs for selected Sandretto iPP mouldings showing a distinct shift from edge initiation to centre initiation at 21mm and 70mm along the flow direction for low and high melt temperature mouldings respectively.

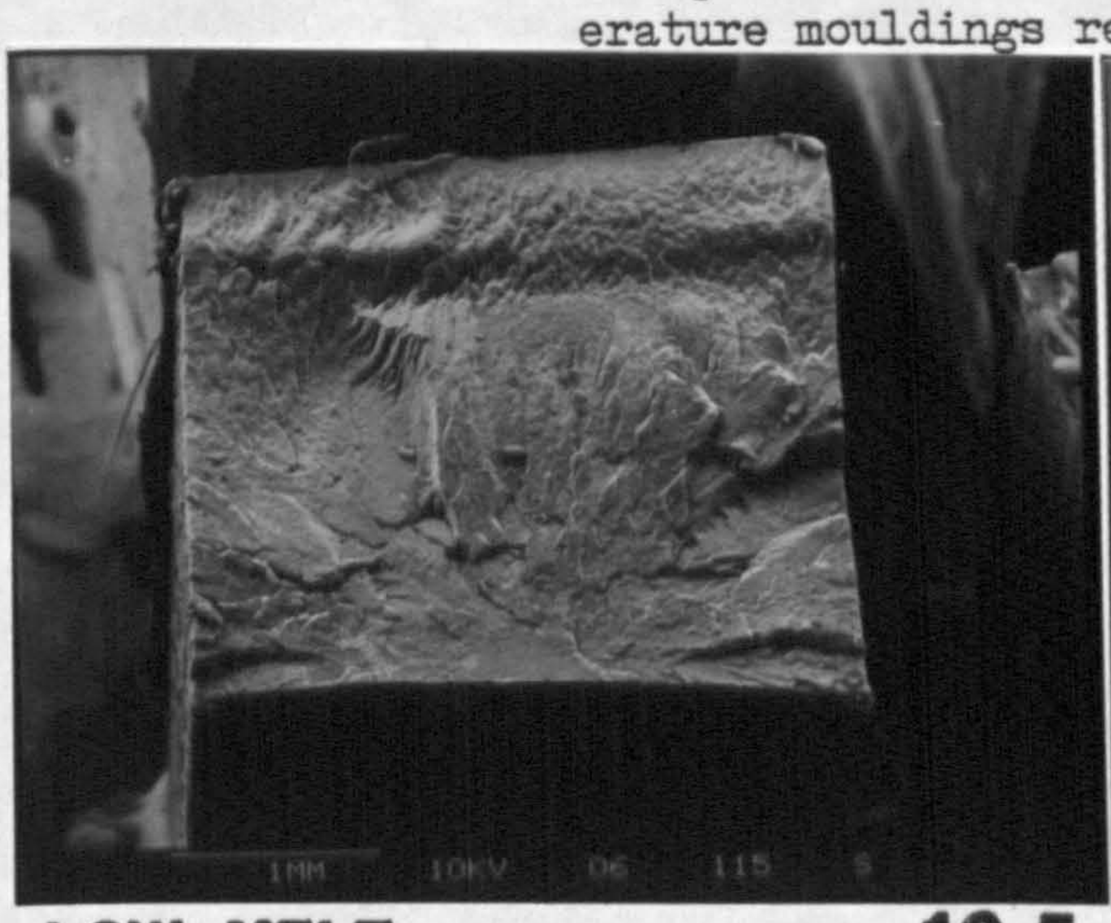

LOW MELT

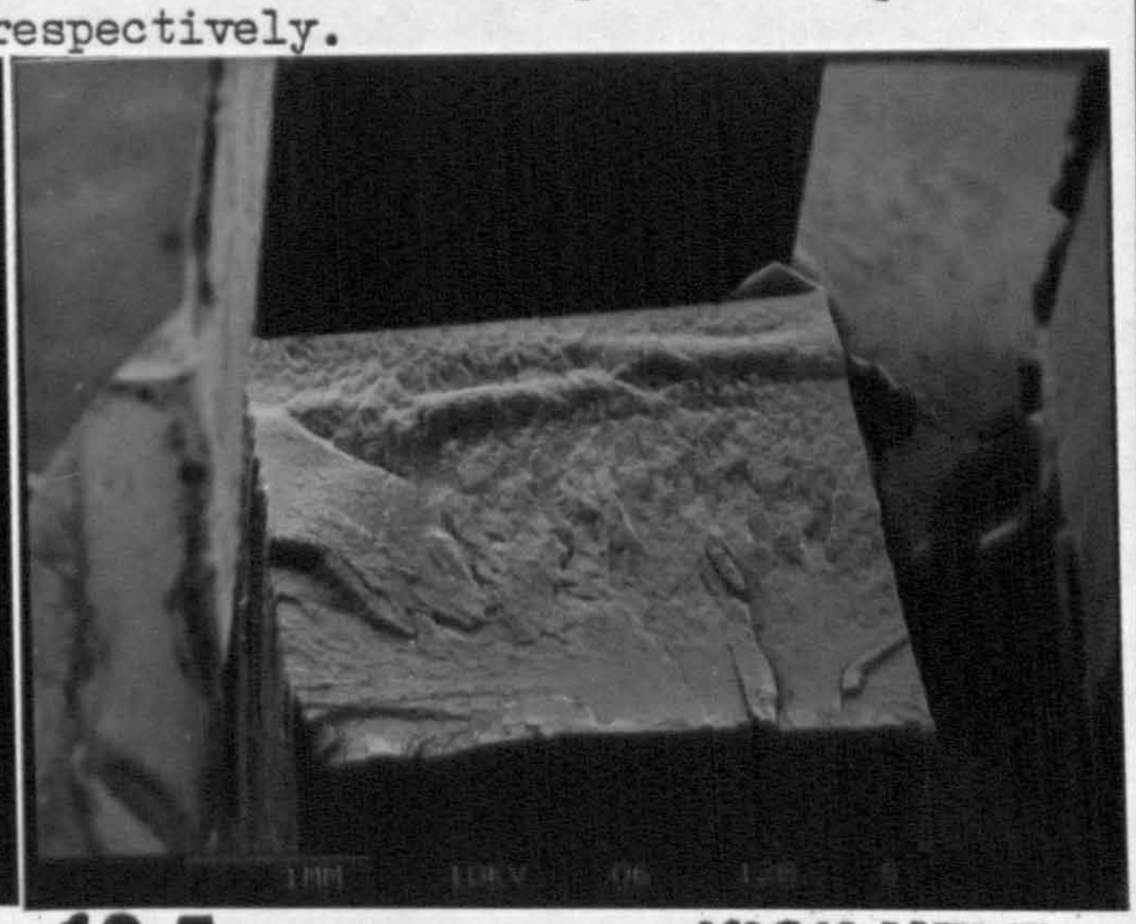

HIGH MELT

10.5—13.5mm

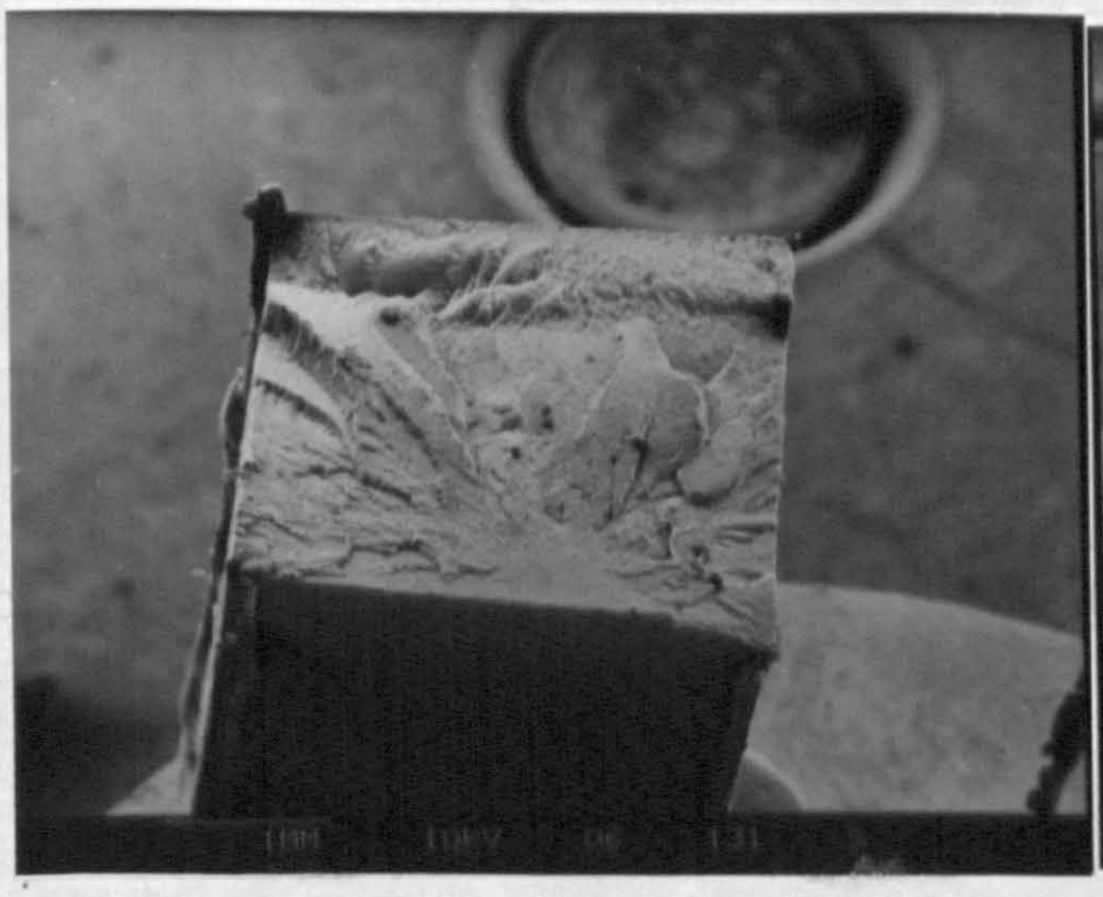

66.5—69.5mm

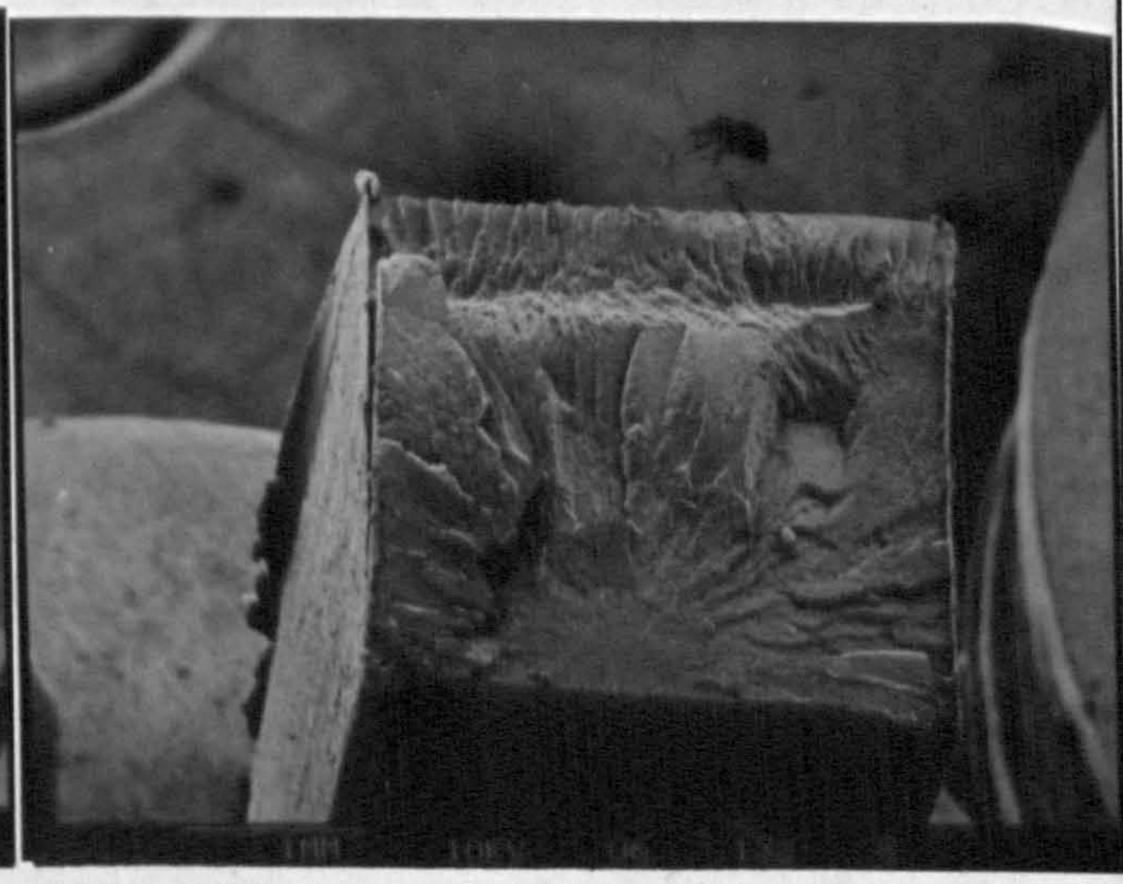

17.5—20.5mm

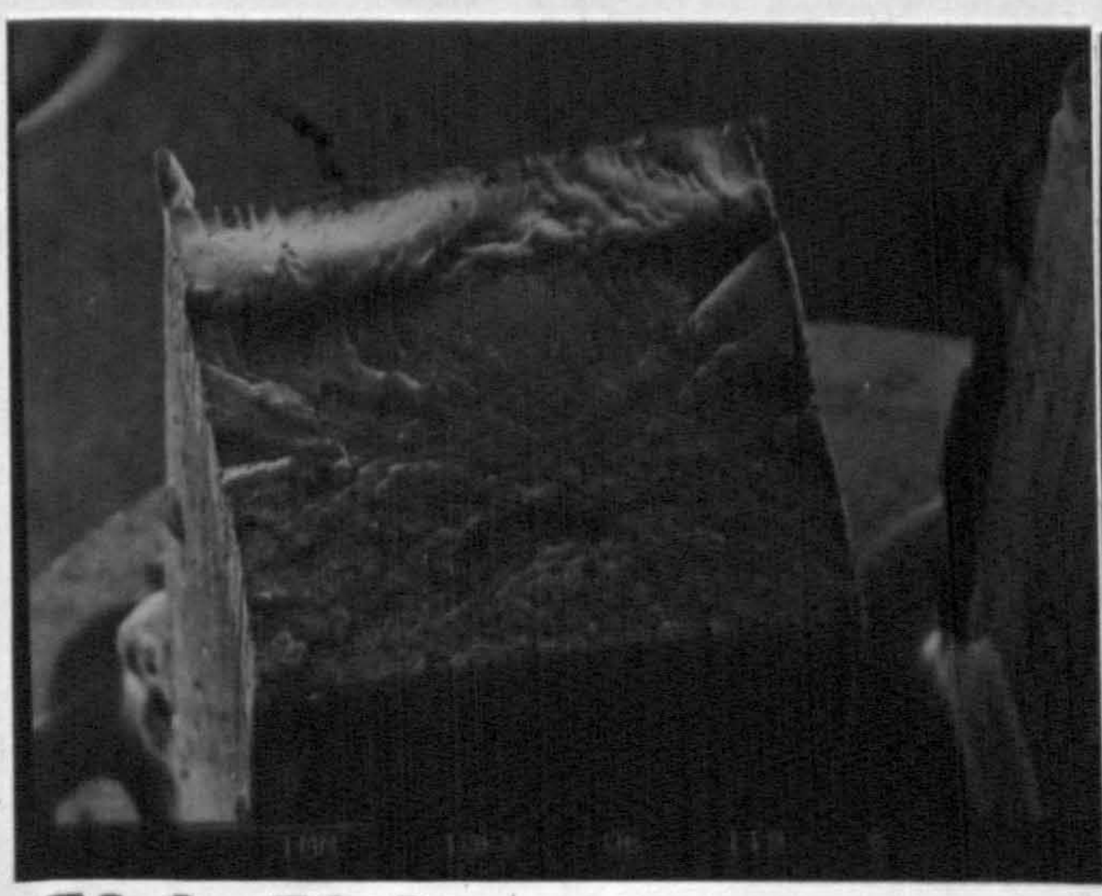

70.0—73.0mm

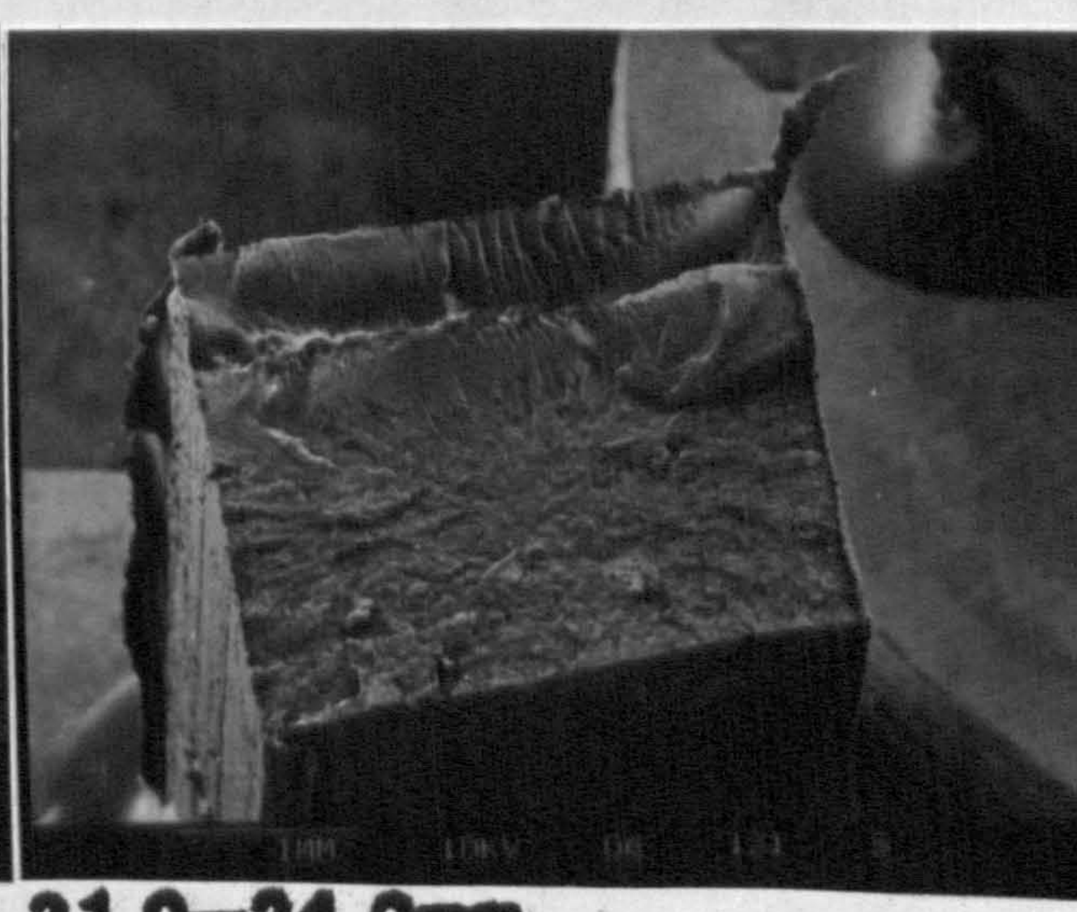

21.0—24.0mm

initiation sites from the edge to the centre of the moulding at 21 mm and 70 mm along the flow direction as revealed in Figure 95(b) , this also corresponded to the transition in impact properties shown in Figure 53.

The improved toughness of the mouldings is related to the absence of banded morphologies, in particular row nucleated β phase spherulites. The structure in these sections of the flow path reveal skin core morphologies, the skin is comprised of apparently tough oriented material whereas the core consists of large α -phase spherulites.. The possibility of cracks initiating at the boundary of large spherulites is well documented. Way et al., (7) discovered that slower cooling rates result in the segregation of impurities and the formation of contraction voids at spherulite boundaries, consequently weakening these regions. However, in fine spherulitic textures crack propagation is chiefly controlled by craze formation. A more detailed discussion of spherulite size effect on fracture mechanisms in iPP is given in Chapter VI with reference to the work of other authors.

3.6 MICROHARDNESS TESTING OF iPP MOULDINGS

Microhardness measurements were made on the sample used for etching and replication in TEM studies. A surface through the thickness of the moulding and parallel to the flow direction was microtomed prior to polishing to a 1 μm finish according to the procedure explained in Section 2.9.4. The microhardness test procedure for the Vickers pyramid indenter adopted was that defined also in Section 2.9.4, namely, that a load of 10 grammes is applied for 1 minute followed by a subsequent 2 minute recovery period before measurement of diagonals parallel and perpendicular to the flow direction.

TABLE 26 Microhardness profile through the thickness of an iPP moulding 2mm along the flow direction.

DISTANCE FROM SKIN (μm)	MEAN DIAMOND LENGTH II TO I.D (μm)	MEAN VHN (Kgmm^{-2})	MEAN DIAMOND LENGTH L TO I.D (μm)	MEAN VHN (Kgmm^{-2})	ΔVHN (Kgmm^{-2})
100	38.80	12.32	37.60	13.12	.800
200	32.13	17.96	30.67	19.71	1.747
275	30.94	19.37	30.13	20.43	1.059
350	33.20	16.82	32.40	17.67	.846
425	33.86	16.17	32.53	17.52	1.346
500	32.93	17.10	31.60	18.57	1.470
575	33.60	16.43	32.00	18.11	1.685
650	33.20	16.82	32.80	17.24	.416
725	33.46	16.56	34.00	16.04	-.524
800	34.26	15.80	34.26	15.80	.001
875	34.26	15.80	34.00	16.04	.241
950	33.46	16.56	33.20	16.82	.256
1025	32.97	17.10	33.80	16.23	-.870
1100	33.07	16.96	33.60	16.43	-.526
1175	32.13	17.96	33.60	16.43	-1.533
1250	32.40	17.67	32.93	17.10	-.565
1325	32.80	17.24	33.07	16.96	-.277
1400	32.67	17.37	32.33	16.93	-.444
1475	32.67	17.37	32.80	17.37	-.004
1550	31.47	18.72	31.34	18.90	.176

TABLE 27 Microhardness profile through the thickness of an iPP moulding 5mm along the flow direction.

DISTANCE FROM SKIN (μm)	MEAN DIAMOND LENGTH II TO I.D (μm)	MEAN VHN (kgmm^{-2})	MEAN DIAMOND LENGTH L TO I.D (μm)	MEAN VHN (kgmm^{-2})	ΔVHN (kgmm^{-2})
100	38.53	12.49	36.53	13.89	1.400
200	35.60	14.63	34.13	15.92	1.289
275	34.00	16.04	34.73	15.37	-.670
350	31.42	18.79	32.87	17.16	-1.630
425	33.72	16.31	33.59	16.43	.120
500	33.73	16.29	33.66	16.37	.080
575	33.57	16.45	33.28	16.74	.290
650	33.39	16.63	33.36	16.66	.030
725	33.73	16.29	33.36	16.66	.370
800	33.07	16.96	33.34	16.68	-.280
875	33.12	16.91	33.33	16.69	-.220
950	33.11	16.92	33.19	16.83	-.090
1000	32.81	17.23	32.67	17.37	.140
1025	33.33	16.69	32.67	17.37	.680
1500	31.87	18.26	31.61	18.56	.300
1550	31.47	18.72	31.34	18.88	.160

At least three sets of indentations, 75 μm centre to centre apart, were made across each specimen at consecutive 75 μm intervals. Two such plots were made one at 2 mm and the other at 5mm from the gate and the Vickers Hardness Number, VHN, values calculated are presented in Tables 26 and 27.

The microhardness profiles from each plot are illustrated in Figures 96 and 97. The abscissa plots the mean value of the VHN from the mean diamond diagonal length parallel to the injection direction with respect to the structural variations. A microhardness plot, measuring the difference in the VHN parallel and perpendicular to the injection direction for this moulding reflects the changes in orientation, as can be seen in Figure 98. A reflected light micrograph of a typical microhardness scan is shown in Figure 99, illustrating the ease of discernibility of bright row nucleated β phase spherulites.

The microhardness profiles shown revealed:-

(i) A relatively soft surface skin, with VHN values in the order of 12 $kgmm^{-2}$. This skin has been revealed already as a highly oriented layer with its c-axis parallel to the injection direction, this is reflected in the large difference in length of diagonals parallel and perpendicular to the injection direction.

(ii) A hard region corresponding to the row nucleated band close to the gate region in the moulding, with VHN values in the order of 19 $kgmm^{-2}$. This appears to be the most highly oriented region in the mouldings.

(iii) Row nucleated β -phase spherulites, clearly visible in reflected light, with a VHN of almost 19 $kgmm^{-2}$. These spherulites also appear to be showing anisotropy.

Figure 96

Microhardness profile through the thickness of an iPP moulding made at 2mm from the gate.

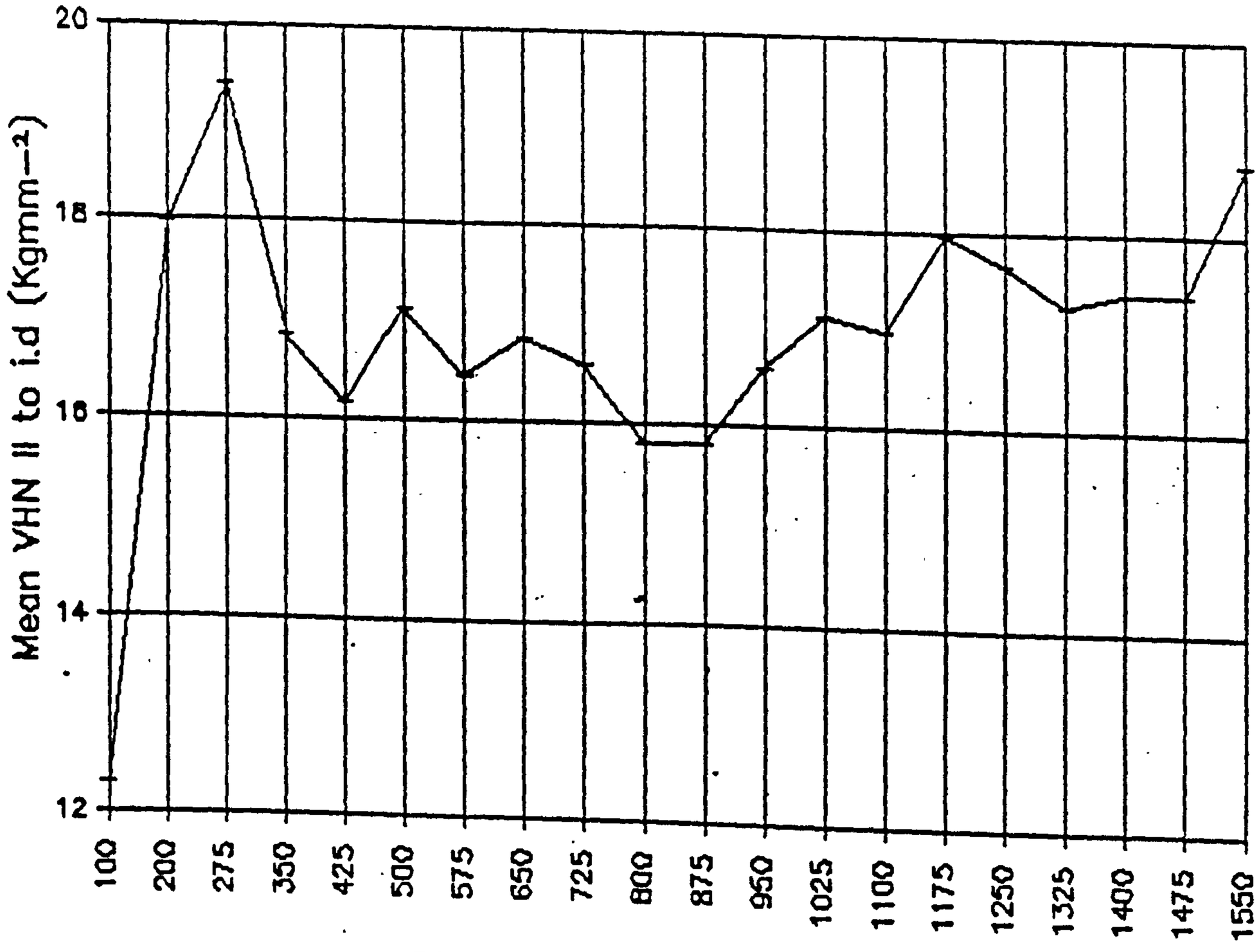

Figure 97

Microhardness profile through the thickness of an iPP moulding made at 5mm from the gate.

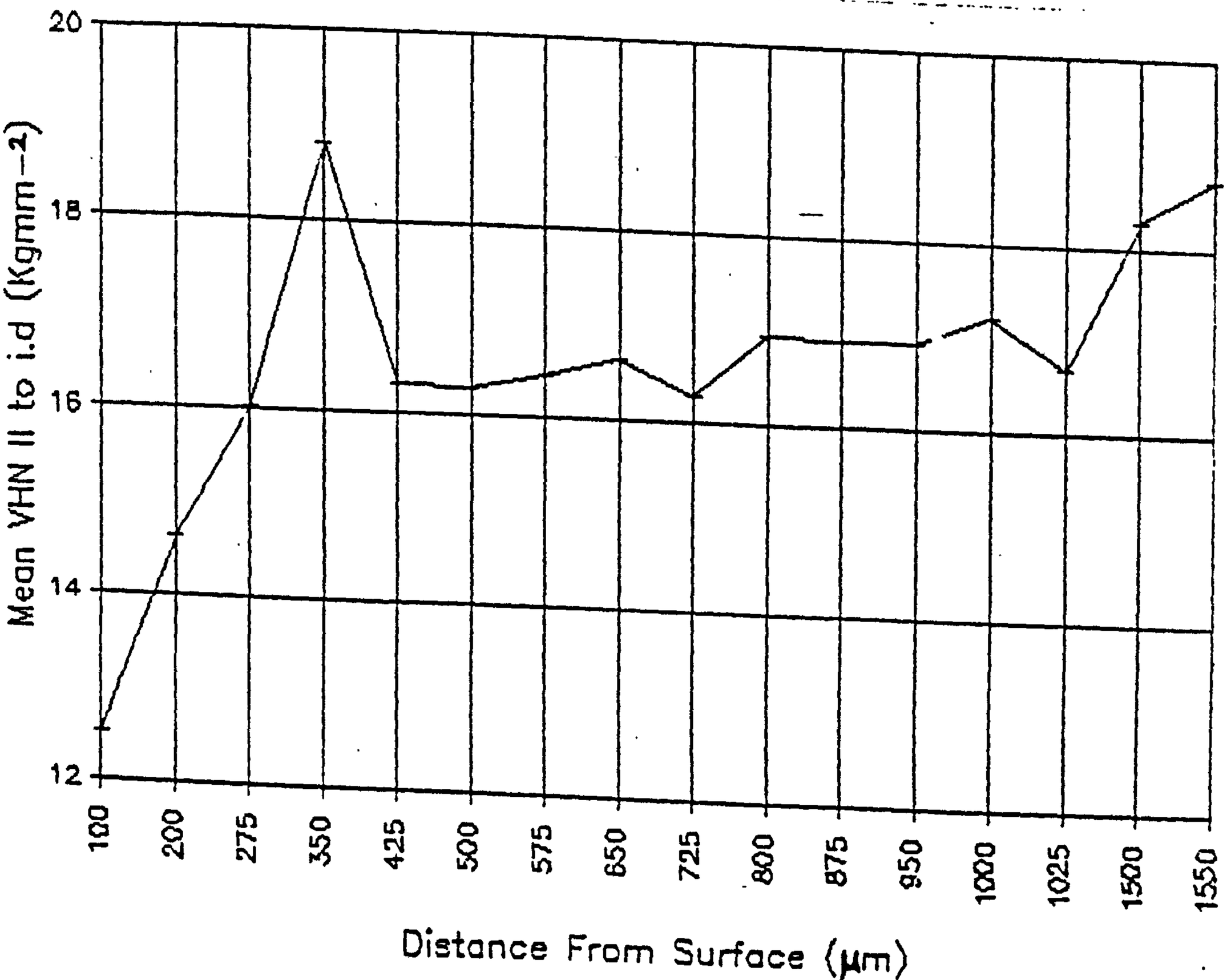

Figure 98

Difference in VHN parallel and perpendicular to the injection direction versus distance from the gate.

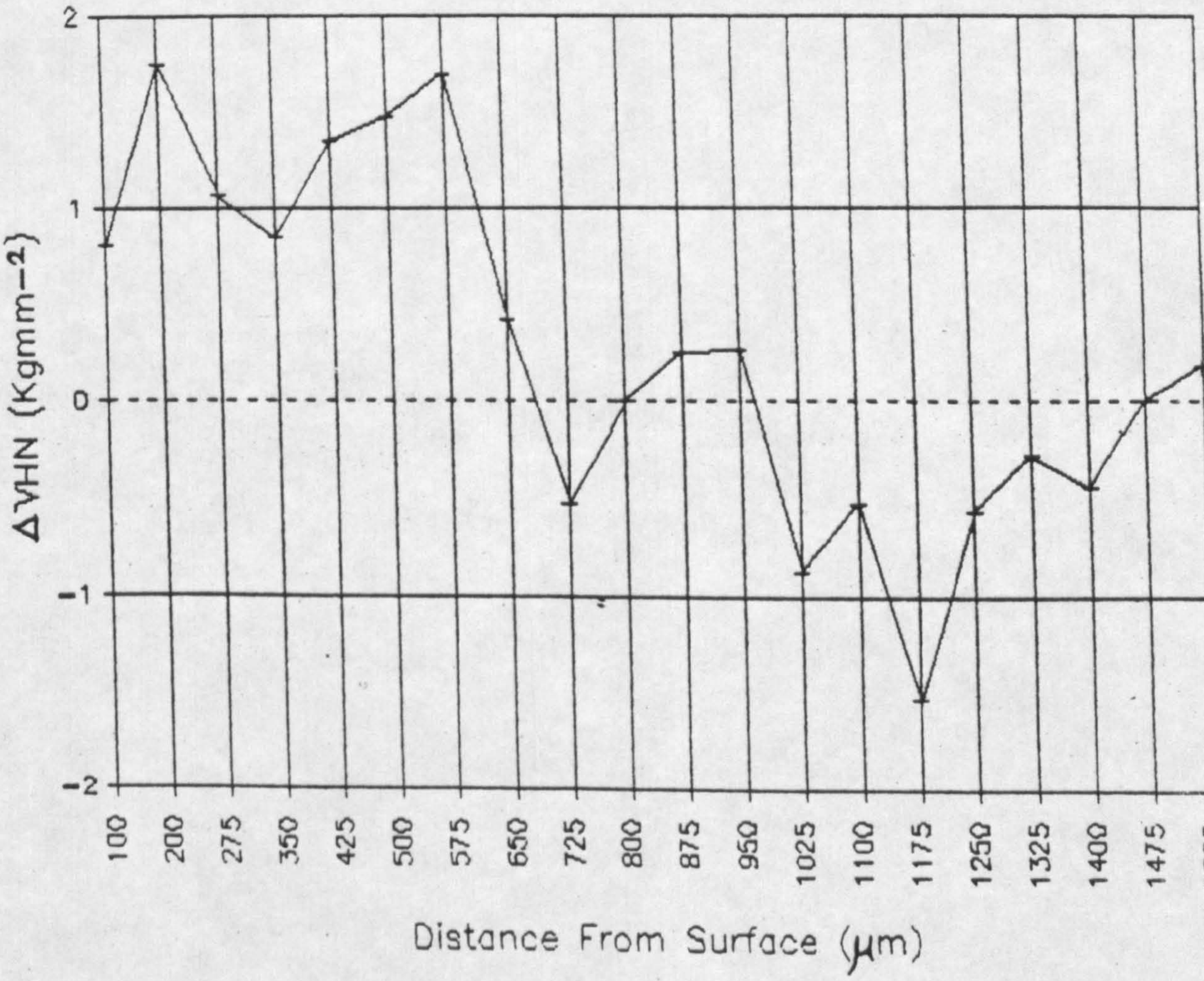

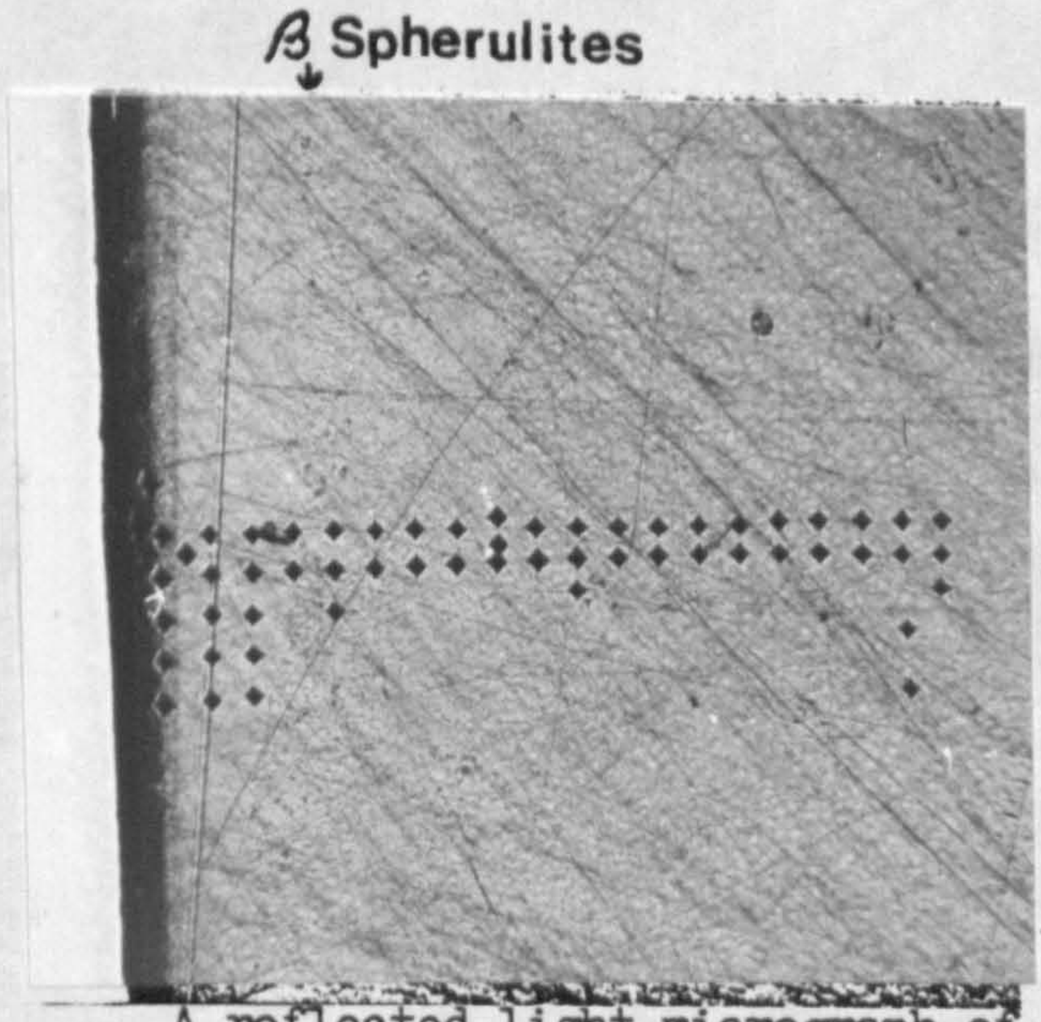

Figure 99

A reflected light micrograph of a typical microhardness plot.

(iv) A relatively soft region between row nucleated structures and well developed α -phase core spherulites. The spherulites in this region are small and underdeveloped and show little anisotropy.

(v) The core region of mouldings which appears to be quite hard with a VHN in the order of 18 $kgmm^{-2}$. The spherulites in this region are upto 40 μm in diameter.

3.7 X-RAY DIFFRACTION OF INJECTION MOULDED iPP

3.7.1 Introduction

It has been illustrated by polarised light microscopy that the morphology of injection moulded iPP is complex particularly in areas close to the gate where upto six discrete morphological bands are revealed. The presence of bright row nucleated β -phase spherulites in varying amounts, depending on the processing history, has been linked to significant reductions in impact properties. Since the nucleation of the β form is in the few percent level it has not been an easy task to assess the concentration or distribution of it throughout mouldings, but because these structures occur within 600 μm of the surface an attempt to quantify the concentration and distribution of the β phase by x-ray diffraction techniques was proposed, based on the work by Trotignan et al., (149). The indexing technique used by the latter (based on diffractogram peak heights) provides a quick and effective assessment of β -phase concentration, α -phase orientation parallel to the surface and crystallinity indexed as described in Section 2.8.7.

3.7.2 Through the Thickness Variations in Orientation and Crystallinity Determined by X-Ray Diffractometry

An initial x-ray investigation was made on the gate sample prepared for microhardness and TEM characterization. It involved sectioning 500 μm thick layers off the moulded surface

using a diamond saw. These surfaces were then exposed to the x-ray beam to determine orientation and crystallinity variations through the thickness of this sample.

The analysis of the diffractograms presented in Figure 100 gave the results shown in Table 28. From the results of Table 28 it was assumed that:-

(i) the x-ray beam penetrates far enough into the moulded surface to give strong reflections from the β phase (300) plane found some 500-600 μm below the surface. There is no indication of any β-form below this depth,

(ii) that the crystallinity index C increases marginally towards the core of the moulding,

(iii) the orientation is reduced significantly towards the core of the moulding, and

(iv) on the basis of these results it can be further concluded that x-ray diffractometry is a useful quantitative technique to study the distribution and orientation of the different polypropylene crystalline phases within the surface layers of injection mouldings.

3.7.3 Crystalline Polymorphism and Orientation in Daniels Injection Mouldings

Following this initial experiment one plaque from each of the processing conditions used was selected for detailed x-ray analysis. The samples were sectioned through the gate as shown previously in Figure 31 to give nine 10mm x 10mm x 3mm samples which were then exposed to x-rays. The resultant analysis of peak heights is given in Table 29 for each processing condition. The β-phase index B, crystallinity index C and orientation index A were plotted against distance along the flow direction for each processing condition as shown in Figures 101 to 106.

Figure 100 Diffractograms of consecutive 500 μm thick layers removed from the surface of an iPP moulding in a region close to the gate.

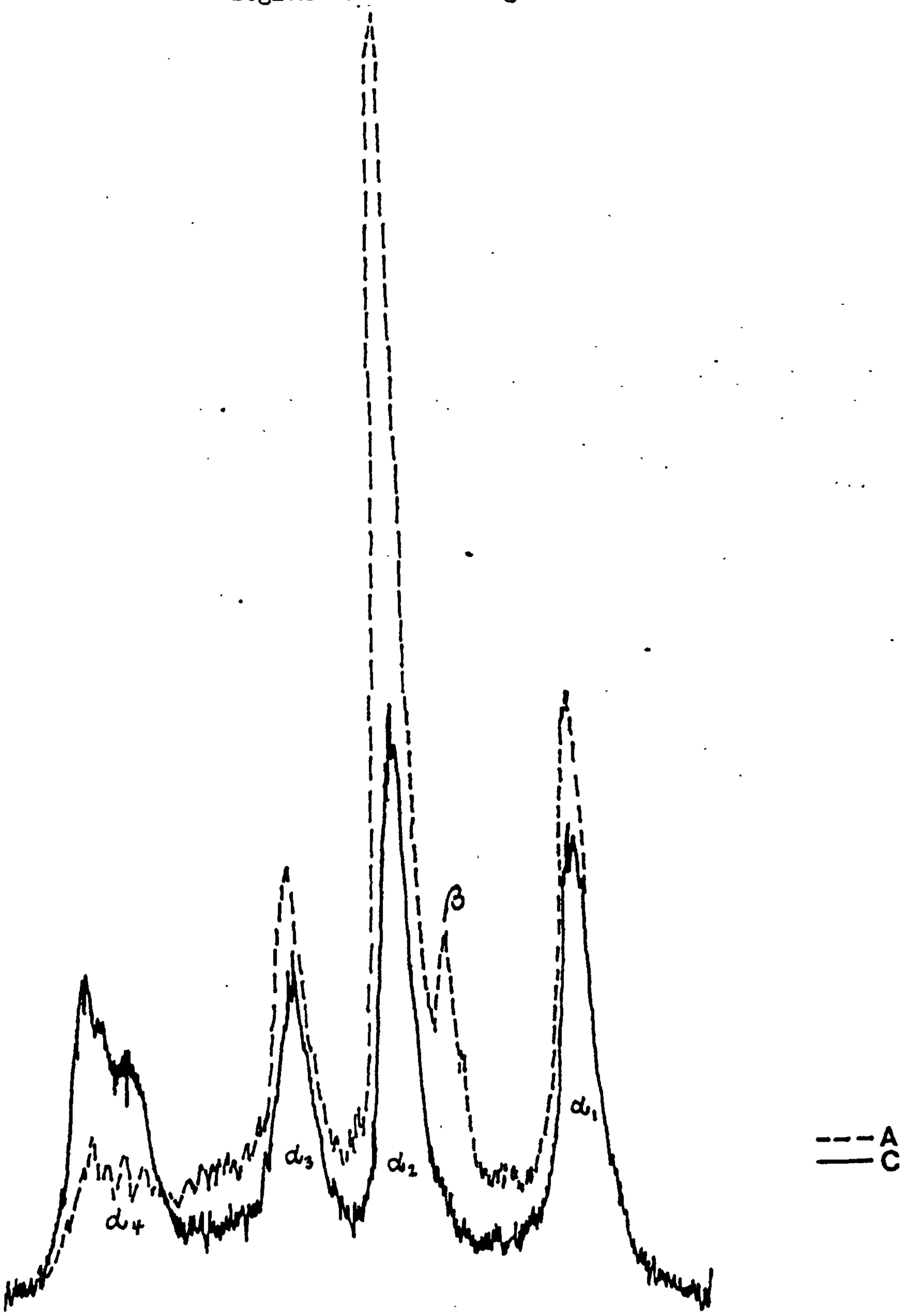

TABLE 28 X-ray diffraction analysis through the thickness of an iPP injection moulding by layer removal.

	DEPTH FROM SURFACE (μm)	PEAK HEIGHTS (mm) hα1	hα2	hα3	hα4	hβ	CRYST. INDEX ha	C	β-PHASE INDEX B	α-PHASE INDEX A
A	0- 550	84	198	48	18	40	33	2.35	.108	.824
B	920-1390	57	90	40	37	0	18.5	2.42	.000	.606
C	1790-2290	69	85	46	47	0	21	2.35	.000	.595
	0-3000	96	208	56	24	45	38	2.26	.111	.800

TABLE 29 X-ray diffraction results for Daniels injection mouldings.

MOULDING CONDITION	DISTANCE FROM GATE (mm)	PEAK HEIGHTS hα1	hα2	hα3	hα4	hβ	CRYST. INDEX ha	β-PHASE INDEX C	α-PHASE INDEX B	A
	0-10	133	285	69	29	76	43	2.75	.135	.821
	10-20	92	83	43	47	83	30	2.32	.276	.662
	20-30	90	75	36	47	36	30	1.89	.152	.657
80/280/4.00	30-40	97	84	45	51	28	31	1.97	.110	.655
	40-50	81	66	40	49	25	29.5	1.77	.118	.623
	50-60	86	73	42	54	0	32	1.59	.000	.614
	60-70	87	75	45	56	0	32	1.64	.000	.608
	70-80	92	73	39	58	0	33	1.59	.000	.613
	80-90	75	59	37	53	0	29	1.54	.000	.586
	0-10	115	206	68	33	63	45	2.16	.139	.777
	10-20	83	153	50	38	34	40	1.79	.106	.686
	20-30	87	139	46	42	36	42	1.67	.117	.674
	30-40	60	100	33	44	36	38	1.44	.157	.577
35/220/1.35	40-50	53	68	32	48	25	37	1.22	.140	.525
	50-60	49	56	32	54	0	36	1.06	.000	.476
	60-70	49	49	29	56	0	36	1.02	.000	.467
	70-80	52	48	28	57	0	35	1.06	.000	.477
	80-90	44	37	25	48	0	33	.93	.000	.478
	0-10	92	169	56	40	42	41	1.95	.117	.697
	10-20	61	90	37	46	25	35	1.48	.117	.570
	20-30	59	52	31	54	20	34	1.27	.123	.522
	30-40	60	67	33	48	17	34	1.32	.096	.556
35/280/1.35	40-50	60	61	33	50	0	33	1.24	.000	.545
	50-60	59	53	32	55	0	35	1.14	.000	.518
	60-70	57	57	34	52	0	33	1.21	.000	.523
	70-80	59	47	32	52	0	32	1.19	.000	.532
	80-90	51	39	26	52	0	31	1.08	.000	.495
	0-10	146	271	72	31	120	49	2.61	.197	.825
	10-20	114	212	58	35	77	38	2.61	.167	.765
	20-30	81	152	44	39	64	35	2.17	.188	.675
	30-40	66	100	38	45	66	32	1.97	.244	.595
80/220/1.35	40-50	72	98	39	46	64	29	2.20	.234	.610
	50-60	81	97	42	50	45	31	2.03	.170	.618
	60-70	76	88	43	51	24	31	1.82	.104	.598
	70-80	70	76	36	48	0	29	1.59	.000	.593
	80-90	72	76	35	47	0	30	1.53	.000	.605
	0-10	112	208	54	31	89	37	2.67	.192	.783
	10-20	80	79	41	45	74	28	2.28	.270	.640
	20-30	80	77	39	48	49	30	1.95	.200	.625
80/280/1.35	30-40	80	69	38	46	38	30	1.81	.169	.635
	40-50	87	76	42	52	29	28	2.04	.124	.626
	50-60	84	69	42	50	21	30	1.77	.097	.627
	60-70	88	69	42	55	0	30	1.69	.000	.615
	0-10	103	250	67	26	36	43	2.24	.079	.79E
	10-20	57	75	31	43	27	31	1.50	.142	.57C
	20-30	55	70	33	46	24	32	1.43	.132	.54E
	30-40	54	68	32	46	15	32	1.34	.089	.54C
35/280/4.00	40-50	55	68	34	52	10	32	1.37	.060	.514
	50-60	55	58	31	50	0	33	1.18	.000	.524
	60-70	57	56	33	53	0	32	1.24	.000	.51E
	70-80	54	49	28	55	0	33	1.13	.000	.49E
	0-10	128	293	78	27	44	47	2.43	.081	.82E
	10-20	71	159	43	39	27	38	1.78	.090	.64E
	20-30	54	86	34	41	24	34	1.41	.121	.56E
	30-40	45	72	31	45	21	34	1.26	.124	.50C
35/220/4.00	40-50	48	59	26	45	20	35	1.13	.131	.51E
	50-60	46	53	26	46	0	31	1.10	.000	.50C
	60-70	50	53	26	50	0	32	1.12	.000	.50C

Figure 101 The longitudinal distribution of B values for Daniels iPP mouldings; 35/220/1.35, 35/280/1.35, 80/220/1.35, 80/280/1.35.

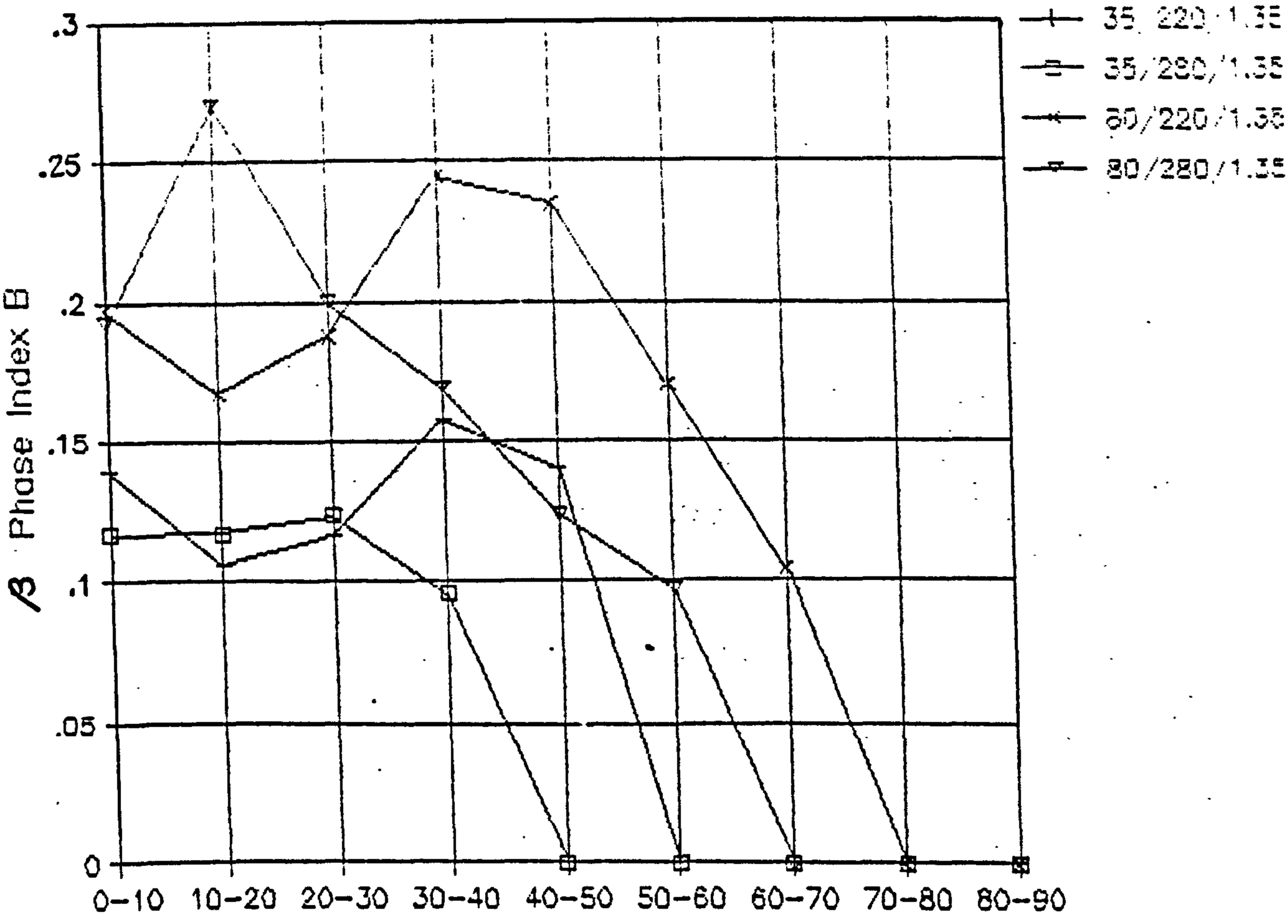

Figure 102 The longitudinal distribution of B values for Daniels iPP mouldings; 80/280/4.00, 35/280/4.00, 35/220/4.00.

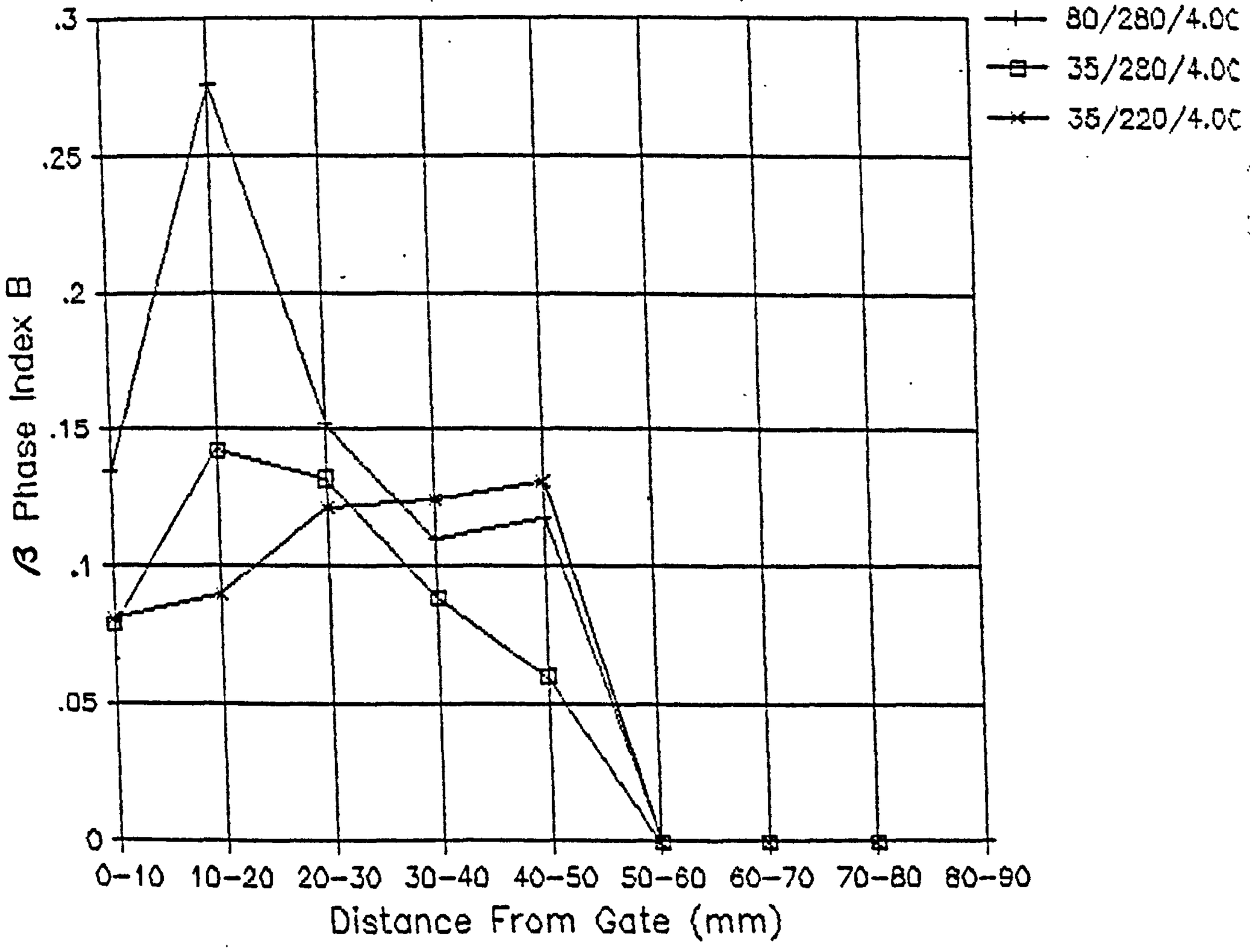

Figure 103 The longitudinal distribution of C values for Daniels iPP mouldings; 35/220/1.35, 35/280/1.35, 80/220/1.35, 80/280/1.35.

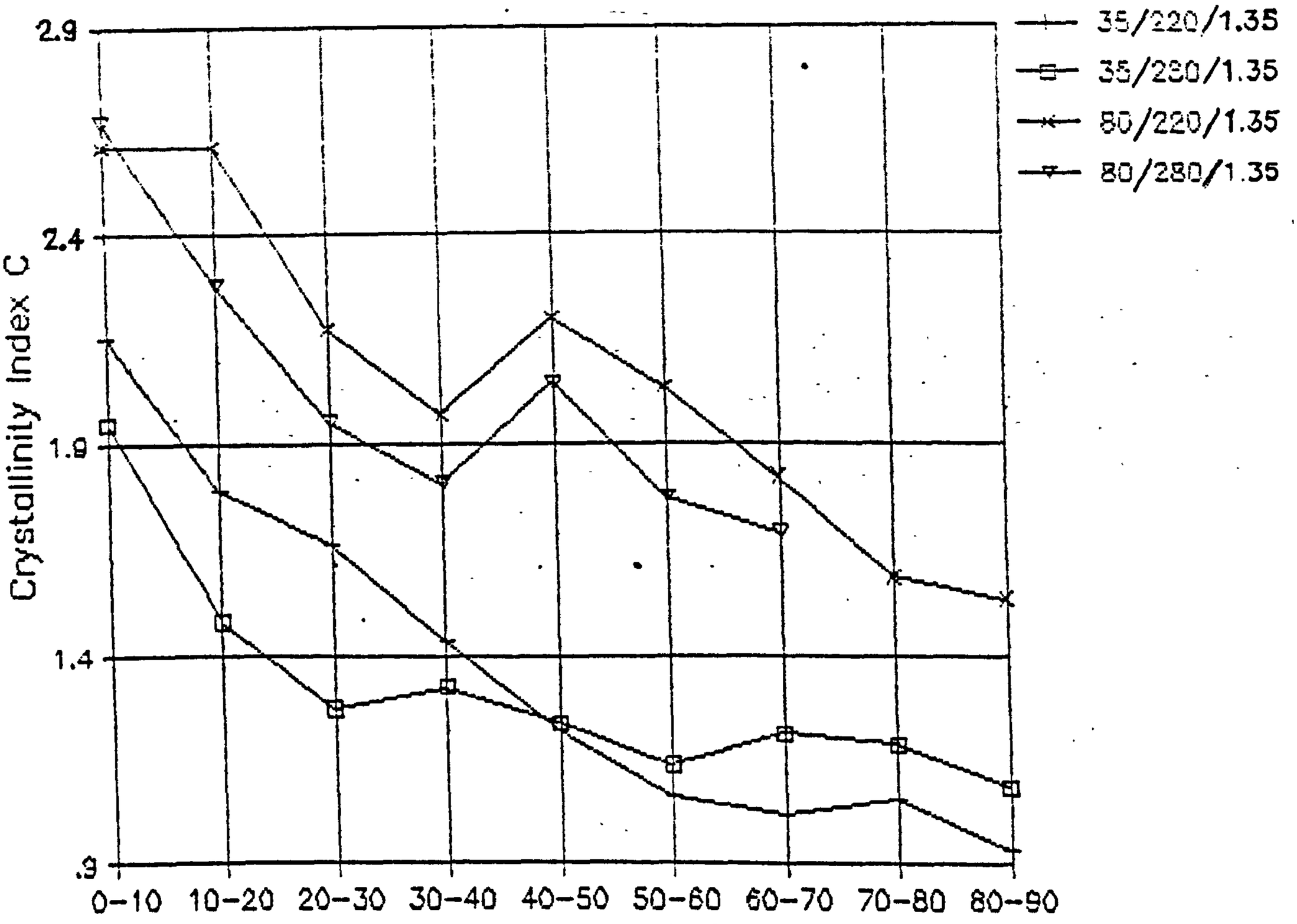

Figure 104 The longitudinal distribution of C values for Daniels iPP mouldings; 80/280/4.00, 35/280/4.00, 35/220/4.00.

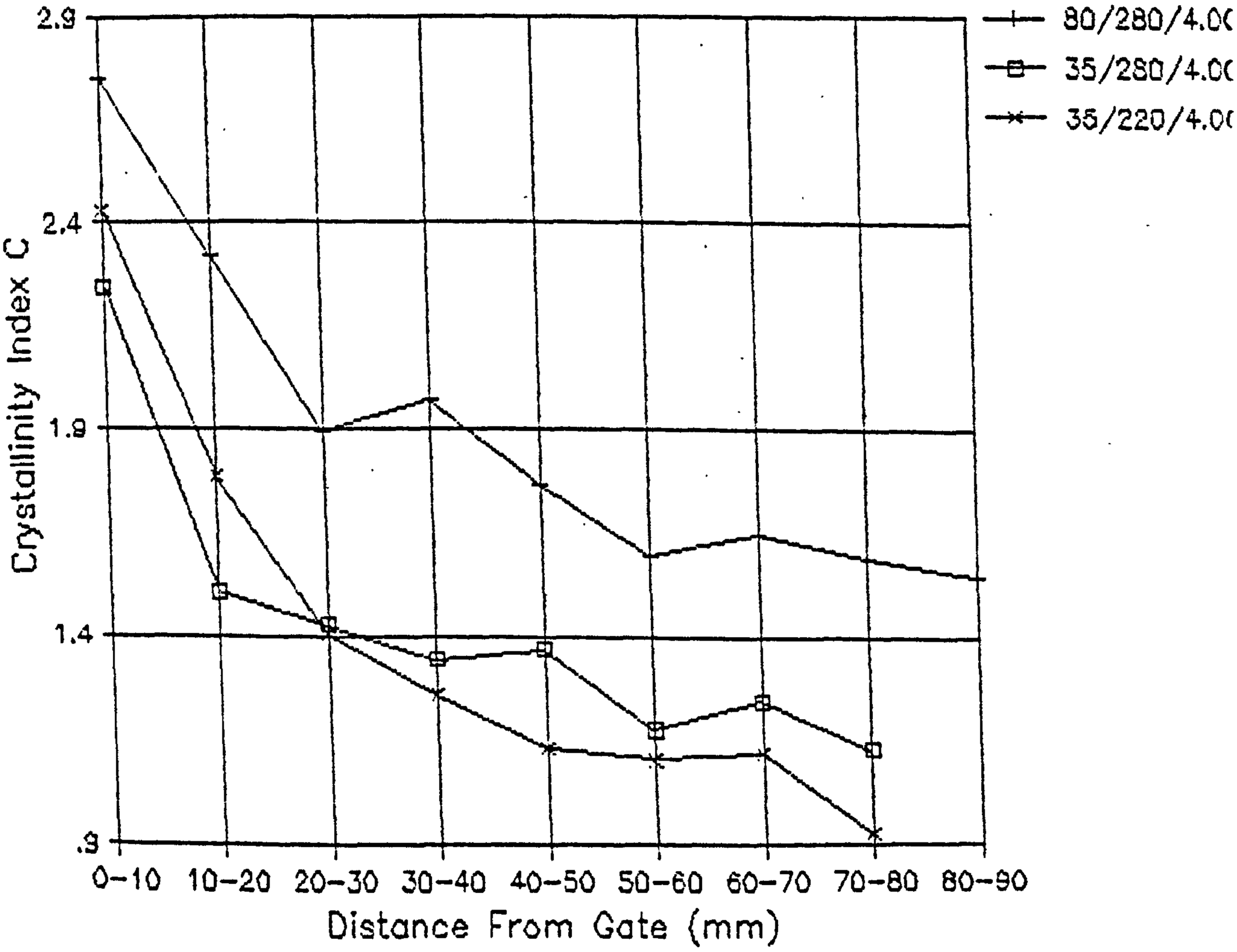

Figure 105 The longitudinal distribution of A values for Daniels iPP mouldings; 35/220/1.35, 35/280/1.35, 80/220/1.35, 80/280/1.35.

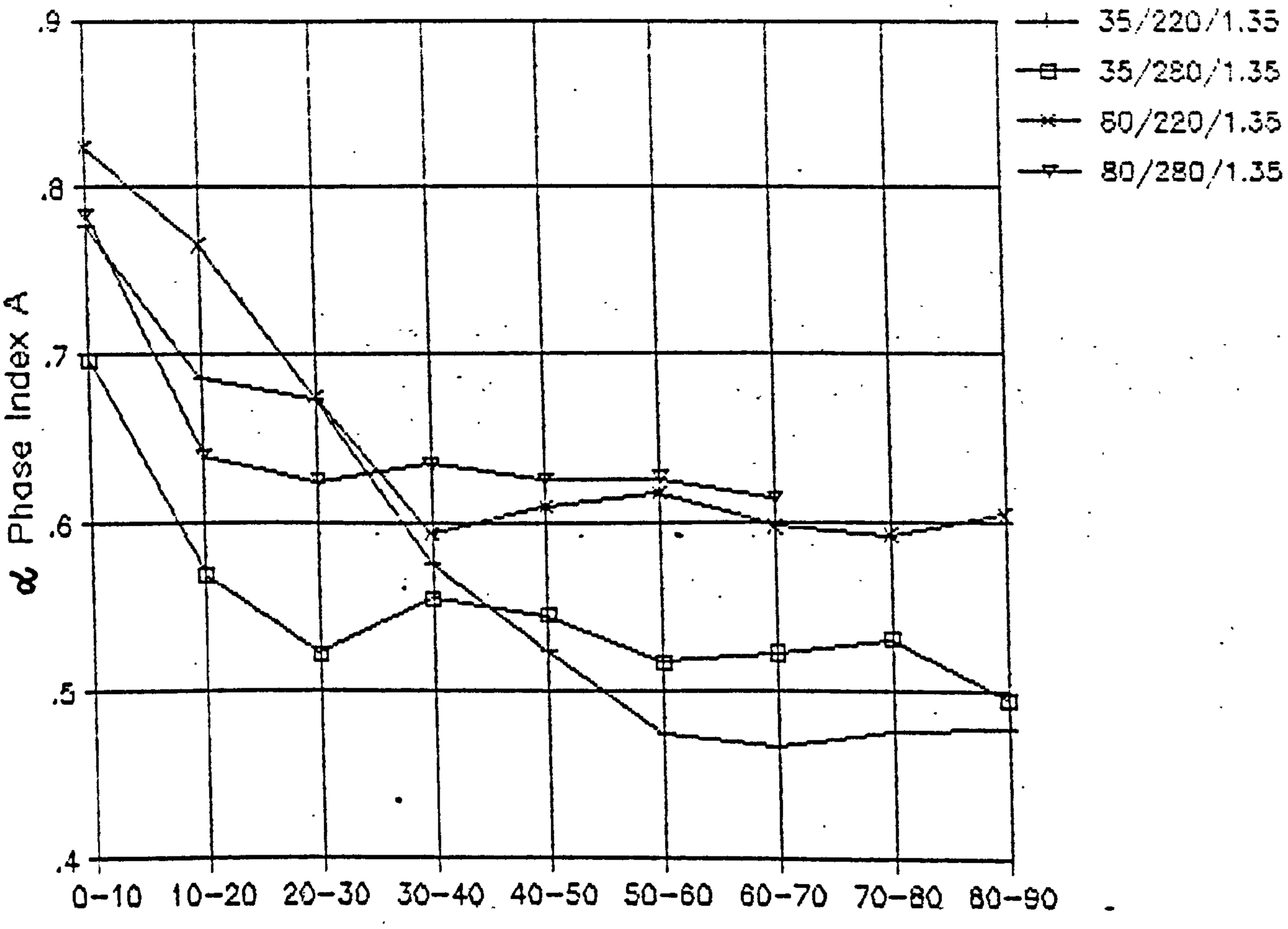

Figure 106 The longitudinal distribution of A values for Daniels iPP mouldings; 80/280/4.00, 35/280/4.00, 35/220/4.00.

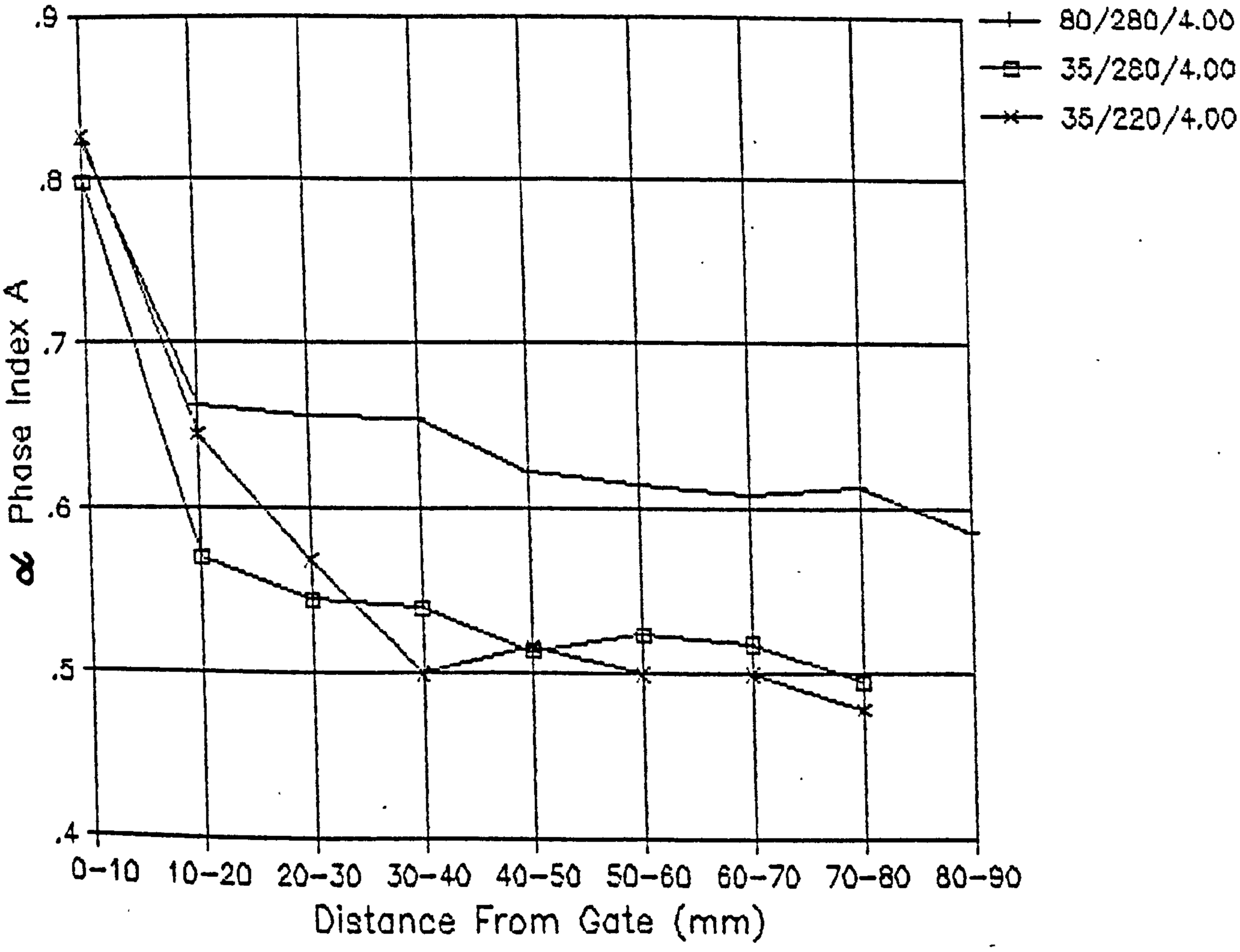

The following observations were made for the distribution of B, C and A indexes respectively:-

1. β-phase Index

The longitudinal distribution of the B values are given in Figures 101 and 102. The following observations were made:-

(i) The β phase concentration reaches a maximum before it decreases to zero at a certain point along the flow direction.

(ii) The β phase concentration increases with increasing mould temperatures and with decreasing melt temperatures. No trend could be found with changes in injection velocity.

(iii) Low mould temperatures, high melt temperatures and fast injection velocities when used to produce mouldings give the lowest concentration and shortest distribution of the β-phase along the melt flow direction.

2. Crystalline Fraction

The longitudinal distribution of C values is given in Figures 103 and 104. The following observations were made:-

(i) In all mouldings the maximum degree of crystallinity is found in the zones near to the injection gates.

(ii) The overall crystalline fraction increases with mould temperatures used to produce mouldings.

(iii) These mouldings produced at low melt temperatures and low mould temperatures are noticably more heterogeneous than other mouldings under investigation.

(iv) Slow injection speeds appear to increase the crystallinity overall but particularly at the injection gates of mouldings.

(v) The most homogeneous mouldings were produced using low mould temperatures, high melt temperatures and slow injection speeds. The crystallinity at these mouldings was noticeably lower.

3. Orientation of the α-phase

Measurement of isotropic samples such as granules give A = 0.57, with this in mind it was found that:-

(i) Orientation of the c-axis with respect to the flow direction was observed in the gate regions of all mouldings i.e. values of A higher than 0.57.

(ii) High mould temperatures lead to mouldings with preferred orientation of the c-axis with respect to the flow direction across the entire moulding.

(iii) Mouldings produced at high melt temperatures exhibit the least preferred molecular orientation in the flow direction.

(iv) A slight increase in the degree of preferred orientation is shown with slower injection velocities.

Correlations between A, B and C confirm the importance of orientation on crystallization processes during injection moulding. The β-phase crystallization is clearly favoured by a strong orientation of the melt as is the overall crystalline fraction. It has been shown that a strong morphological heterogeneity exists along the melt flow direction which is in complete agreement with light microscopy observations.

3.7.4 Crystalline Polymorphism and Orientation in Sandretto Mouldings

The same x-ray experiment was carried out on Sandretto injection moulded plaques from each respective processing condition. The results of this study are presented in Table 30 and plots of β-phase Index B, Crystallinity Index C, and Orientation Index A,

TABLE 30 X-ray diffraction results for Sandretto injection mouldings.

MOULDING CONDITION	DISTANCE FROM GATE (mm)	hα1	hα2	hα3	hα4	hβ	ha	CRYST. INDEX C	β-PHASE INDEX B	α-PHASE INDEX A
	0-10	79	161	49	34	33	37	1.924	.102	.699
	10-20	87	175	53	46	33	40	1.970	.095	.654
	20-30	76	151	48	34	29	38	1.779	.095	.691
30/220/30	30-40	61	113	36	39	34	36	1.572	.139	.610
	40-50	52	78	30	46	28	35	1.337	.149	.531
	50-60	57	55	32	48	5	36	1.094	.034	.543
	60-70	57	56	35	52	0	35	1.143	.000	.523
	70-80	56	56	30	55	0	34	1.159	.000	.505
	0-10	67	137	42	38	25	34	1.818	.092	.638
	10-20	61	108	40	46	24	33	1.691	.103	.570
	20-30	57	70	33	50	32	33	1.467	.167	.533
	30-40	55	64	25	48	22	31	1.381	.133	.534
30/250/30	40-50	52	52	30	52	11	33	1.194	.076	.500
	50-60	57	47	28	51	0	33	1.109	.000	.528
	60-70	58	49	31	52	0	32	1.188	.000	.527
	70-80	62	46	31	58	0	34	1.159	.000	.517
	0-10	73	139	42	46	36	39	1.723	.124	.613
	10-20	56	59	32	46	37	34	1.353	.201	.549
	20-30	59	57	32	51	22	32	1.381	.129	.536
	30-40	59	56	36	50	0	32	1.256	.000	.541
30/280/30	40-50	40	35	22	35	0	21	1.257	.000	.533
	50-60	53	43	31	45	0	9	1.186	.000	.541
	60-70	61	45	35	58	0	34	1.171	.000	.513
	70-80	60	45	35	54	0	31	1.252	.000	.526
	0-10	74	144	47	38	21	36	1.800	.073	.661
	10-20	75	171	51	34	26	35	2.040	.080	.688
	20-30	69	135	43	41	25	37	1.692	.092	.627
	30-40	52	90	32	42	28	32	1.525	.139	.553
30/220/15	40-50	47	66	27	42	29	34	1.241	.172	.528
	50-60	51	64	30	48	21	34	1.259	.127	.515
	60-70	50	49	27	50	0	34	1.035	.000	.500
	70-80	52	44	26	51	0	33	1.048	.000	.505
	0-10	81	172	51	35	37	35	2.149	.109	.698
	10-20	80	146	49	33	32	35	1.943	.104	.708
	20-30	85	157	49	35	34	36	2.000	.105	.708
30/220/45	30-40	61	111	36	36	35	34	1.641	.144	.629
	40-50	51	58	23	41	22	31	1.258	.143	.554
	50-60	55	49	26	45	0	33	1.061	.000	.550
	60-70	54	44	30	47	0	33	1.061	.000	.535
	70-80	60	44	26	46	0	32	1.100	.000	.566
	0-10	130	240	85	24	55	38	2.811	.108	.844
	10-20	101	213	58	38	51	36	2.561	.121	.727
	20-30	84	160	49	42	53	32	2.425	.153	.667
	30-40	68	107	42	44	47	30	2.053	.178	.607
70/220/30	40-50	69	99	41	47	55	30	2.073	.208	.595
	50-60	78	109	47	48	25	32	1.919	.097	.619
	60-70	77	97	46	48	11	31	1.800	.048	.616
	70-80	80	88	45	51	0	31	1.703	.000	.611
	0-10	101	185	60	30	30	35	2.320	.080	.771
	10-20	95	200	55	36	41	37	2.308	.105	.725
	20-30	86	173	48	36	41	35	2.194	.118	.705
	30-40	72	111	43	42	46	34	1.847	.169	.632
50/220/30	40-50	65	88	37	45	33	33	1.624	.148	.591
	50-60	66	76	35	46	16	31	1.542	.083	.589

Figure 107 The longitudinal distribution of B values with melt temperature.

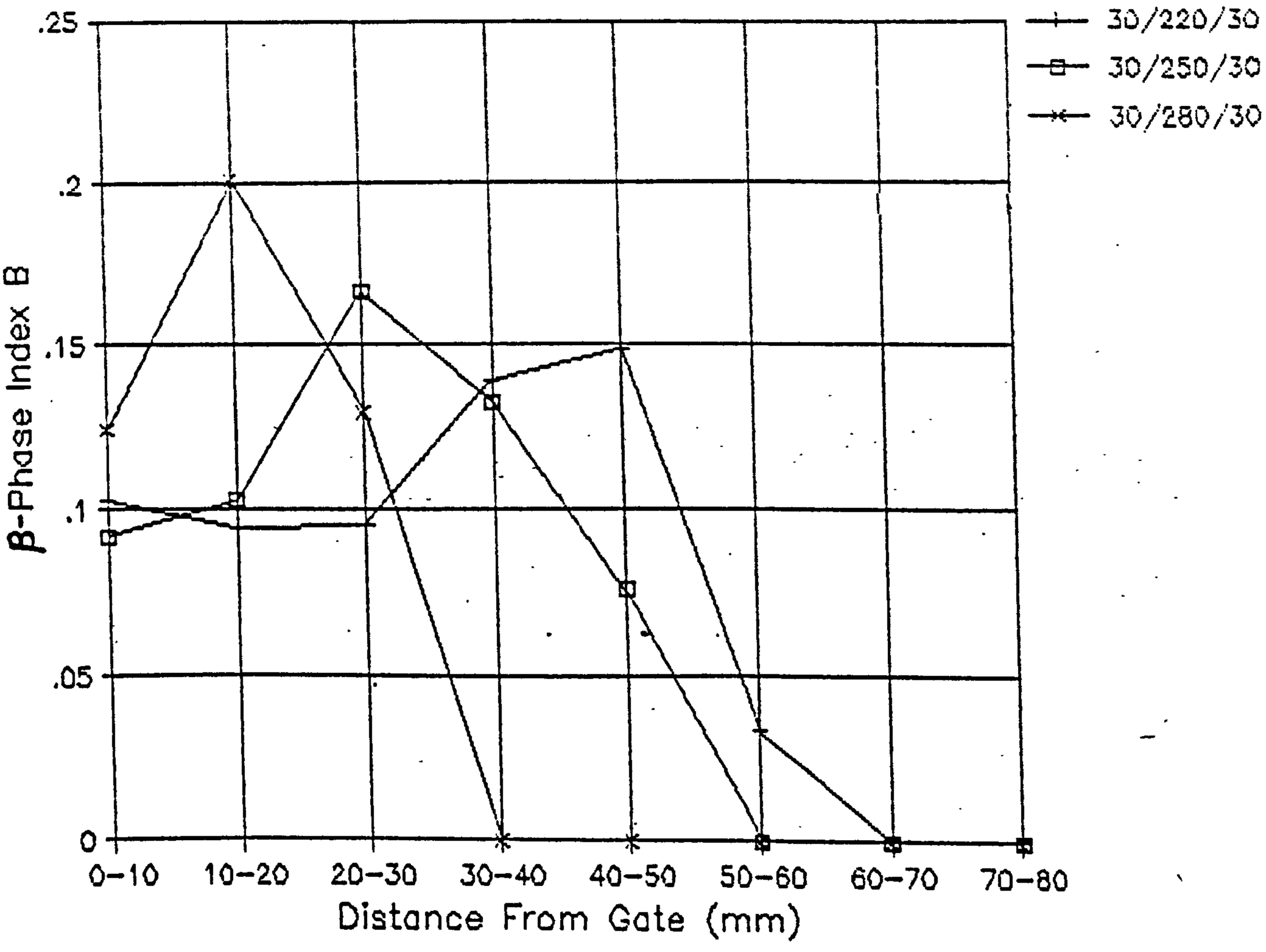

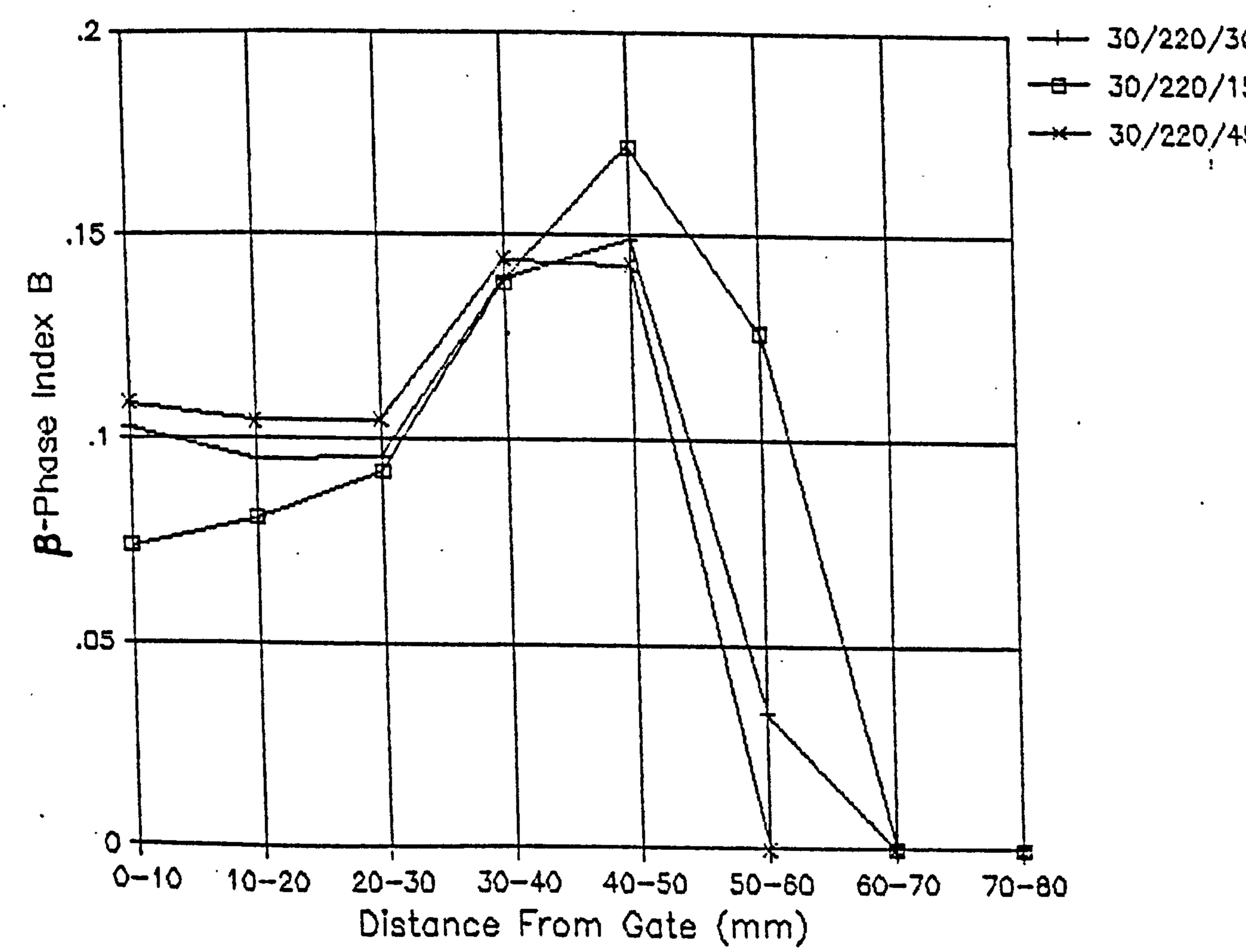

Figure 109 The longitudinal distribution of B values with injection velocity.

Figure 108 The longitudinal distribution of B values with mould temperature.

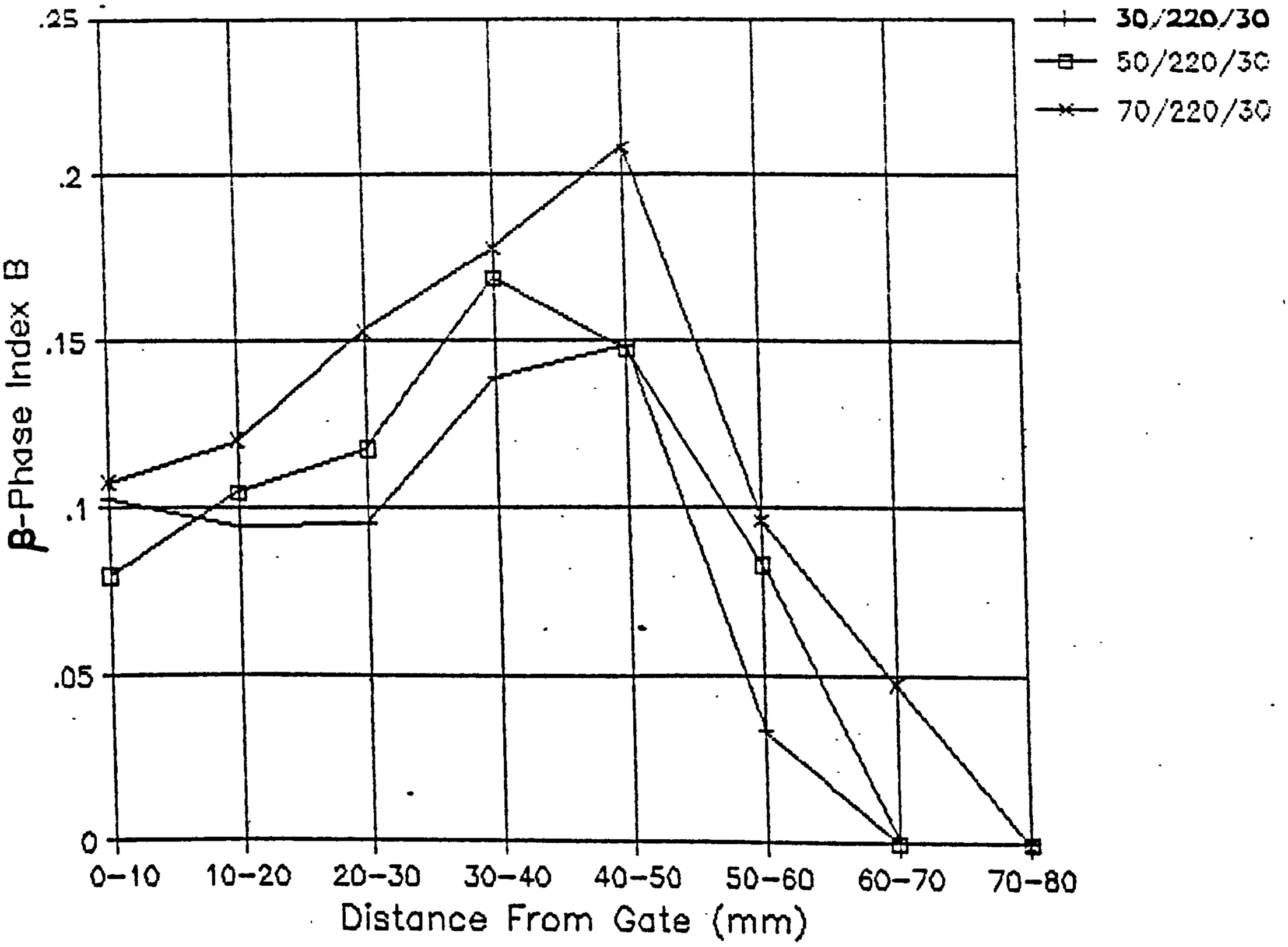

Figure 110 The longitudinal distribution of C values with melt temperature.

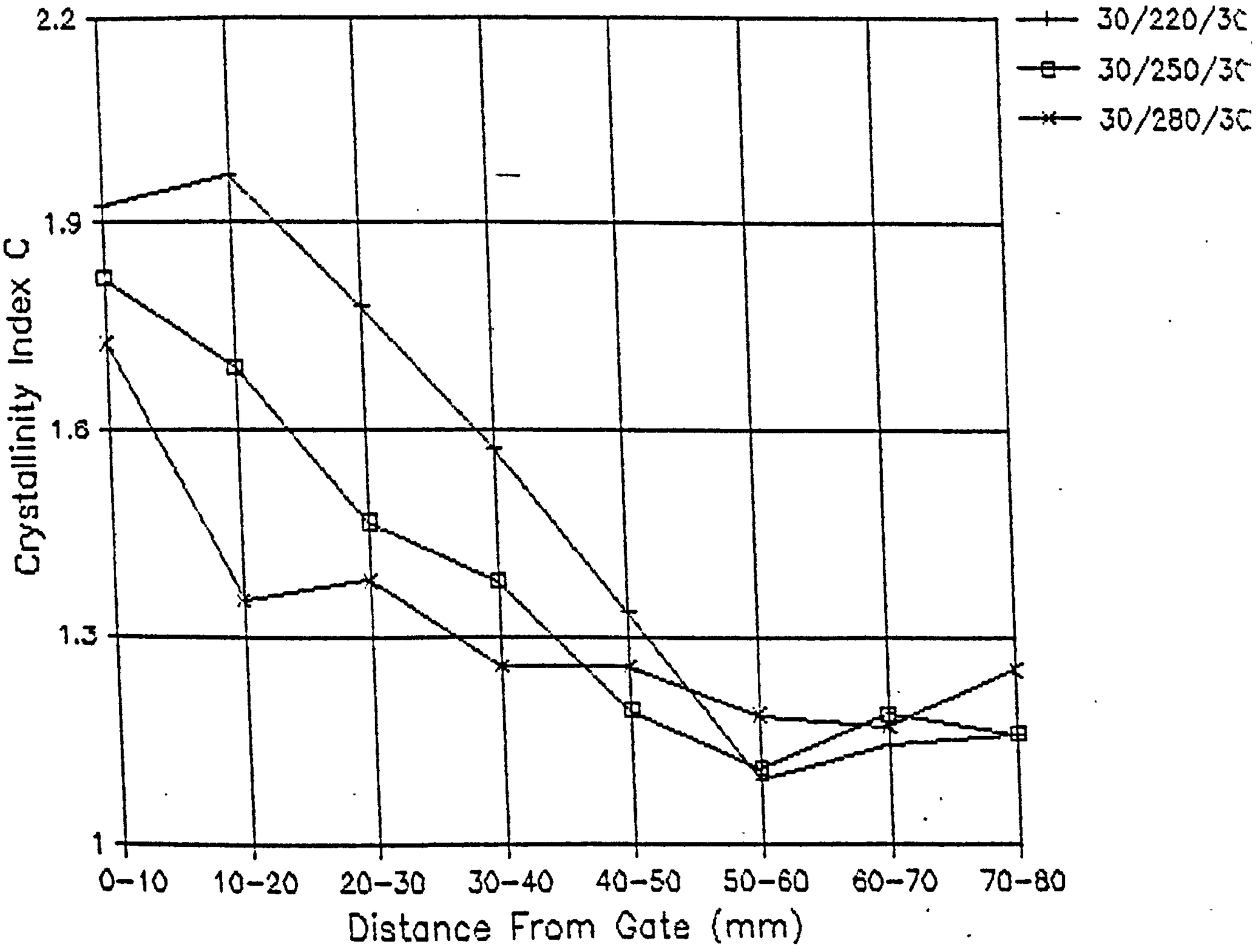

Figure 112 The longitudinal distribution of C values with injection velocity.

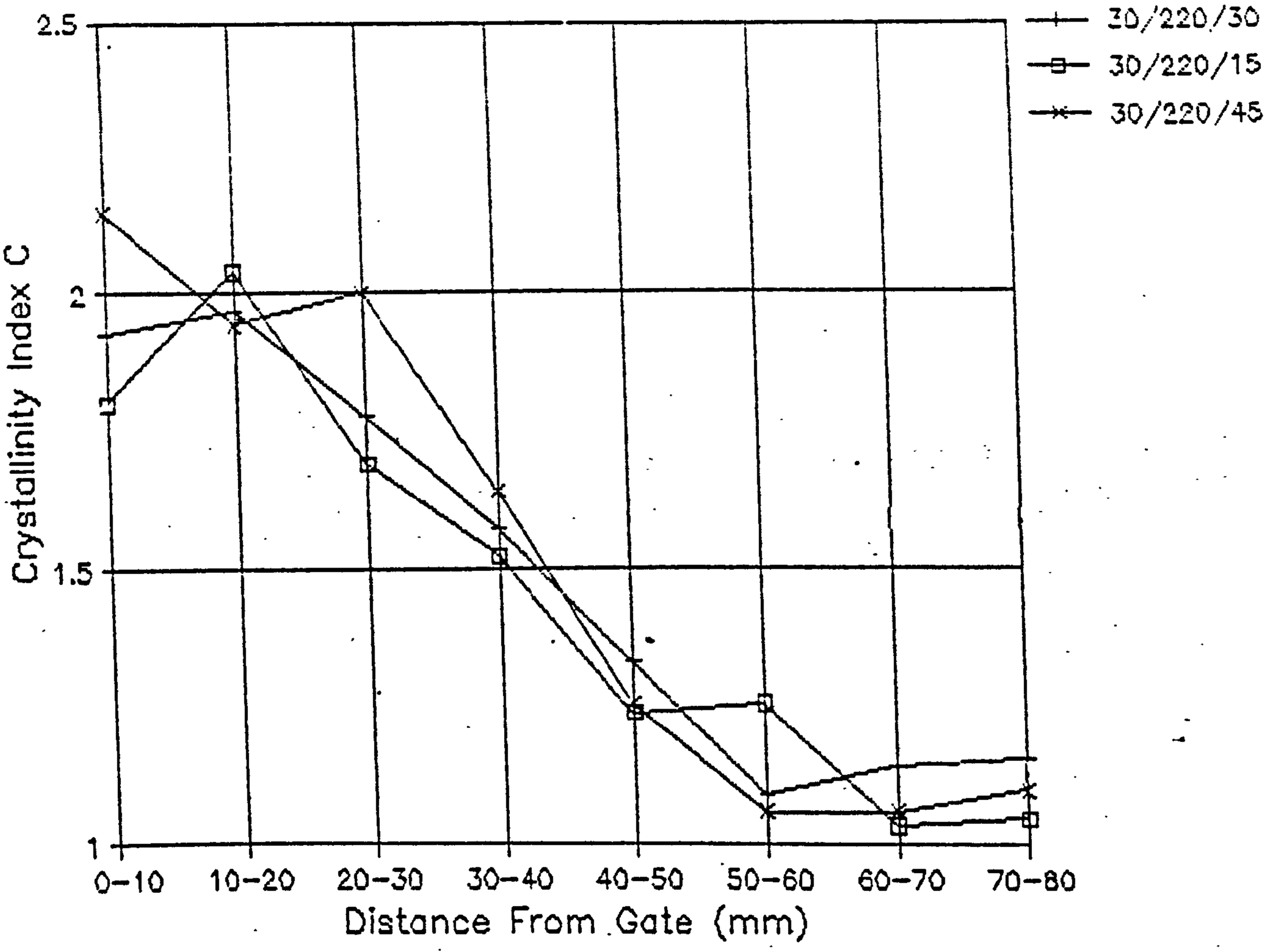

Figure 111 The longitudinal distribution of C values with mould temperature.

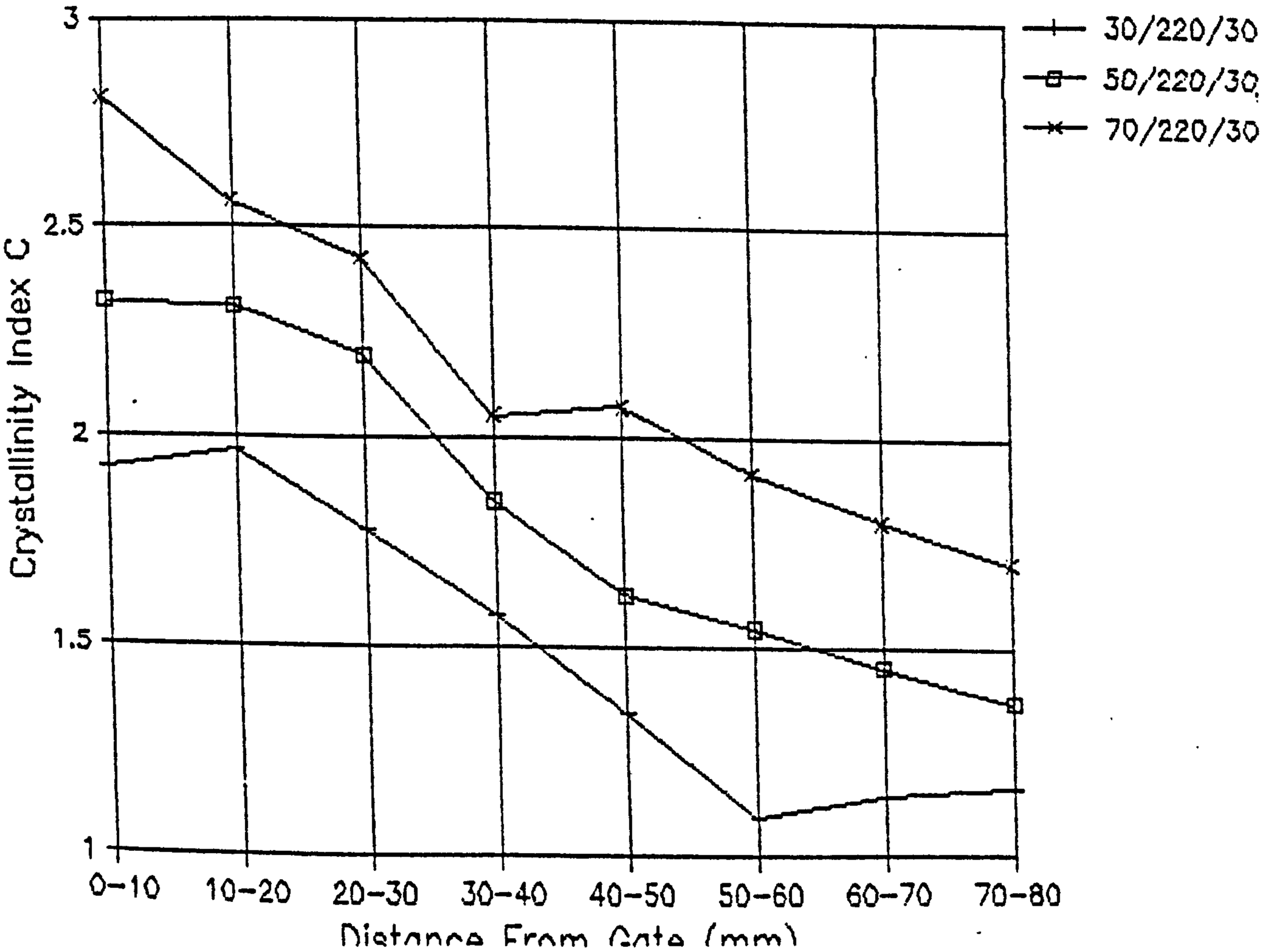

Figure 113 The longitudinal distribution of A values with melt temperature.

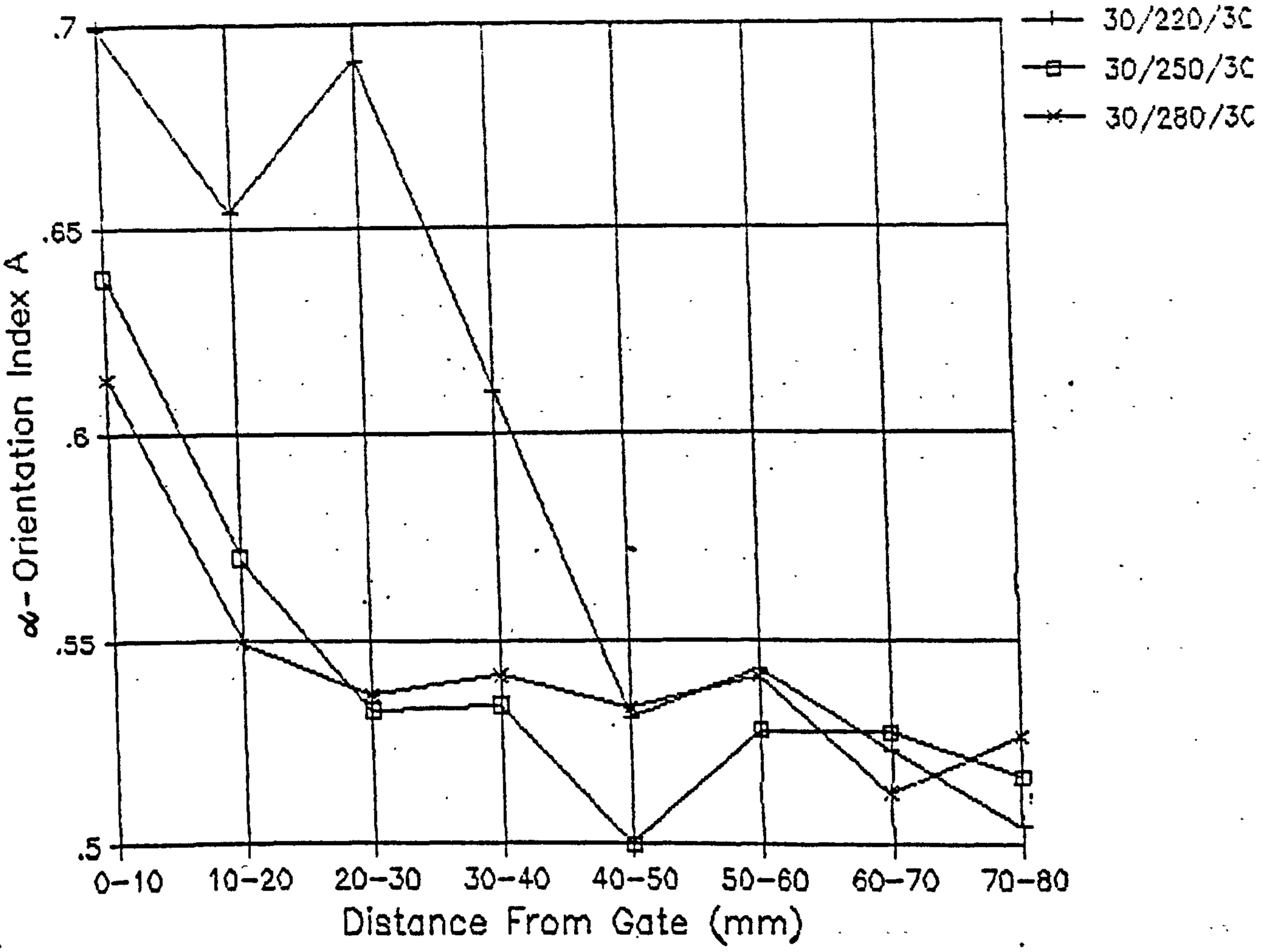

Figure 115 The longitudinal distribution of A values with injection velocity.

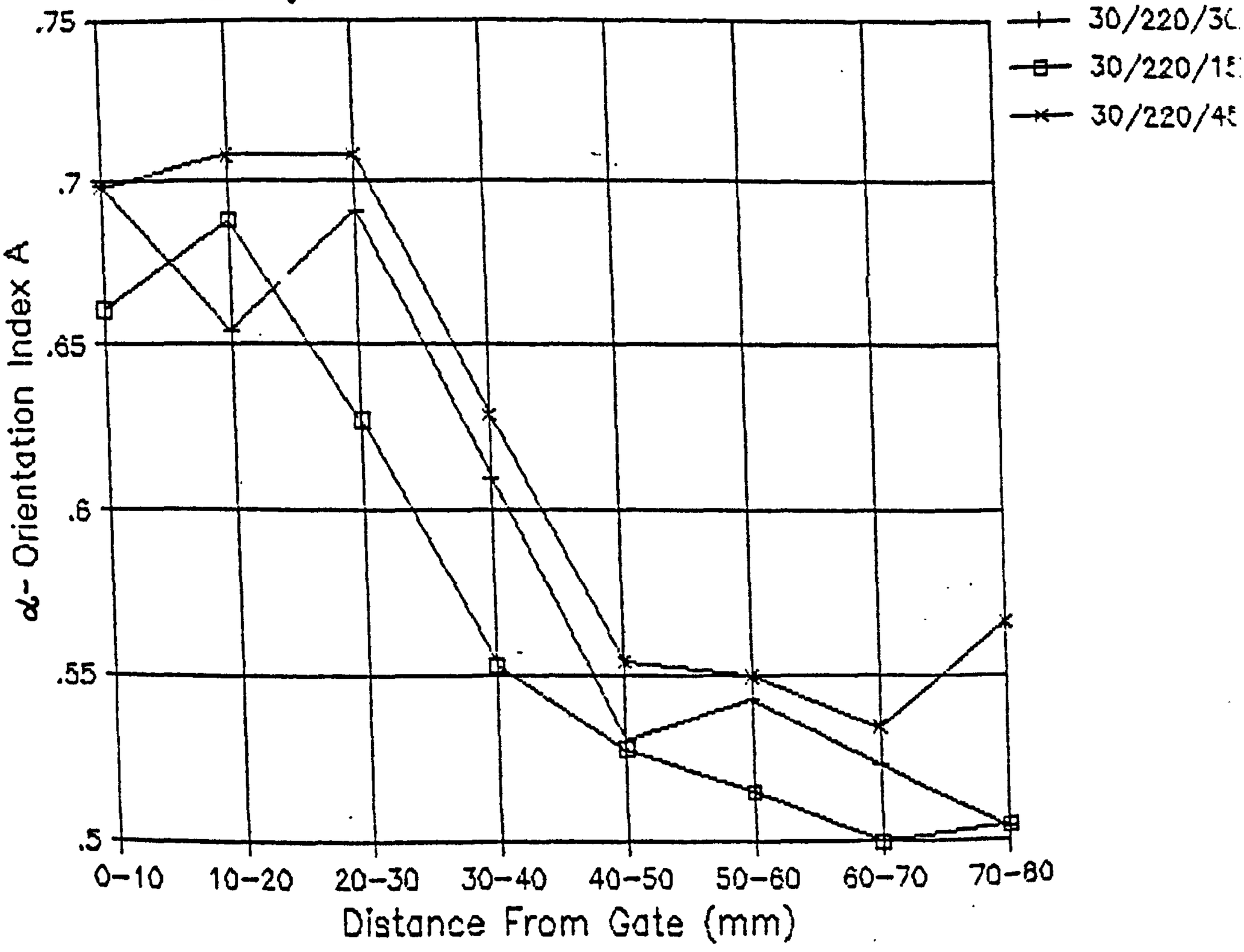

Figure 114 The longitudinal distribution of A values with mould temperature.

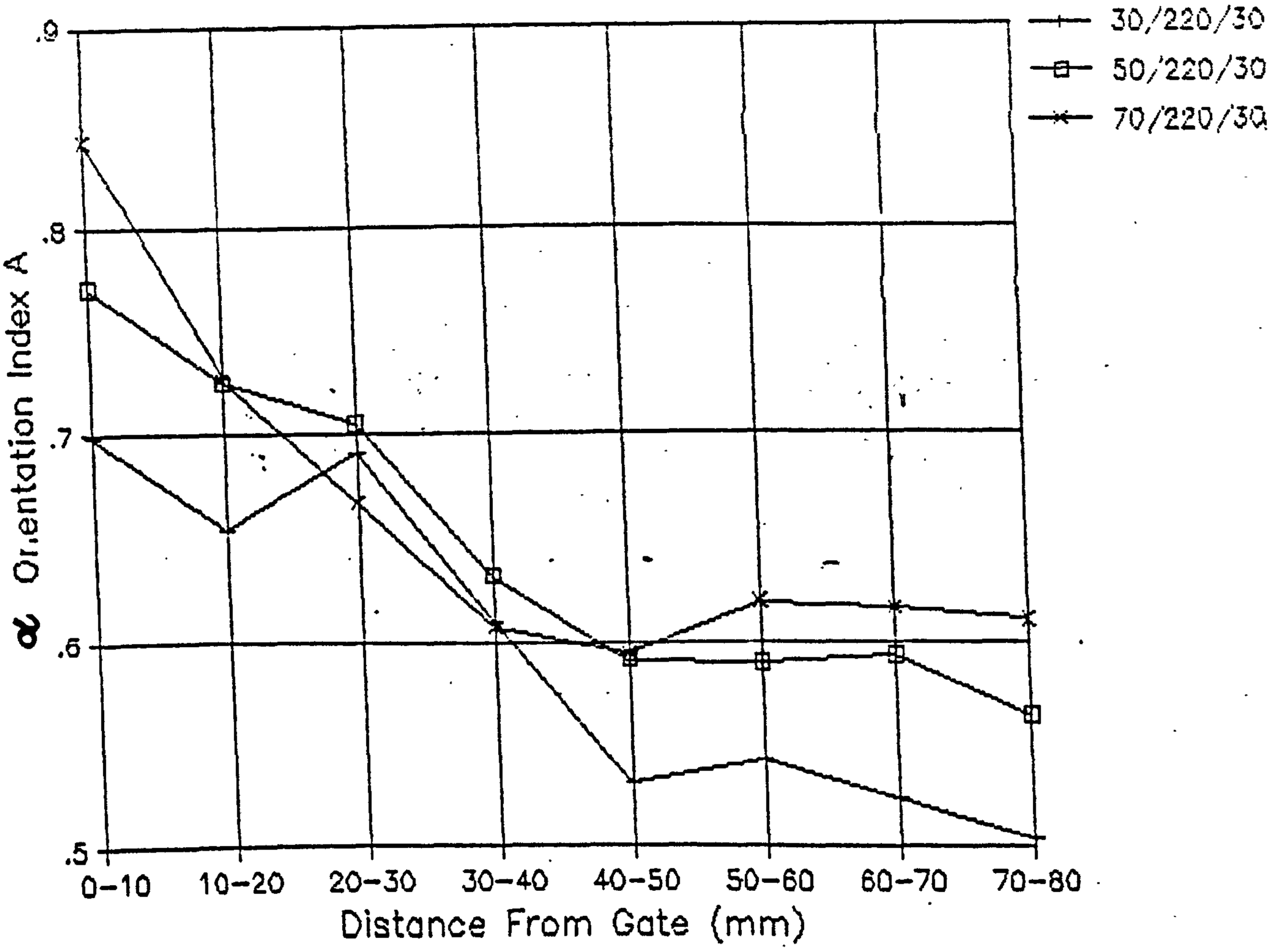

TABLE 31 Correlation between transition in impact properties and phase distribution along the flow direction in iPP injection mouldings.

MOULDING CONDITION			B-PHASE DISTRIBUTION	TRANSITION IN IMPACT
°C	°C	%	(mm)	PROPERTIES (mm)
30	220	30	50-60	70
30	250	30	30-40	20-40
30	280	30	20-30	21
50	220	30	50-60	40-70
70	220	30	60-70	>70
30	220	15	50-60	40-70
30	220	45	40-50	40-60

versus distance along the flow direction are presented in Figures 107 to 115 for each processing condition. The following observations were made:-

1. <u>β-phase Index</u>

   β-phase index distribution as illustrated in Figures 107 to 109 revealed that:-

   (i) The β phase concentration reaches a maximum before it decreases to zero at a certain point along the flow direction.

   (ii) The nucleation of the β phase is particularly sensitive to changes in mould temperature and melt temperature. A significant increase in distribution along the flow direction is noted for increasing mould temperatures and reduction in melt temperatures.

   (iii) Little effect is seen of injection velocity on β phase nucleation, it is perhaps slightly enhanced with fast cavity injection speeds.

2. <u>Crystalline Fraction</u>

   The longitudinal distribution of C values is shown in Figures 110 to 112. It was noticed that:-

   (i) In all mouldings the maximum degree of crystallinity was found in the vicinity of the gate.

   (ii) The degree of crystallinity is increased drammatically with increasing mould temperatures.

   (iii) A reduction in the degree of crystallinity was found with increasing melt temperatures particularly in the first half of the flow path away from the gate.

   (iv) Little change in degree of crystallinity was observed with injection velocity variations.

3. Orientation of the α-phase

As illustrated in Figures 113 to 115.

(i) Orientation of the c-axis with respect to the flow direction is observed close to the gate regions in all mouldings.

(ii) The highest degree of preferred orientation was observed in high mould temperature mouldings and low melt temperature mouldings.

(iii) No significant variation in preferred molecular orientation was found when changing injection velocities.

3.7.5 Summary of Results

The results for Daniels mouldings are in almost complete agreement with those found for Sandretto injection moulded plaques. In both cases a large degree of structural heterogenity exists along the melt flow direction which is particularly sensitive to variations in the mould and melt temperatures used during injection moulding. In all cases the x-ray observations agree with optical studies with respect to the β phase concentration and distribution across mouldings. It can be concluded therefore that x-ray diffractometry is indeed a powerful technique in characterization of surface polymorphisms and orientation in injection moulded articles.

It has been shown that the impact properties of injection mouldings of isotactic polypropylene can be markedly reduced by the presence of row nucleated β-phase spherulites,and by nucleation of large crystallites, in the surface layers.x-ray diffraction results can therefore be used to predict failure anywhere in the calibrated moulded part, for example see Table 31 which relates the transition in impact strength from low to high with β phase distribution along the flow direction.

3.8 DSC ANALYSIS OF INJECTION MOULDED iPP PLAQUES

The effects of processing conditions on the melting behaviour of GXM43 polypropylene mouldings was determined by use of the DSC 2 according to the procedure given in Section 2.6.4. Thermal analysis of thin films of approximately 5mg weight taken from Daniels injection moulded Izod test pieces 20mm along the flow direction and through the thickness was made for each processing condition. The melting curves exhibited upto 4 peaks, one major peak corresponding to the α-phase melting endotherm at 437K and three minor peaks on the shoulder of the major peak at 414K, 423K. and between 430 and 432K respectively. The peak of 423K agrees with the β phase melting endotherm reported by Lovinger (59). Figure 116 shows the melting behaviour of a sample moulded using high mould and melt temperatures, note the multiple melting peaks.

A summary of the melting peak positions and heats of fusion for polypropylene samples moulded at different processing conditions is given in Table 32. From this Table it is noticed that processing parameters that lead to high degrees of β phase formation with spherulites upto 40 μm in diameter, namely high mould temperatures, reveal two extra peaks at 413K and 423K which are both due to the β phase.

From the results it was concluded that two peaks occur for the α phase melting and two for the β phase, these doublets are probably due to preferred molecular orientation. The heats of fusion suggest that a higher degree of crystallinity is present in samples moulded at high mould temperatures, whereas low mould temperatures and low melt temperatures give the least crystallinity. These findings are in good agreement with x-ray observations reported in Section 3.7.

TABLE 32 DSC analysis of Daniels injection mouldings.

MOULDING CONDITION °C	°C	secs	MELTING PEAK TEMPERATURE (C) β1	β2	α1	α2	HEAT OF FUSION cal/gram
35	220	1.35			~429	437.47	19.63
35	220	4.00			~429	437.70	20.22
80	220	1.35	413.00	423.39	~429	436.77	20.18
35	280	1.35			~429	437.29	20.41
35	280	4.00			429.82	437.87	19.65
80	280	1.35	413.97	423.16	432.15	437.81	22.85
80	280	4.00	413.13	423.00	432.08	438.04	20.11

Figure 116 The melting behaviour of an iPP moulding produced using high mould and melt temperatures. Note the multiple melting peaks.

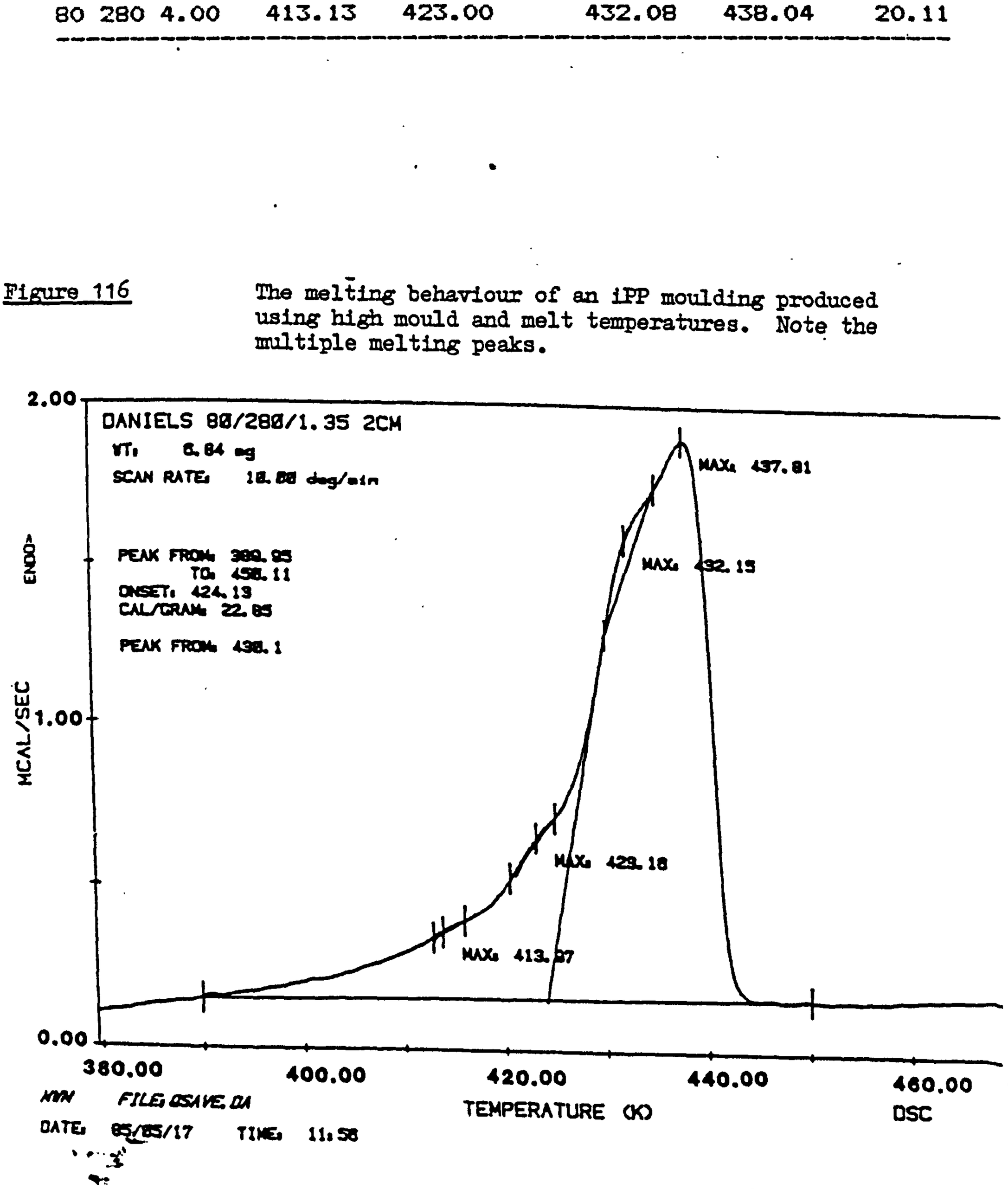

CHAPTER 4

EFFECT OF MOLECULAR WEIGHT DISTRIBUTION ON MICROMORPHOLOGY AND IMPACT PROPERTIES OF INJECTION MOULDED iPP.

4.1 INTRODUCTION

With a view to establishing a general way of improving the impact resistance of GXM43 polypropylene injection mouldings the addition of various percentages of a high and low molecular weight polyproplylene was considered. The aims of this study were to assess the effect of molecular weight on:-

(i) the nucleation of row structures and the β phase in the vicinity of the gate,

(ii) the extent and width of banded morphologies along the flow direction,

(iii) the size of α -phase core spherulites, and

(iv) the changes in impact performance resulting from any modification in the morphology of mouldings observed.

The two polypropylenes chosen for this experiment were GYM45 and GSE16 with Melt Flow Indices of 15.0 grammes per 10 minutes and 0.8 grammes per 10 minutes respectively. Technical data and selection criteria for each polypropylene are given in Section 2.1.2.

4.2 INJECTION MOULDING

Feedstocks consisting of 5, 10, 20 and 30 wt.% of GSE16 and GYM45 were prepared. The compounds were simply tumble mixed with virgin granules of GXM43 polypropylene prior to moulding on the Sandretto using the set processing conditions given in Table 12 but with a modified packing pressure profile in an attempt to improve the volume shrinkage of mouldings. The mean peak cavity pressure for GXM43 polypropylene moulded at 220°C melt temperature, using a 30°C mould temperature and injection velocity of 30%, was increased from 25.23 to 28.65 MNm^{-2} which resulted in slightly better packing of the mould and a subsequent increase in the weight of mouldings in the

order of 3 grammes. The processing conditions were kept constant for all polypropylene blends since it would have been impractical to consider using a range of processing conditions in the time available. For completeness granules of both GSE16 and GYM45 were also moulded.

The mean peak cavity pressure, mean shot weight and percent volume shrinkage data for the moulding programme are given in Table 33. As with previous moulding a good proportional correlation between shot weight and peak cavity pressure was found.

From Table 33 it can be seen that the mean shot weight was found to decrease with increasing molecular weight. This was probably due to the higher viscosity of the associated melt which leads to faster cooling and consequently more shrinkage with reduced crystallinity. In low molecular weight 100% GYM45 mouldings a lower viscosity leads to slow cooling of the melt and consequently large spherulites and reduced shrinkage in the cavity during mould filling leading to denser mouldings.

4.3 CHARACTERISATION OF iPP BLENDS

To assess the degree of mixing/dispersion of high and low molecular weight additions, and to determine the overall thermal degradation during the injection moulding programme, plaques were granulated and sent to the Polymer Supply and Characterisation Centre at RAPRA for Gel Permeation Chromatographic (GPC) analysis. Samples were also granulated for the purpose of routine Melt Flow Index (MFI) measurements according to ASTM D1238 to also provide a measure of the molecular weight characteristics of each blend.

TABLE 33 Summary of data monitored for injection moulding of iPP blends.

iPP BLEND	MEAN SHOT WEIGHT (g) $\bar{x}$	s.d	MEAN PEAK CAVITY PRESSURE (MNm^{-}) $\bar{x}$	s.d	VOLUME SHRINKAGE (%)
100% GSE16	39.87	.290	26.99	.328	5.071
V+30% GSE16	39.93	.266	27.21	.372	4.929
V+20% GSE16	39.92	.227	27.19	.435	4.952
V+10% GSE16	39.94	.437	27.24	.511	4.905
V+ 5% GSE16	39.97	.353	27.31	.911	4.833
100% GXM43=V	40.52	.359	28.65	.925	3.524
V+ 5% GYM45	40.82	.107	28.78	.549	2.810
V+10% GYM45	40.89	.112	28.85	.358	2.643
V+20% GYM45	40.94	.137	29.05	.501	2.524
V+30% GYM45	41.02	.230	29.21	.412	2.333
100% GYM45	41.21	.113	30.33	.172	1.881

TABLE 34 Results from RAPRA GPC molecular weight distribution analysis and subsequent MFI measurements.

iPP BLEND	NUMBER AVERAGE MOL.WT. $\bar{M}n$*10E4	WEIGHT AVERAGE MOL.WT. $\bar{M}w$*10E5	AVERAGE MOL.WT. $\bar{M}z$*10E5	D	MELT FLOW INDEX (MFI) (g/10min)
GXM43 gran.	5.02	2.84	8.62	5.665	9.20
GYM45 gran.	3.28	2.49	9.10	7.584	15.00
GSE16 gran.	7.26	4.90	12.60	6.756	.78
100% GXM43=V	3.95	2.65	7.78	6.704	12.32
100% GYM45	3.04	2.31	7.99	7.250	18.92
100% GSE16	6.96	4.70	12.09	6.992	1.53
V+ 5% GYM45	3.91	2.64	7.92	6.900	12.65
V+10% GYM45	3.80	2.62	7.98	6.900	12.98
V+20% GYM45	3.71	2.60	7.79	6.998	13.65
V+30% GYM45	3.81	2.58	7.98	6.780	14.30
V+ 5% GSE16	4.02	2.75	8.85	6.779	11.78
V+10% GSE16	4.37	2.99	9.30	6.837	11.09
V+20% GSE16	4.66	3.10	9.13	6.644	10.16
V+30% GSE16	5.14	3.17	9.19	6.161	9.08

4.3.1 GPC Analysis

The GPC column was set up in accordance with the following conditions:-

Column	Styragel pore sizes 10^6, 10^4, 500A
Flow Rate	1.0 ml/min
Solvent	1,2,4 Trichlorobenzere stabilised with 2,6 - di - tert - butyl - p - cresol.
Temperature	140°C
Calibration	Derived from polystyrene standards. Mark-Houwink constants ($[\eta] = kM^{\alpha}$) used for conversion via Universal calibration:-
	Polystyrene $k = 1.38 \times 10^{-4}$ $\alpha = 0.7$
	Polypropylene $k = 1.03 \times 10^{-4}$ $\alpha = 0.78$

(where $\alpha = 0.5$ for a theta solvent).

The different molecular species eluted from the column in order of their molecular size, as distinguished from their molecular weight, gave typical molecular weight distribution curves as shown in Figure 117. The results provided included a measure of Number Average ($\bar{M}n$), Weight Average ($\bar{M}w$) and average ($\bar{M}z$) molecular weights and a diffusion constant D as derived from the rate of diffusion of each blend.

Plots of weight average molecular weight versus percent GSE16 and GYM45 are given in Figures 118 and 119 taken from the results presented in Table 34. A linear relationship is shown in both cases with; increasing molecular weight with percent GSE16 and decreasing molecular weight with percent GYM45. A good overall dispersion of low and high molecular weight additions was assumed from these results. However, some loss in molecular weight is noticed arising from thermal degradation during injection moulding.

Figure 117 Typical molecular weight distribution curves for three different polypropylene grades.

PSCC GPC SYSTEM CALIBRATION: ODCB09B

D348 GSE16 14:00 05/11/84

PEAK START:	730	MN:	7.26E+04
PEAK FINISH:	1280		
		MW:	4.00E+05
BASELINE START:	660		
BASELINE FINISH:	1640	MZ:	1.26E+06
FLOW CORRECTION:	1.000	MP:	7.26E+05
KP:	$1.030X10^{-4}$	D:	6.756
AP:	.78		

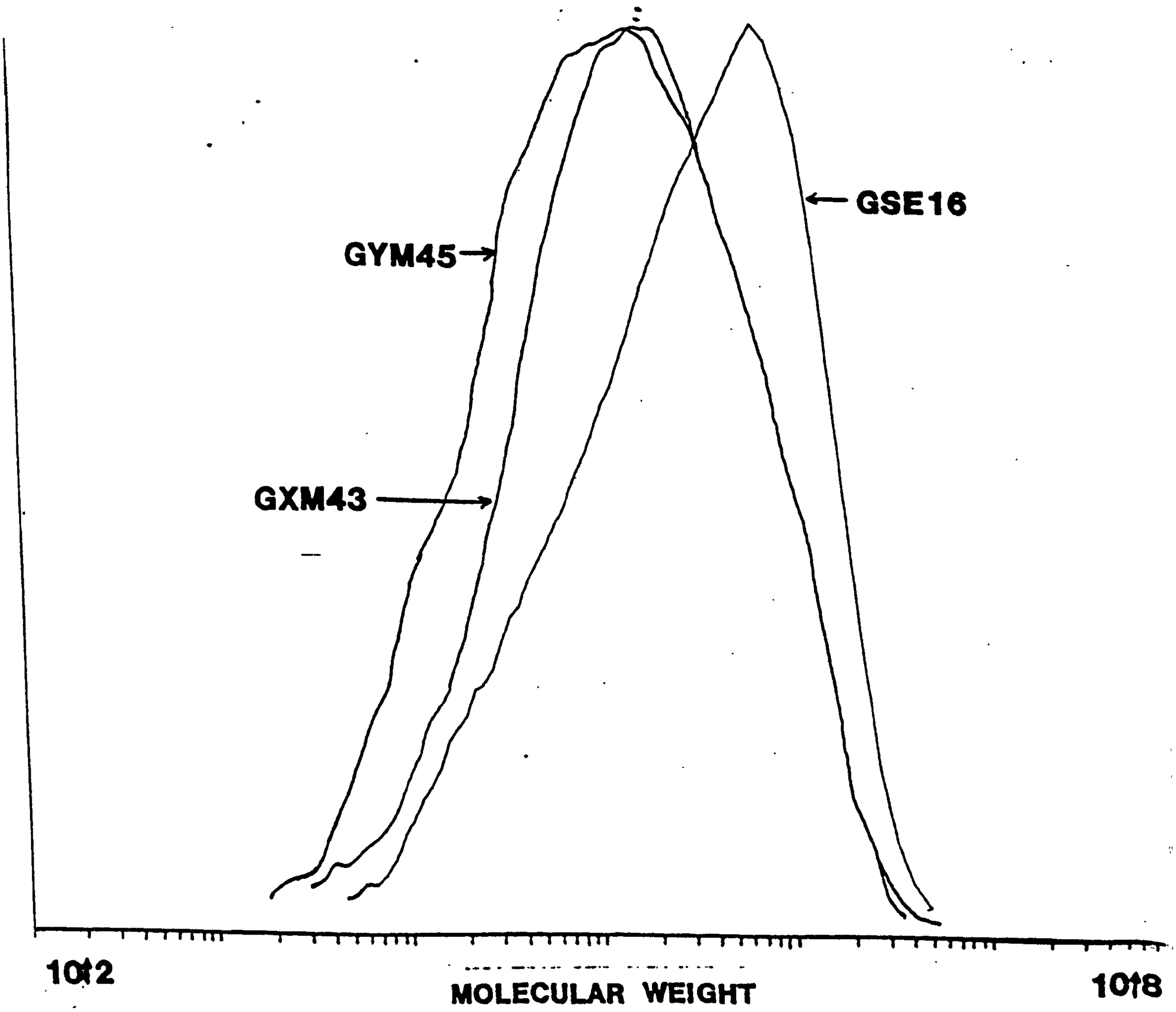

Figure 118 Weight average molecular weight versus weight percent G3E16 iPP added to GXM43 iPP.

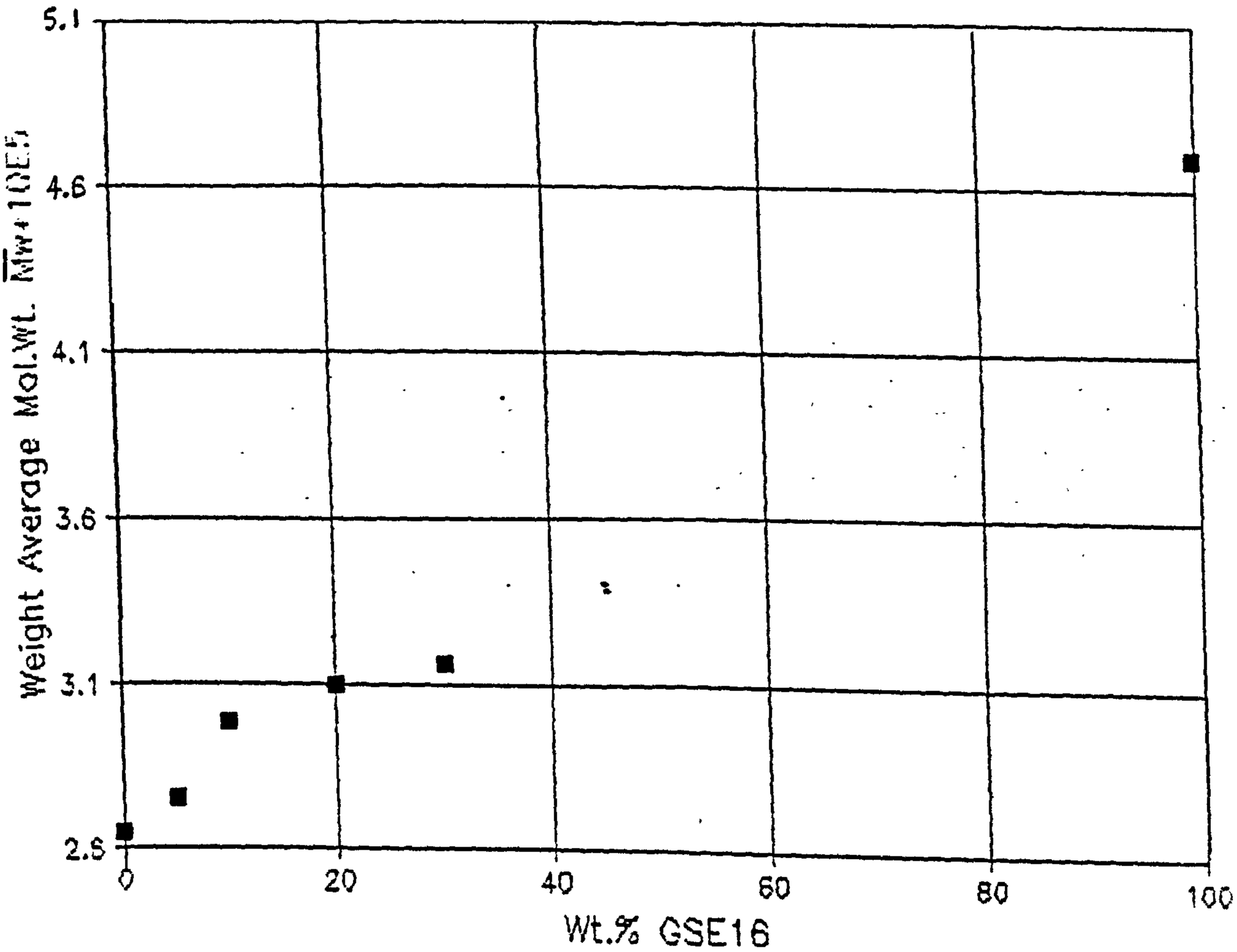

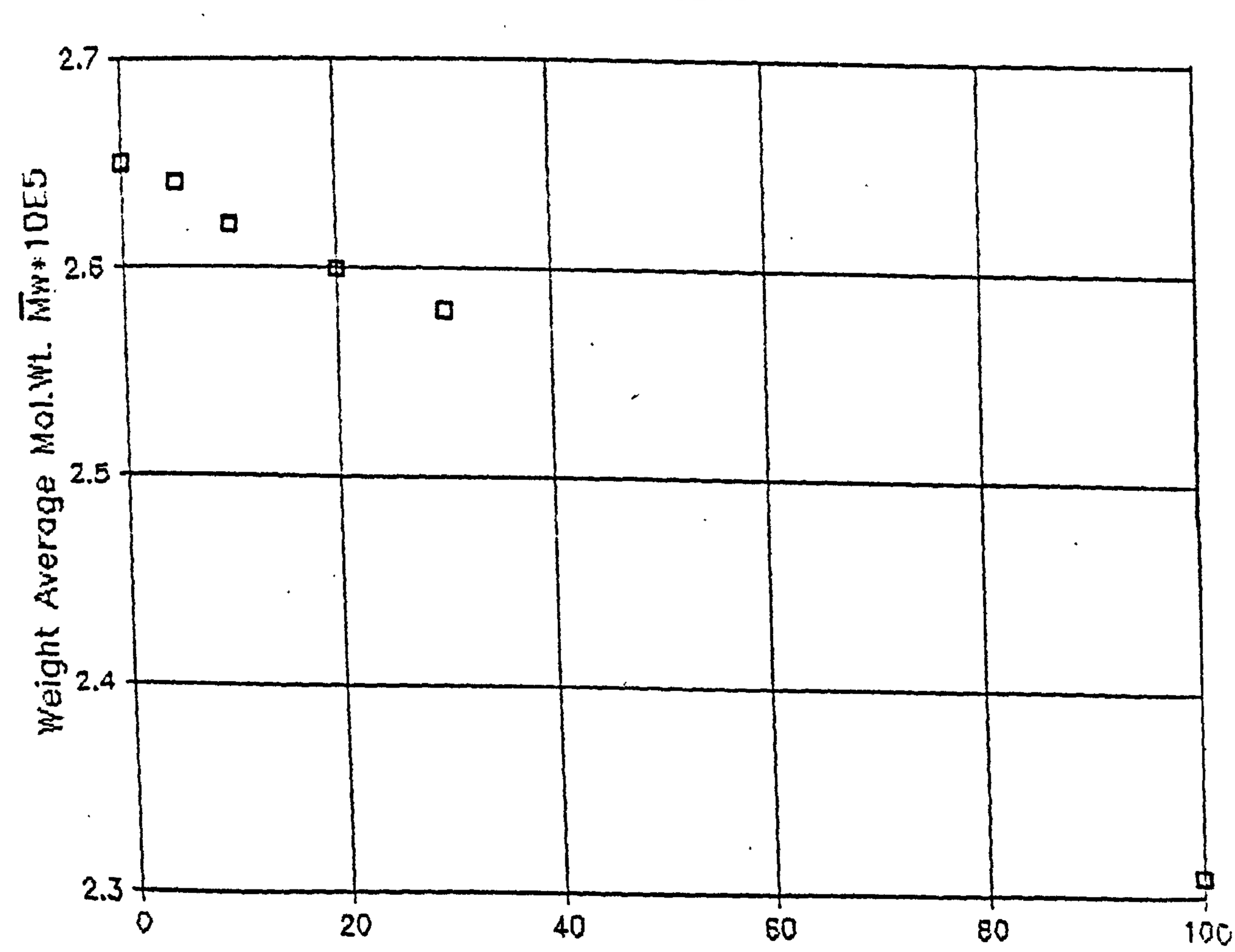

Figure 119 Weight average molecular weight versus weight percent GYM45 iPP added to GXM43 iPP.

4.3.2 MFI Measurement

The MFI of each polypropylene blend was determined at 230°C using a load of 2.16 Kg and a standard, 8mm long, 2.096mm internal diameter, die according to ASTM D 1238. Five measurements were made on each blend, the average weight of the extrudates for each blend was then used to calculate the MFI from the equation:-

$$MFI = \frac{10W}{T}$$

where MFI = Flow in grammes per 10 minutes.

W = Average weight of extrudate in grammes.

T = Extrusion time for each sample in minutes

The melt flow indices are also presented in Table 34 for comparison.

The MFI and number average molecular weight are seen to be indirectly proportional as expected, giving confidence in MFI as a characterisation technique.

4.4 IMPACT TESTING OF INJECTION MOULDED iPP BLENDS

4.4.1 Instrumented Izod Impact Testing

As with GXM43 virgin polypropylene moulded plaques Izod impact tests on miniature (3mm x 3mm x 12mm) test pieces cut from selected areas 20mm, 40mm and 70mm along the flow direction were performed on five plaques of each blend. The results are presented in Table 35 and Mean Izod impact strength versus distance from gate curves are presented in Figures 120 and 121.

Figure 120 shows that with increasing percentages of low molecular weight material the impact properties improve slightly at the gate but are inferior at the centre and far side of the moulded plaques. The transition point from low to high impact

TABLE 35 Instrumented Izod impact test results for injection moulded iPP blends.

iPP BLEND	I.S 20 mm (kJm^{-2}) x	s.d	I.S 40 mm (kJm^{-2}) x	s.d	I.S 70 mm (kJm^{-2}) x	s.d
100% GXM43=V	5.26	.96	17.90	.53	22.28	1.06
V+ 5% GYM45	5.43	.34	17.85	.21	21.29	.34
V+10% GYM45	5.53	.35	17.75	.59	20.77	.75
V+20% GYM45	6.12	.14	15.11	1.32	19.91	.83
V+30% GYM45	5.94	.19	15.09	1.27	19.71	1.23
100% GYM45	6.66	.34	14.73	1.82	18.41	.73
V+ 5% GSE16	5.06	.26	7.00	1.19	22.13	.99
V+10% GSE16	5.02	.33	7.05	1.13	23.21	.76
V+20% GSE16	5.16	.31	5.82	.36	26.08	1.35
V+30% GSE16	4.67	.27	5.25	.31	26.99	1.21
100% GSE16	4.59	.87	5.12	1.40	31.29	1.47

Figure 120 Mean Izod impact strength versus distance from gate curves for GXM43 iPP with various weight percent additions of low molecular weight GYM45 iPP.

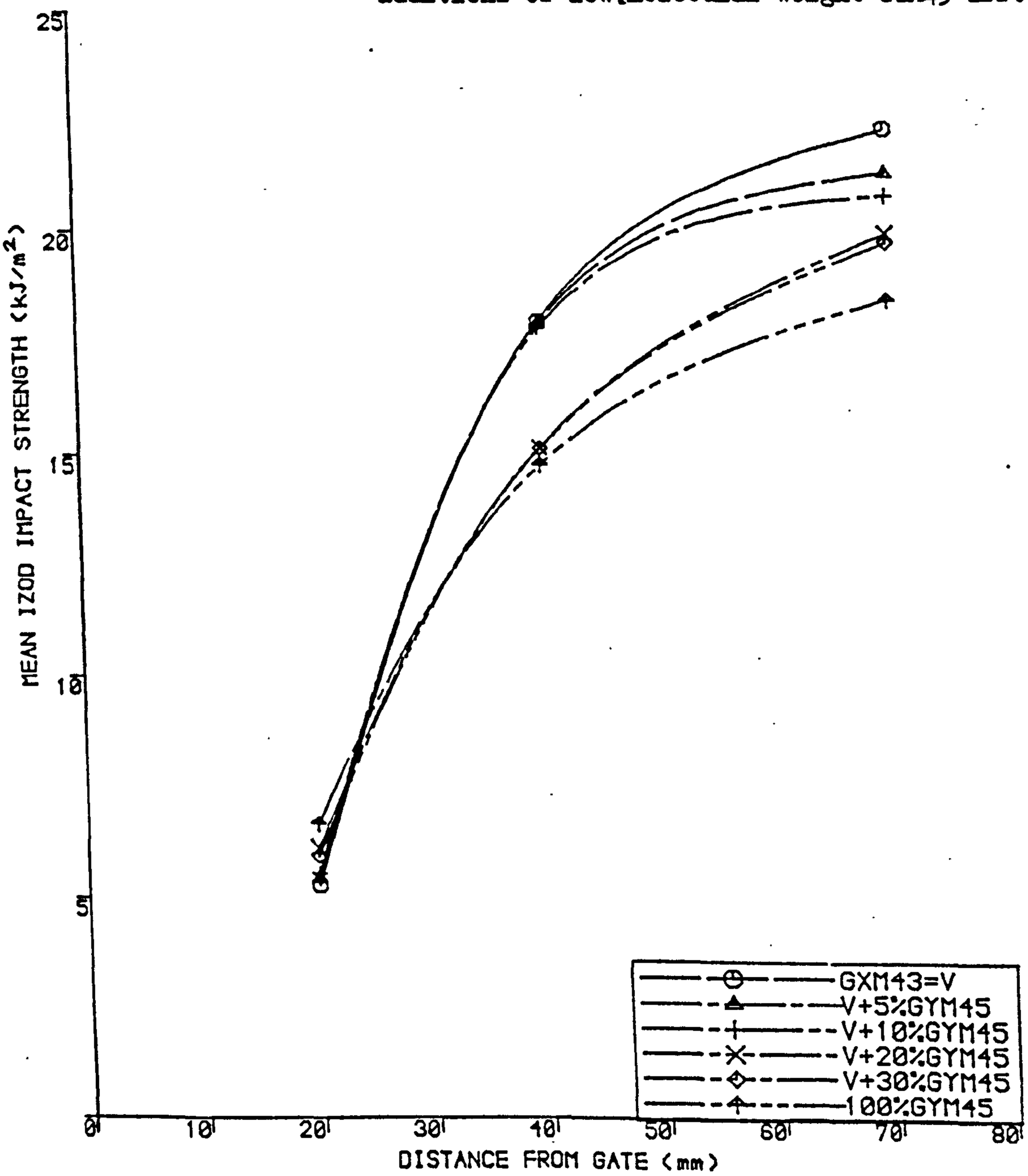

Figure 121

Mean Izod impact strength versus distance from gate curves for GXM43 iPP with various weight percent additions of high molecular weight GSE16 iPP.

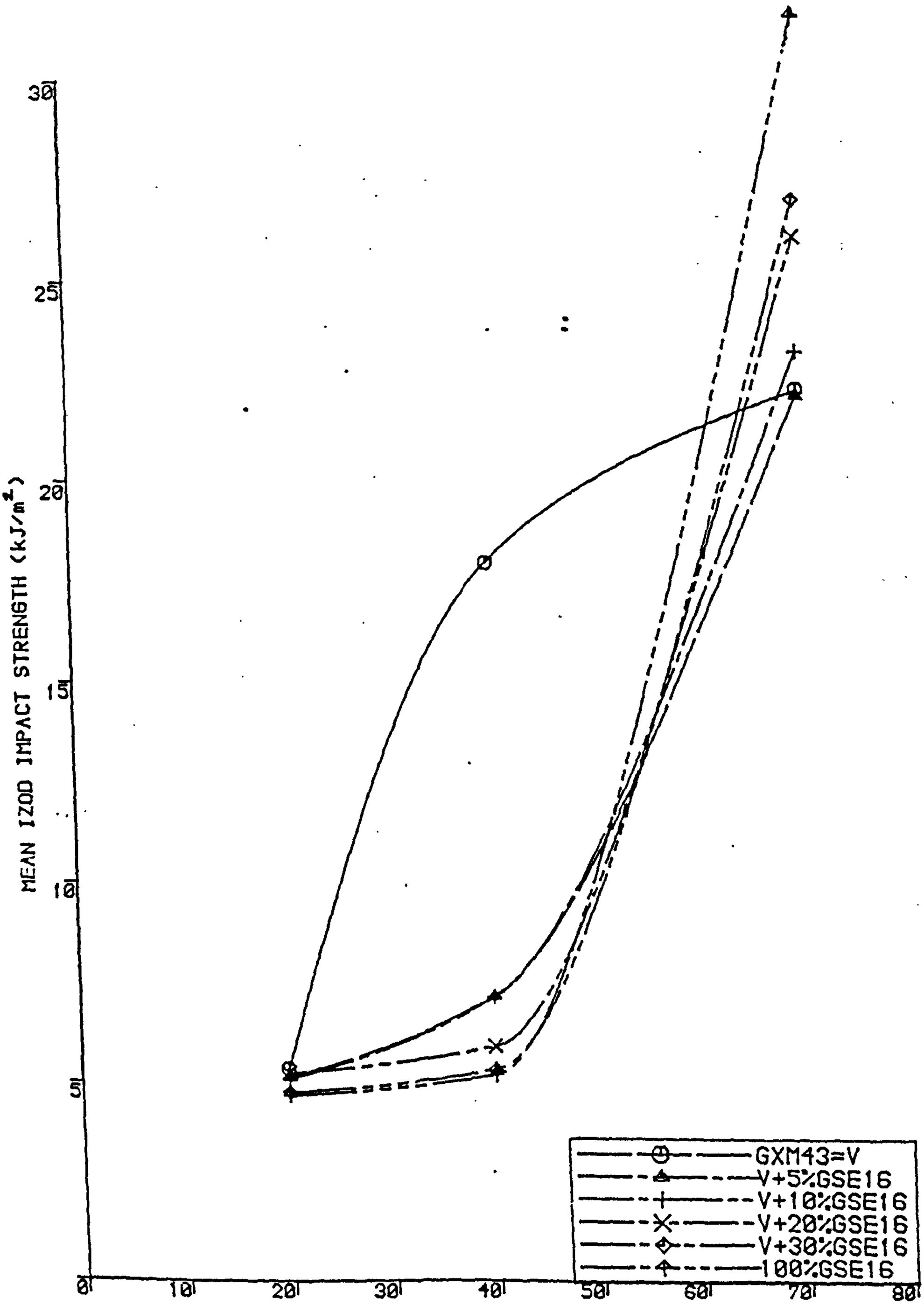

Figure 122

Typical Izod impact force/time curves for each iPP homopolymer to illustrate the differences in properties 70mm along the flow direction.

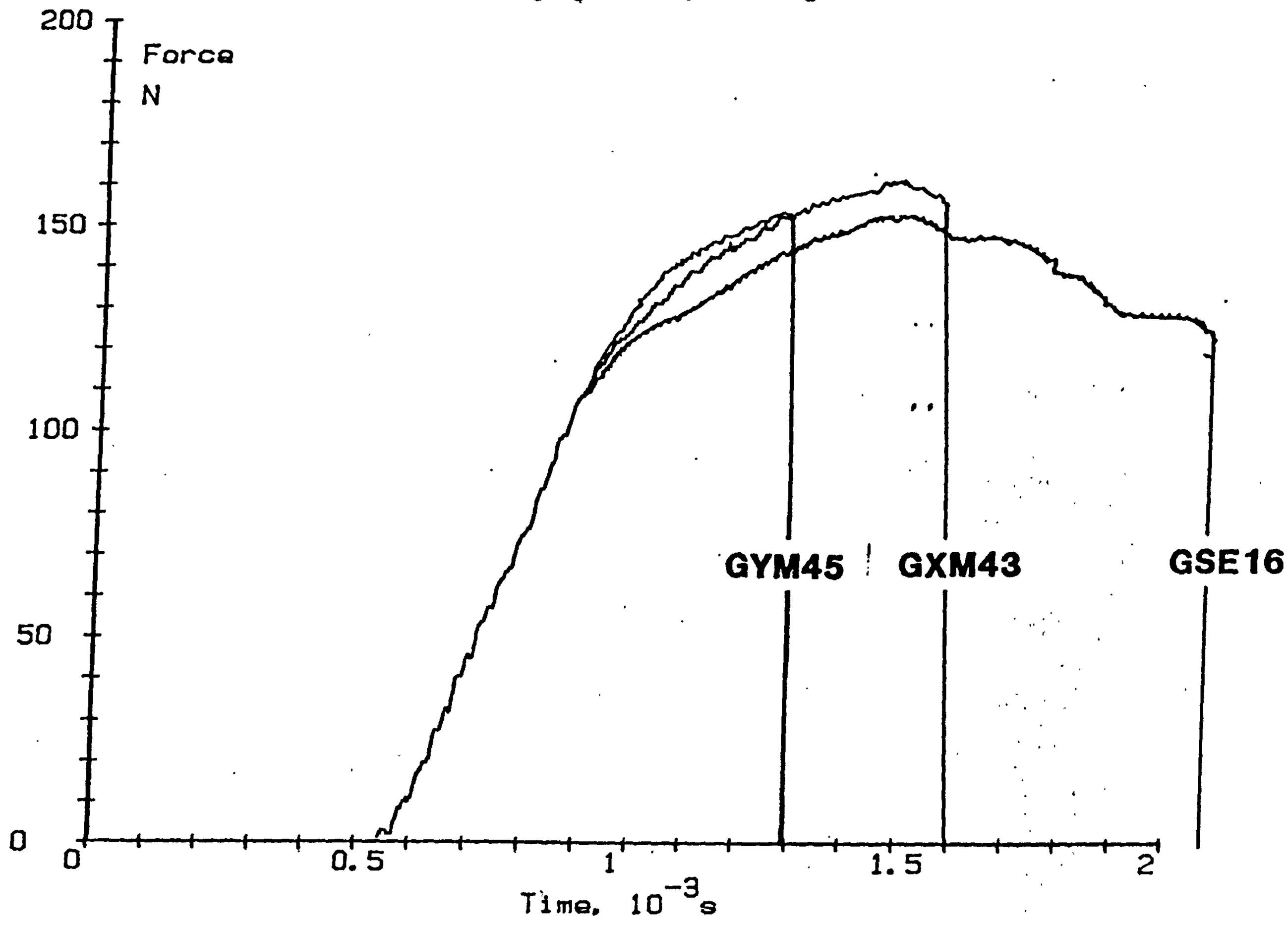

strength values appears to occur closer to the gate with reduced molecular weight polypropylene blends, however, the final impact strength reached is lower than that attained in GXM43 homopolymer mouldings.

Figure 121 shows that with increasing percentages of high molecular weight material the impact strength close to the gate is reduced but at the far side of the mouldings is significantly improved. Impact properties at the centre of the mouldings are dramatically reduced with increasing molecular weight suggesting a shift of the transition point from low to high impact strengths along the flow direction. Typical Izod Impact Force v's Time curves are shown in Figure 122 for each homopolymer to illustrate the difference in properties at 70mm along the flow direction.

4.4.2 Instrumented Drop-Weight Impact Testing

In order to provide more information on drop-weight impact properties within a moulding, 50mm x 60mm x 3mm impact samples were cut from plaques, each sample having its centre at either 25mm, 40mm or 55mm away from the gate as shown in Figure 123. These dimensions are closer to conformation with ISO/DIS 6603/1 specifications which suggest a 60mm side for square specimens. Five samples from each of the three positions were prepared from each polymer blend and polypropylene homopolymer mouldings. Each sample was tested in accordance with the procedure explained in Section 2.4.3. In this way both directional and positional weakness could be identified within mouldings using the drop-weight test.

Since the first peak on the force/distance curves corresponds to the energy required to initiate major cracks the mean peak impact energy versus distance along flow direction data only

Figure 123 Schematic representation of position of drop weight impact test on 50 x 60 x 3mm impact samples.

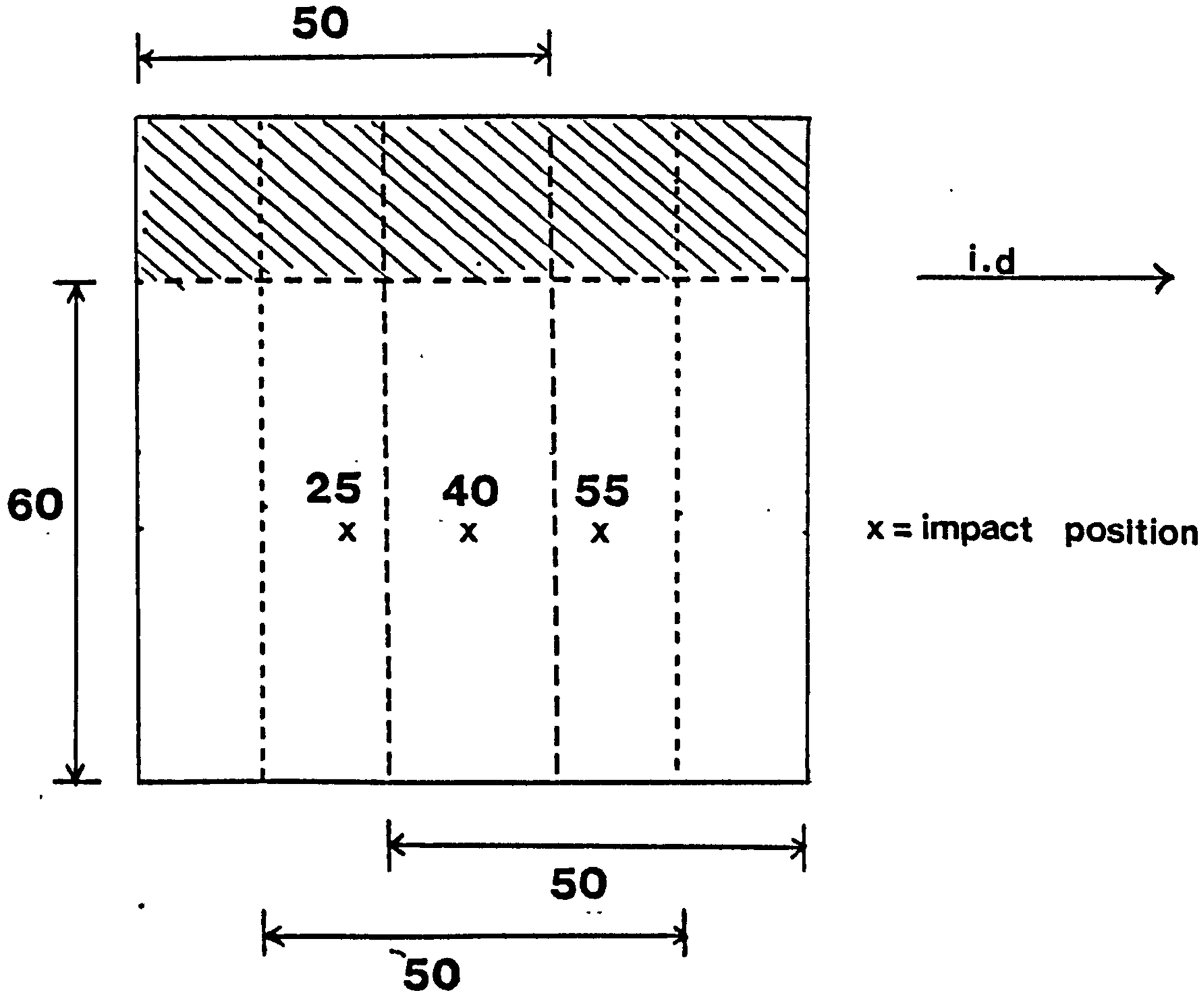

was collated. These results are given in Table 36 and graphically represented in Figures 124 and 125 for low and high molecular weight additions respectively.

The following observations were made from these results:-

(i) Increasing the molecular weight of polypropylene by dosing GXM43 with GSE16 polypropylene leads to inferior properties up to and beyond the centre of moulded plaques.

(ii) Reducing the molecular weight by dosing GXM43 with GYM45 polypropylene marginally improves the properties up to half way across the mouldings but beyond this the properties are inferior.

4.4.2.1 Analysis of Fracture Behaviour

An analysis of the fracture patterns revealed distinct changes in appearance between low and high molecular weight polypropylene blends. A summary of the variation in number of major and minor cracks found for each blend at selected areas is given in Table 37. Typical fracture patterns are presented in Figure 126 for GSE16, GXM43 and GYM45 polypropylene injection moulded plaques. It is again noticed that an increase in drop-weight impact strength is accompanied by substantial increase in minor crack formation and to a less extent major crack formation. In the high molecular weight polypropylene where only one major crack was found it was seen to propagate towards the gate confirming the previously defined direction of weakness.

The Force/time data plotted revealed a distinct increase in energy of first peak followed by only a small propagation peak for tough plaques, compared to, a small first peak and a more

TABLE 36 Instrumented drop-weight impact test results for injection moulded iPP blends.

iPP BLEND	PEAK ENERGY (Nm) 25mm $\bar{x}$	s.d	PEAK ENERGY (Nm) 40mm $\bar{x}$	s.d	PEAK ENERGY (Nm) 55mm $\bar{x}$	s.d
100% GSE16	0.354	.030	0.458	.075	0.517	.072
V+30% GSE16	0.365	.020	0.477	.076	0.536	.100
V+20% GSE16	0.415	.055	0.595	.090	0.626	.088
V+10% GSE16	0.471	.058	0.665	.240	0.653	.049
V+ 5% GSE16	0.488	.113	0.772	.202	0.768	.137
100% GXM43=V	0.574	.157	1.133	.227	1.975	.479
V+ 5% GYM45	0.593	.067	1.048	.084	1.648	.314
V+10% GYM45	0.578	.099	1.107	.211	1.358	.790
V+20% GYM45	0.665	.105	1.073	.180	1.908	.352
V+30% GYM45	0.702	.098	0.838	.146	1.690	.472
100% GYM45	0.755	.092	0.814	.200	1.440	.355

TABLE 37 Results of fracture pattern analysis of drop-weight impact tested plaques of iPP blends.

iPP BLEND	NUMBER OF CRACKS AT 25mm MINOR	MAJOR	NUMBER OF CRACKS AT 40mm MINOR	MAJOR	NUMBER OF CRACKS AT 55mm MINOR	MAJOR
100% GSE16	1	1-2	1	2-3	1	4
V+30% GSE16	3-4	4	2	5	4-5	5
V+20% GSE16	3-4	4	4	5	5	5
V+10% GSE16	4-6	4	8-10	5	6-8	5-6
V+ 5% GSE16	4-6	4	6-10	5	6-10	5
100% GXM43=V	4-5	4-5	8-10	5	>20	6-7
V+ 5% GYM45	5-7	4-5	10-12	4	15	4-6
V+10% GYM45	7-9	4-5	12-14	5	>20	7
V+20% GYM45	8-10	5	12-14	5	16-20	7
V+30% GYM45	10	5	12-14	5	>20	6-7
100% GYM45	12	5-6	15	5-6	>20	6-7

Figure 124

Mean drop-weight impact energy versus distance from the gate with increasing additions of low molecular weight GYM45 iPP.

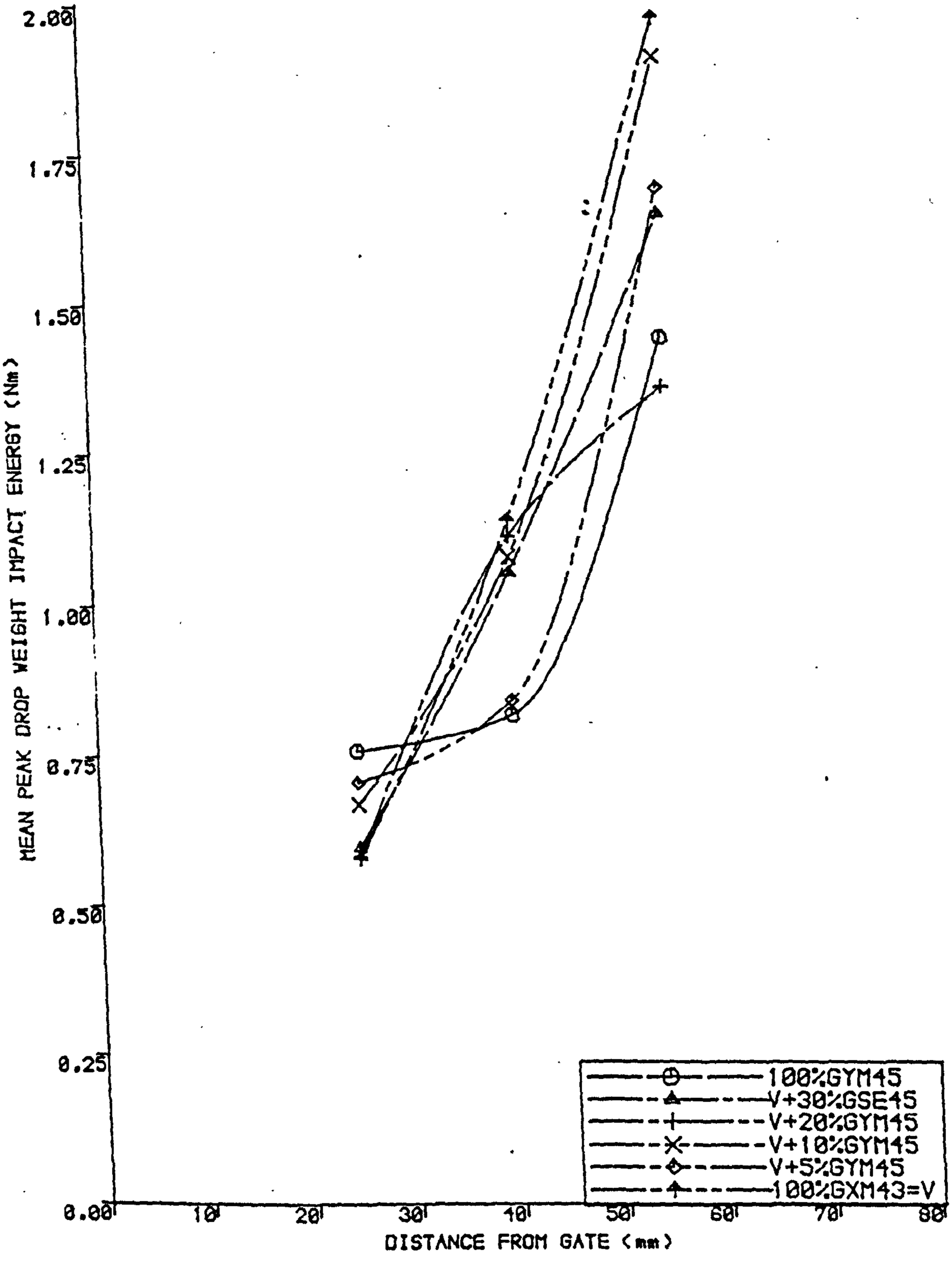

Figure 125

Mean drop-weight impact energy versus distance from the gate with increasing additions of high molecular weight GSE16 iPP.

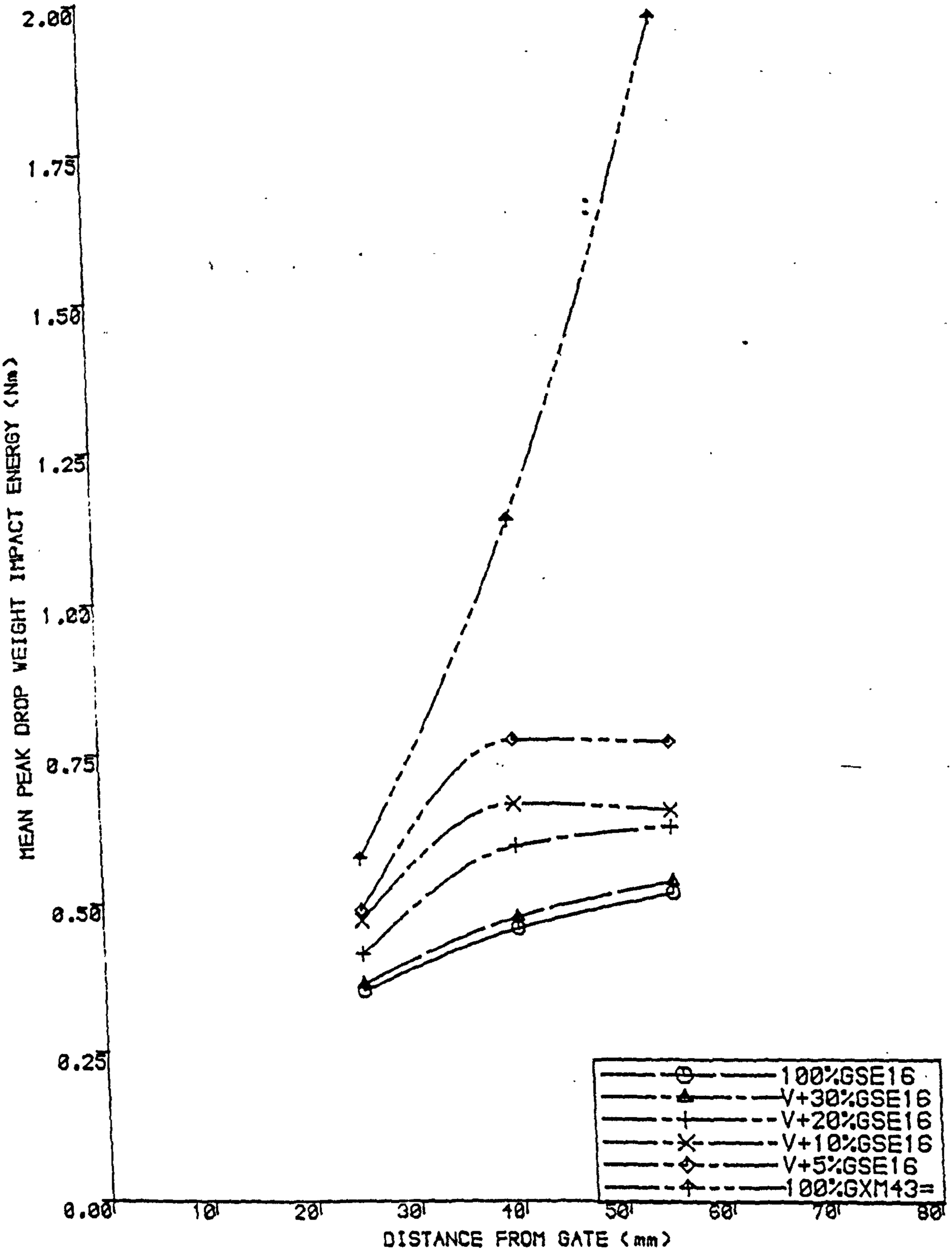

Figure 126 Typical fracture patterns for GSE16 GXM43 and GYM45 iPP injection moulded plaques.

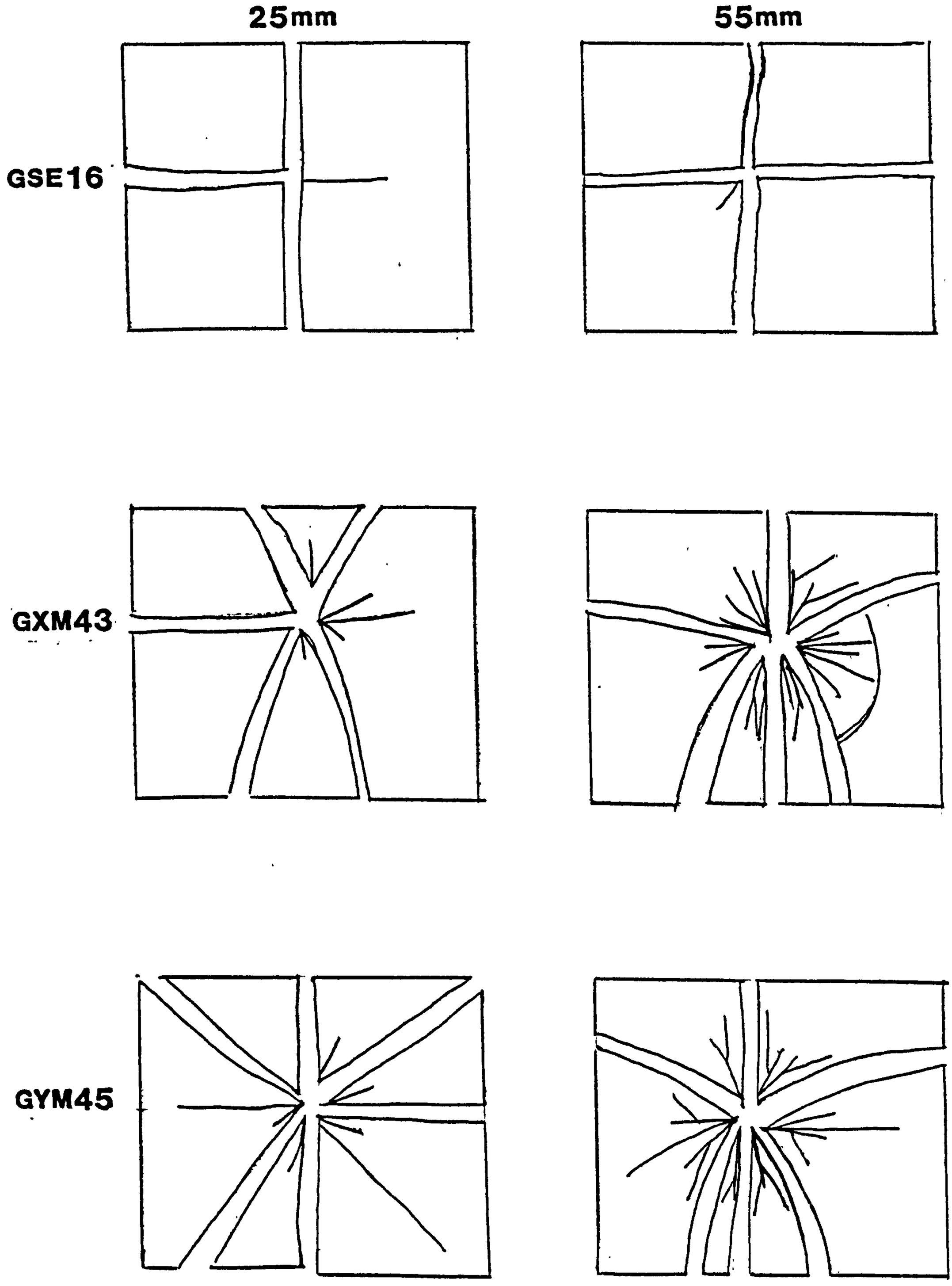

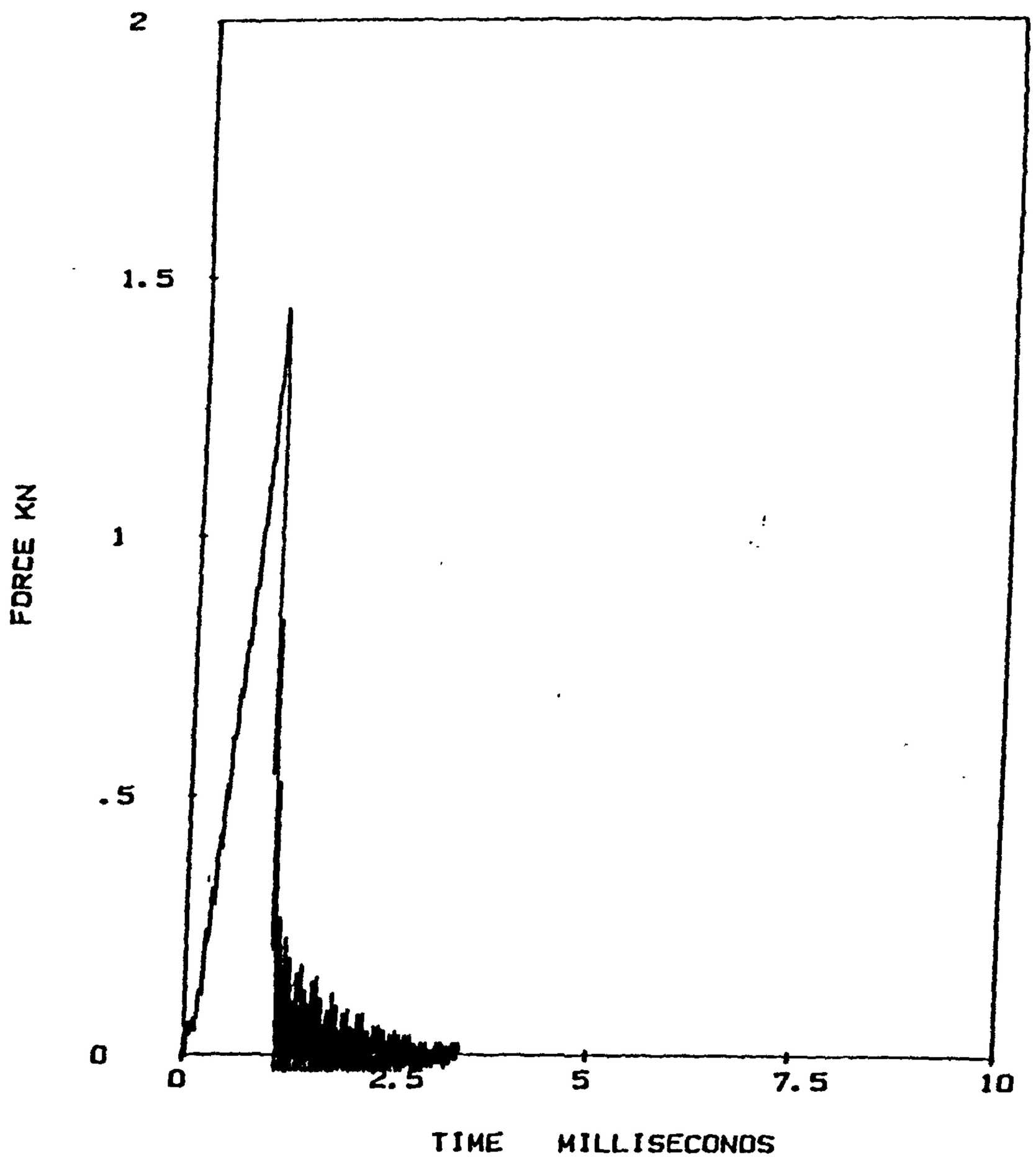

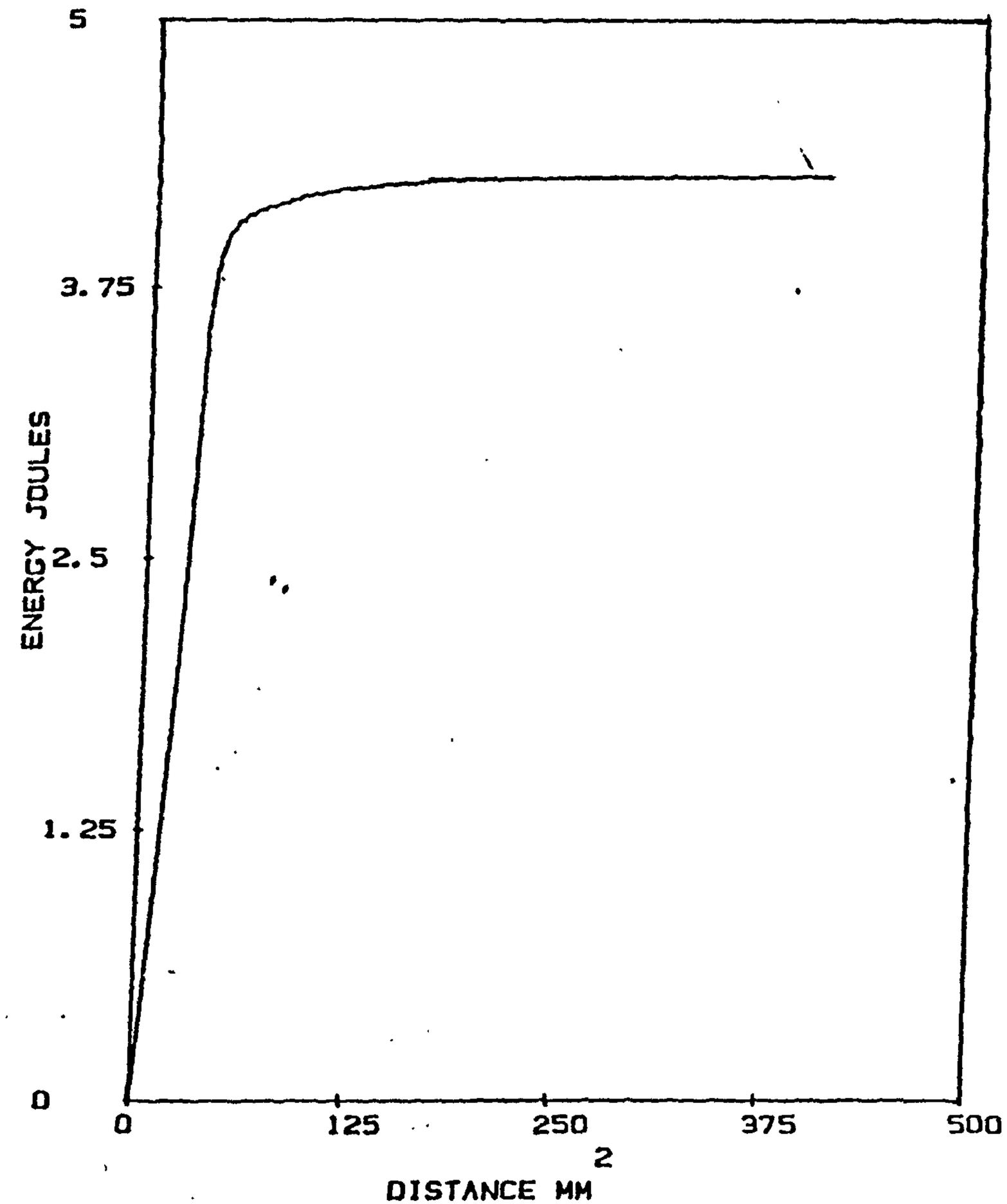

Figure 127 Force/time and energy/distance^2 curves for a tough iPP plaque.

MATERIAL CODE GXMNEW SAMPLE DETAILS GXM43 30/220/30

DATE 23/11/84 TEMP 23 DEG C IMPACT VELOCITY 3 M/S

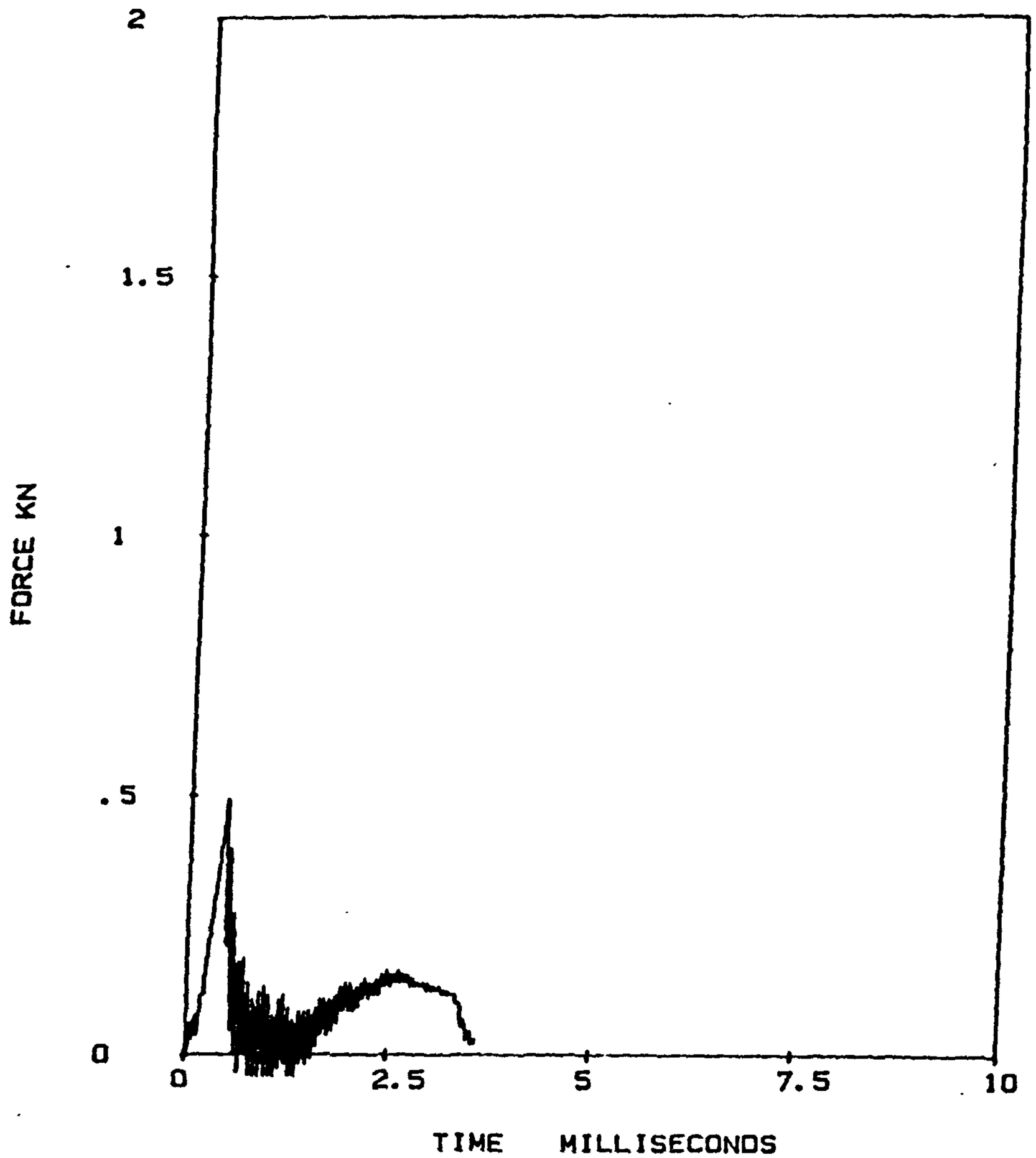

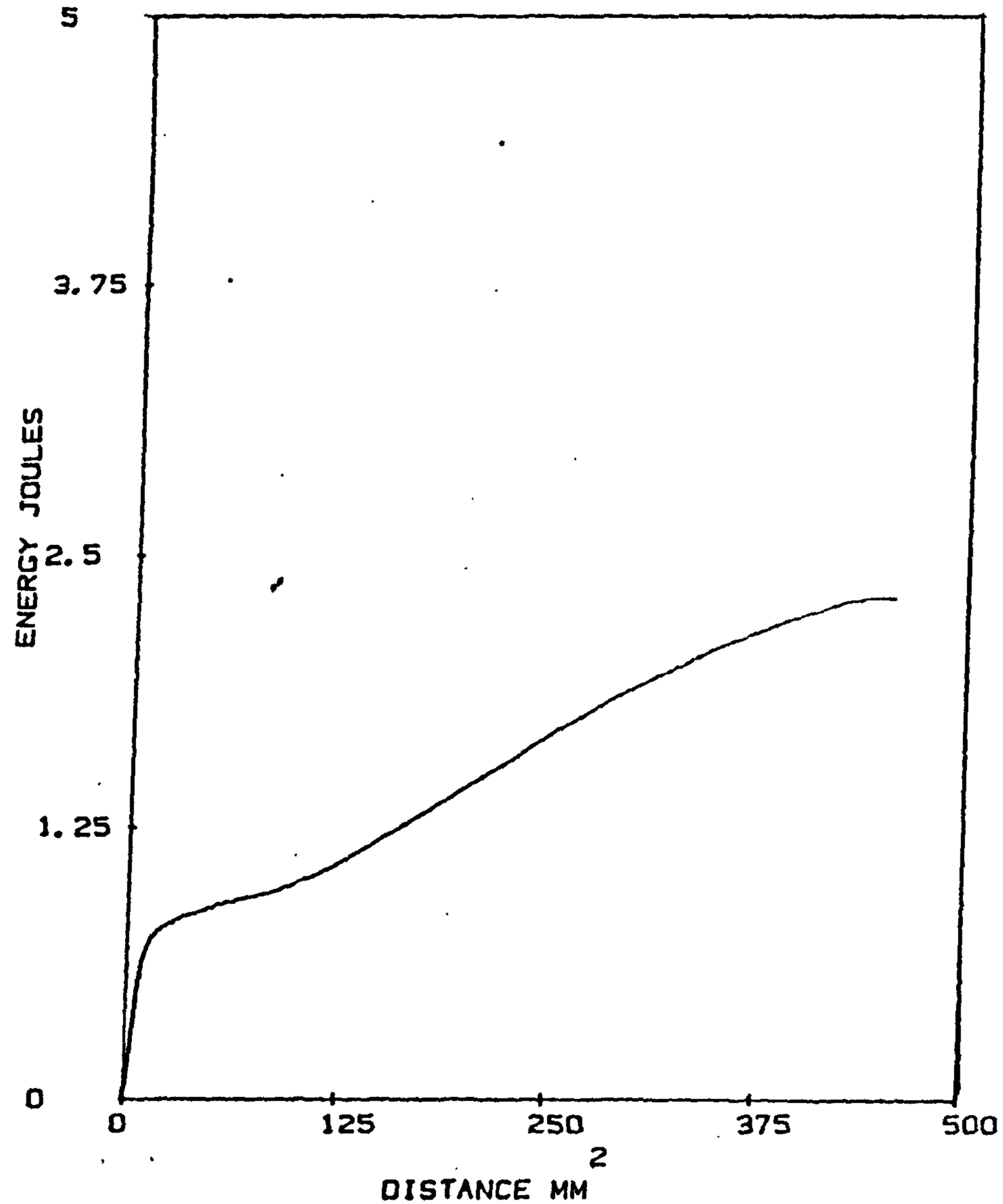

Figure 128 Force/time and energy/distance^2 curves for a weak iPP plaque.

significant propagation peak in weaker samples. The energy required to initiate cracks appears therefore to be the deciding factor as to whether a plaque will have high or low drop-weight impact resistance. In all cases only one propagation peak was observed after the first peak, this is probably due to the reduction in lateral dimensions of the plaque i.e. the crack has less distance to travel before reaching the edge of the moulding. Force/time and Energy/distance^2 curves are shown in Figures 127 and 128 for a tough and a weak plaque respectively.

These results are in very good agreement with the Izod Impact test results if one assumes that the high molecular weight blends exhibit superior properties beyond 55mm along the flow direction. Drop-Weight Tests beyond 55mm would unfortunately have put some doubt as to the test procedure consistency due to reduced sample sizes.

4.5 OPTICAL CHARACTERISATION OF INJECTION MOULDED iPP BLENDS

A polarised light microscopy study of representative microtomed sections taken from Izod test pieces of each polypropylene blend was made. Sections taken at selected areas along the melt flow direction revealed typical skin-core banded morphologies which were found to be particularly sensitive to molecular weight variations.

Micrographs of the sections taken from 20mm, 40mm and 70mm along the melt flow direction are presented in Figures 129 to 131. The gate area micrographs reveal a gradual increase in the width of the fibrous row nucleated band with increasing molecular weight accompanied by an increase in β-phase nucleation at the boundary of this fibrous band with the core.

Figure 129

Micrographs of sections taken from 20mm along the melt flow direction for each iPP blend.

100% GXM43=V

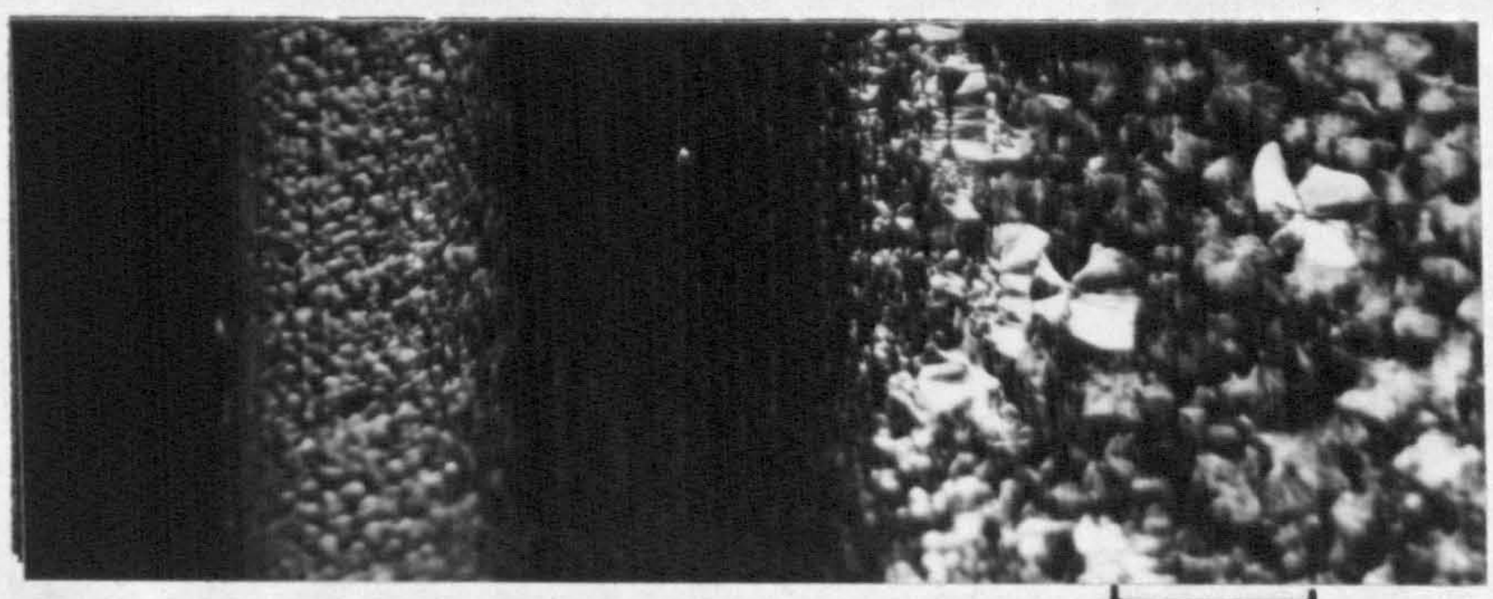

V+5% GSE16

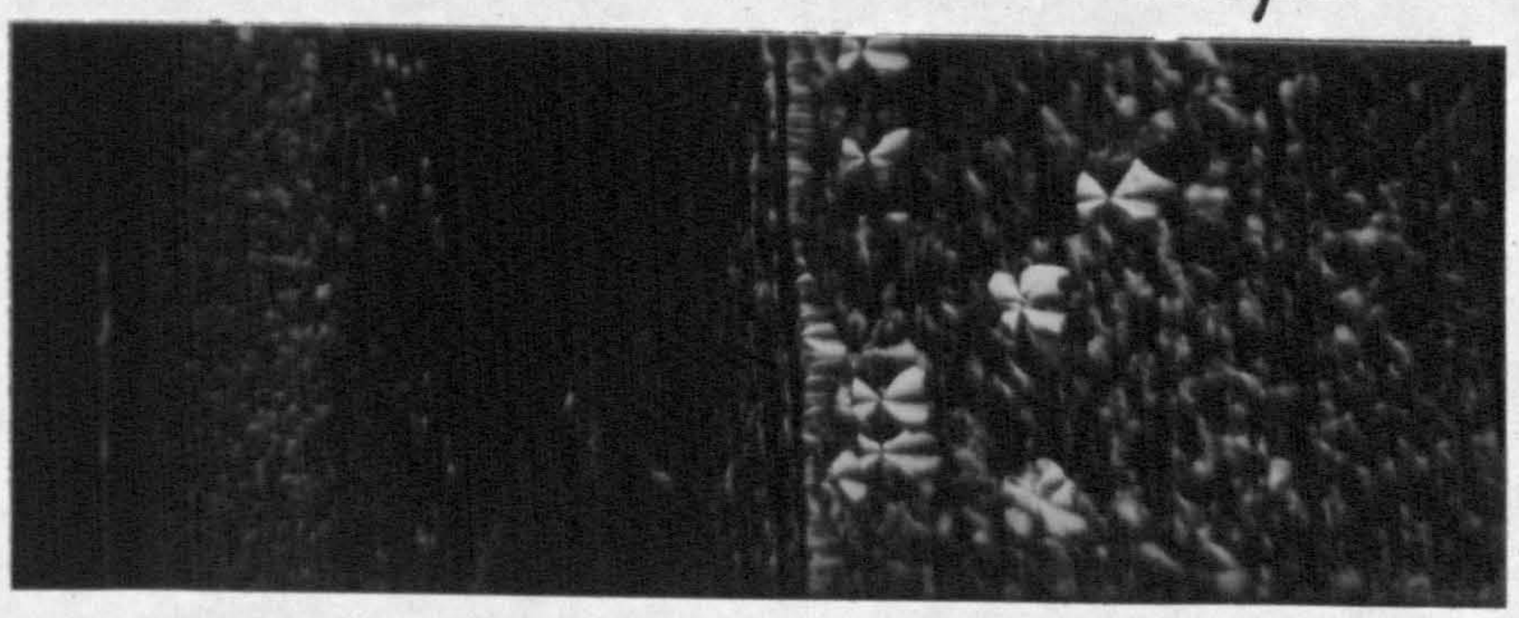

V+10% GSE16

V+20% GSE16

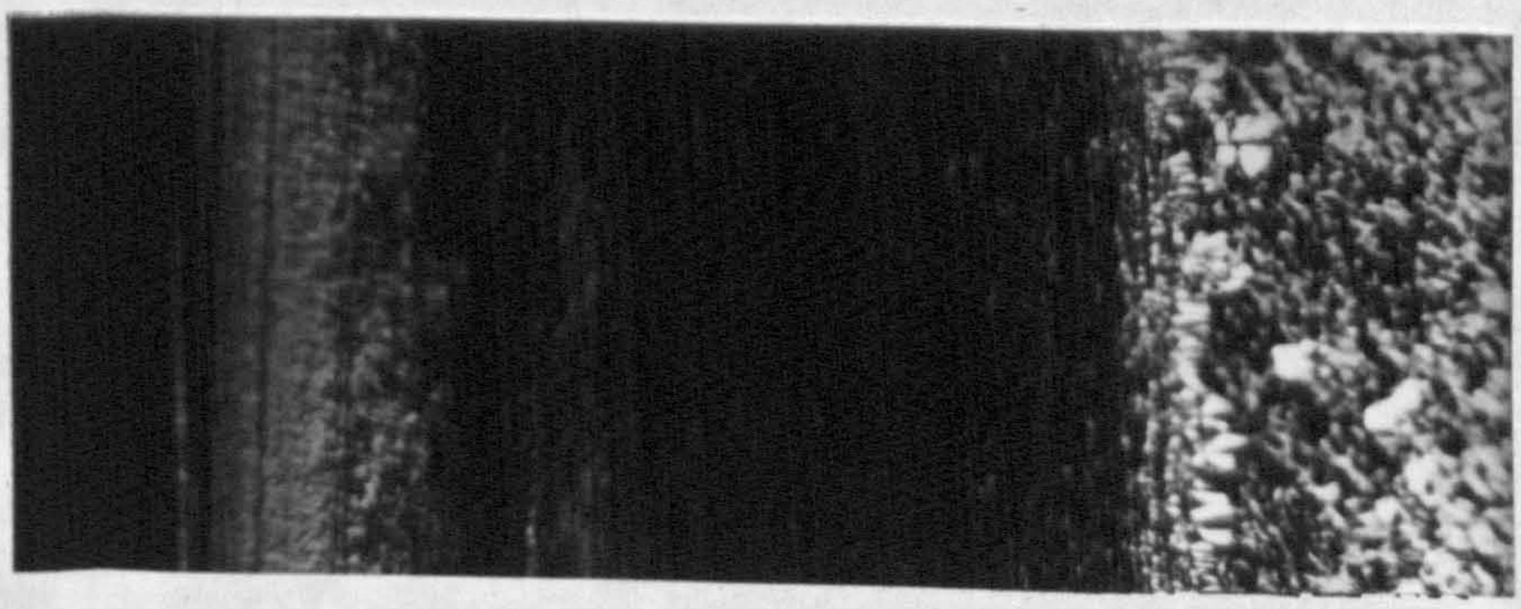

V+30% GSE16

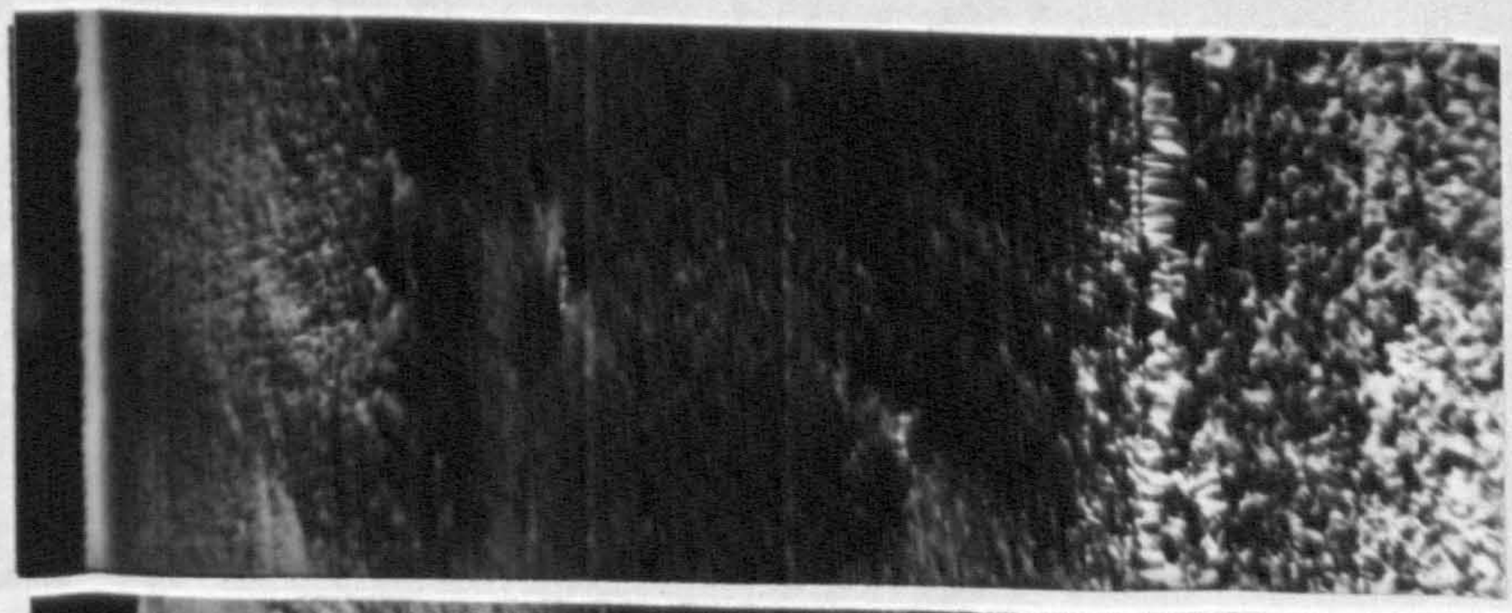

100% GSE16

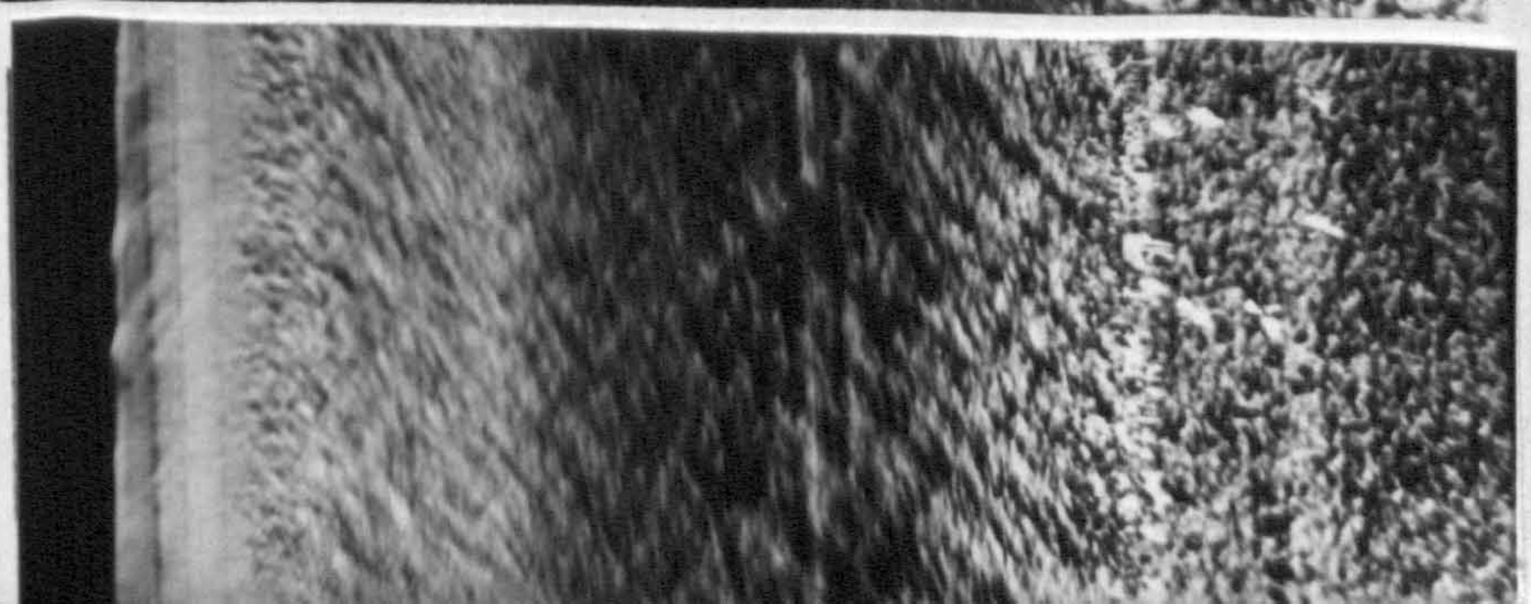

100% GXM43=V

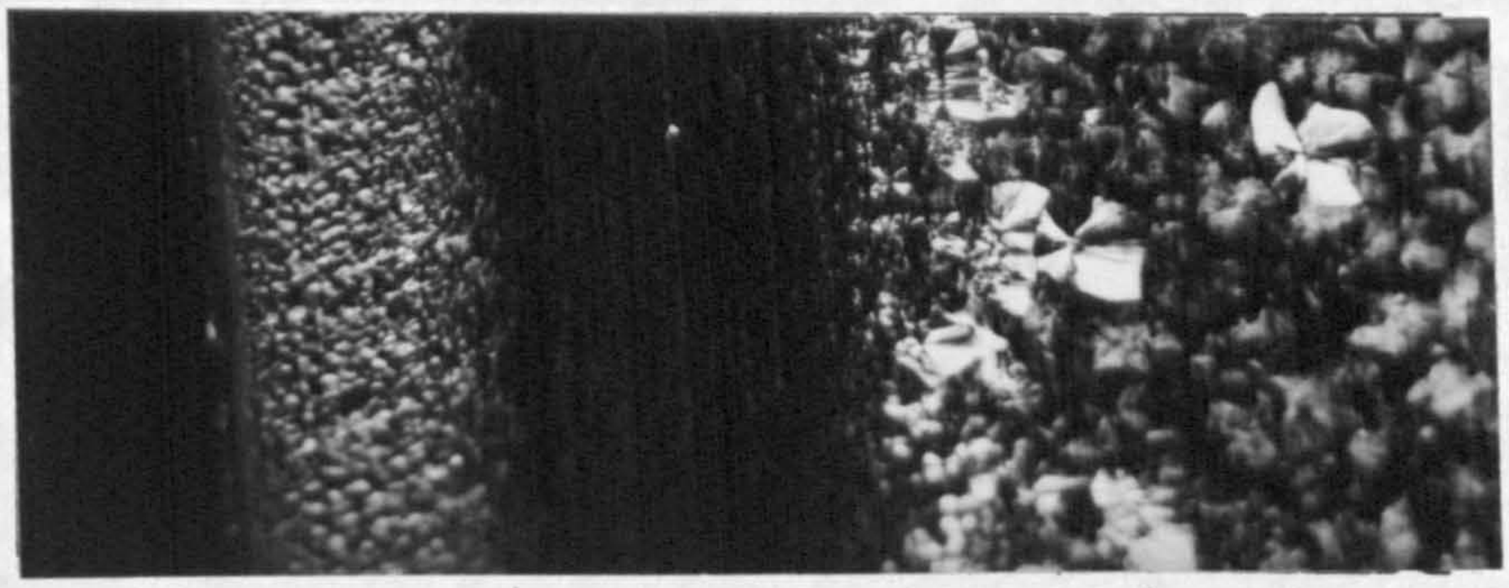

100μm

V+5% GYM45

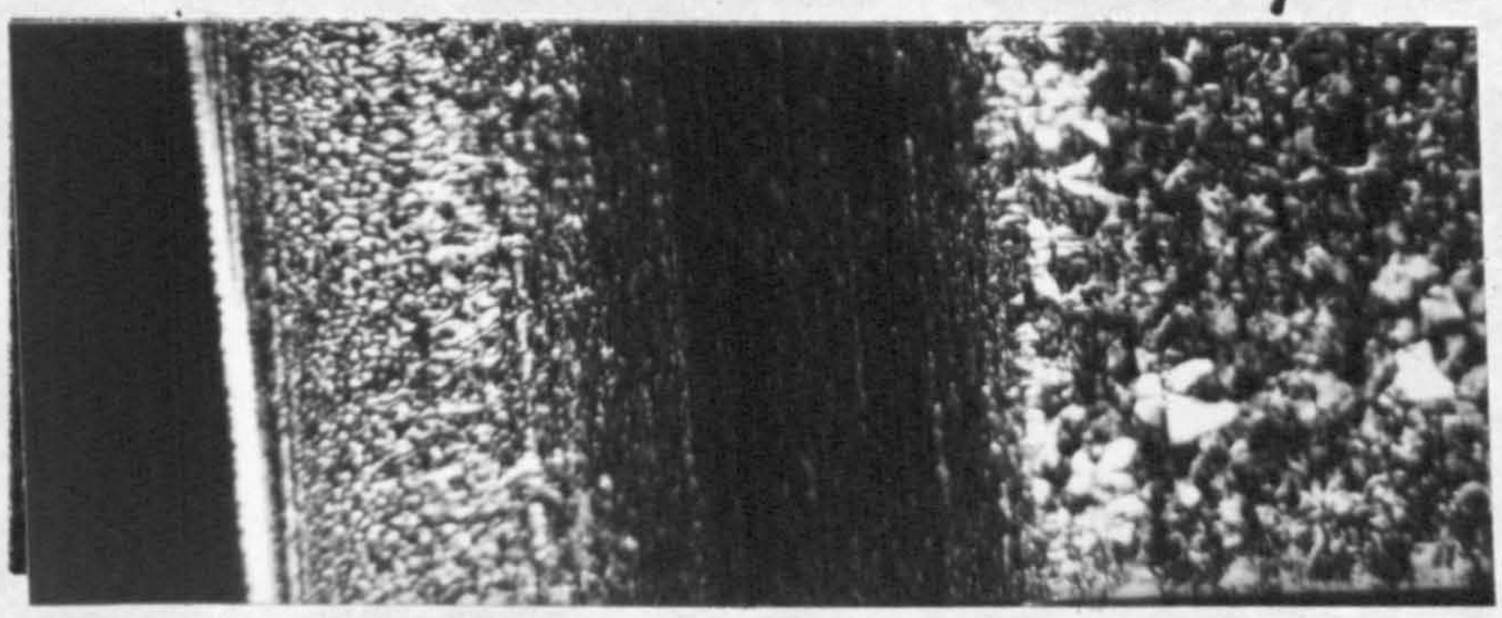

V+10% GYM45

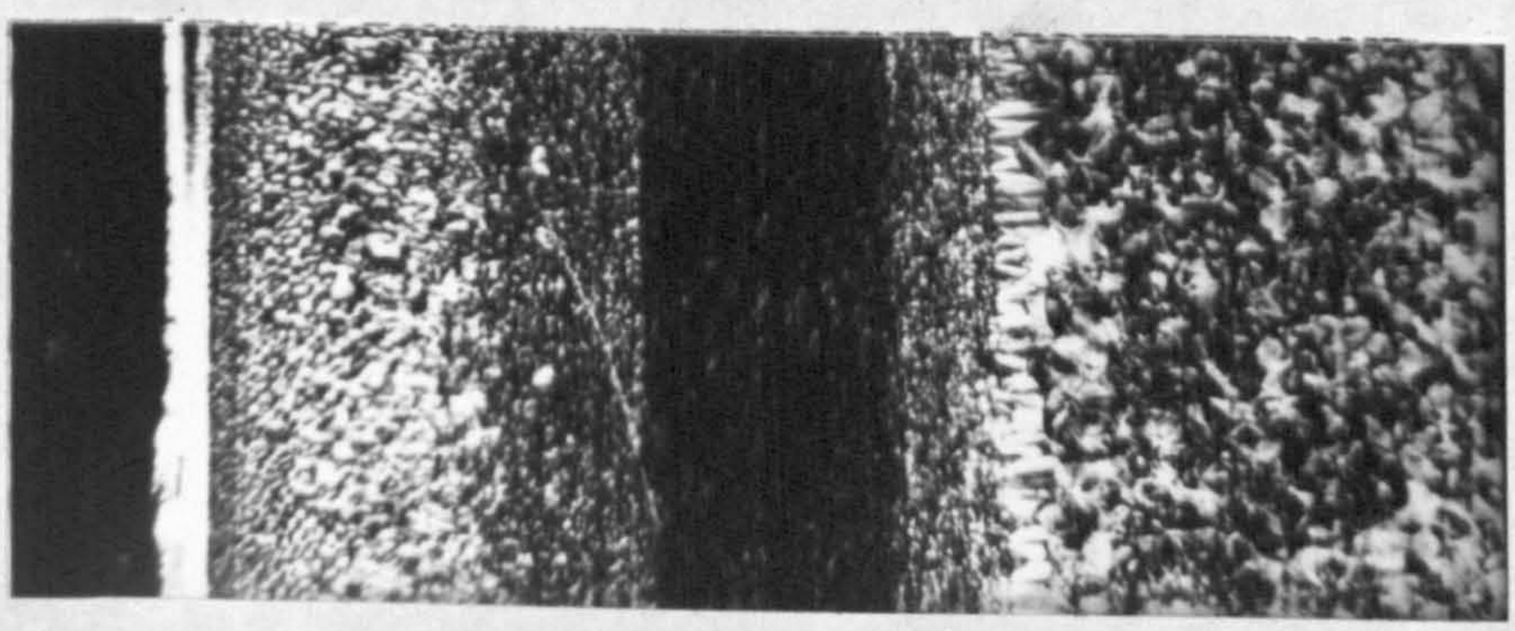

V+20% GYM45

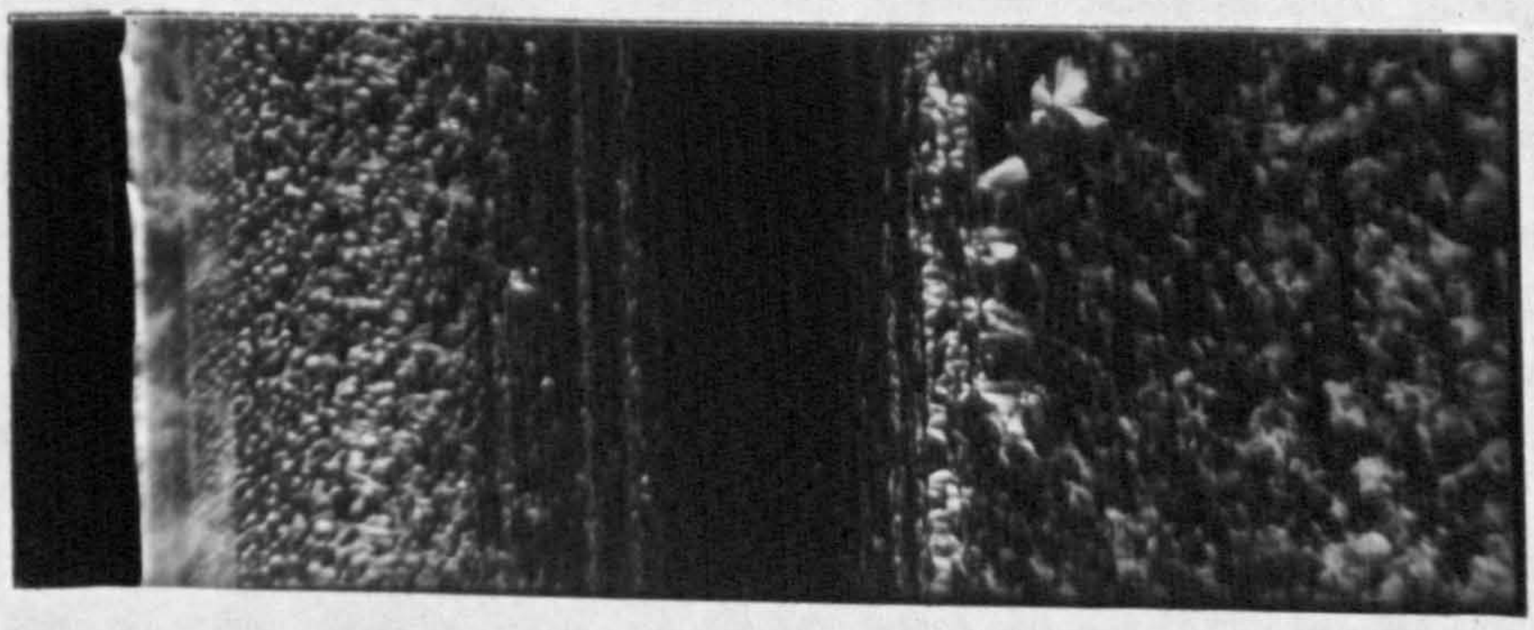

V+30% GYM45

100% GYM45

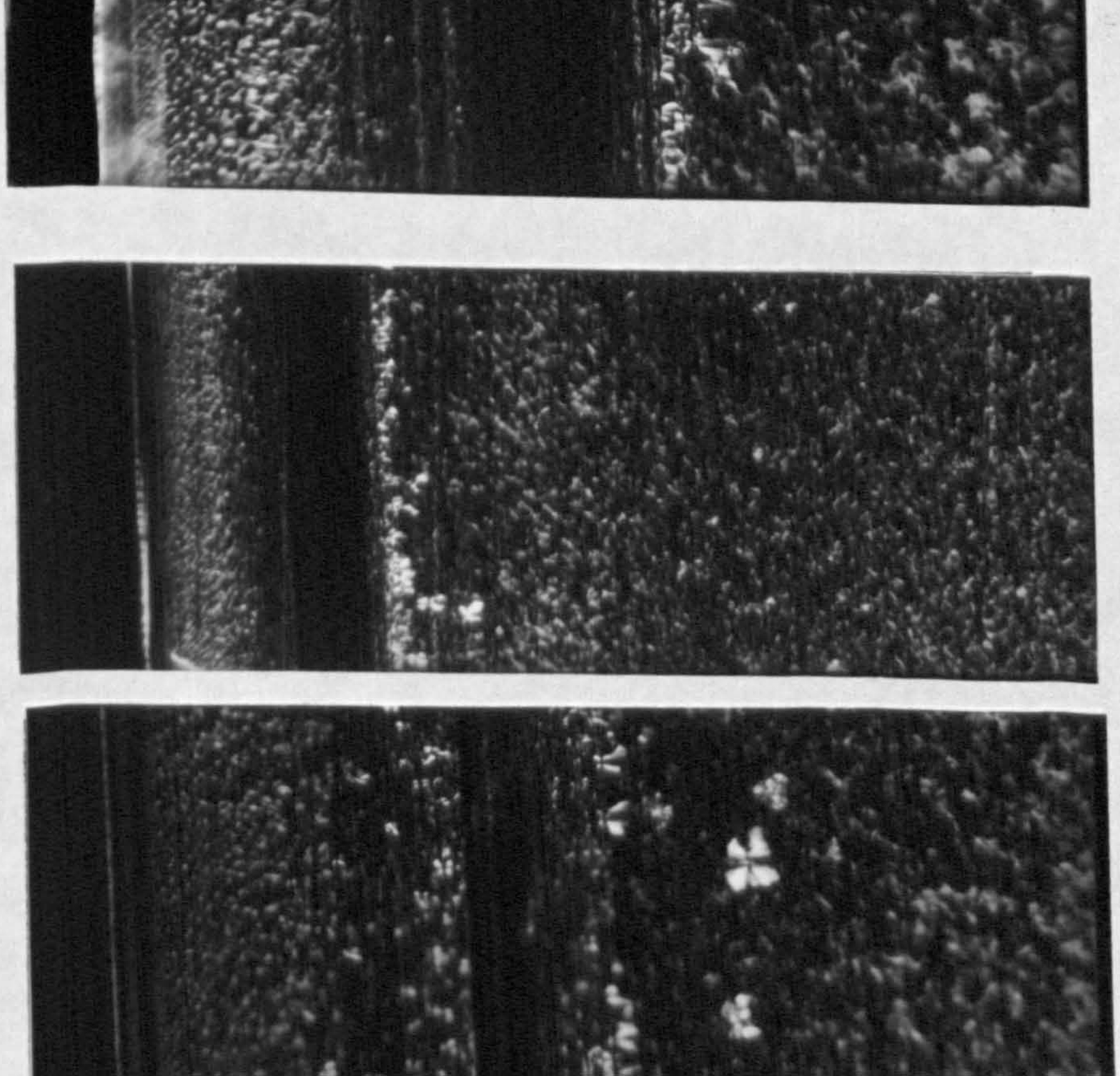

Figure 130

Micrographs of sections taken from 40mm along the melt flow direction for each iPP blend.

100% GXM43=V

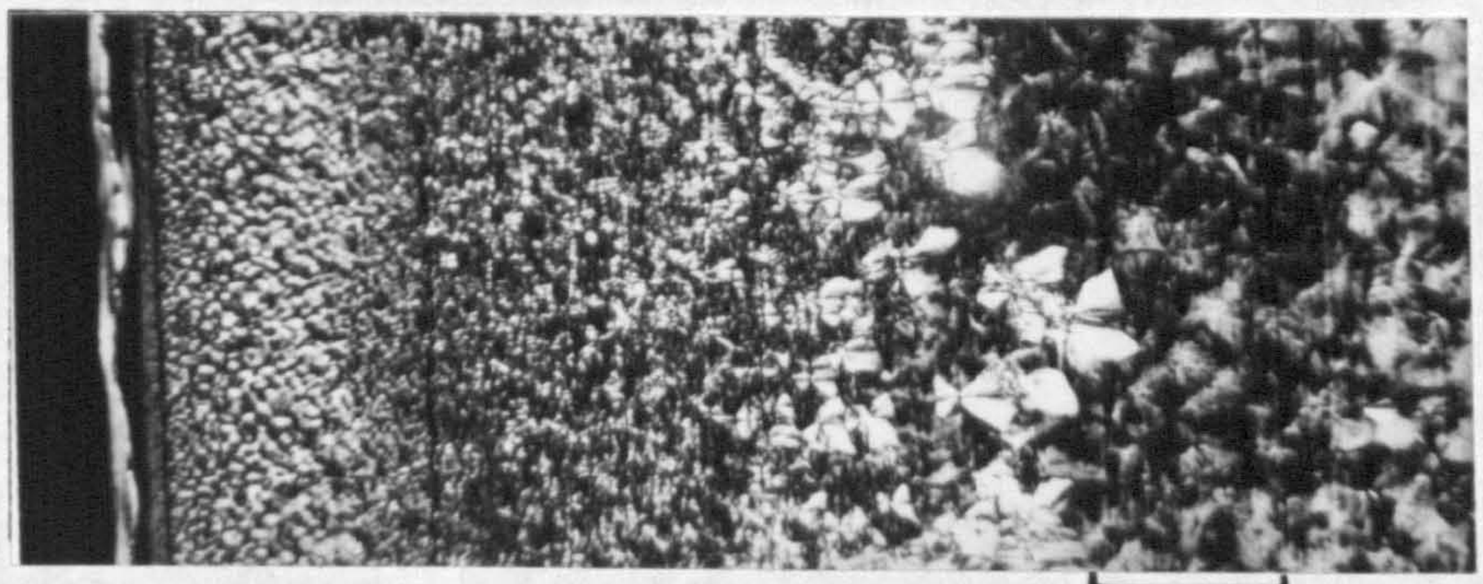

V+5% GSE16

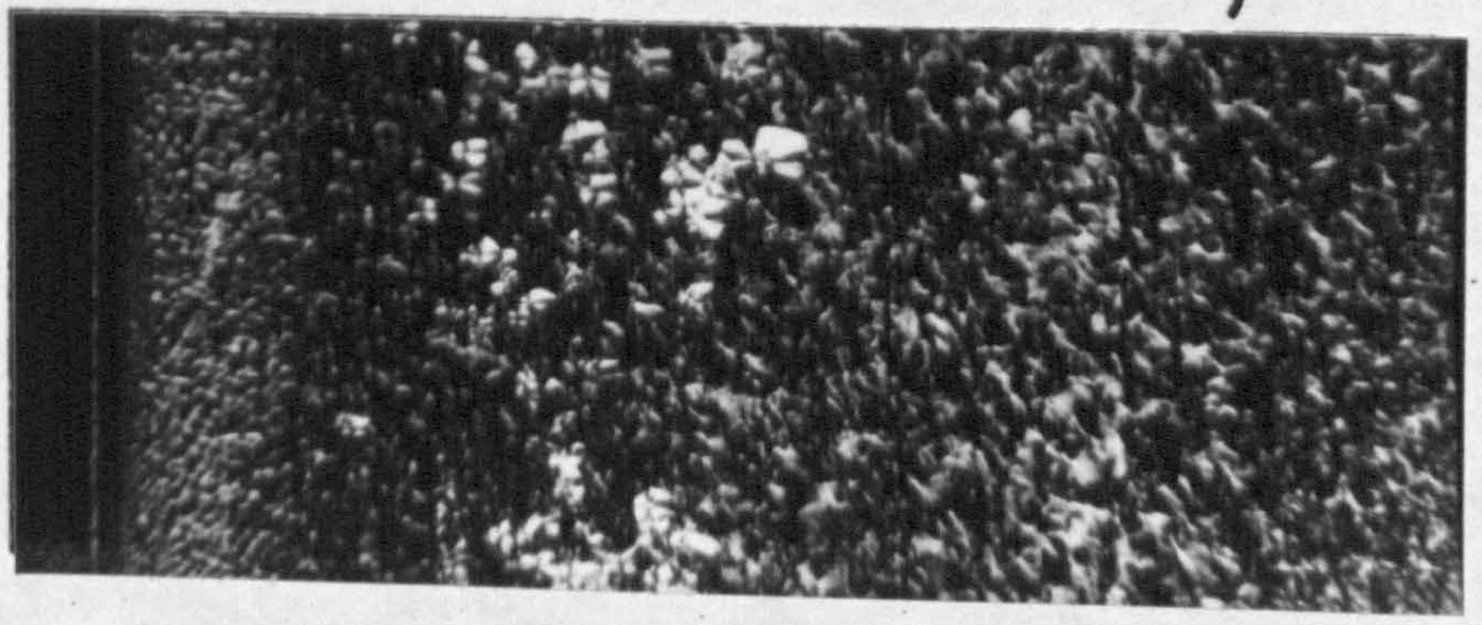

V+10% GSE16

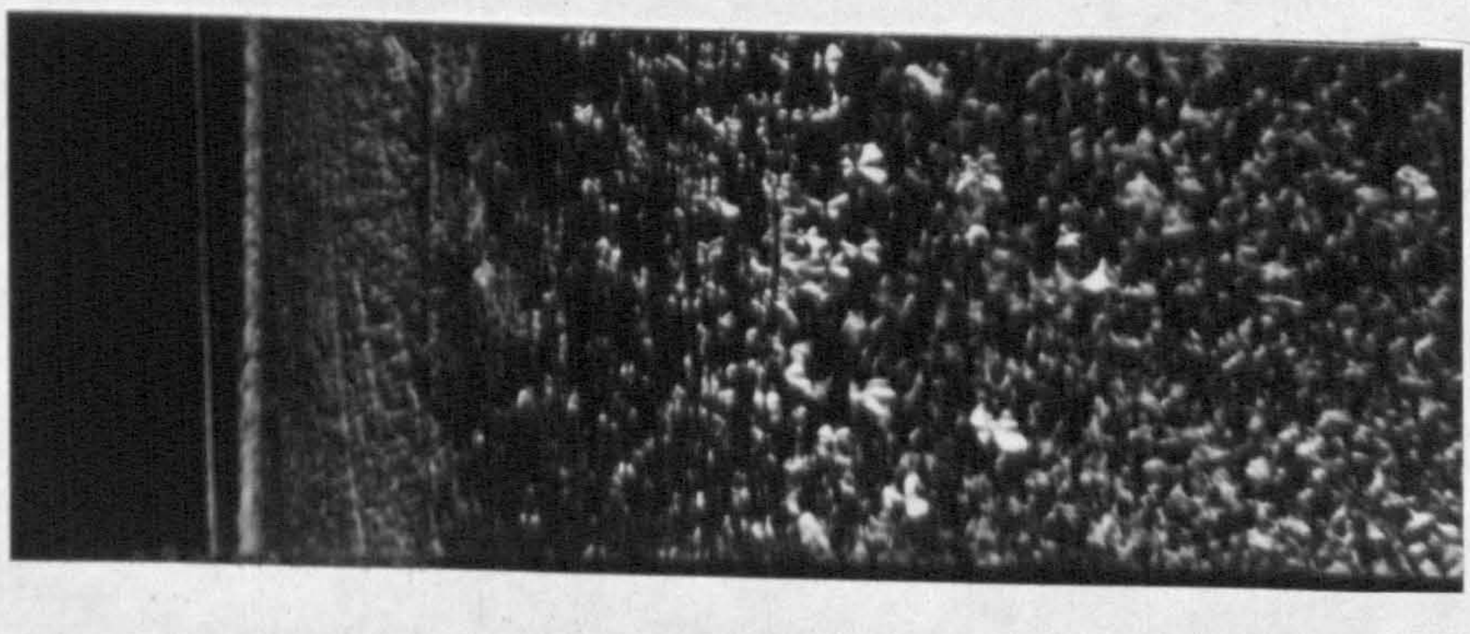

V+20% GSE16

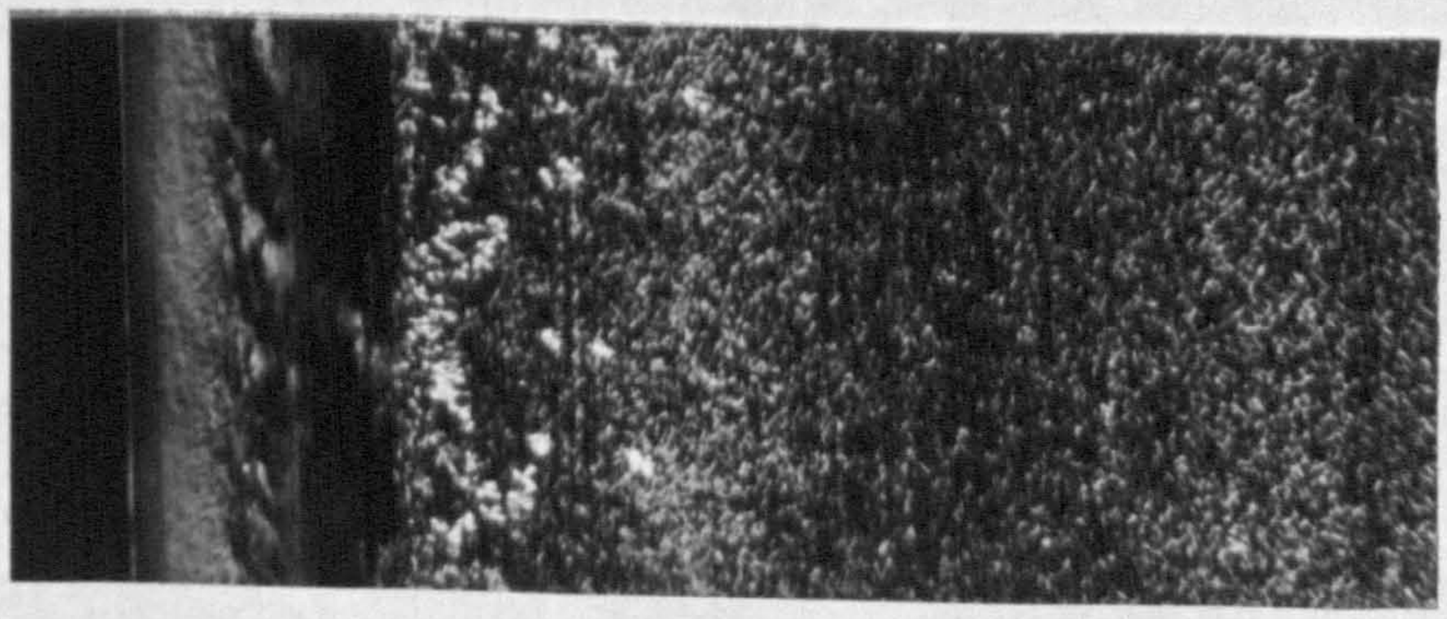

V+30% GSE16

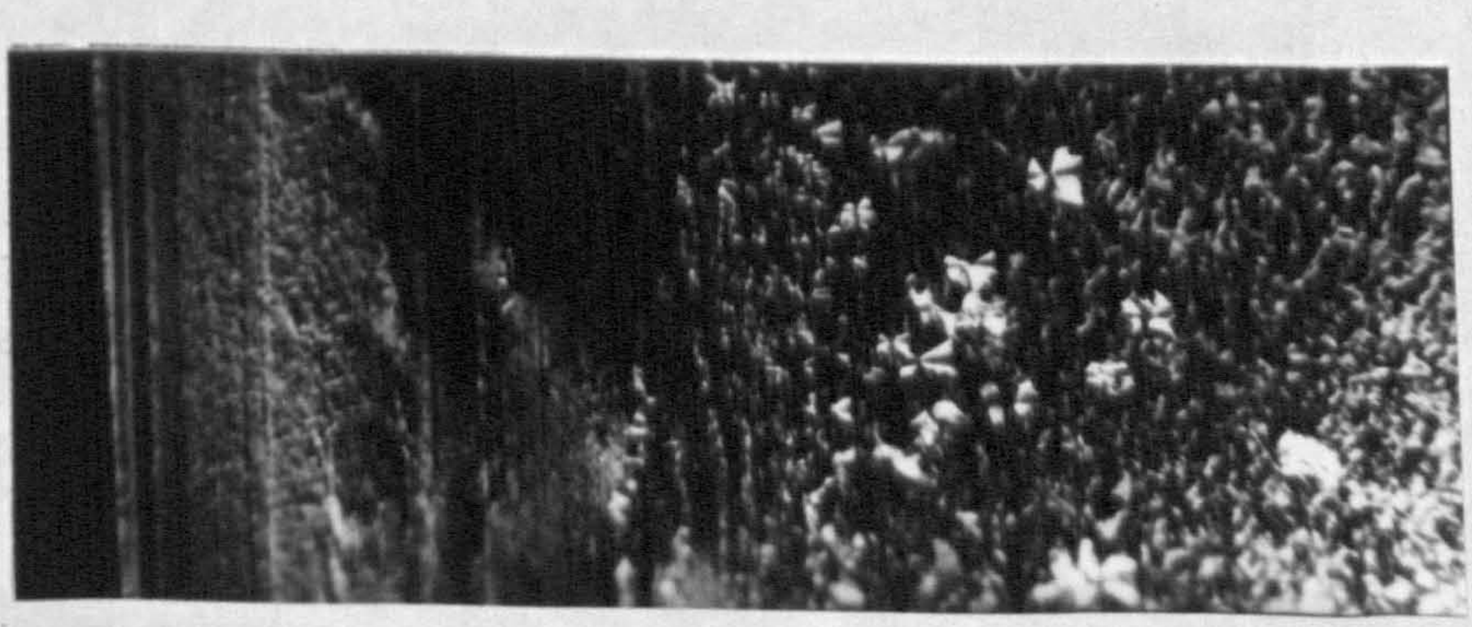

100% GSE16

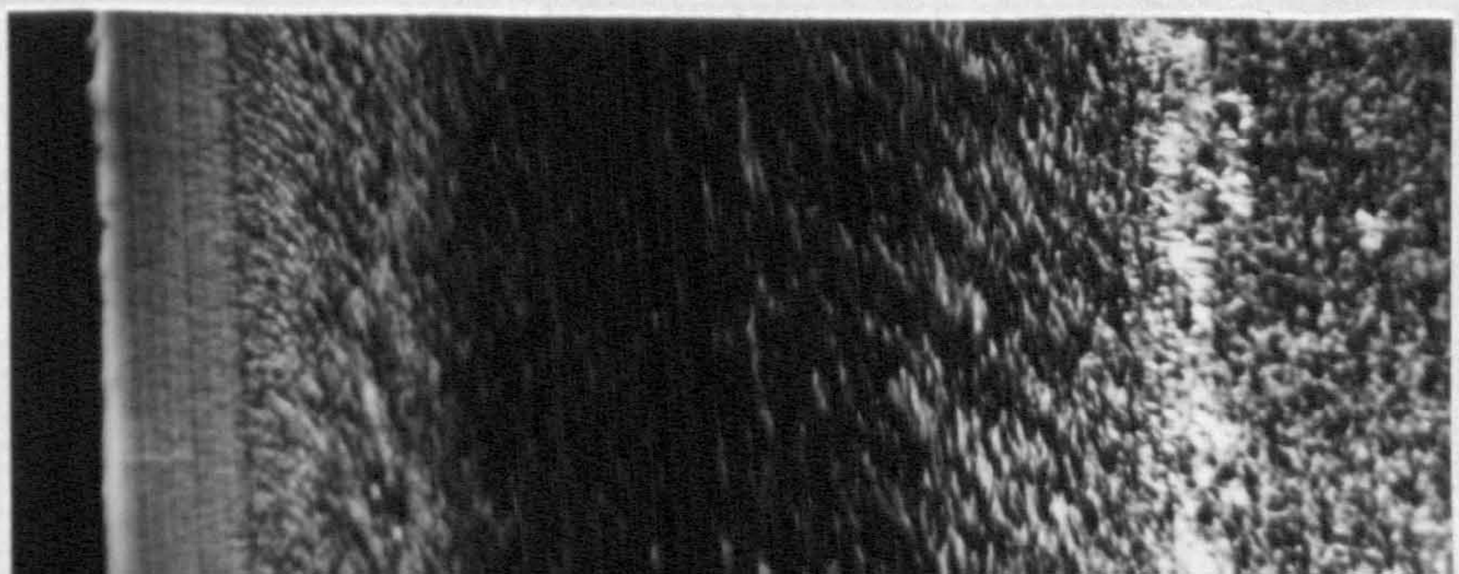

100% GXM43=V

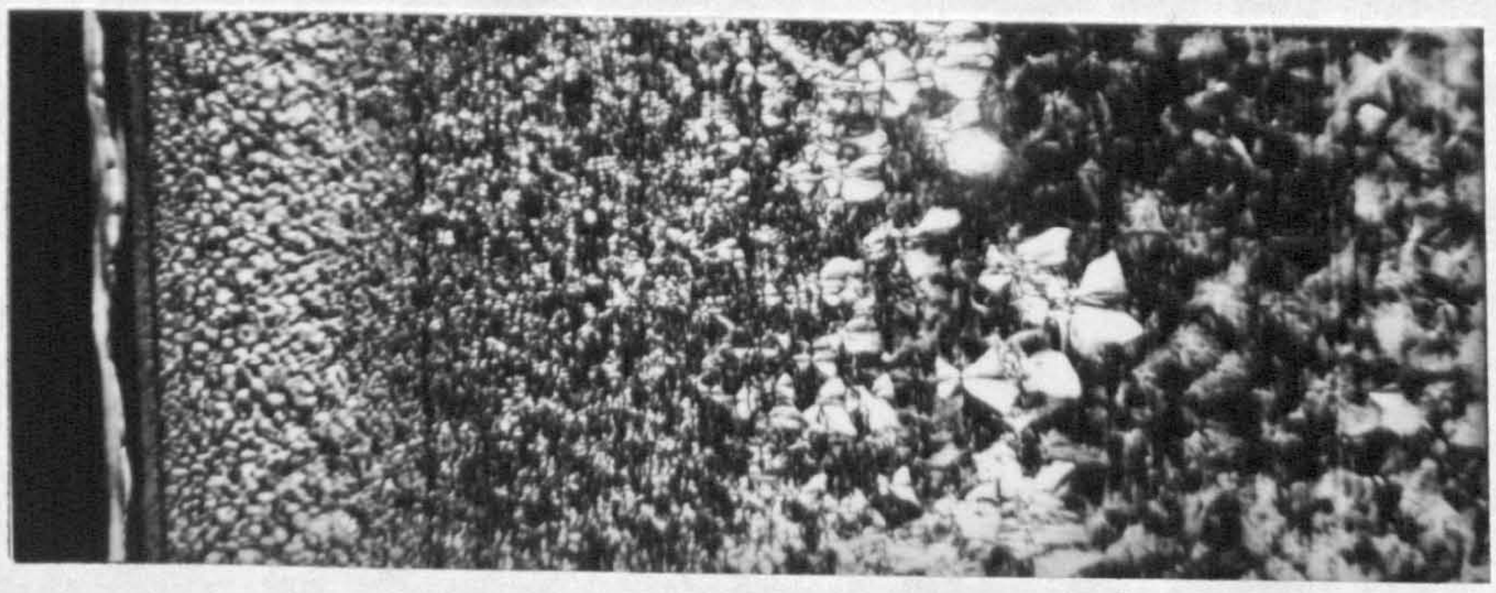

100μm

V+5% GYM45

V+10% GYM45

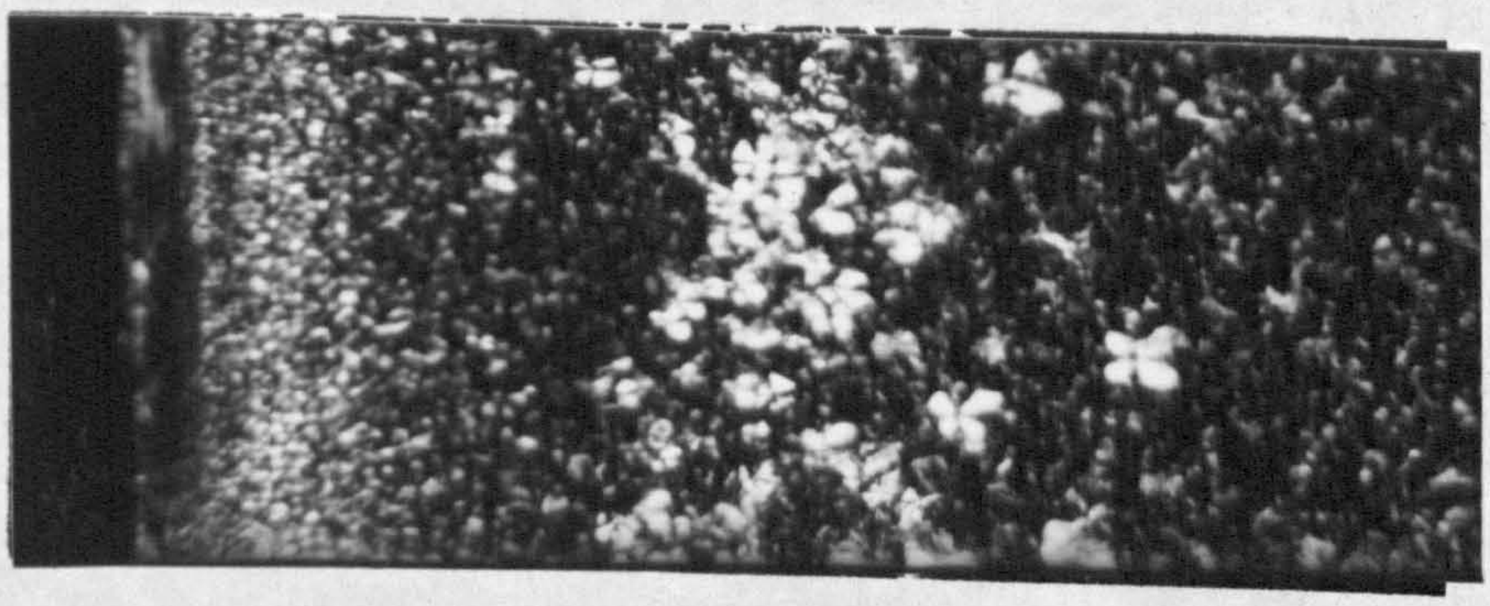

V+20% GYM45

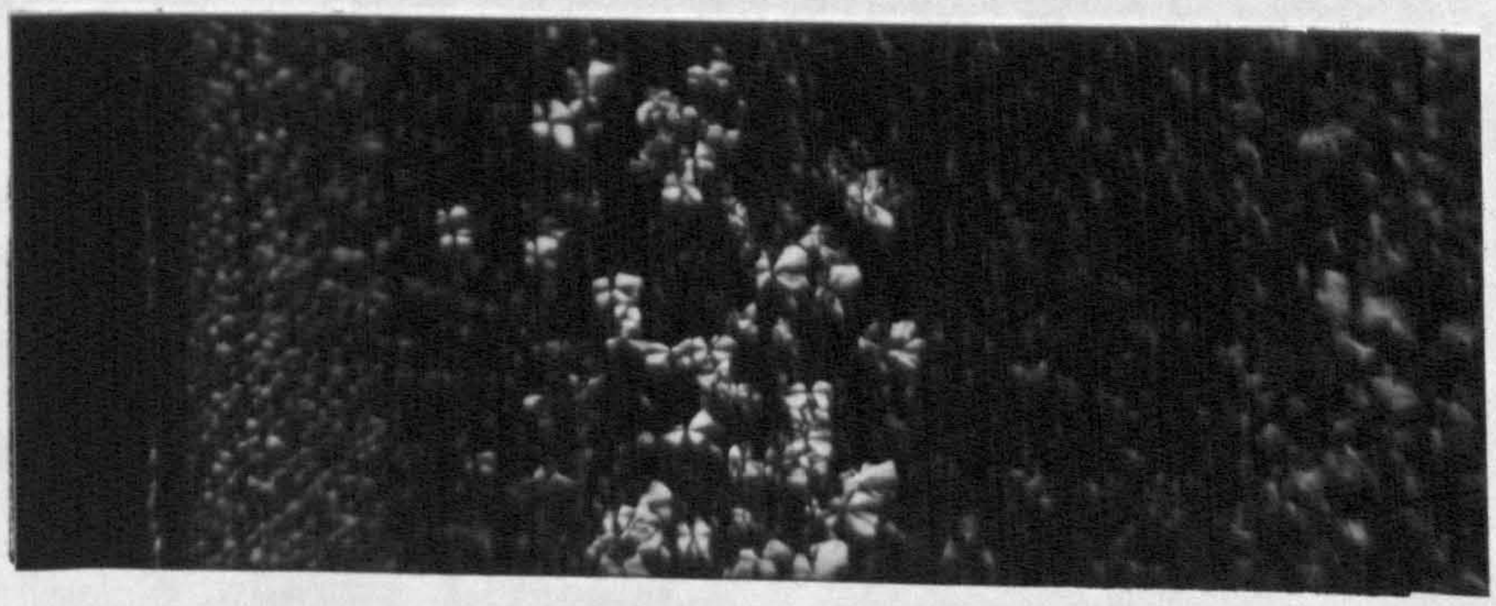

V+30% GYM45

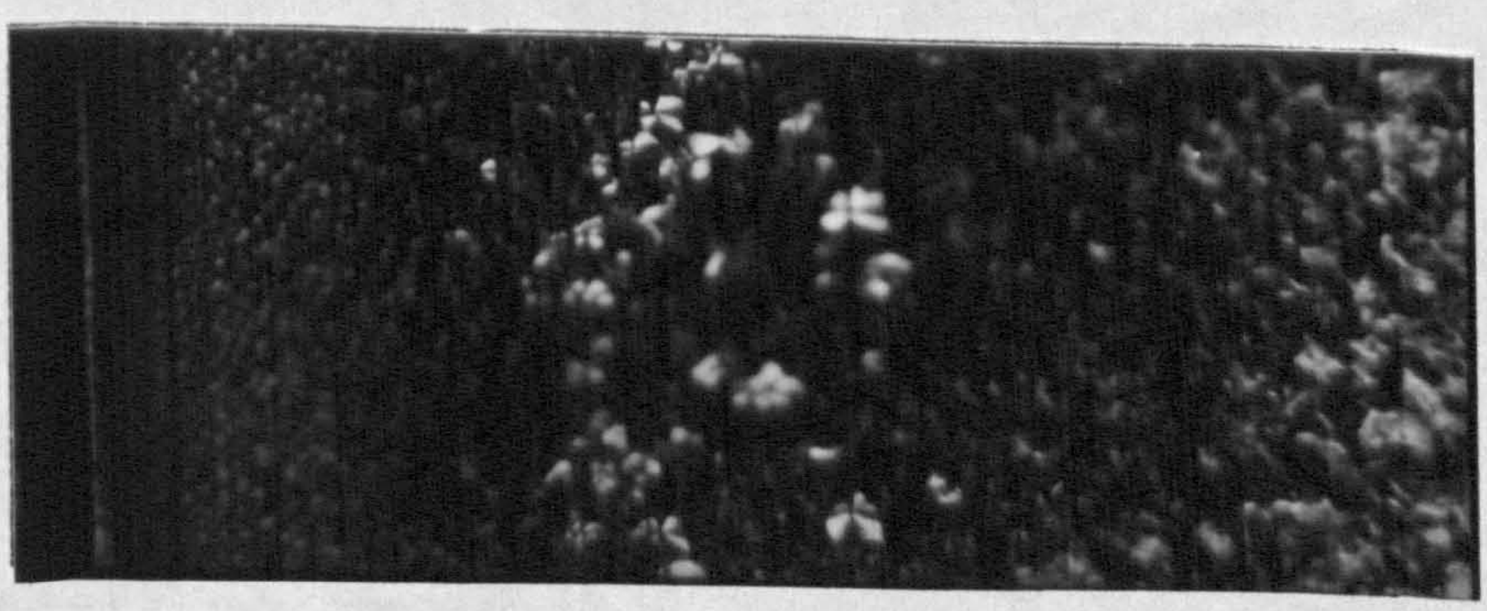

100% GYM45

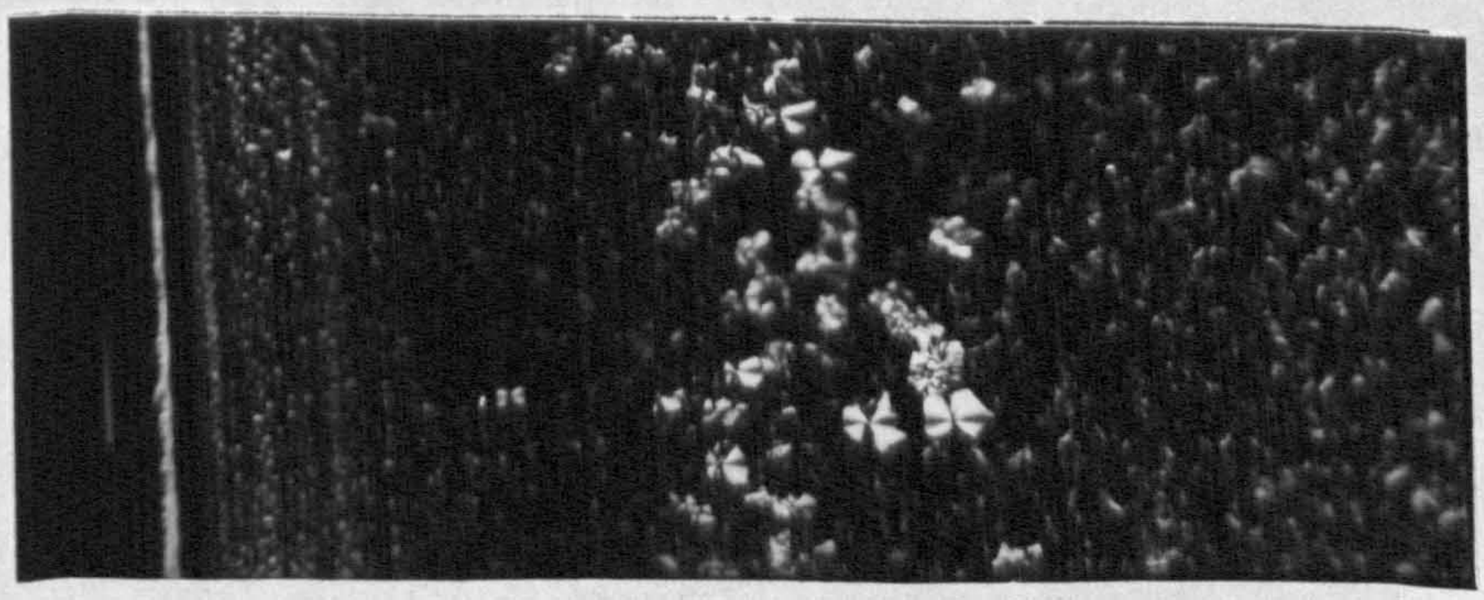

Figure 131 Micrographs of sections taken from 70mm along the melt flow direction for each iPP blend.

100% GXM43=V

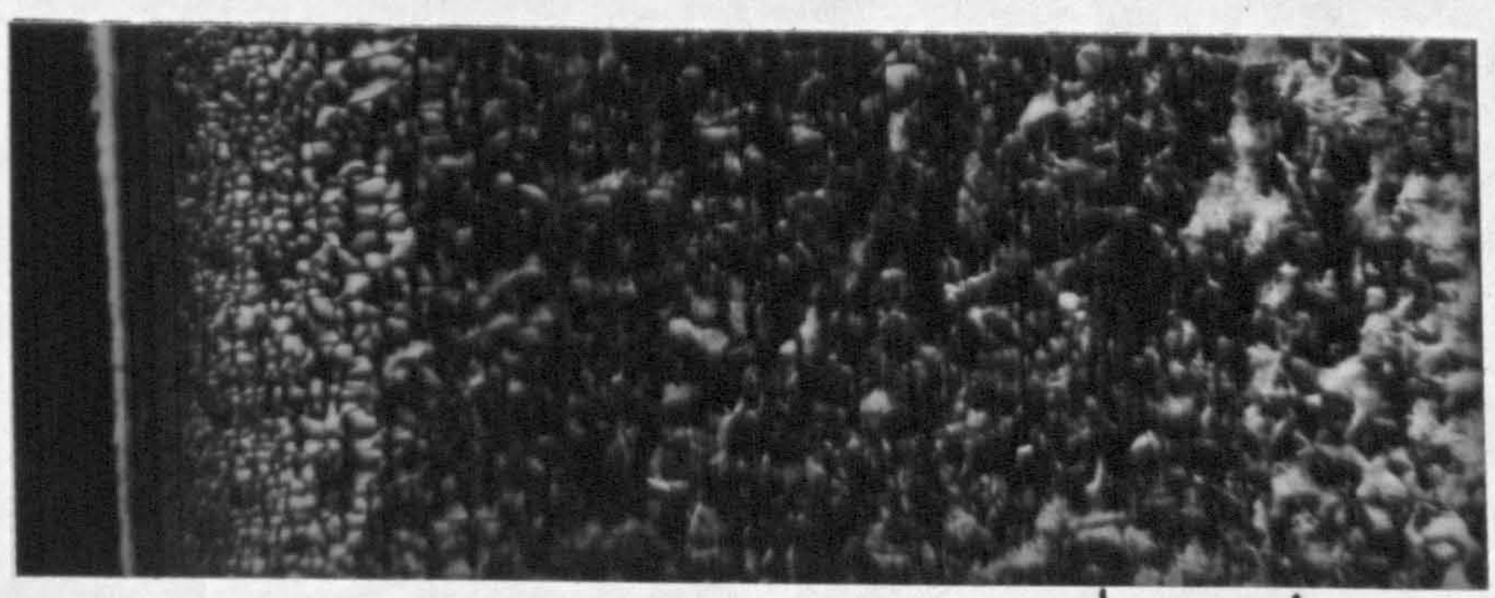

V+5% GSE16

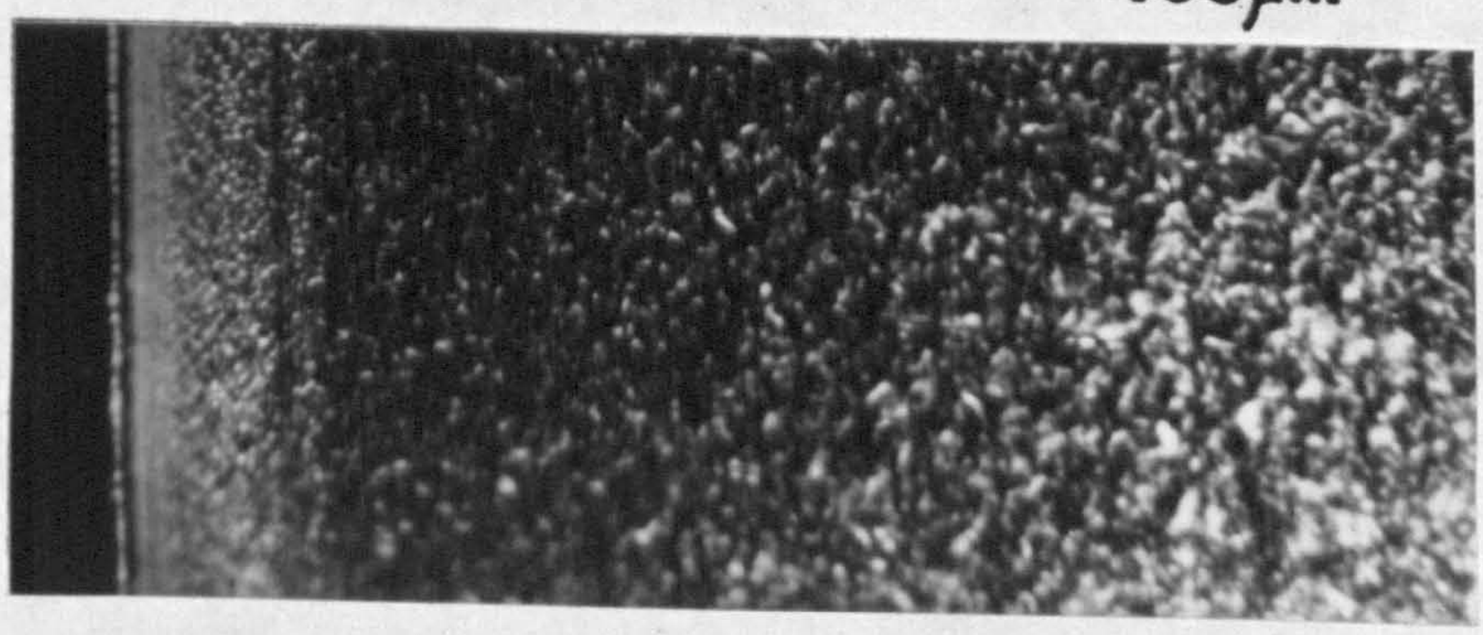

V+10% GSE16

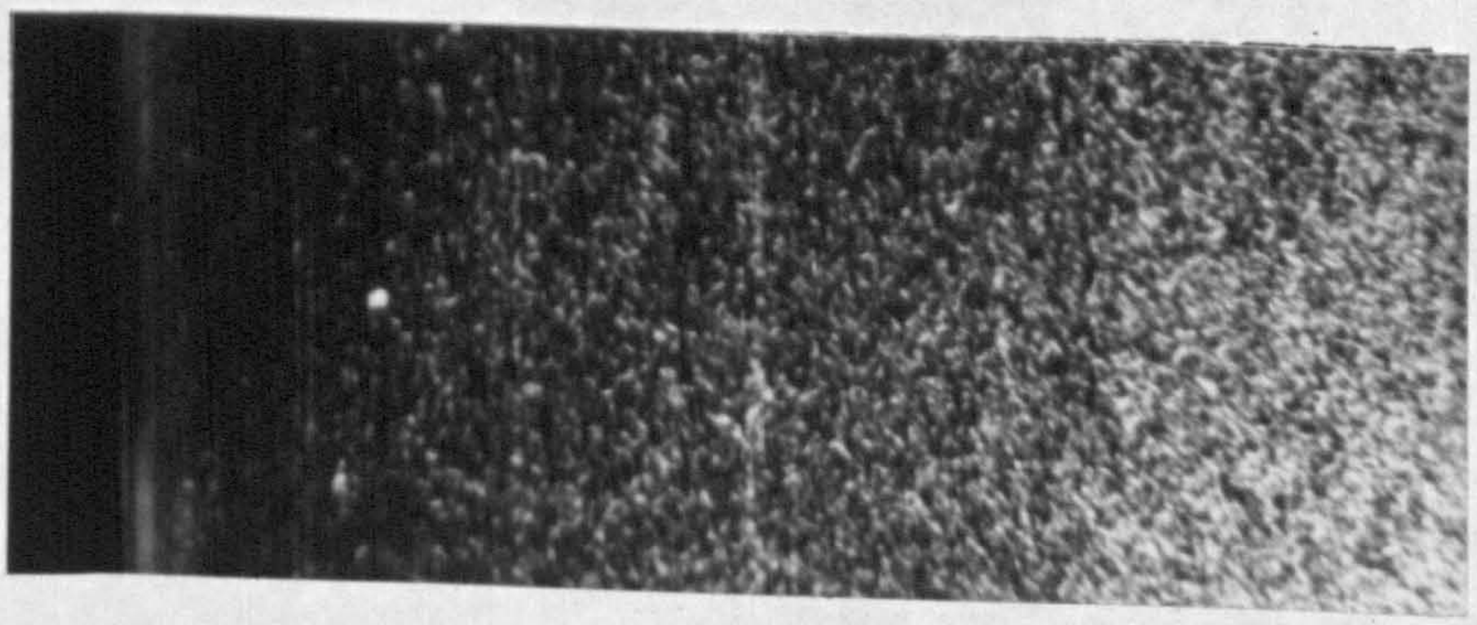

V+20% GSE16

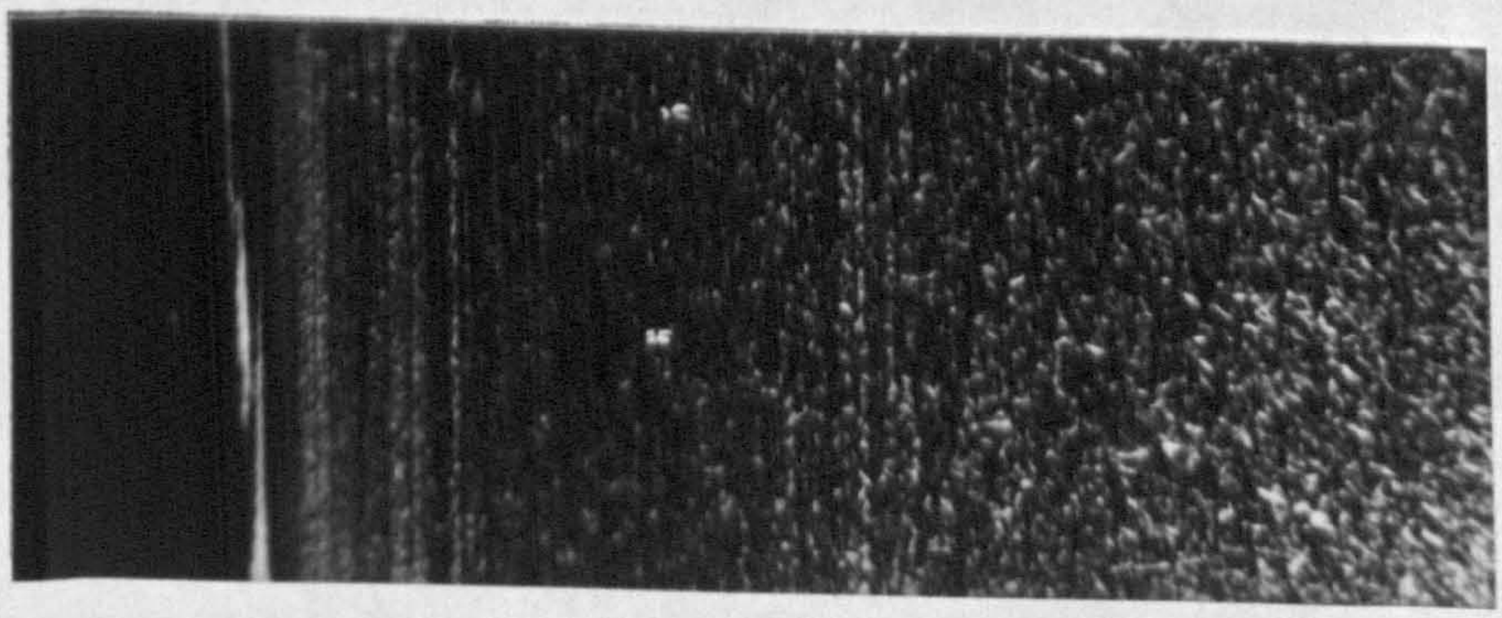

V+30% GSE16

100% GSE16

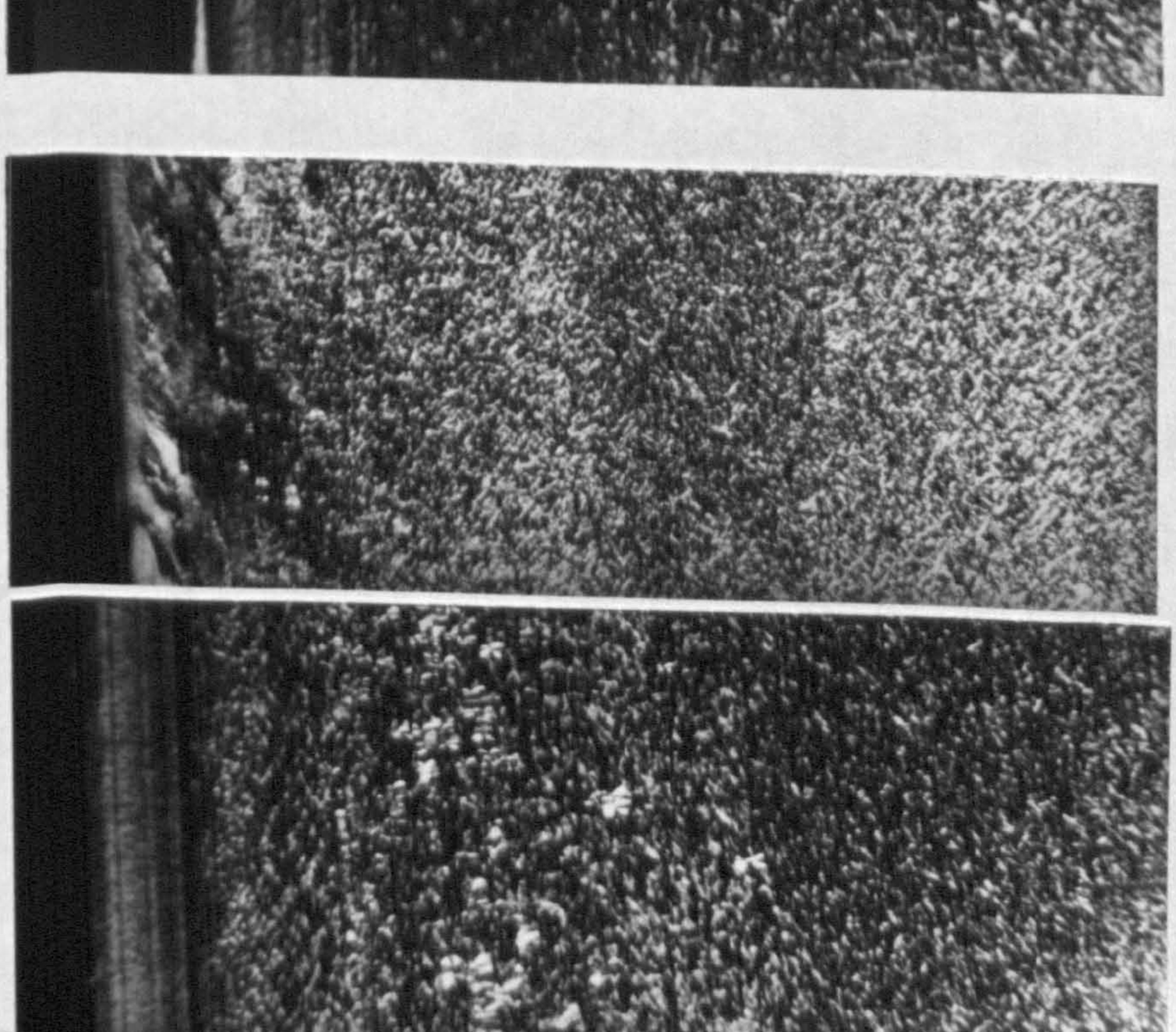

100% GXM43=V

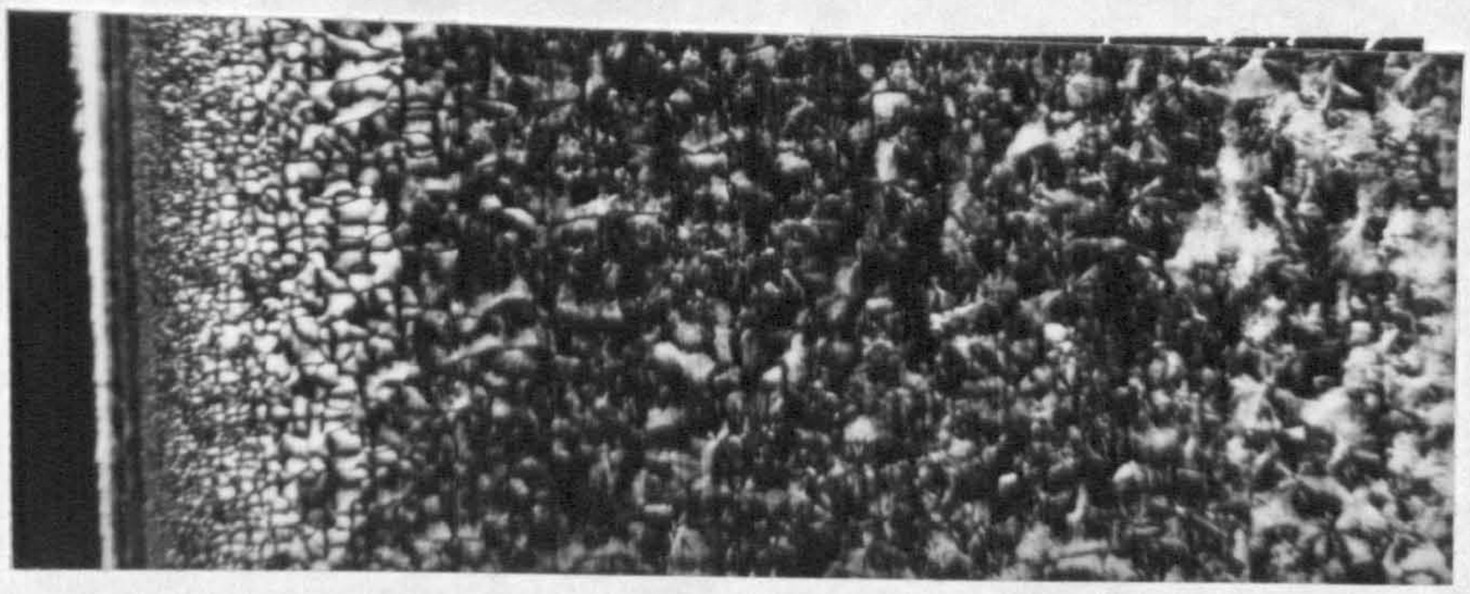

100μm

V+5% GYM45

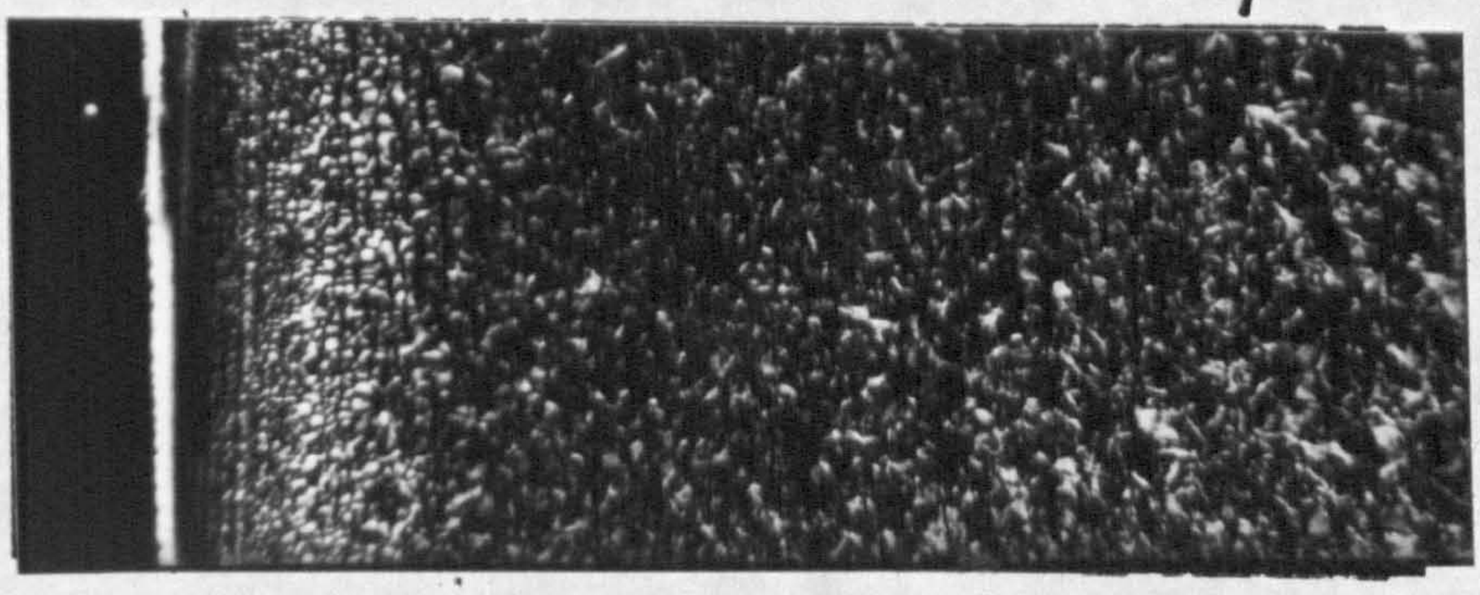

V+10% GYM45

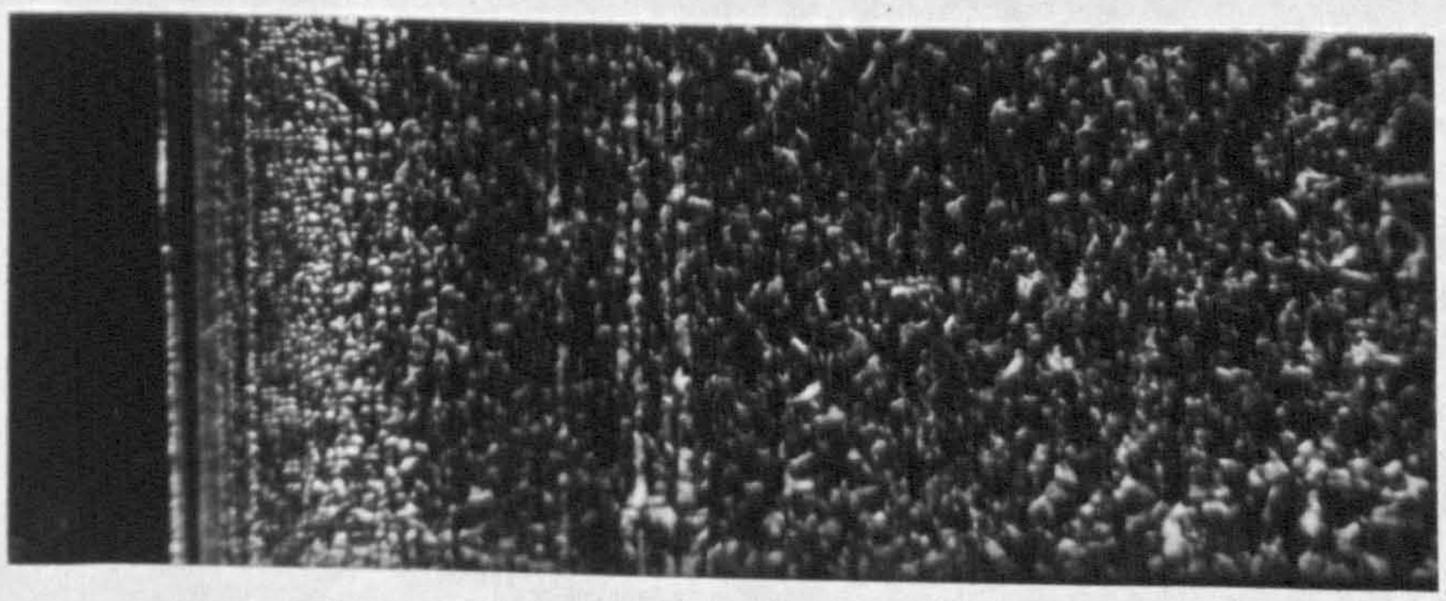

V+20% GYM45

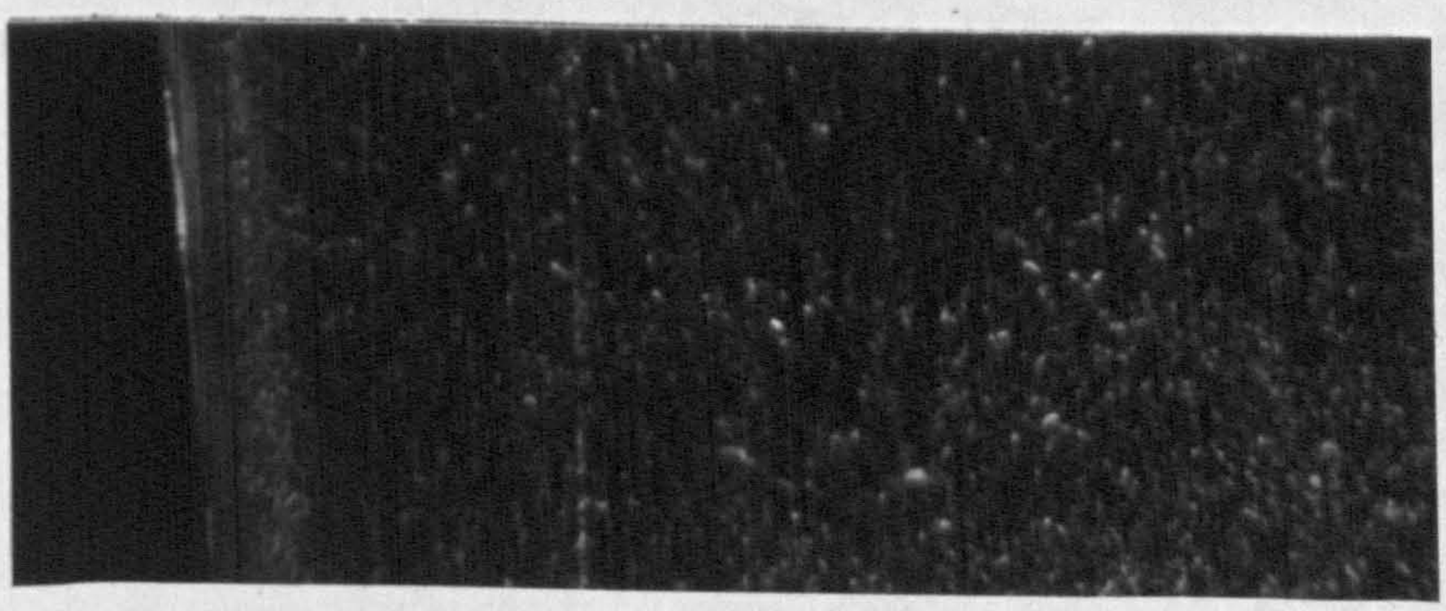

V+30% GYM45

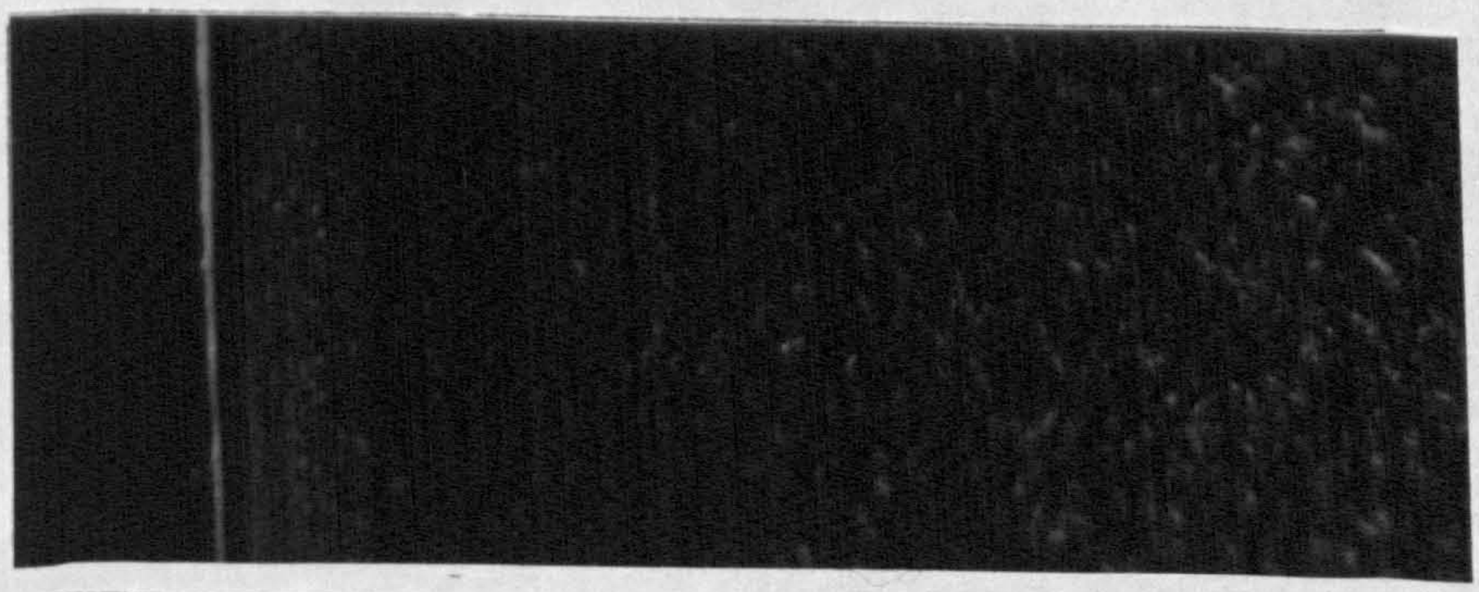

100% GYM45

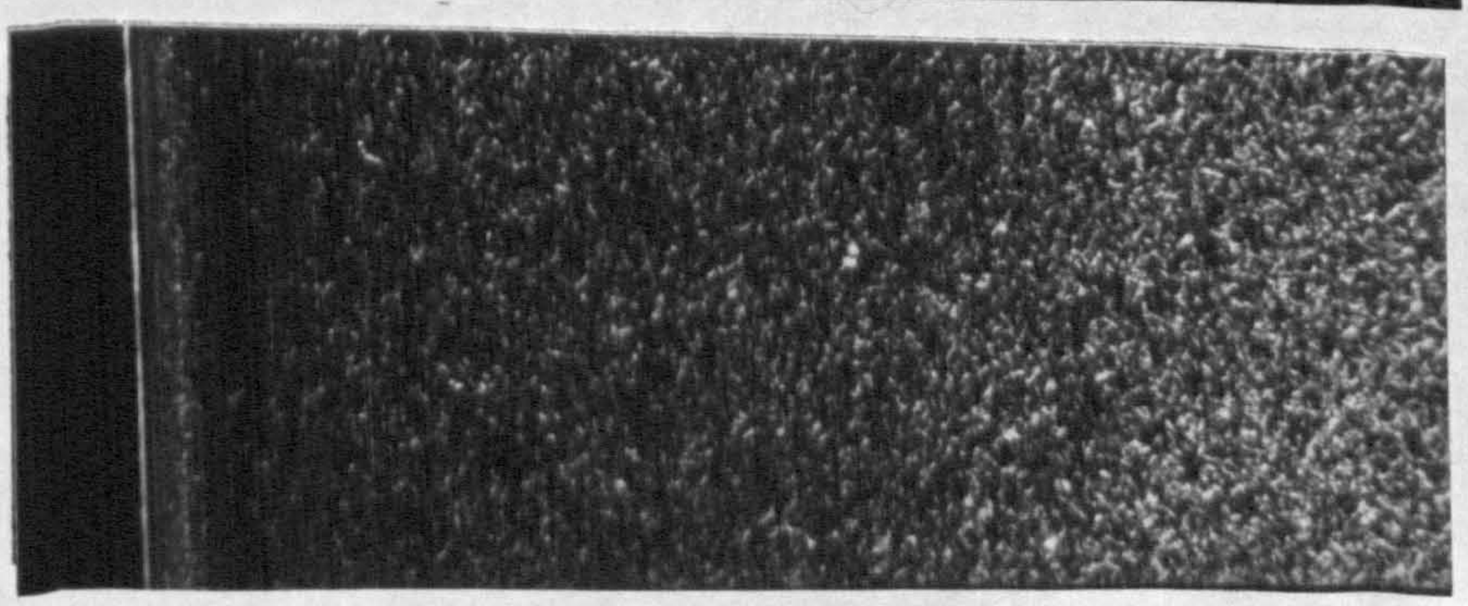

Figure 132 Core α -spherulite size variation with iPP molecular weight.

100% GXM43=V

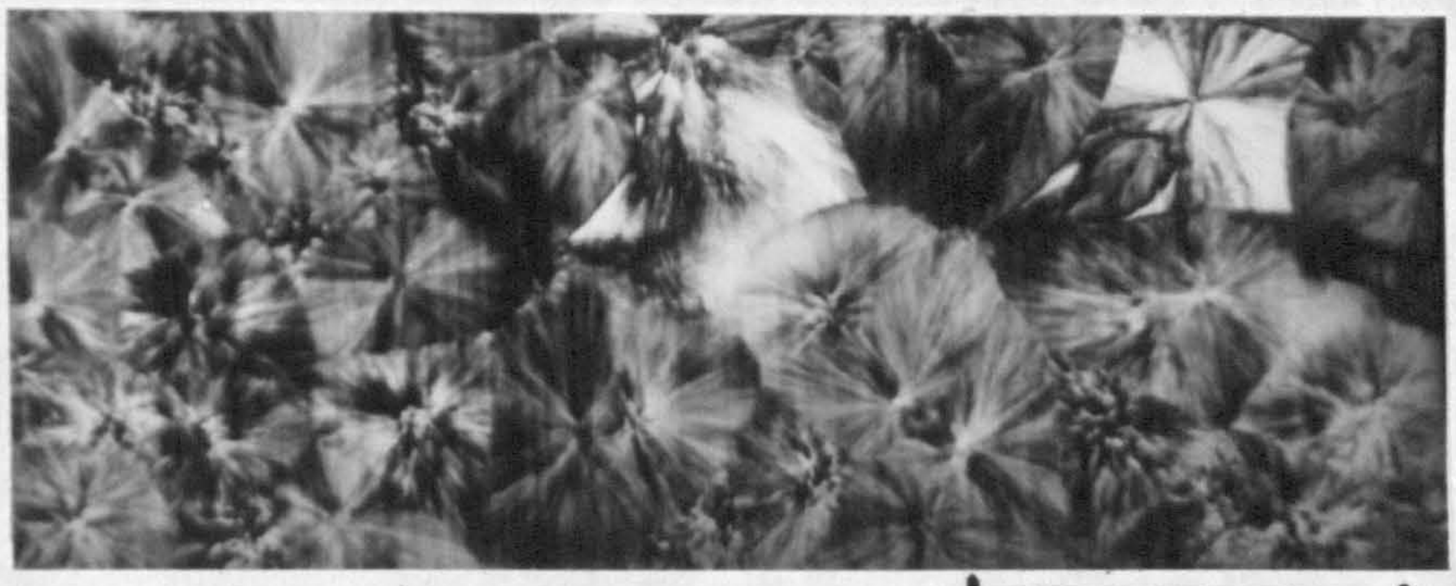

V+5% GYM45

V+10% GYM45

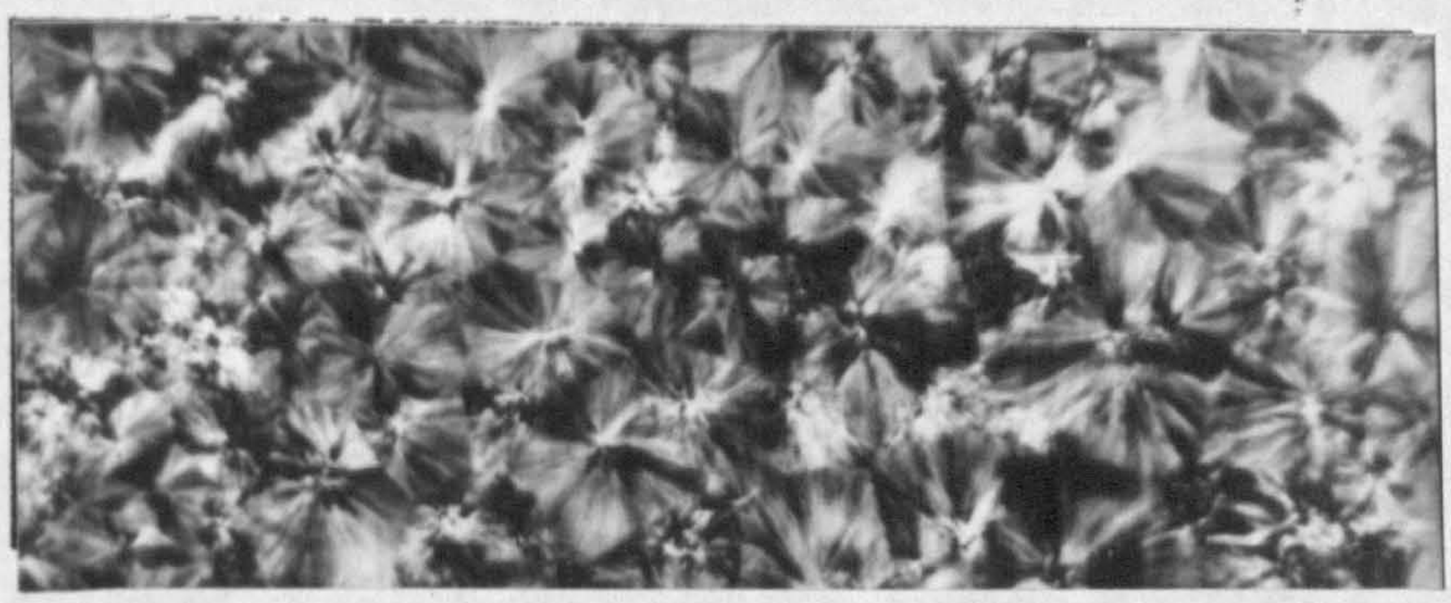

V+20% GYM45

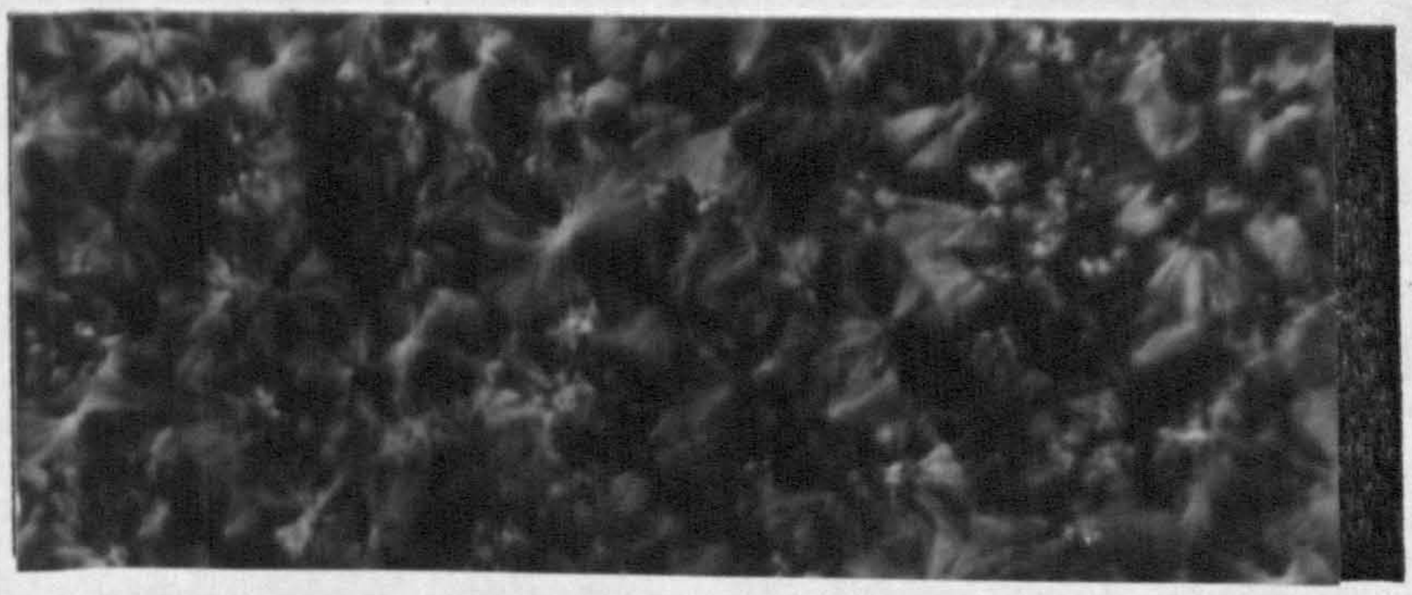

V+30% GYM45

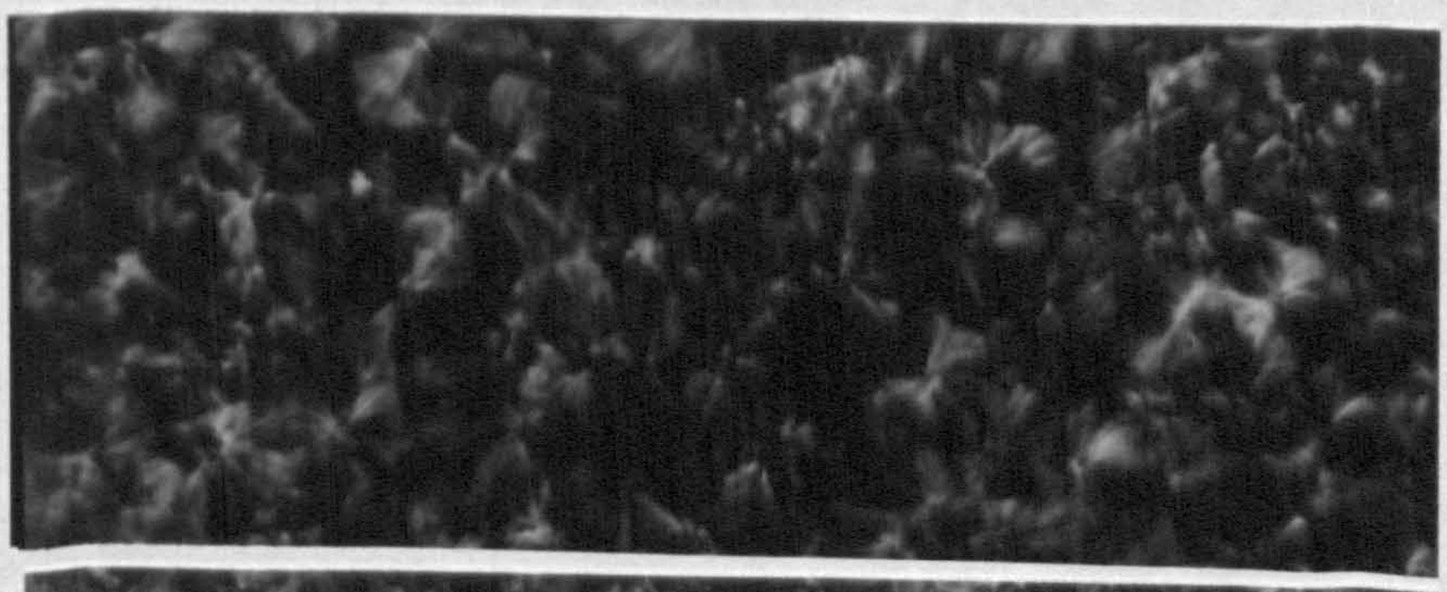

100% GYM45

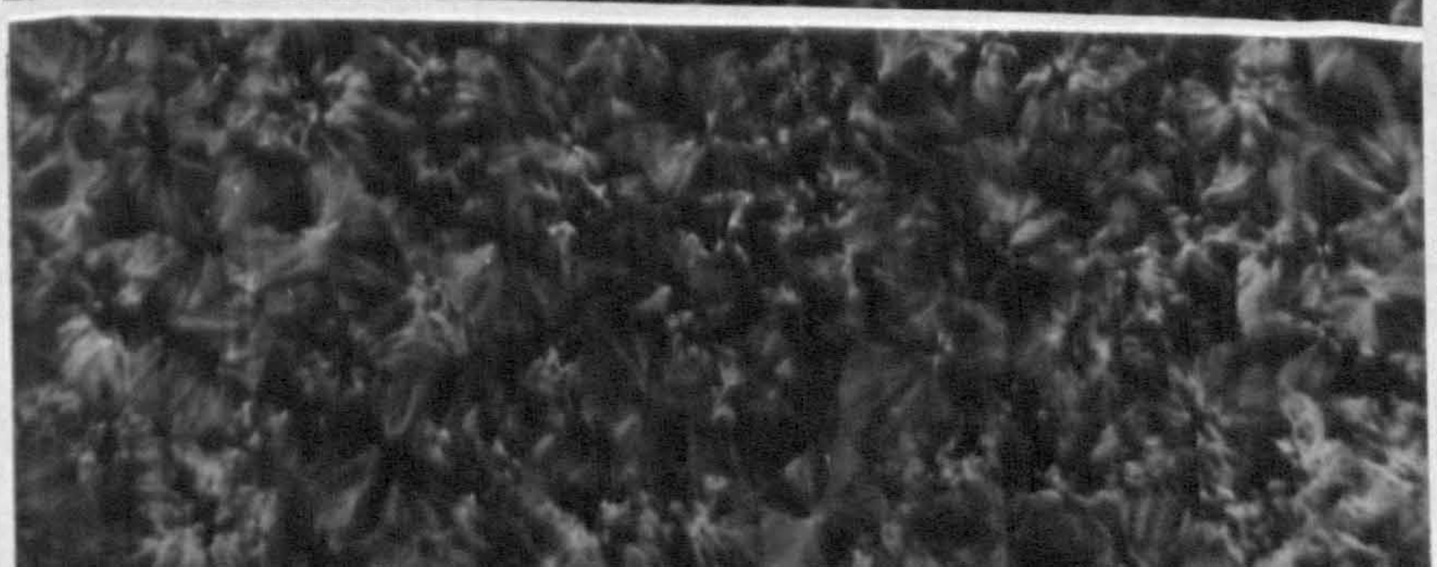

100% GXM43=V

V+5% GSE16

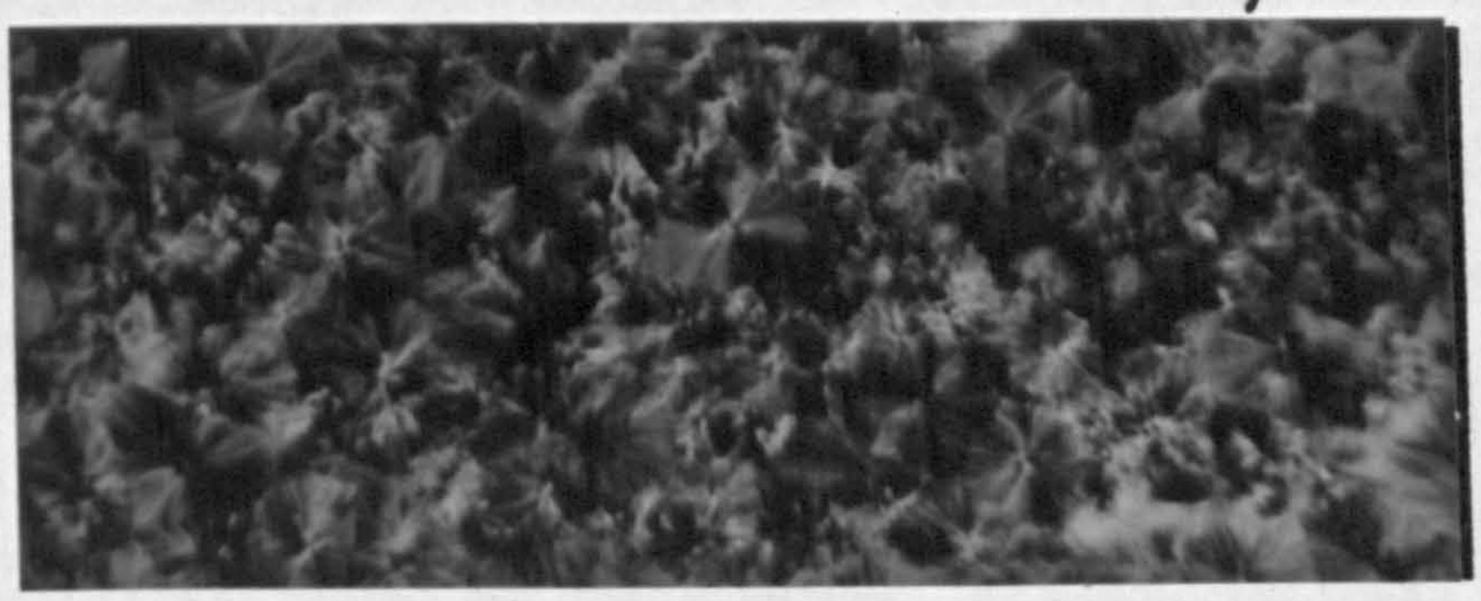

V+10% GSE16

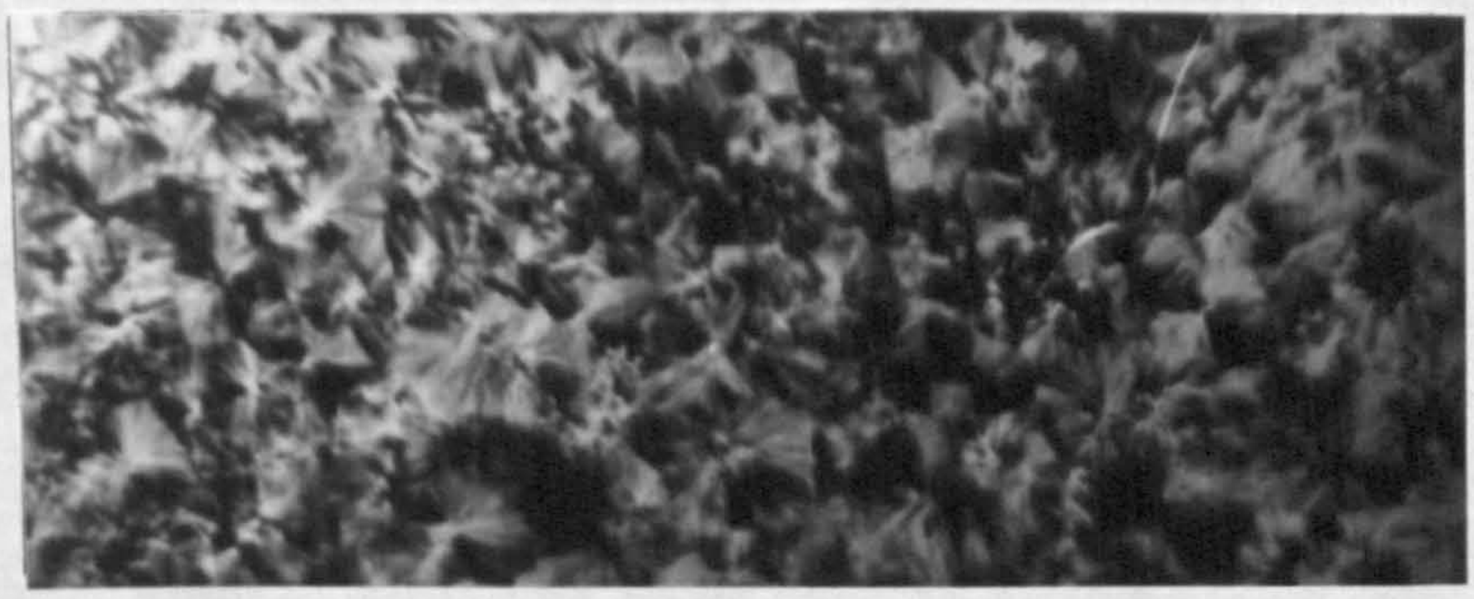

V+20% GSE16

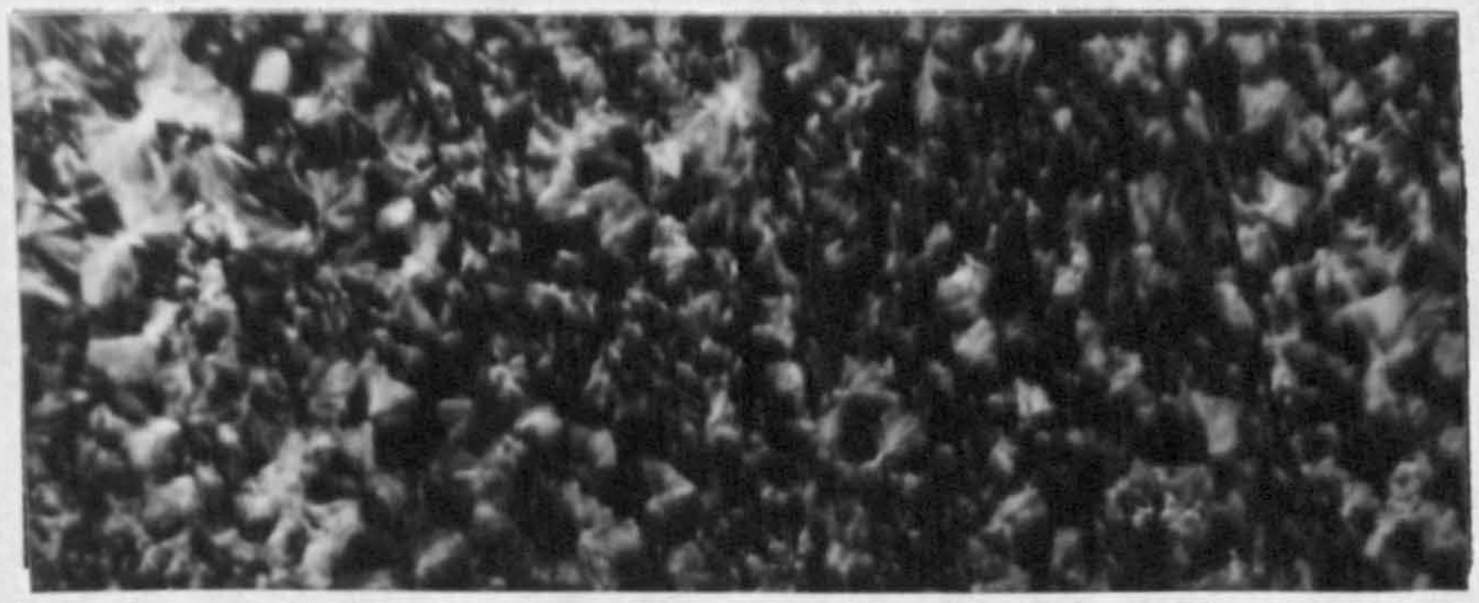

V+30% GSE16

100% GSE16

The central area of mouldings showed an increase in the extent and width of the fibrous row nucleated band with increasing molecular weight also. Mouldings with a weight average molecular weight below c.a. 3.10×10^5 did not exhibit this row nucleated band in the central areas of mouldings. The β phase spherulites in the centre of mouldings were seen to be much more random and less concentrated as the molecular weight was reduced, in high molecular weight GSE16 iPP mouldings dense populations of small β phase structures were found at the fibrous band to core interface this is probably due to the number of nucleation sites provided by this fibrous band.

The far side of mouldings revealed little variation in micro-morphology with molecular weight exhibiting a skin core micro-structure with no β phase row nucleated spherulites present. However, it was found that some row nucleated β phase spherulites were seen in the high molecular weight GSE16 homopolymer mouldings as shown in Figure 131(k).

In addition, the core α -phase spherulites were found to be nucleated at higher concentrations as the molecular weight was increased, Figure 132 exhibits the dramatic difference in size and nucleation of core spherulites in each polypropylene blend used.

4.6 DSC ANALYSIS OF INJECTION MOULDED iPP'S OF DIFFERENT MOLECULAR WEIGHTS

Izod impact test samples, at 20mm and 70mm along the flow direction, of each homopolymer GXM43, GYM45 and GSE16 were sectioned through their thicknesses for DSC thermal analysis according to the procedure of Section 2.6.4. As with the thermal study of Daniels injection moulded polypropylene GXM43

multiple melting peaks associated with the different crystalline forms were observed. In this work however the β peak at around 414K was not identified in any of the polypropylene samples. The melting curves revealed only the α polypropylene melting endotherm at 437K and a β endotherm at around 420K, in addition, a shoulder on the main α endotherm at 430K was also observed. The relative sizes of the α and β peaks were shown to depend very much on the molecular weight and position along the melt flow direction. A summary of the melting behaviour of each polypropylene is given in Table 38.

From these results it was found that the less perfectly formed crystallites (due to the number of nucleation sites) found in high molecular weight polypropylene melt at lower temperatures than the larger well formed crystallites of low molecular weight polypropylene. In addition, the overall degree of crystallinity in the bulk sample is lower in higher molecular weight material as a result. The presence of a β melting peak in GSE16 at 70mm along the flow direction is in good agreement with optical and x-ray diffraction observations presented in Sections 4.5 and 4.7 respectively.

The recrystallisation behaviour of each polypropylene was also studied to assess the rate of recrystallisation dependence on molecular weight. The results of this study given also in Table 38 shows that there appears to be no significant difference in crystallisation temperatures despite the different crystallite sizes produced during nucleation.

TABLE 38 DSC analysis of different moulded isotactic polypropylenes at selected areas along the flow direction.

INJECTION MOULDING iPP	POSITION	MELTING PEAK β_2 (°C)	α_1	α_2	HEAT OF CRYST. FUSION ΔH (Jg-1)	(%)	ONSET Tc (°C)	Tc (°C)
GXM43	20mm	421.64	430.16	437.91	82.62	59.01	390.24	385.51
GYM45	20mm	421.44	429.77	437.47	83.12	59.37	389.99	384.68
GSE16	20mm	419.10	429.00	435.86	77.85	55.61	390.10	384.72
GXM43	70mm		429.00	437.50	82.29	58.78		
GYM45	70mm		429.66	437.34	82.79	59.14		
GSE16	70mm	417.15		436.97	77.52	55.37		

TABLE 39 X-ray diffraction results for moulded iPP's

MOULDED iPP	DISTANCE FROM GATE (mm)	hα1	hα2	hα3	hα4	hβ	CRYST. INDEX ha	C	B-PHASE INDEX B	-PHASE INDEX A
	0-10	88	184	49	36	32	40	1.945	.091	.710
	10-20	63	158	38	40	32	35	1.891	.110	.612
	20-30	60	80	32	47	29	34	1.459	.144	.561
GYM45	30-40	58	72	32	45	27	34	1.376	.143	.563
	40-50	58	70	34	50	18	32	1.438	.100	.537
	50-60	59	66	34	54	0	33	1.291	.000	.522
	60-70	61	64	33	53	0	34	1.241	.000	.535
	70-80	63	56	34	55	0	33	1.261	.000	.534
	0-10	81	160	49	36	39	35	2.086	.119	.692
	10-20	66	159	41	43	33	36	1.900	.110	.606
	20-30	55	77	31	45	32	32	1.500	.164	.550
	30-40	57	74	37	51	28	35	1.411	.143	.528
GXM43	40-50	56	62	31	49	16	34	1.259	.097	.533
	50-60	54	55	32	50	0	32	1.194	.000	.519
	60-70	59	58	32	57	0	34	1.212	.000	.509
	70-80	56	42	28	55	0	34	1.065	.000	.505
	0-10	161	181	85	24	48	41	2.434	.101	.870
	10-20	192	222	98	22	69	43	2.805	.119	.897
	20-30	196	203	95	23	86	43	2.805	.148	.895
	30-40	175	171	83	23	96	45	2.436	.183	.884
GSE16	40-50	180	157	77	23	141	41	2.820	.254	.887
	50-60	155	122	61	23	164	37	2.838	.327	.871
	60-70	106	121	42	32	151	38	2.379	.360	.768
	70-80	52	165	34	42	46	38	1.784	.155	.553

4.7 EFFECT OF MOLECULAR WEIGHT ON CRYSTALLINE POLYMORPHISM AND ORIENTATION IN iPP INJECTION MOULDINGS BY X-RAY DIFFRACTION

The x-ray diffractometer was used to investigate the β phase concentration and distribution, the degree of preferred orientation and the crystallinity as a function of molecular weight in as-moulded plaques of GXM43, GSE16 and GYM45. Mouldings were sectioned into eight 10mm x 10mm x 3mm squares running the length of the flow path, these were exposed to x-rays and the resulting diffractograms indexed according to the procedure given in Section 2.8.7. The results are presented in Table 39 and plots of β phase index, crystallinity index and α -phase orientation index versus distance from gate are shown in Figures 133 to 135 respectively for the three polypropylenes. The following observations were made:-

(i) β -phase Concentration and Distribution

Figure 133 shows that the β -phase concentration and distribution is very much dependent on the molecular weight of the polypropylene injection moulded. High molecular weights lead to high concentrations and extensive distribution of these β row nucleated spherulites, the reverse is found with low molecular weight polypropylene where lower concentrations and less extensive β row nucleation occurs. The high concentration of the β phase is again associated with high degrees of crystallinity and preferred orientation in the direction of flow. The β -phase concentration was also found to increase to a maximum at a certain point along the flow direction consistent with optical microscopy findings.

(ii) Crystalline Fraction

The longitudinal distribution of crystallinity, shown in Figure 134, reveals much higher crystallinity in high molecular weight mouldings particularly close to the gate area. All mouldings regardless of molecular

Figure 133. Longitudinal distribution of B values with molecular weight.

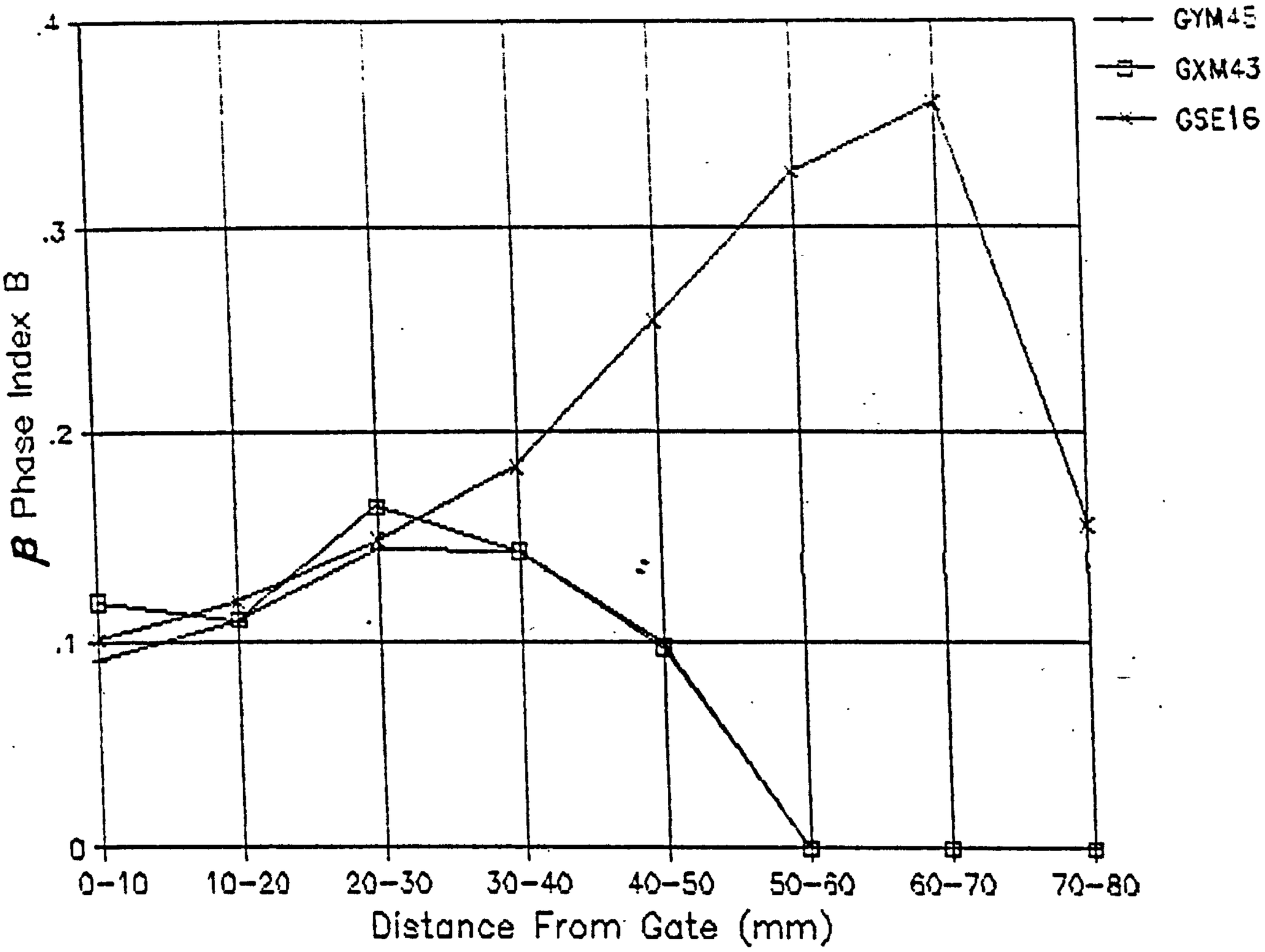

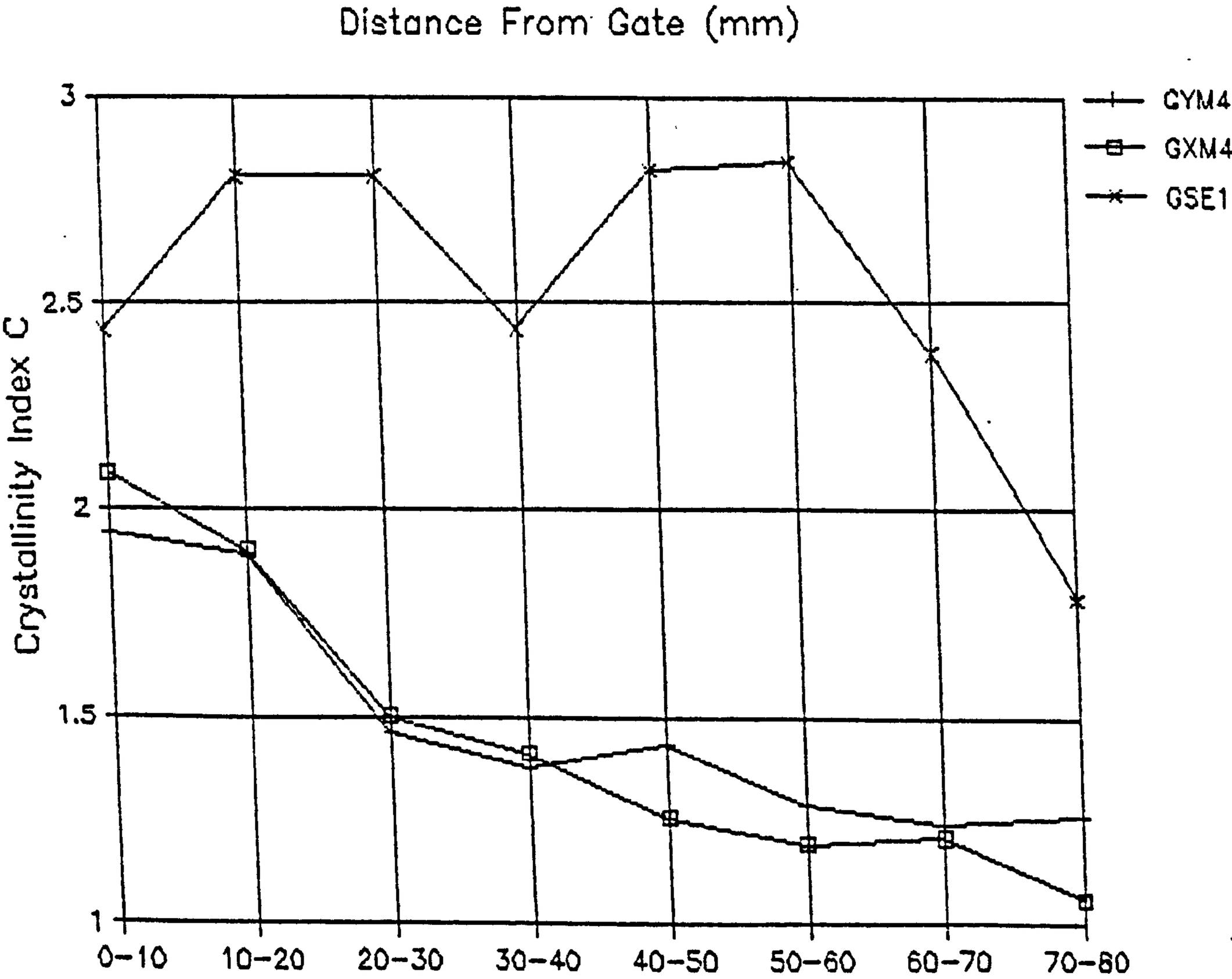

Figure 134 Longitudinal distribution of C values with molecular weight.

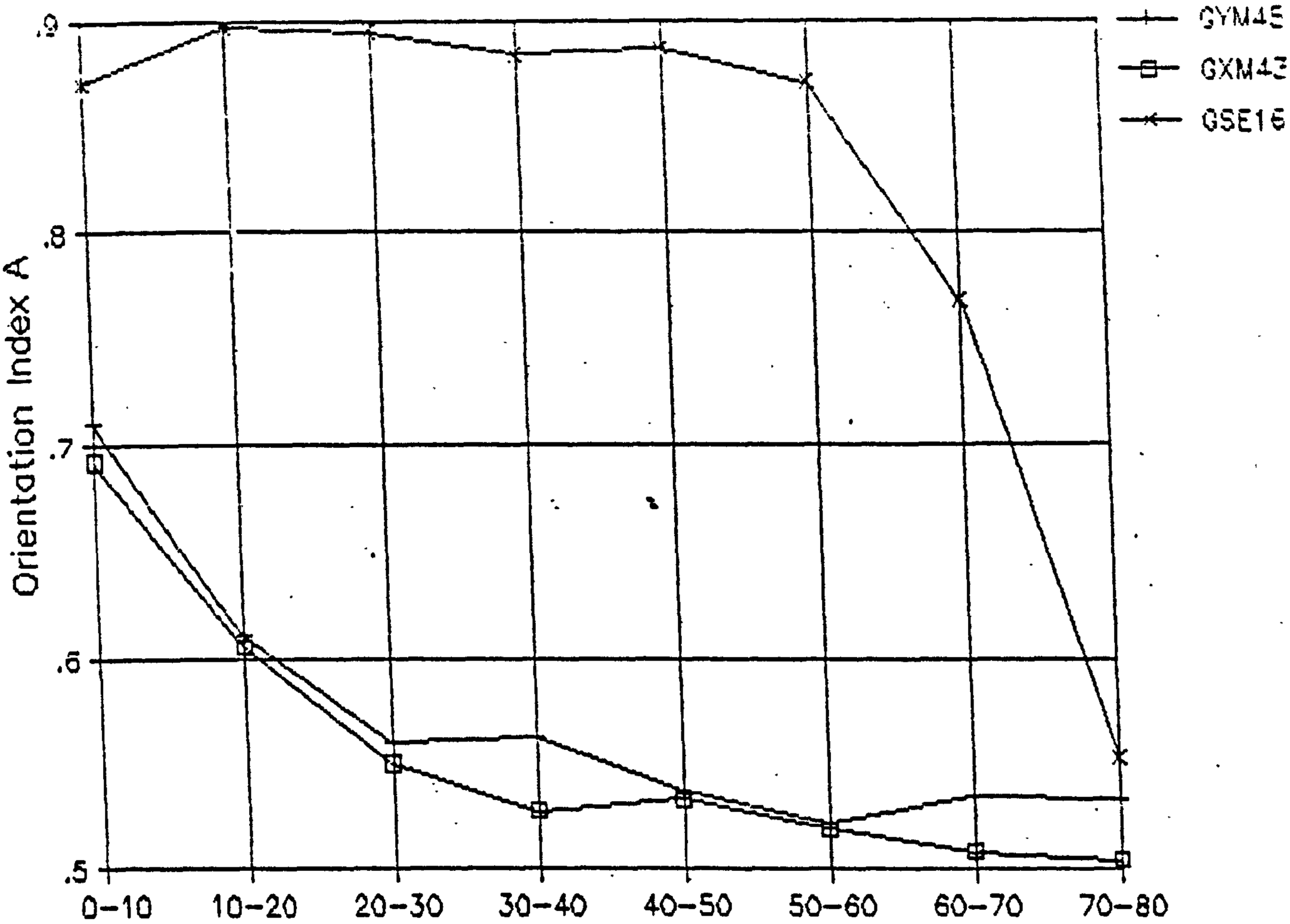

Figure 135 Longitudinal distribution of A values with molecular weight.

weight exhibited heterogeneity along the melt flow path. This result is in contradiction to the findings of DSC studies. However, since x-ray diffraction is a surface crystallinity measurement the β phase found is expected to significantly increase the crystalline fraction in high molecular weight mouldings.

(iii) Orientation of the α -phase

Figure 135 shows that orientation of the c-axis with respect to the flow direction is noticeably more pronounced in high molecular weight mouldings. However, the low molecular weight moulding revealed more preferred orientation than the intermediate molecular weights GXM43 mouldings.

These x-ray diffraction results are once again found to correlate particularly well with optical microscopy studies and Impact test results. The impact strength is seen to improve markedly at the point where β -phase spherulites die away to leave a skin core morphology with high levels of crystallinity and significant surface preferred orientation. The β phase distribution in high molecular weight mouldings is the most significant factor that can be attributed to the low impact properties at 70mm along the flow direction.

4.8 FRACTURE SURFACE ANALYSIS BY SEM

The selected area Izod impact fracture surfaces of a high and a low molecular weight polypropylene were splutter coated and analysed using the Cambridge Stereoscan SEM according to the procedure described in Section 2.7.3. The impact fracture surfaces at 20mm, 40mm and 70mm along the melt flow direction revealed are illustrated in the low magnification micrographs of Figures 136 and 137 for GYM45 and GSE16 respectively.

Figure 136

Fracture surfaces at 20mm, 40mm and 70mm for GYM45 iPP mouldings.

Figure 137

Fracture surfaces at 20mm, 40mm and 70mm for GSE16 iPP mouldings.

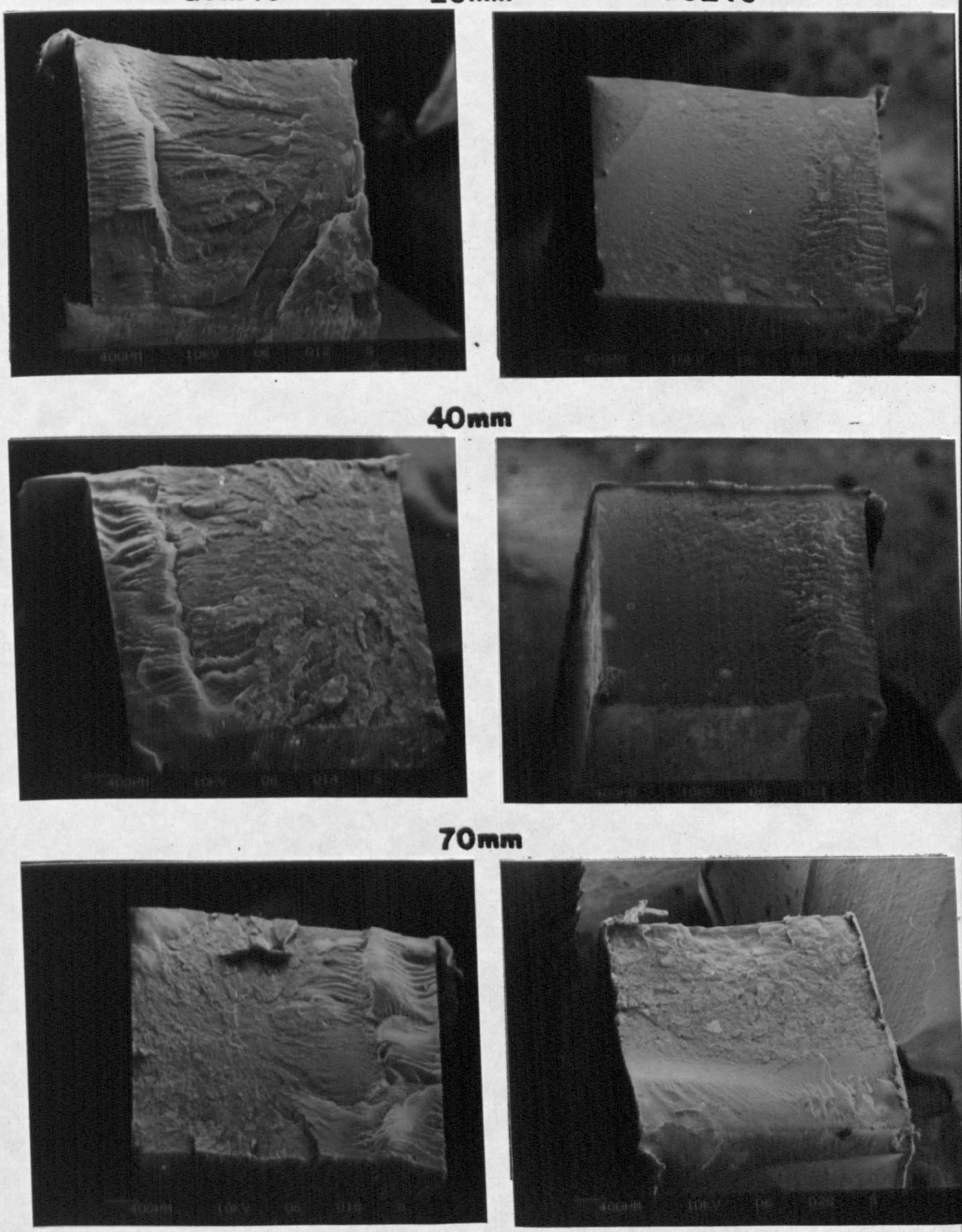

The low molecular weight GYM45 polypropylene mouldings revealed coarse fibrillar fracture surfaces with apparently random crack initiation found in all areas of testing. However, the initiation site was observed to change position moving in towards the core of mouldings as the flow direction was traversed. In contrast, high molecular weight GSE16 polypropylene mouldings exhibited the smooth fracture surfaces associated with brittle low impact energy failures up to 40mm across the flow direction, the initiation site was seen as a very smooth half moon shape at the surface in these samples. At 70mm along the flow direction a transition to a fibrillar fracture surface with crack initiation occuring close to the centre occured in high molecular weight samples, this was associated with the dramatic increase in Izod impact strength observed during testing.

From these observations it can be concluded that:-

(i) in samples where high concentrations of the β phase and row nucleated banded structures are present low impact properties and smooth, skin area, initiated brittle fracture surfaces occur.

(ii) in samples where there is an absence of structural heterogeneity a much tougher fibrillar core initiated fracture surface occurs.

4.9 SUMMARY OF RESULTS

The following observations have been made regarding the effects of molecular weight distribution on the micromorphology and impact properties of injection moulded iPP:-

(i) The impact properties in the vicinity of the gate in GXM43 iPP mouldings were not significantly affected by changes in molecular weight. However, higher molecular weight mouldings lead to enhanced row nucleated lamellar

and β spherulite structures in the shear zones which tend to supress the normally low impact properties still further.

(ii) The impact properties in the centre of GXM43 iPP mouldings were dramatically reduced with the addition of as little as 5wt.% of a high molecular weight tail. This reduction in properties was found to be associated with enhanced β spherulite nucleation as detected by optical and x-ray methods.

(iii) The impact properties at the far end of the melt flow path (beyond 70mm) were found to increase significantly with increasing molecular weight. This improvement was associated with a gradual increase in the skin thickness and the nucleation of α phase core spherulites in the absence of shear nucleated structures.

(iv) The β -phase distribution in iPP injection mouldings is particularly sensitive to variations in molecular weight. Increasing the molecular weight from $Mw = 2.65 \times 10^5$ to $Mw = 4.70 \times 10^5$ revealed a change in β phase distribution from 40mm up to 80 mm along the melt flow path.

****

CHAPTER 5

EFFECTS OF PIGMENTS AND MINERAL FILLERS ON MICROMORPHOLOGY AND IMPACT PROPERTIES OF INJECTION MOULDED iPP

5.1 INJECTION MOULDING

Polypropylene feedstocks containing 0.1 wt.% of the various pigments, 5 wt.% talc and 1 wt.% chalk, prepared according to the procedure given in Section 2.2, were injection moulded on the Sandretto machine using the previously described instrumentation and set processing conditions given in Table 12. As with molecular weight studies the processing conditions were kept constant for all feedstocks since it would have been impractical to consider using a range of processing conditions in the time and with the finance available. The mean peak cavity pressure and mean shot weight data for the moulding programme are given in Table 40. A good correlation between shot weight and peak cavity pressure was found as well as excellent reproducibility of mouldings with a shot weight standard deviation maximum of 0.16 grammes.

5.2 INSTRUMENTED IMPACT TESTING OF PIGMENTED AND MINERAL FILLED POLYPROPYLENE INJECTION MOULDINGS

5.2.1 Instrumented Izod Impact Testing

Five Izod test bars (3mm x 3mm x 12mm) were prepared as before at each of the three selected positions of 20mm, 40mm and 70mm along the melt flow direction from each of the modified polypropylene moulded plaques. These bars were impact tested in accordance with the procedure given in Section 2 providing the results presented in Table 41, the mean Izod impact strength versus distance from gate curves are illustrated in Figures 138 and 139. From these impact test results it was found that Ultramarine Blue pigment was the only additive to markedly improve impact properties. However, even with this pigment a transition from low to high impact strength values occurred as the melt flow direction was traversed, indicating structural heterogeneities close to the gate. The addition of

KEY

S.S single screw extruded

T.S twin screw extruded

U.M ultramarine

P.B phalocyanine blue

Q.R quinacridone red

Q.P quinacridone pink

TABLE 40 Summary of data monitored for injection moulded iPP compounds.

iPP COMPOUND	MEAN SHOT WEIGHT (g)		MEAN PEAK CAVITY PRESSURE (MNm^{-2})		VOLUME SHRINKAGE (%)
	$\bar{x}$	s.d	$\bar{x}$	s.d	
GXM43 S.S=V	40.04	.141	24.43	.419	4.667
GXM43 T.S=V'	40.56	.064	29.78	.219	3.429
V+0.1% U.M	39.79	.082	23.52	.459	5.262
V+0.1% P.B	39.85	.145	24.02	.411	5.119
V+0.1% Q.R	40.85	.163	30.28	.270	2.738
V+0.1% Q.P	40.45	.118	27.99	.549	3.690
V+1% CHALK	40.17	.084	25.34	.729	4.357
V'+5% TALC	42.24	.060	30.66	.515	.571

TABLE 41 Instrumented Izod impact test results for injection moulded iPP compounds.

iPP COMPOUND	I.S 20mm (kJm^{-2})		I.S 40mm (kJm^{-2})		I.S 70mm (kJm^{-2})	
	$\bar{x}$	s.d	$\bar{x}$	s.d	$\bar{x}$	s.d
GXM43 S.S=V	4.481	.229	5.953	.986	15.068	1.605
GXM43 T.S=V'	7.852	.091	19.242	1.195	22.174	2.651
V+0.1% U.M	5.459	.362	8.195	1.546	20.903	.802
V+0.1% P.B	4.296	.046	5.033	.373	9.142	1.926
V+0.1% Q.R	3.945	.098	4.422	.121	8.643	1.075
V+0.1% Q.P	4.472	.188	5.428	.309	8.238	1.107
V+1% CHALK	5.022	.327	5.714	.363	14.747	.926
V'+5% TALC	5.347	.776	4.894	.314	7.740	.408

TABLE 42 Instrumented drop-weight impact test results for injection moulded iPP compounds.

iPP COMPOUND.	PEAK ENERGY 25mm (Nm)		PEAK ENERGY 40mm (Nm)		PEAK ENERGY 55mm (Nm)	
	x	s.d	x	s.d	x	s.d
GXM43 S.S=V	0.349	.112	0.391	.068	0.722	.128
GXM43 T.S=V'	0.493	.082	0.796	.171	0.956	.420
V+0.1% U.M	0.373	.018	0.438	.049	0.747	.049
V+0.1% P.B	0.304	.026	0.368	.056	0.509	.070
V+0.1% Q.R	0.332	.018	0.326	.033	0.426	.049
V+0.1% Q.P	0.267	.038	0.365	.072	0.434	.059
V+1% CHALK	0.332	.047	0.366	.078	0.600	.109
V'+5% TALC	0.277	.016	0.269	.090	0.275	.062

Figure 138 Mean Izod impact strength versus distance from the gate for single screw extruded pigmented and chalk filled GXM43 iPP plaques.

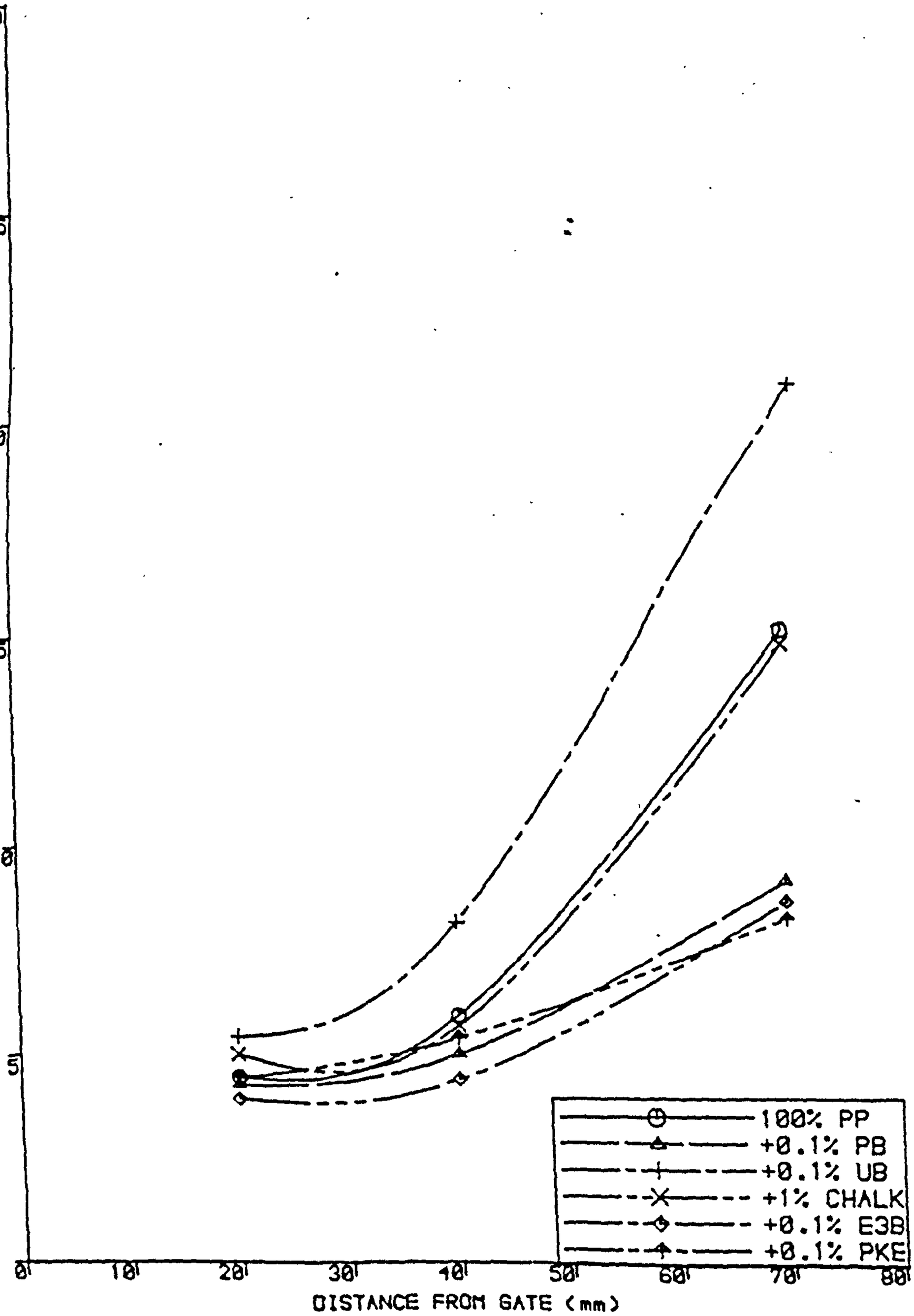

Figure 139 Mean Izod impact strength versus distance from the gate for twin screw extruded and injection moulded talc filled iPP plaques.

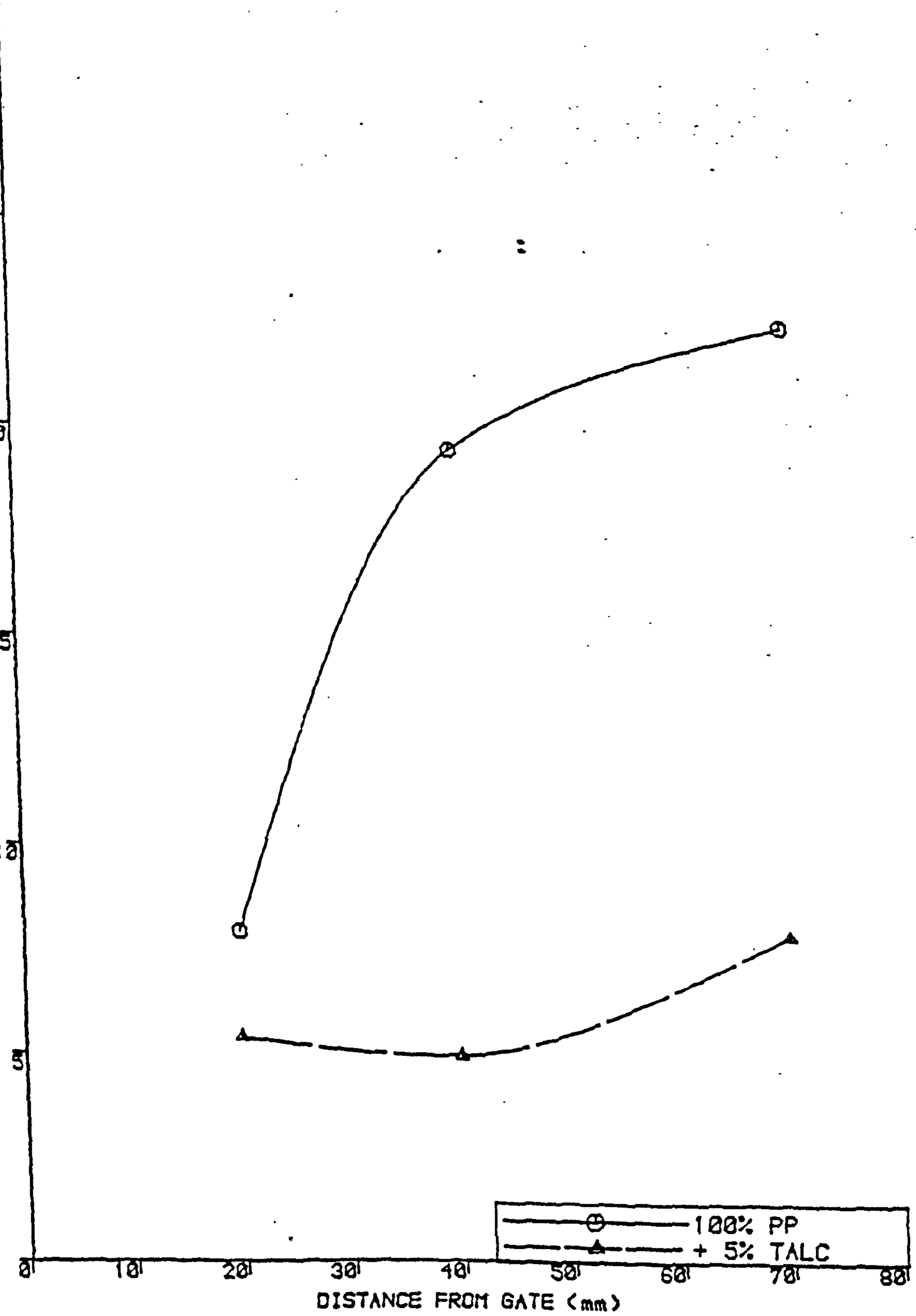

1 wt.% chalk does not appear to have had any effect on the impact properties of the polypropylene mouldings. However, the addition of 0.1 wt.% of the Quinacridone and Phthalocyanine pigments and 5 wt.% talc to polypropylene has a severe detrimental effect on the properties of the moulded plaques, particularly at the far side of the moulding where high impact strengths are usually found.

5.2.2 Instrumented Drop-Weight Impact Testing

Drop Weight impact test samples of dimensions 50mm x 60mm x 3mm were prepared from injection moulded plaques of polypropylene containing low percentage additions of the varicus additives. Five impact samples from each of three positions at 25mm, 40mm and 55mm along the melt flow direction were prepared and tested, according to the procedure explained in Section 2.4.3, for each of the modified GXM43 polypropylene mouldings. As with previous drop weight impact testing the first peak on the force/distance curves corresponded to the energy required to initiate major cracks and so only the mean peak impact energy data was given detailed analysis. The resulting mean peak drop weight impact energies for selected area testing are presented in Table 42 for each injection moulded feedstock and presented graphically in Figures 140 and 141.

A good overall agreement was found between Izod and drop-weight impact test result trends i.e. an improvement in impact properties with low percentage additions of Ultramarine Blue pigment, no change in properties with the addition of 1 wt.% chalk, but a deleterious effect upon impact properties with small additions of the Phthalocyanine pigment, Quinacridone pigments and talc filler to the GXM43 polypropylene homopolymer.

Figure 140 Mean drop-weight impact energy versus distance from (a) the gate for single screw extruded pigmented and (b) chalk filled GXM43 iPP moulded plaques.

(a)

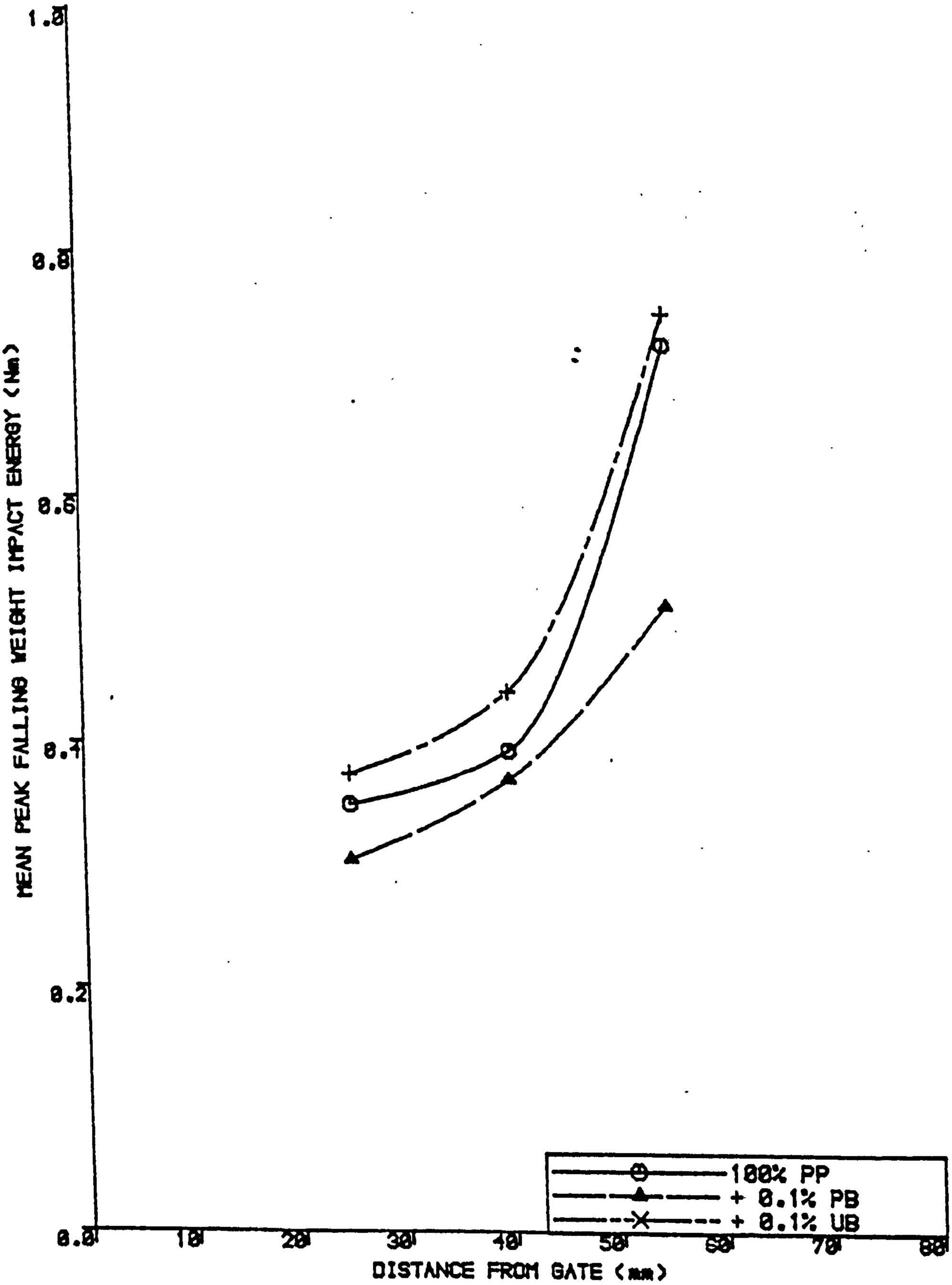

Quinacridone Pigments

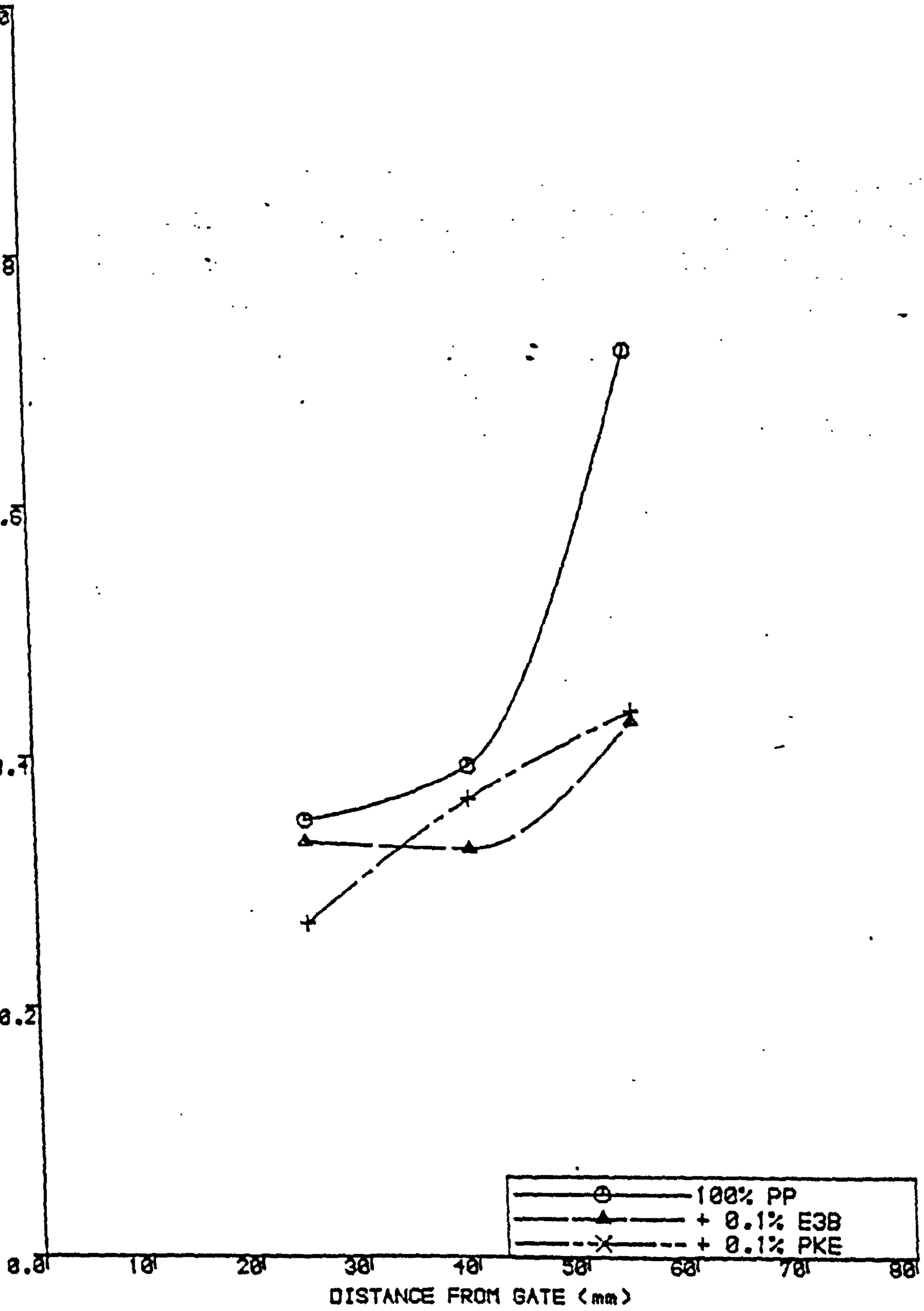

(b)

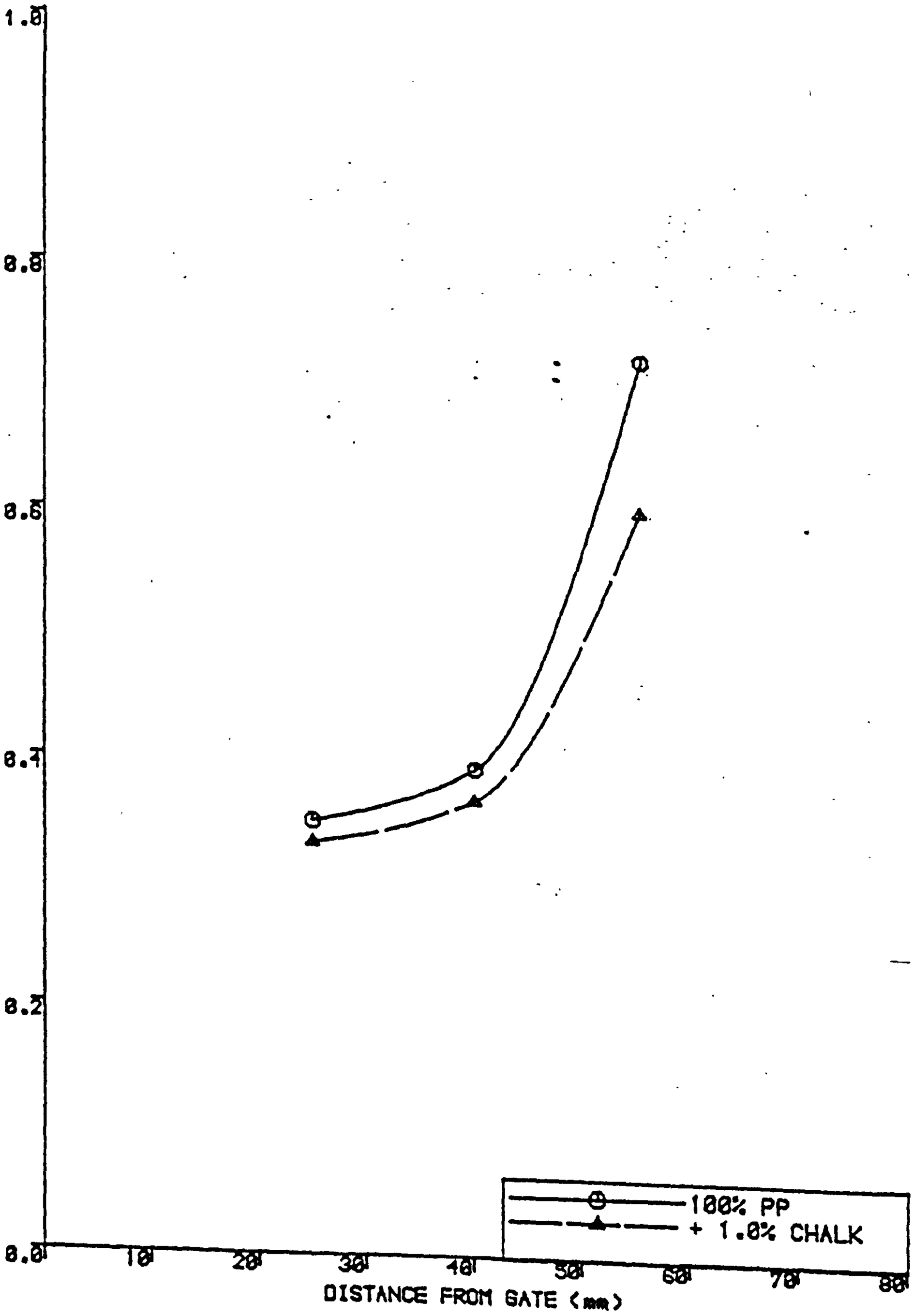
1.0
0.8
0.6
0.4
0.2
0.0
MEAN PEAK FALLING WEIGHT IMPACT ENERGY (Nm)
10
20
30
40
50
60
70
80
DISTANCE FROM GATE (mm)
100% PP
+ 1.0% CHALK

Figure 141

Mean drop-weight impact energy versus distance from the gate for twin screw extruded and injection moulded talc filled GXM43 iPP plaques.

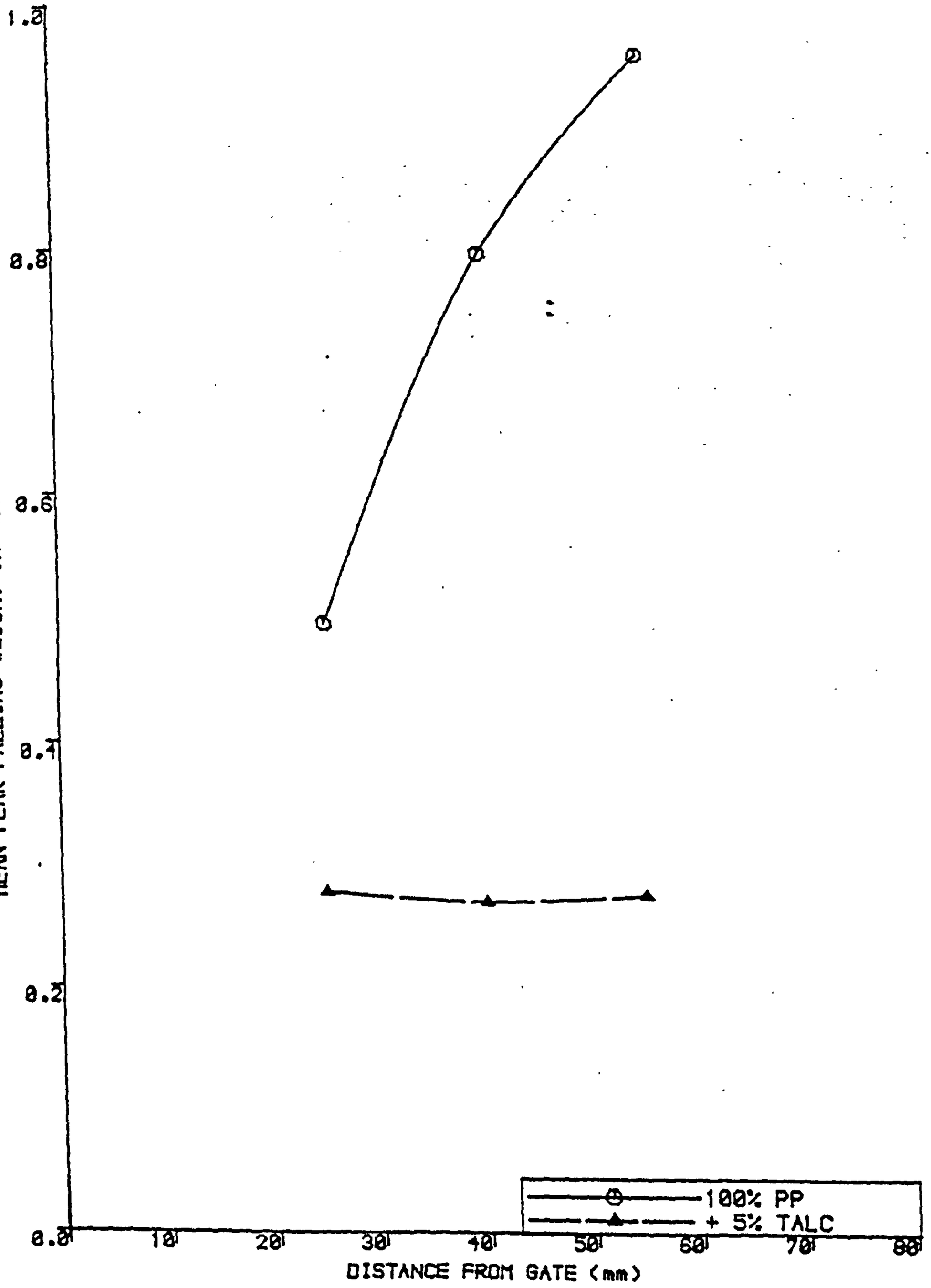

TABLE 43 Results of fracture pattern analysis of drop-weight impact tested plaques of iPP compounds.

iPP COMPOUND	NUMBER OF CRACKS AT 25mm		NUMBER OF CRACKS AT 40mm		NUMBER OF CRACKS AT 55mm	
	MINOR	MAJOR	MINOR	MAJOR	MINOR	MAJOR
GXM43 S.S=V	7	5	9	5	15	5
GXM43 T.S=V'	16	5	16	5-6	16-20	6
V+0.1% U.M	1-3	5-7	6	6	12-15	6
V+0.1% P.B	4	5	4	5	4	5
V+0.1% Q.R	1-2	5	1-2	5-6	3	5-6
V+0.1% Q.P	3	5	3-4	5	5	5
V+1% CHALK	2	5	4	5	6	5
V'+5% TALC	0	5	0	6	1	6

In addition, it was noted that a reduction in impact properties occurred with increased thermo-mechanical working of the homopolymer, this is probably associated with a reduction in molecular weight.

An analysis of fracture patterns revealed an increase in minor crack formation with impact strength. For example, in the case of talc filled polypropylene no minor crack formation was found and this was reflected by low impact energies. A summary of major and minor crack variations exhibited by each injection moulded feedstock is given in Table 43.

The force/time data revealed an increase in first peak force with increasing minor crack formation accompanied by a reduction in the propagation energy after the first peak. In all cases only one propagation peak was observed after the initiation of major cracks and time of reduced rigidity, i.e. the more minor cracks produced the less energy required to propagate them through the lateral dimensions of the plaque.

5.3 OPTICAL MICROSCOPY OF GXM43 iPP MOULDINGS CONTAINING LOW PERCENTAGE ADDITIONS OF PIGMENTS AND MINERAL FILLERS

A polarised light microscopy study of microtomed sections taken from Izod test pieces of the pigmented and filled polypropylene mouldings was made. Typical micrographs taken at selected areas along the flow direction of each moulded feedstock are shown in Figures 142 to 147. It was anticipated that the microstructural detail revealed by these sections would give an indication of the reasons why the impact properties of the moulding are caused to change with changes in compound formulations.

5.3.1 Ultramarine Blue

The effect of incorporating 0.1 wt.% Ultramarine Blue pigment on the microstructure of injection mouldings is illustrated in Figure 142. The micrographs show that Ultramarine Blue pigment caused an increase in the nucleation of β phase spherulites in the skin-core region of the mouldings. The structure of the core spherulites and the skin remained essentially the same as unpigmented plaques and therefore independent of pigmentation. However, the proportion of β spherulites extending into the core of the moulding, despite the reduction of shear forces, was found to be surprisingly high. In addition, an increase in the longitudinal distribution of these row nucleated β structures along the melt flow direction was also found.

The dispersion of Ultramarine Blue was assessed by viewing sections in transmitted light with the polariser removed. A micrograph showing typically well dispersed pigment particles is shown in Figure 142(d). The improved impact properties of these mouldings is at present not fully understood.

5.3.2 Phthalocyanine Blue

Light micrographs from mouldings containing the Pthalocyanine Blue pigment revealed that the pigment acted as a strong nucleating agent which caused a marked reduction in the size of spherulites in the core of the mouldings compared with that observed in the unpigmented mouldings. Figure 143(a) and 143(b) illustrate the structure of the 0.1 wt.% Phthalocyanine Blue injection mouldings in the surface regions and in the core respectively. The powerful nucleating effect is accompanied by relatively poor dispersion of the Pthalocyanine Blue pigment in polypropylene, a characteristic feature of this pigment,

Figure 142

Typical micrographs from selected areas of Ultramarine Blue pigmented iPP plaques.

Figure 143

Typical micrographs from selected areas of Pthalocyanine Blue pigmented plaque showing;
(a) surface region
(b) core region
(c) illustration of the poor dispersion.

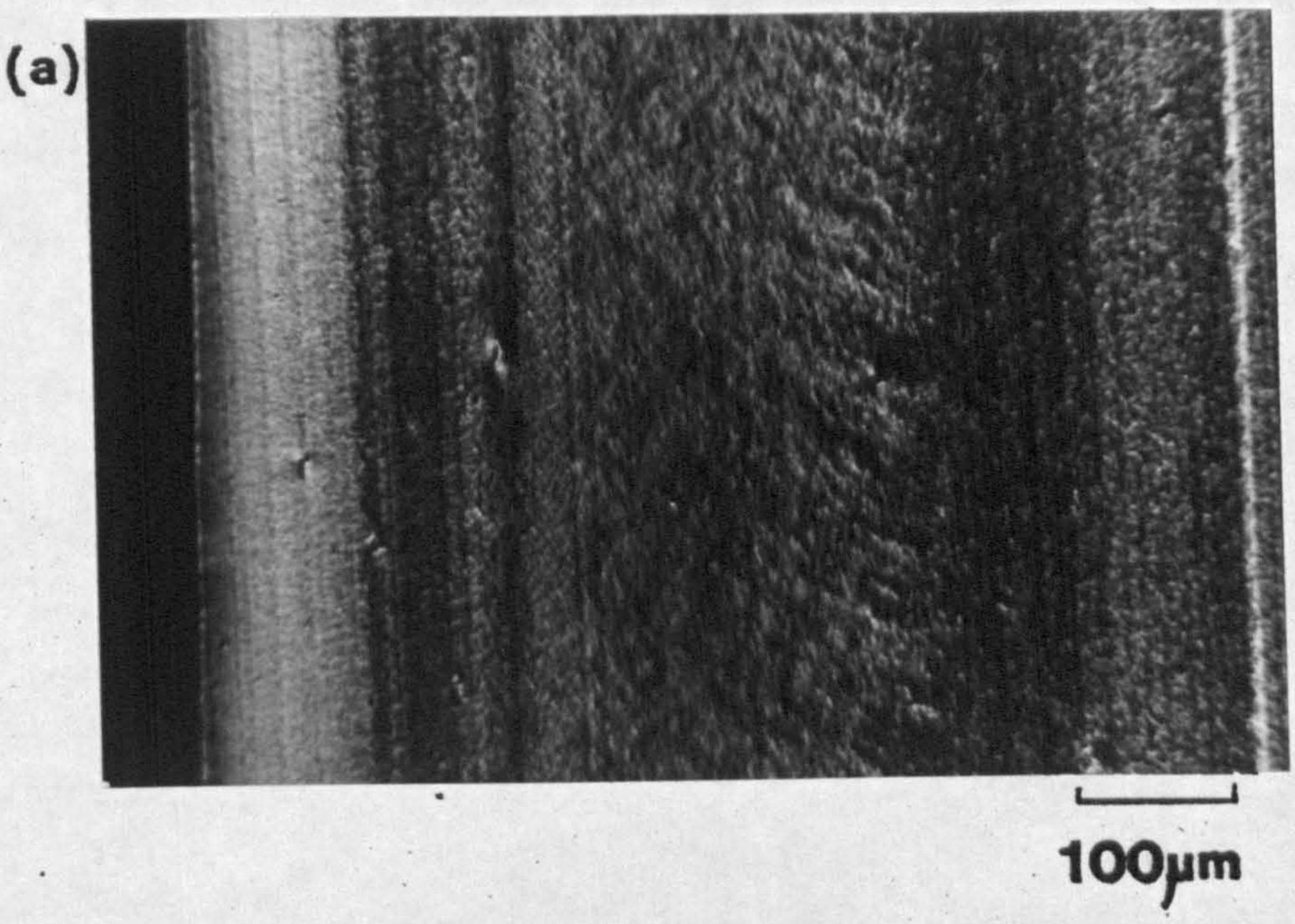

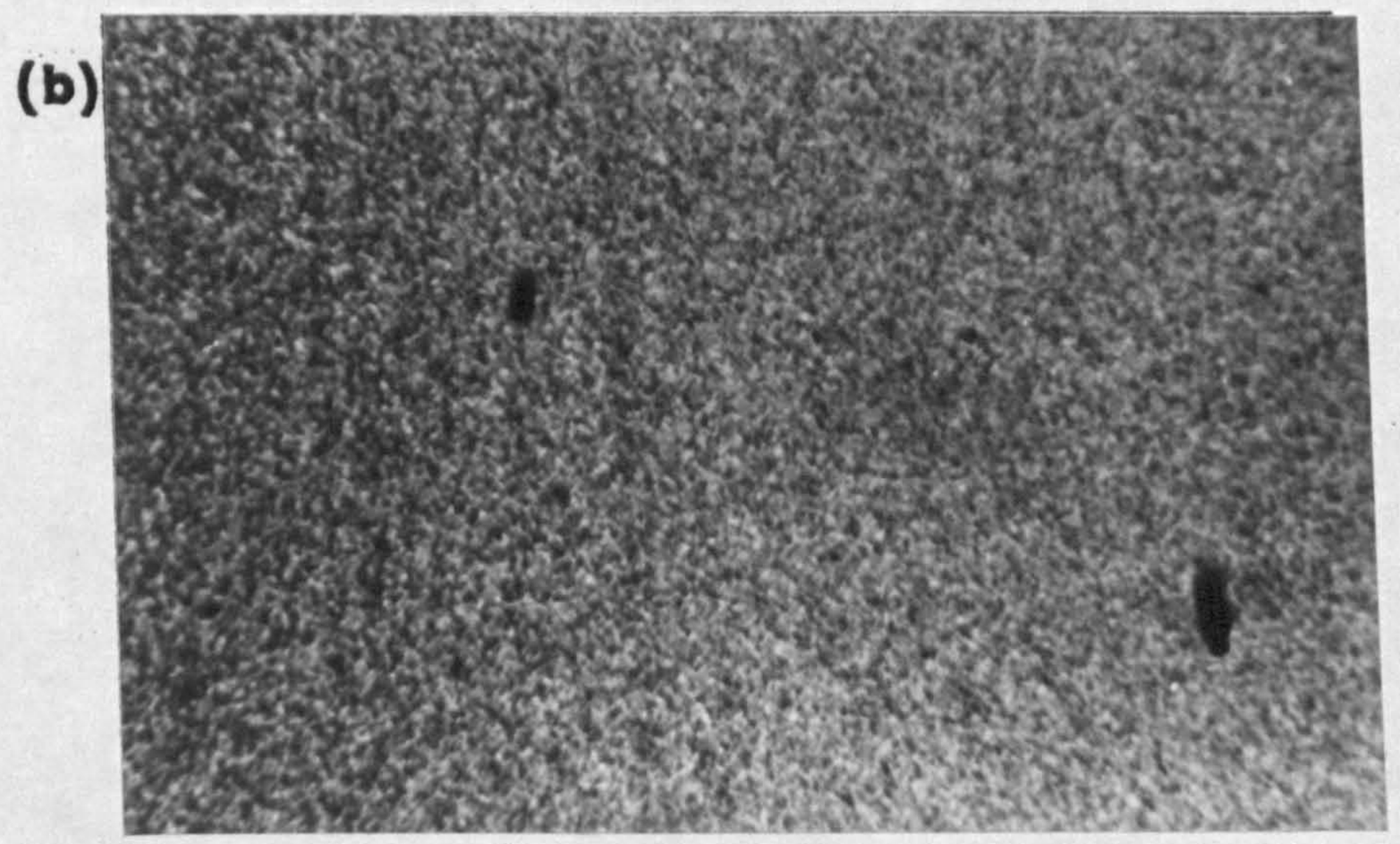

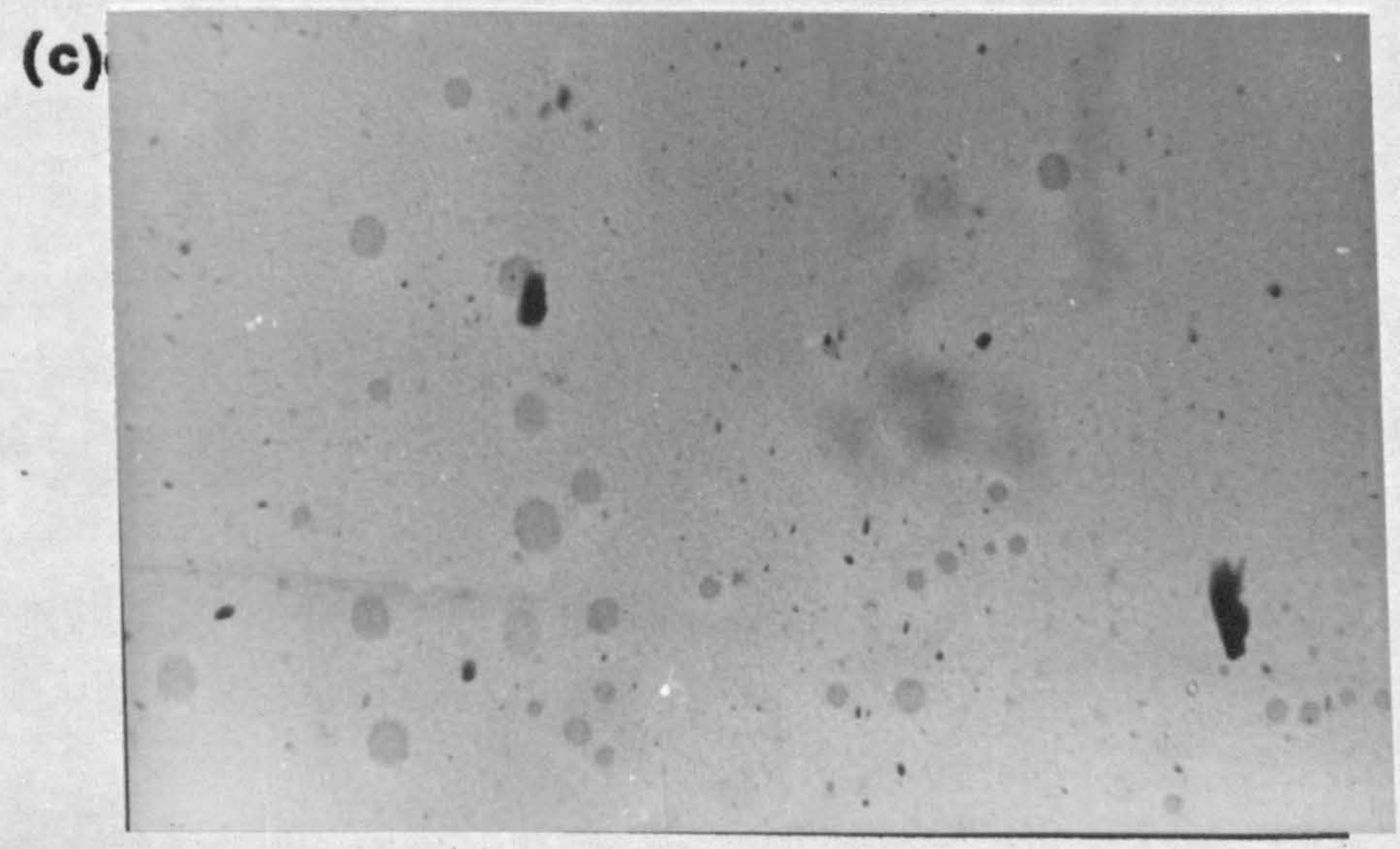

despite efforts to improve matters by extrusion prior to injection moulding. Figure 143(c) illustrates this poor dispersion even at such low loadings showing distinct agglomeration of the pigment particles. This observation indicated that apart from the nucleating effect the presence of pigment agglomerates may be attributed to the marked reduction in the impact strength of mouldings.

5.3.4 Quinacridone Red E3B

The effect of adding 0.1 wt.% of Quinacridone Red pigment to polypropylene on the microstructure of injection mouldings is illustrated in Figures 144(a) and 144(b). The former shows a low magnification micrograph taken 20mm along the flow direction, the width of the skin and the row nucleated band do not appear to be effected, however, no noticeable β phase nucleation can be seen. The latter shows a higher magnification micrograph of the core spherulites revealing a powerful α nucleation effect.

The size of core spherulites are even smaller than those found in Pthalocyanine Blue pigmented plaques. The dispersion of the pigment was in this case excellent as shown in Figure 144(c). It appeared at this stage that the marked reduction in impact properties could be simply attributed to the nucleating effect of the pigment.

5.3.5 Quinacridone Pink E

The micrographs taken from Quinacridone Pink pigmented polypropylene injection mouldings revealed similar microstructures to those found in Quinacridone Red pigmented polypropylene mouldings i.e. significant nucleation of core spherulites aided by excellent dispersion of the pigment. A typical microstructure

Figure 144

Typical micrographs from selected areas of Quinacridone Red E3B pigmented iPP plaques showing;
(a) surface region
(b) core region
(c) illustration of the excellent pigment dispersion.

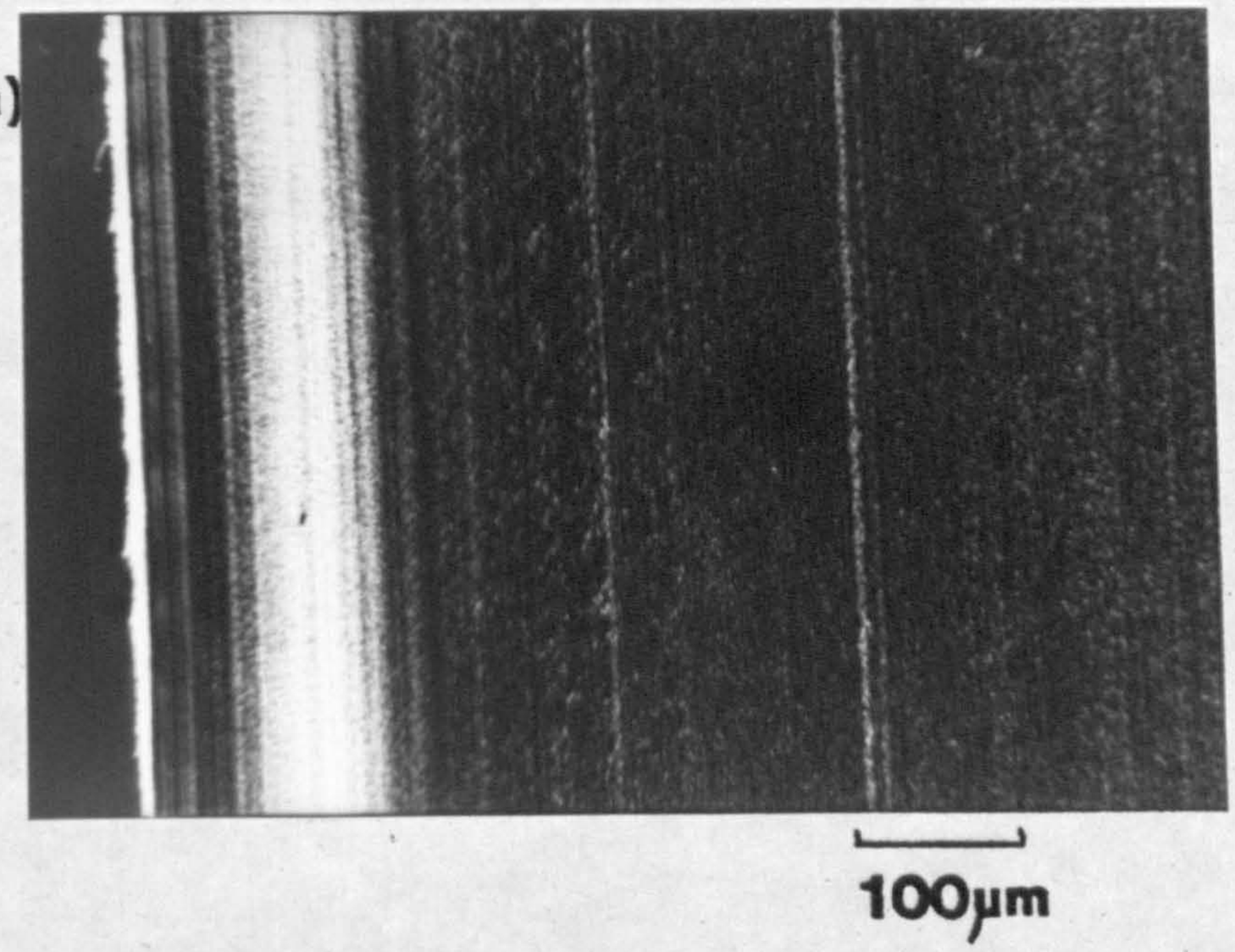

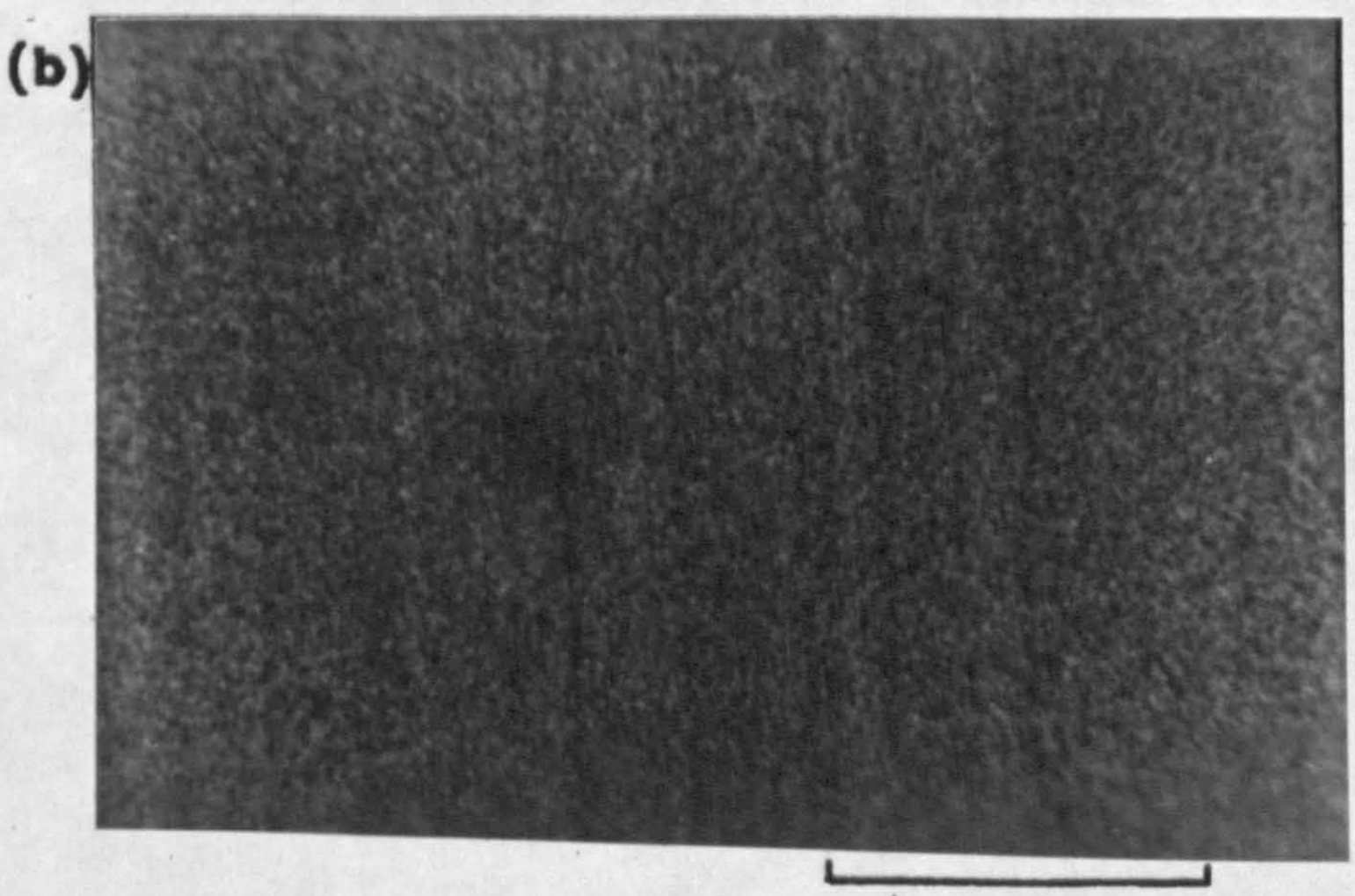

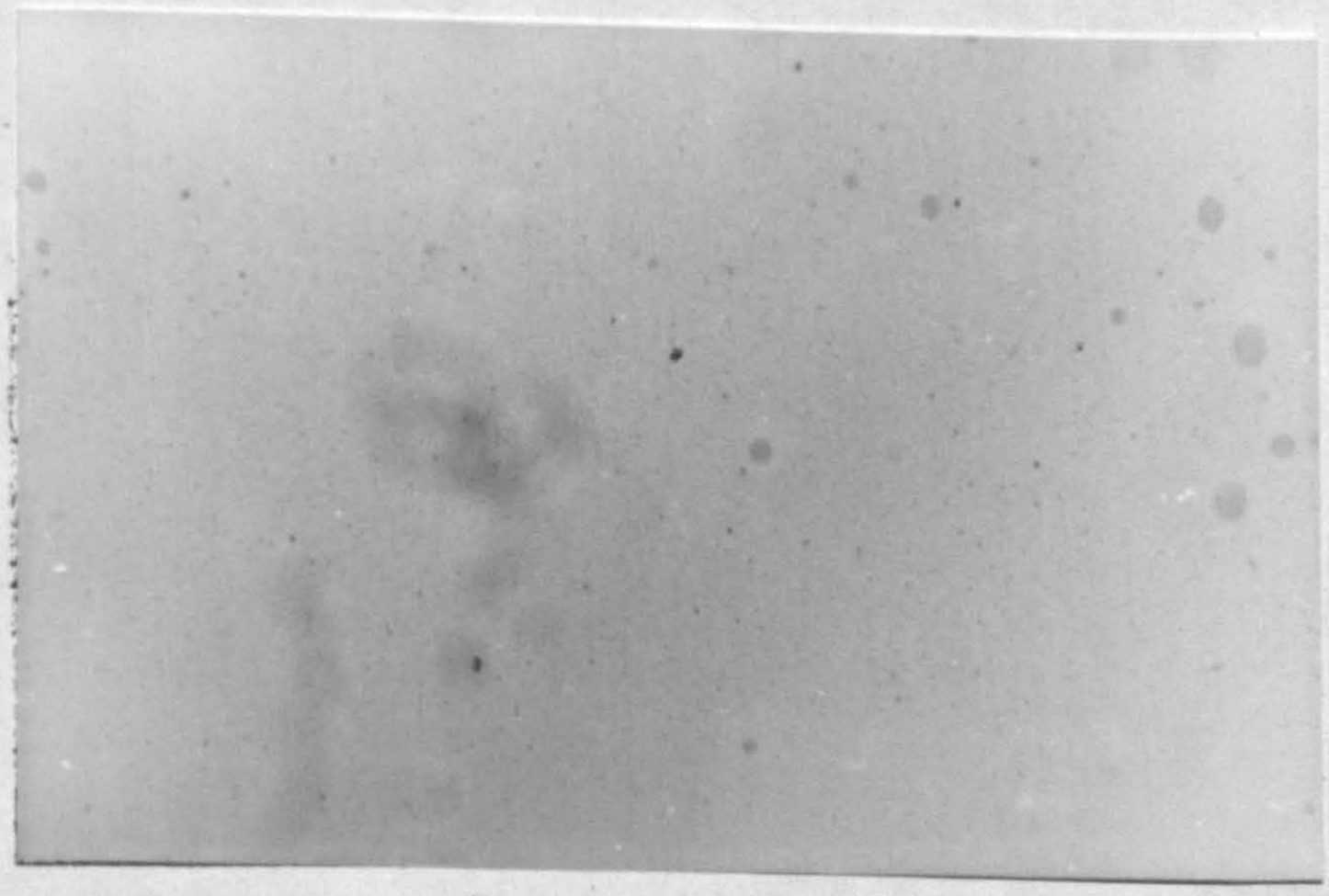

Figure 145

A typical Quinacridone Pink E pigmented iPP microstructure.
(a) surface region
(b) core region
(c) illustration of the excellent pigment dispersion.

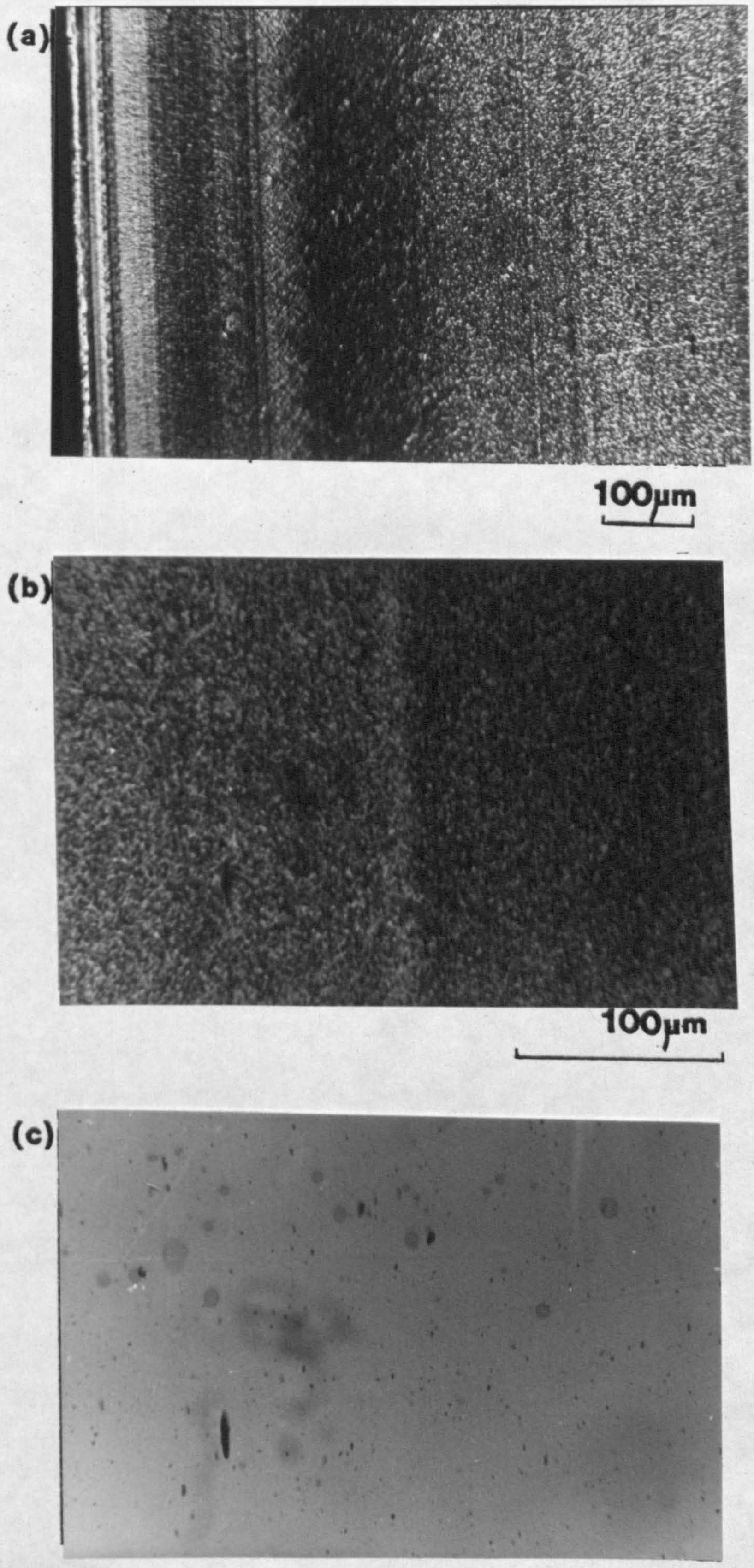

is illustrated in Figure 145. No β phase nucleation was observed in these pigmented mouldings.

5.3.6 Chalk

Injection mouldings containing 1 wt.% of chalk filler revealed an increase in the proportion of β negatively birefringent spherulites in the skin-core region of the mouldings as shown in Figure 146(a). The structure of the core spherulites shown in Figure 146(b) appeared essentially unchanged except for the deposition of small chalk particles. In the gate region of mouldings a normal β phase row nucleation effect occurred which suprisingly extended beyond 70mm along the flow direction, the β spherulites did however appear to be much more randomly nucleated beyond 40mm in a similar manner to that found in Ultramarine Blue pigmented plaques.

The impact properties of chalk filled polypropylene mouldings do not appear to be significantly affected by this higher concentration of randomly nucleated β phase spherulites in the same way as Ultramarine Blue pigmented plaques were. This may be due simply to dispersion problems.

5.3.7 Talc

Light micrographs shown in Figure 147 revealed the powerful nucleating ability of talc in polypropylene. The presence of small α phase spherulites in the core of mouldings illustrates this nucleating effect despite the apparent absence of any β phase spherulites. As with Phthalocyanine Blue the poor impact properties may also be attributed to the dispersion problems that occurred despite careful preparation of talc filled iPP feedstocks using the twin screw extruder. An example of the dispersion problems is shown in Figure 147(c)

Figure 146

Typical micrographs from a Chalk filled iPP moulded plaque showing;
(a) surface region
(d) core region

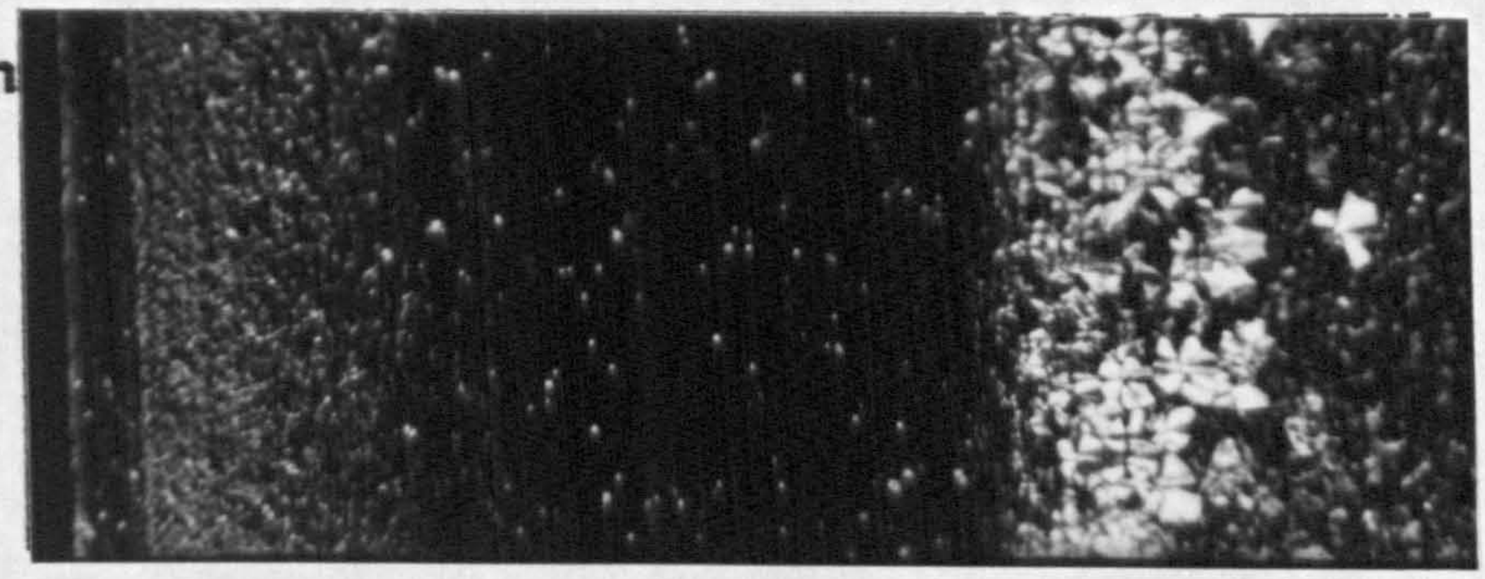

Figure 147

Typical micrographs from talc filled iPP moulded plaque showing;
(a) surface region
(b) core region
(c) an illustration of the dispersion problems encountered.

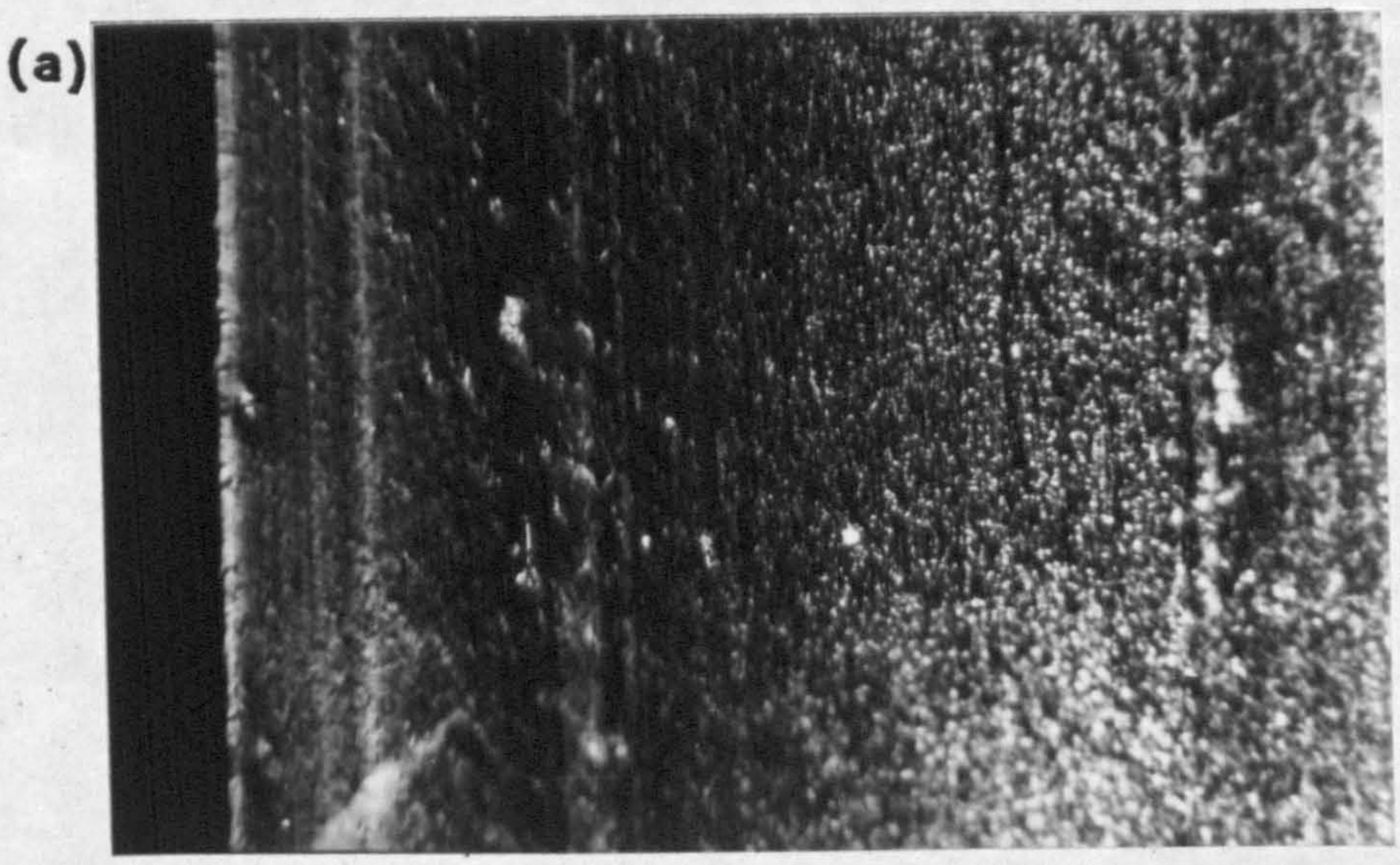

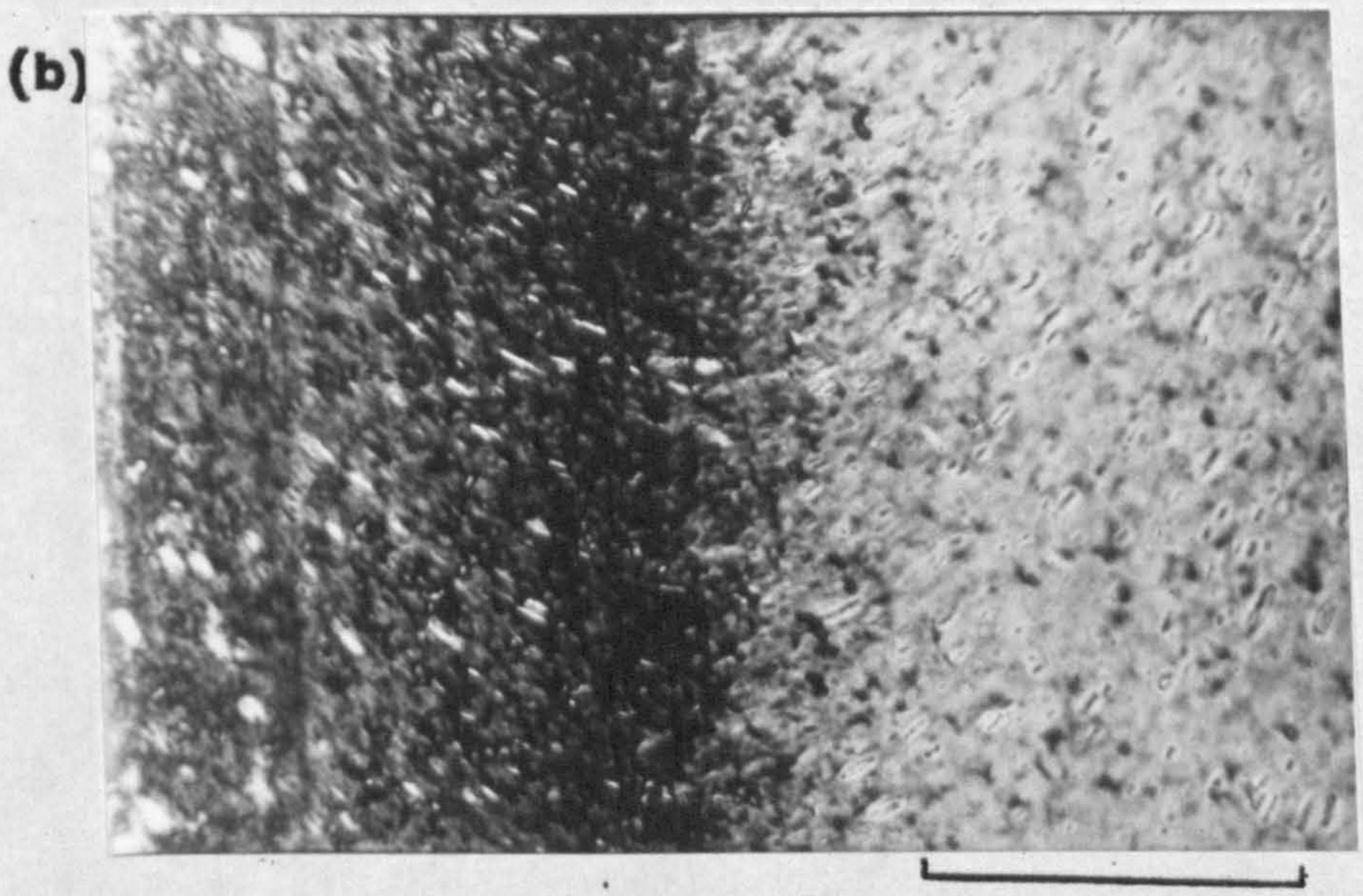

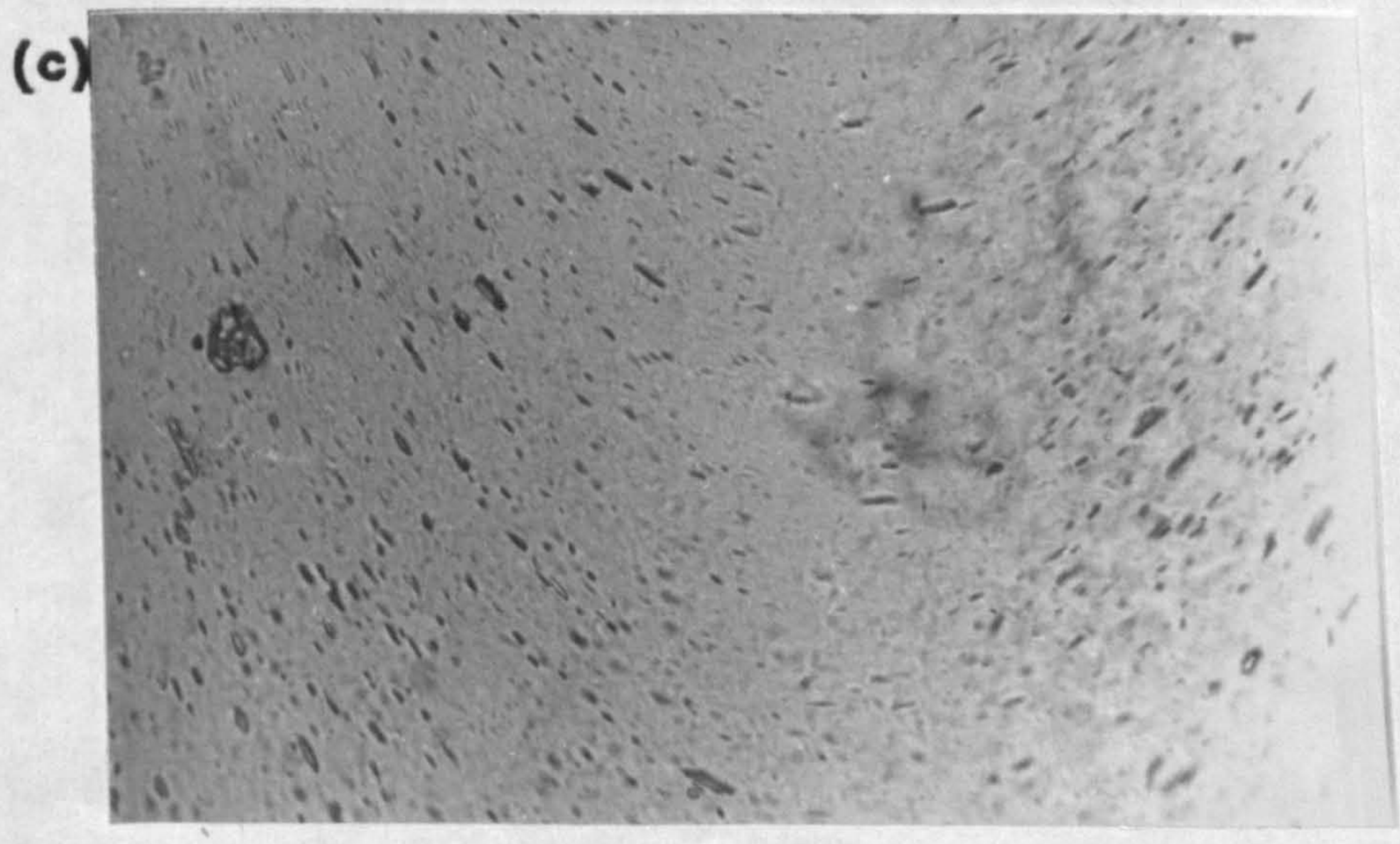

where some talc agglomeration occurred during processing is illustrated.

5.4 EFFECT OF NUCLEANTS ON CRYSTALLINE POLYMORPHISM AND ORIENTATION IN iPP GXM43 INJECTION MOULDINGS

The x-ray diffractometer was again used to determine the longitudinal distribution and degree of crystallinity, β phase nucleation and α phase orientation, in the surface layers of mouldings incorporating low percentages of mineral fillers and pigments. The diffractograms of eight 10mm x 10mm x 3mm samples cut from each moulding were indexed as before (Section 2.8.7.) and the results are given in Table 44. Plots of β phase Index B, Crystallinity Index C and Orientation Index A versus distance along the flow direction are given in Figures 148 to 150 for each of the filled mouldings. The following observations were made as regards each additives effect on the x-ray diffraction results of GXM43 iPP injection mouldings:-

Prior to x-ray diffraction studies on these mouldings powder diffractograms for each additive were recorded using copper Kα radiation. These diffractograms are presented in Figure 151 (a) - (f).

5.4.1 Ultramarine Blue

1. β Phase Concentration and Distribution

The β phase concentration and distribution was greatly enhanced with the addition of 0.1 wt.% of Ultramarine Blue pigment. The β spherulites appear to be nucleating across the entire melt flow direction in the pigmented mouldings with an Index maximum reaching 0.341 compared to 0.179 in the unpigmented plaques. This result is in good agreement with polarised light microscopy observa-

TABLE 44 X-ray diffraction results for iPP compounds.

MOULDING CONDITION	DISTANCE FROM GATE (mm)	PEAK HEIGHT (mm) hα1	hα2	hα3	hα4	hβ	CRYST. INDEX ha	C	B-PHASE INDEX B	-PHASE INDEX A
	0-10	100	190	64	28	42	38	2.232	.106	.781
	10-20	85	188	54	36	62	40	2.125	.159	.702
	20-30	75	160	46	38	49	36	2.044	.148	.664
	30-40	61	94	32	40	72	33	1.812	.278	.604
V+0.1% U.M	40-50	56	84	32	46	89	33	1.861	.341	.549
	50-60	56	68	34	47	63	32	1.675	.285	.544
	60-70	57	61	33	52	20	32	1.394	.117	.523
	70-80	65	54	34	55	0	33	1.261	.000	.542
	0-10	92	158	55	33	27	39	1.872	.081	.736
	10-20	97	241	58	32	67	39	2.538	.145	.752
	20-30	81	152	41	38	31	38	1.805	.102	.681
	30-40	77	140	40	43	0	34	1.765	.000	.642
V+0.1% P.B	40-50	78	154	42	41	0	36	1.750	.000	.655
	50-60	75	148	38	38	0	35	1.709	.000	.664
	60-70	77	143	38	37	0	35	1.686	.000	.675
	70-80	76	126	35	41	0	33	1.685	.000	.650
	0-10	92	270	55	22	132	42	2.719	.240	.807
	10-20	65	272	40	25	162	37	3.049	.301	.722
	20-30	55	270	32	25	175	37	3.011	.329	.688
	30-40	35	265	22	30	195	35	3.126	.377	.538
V+0.1% Q.R	40-50	32	307	20	27	255	40	3.205	.415	.542
	50-60	27	342	17	27	315	40	3.640	.449	.500
	60-70	32	342	17	25	315	42	3.481	.446	.561
	70-80	35	312	28	30	305	41	3.463	.449	.538
	0-10	110	222	59	29	42	40	2.310	.097	.791
	10-20	89	203	49	33	33	38	2.142	.088	.730
	20-30	79	151	42	39	0	34	1.829	.000	.669
	30-40	66	124	36	45	0	36	1.506	.000	.595
V+0.1% Q.P	40-50	71	154	37	41	0	35	1.731	.000	.634
	50-60	75	159	43	39	0	36	1.756	.000	.658
	60-70	70	131	40	35	0	32	1.725	.000	.667
	70-80	85	149	44	43	0	37	1.735	.000	.664
	0-10	85	152	54	25	36	31	2.271	.110	.773
	10-20	78	182	52	29	60	32	2.506	.161	.729
	20-30	69	133	40	29	51	28	2.300	.174	.704
V+1% CHALK	30-40	55	93	32	34	72	28	2.043	.286	.618
	40-50	46	69	26	31	99	25	2.168	.413	.597
	50-60	41	61	25	35	112	27	2.030	.469	.539
	60-70	44	53	24	37	53	25	1.688	.305	.543
	70-80	33	31	17	30	0	15	1.480	.000	.524

TABLE 44 X-ray diffraction results for iPP compounds. cntd.

MOULDING CONDITION C C %		PEAK (mm) hα1	hα2	hα3	hα4	hβ	ha	C	B	A
V+5% TALC	0-10	52	377	30	20	35	37	2.778	.071	.722
	10-20	35	395	32	12	37	32	3.194	.074	.745
	20-30	35	435	42	20	37	35	3.251	.067	.636
	30-40	35	457	42	15	35	35	3.337	.062	.700
	40-50	35	417	40	15	37	35	3.109	.070	.700
	50-60	27	490	35	15	45	35	3.497	.075	.643
	60-70	25	497	35	17	0	32	3.588	.000	.595
	70-80	23	495	37	17	0	35	3.269	.000	.575
GXM43=V	0-10	110	207	70	32	41	41	2.244	.096	.775
	10-20	94	262	63	36	68	41	2.551	.140	.723
	20-30	78	154	46	43	45	39	1.877	.139	.645
	30-40	67	104	40	47	46	35	1.737	.179	.588
	40-50	62	82	36	51	32	34	1.547	.151	.549
	50-60	66	70	38	54	0	33	1.382	.000	.550
	60-70	67	71	38	56	0	35	1.326	.000	.545
	70-80	62	53	32	56	0	34	1.194	.000	.525
GXM43 T.S=V'	0-10	84	205	53	41	29	42	1.962	.078	.672
	10-20	57	118	35	47	24	34	1.653	.103	.548
	20-30	64	88	35	51	20	35	1.474	.097	.557
	30-40	61	86	37	50	23	35	1.469	.111	.550
	40-50	59	74	35	46	13	35	1.297	.072	.562
	50-60	58	64	30	50	0	34	1.188	.000	.537
	60-70	66	62	33	54	0	34	1.265	.000	.550
	70-80	60	59	36	51	0	31	1.329	.000	.541

Figure 148 Longitudinal distribution of B values for the various iPP compounds.

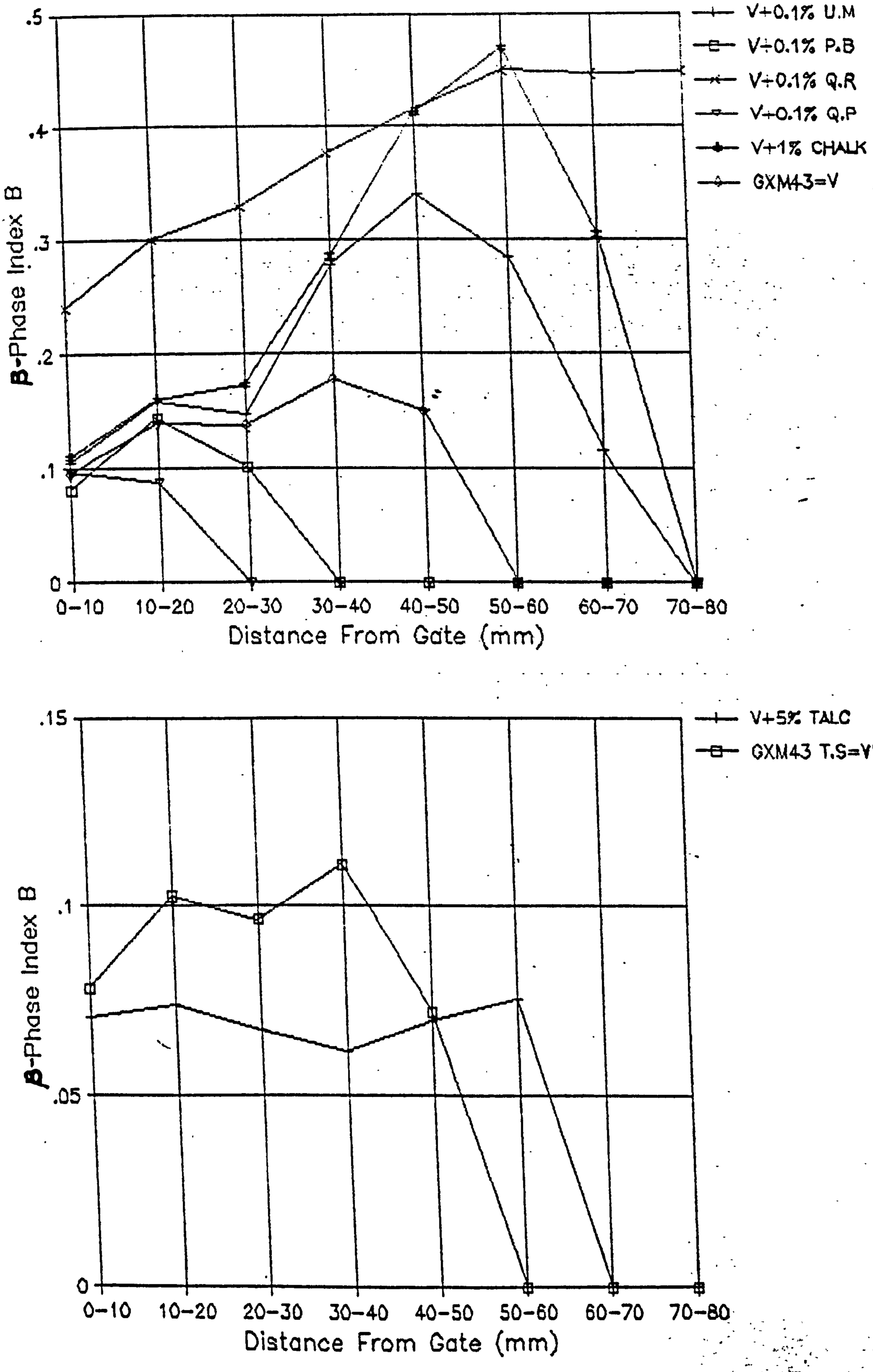

Figure 149 Longitudinal distribution of C values for the various iPP compounds.

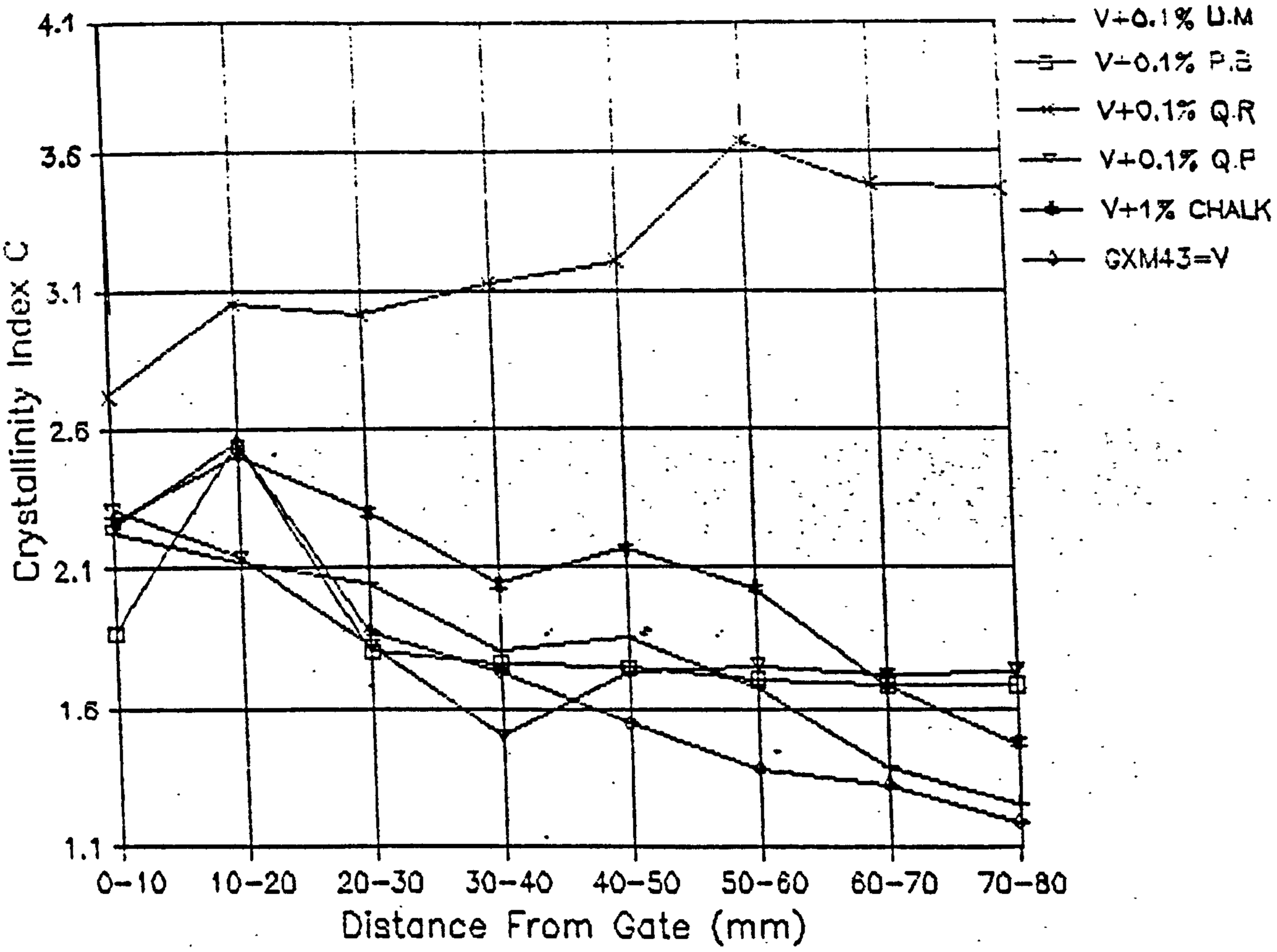

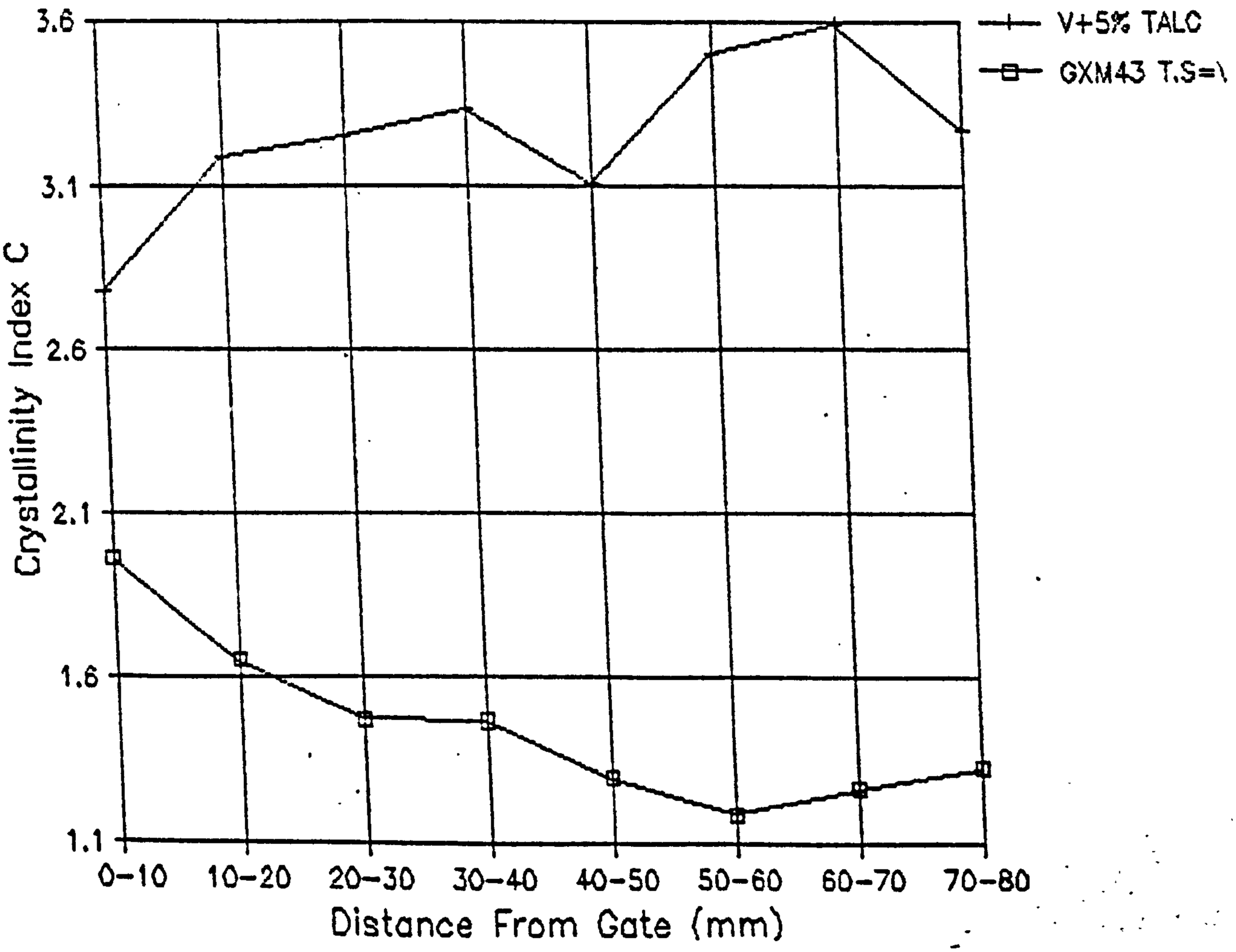

Figure 150 Longitudinal distribution of A values for the various iPP compounds.

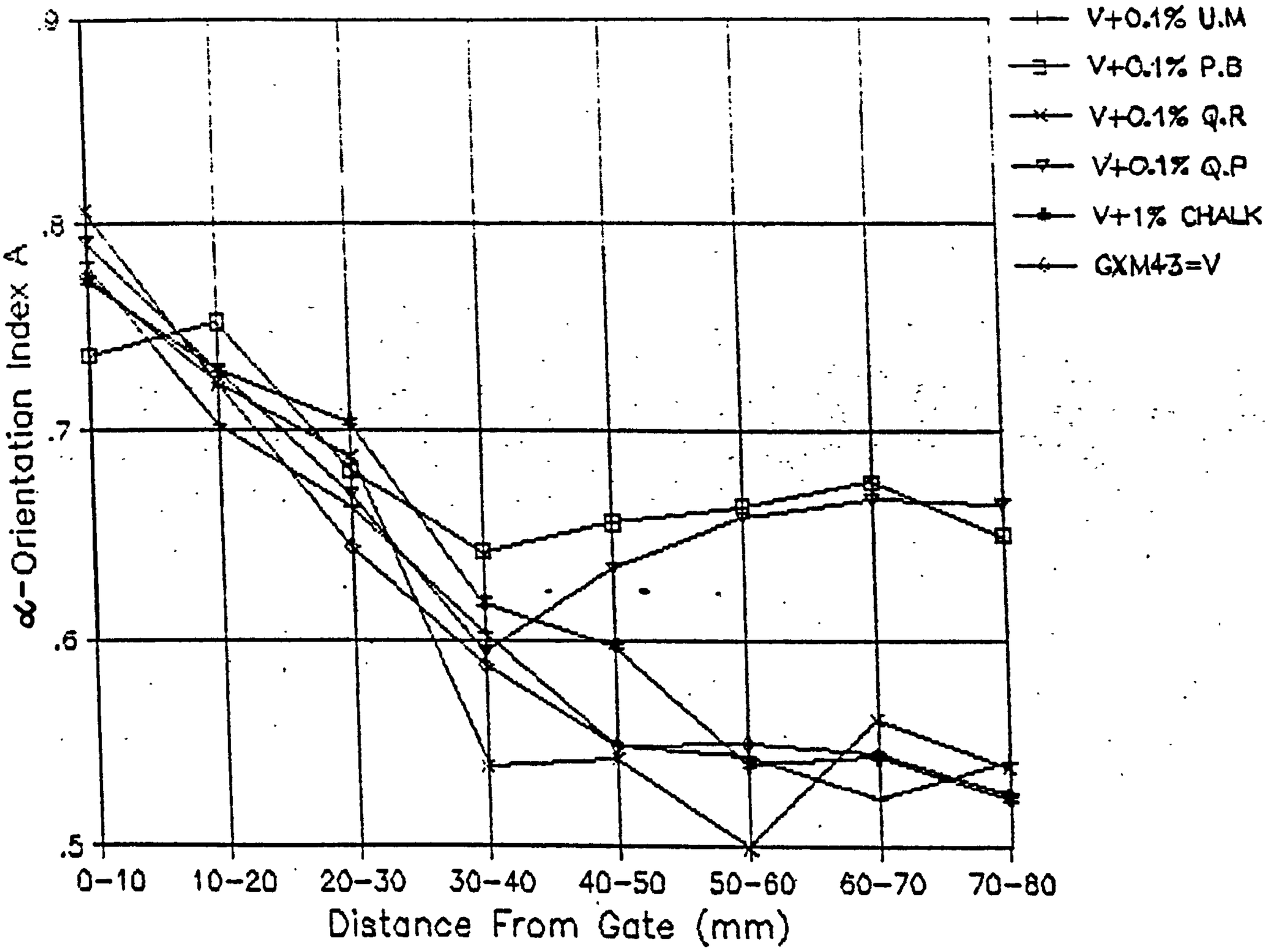

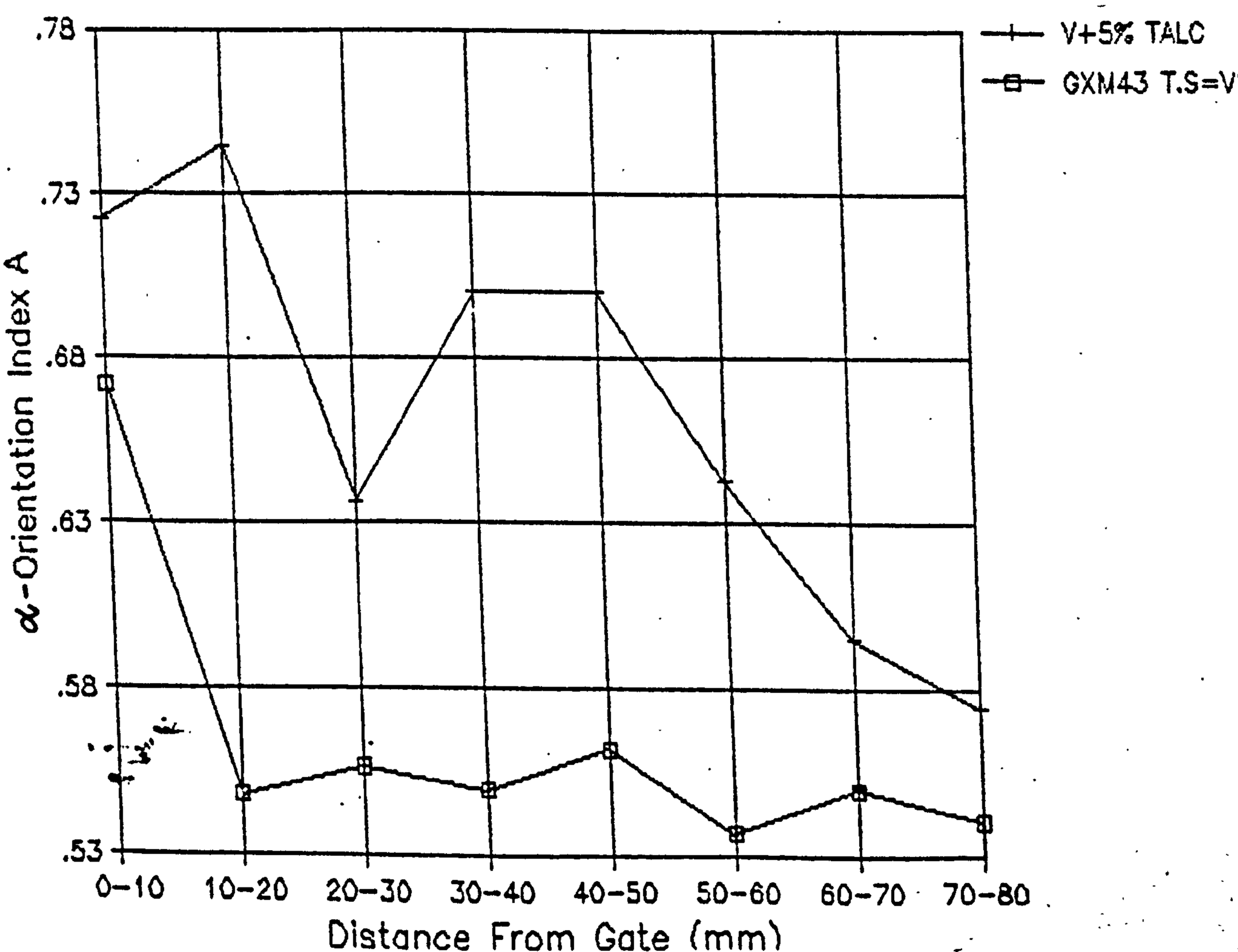

Figure 151 (a - e) Powder x-ray diffractograms for each additive incorporated.

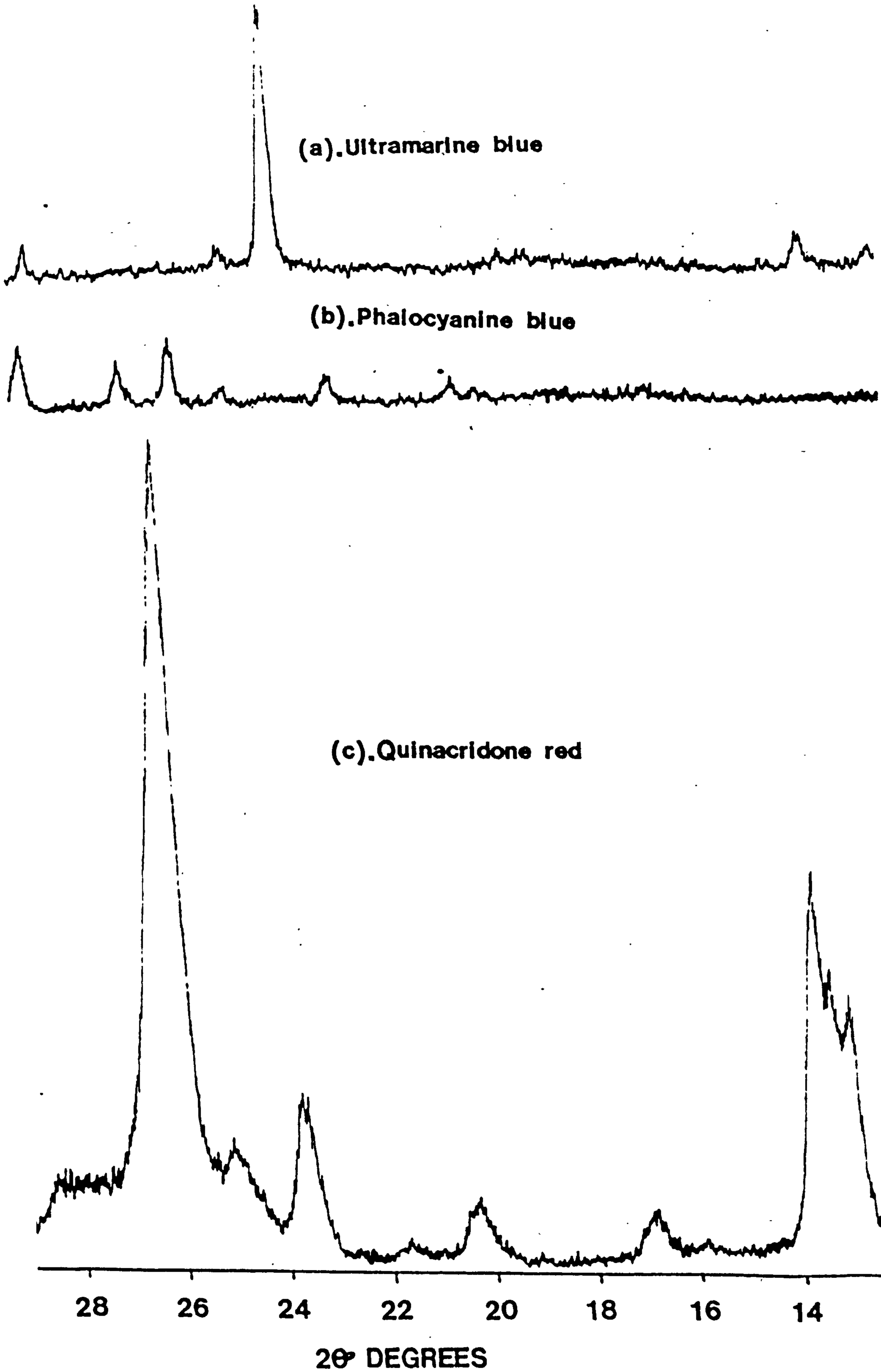

(d).Quinacridone pink

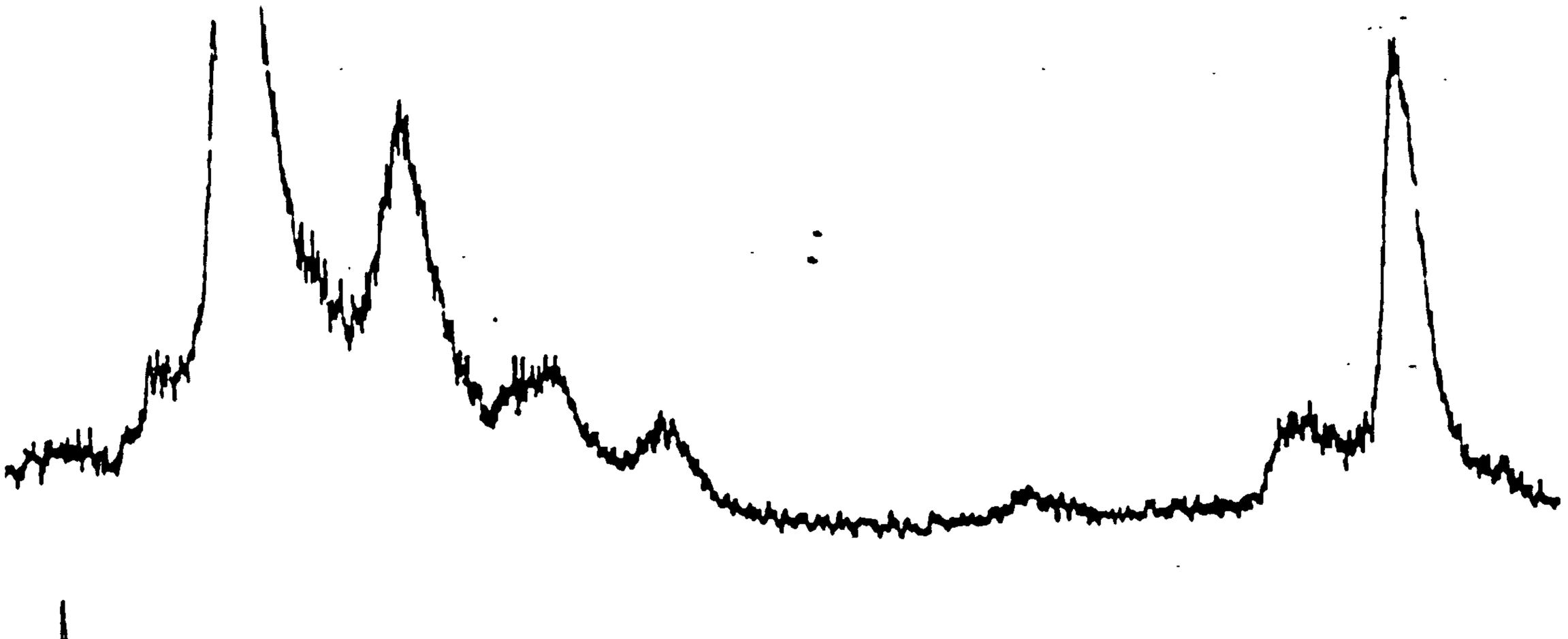

(e).Chalk

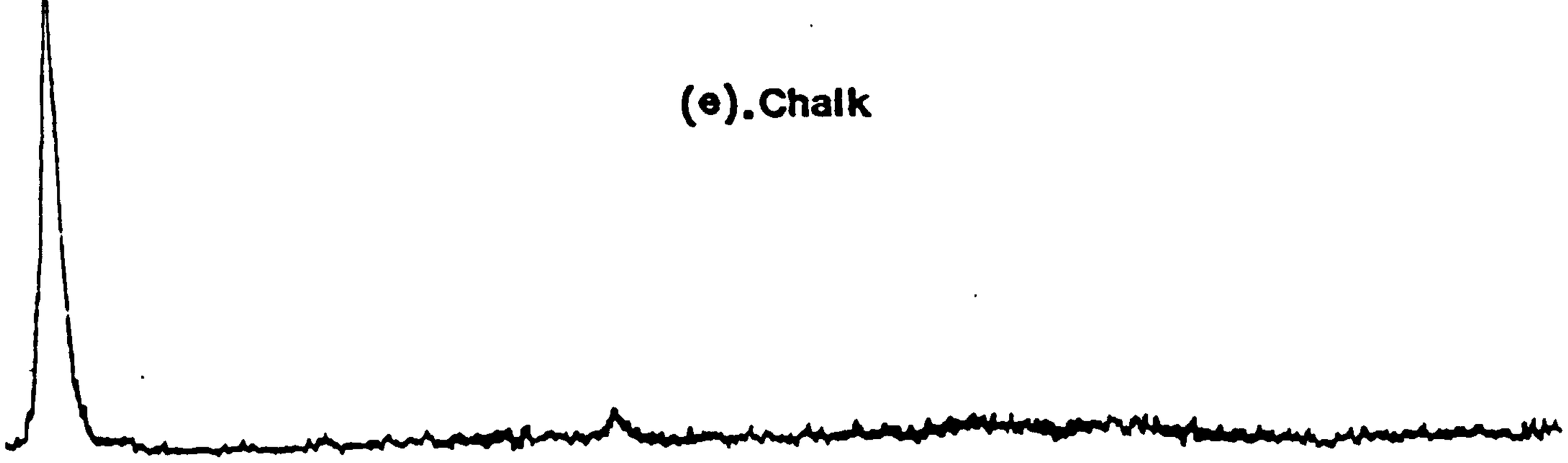

(f).Talc

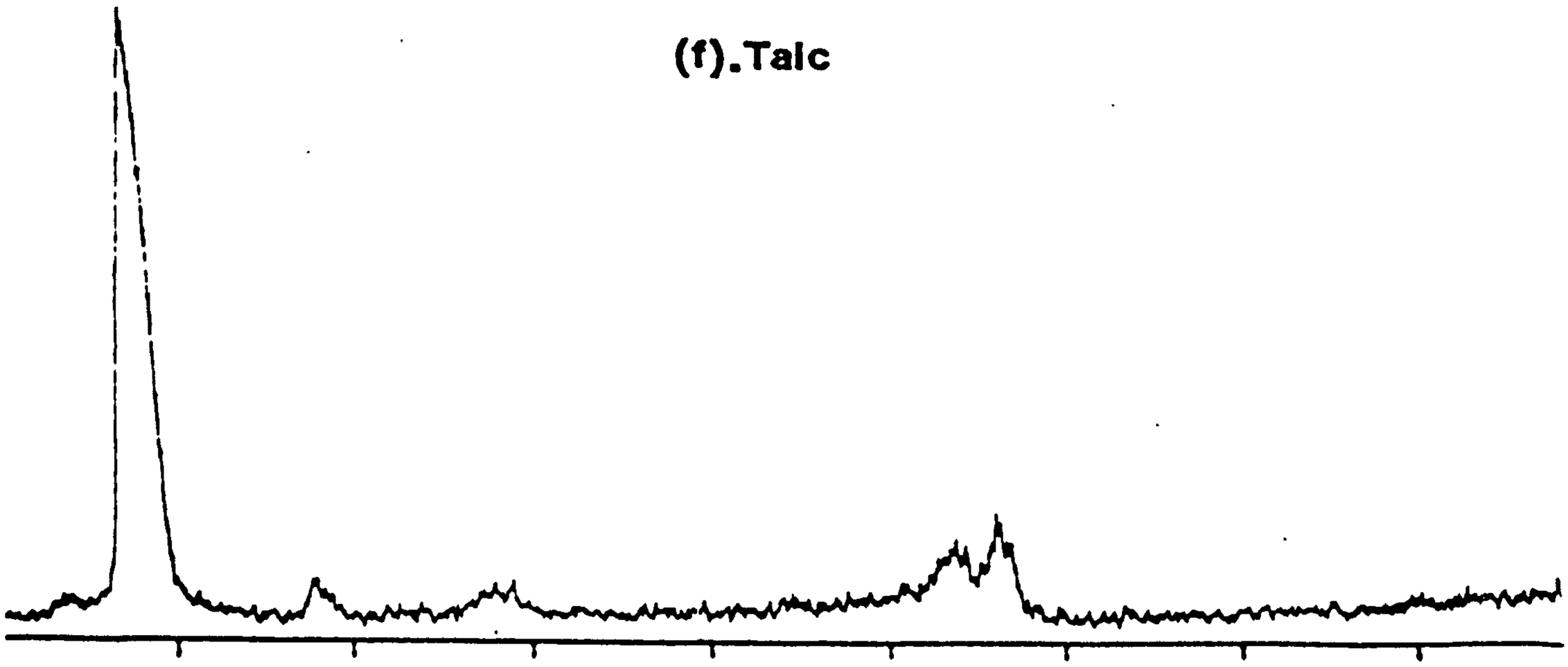

2θ° DEGREES

tions which revealed high concentrations of randomly nucleating β phase spherulites.

2. Crystalline Fraction

A marginal increase in the longitudinal degree of crystallinity was observed in pigmented mouldings. This enhanced crystallinity corresponds to a noticed increase in α-spherulite size found in optical studies. The large contribution of the β phase to surface crystallinity is also a factor to consider.

5.4.2 Phthalocyanine Blue

1. β-phase Concentration and Distribution

The β phase concentration in the gate area of pigmented mouldings does not appear to be significantly different to that found in unpigmented mouldings. However, the distribution across the melt flow direction of the β phase was reduced with the incorporation of the pigment.

2. Crystalline Fraction

The overall longitudinal concentration of crystallinity was increased with pigmentation of mouldings particularly at the far end of the melt flow path. This increase in crystallinity was observed optically as a dramatic reduction in spherulite sizes indicating a massive nucleation effect. The phthalocyanine Blue pigmented mouldings have shown a generally improved homogeneity of crystallinity across the melt flow direction.

5.4.3 Quinacridone Pink E

1. β phase Concentration and Distribution

The level of β phase nucleation was very similar in the gate area samples of pigmented and unpigmented mouldings. However, as with the Phthalocyanine Blue pigmented plaques the longitudinal distribution of the β phase was

significantly reduced with low percentage additions of this quinacridone pigment.

2. Crystalline Fraction

The addition of Quinacridone Pink E in low percentages appears to have had little effect on the degree of crystallinity in the first half of the mouldings, up to 50mm along the flow direction. The crystallinity between 50mm and 80mm though was somewhat higher in pigmented mouldings leading to an overall improvement in homogeneity of crystallinity as found with the Phthalocryanine Blue pigmented plaques.

5.4.4 Quinacridone Red E3B

1. β -phase Concentration and Distribution

The addition of 0.1 wt.% of this pigment led to a dramatic increase in the concentration and distribution of the β phase spherulites across the melt flow direction. This pigment was clearly the most powerful β phase nucleant for isotactic polypropylene found.

2. Crystalline Fraction

The crystallinity of E3B pigmented mouldings was found to be very high and reasonably homogeneous across the melt flow direction. Optical studies revealed massive nucleation and consequently very small spherulitic structures in these mouldings.

5.4.5 Chalk

1. β phase Concentration and Distribution

The β phase concentration and distribution was suprisingly high in chalk filled polypropylene mouldings since no nucleation effect was expected. The concentration of the β form gave an Index as high as 0.469 which was not surpassed

by any other additive used. The extent of β nucleation suggests that chalk, contrary to previous publications, can act as a nucleant. Optical studies on chalk filled mouldings revealed no noticeable α phase nucleation effect, but in agreement with these x-ray diffraction results an increase in the proportion of β phase spherulites throughout was shown.

2. Crystalline Fraction

The degree of crystallinity in the vicinity of the gate was not significantly altered with the addition of 1% by wt. of chalk to polypropylene injection mouldings. However, a contribution of the β phase spherulities to the overall surface crystalline fraction at the far side of the moulding was observed.

5.4.6 Talc

1. β phase Concentration and Distribution

Injection moulding of twin screw extruded iPP containing 5% by wt. of talc resulted in an increase in β phase distribution along the melt flow direction, but a reduction in its concentration.

2. Crystalline Fraction

Talc is clearly a good heterogeneous nucleating agent for polypropylene crystallisation. A high degree of crystallinity was found across the entire moulding of talc filled plaques despite the low percentage of β phase crystallites.

5.4.7 Summary of X-ray Diffraction Results On Pigment And Mineral Filled Polypropylene Injection Mouldings

(i) Low percentage additions of fine particle sizes of Quinacridone Red E3B, Chalk and Ultramarine Blue in GXM43 iPP homopolymer caused a significant increase in the nucleation of the β phase crystallites during the moulding process.

(ii) Low percentage additions of Phthalocyanine Blue and Quinacridone Pink E pigments caused a reduction in the concentration and distribution of the β phase along the melt flow direction in polypropylene injection mouldings accompanied by an increase in α nucleation.

(iii) The incorporation of 5 wt.% talc and 0.1 wt.% Quinacridone E3B in iPP injection mouldings caused a dramatic increase in the degree of crystallinity within the surface layers of plaques.

(iv) Despite the large differences in nucleation effects produced by incorporating low percentages of pigments and fillers in polypropylene feedstocks prior to moulding, no noticeable effects were observed on the preferred α phase orientation of the c-axis with respect to the flow direction. However, in all mouldings a gradual reduction in surface preferred orientation was observed with distance along the flow direction from the gate area.

(vi) In all cases the x-ray observations agree with optical studies with respect to the large degree of structural heterogeneity along the melt flow direction and the variations in nucleation of the α and β crystallites within polypropylene injection mouldings.

5.5 DSC STUDIES ON PIGMENTED AND MINERAL FILLED iPP INJECTION MOULDINGS

A large degree of super cooling has been observed in polypropylene injection mouldings by analysis of the re-crystallisation behaviour using the DSC. The presence of heterogeneous nucleating agents can alter the amount of supercooling given that the more effective the nucleant the greater the reduction in supercooling i.e. the higher the polymer freezing point. A thermal analysis of the polypropylene injection mouldings

containing low percentages of various additives was made to not only give some information on the melting behaviour, but also on the nucleating effect of each additive by observing their effect upon the polymer recrystallisation temperature T_c.

5.5.1 Melting And Recrystallisation Behaviour Of iPP Compounds

Samples (~5mg) were taken from an area 20mm along the flow direction, through the thickness of injection mouldings, and analysed using the DSC according to the procedure given in Section 2.6.4. A summary of the melting and recrystallisation characteristics are given in Table 45 and typical melting and recrystallisation curves are shown in Figures 152 to 158. From these curves and the results presented in Table 45 the following observations were made:-

(i) Polypropylene mouldings incorporating 0.1 wt.% of Ultramarine Blue or 1 wt.% Chalk have an increased concentration of the β form as shown by the well defined melting endotherms at 415, and 422k. However, in both cases the overall degree of supercooling was slightly increased indicating a reduction in the α form nucleation. Similar degrees of crystallinity are found in these mouldings.

(ii) Polypropylene mouldings incorporating 0.1 wt.% of Quinacridone E3B exhibited some β formation as seen by a small β endotherm. However, the degree of supercooling was reduced by some 14° indicating enhanced α form nucleation.

(iii) Polypropylene mouldings incorporating 0.1 wt.% of Quinacridone Pink E or 0.1 wt.% Phthalocyanine Blue caused a reduction in the level of β formation, no β endotherms were identified as a result. However, the degree of supercooling was reduced by 15° and 13° for

TABLE 45 DSC analysis of iPP moulded compounds.

iPP COMPOUND	MELTING PEAK TEMPERATURE β1	β2	α1	α2	HEAT OF FUSION (cal/gram)	ONSET Tc	Tc	DEGREES SUPERCOOL
GXM43=V		422.66	431.00	437.66	20.68	387.88	384.46	49.78
V+0.1% U.B	415.14	422.71	430.54	438.30	18.29	387.82	383.58	54.72
V+0.1% P.B				436.41	19.15	403.55	399.86	36.55
V+0.1% Q.B	415.64			436.78	19.98	404.71	400.87	35.91
V+0.1% Q.P				434.69	19.61	403.30	399.94	34.75
V+1% CHALK	415.15	422.32	430.96	437.09	18.14	388.05	384.51	52.58
V+5% TALC	414.76	422.38	431.19	434.88	17.09	399.24	395.67	39.21

Figure 152 Melting behaviour of Ultramarine Blue pigmented PP moulded plaques.

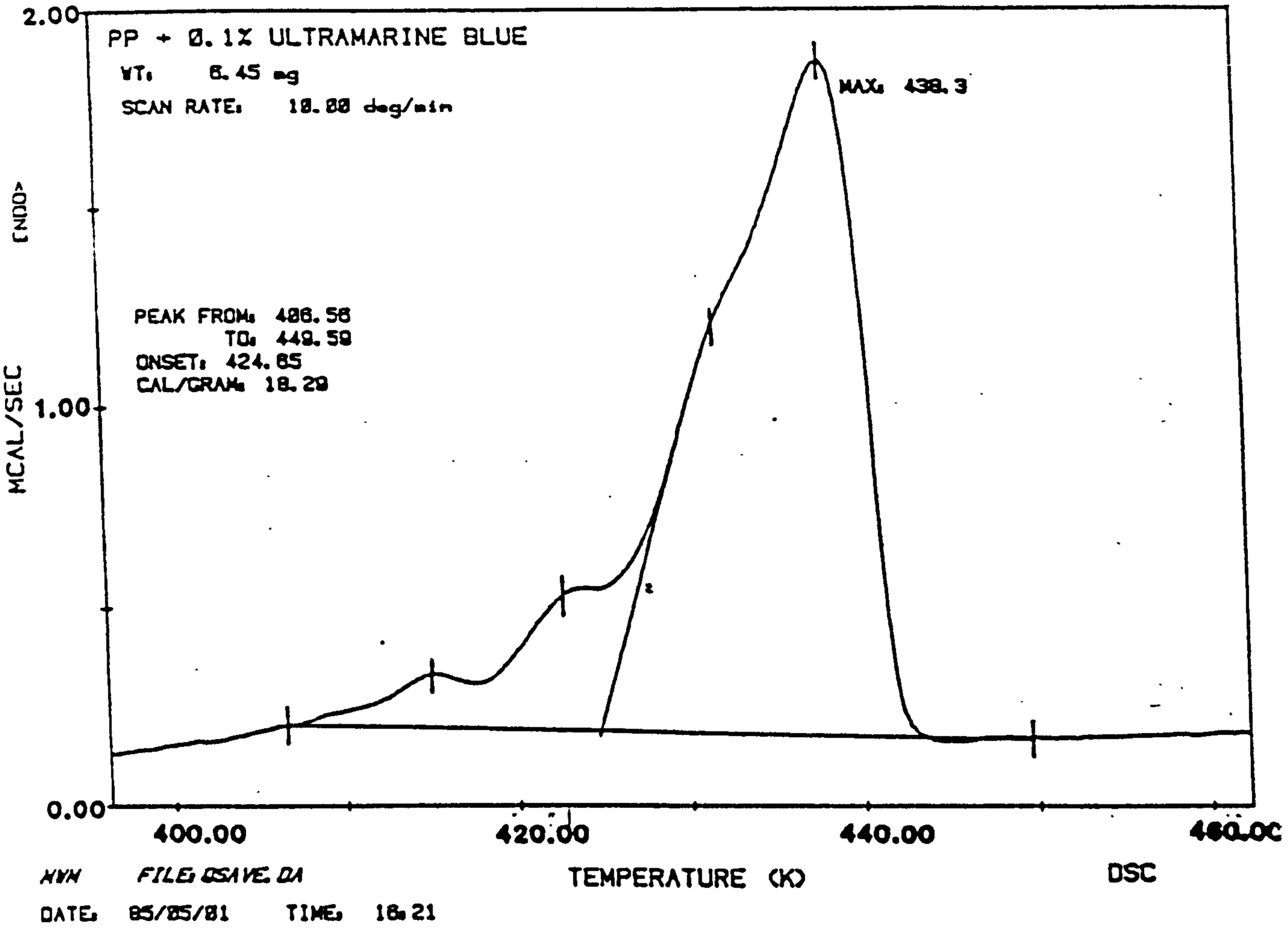

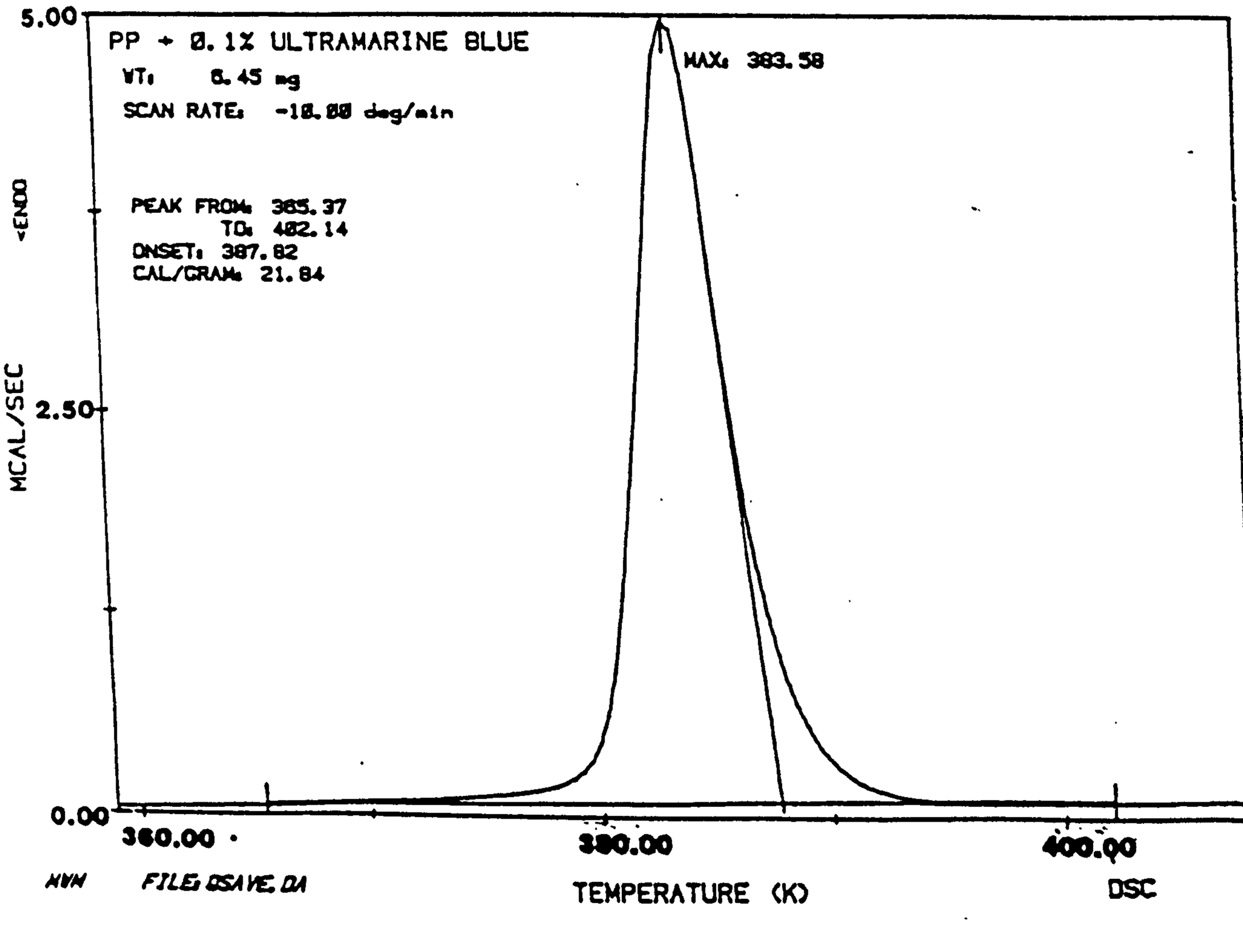

Figure 153 Melting and recrystallisation behaviour of Phthalocyanine Blue pigmented iPP moulded plaques.

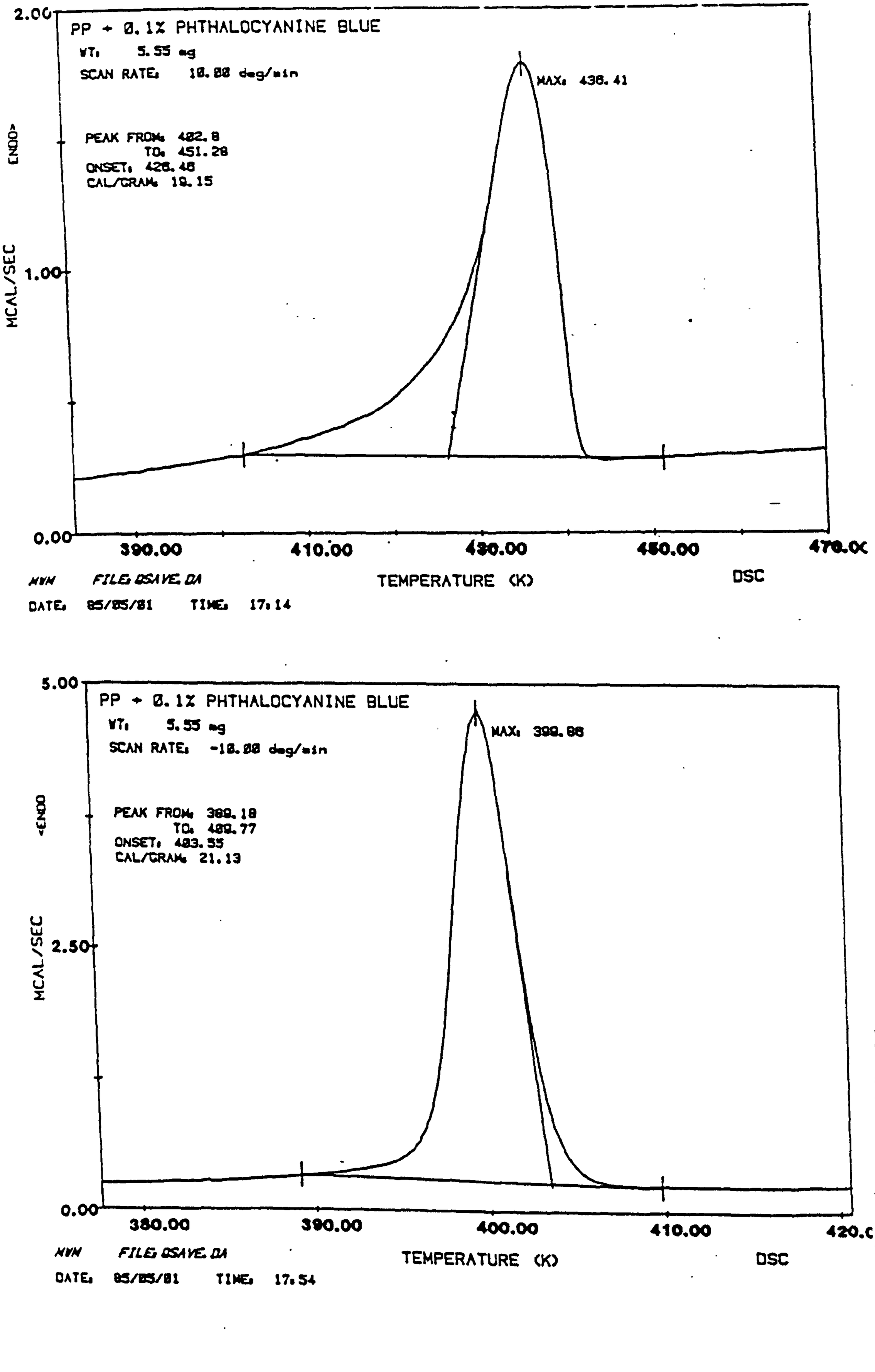

Figure 155 Melting and recrystallisation behaviour of Quinacridone Pink pigmented iPP moulded plaques.

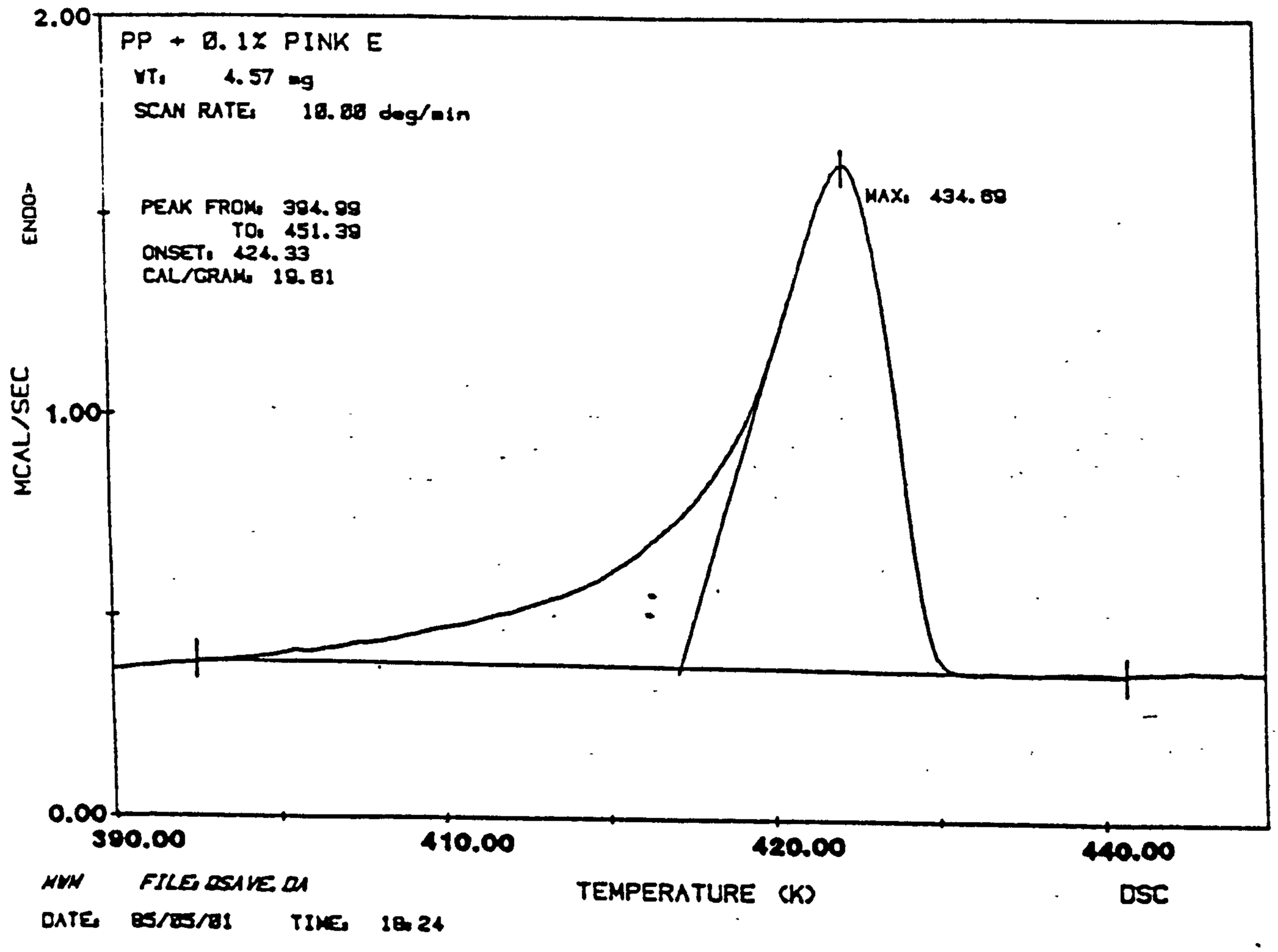

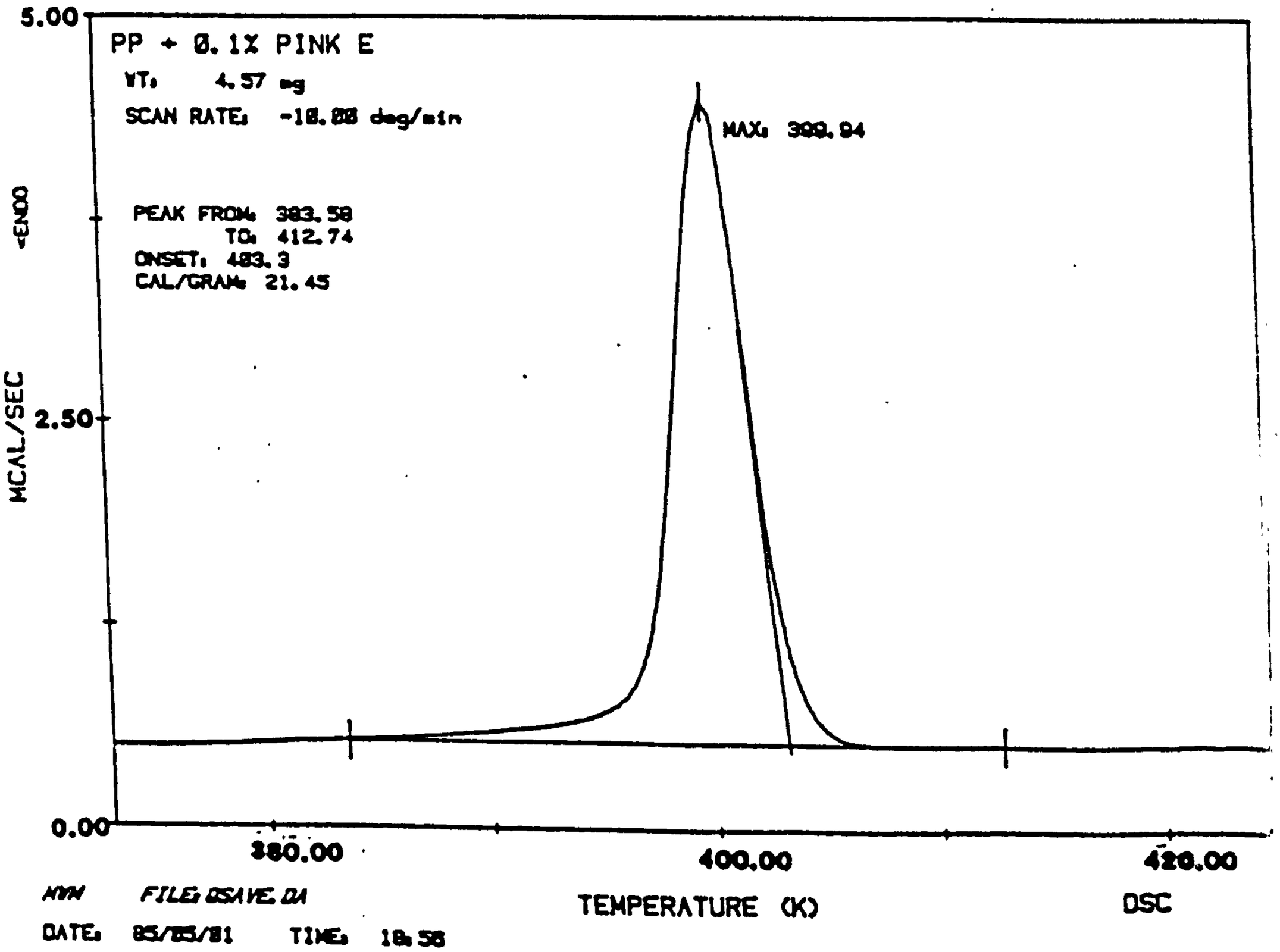

Figure 155 Melting and recrystallisation behaviour of Quinacridone Pink pigmented iPP moulded plaques.

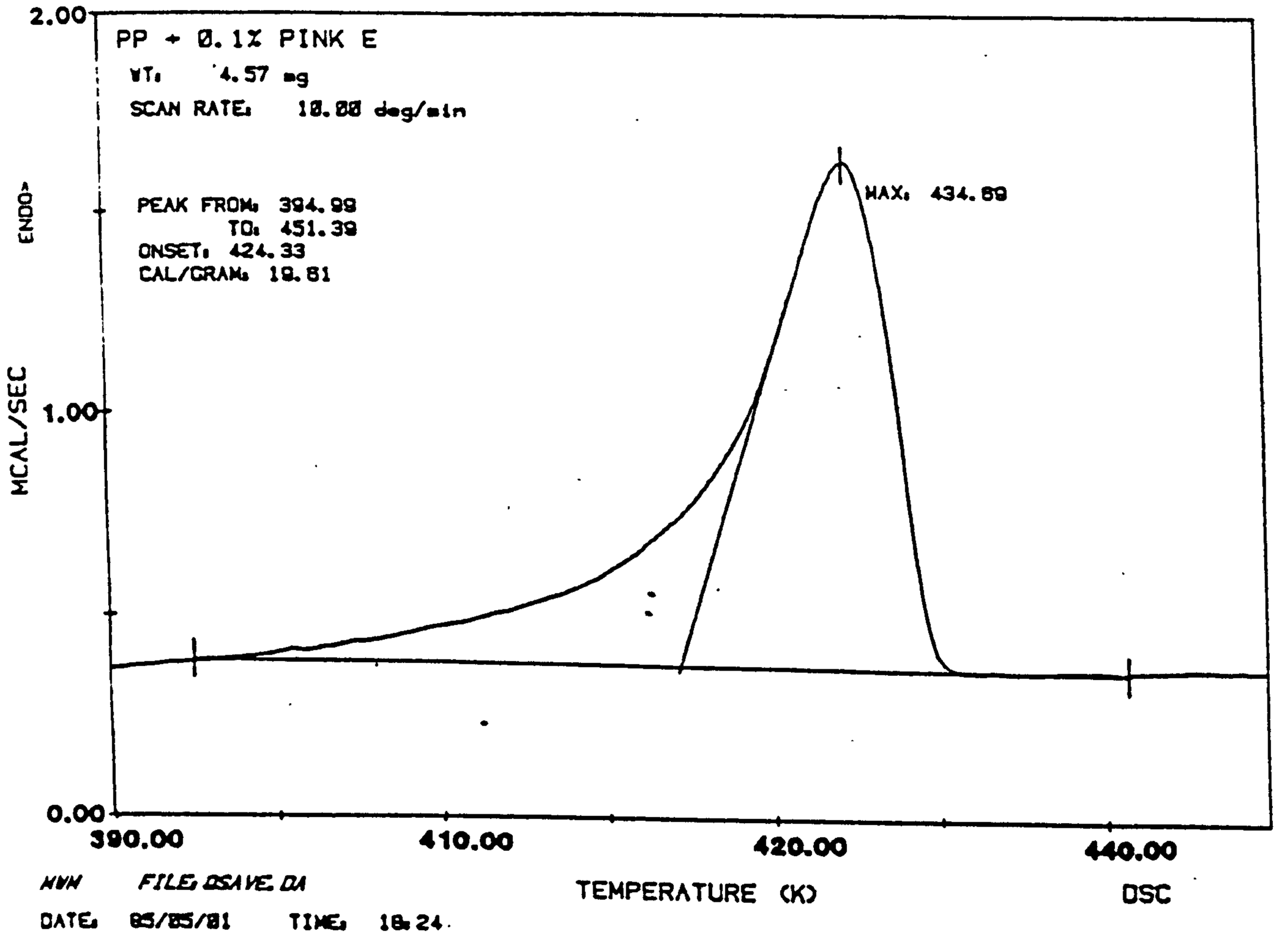

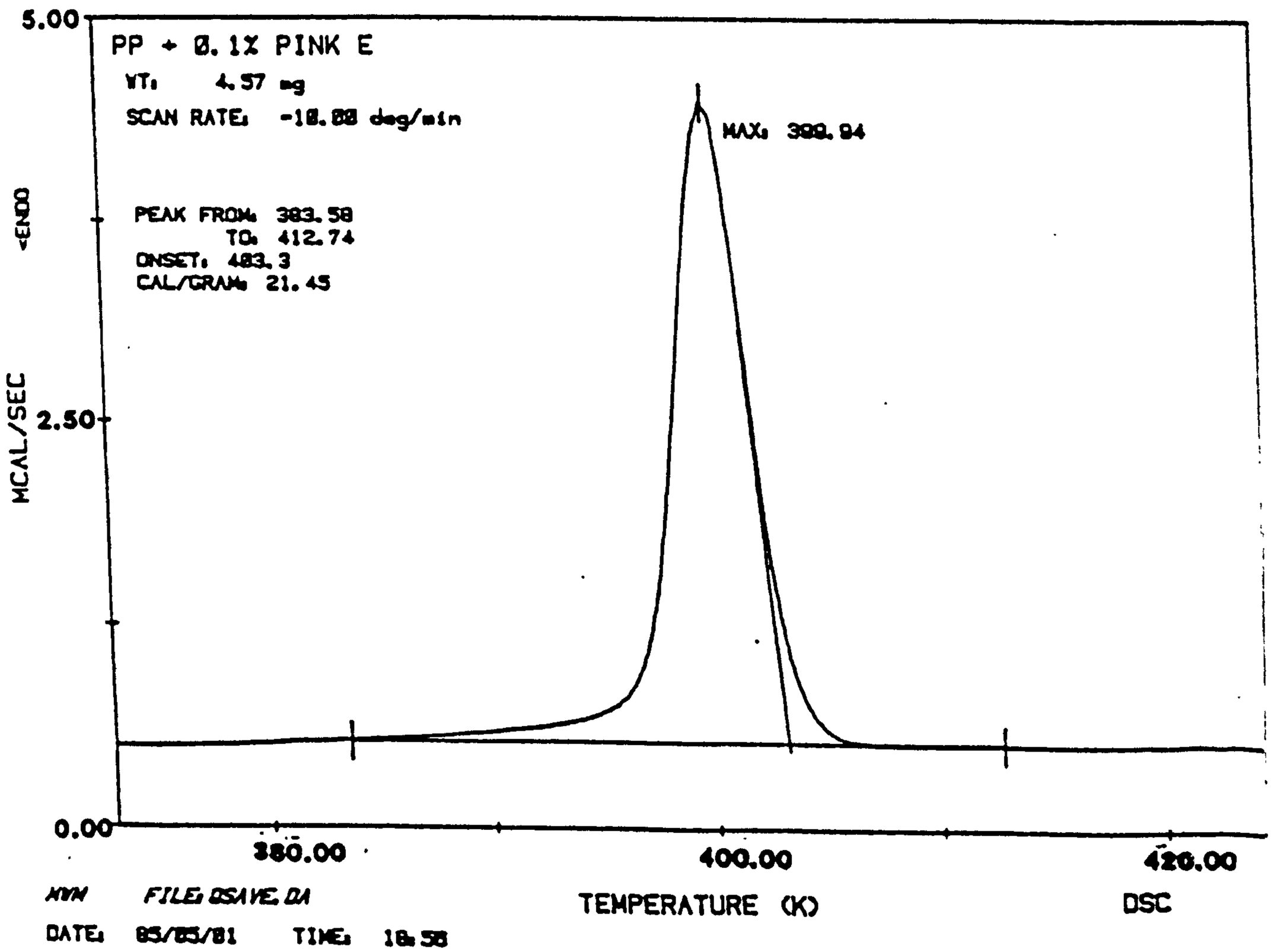

Figure 156 Melting and recrystallisation behaviour of Chalk filled iPP moulded plaques.

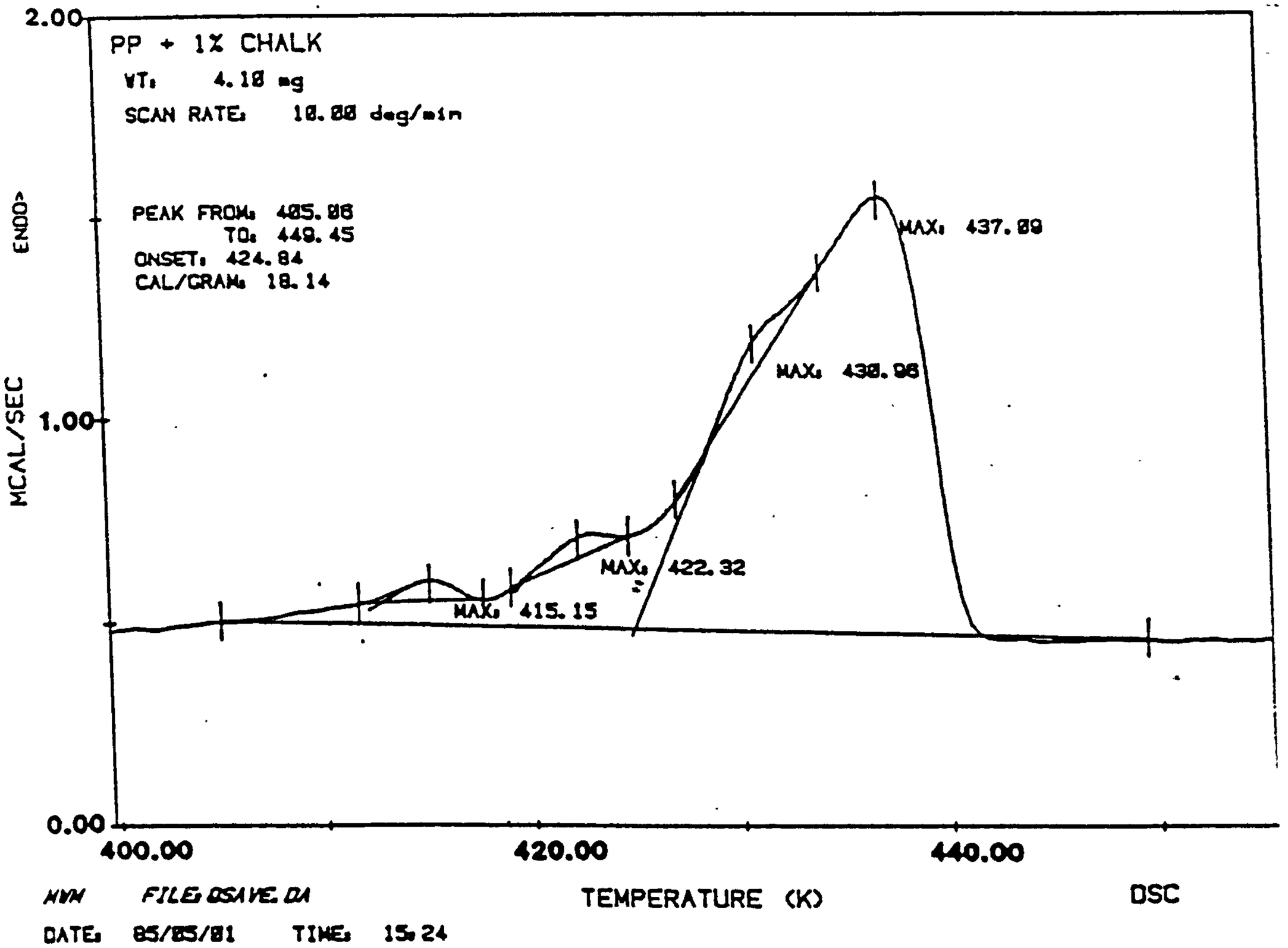

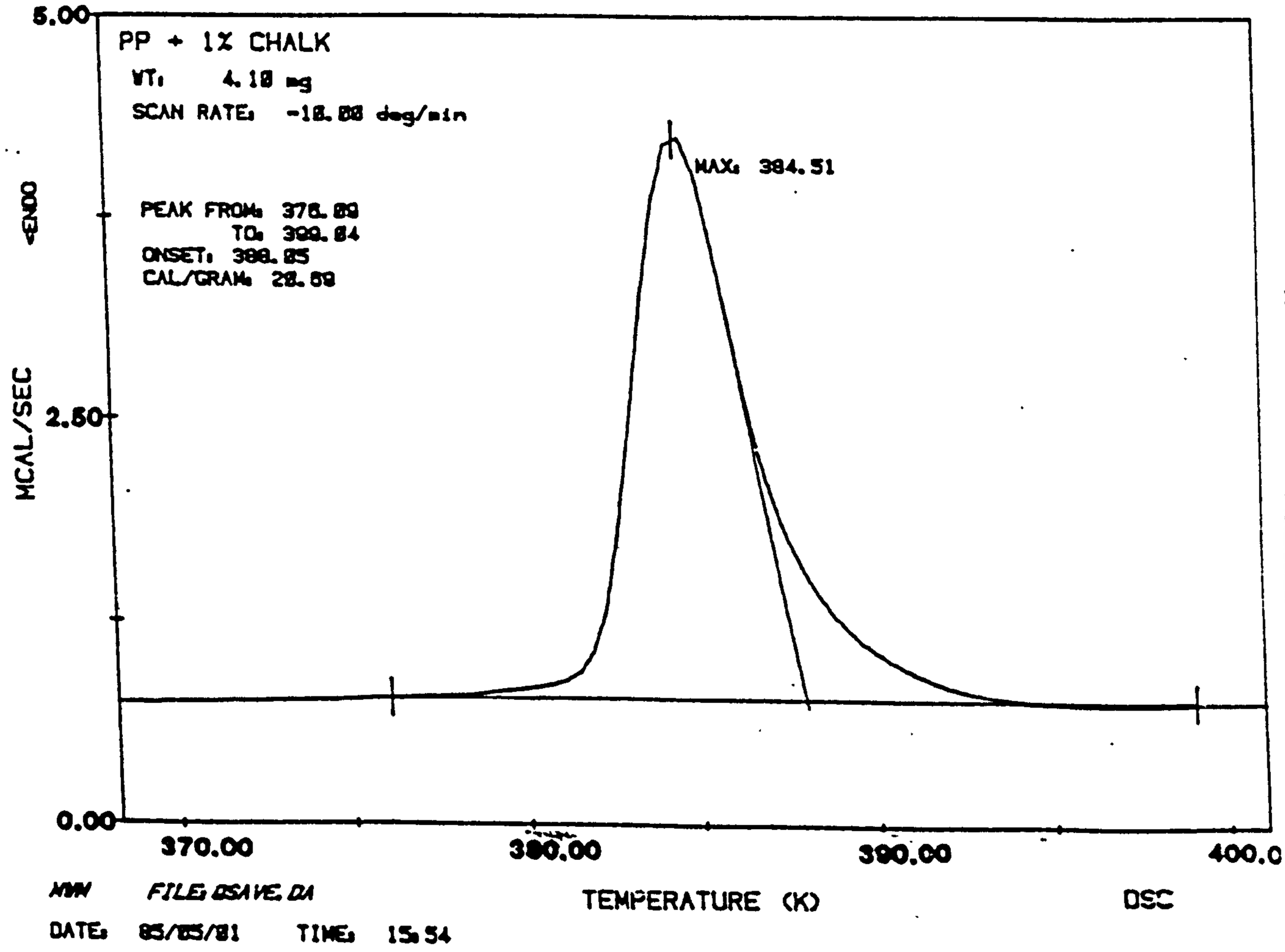

Figure 157 Melting and recrystallisation behaviour of talc filled iPP moulded plaques.

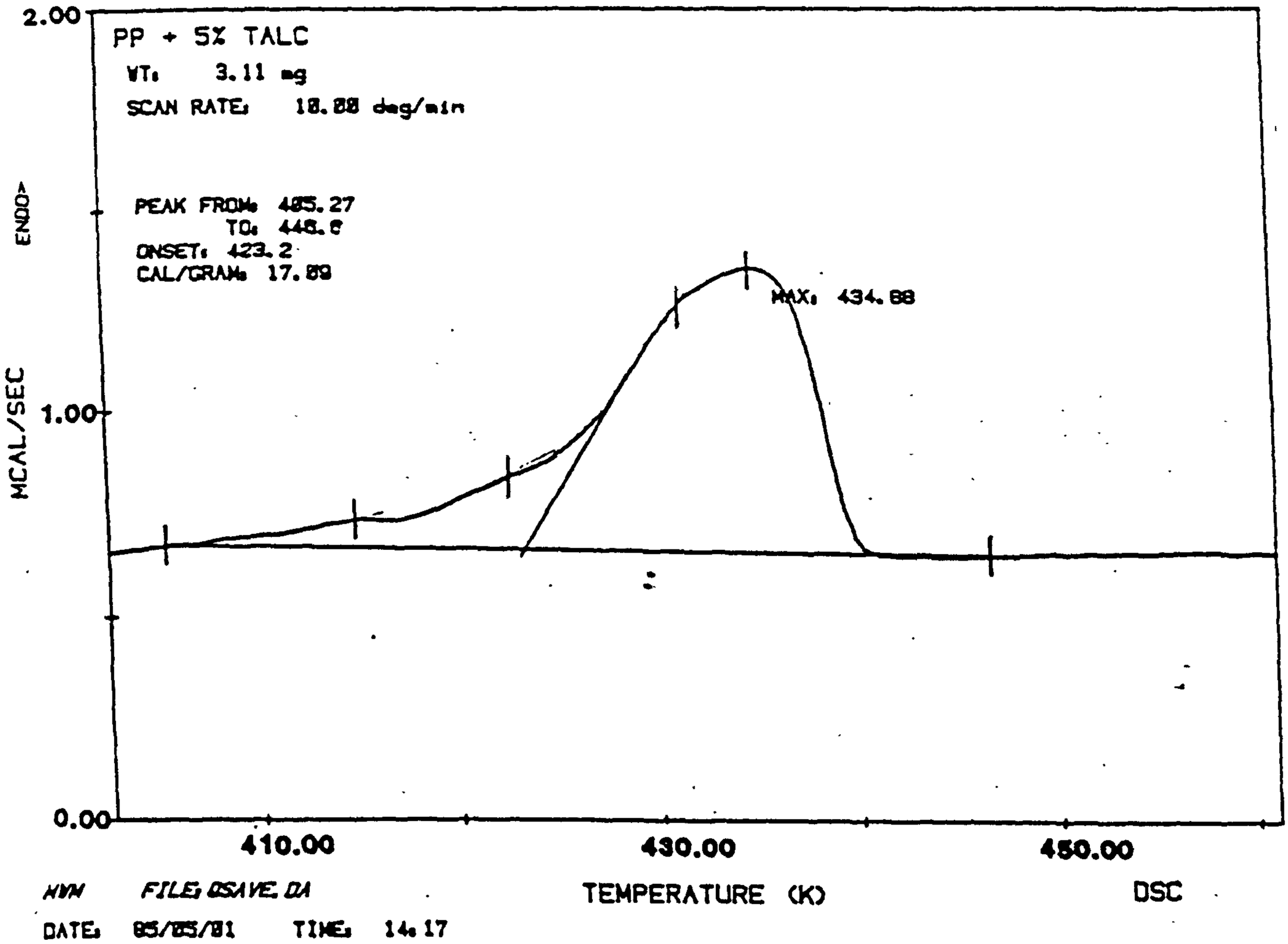

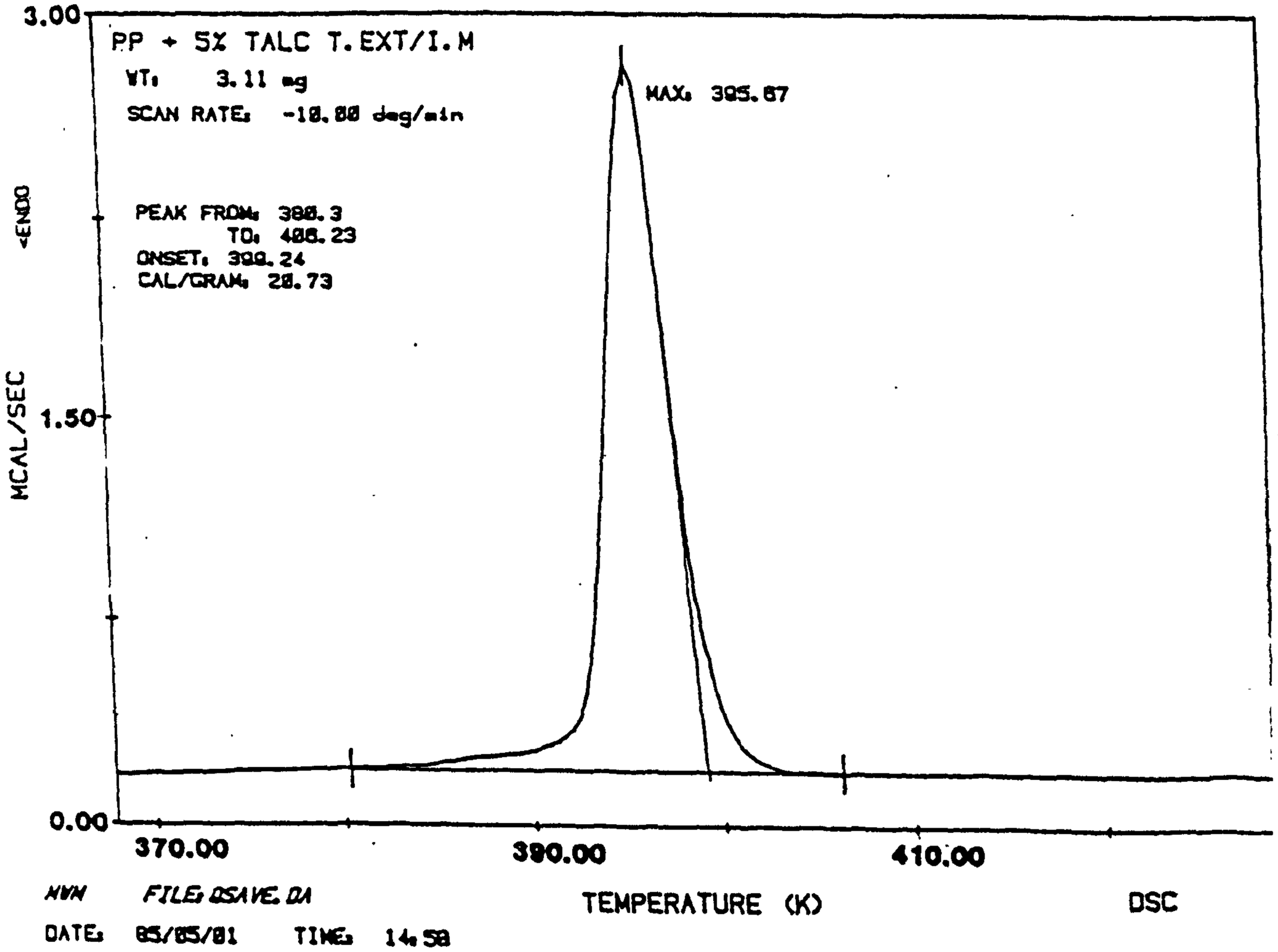

Figure 158 Melting and recrystallisation behaviour of extruded iPP moulded plaques.

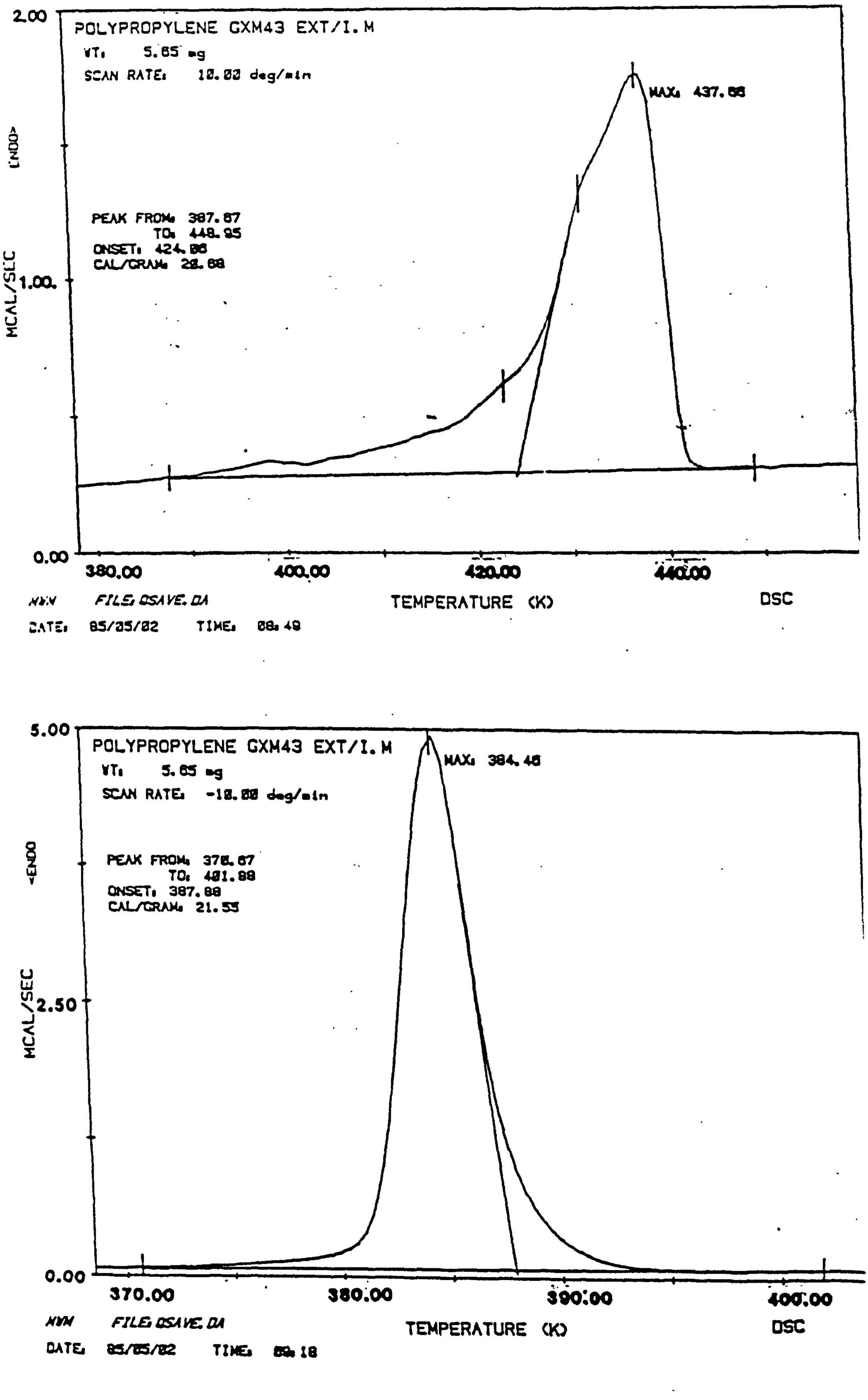

the Pink E and Phthalocyanine Blue pigmented plaques respectively; revealing enhanced α form nucleation.

(iv) The addition of 5 wt.% talc to polypropylene led to mouldings with some β form but with enhanced nucleation of the α form. The degree of supercooling in these mouldings was reduced by some 10.5°. The degree of crystallinity does appear to be somewhat lower than expected.

From this study it can be concluded that Ultramarine Blue and Chalk are good β phase nucleants whereas Quinacridone Pink E, Quinacridone Red E3B, Talc and Phthalocyanine Blue are excellent α phase nucleants. The degree of crystallinity does not appear to be significantly changed by changes in nucleation levels.

These results agree reasonably well with x-ray diffraction results with the exception that E3B Quinacridone was not identified as a strong β phase nucleant by DSC analysis.

5.5.2 Relationship Between Polypropylene Recrystallisation Behaviour And Impact Properties

The implication of the varying T_c values is that there is some nucleating phenomenon occurring in these compounds, and it is conceivable that this not only gives rise to enhanced rates of crystallisation, but also to a morphology which exhibits differing impact properties. To investigate this the crystallisation temperature versus falling weight impact strength and Izod impact strength curves in Figures 159 and 160 respectively were drawn from the data given in Tables 41,42 & 43. The values of impact strength were taken from samples at the far side of mouldings where banded morphologies were generally

Figure 159 — Crystallisation temperature T_c versus falling weight impact strength for the various iPP compounds.

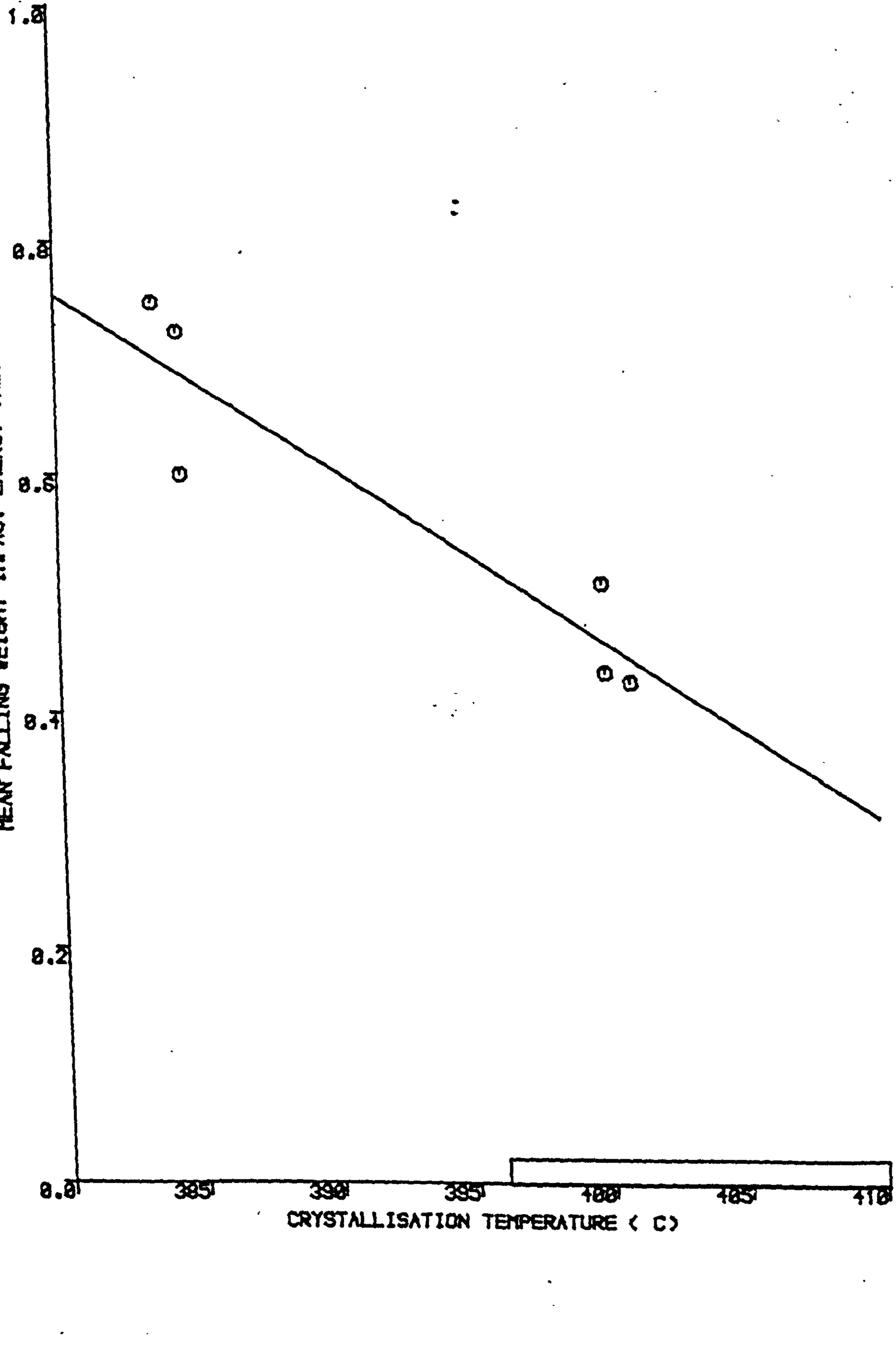

Figure 160 Crystallisation temperature T_c versus mean Izod impact strength for the various iPP compounds.

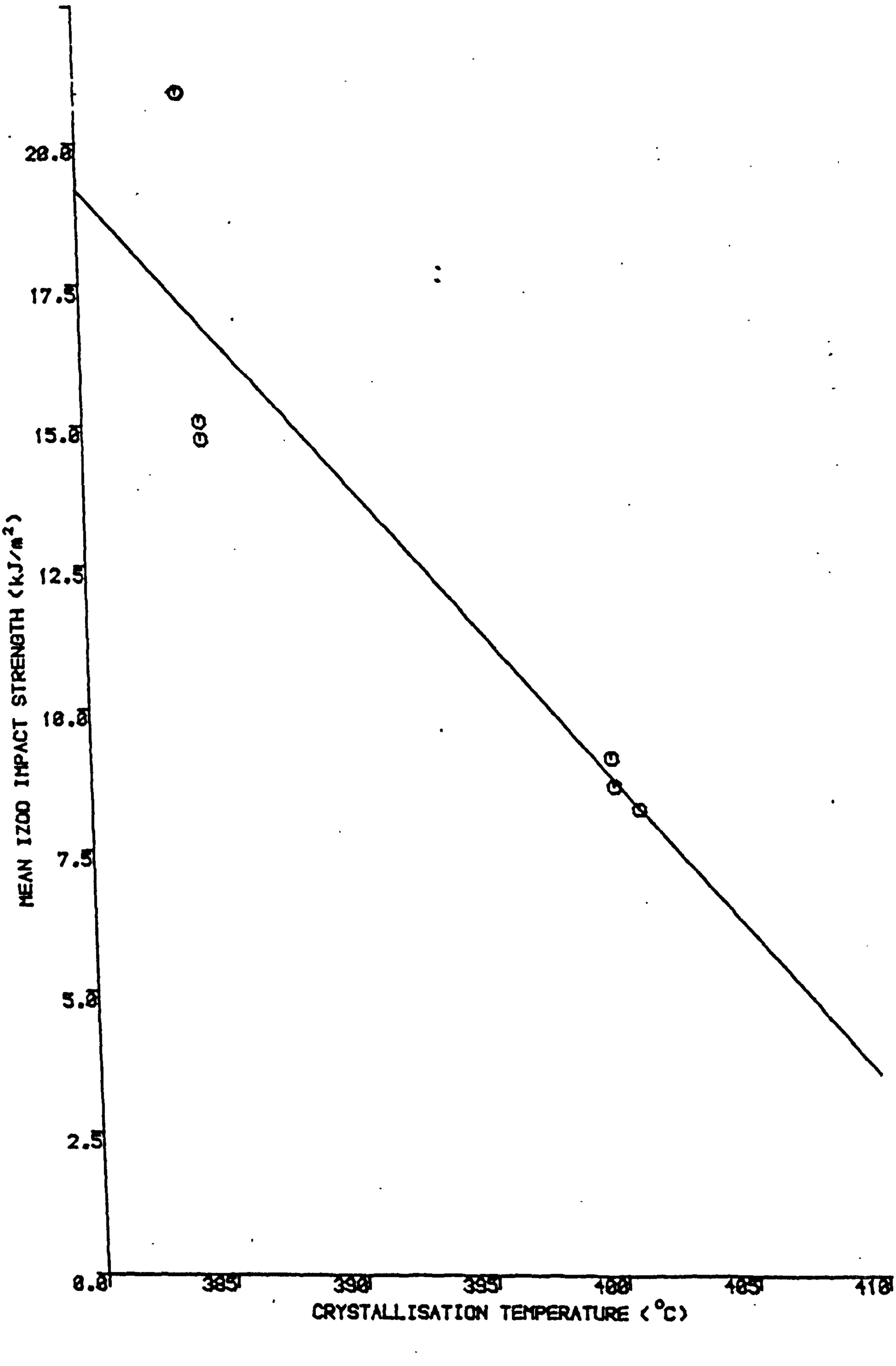

absent since the T_c values used were determined for samples relieved of thermal history.

For these compounds the crystallisation temperature, T_c, was found to increase with decreasing FWIS and Izod impact strength. The relationship gives a good Least squares straight line fit. Overall, the evidence from these albeit limited studies is overwhelmingly in favour of an apparent inverse relationship between T_c and impact strength for these six compounds.

5.6 FRACTURE SURFACE ANALYSIS BY SEM

Selected area Izod impact fracture surfaces of each polypropylene compound were splutter coated and analysed using the Cambridge Stereoscan SEM according to the procedure described in Section 2.7.3. Typical fracture surface micrographs are presented in Figures 161 to 166 and the following observations were made:-

(i) Ultramarine blue pigmented and chalk filled iPP plaques revealed a transition in fracture initiation site from the surface to the core as the flow direction was traversed. As with virgin iPP plaques the fracture surface was seen to transform from smooth and brittle to fribrillar and ductile.

(ii) Quinacridone and pthalacyanine pigmented and talc filled iPP plaques exhibited fracture initiation close to the surface skin regardless of position of Izod test piece relative to the flow direction.

These observations again link well with the trends in impact properties, i.e. fracture initiation close to the moulded skin is reflected in poor impact properties whereas fracture initiation in the spherulitic core region is reflected in good impact properties. The presence of large or pigment filler particles does not appear to have influenced the crack initiation site position or the crack propagation mode.

Figure 161 (a - b) Fracture initiation site changes with distance from gate for Ultramarine Blue pigmented plaques.

(a).20mm

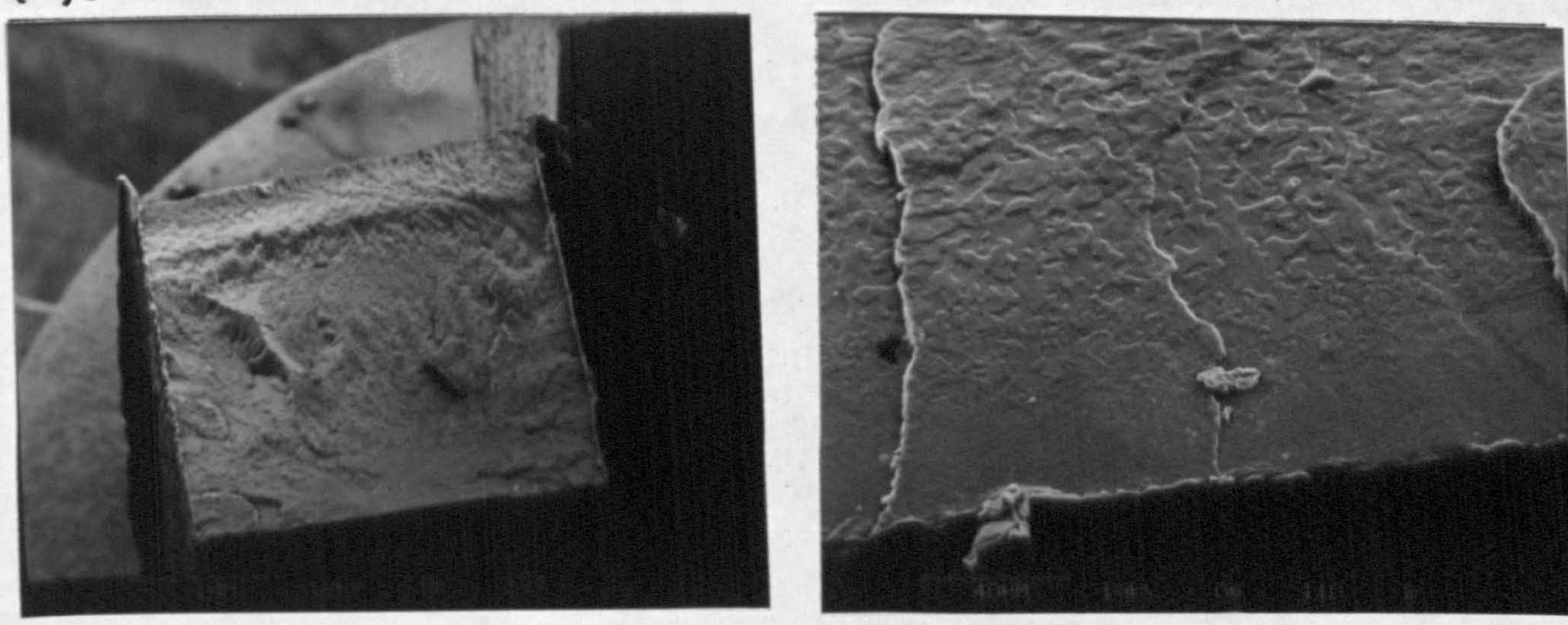

(b).70mm

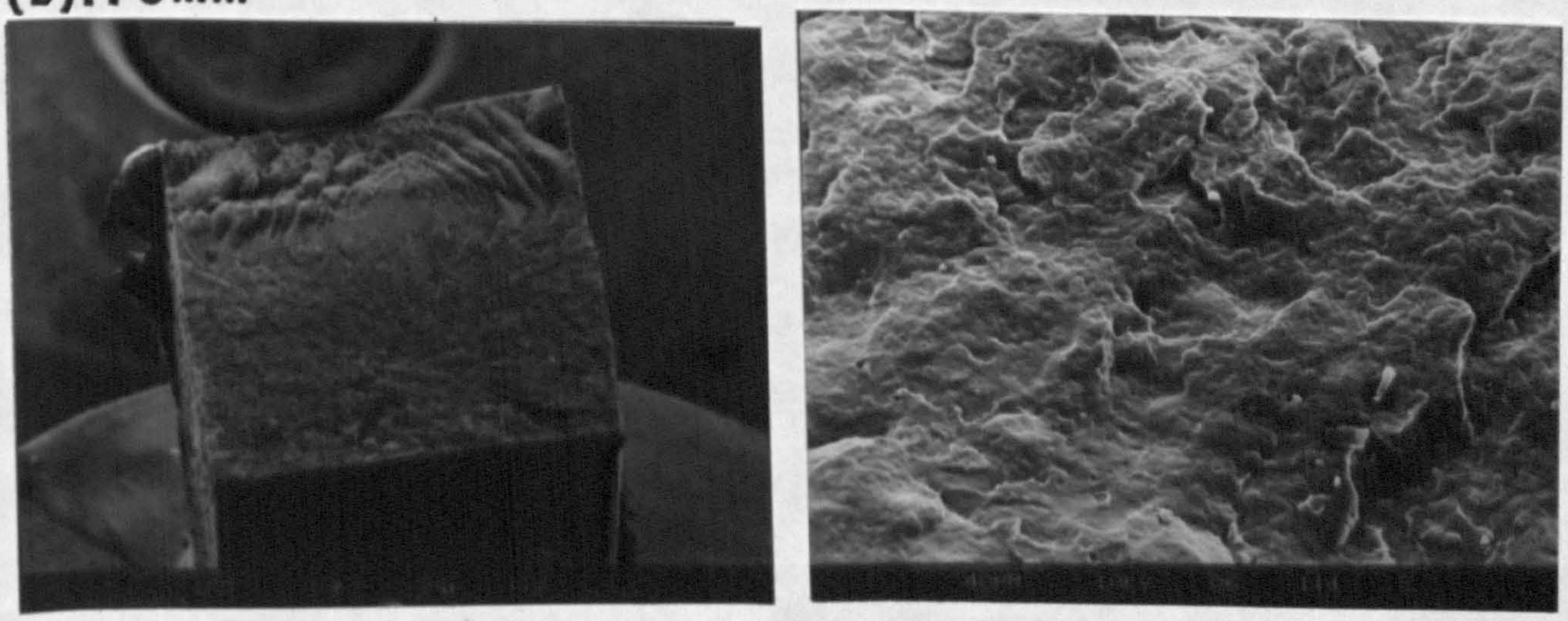

Figure 162 Typical fracture initiation found for Phthalcyanine Blue pigmented plaques.

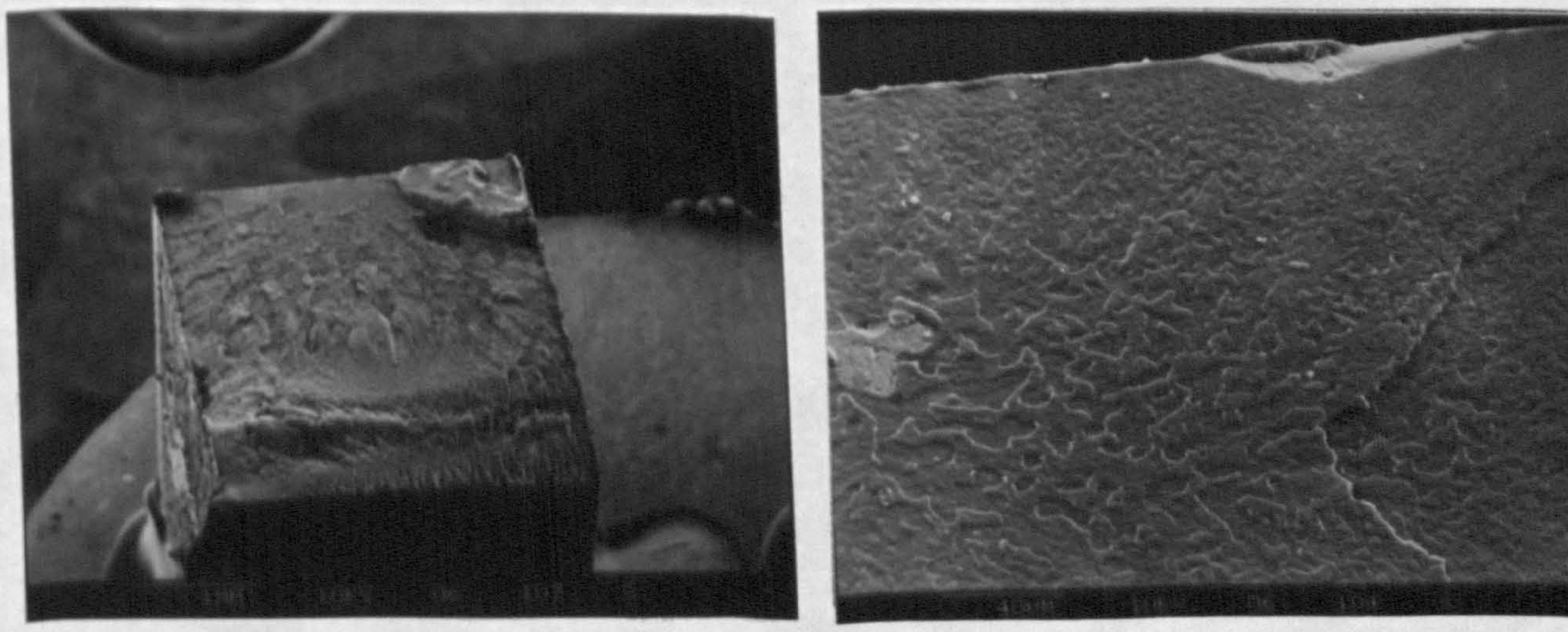

Figure 163 Typical fracture initiation found for Red E3B pigmented iPP plaques.

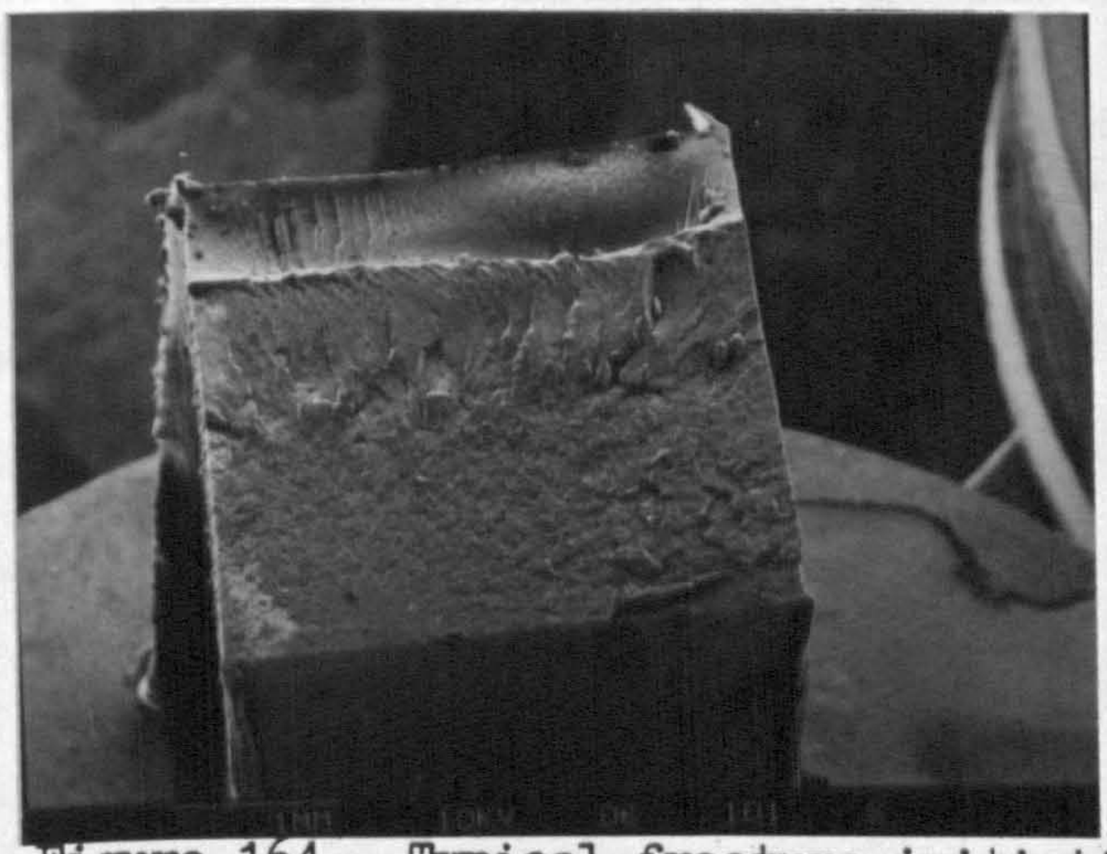

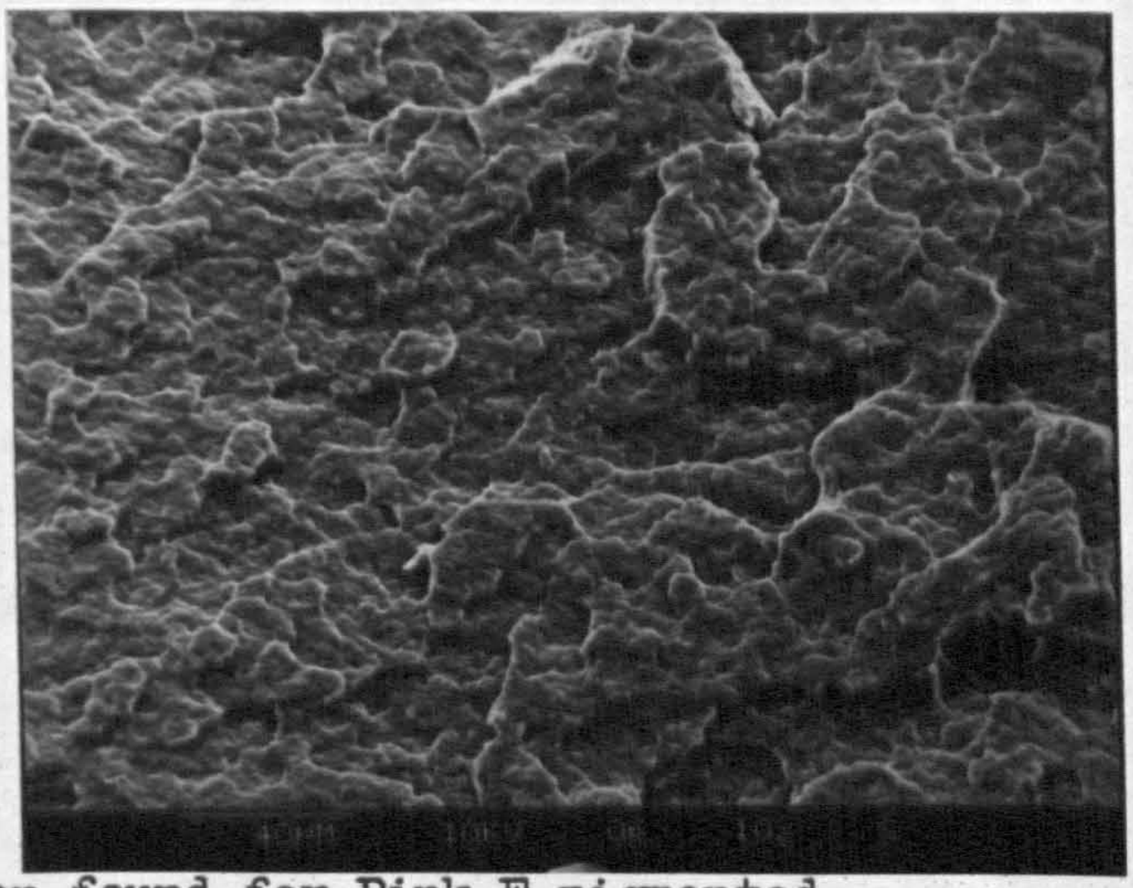

Figure 164 Typical fracture initiation found for Pink E pigmented plaques.

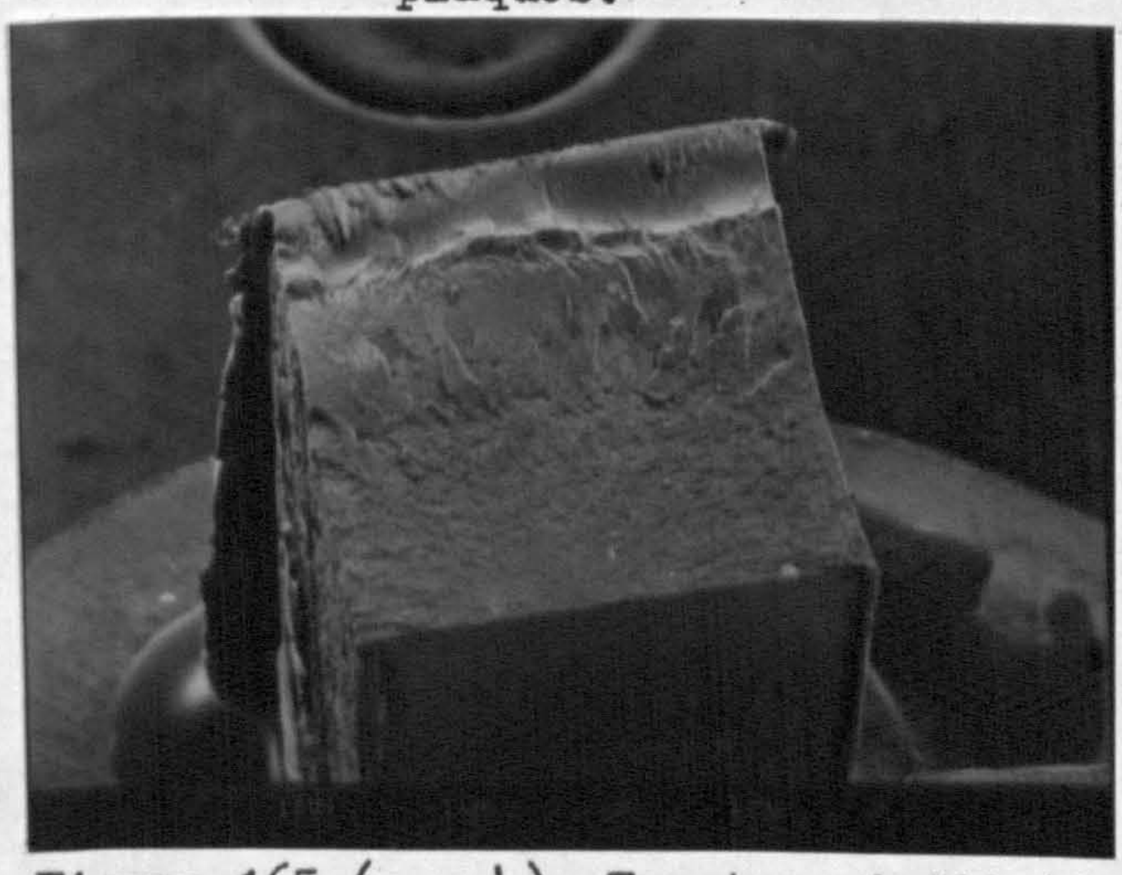

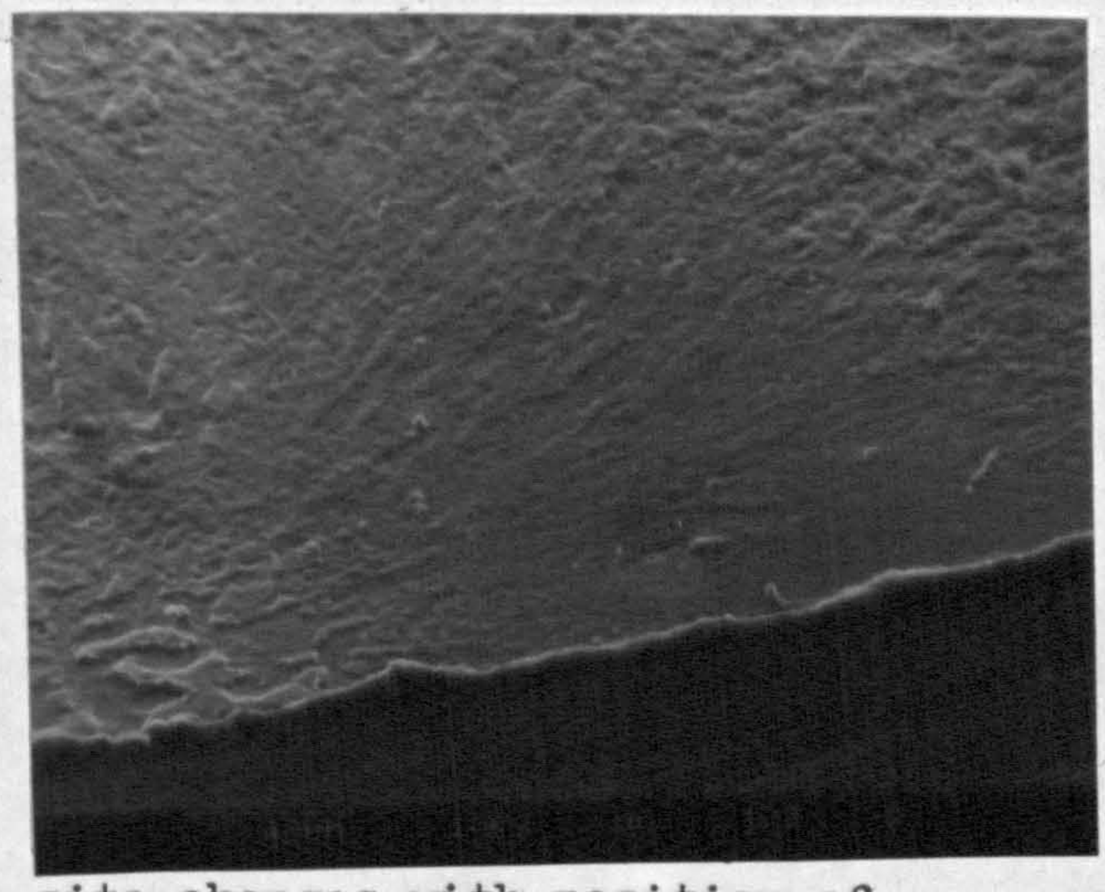

Figure 165 (a - b) Fracture initiation site changes with position of test for Chalk filled iPP plaques.

a) 20mm

b) 70mm

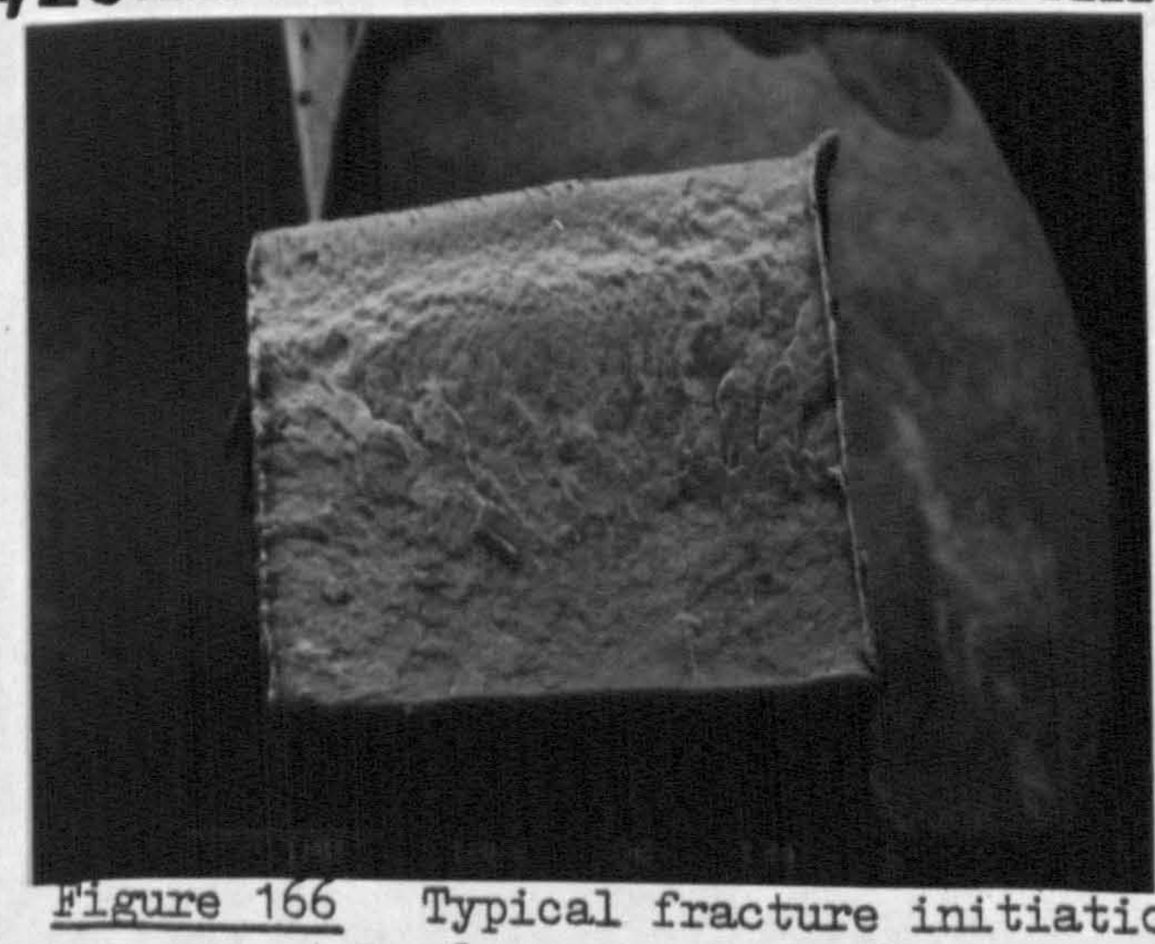

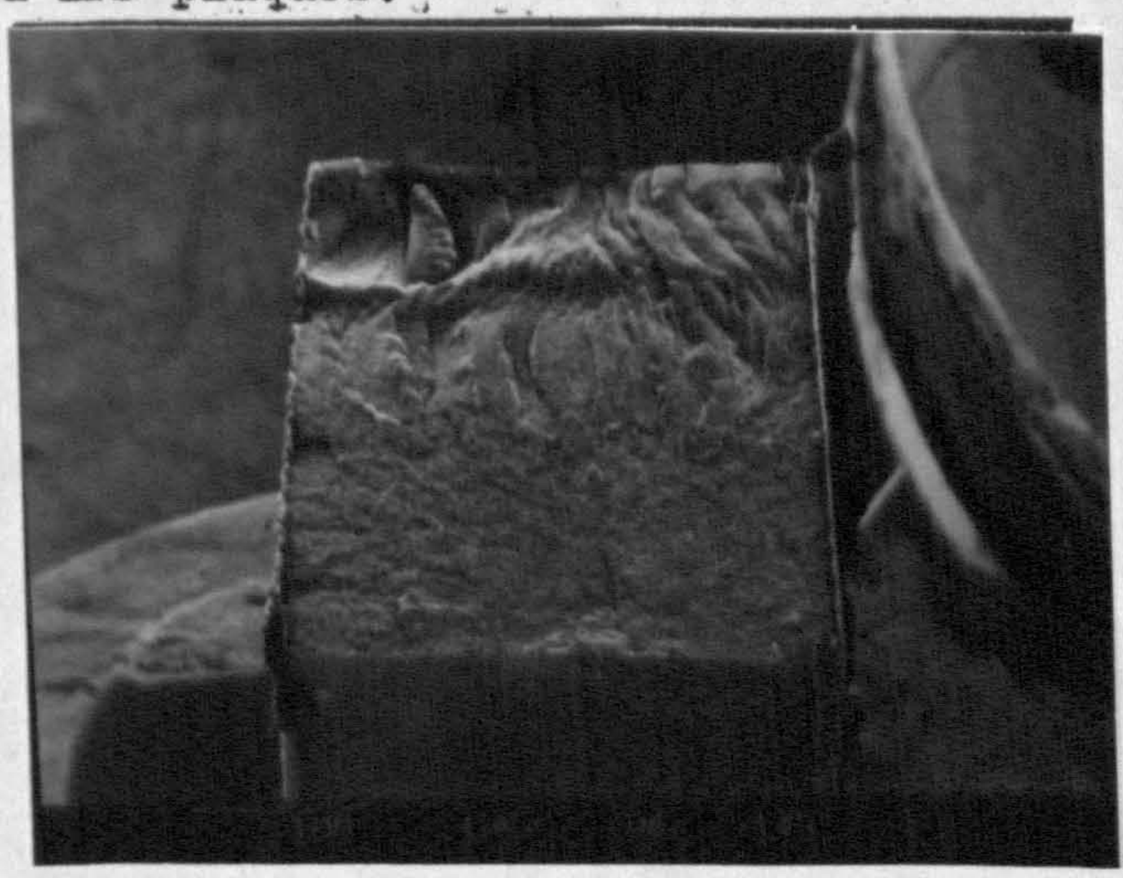

Figure 166 Typical fracture initiation found for talc filled iPP plaques.

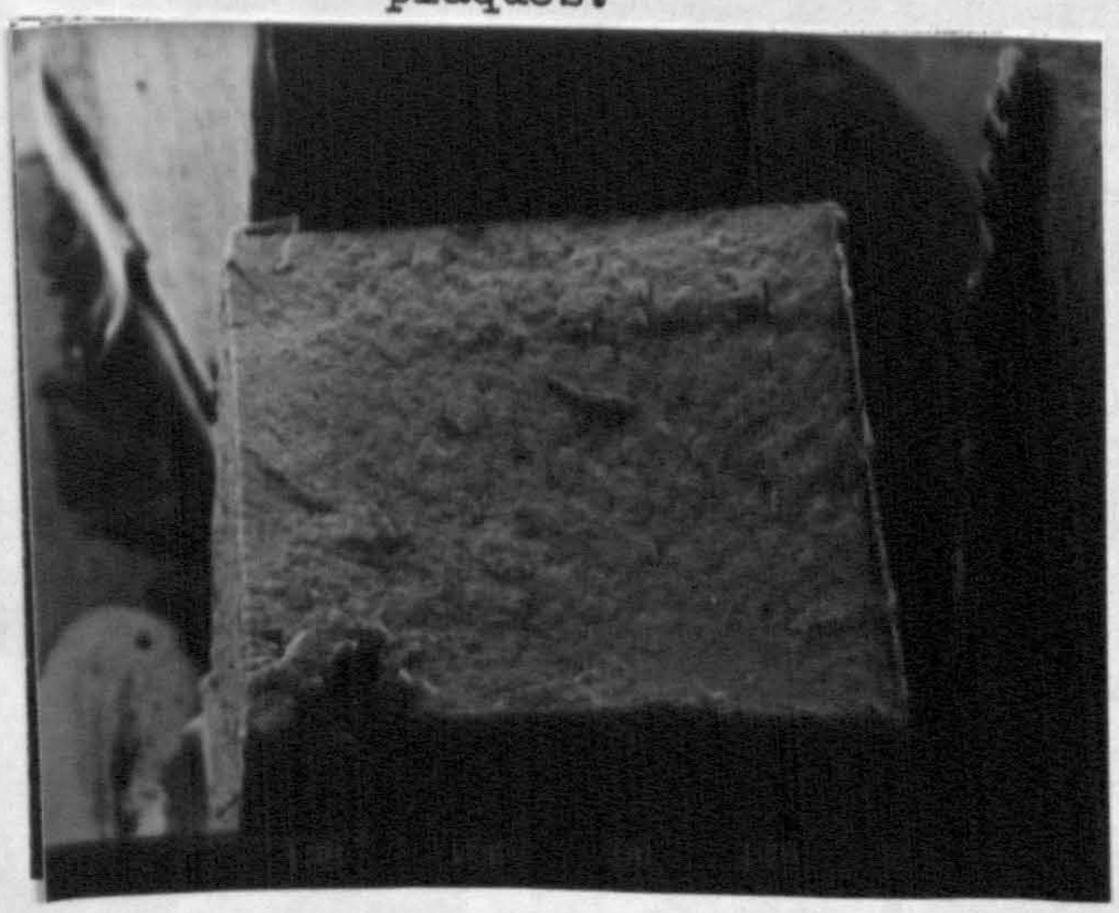

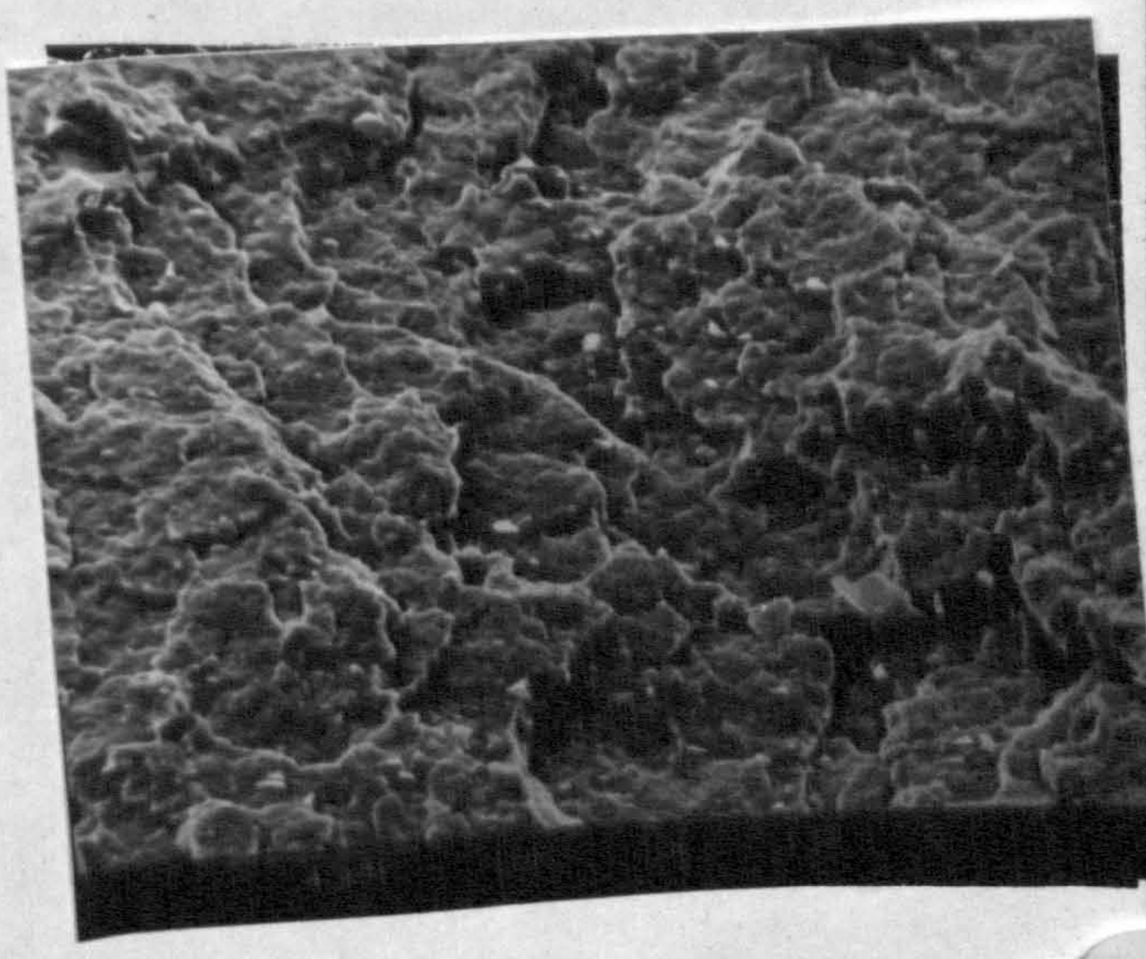

CHAPTER 6

DISCUSSION

The original aim of the research project was to identify the micromorphology of regions in polypropylene injection mouldings, associated with processing factors, which give rise to poor impact properties. To this end, the morphology of isotactic polypropylene homopolymer, grade GXM43, has been varied by systematically changing carefully controlled processing conditions, or by the incorporation of certain additives in minor concentrations. A range of analytical techniques was used to characterise the as-moulded micromorphology in particular the surface morphology which plays an important rôle in determining impact resistance. The experimental data generated from impact studies suggested a strong relationship between processing conditions, micromorphology and impact behaviour which is now discussed with reference to previously published work. The discussion will be divided into four sections namely; the effect of processing parameters, molecular weight and additives on micromorphology and impact properties and lastly the application of our research findings to a commercial pigmented moulding of GXM43 iPP.

6.1 EFFECT OF PROCESSING PARAMETERS ON THE MICROMORPHOLOGY AND IMPACT PROPERTIES OF ISOTACTIC POLYPROPYLENE

6.1.1 Structure Development

Tadmor (70) proposed a mould filling model that has been applied by Bowman (25) to explain the texture and morphology present in injection mouldings of a polyoxymethylene copolymer. This model may similarly be applied to polypropylene injection mouldings which exhibit an oriented skin-equiaxed core type of morphology. In this model the flow at the front of the advancing melt is termed extensional in character, a mode of polymer flow capable of producing significant molecular chain uncoiling and extension. This "molecularly extended" melt is shock cooled on contacting the cold mould wall and retains the orientation induced by the flow. Clark (2,3,4) proposed that

under a high stress from quasi-extensional flow, lamellae develop with a planar conformation in this frozen oriented skin layer.

A number of workers have attempted to reveal the micro-morphology of the skin layer of injection mouldings with very limited success. However, using the permanganic etching and replicating technqiue in this research programme the skin layer has indeed been revealed as a region of highly aligned material with lamellae and fibrils being parallel to the injection direction. The skin can therefore be interpreted as that portion of the polymer crystallised during the filling stage, whereas further structural development is due to the packing and cooling stages of the moulding process.

The material behind the advancing melt front and between the solidified layers experiences a velocity and shear rate profile (according to Tadmor) that has a zero shear adjacent to the skins and at the centre of the moulding, with maximum shear in between, this was illustrated in Figure 14. The layer immediately below the skin of polypropylene injection mouldings was found to be spherulitic in many cases, even close to the gate, but with growth constrained to a direction away from the cold mould wall. The presence of a skin reduces the cooling rate in this layer delaying crystallisation and allowing some melt relaxation. The reduced cooling rate and the loss of some melt orientation combined allowed growth of these oriented spherulites from the nuclei that had formed.

The extent of the finely structured layer 3 as a function of distance from the gate was examined for all processing conditions, in every case this layer was present near, but absent

far from the gate. This observation was also made by Scherpereel (148) for polypropylene and by Bowman (25) for a polyacetal copolymer. Both authors attributed this finely structured layer to material that is last to enter the mould during the filling stage so that it is unaffected by flow of additional material. The drop in pressure and the lack of material flow do not allow sufficient molecular reorganisation for the development of a spherulitic morphology but do encourage the row nucleation of fibrils perpendicular to the flow direction as revealed in TEM replica micrographs (see Figure 86). Bowman (25) referred to this layer as a stationary skin formed by continual 'laying down' of material from the core flowing melt.

Returning to the Tadmor model one must assume a steady increase in the shear stresses away from the mould surface to a maximum. The β hexagonal crystal modification identified in iPP is associated with fast cooling and shearing of polypropylene melts and the nucleation of these bright negatively birefringent spherulities (as viewed optically) suggests that shear stresses in the flowing melt are responsible for their formation. The crystallites appear to be nucleated epitaxially on bundles of molecules oriented along the shear band. The nucleation density along the length of this row nucleated shear band is so high that crystallites are constrained to grow predominantly in one direction, namely perpendicular to the flow direction. This type of growth is termed transcrystallinity.

It has not been possible during this research programme to identify optimum shear stress levels for β formation, but certainly the extent of nucleation was favoured by higher viscosity melts i.e. where higher shear stresses occur.

However, Dragaun et. al., (44) examined extruded, injection moulded, unoriented crystallised specimens and capillary rheometer efflux strands of commercially stabilized polypropylene by optical microscopy and x-ray diffraction, to determine the conditions for β form crystallisation as a function of the distance from the surface and of the shear rate at commercial processing conditions. Results demonstrated that at all "cooling conditions" $\Delta T = Tm - T_b$ (defined as the melt temperature Tm and the bath temperature T_b) effects of strain flow initiate nucleation of β-form crystals. The shear rate was demonstrated to be important for β-form crystallisation in that a critical average threshold value for the shear rate of approximately 3×10^2 sec^{-1} had to be exceeded using ΔT values of 130 to 210°C for their formation.

The extent of β nucleation as a function of distance from the gate in our iPP mouldings was examined optically, in all cases the concentration of β spherulites increased to a maximum as layer 3 width reduced supporting Scherpereels (148) prediction of a transformation along the flow path of row nucleated fibrils to β spherulites. These row nucleated spherulites were observed to die-away at some point along the flow direction depending on processing conditions used. It is a point of interest to note the high degree of random formation in the gate region of all mouldings, this gives further evidence of shear induced nucleation during the packing stage of the moulding process.

The mode of flow in the core of mouldings produced little preferred orientation. This, combined with the low rates of cooling, gave rise to the essentially equiaxed structure present in the core of most injection mouldings as predicted

by Schmidt (23) and Tadmor (70). In the case of polypropylene the stable monoclinic α phase spherulites of the positively birefringent form were identified.

6.1.2 The Influence of Processing Conditions on Structure Distribution

(i) Melt Temperature

The effect of melt temperature on the thickness of the highly oriented non-spherulitic skin of polypropylene injection mouldings is well documented by Kantz et. al., (6), Fitchmun et. al., (77, 78), Sherpereel (148), Fujiyama et. al., (10-14), Okamoto (15) and Williams (16-20). Namely, that the thickness of the skin decreases with increasing melt temperatures. The same trend has been reported and reviewed in this thesis for several other polymers; polyethylene (71-76) polyoxymethylene (25, 4), polypropylene ethylene copolymers (8) and polybutylene (22). In general, increasing the melt temperature increases melt heat content and reduces the cooling rate at those temperatures where the nucleation density is low and growth is fast, thus favouring growth to nucleation. The loss of preferred crystal orientation at the surface with increasing barrel temperature is due primarily to melt relaxation i.e. the extra heat content and temperature of the melt delaying cooling and reducing relaxation times.

The extent of the highly oriented sheared layers revealed in polypropylene injection mouldings close to the gate are also significantly reduced by increasing melt temperatures. This again reflects the preference for spherulitic growth to fibril nucleation at the

slower cooling rates, which is associated with relaxed preferred chain axis orientation. The nucleation of the β phase is certainly enhanced by use of low melt temperatures as revealed in this research programme which is in good agreement with the observations of Williams and Bevis (16-20) and supports the theory of shear induced β-phase growth.

(ii) Mould Temperature

Henke and co-workers (8) studied the effect of mould temperature on the morphology and tensile properties of a polypropylene ethylene copolymer. They found that the width of the skin did not vary with mould temperatures employed between 40°C and 80°C, at constant melt temperatures. This result was in contradiction to the observations of Kantz et. al., (6) and those made in this research programme for polypropylene homopolymer mouldings. However, the authors did report that the highly oriented non-spherulitic skin layer of the specimens possessed a molecular weight higher than that of the interior regions, a phenomenon which had not previously been noted in the literature for injection moulded polymers.

The general conclusions drawn from the latter study were that small spherulites and wide shear bands are characteristic of low mould temperatures whereas larger spherulites and thinner shear zones are characteristic of higher mould temperatures. In this respect our research findings are in complete agreement since in high mould temperature mouldings little evidence of a row nucleated shear band was found, but large α and β spherulites were.

The influence of mould temperature on structure development was explained by Guo and Bowman (22) in terms of the effects of temperature gradient. As the temperature gradient between the melt and mould is reduced, so the rate of heat withdrawal decreases and consistent with the melt temperature effect the thickness of the skin decreases and the preference for spherulitic rather than fibril growth is achieved. For polypropylene moulded at high mould temperatures ~80°C the melt adjacent to the mould wall crystallises rapidly causing a 'burst' of spherulitic nucleation in the direction normal to the wall since the spherulites are constrained by their neighbours to do so. This type of spherulitic growth is termed 'transcrystallinity' and has been clearly illustrated for polypropylene in Figure 52(e).

Transcrystallinity has been observed in many other semi-crystalline polymers. It is generally acknowledged that such structures are initiated by crystallisation conditions which induce a high density of nuclei on the melt surface. Once these nuclei are formed, their proximity to one another permits only undirectional growth of the spherulite into the melt. For the thermal history employed above, it is evident that the nature of the mould material and in particular its nucleating activity can have a profound influence on the morphology developed at the surface of the polymer. Rapid cooling has often been suggested as a factor in the formation of trans-crystallinity.

Barriault and Gronholz (163) reported that extruded nylon 66 transcrystallizes under nearly all cooling conditions except severe quenching. This they believed, indicates that a nucleating agent is not required and proposed that a

temperature gradient is sufficient to induce a high nucleation density on the surface.

Eby (164) reported that a transcrystalline surface layer developed in polyethylene when the polymer was crystallised under a temperature gradient. Furthermore, the thickness of this layer could be increased by increasing the temperature gradient between the surface and the interior of the melt.

Fitchmun and Newman (99) investigated the effect of different cooling rates on the surface morphology of compression moulded polypropylene and found that a temperature gradient alone was ineffective as a catalyst for transcrystalline growth. The authors proved that the nucleating activity of the mould surface plays an important rôle in determining the degree of transcrystallinity of the mould surface, Mylar (poly(ethylene-terephthalate)) and TFE - Teflon surfaces were the most active surfaces inducing transcrystallinity.

In order to explain the transcrystalline growth revealed in mouldings of polypropylene produced in this research project one must consider the shear flow induced molecular orientation that occurs during the mould filling stage. Applying the Tadmor model to conditions of a hot mould (80°C) and hot melt (220-280°C) one would expect the level of maximum shear stress to occur closer to the mould surface than in low mould temperature mouldings. As the temperature gradient is reduced, so the rate of heat withdrawal decreases, and consequently the level of elongational flow at the surface is reduced but the level of shear flow is increased. The time for relaxation of molecular orientation induced by shear stresses is increased at higher mould temperatures permitting the spherulitic growth from the oriented twisting lamellae. Micrographs of this transcrystalline

surface shown in Figures 87 and 88 reveal large β phase spherulites which confirm the presence of high shear stresses close to the mould surface and illustrate the increase in transcrystallinity with reduction in temperature gradient between the surface and the interior of the melt.

6.1.3 Impact Property - Micromorphology and Process Condition Relationship

Process variables have significant effects on the microstructure and, hence, on the impact properties of a moulded article. Okamoto et. al., (15) reported a relationship between Izod impact strength and various moulding conditions for high density polyethylene injection mouldings. The authors found that as melt temperature increases Izod impact strength in the longitudinal direction decreases while the strength in the direction transverse (i.e. through the thickness) increases. This result corresponded to their earlier conclusions that the percentage of skin layer was reduced with mould temperature, melt temperature and injection speed. The results of Kantz et. al., (6) also revealed a linear increase in tensile impact strength with melt temperature and area fraction of skin.

Williams (16) noted the effect of variations in barrel temperature on microstructure and morphology during a study of polypropylene copolymer injection mouldings. Increasing the melt temperature from as low as 185°C up to 225°C not only reduced the skin thickness, but also reduced the degree of molecular orientation in the mouldings, as observed by the elimination of the rows of shear nucleated β phase spherulites. At temperatures below the ductile failure mode (at -10°C) the influence of the β phase and internal stresses was clearly demonstrated by a reduction in impact strength of plaques prepared at 185°C and a marked rise in impact strength of

mouldings prepared at higher melt temperatures of 225°C. At melt temperatures above 245°C the character of the moulded skin changed from that of a featureless oriented structure to one more characteristic of a spherulitic transcrystalline structure. The highly oriented featureless skin offered greater impact resistance than the transcrystalline skin indicating an optimum melt temperature of 245°C for maximum impact resistance. The results of Williams et. al., (16) for a polypropylene copolymer infer that for polypropylene GXM43 injection mouldings used in this research project, there is an optimum melt temperature around 280°C above which transcrystalline surface layers will develop and seriously impair the impact performance.

Henke and co-workers (8) studied the relationship of mould temperature with Izod impact strength and relative spherulite size for a propylene-ethylene copolymer. The authors found that average spherulite size appeared to correlate well with most physical properties; good impact properties were related to small average sizes associated with low mould temperatures. The authors attempted to explain this physical property shift caused by mould temperature variance on the basis of different fracture mechanisms associated with different spherulite sizes assuming that the polymer will fracture interspherulitically, basically by rupture of the tie molecules. For example, if the sample has large spherulites the number of tie molecules will be reduced and consequently will reduce the impact strength.

Way, Atkinson and Nutting (7) studied in more detail the effect of spherulite size on the fracture morphology of compression moulded polypropylene and found that an average spherulite radius of R = 0.08 mm gave optimum tensile properties. Slow cooling rates resulted in the segregation of impurities and the

formation of contraction voids at the boundaries, consequently weakening these regions and having a detrimental effect on the whole structure. Fast cooling rates produced smaller spherulites which tended to fracture in a fibrillar fashion. It was proposed by the authors that at the faster cooling rates there is not enough time for significant segregation of low molecular weight species or uncrystalliseable impurities and, consequently, these weaken the spherulites. In addition to this theory it could be that lack of crystallinity and "cross hatched" lamellar growth within small spherulites reduces the stiffness and strength, this hypothesis is discussed below.

The most recent publication on the effects of processing parameters on the impact strength of injection moulded polypropylene homopolymer was given by Crawford and McGonagle (84) previously discussed. The authors found consistent reductions in impact strength for increasing mould temperatures from 20 to 60°C and established an impact strength maximum at a melt temperature of 190°C, but little variation in impact properties with injection rate. Crawford simply explained the impact property trends in terms of molecular orientation variations although no actual measurements were made. Similar trends were also reported by the author for a polypropylene copolymer.

The impact test results collated from this research programme can be discussed with reference to micromorphology, molecular orientation and crystallinity due to the comprehensive nature of characterization techniques employed. There is excellent agreement with previous research as regards the effects of processing conditions on structure and impact properties but the understanding of an impact property micromorphology relationship is somewhat more complex than previously realised.

The nature of the polypropylene crystallites and the consideration of the spherulite itself as an inhomogeneous stress system are among many factors that are not as yet accounted for.

As far as is known, isotactic polypropylene is unique in having a unit cell whose similar a and c repeat distances permit the epitaxial cell fit which gives rise to the monoclinic, "cross hatched" lamellar, spherulitic structure. However, fast cooling rates and high shear stresses experienced by polypropylene melts in the injection moulding process give rise to the formation of the β hexagonal, entirely radially organised lamellar, spherulitic structure in addition to the normal equiaxed α phase spherulites. The fact that isotactic polypropylene mouldings contain these two quite different polymorphs has been known for some time, but their importance has not been fully realised. We believe that the lamellar organisation of spherulites can be used to explain the anomolous impact properties exhibited by polypropylene injection mouldings.

Based on the work by Way et. al., (7) on deformation processes in α spherulitic polypropylene it can be proposed that the greater the degree of isotropy implied by the cross-hatched structure may explain the extremely high impact resistance of core material found in our fly-cutting exercise of Section 3.3.4. The tangential oriented lamellae will bind the radial lamallae together and impede crack growth between the lamellae, i.e. the tangential branching of lamellae during the growth of the α phase will give strength to those otherwise weak and generally amorphous regions. It then follows, that the reason

for the β phase acting as a weakening factor reducing the impact strength of injection mouldings is because crack propagation will occur most readily between radial lamellae where there are only weak tie molecules offering any resistance.

The microhardness of regions containing the β spherulites was found to be significantly higher than that of material at the skin and between these regions and the core of mouldings. The hardness values exhibited by the β phase implies increased brittleness, but low impact resistance. It has been reported by Way et. al., (7) that in general, the larger the α phase spherulite size the fewer are the interspherulitic links and this also results in a more brittle, low strength material due to the ease of crack propagation along spherulite boundaries. Our microhardness test results revealed a gradual increase in hardness/brittleness with spherulite size as the core of mouldings was approached, this is in good agreement with the afore mentioned work.

The lamellar organisation and consequent properties of spherulites also provides a reason for the transition in impact fracture initiation sites and fracture surface topography noticed with distance along the melt flow direction of polypropylene injection mouldings. In areas of mouldings where the β phase was identified (seen optically as row nucleated bright spherulites) fracture was found to iniatiate in the vicinity of them, whereas in areas away from the gate where no β phase was found crack initiation occurred in the core region of mouldings in the vicinity of the largest α phase spherulites. The accompanying fracture patterns were distinctly different the β phase crack initiation site appearing as a typically smooth brittle fracture, whereas the core α phase crack

initiation was seemingly fibrillar and random in propagation possibly indicating the interspherulitic fracture mechanism discussed.

Having emphasised the need to consider the nature and size of the crystallites it is also necessary to determine the rôle of the surface microstructure and the highly oriented row nucleated lamellar region, found some 500 μm below the surface, in determining the impact performance of polypropylene mouldings. Microhardness profiles through the thickness of moulded plaques reveal that the highly oriented frozen skin layer is infact very soft in contrast to the interior microstructure. This finding links well with Henke and Co-workers (8) observation of a skin layer exhibiting a higher molecular weight than that of interior regions of an injection moulded polypropylene. It can be concluded therefore that a fast cooled oriented non-spherulitic skin has good energy absorbing characteristics.

In our polypropylene mouldings produced at high mould temperatures (in excess of 70°C) the formation of a transcrystalline surface layer resulted in dramatic reductions in impact properties. An analysis of fracture surfaces revealed crack initiation sites at the surface illustrated by small cracks running perpendicular to the surface through a smooth typically brittle initiation zone.

Hobbs (81) studied the morphology and fracture characteristics of knit lines in isotactic polypropylene and revealed one or more bands of transcrystalline growth nucleated on highly ordered material running along the weld line. During tensile tests it was found that transcrystalline and shear induced morphologies rather than poor bonding of melt fronts were

responsible for deformation and it was proposed that these morphologies were the determining factor in failure which strongly supports our findings.

In addition, studies on the effect of interfacial microstructure on composite properties have also revealed curious anomolies regarding transcrystalline layers. One of the earliest systemmatic studies was reported by Bessel et. al., (165) using nylon 6 as the matrix polymer loaded with 15% by volume of glass fibres. It was noticed that in tensile tests the propagating cracks were occasionally redirected parallel to the fibres at a distance of about 2μm from the actual fibre-matrix interface. These workers suggested that there is a surface of weakness some distance from the fibre surface which may be related to the columnar transcrystalline region around the fibre.

Ritchie and Cherry (166) and Masuoko (167) have investigated the possible rôle of transcrystallinity as a factor in controlling adhesive bond strengths in glass fibre filled high density polyethylene and nylon 12 respectively. Both authors concluded that changes in bond strength arose from the change in degree of crystallinity. In addition Kardos (168) examined the microstructure and mechanical properties of glass and carbon fibre reinforced polycarbonate and using a special moulding and annealing sequence, the latter reported that the tensile modulus and strength of test bars are enhanced due to the localized formation of crystalline entities on the fibre surface.

More recently, Folkes and Wong (169) have developed an experimental technique for the systematic determination of critical

fibre length and hence interfacial shear strength. In the case of glass fibre filled polypropylene and carbon fibre filled polyamide composites the formation of a transcrystalline layer around the fibres led to a reduction in interfacial shear strength. In related work Folkes and Hardwick (170) have shown the dependence of transcrystalline formation on molecular weight of the polypropylene matrix in terylene fibre reinforced composites.

It can be concluded that the exact mechanism of impact fracture occurring at the transcrystalline surface of polypropylene injection mouldings is not yet fully understood. However, two possible fracture mechanisms are now proposed based on the literature survey and experimental work carried out in this research project. Firstly, that cracks initiate as a result of the weak amorphous regions between the embryonic spherulitės, these regions acting as effective surface notches and causing delamination between the spherulites perpendicular to the surface, or secondly, that the lamellar growth nature of these transcrystalline entities is entirely radial permiting crack initiation and propagation between radial lamellae where there are only weak tie molecules offering any resistance. The latter mechanism coincides with that proposed for the fracture of brittle β phase spherulites and since numerous large β crystallites were found at the surface this already established mechanism appears to be the most likely.

The apparent weakness in the row nucleated shear band found close to the gate in all mouldings can possibly be explained with reference to the recent work of Bashir et al., (69) on high modulus chain extended polyethylene. The former found that oriented polyethylene plugs produced by extrusion

revealed an underlying structure which was found to be essentially lamellar with the lamellar oriented normal to the plug or fibre axis similar to that revealed in our work. This largely lamellar structure, representing chain folded crystallisation was in fact found to produce high modulus materials, in contrast to the usual belief that the attainment of high modulus requires a high level of chain extension. The enhanced modulus associated with parallelism of lamellae was not measured for the polypropylene shear nucleated morphology revealed in this work, but microhardness values indicate an apparent increase in embrittlement as a result of its formation.

In summary, for optimum impact performance in polypropylene homopolymer injection mouldings one must strive to produce mouldings with a thick (~50μm) highly oriented non-spherulitic surface skin and an underlying well formed cross hatched spherulitic morphology with as little production of shear nucleated structures as possible. To assist the moulder in achieving these requirements two models based on this research work were proposed on the effects of melt temperature and mould temperature on impact properties as illustrated overleaf.

6.2 THE EFFECT OF MOLECULAR WEIGHT ON THE MICROMORPHOLOGY AND IMPACT PROPERTIES OF ISOTACTIC POLYPROPYLENES

The application of a shear stress to a polymer melt results in molecular orientation. In accord with the theories of Flory (171) and Krigbaum and Roe (172), the associated decrease in the entropy of the melt may be considered to increase the melting temperature and hence, the supercooling. Hans and Maxwell (173) and Fritzsche and Price (174) concluded that for polyethylene, polybutylene and polyethylene oxide melts under high shear stresses at which large increases in supercooling apparently

MODEL 1 Effect of melt temperature on the impact properties and micromorphology of injection moulded GXM43 iPP.

	MELT TEMPERATURE			
	220 C	250 C	280 C	>280 C
Centre of moulding impact strength	— increasing ⟶		maximum —	decreasing ⟶
Skin morphology	frozen	non spherulitic		transcrystalline
Thickness (μm)	20	10-15	5-10	0
Row nucleated shear band	decreasing in thickness and extent ⟶			
β phase row spherulites	decreasing in concentration and extent ⟶			
Preferred orientation	marginal decrease ⟶		increasing ⟶	
Crystallinity	marginal decrease ⟶		dramatic increase	

MODEL 2 Effect of mould temperature on the impact properties and micromorphology of injection moulded GXM43 iPP.

	MOULD TEMPERATURE			
	30 C	50 C	70 C	80 C
Centre of moulding impact strength	——decreasing⟶			very poor
Skin morphology	frozen	non spherulitic⟶		transcrystalline
	decreasing in thickness			
Row nucleated shear band	decreasing in thickness and extent ⟶			
β phase row spherulites	increasing in size and extent ⟶			
Preferred orientation	increasing ⟶			
Crystallinity	—— increasing ⟶			dramatic increase

result, crystallization rate is favoured by use of higher temperatures and with polymers of low molecular weight. Low molecular weight samples crystallise more rapidly under shear stress due to increased molecular chain mobility providing faster orientation and shorter relaxation times. In contrast, increasing molecular weight increases relaxation times so that preferred orientation introduced by extensional and shear flow is retained for longer periods to allow crystallisation and growth from oriented melts. Therefore, under conditions of equal temperatures and shear rates, the shear stress would be less in a lower molecular weight system than in a high molecular weight one.

In injection mouldings of iPP prepared in this present research study it was revealed that the skin thickness increased markedly with molecular weight. Guo and Bowman (22) observed a similar trend for two grades (molecular weights) of polybutylene and simply related it to the changes in relaxation times. Fujiyama and Kimura (10-14) however, discussed a similar effect in iPP injection mouldings in terms of recoverable shear strain γ_e, relaxation time λ, crystallisation time t_c, and mould shrinkage. The authors concluded that since viscosity becomes higher as the molecular weight becomes higher, γ_e and λ also become higher. Since iPP meltscrystallise under a high shear stress in injection moulding, their molecular chains crystallize in an expanded state. At this time, not all expanded molecular chains orientation crystallize, but a portion become random coils due to their relaxation during the time before crystallisation and cause spherulitic growth (found below the immediate surface). The number of molecular chains that orientation crystallize (proportional to the thickness of the skin layer) must become larger as the degree of the expansion of the molecular

chains becomes higher, their relaxation becomes slower and the time before they crystallize becomes shorter. The thickness of the skin layer must become higher than as γ_e becomes higher, λ becomes longer, and t_c becomes shorter i.e. as the molecular weight increases.

It can be said that in the present study as with Fujiyama and Kimura's (9-14) work that shrinkage correlates closely with thickness of the skin layer through the recoverable shear strain γ_e is governed by rheological and crystallisation characteristics. These, in turn, are governed finally by the molecular structure of iPP.

The width and extent of the highly sheared row nucleated lamellae zone, found some 500 μm below the surface of our injection moulded iPP samples, was found to be significantly enhanced by increasing the molecular weight. Applying the theories discussed above this trend can be explained simply in terms of the increased shear stress, preferred orientation and relaxation times associated with increasing molecular weight. As a consequence the row nucleation of the β-phase crystallites ahead of this zone increased revealing dense populations of small spherulites across the entire flow path of the highest molecular weight mouldings. X-ray diffraction studies confirmed an increase in preferred molecular orientation, β phase concentration and crystallinity in the surface layers of these samples. In low molecular weight mouldings reduced shear stresses allowed relaxation and growth of larger more random β spherulites in the shear zone which were seen to die away a short distance from the gate.

The lamellar morphology resulting from high levels of chain extension was studied recently by Bashir et al., (69) for

extruded polyethylene plugs. The authors also related the process of chain extension to the competing process of chain relaxation and found that one of the ways of increasing the proportion of molecules undergoing chain extension was to increase the molecular weight. In fact, it was found that a small quantity such as 3% of added high molecular weight material can have a disproportionate effect on processing and end product by setting the pattern for the lamellar crystallisation. In our studies an almost proportional effect of percentage high or low molecular weight tail in the bulk polypropylene was found with very little noticeable effect of low percentage additions.

The noticeable decrease in core α spherulite size with molecular weight must be related to the difficulty of the polymer to crystallize rapidly with longer chains and entanglements inhibiting lateral development. A similar effect was recently reported by Hardwick and Folkes (170) who have shown that the lateral development of transcrystalline iPP layers off Terylene fibres depends on molecular weight. For the highest molecular weight sample, it was difficult to discern any difinitive transcrystalline layer.

In conclusion it does appear that molecular weight has a profound effect upon structural heterogeneity in iPP injection mouldings particularly as regards surface and shear band morphologies.

The impact properties of injection moulded iPP have also been shown to depend on the molecular weight and resultant micromorphology. In regions between the gate and beyond half way along the flow direction a significant increase in the width

of the shear row nucleated zone and β phase nucleation with increasing molecular weight resulted in very poor impact properties compared to low molecular weight iPP mouldings prepared under the same processing conditions. However, in regions at the far end of the flow path in high molecular weight plaques a six fold improvement in Izod impact strength led to far superior impact properties than the low molecular weight mouldings. The reason for this vast improvement was shown optically to be due to the absence of shear nucleated structures but the presence of a thick skin/small core α spherulite morphology.

These results again highlight the overiding role of shear induced morphologies, and in particular β phase spherulite nucleation, on impact properties regardless of skin thickness or core spherulite size in iPP injection mouldings.

6.3 THE EFFECT OF NUCLEANTS ON THE MICROMORPHOLOGY AND IMPACT PROPERTIES OF ISOTACTIC POLYPROPYLENE

6.3.1 Discussion of Results

As previously discussed, it has been shown by Henke et al., (8) and Way et al., (7) that the spherulite size correlates well with most physical properties in compression moulded polypropylene parts. Good impact properties in injection moulded iPP plaques were shown in this research project to be dependant on surface morphology which can be similar to or substantially different from that in the core as a consequence of the molecular weight of the resin and or the processing conditions employed. It has also been proposed that for good impact performance in iPP injection mouldings one must strive to produce mouldings with a well formed cross-hatched α spherulitic morphology with as little shear induced row nucleated crystallites as possible. It was therefore of

interest to modify the micromorphology of mouldings by the incorporation of low percentages of commercially available additives to assess the effect of degree of crystallisation and size, type and perfection of spherulites on the impact properties. Of particular interest was the relationship between size and concentration of the α and β phase crystallites and impact performance.

From x-ray diffraction and DSC thermal studies the effectiveness of each additive as a heterogeneous iPP nucleant was assessed and related to the resultant impact properties. It was noticed that those additives that enhanced the nucleation of α phase spherulites also lead to mouldings with reduced impact strength which is in excellent agreement with recent publications by Hutley et al., (108, 109) on mineral filled polypropylene copolymer compounds. In fact, the inverse relationship between crystallization temperature and impact strength shown in Figure 159 provided a much tighter least squares straight line fit than that given by the latter authors. The explanation for this loss in impact performance must surely be given with reference to the observed reduction in spherulite size. The massive nucleation revealed embryonic type spherulites which due to enhanced crystallisation rates probably have very little cross-hatched lamellar growth or segregation of impurities required for optimum properties.

In contrast to the well nucleated Quinacridone, talc, and phthalocyanine filled polypropylene mouldings the ultramarine blue pigmented mouldings revealed an apparent reduction in degree of crystallisation and an associated increase in spherulite size. It is significant that the impact properties were better than the unpigmented polypropylene plaques and it was assumed therefore that the larger α spherulites in the

ultramarine blue pigmented samples had a somewhat more developed cross-hatched morphology.

This assumption was based on previous work by Binsbergen and De Lange (116) who measured the relative amounts of radial and tangential lamellae as functions of temperature of crystallisation in polypropylene melts by use of birefringence measurements. The fraction of tangential lamellae in mixed or non-birefringent spherulites is about a third, as deduced from refractive index equations. Spherulites crystallised below 403K have a higher fraction (up to a half) and those crystallised above 413K a lower fraction of tangential lamellae. So the fraction of tangential lamellae tends to be lower at smaller degrees of supercooling. Also, crystallisation at 433K did not produce cross-hatched morphologies, only sheaves of lamellae, and cross-hatched morphologies seem to have a more open structure when crystallised at a smaller degree of supercooling.

In addition to the enhanced α phase nucleation observed for some of the compounds the degree of β phase nucleation was also significantly altered by each additive. Ultramarine blue, chalk and Quinacridone Red E3B incorporated in polypropylene mouldings significantly enhanced β formation. Micrographs taken of Ultramarine blue pigmented and Chalk filled plaques revealed a distinct increase in the concentration of randomly nucleated β crystallites extending into the core with little evidence of increased row nucleated β structures in the highly sheared regions. Micrographs of the Quinacridone Red pigmented plaques revealed a highly nucleated spherulitic morphology and despite the high levels of the β polymorph indicated by x-ray diffraction studies no β spherulites were discernable.

This specific β phase nucleating characteristic was reported for Ultramarine blue pigment by Williams et al., (20) in an injection moulded polypropylene copolymer and for Quinacridone Red E3B pigmented polypropylene melts by Leugering (46) and Duswalt et al., (47). However, a search of the literature revealed that this specific nucleating effect has not been previously observed for commercially used chalk filler in polypropylene. The increase in random β phase formation does not appear to have had any deletereous effect on the impact properties of Ultramarine blue or Chalk filled compounds which again highlights the association of brittle impact behaviour with shear row nucleated β and small underdeveloped α phase structures. It does appear that the randomly nucleated β spherulites form as a result of increased cystallisation rates which is a mechanism proposed by other workers in the field, including Kieth and Padden (40) and Turner-Jones (42).

6.3.2 Heterogeneous Nucleating Mechanisms

The basic idea underlying most pictures of heterogeneous nucleation is that the total interfacial free energy of the crystalline embryo is reduced by a foreign phase which already provides part of the interface to be formed, this brings about a reduction in the activation free energy for nucleation and thereby a decrease in the degree of supercooling required for nucleation. The higher the preference of the crystalline phase to absorb at the foreign material rather than the liquid phase the lower the activation free energy for nucleation will be. The amount of reduction in interfacial free energy is dependent on both the geometrical form of the foreign phase and its chemical nature.

Extensive investigations of nucleating agents reviewed already have been carried out by other workers for polypropylene.

Beck (96) and Binsbergen (97, 98) for instance have ranked materials on the basis of the crystallisation temperature Tc observed by differential thermal analysis in experiments at constant cooling rates. The best known nucleating agents are the sodium salts of carboxylic acids and the poorest are the oxides of aluminium and titanium.

From the above studies Tc values of up to 404K were quoted for heterogeneously nucleated polypropylene, in the present study incorporation of 0.1 wt.% Quinacridone and Phthalocyanine pigments exerted the greatest influence on the morphology with Tc values in the region of 400K, with 5 wt.% talc filled samples giving Tc values of 395K. We may assume that the overall crystallisation rates indicated by the shifts in the degree of supercooling reflect the influence of the foreign material on the nucleation rate.

Binsbergen (98) provided evidence that the nucleating agents for polypropylene have the following features in common based on extensive studies on the chemical and physical nature of the nucleating agents:-

(i) The crystals of the nucleating agents expose faces of hydrocarbon groups. These groups resemble moderate to good solvents for polyolefins i.e. aromatic chlorinated aromatic, cycloaliphatic and branched chain aliphatic hydrocarbons.

(ii) The nucleating agents are, nevertheless, insoluble in the polymer melt due to a polar group attached to the hydrocarbon group or to a condensed aromatic structure.

The author proposed that the nucleating effect is in all probability linked up with a general feature of the crystal structure of the nucleating agents since the crystals of

nucleating agents expose faces of hydrocarbon groups, the latter being arranged in rows or stacks parallel to the faces. As a result, the faces show shallow ditches in which absorbed polymer molecules can be forced to assume a stretched conformation over some distance allowing crystallisation to occur that much easier. From the experimental observations it was concluded that a good nucleating agent has a physical state consisting of a fine dispersion of small crystals and that the crystals are built up of polar (p) and non-polar (n) layers.

The proposals made by Binsbergen for a good nucleating agent agreed extremely well with the earlier statements by Beck (96) and one must therefore place confidence in applying their nucleation theories to explain the effects of the three strong nucleants identified in the present study:-

(i) Phthalocyanine Blue is a crystalline organic pigment with an extremely stable copper complex structure . It is a condensed aromatic compound which was shown by Honigmann et al., (175) to exhibit regular packing of parallel stacks of the flat ring systems in a (n-p—n-p) arrangement . This pigment has been observed to cause highly oriented crystallisation in injection moulded polyethylene nucleated by copper phthalocyanine needles. As a nucleant it fulfils the requirements proposed by Beck.

(ii) Quinacridones are crystalline organic pigments for which there is evidence for the existence of seven polymorphic forms. The features of exposed faces of non polar carbonyl groups and the polar -NH- attached to the condensed aromatic structure provide the requirements for a good polypropylene heterogeneous nucleator. The preferential nucleation of the β phase spherulites by

Quinacridone Red E3B is well documented but little is known about the factors governing this preference. It may simply be a better match of lattice parameters with the hexagonal rather than monoclinic crystal structure. Insufficient crystal structure data on the Quinacridones examined are available to allow a firm conclusion. Certainly the type of crystalline structure is of importance as highlighted by Beck (96) where sodium formate and lithium benzoate nucleants revealed monoclinic structures close to those of polypropylene α phase spherulites.

(iii) Talc, $Mg_3(OH)_2\ Si_4\ O_{10}$, has a charged structure which possesses a zeta potential. Vesely and Shipley (176) proposed a nucleation mechanism on the basis of experiments involved with applying a small voltage to electrodes embedded in polypropylene films crystallised on a layer of talc substrate. A small applied potential caused enhanced nucleation. The authors suggested that whilst the polypropylene is molten it is believed that electrostatic forces originating from the surface of the nucleator induce dipoles in the atoms of the polymers main chain. The intermolecular forces, are thought to restrict the motion of the polymer chains in the melt phase allowing crystallisation to occur at a higher temperature. This mechanism differs from that proposed by Binsbergen and Beck in that the most polar groups are situated on the materials surface i.e. at the ends of talc platelets where bonds have been broken, as illustrated in Figure 16 previously.

The explanation of the apparent preferential nucleation of the β hexagonal phase spherulites by chalk and Ultramarine blue and Quinacridone Red is not yet fully understood. However, Geil (57)

stated that in crystallisation of polypropylene one can have crystallised spherulites in the hexagonal unit cell or the monoclinic unit cell independently by using specific types of heterogeneous nuclei, and that it is the structure of the nucleus which determines the unit cell throughout the entire spherulite. However, the author does not quote any specific nucleant or reference to support this claim. The studies reviewed in this discussion have not revealed specifically what types of interaction with the polymers render the nucleating agent active. Epitaxy or lattice matching has been recurrently invoked but it has never been firmly established as a mechanism. Although Binsbergen (97, 98) has excluded lattice matching type epitaxy as the major mechanism for heterogeneous nucleation, Wittman and Lotz (103) in a recent publication suggested that structural similarities between some of the apolar parts of the well known nucleants and polyethylene are striking and indicates a need for re-examination of the experimental evidence on which the up to date conclusions rest. The authors based their proposal on studies of the nucleating effect of benzoic acid for various polymers. They reported an epitaxial relationship between polyethylene, n-paraffins or aliphatic polyesters and benzoic acid which was characterised by a unique orientation of the polymer mass parallel to the substrate plane.

Garborczyk and Paukszta (177) studied the influence of small amounts (0.5%) of stabilizers on the crystal structure of iPP during crystallisation from a melt and examined the relationship between the molecular and crystal structure of stabilizers and iPP by means of x-ray diffraction techniques. For polypropylene samples containing 2-mercaptobenzimidazole (MBIM) and Triphenodithiazine (TPDT) the degree of β -form was significantly enhanced. The authors proposed that the shape of the stabilizer crystal is one of the reasons why the β -form of iPP is formed.

The crystals of compounds which initiate hexagonal iPP have the form of plates or needles elongated in the c-axis direction and belong to the centrosymmetric space groups. In addition these compounds have similar structures in which sulphur atoms are placed above the planes of the phenyl rings. It is interesting that Permanent Red E3B, mentioned above, which also initiates the hexagonal β form of iPP, has a similar molecular structure to TPDT as shown in Figure 167.

Ronca (107) more recently established an epitaxial relationship for polyethylene, polypropylene, polyoxymethylene (POM) and polyhydroxybutyrate (PHB) nucleated with talc and boron nitride. The relationship was made after taking electron micrographs from theparticles which form the centre of spherulites produced by melting and recrystallisation of solvent cast films of the compounds. With respect to iPP (grade GXM43), preferential growth of spherulites along the (040) plane with the chain axis oriented parallel to the surface of the substrate was observed and two dimensional lattice matching of the polymer with talc and boron nitride was identified. The former substrate revealed a repeated configuration with a periodicity of nine polymer chains and the latter with a periodicity of thirteen polymer chains. The author also demonstrated a close epitaxial growth of polyethylene POM and PHB with talc and boron nitride with excellent crystal matching between polymer and substrate. Ronca concluded that the epitaxial growth is the most probable mechanism for induced nucleation and that perfect crystal matching of the polymer and substrate will ensure a maximum shift in the crystallisation temperature T_c.

The results of the investigations made in this present study show that the preferential nucleation of α or β isotactic polypropylene may be caused by small amounts of additives.

Figure 167 Molecular structures of TPDT and Quinacridone red E3B

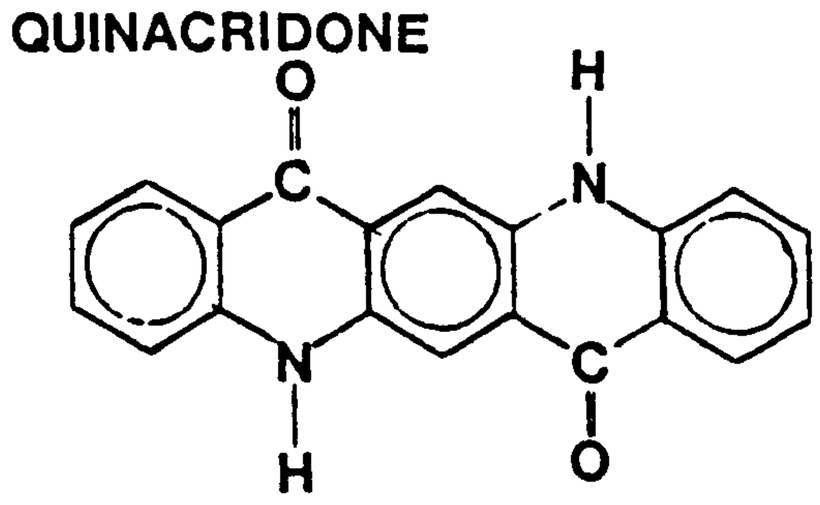

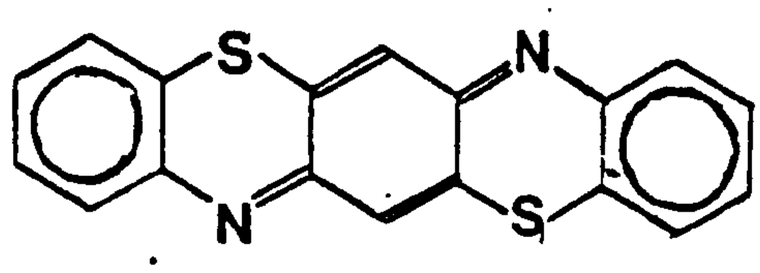

Figure 168 Sectioning of dust pans for impact testing and microscopy.

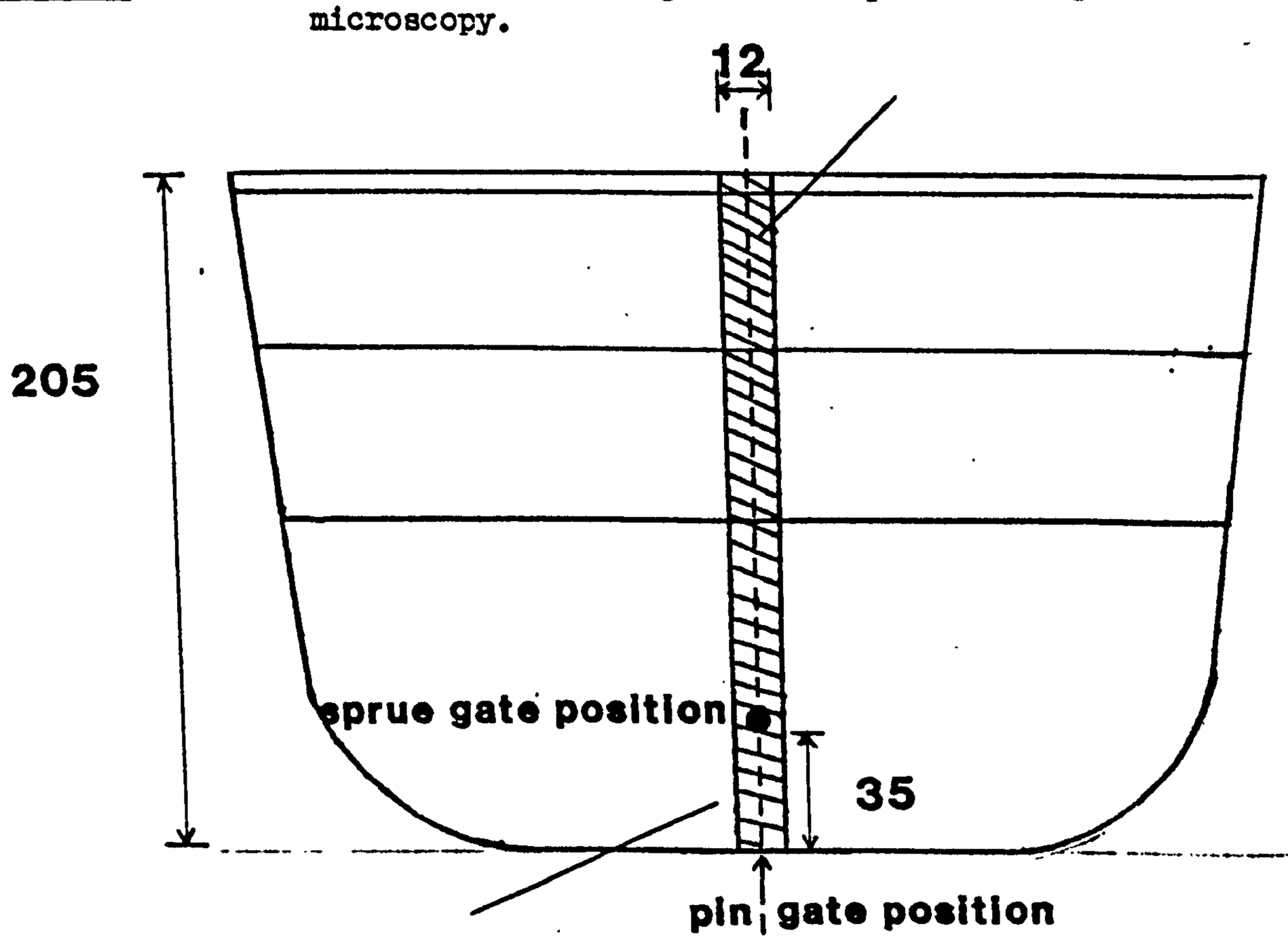

The contribution of the β form in iPP depends upon the type of additive and is undoubtedly connected with the observed epitaxial relationship phenomena but at this stage of our research it is impossible to determine a close relationship between molecular structure and crystal shape of additives and space arrangements of iPP during crystallisation in the injection moulding process. This problem is a subject for further investigation.

6.4 APPLICATION OF RESEARCH FINDINGS TO COMMERCIAL PIGMENTED INJECTION MOULDINGS OF GXM43 iPP

6.4.1 Introduction

In the past it has proved difficult to make definitive statements on the effects of injection moulding variables on the morphology and properties of a moulded product, due to the complexities which arise when one considers the many interdependent combinations of machine settings and their effect on the mechanical working and thermal history of the material. In most cases, as with ours, the problem has been tackled by moulding standard test pieces using a variety of moulding conditions and relating their mechanical properties to the process variables. Unfortunately, moulders have tended to be sceptical of the results of such tests because it is argued that simple geometries of laboratory test pieces do not simulate the flow paths which are experienced by the melt in practical mouldings.

In an effort to support our results and convince industry of their relevance to real iPP moulded articles, a brief programme of work was initiated to see whether impact property-morphology relationships established for GXM43 iPP injection mouldings could be applied to a commercial pigmented moulding of the same polymer. Addis (26) kindly supplied two standard dust pans moulded in GXM43 iPP as used in our research studies, for this

work. The two mouldings differed only in that one was pigmented green and sprue gated (5mm diameter) and the other pigmented red and pin gated (1mm D x 1mm W). Addis assured us that the pigments used to colour the mouldings were carefully selected by I.C.I. and do not heterogeneously nucleate iPP.

6.4.2 Experimental Procedure

The two commercial mouldings were sectioned according to Figure 168, to provide 80 consecutive Izod test pieces (approximately 2mm x 2mm x 12mm) along the flow direction from the flat area base of the dust pans. The cross-sectional area of each selected test piece was recorded prior to Instrumented Izod impact testing and Optical microscopy studies according to the procedure used in previous experiments. The Izod impact test results are collated in Table 46 and represented graphically in Figure 169. Selected micrographs for each moulding are also presented in Figures 170 and 171

6.4.3 Analysis of Results

From the Izod impact test results, plotted in Figure 169 , it is clearly evident that the impact strength varies considerably with position relative to the gate which is in turn dependent on the type of gate and the flow path length. The following general observations were made from these results:-

(i) The impact prcperties directly at the gate were very low, particularly with the sprue gate geometry where significant voids were observed.

(ii) The red pin gated moulding revealed a steady improvement in impact properties up to 175mm away from the gate, from c.a. 1.6 kJm^{-2} to c.a. 4 kJm^{-2}. Beyond 175mm the impact properties increased dramatically to c.a. 12 kJm^{-2}.

TABLE 46 Instrumented Izod impact test results for two commercial mouldings of GXM43 iPP.

SPRUE GATED MOULD		PIN GATED MOULD	
DISTANCE FROM GATE (mm)	I.S (kJm-2)	DISTANCE FROM GATE (mm)	I.S (kJm-2)
37.5-35.5	6.42	0.0- 2.0	1.61
35.0-33.0	7.78	2.5- 4.5	2.08
32.5-30.5	5.53	5.0- 7.0	1.94
30.0-28.0	6.92	7.5- 9.5	1.81
27.5-25.5	6.09	10.0-12.0	1.82
25.0-23.0	5.33	12.5-14.5	1.94
22.5-20.5	3.08	15.0-17.0	2.52
20.0-18.0	2.49	17.5-19.5	2.77
17.5-15.5	2.02	20.0-22.0	2.09
15.0-13.0	1.76	22.5-24.5	2.71
12.5-10.5	0.84	25.0-27.0	2.74
10.0- 8.0	1.01	27.5-29.5	2.80
7.5- 5.5	1.75	30.0-32.0	2.76
5.0- 3.0	1.44	32.5-34.5	2.69
2.5- 0.5	1.50	35.0-37.0	2.59
0.0- 2.0	1.14	37.5-39.5	2.60
2.5- 4.5	1.76	40.0-42.0	2.90
5.0- 7.0	1.66	42.5-44.5	2.90
7.5- 9.5	2.00	45.0-47.0	2.48
10.0-12.0	1.92	47.5-49.5	2.60
12.5-14.5	1.82	50.0-52.0	3.00
15.0-17.0	1.98	52.5-54.5	2.38
17.5-19.5	2.06	55.0-57.0	3.10
20.0-22.0	2.19	57.5-59.5	3.60
22.5-24.5	2.03	60.0-62.0	3.00
25.0-27.0	2.01	62.5-64.5	2.69
27.5-29.5	2.32	65.0-67.0	2.85
30.0-32.0	2.07	67.5-69.5	3.00
32.5-34.5	2.26	70.0-72.0	2.95
35.0-37.0	3.07	72.5-74.5	2.96
40.0-42.0	2.08	85.0-87.0	2.95
47.5-49.5	2.31	97.5-99.5	2.94
60.0-62.0	2.58	110.0-112.0	2.90
72.5-74.5	2.07	122.5-124.5	2.88
85.0-87.0	2.54	135.0-137.0	2.87
97.5-99.5	2.92	147.5-149.5	3.70
110.0-112.0	3.17	160.0-162.0	3.84
122.5-124.5	3.15	172.5-174.5	3.59
135.0-137.0	2.69	185.0-187.0	10.00
147.5-149.5	4.07	187.5-189.5	9.71
150.0-152.0	5.09	190.0-192.0	9.95
152.5-154.5	6.16	192.5-194.5	12.00
155.0-157.0	10.15	195.0-197.0	12.41
157.5-159.5	9.43	197.5-199.5	12.30
160.0-162.0	10.37		

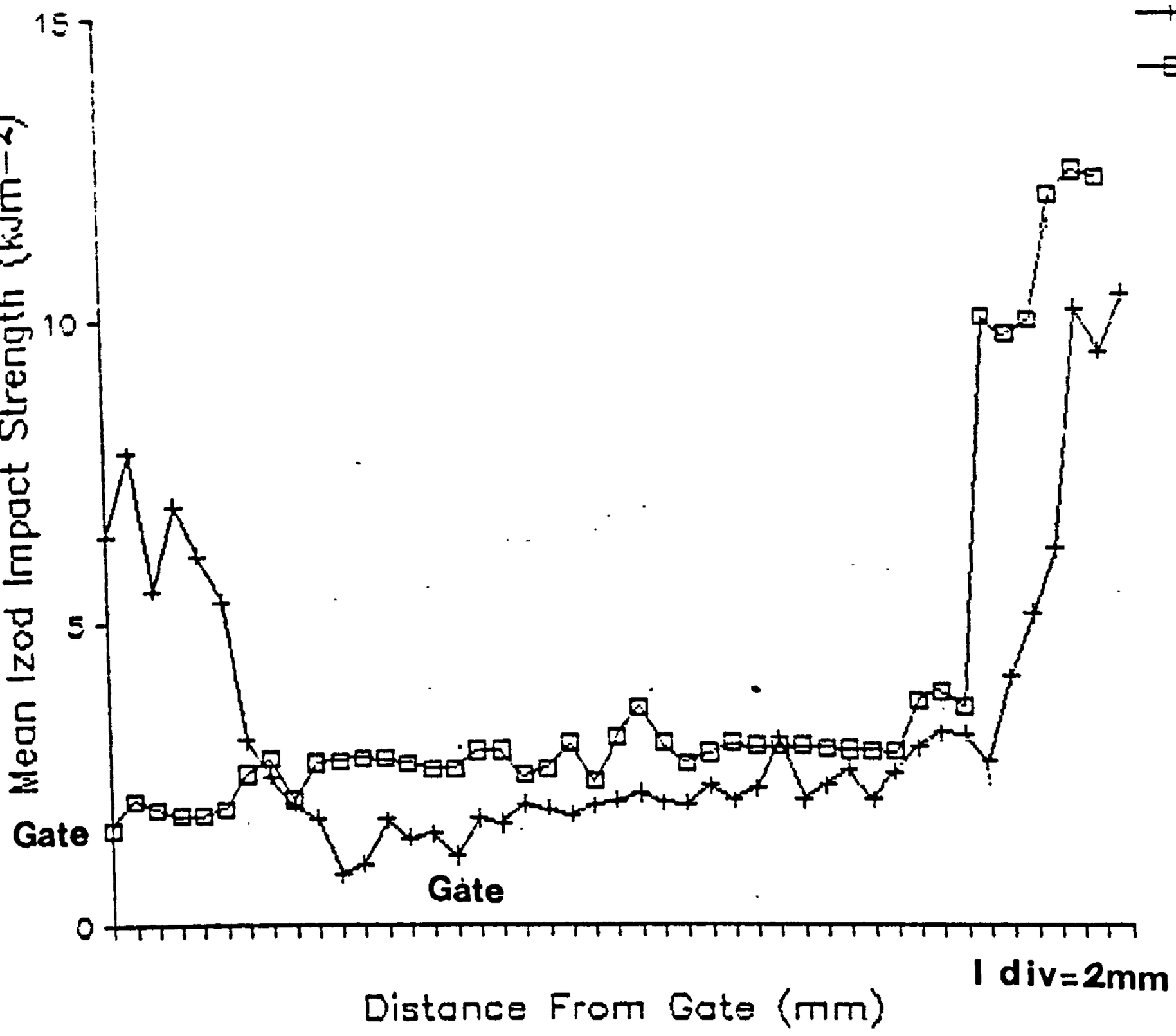

Figure 169 Mean Izod impact strength versus distance from the gate for the two commercial mouldings of GXM43 iPP.

Figure 170 Typical micrographs from selected areas of the red moulding:

(a) in the vicinity of the gate

300µm

(b) 50mm from the gate

(c) 185mm from the gate

(d) At the extremity of the flow direction.

Figure 171 Typical micrographs from selected areas of the green moulding:

300μm

(a) in the vicinity of the gate

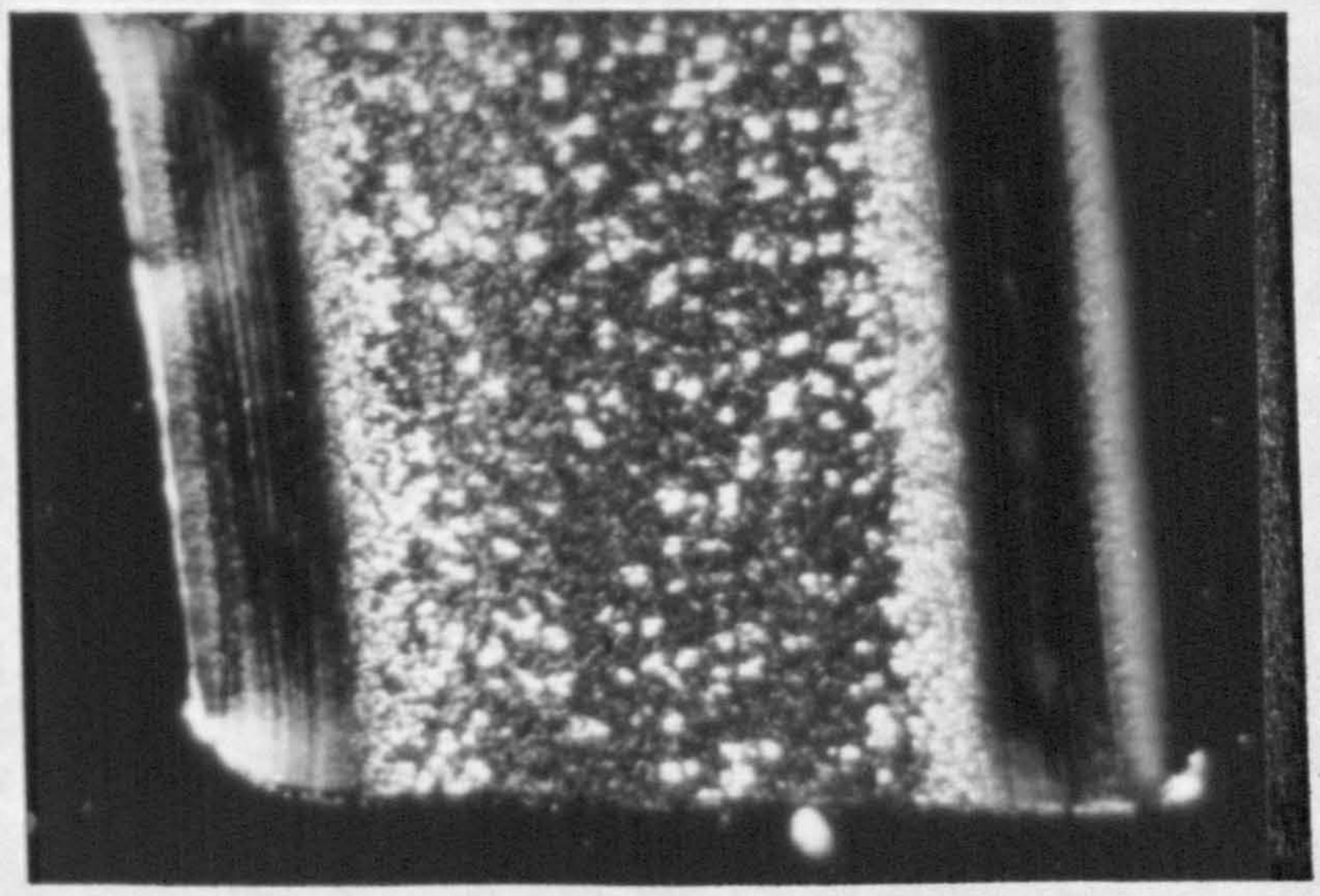

(b) 60mm from the gate

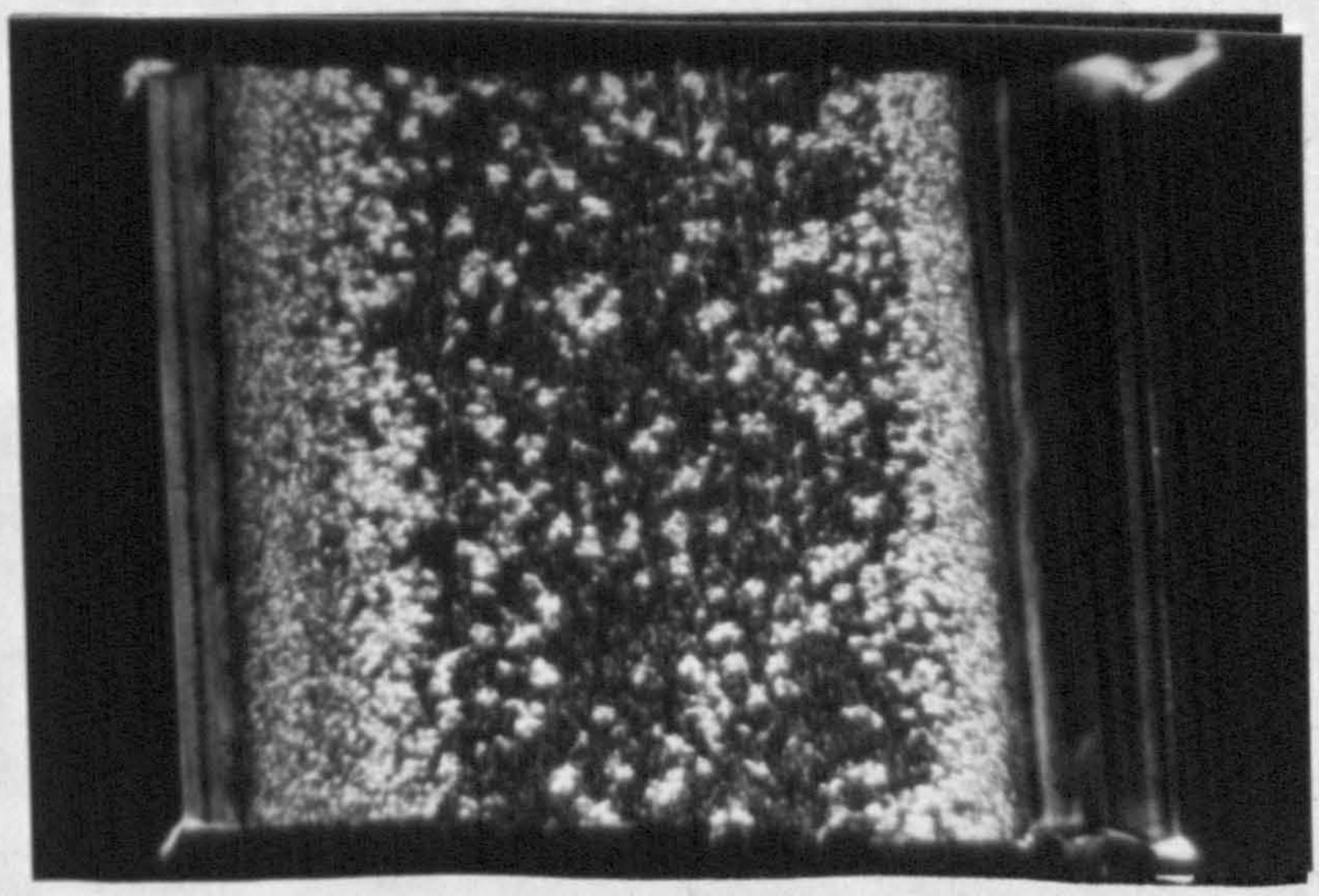

(c) 150mm from the gate

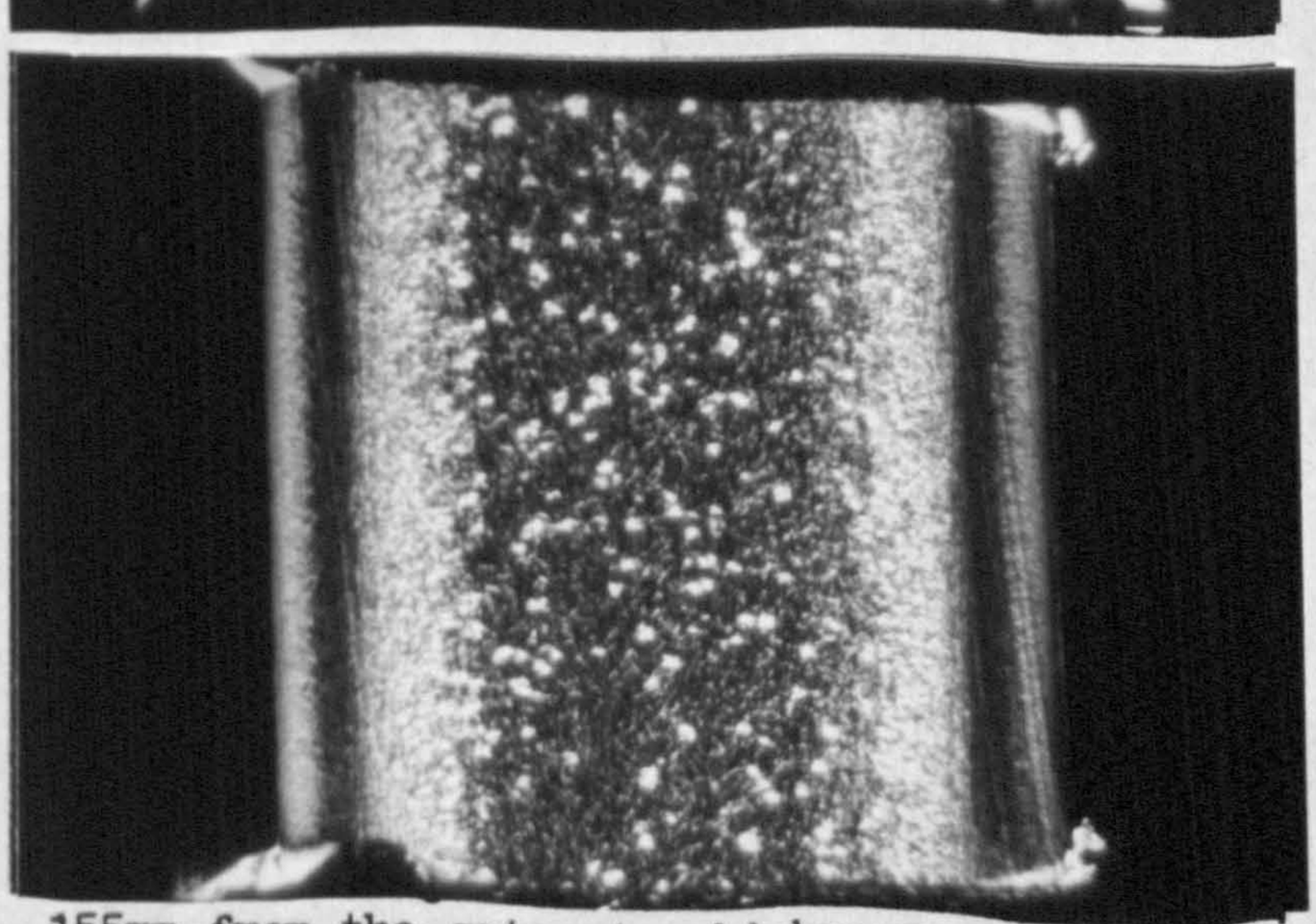

(d) 155mm from the gate at a higher magnification.

100μm

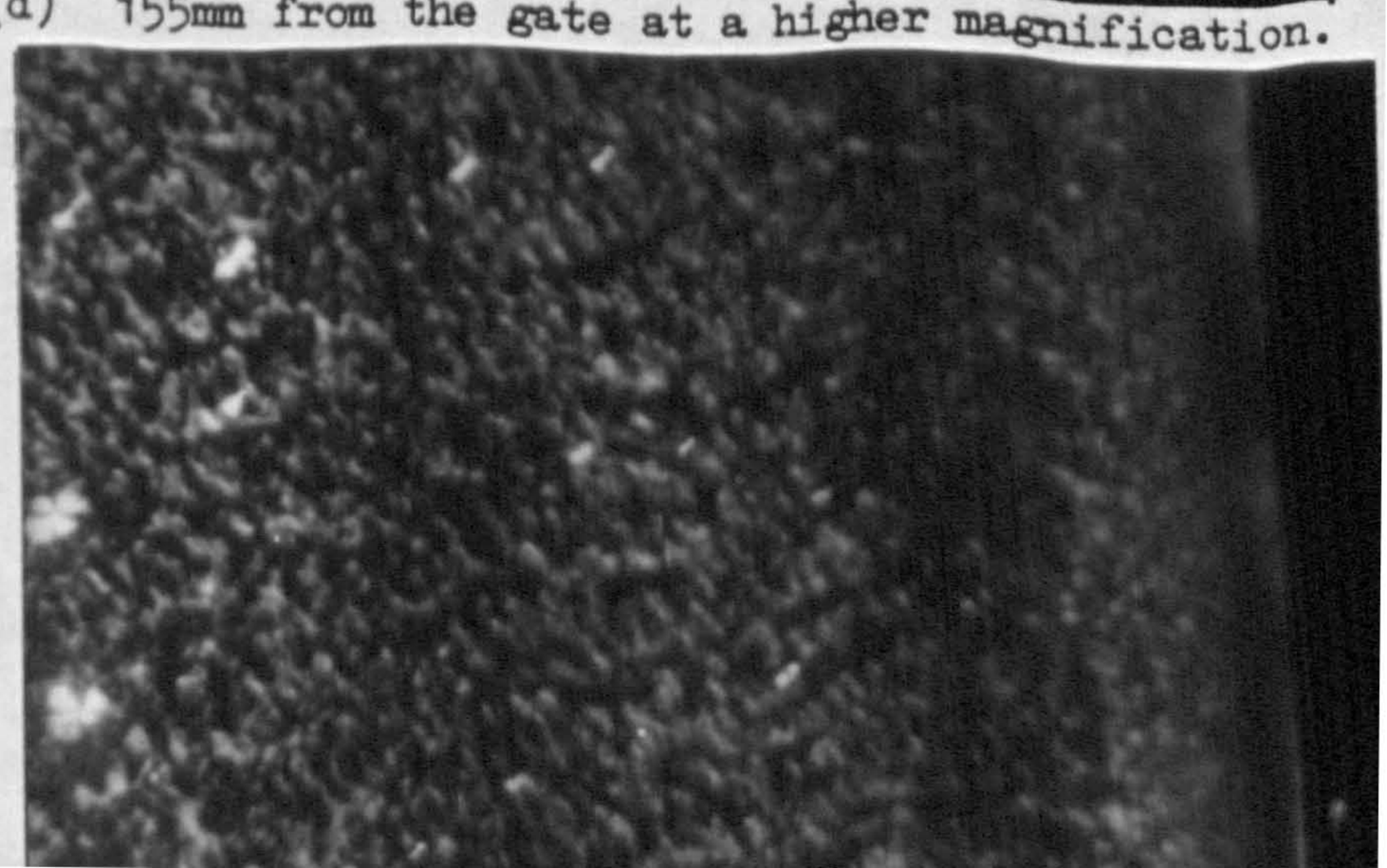

(iii) The green sprue gated moulding revealed a steady improvement in impact properties up to 150 mm away from the gate, from c.a. 1 kJm^{-2} to c.a. 4 kJm^{-2}. Beyond 150mm the impact properties increased dramatically to c.a. 10 kJm^{-2}. However, in the opposite direction away from the gate the increase in impact strength appeared to occur over a much shorter distance with values of 7 kJm^{-2} recorded at 35mm away from the gate.

(iv) The impact properties compare extremely well with those measured for the Daniels injection moulded iPP 2mm plaques, moulded using low melt temperatures (220°C) and low mould temperatures (35°C) presented in Table 24.

The optical micrographs presented in Figures 170 and 171revealed as expected, the complex banded morphologies associated with iPP injection mouldings. In regions which exhibited poor impact properties wide shear bands with massive row nucleation of the β polymorph were apparent. The level of β nucleation was much higher than that observed for any test piece moulded in this research project, the reason for this is probably due to the extremely fast injection speeds used in industry to achieve fast cycle times. In regions furthest from the gate in both mouldings the level of β nucleation is much lower and decidedly random with no shear row nucleated banded morphologies present. These regions exhibited good impact properties.

This brief, but informative study has provided conclusive evidence to support the observations made on simple geometry iPP test pieces. It is now certain that structural heterogeneities, particularly the presence of row nucleated β structures can have a profound effect upon the impact properties of real injection moulded iPP parts. This effect being enhanced with use of fast injection and low melt and mould temperatures,

which are employed for fast cycle times to produce economically viable moulded products.

Whether the moulder should utilise this knowledge to achieve maximum impact resistance in moulded articles will depend on the end use and complexity of the product. However, process condition-structure-property relationships must surely serve as a useful tool in the trouble-shooting area of injection moulding of polypropylene parts.

CONCLUSIONS

A comprehensive, systematic study for one polymer - namely a polypropylene homopolymer - on the influence of processing conditions, molecular weight,and low percentage incorporation of commercially used additives,upon the impact properties of injection mouldings has been carried out. The following conclusions have been made from the results of this research project:-

(i) The impact strength of injection moulded GXM43 iPP homopolymer was determined by the processing conditions used, molecular weight distribution of the polymer, additives incorporated and the resultant micromorphology.

(ii) The impact strength may increase substantially part way across mouldings where banded morphologies and in particular row nucleated β phase spherulites disappear. This transition point in properties was always accompanied by a shift in the position of fracture initiation site towards the centre and a change in the fracture topography of initiation sites from smooth and brittle to fibrillar and tough.

(iii) The extent and depth of the highly sheared regions below the highly oriented skin varied considerably with processing conditions and resulted in variations in the impact performance.

(iv) Increasing the melt temperature used during moulding reduced the extent and depth of the row nucleated lamellar shear band and nucleation of β phase spherulites. This resulted in an improvement in impact properties by shifting the transition point closer to the gate. In addition, the size of core α-phase spherulites was enhanced with increasing melt temperatures and the skin thickness reduced.

(v) Increasing the mould temperature to above 70°C did not significantly effect the extent and width of banded morphologies. However, it resulted in the formation of a transcrystalline brittle surface layer in contrast to the usual tough/soft

surface skin found in low mould temperature mouldings. This transcrystalline surface layer caused dramatic reductions in impact resistance regardless of the underlying morphology. The size of β and core α spherulites were also observed to increase with mould temperature.

(vi) Reducing the cavity fill time increased the skin thickness and row nucleation of β spherulites. This resulted in some confusion as to the trends in impact properties with injection velocity since, a thick skin favoured good properties whereas extensive β formation favoured poor impact properties. Generally, little change in impact properties was found with variation in injection velocity. However, fast cavity filling did consistently improve centre of moulding impact properties.

(vii) The optimum impact strength distribution along the melt flow direction was found when high melt temperatures, low mould temperatures with fast injection times were used in combination to produce the iPP moulding. The microstructure of such a moulding was revealed as one with a relatively thick highly oriented skin ($\sim$20μm) and an underlying banded morphology which only extended some 20mm in from the gate.

(viii) It was proposed that the greater degree of isotropy implied by the α-phase cross-hatched lamellar structure revealed in TEM studies explained the extremely high impact resistance of the core material.

(ix) It was also proposed that the β phase spherulite caused an embrittlement of mouldings because of its entirely radial organisation of lamellae. Crack propagation will occur most readily between radial lamellae where there are only weak tie molecules offering any resistance.

(x) The skin thickness and the extent and depth of highly shear nucleated row structures were found to increase markedly with increasing molecular weight. As a consequence impact properties were supressed in the highly sheared gate region of high

molecular weight mouldings, but enhanced in regions furthest from the gate, where sheared structures were absent. This trend was explained in terms of increased shear stress, preferred orientation and relaxation times with the increase in molecular weight.

(xi) A noticeable decrease in core α spherulite size with molecular weight of polypropylene was also revealed. It was proposed that the perfection of small α-phase spherulites and the presence of a thick skin were responsible for the improvement in impact properties in regions further from the gate.

(xii) Low percentage additions of Quinacridone, talc and phthalocyanine compounds to GXM43 iPP injection mouldings caused massive nucleation of the α phase due to enhanced crystallisation rates. The impact properties of mouldings containing these additives were very poor. It was suggested that the spherulites nucleated in these compounds were underdeveloped with little cross hatched lamellar growth.

(xiii) Ultramarine blue pigmented iPP mouldings revealed an apparent reduction in degree of crystallinity with an increase in α spherulite size. The impact properties of Ultramarine blue pigmented plaques were slightly better than unpigmented ones. It was suggested that the α spherulites in the pigmented samples had a well developed cross-hatched lamellar morphology.

(xiv) Ultramarine blue pigmented and Chalk filled polypropylene injection mouldings revealed significantly enhanced random nucleation of β phase spherulites. This specific β phase nucleating characteristic did not alter the level of β row nucleation in the shear zone or the impact properties.

(xv) Several nucleating mechanisms have been reviewed in this thesis. It appears that the most probable explanation for the preferential nucleation of either the α or β polymorph could be connected with an epitaxial growth mechanism.

(xvi) Commercial mouldings of GXM43 iPP also revealed these structural heterogeneities in the form of skin-shear-core banded morphologies. In agreement with our observations the presence of shear nucleated β phase spherulites dramatically supressed the impact properties of the moulded part.

In conclusion, it can be stated that the research project fulfilled its original objective in relating the micromorphology of a range of iPP injection mouldings to the impact properties, to a depth not previously reported, using novel techniques of characterisation and only recently established impact testing procedures.

RECOMMENDATIONS FOR FUTURE WORK

Recommendations for future work arising from the studies presented in this thesis are as follows:-

(i) A strong case can be made for studying the effect of other pigments and nucleants on the micromorphology and properties of iPP mouldings. FBC Industrial Chemicals forwarded a preliminary applications data sheet for FIC MDBS which is an alkyl substituted di-benzylidene sorbital developed specifically as a nucleating agent for use in crystalline polyolefines. FIC MDBS is claimed to improve crystallisation rates and result in improved tensile strength and modulus, improved impact resistance, as well as improvements in processing factors such as dimensional stability. Pigments based on chromium and iron compounds especially should be studied together with rutile which is extensively used as a white filler in industry.

(ii) To investigate the effect of incorporating various loadings of short and continuous glass and carbon fibres into polypropylene feedstocks on the micromorphology and impact properties of injection mouldings. A similar systematic study has recently been initiated at Brunel incorporating liquid crystal fibres in GXM43 and GYM45 iPP, to assess the effects of various volume percentages on the morphology and properties, as an extension to this work.

(iii) To determine whether there is a close relationship between molecular structure and crystal shape of additives and space arrangements of iPP which facilitate an epitaxial growth mechanism for induced nucleation of either the α or β crystalline form. This will involve extensive electron diffraction studies on particles which form the centre of spherulites produced by melting and recrystallisation of solvent cast films of the compounds.

(iv) More definitive information about the primary cause and mechanism of brittle fracture in mouldings which contain row nucleated β spherulites would be desirable. Systematic studies of low temperature tensile tests and bend tests on mouldings produced under a range of processing conditions together with associated microstructure studies may provide the required information i.e. whether brittle failure is due to the entirely radial lamellar organisation of the spherulite.

(v) In addition to (iv) more information on the rôle of the α phase cross-hatched morphology on properties is desirable. To this end, use of optical birefringence measurements and TEM could be used in conjunction on a series of compression moulded plaques prepared and conditioned over a range of temperatures. The degree of cross-hatch measured could then be related to physical properties measured.

(vi) All the work reported in this thesis applies to isotactic polypropylene homopolymers. Similar systematic studies on the effect of processing conditions and nucleants upon the impact properties and microstructures of other polyolefines such as polybutylene, polyacetate, TPX and polyethylene should be carried out.

****

REFERENCES

1. S.M. Ohlberg, J. Roth, R. Raff, J. Mat.Sci.9,(1974),293.
2. E.S. Clark, SPE J. 23,(1967),46.
3. E.S. Clark, C.A. Garber, Int.J. Polym. Mater.1,(1971),31.
4. E.S. Clark, Appl. Polym. Symp. No 20,(1973),325.
5. M.R. Kantz, Int.J. Polym. Mater,3,(1974),245.
6. M.R. Kantz, H.D. Newman, F.H. Stigale, J.App.Polym.Sci.16,(1972),1249.
7. J. Way, J. Atkinson, T. Nutting, J.Mat.Sci.9,(1974),293.
8. S.J. Henke, C.E. Smith, R.F. Abbott, Polym.Eng.Sci.15,(1975),79.
9. J. Bowman, N. Harris, M. Bevis, J.Mat.Sci.10,(1975),63.
10. M. Fujiyama, S. Kimura, Kobunshi Ronbunshu, 32,(10),(1975),581.
11. M. Fujiyama, S. Kimura, Kobunshi Ronbunshu, 32,(10),(1975),591.
12. M. Fujiyama, S. Kimura, J.App.Polym.Sci.21,(1977),2285.
13. M. Fujiyama, H. Awaya, S. Kimura, J.App.Polym.Sci.21,(1977),3291.
14. M. Fujiyama, S. Kimura, J.App.Polym.Sci.22,(1978),1225.
15. T. Okamoto, Japan plastics age, issue II,July,(1977),22.
16. D. Williams, Ph.D Thesis, Liverpool University, (1979).
17. D. Williams, M. Bevis, J.Mat.Sci.15,(1980),2834.
18. D. Williams, M. Bevis, J.Mat.Sci.15,(1980),2843.
19. D. Williams, M. Bevis, J.Mat.Sci.15,(1981),3335.
20. D. Williams, M. Bevis, J.Mat.Sci.17,(1982),1915.
21. K. Watkinson, A. Thomas, M. Bevis, J.Mat.Sci.17,(1982),347.
22. M. Guo, J. Bowman, J.App.Polym.Sci.28,(1983),2341.
23. L. Schmidt, J. Opfermann, G. Menges, Polym.Eng.Rev.1,(1),(1981),1.
24. S.F. Xavier, D. Tyagi, A. Misra, Polym.Composites,3,(1982),88.
25. J. Bowman, J.Mat.Sci.16,(1981),1151.
26. Private communication with Mr. R. Addis.
27. O.C. Oppenlander, Science, 159,(1968),1311.
28. R.S. Stein, SPE Trans,(1964),178.
29. B. Wunderlich, Macromol. Phys.,1,(1973) Academic Press.N.Y.69.
30. H.D. Keith, F.J. Padden, J.Polym.Sci.,39,(1959),101.
31. H.D. Keith, F.J. Padden, J.Polym.Sci.,39,(1959),123.
32. A. Keller, J.Polym.Sci.,39,(1959),151.
33. F.P. Price, J.Polym.Sci.,39,(1959),139.
34. H.D. Keith, F.J. Padden, J.Appl.Phys.,34,2409.
35. D.C. Bassett, "Principles of Polymer Morphology". Cambridge University Press.(1981),146.
36. J.D. Hoffman, G.T. Davis, J.I. Lauritzen "Treatise on solid state Chemistry", N.Y.Plenum,3,Chap.7,(1976).
37. I.C. Sanchez, J. Macromol. Sci.Rev. Macromol Chem.,10,(1974),113.
38. J.M. Schultz, Polymer Materials Science, Englewood Cliffs, NJ: Prentice Hall (1974).
39. G. Natta, P. Corradini, Nuovo.Cim.Supp.15,(1960),1.
40. H.D. Keith, F.J. Padden, N.M. Walter, M.W. Wycoff, J.Appl.Phys. 30,(1959),1485.
41. A. Turner-Jones, J.M. Aizlewood, D.R. Beckett, Makromol.Chem. 75,(1964),134.
42. A. Turner-Jones, A.J. Cobbold, J.Polym.Sci.6,(1968),539.
43. R.J. Samuels, R.Y. Yee, J.Polym.Sci.A-2,10,(1972),385.
44. H. Dragaun, H. Hubeny, H. Muschik, J.Polym,Sci.Phys.15,(1977),1779.
45. A.J. Lovinger, T.O. Chua, C.C. Gryte, J.Polym,Sci.15,(1977),641.
46. H.J. Leugering, Die Makromol. Chem.109,(1967),204.
47. A.A. Duswalt, W.W. Cox, ACS Polym.Pre prints,11,(2),(1970),1154.
48. H.J. Leugering, G. Kirsch, Die.Ang. Makromol. Chem.33,(1973),17.
49. D.R. Morrow, B.A. Newman, J.Appl.Phys.39,(1968),4944.
50. J.L. Kardos, A.W. Christiansen, E. Baer, J.Polym.Sci.A-2,4,(1966),777.
51. J.A. Sauer, K.D. Pae, J.Appl.Phys.30,(1968),4950.
52. E.J. Addinck, J. Beintema, J.Polymer,2,(1961),185.
53. F.J. Padden, H.D. Keith, J.Appl.Phys.30,(1959),1479.
54. J.A. Sauer, D.R. Morrow, S.C. Richardson, J.Appl.Phys.36,(1965),3017.
55. F.J. Khoury, Res.Natl.Bur.Stand.(1966),A70,29.
56. F.J. Padden, H.D. Keith, J.Appl.Phys.44,(1973),1217.

57. P.M. Geil, 'Polymer Single Crystals', Interscience,N.Y,(1963),211.
58. F.J. Padden, H.D. Keith, J.Appl.Phys.37,(1966),4013.
59. A.J. Lovinger, J.Polym.Sci.,Polym.Phys.Edn.,21,(1983),97.
60. R.M. Olley, A.M. Hodge, D.C. Bassett, J.Polym.Sci.,Polym.Phys. Edn.,17,(1979),627.
61. D.C. Bassett, A.M. Hodge, R.H. Olley, Proc.Roy.Soc.A377;(1981); I,25;II,39; III, 61.
62. D.C. Bassett, R.H. Olley, Polymer, 25,(1984),935.
63. D.R. Norton, A. Keller, Polymer,26,(1985),704.
64. E.S. Clark, J.E. Spruiell, Polym.Eng.Sci,16,(1976),176.
65. A.A. Duswalt, W.W. Cox, Polym.Character.,Interdisciplinary Approaches, Prac.Symp.,(1970),147.
66. Y. Fujiwara, Colloid.Polym.Sci.,253,(1975),273.
67. W. Ullman, J.H. Wendorff, Progr.Colloid.Polym.Sci,66,(1979),25.
68. J.A. Odell, D.T. Grubb, A. Keller, Polymer,19,(1978),617.
69. Z. Bashir, J.A. Odell, A. Keller, J.Mat.Sci,19,(1984),3713.
70. Z. Tadmor, J.Appl.Polym.Sci.18,(1974),1753.
71. V. Tan, M. Kamal, J.Appl.Polym.Sci.22(1978),2341.
72. M. Kamal, F.H. Moy, Polym.Eng.Review,2,(1983),No 4,381.
73. B. Heise, H.G. Kilian, G. Lupke, P. Schultz,W. Woebeken, Kolloid -Z,250,(1972),120.
74. B. Heise, Colloid.Polym.Sci.254,(1976),279.
75. S. Katti, J. Schultz, Polym.Eng.Sci.22,(1982),1001.
76. W. Heckmann, U. Johnsen, Colloid.Polym.Sci.,252,(1974),826.
77. D.R. Fitchmun, Z. Mencik, J.Polym.Sci.,Polym.Phys.Edn,11,(1973),951.
78. Z. Mencik, D.R. Fitchmun, J.Polym.Sci.,Polym.Phys.Edn,11,(1973),973.
79. G. Menges, A. Wubken, B. Horn, Colloid.Polym.Sci.,254,(1978),267.
80. J.E. Collear, J.B. Shorthall, J. Mater.Sci.,12,(1977),141.
81. S.Y. Hobbs, C.F. Pratt, J.Appl.Polym.Sci.,19,(1975),1701.
82. G. Menges, G. Wubken, SPE Antec tech.papers,19,(1973),519.
83. E.A. Cole, Plastics and Polymers,Oct,(1975),181.
84. R.J. Crawford, K. McGonagle, Plast.Rubb.Proc.App.3,(1983),43.
85. R.J. Crawford, V. Klewpantinond, P.P. Benham, Plastics and Rubber: Processing,April,(1978),133.
86. R.J. Crawford, V. Klewpantinond, P.P. Benham, Plastics and Rubber: Processing April,(1979),151.
87. R.J. Crawford, A.Ali,Proc.PRI conf. 'Moulding of Polyolefins', November,1980,London.
88. R.J. Crawford, Plastics and Rubber: Processing,June,(1980),61.
89. P.J. Cloud, I. McDowell, G. Gerakaris, Plast.Tech.,22,(1976),9.
90. J.R.F. Andrews, M. Bevis, J.Mat.Sci.,19,(1984),653.
91. C.R. Lindsey, J.Appl.Poly.Sci.,26,(1981),1.
92. R.C. Thamm, Rubb.Chem.Tech.April,(1977),50.
93. S.C. Kofard, Soc.Plast.Ind. 36th Annual.Conf. - Reinforced Plastics Feb.(1981).
94. R.J. Crawford, P.P. Benham, J.Mech.Eng.Sci.,16,(1974),178.
95. P.C. Emeanuwa, M. Bevis, to be published.
96. H.N. Beck, J. Appl.Polym.Sci.,11,(1967),673.
97. F.L. Binsbergen, J.Polym.Sci.,Polymer Symposium.59,(1977),11.
98. F.L. Binsbergen, Polymer.11,(1970),253.
99. D.R. Fitchmun, S. Newman, J.Polym.Sci.,A-2,8,(1970),1545.
100. A.M. Chaterjee, F.P. Price, J.Polym.Sci.,Polym Phys Ed.,13,(1975),2369.
101. A.M. Chaterjee, F.P. Price, J.Polym.Sci.,Polym.Phys.Ed.,13,(1975),2385.
102. S.Y. Hobbs, Nature.Phys.Sci.,239,(1972),89,28.
103. J.C. Wittman, B. Lotz, A.M. Hodge, J.Polym.Sci.,Phys.,21,(1983),2495.
104. J. Garbarczyk, D. Paukszta, Polym.Reports,22,(1981),562.
105. F. Rybnikar, J.Appl.Polym.Sci.,13,(1969),827.
106. F. Rybnikar, J. Macromol. Sci.,Phys,B19,1,(1981),1.
107. G. Ronca, PhD Thesis, (1985), Brunel University.
108. T.J. Hutley, M.W. Darlington, Polymer(Commun.),25,(1984),226.
109. T.J. Hutley, M.W. Darlington, Polymer(Commun.),26,(1985),264.
110. I.C.I. Technical Data Summary Leaflet, PP34.
111. I.C.I. Technical Data Summary Leaflet, PP36.

112. Omya, Technical Data Sheet "Hydrocarb" 12/76.
113. Telephone Communication. Mr. K. Tuck, I.C.I.
114. Reckitts Colours Ltd. Information Sheet 307/2/08.
115. D.R. Morrow, J. Macromol. Sci.,Phys.,1,B3,(1969),53.
116. F.L. Binsbergen, B.G.H. De Lange, Polymer,9,(1968),23.
117. Hoechst Information Booklet "Organic Pigments for the Paint Industry" (1982).
118. Hoechst Information Sheet "Hostaperm Red E3B For The Automotive Industry."
119. Hoechst Information Sheet "Hostaperm Red E3B For The Printing Industry."
120. Hoechst Information Booklet "Pigments And Special Dyes",(1984).
121. Patent Specifications, 1577 034,Inv.K. Thomas.,(1977).
122. W.E. Wolstenholme, J.Appl.Polym.Sci.,6,(1962),332.
123. P.P. Kelly, T.J. Dunn, Mater.Res.Stand.3,(1963),545.
124. C.B. Arends, J.Appl.Polym.Sci.,9,(1965),3531.
125. C.J. Hooley, M.J. Williams, I.C.I. Communication (1978).
126. L.C. Cessna, J.P. Lehane, R.H. Ralston, T. Prindle, Polym.Eng. Sci.,16,(1976),419.
127. T. Casiraghi, Polym.Eng.Sci.,18,(1978),833.
128. T. Casiraghi, G. Castiglioni, G. Ajrold, Plast.Rubb.Proc.App.2, (1982),353.
129. P. Zoller, Polym.Testing,3,(1983),197.
130. J.J. Mooij, Polym.Testing,1,(1981),69.
131. S. Turner, M. Money, P.E. Reed, Plast.Rubb.Proc.App.,4,(1984),369.
132. Rosand Technical Leaflet (1984).
133. K. Thomas, D.E. Meyer, Proc. 5th European Conf. on Plast. x Rubb, Paris. 12-15 June (1978).
134. G.C. Stevens, K. Thomas, PRI Int.conf. Impact Testing and Performance of polymeric materials Sept(1985),12/1.
135. L.B. Morgan, J.Appl.Chem.,4,(1954),160.
136. H.N. Beck, H.D. Ledbetter, J.Appl.Polym.Sci.,9,(1965),2131.
137. M.J. Richardson, D.A. Blackadder, N.G. Savill, Makromol.Chem. 25,(1984),226.
138. G. Ronca, D. Vesely. submitted to J.Poly.Sci.,(1984).
139. M.J. Oliveira, D.A. Hemsley, British Polymer Journal,17,(3),(1985),269.
140. R.P. Palmer, A.J. Cobbolds, Makromol.Chem.74,(1964),174.
141. D.R. Fitchmun, Z. Mencik, J.Polym.Sci.,Polym.Phys.Ed.11,(1973),951.
142. V.J. Armond, J.R. Atkinson, J.Mat.Sci.,4,(1969),509.
143. G. Kanig, Kolloid Z, 251, (1973),782.
144. F. de Korosy, E. Zeigerson, J.Appl.Polym.Sci.,11,(1967),909.
145. R.H. Olley, A.M. Hodge, D.C. Bassett, J.Polym.Sci,Polym.Phys.Ed. 17,(1979),627.
146. D.R. Norton, PhD Thesis, Bristol University, (1984).
147. H. Uejo, S. Hoshino, J.Appl.Polym.Sci.,14,(1970),317.
148. D.E. Scherpereel, Plast.Eng.,(1973),46.
149. J.P. Trotignan, J.L. Lebrun, J. Verdu, Plast.Rubb.Proc.App.2, (1982),247.
150. A. Weidinger, P.H. Hermans. Makromol.Chem.24,(1961),44.
151. R. Ullman, J.Polym.Sci.,45,(1960),91.
152. B.W. Mott, Micro-Indentation Hardness Testing, Butterworths, London, (1956).
153. R.J. Kent, K.E. Puttick, J.G. Rider, Plast. & Rubb.Int.6,(1981),104.
154. R.J. Crawford, D. Paul, Y. Adeebnia, European.Polym.J.16,(1980),401.
155. J. Bowman, M. Bevis, Plast.Rubb:Mats. App.(1976),177.
156. J. Bowman, M. Bevis, Colloid and Polym.Sci.,255,(1977),954.
157. R.J. Kent, K.E. Puttick, J.G. Rider, Plast.Rubb.Proc.App.,1,(1), (1981)I.55-61, II,113-117.
158. P. Eyerer, G. Lang, German Plastics, 62,(1972),19.
159. R.J. Crawford, Polym Testing.,3,(1982),37.
160. R.J. Crawford, G. Stevens, Polym Testing, 6,(1985),113.

161. F.J. Balta-Calleja, D.C. Bassett, J.Polym.Sci.,Polym.Symp.58 (1977),157.
162. R.J. Phillips, N.R. Ramakrishnan, Polym.Eng.Sci.,18,(11),(1978),869.
163. R.J. Barriault, L.F. Gronholz, J. Polym,Sci.,18,393,(1955).
164. R.K. Eby, J.Appl.Phys.35,2720,(1964).
165. T. Bessel, J.B. Shorthall, J.Mat.Sci.,10,(1975),2035.
166. P.J.A. Ritchie, B.W. Cherry, 13th and 14th Conf. Adhesion (City Univ. Lond.) 1975/6 Chpt. 15,235.
167. M. Masuoka, Int. J. Adhesion and Adhesives,1,(1981),256.
168. J.L. Kardos, J. Adhesion,5,(1973),119.
169. M.J. Folkes, J. Wong, Internal Report,Brunel University(1985)
170. M.J. Folkes, S. Hardwick, J.Mat.Sci.,Letts.3,(1984),1071.
171. P.J. Flory, J. Chem.Phys.,15,(1947),397.
172. W.R. Krigbaum, R.J. Roe, J.Poly.Sci.,A2,(1964),4391.
173. W. Haas, B. Maxwell, Polym.Eng.Sci.,9,(1969),No. 4.
174. A.K. Fritzsche, F.P. Price, Polym.Eng.Sci.,4,(1974),No. 6.
175. B. Honigmann, H.V. Lenne H.P. Acta.Cryst.17,(1964),1015.
176. D. Vesely, G. Shipley, Internal Report, Brunel University,(1982).
177. J. Garborczyk, D. Paukszta, Polymer.22,(1981),562.